The 12th International Conference of Young Scientists on Energy Issues

Kaunas, Lithuania, May 27–28, 2015

Organized by

Lithuanian Energy Institute

In cooperation with:

AGA
UAB "REO Investment"
UAB BIURO PASAULIS

Chair of the Conference dr. Sigitas RIMKEVČIUS
Chair of the Organizing Committee dr. Viktorija BOBINAITĖ

INTERNATIONAL SCIENTIFIC COMMITTEE

Andres SIIRDE	Estonia	Mantas MARČIUKAITIS	Lithuania
Andris KRESLINS	Latvia	Namejs ZELTINS	Latvia
Alessandro PETRUZZI	Italy	Pierre-Etienne LABEAU	Belgium
Bernhard PETERS	Luxemburg	Panos M. PARDALOS	USA
Bjørn C. HAUBACK	Norway	Ralf EBINGHAUS	Germany
Darius MILČIUS	Lithuania	Sten BERGSTROM	Sweden
Enn MELLIKOV	Estonia	Sigitas RIMKEVIČIUS	Lithuania
Eugenijus UŠPURAS	Lithuania	Sergej ZHDANOK	Belarus
Finn RAVNDAL	Norway	Victor A. ZHOVYANSKY	Ukraine
Florentin PALADI	Moldova	Vaclovas MIŠKINIS	Lithuania
Luis E. HERRANZ	Spain	Virginijus RADZIUKYNAS	Lithuania
Myriam LAZARD	France	Vytautas MARTINAITIS	Lithuania

The Board of the Official Reviewers was formed from the experts in the field of the Conference topics.

BOARD OF THE OFFICIAL REVIEWERS

Robertas ALZBUTAS	Lithuania
Diana ADLIENĖ	Lithuania
Arvydas ADOMAVIČIUS	Lithuania
Tomas DEVEIKIS	Lithuania
Grigorijus DUŠKESAS	Lithuania
Farida DZENAJAVIČIENĖ	Lithuania
Ramūnas GATAUTIS	Lithuania
Viktorija GRIGAITIENĖ	Lithuania
Aleksandras ILJINAS	Lithuania
Audrius JONAITIS	Lithuania
Rolandas JONYNAS	Lithuania
Vytautas JUŠČIUS	Lithuania
Tadas KALIATKA	Lithuania
R. KALPOKAITĖ-DIČKUVIENĖ	Lithuania
Arvydas KANAPICKAS	Lithuania
Jūratė KARBAUSKAITĖ	Lithuania
Žydrūnas KAVALIAUSKAS	Lithuania
Antanas KAVOLYNAS	Lithuania
Inga KONSTANTINAVIČIŪTĖ	Lithuania
Vaclovas KVESELIS	Lithuania
Giedrius LAUKAITIS	Lithuania
Aurimas LISAUSKAS	Lithuania
Narimantas LISTOPADSKIS	Lithuania
Algirdas MAKNICKAS	Lithuania
Liutauras MARCINAUSKAS	Lithuania
Mantas MARČIUKAITIS	Lithuania
Linas MARTIŠAUSKAS	Lithuania
Linas MIKNIUS	Lithuania
Darius MILČIUS	Lithuania
Saulė MILČIUVIENĖ	Lithuania
Mindaugas MILIEŠKA	Lithuania
Violeta MISEVIČIŪTĖ	Lithuania
Vaclovas MIŠKINIS	Lithuania
Žilvinas NAKUTIS	Lithuania
Robertas NAVAKAS	Lithuania
Raimondas PABARČIUS	Lithuania
Robertas POŠKAS	Lithuania
Juozas SAVICKAS	Lithuania
Vytautas STANKUS	Lithuania
Inga STASIULAITIENĖ	Lithuania
Giedrė STRECKIENĖ	Lithuania
Nerijus STRIŪGAS	Lithuania
Marijus ŠEPORAITIS	Lithuania
Audrius ŠIMONIS	Lithuania
Romualdas ŠKĖMA	Lithuania
Artūras ŠMAIŽYS	Lithuania
Dalius TARVYDAS	Lithuania
Aurimas TONKŪNAS	Lithuania
Egidijus URBONAVIČIUS	Lithuania
Gediminas VASILIAUSKAS	Lithuania
Iveta VARNAGIRYTĖ-KABAŠINSKIENĖ	Lithuania

THE ORGANIZATIONAL COMMITTEE OF THE CONFERENCE

Besides the many persons involved in the preparatory work of the Conference the following persons are leading in this process:

Dr. Sigitas Rimkevičius, Director of Lithuanian Energy Institute
Dr. Rolandas Urbonas, Deputy Director of Lithuanian Energy Institute
Dr. Diana Meilutytė-Lukauskienė, Lithuanian Energy Institute
Viktorija Bobinaitė, Lithuanian Energy Institute
Jolanta Kazakevičienė, Studies Administrator of Lithuanian Energy Institute
Young Scientists Association of Lithuanian Energy Institute

Conference secretariat

Dr. Diana Meilutytė-Lukauskienė
Viktorija Bobinaitė

Technical support and programming (conference proceedings, website)

Dr. Darius Jakimavičius
Dr. Tadas Kaliatka
Marius Urbonavičius
Mantas Valantinavičius
Šarūnas Varnagiris
Tomas Vonžodas
Liudvikas Žiemys

Layout

Zita Cvilikienė
Laima Vasiliauskienė

Dear Reader of the Conference Proceedings,

We are pleased to present the original research and review papers from the 12th International Conference of Young Scientists on Energy Issues (CYSENI-2015), which took place on 27–28 May 2015 in Lithuanian Energy Institute, Kaunas, Lithuania.

The Conference aimed at creating a platform where young scientists dealing with energy-related issues could share, create and disseminate knowledge, present the up-to-date research results and familiarize with the research of their colleagues; as well develop their skills to present own ideas and discuss over twelve scientific topics. They are:

I Hydrogen and fuel cells
II Renewable energy sources
III Smart energy networks
IV Energy efficiency and reliability
V Knowledge for energy policy making
VI Investigations in the fields of thermal physics, fluid mechanics and metrology
VII Material sciences and Technology
VIII Investigations of combustion and plasma processes
IX Global change and ecosystems
X Fusion energy
XI Nuclear fission and radiation protection
XII Cross-cutting energy issues

This year the Conference received 76 abstracts, 74 from which were found relevant and approved for the Conference. The Authors of these abstracts prepared the full-length papers. All submitted papers passed a thorough review process. Each paper was reviewed by two reviewers - Official and Young - specializing in the related topic and field. After the review 55 revised papers in various fields of energy have been accepted for the publication in the Conference Proceedings. We kindly invite you to introduce with them.

We would like to heartily thank the Conference Participants who wrote papers and later corrected them based on the Reviewers remarks and according to the Conference guidelines; as well Participants who presented the research results during the Conference event. We are grateful to the Official and Young Reviewers for their responsible viewpoint to review process, well-meant comments, which helped to improve the content of the papers, and their valuable contributions to the Conference Proceedings.

Regarding the next year we invite you to the 13th International Conference of Young Scientists on Energy Issues 2016 (CYSENI-2016), which will be held on 26–27 May 2016 in Kaunas, Lithuania.

Sincerely,
Conference Organizers

CONTENT

I HYDROGEN AND FUEL CELLS (3)

II RENEWABLE ENERGY SOURCES (12)

III SMART ENERGY NETWORKS (1)

IV ENERGY EFFICIENCY AND RELIABILITY (7)

V KNOWLEDGE FOR ENERGY POLICY MAKING (4)

VI INVESTIGATIONS IN THE FIELDS OF THERMAL PHYSICS, FLUID MECHANICS AND METROLOGY (6)

VII MATERIALS SCIENCES AND TECHNOLOGY (6)

VIII INVESTIGATIONS OF COMBUSTION AND PLASMA PROCESSES (5)

IX GLOBAL CHANGE AND ECOSYSTEMS (1)

X FUSSION ENERGY (1)

XI UCLEAR FISSION AND RADIATION PROTECTION (8)

XII CROSS-CUTTING ENERGY ISSUES (1)

CYSENI 2015, May 27–28, Kaunas, Lithuania
ISSN 1822-7554, www.cyseni.com

PHASE-STRUCTURAL TRANSFORMATIONS AND ELEMENTAL COMPOSITION ANALYSIS IN THE TiO$_x$ FILMS EXPOSED IN WATER VAPOUR PLASMA

D. Gimzauskaite
Faculty of Natural Sciences, Vytautas Magnus University
Vileikos str. 8, LT-44404 Kaunas– Lithuania
Email: dovile.gimzauskaite@gmail.com

L. Pranevicius
Centre for Hydrogen Energy Technologies, Lithuanian Energy Institute
Breslaujos str. 3, LT-44403 Kaunas – Lithuania
Email: l.l.pranevicius@gmf.vdu.lt

ABSTRACT

In the presented work the titanium (Ti) films were deposited on monocrystalline silicon substrates by using non-balanced magnetron sputtering technique and then in order to form the photocatalyst the Ti film was oxidized in water vapour plasma. Because of photoelectrochemical water splitting that occurs on the TiOx film surface, phase-structural transformations and elemental composition changes in the films were expected. In order to analyse those processes, deposited films were investigated using modern, high-performance physical research methods: scanning electron microscopy (SEM), energy dispersive X-ray spectroscopy (EDS), X-ray diffraction analysis (XRD), X-ray photoelectron spectroscopy (XPS), optical microscopy, as well as the measurements were performed using nanoprofilometer.

Results obtained with nanoprofilometer and XRD revealed that titanium interaction with water vapour plasma led to intensive structural and compositional transformations of Ti films. Moreover XRD indicated that Ti was oxidized to TiO2. SEM data showed that at higher bias voltage film surface oxidation and hydrogen saturation into the bulk is more intensive. Nevertheless, then the bias voltage is not used, reaction occurs even faster. Studies with optical microscope revealed that it is much easier to saturate the thin film (~175 nm) with hydrogen than the thick one (~ 785 nm). Research with XPS established that regardless of the film thickness, mostly the same thickness of the films (~ 39-42 nm) was oxidized. Also it was found that at higher power (270 W) films oxidation and hydrogen saturation into the bulk occurs more intensive than at lower powers (117 W). Moreover results obtained with XRD revealed that due to the higher power new TiO2 phase formation occurred.

Keywords: water vapour plasma, thin films, oxidation, hydrogen, TiO$_2$

1. INTRODUCTION

The rapidly growing global human population leads to constantly increasing demand for energy. In a broad perspective, energy acts as a key catalyst in the generation of wealth for a nation by making its significant role in developing the technological, industrial, economic and social sectors within the nation [1]. However it should be noted that nowadays most of the energy that we use comes from fossil fuels – limited Earth resources, the use of which causes climate change. Realizing that the rate of energy consumption possibly will increase in the near future and seeking to at least partially solve the environmental problems, we are looking for alternative, environmentally friendly energy sources. Hence by significantly increasing demand for energy, the exploitation of new energy resources has the potential to reshape energy policy at national and international levels – altering energy security, recasting the economics of energy technology investment decisions, and shifting trends in greenhouse gas emissions [2].

Conversion of solar energy into chemical energy in the form of so-called "solar fuels" (such as H_2) is considered one of the most perspective strategies to solve the energy and environmental problems in the future. Hydrogen is the most abundant element on the Earth that has a high energy yield (122 kJ/g) which is triple that of gasoline (40 kJ/g) quadruple that of natural gas [3, 4]. Furthermore, hydrogen is environmentally friendly because no greenhouse gases (CO_2) are produced during the combustion process.

While various technologies can be used to generate hydrogen, only some of them can be considered environmentally friendly [4]. One of them – hydrogen production from water by using semiconductors as photocatalysts. This technology provides a potential efficient way to obtain hydrogen, due to its ecological production process by utilizing solar energy.

Currently TiO_2 has been considered as one of the best photocatalysts due to its good photoactivity, nontoxicity and low cost [5–7], but practical applications of the TiO_2 is still quite limited, mainly because of broad bandgap responding only to UV light [8]. However, the scientists are still looking for the ways to improve photocatalytic TiO_2 properties in order to activate it by daylight.

Typically for research of TiO_2 photocatalytic properties, researches are using already formed TiO_2. But in the presented work the titanium (Ti) films were deposited on monocrystalline silicon substrates by using non-balanced magnetron sputtering technique and then in order to form photocatalysts the Ti film was oxidized in water vapour plasma. The most important factor that the plasma oxidation technique allows us to control the formation of catalytic coating. All these details proves the novelty of this technology. The aim of this work was to analyse phase-structural transformations and elemental composition in the TiO_x films after the exposing in water vapour plasma.

2. METHODOLOGY

The thin Ti films were deposited using non-balanced magnetron sputtering technique (vacuum system PVD – 75) on the crystalline Si (111) substrates (10x20 mm). Pure titanium (99.99 at. %) of 76 mm diameter and 3 mm thickness cathode was used as a target material and distanced 35 mm away from substrate holder. Pure argon gas (99.999 at. %) was used as the sputtering gas. The discharge parameters have been controlled using a variable DC power supply (3 kV, 500 mA). Prior the deposition, the target was plasma cleaned in order to remove surface oxide layers. Sputtering time was chosen in order to obtain 150–750 nm thick Ti films for sputtering power supply of 100 W (200 mA, 500 V), that is corresponding to a power density of 1.2 W/cm^2. The thickness of the films was measured using nanoprofilometer revealing the height of the step with an accuracy of ±10 nm [9].

Samples with the deposited Ti film were placed on the water cooled substrate holder and treated under water vapour plasma for 30 min. Plasma treatment was performed at 63-100 Pa pressure of water vapour using PVD – 75. For plasma generation was used RF power supply. The dissipated power in plasma was verified in the range of 113–270 W. The negative bias voltage was in the range between 0 and -200 V. All samples were located in 18 mm above Ti cathode.

The structure and phase composition of the samples were investigated by the Bruker X-ray diffractometer (Bruker D8). The measurements were performed with 2θ angle in the range 20°–70° using CuKα radiation in steps of 0.01°. All peaks were identified using Search – Match software. After treatment with water vapour plasma, all samples were investigated by the scanning electron (SEM, JEOL JSM-5600) and optical (Nikon Eclipse Lv150) microscopies. The elemental composition of plasma treated films was analysed by energy dispersive X–ray spectroscopy (EDX, Bruker Quad 5040). The depth distribution profiles of

O in Ti films were measured by using the X-ray photoelectron spectroscopy (XPS) equipped with an ion gun. The film was sputtered by using focused 1 keV Ar^+ ion beam at the incidence angle of 45 degrees from surface normal and rotated around the measured spot. The ion current density was around 1 µAcm-^{2}. The film thickness and the surface roughness were measured using the nanoprofilometer (Ambios XP 200).

3. RESULTS AND DISCUSSIONS

To determine the thickness, the film step measurements were done of Ti films before and after the treatment in water vapour plasma. Fig. 1 illustrates typical surface profile. It was found that, the thickness of untreated Ti film is equal to ~ 460 nm and after treatment the thickness increases up to ~ 710 nm. It let us to assume that the redox reaction are successful and films thickness is increasing about 250 nm.

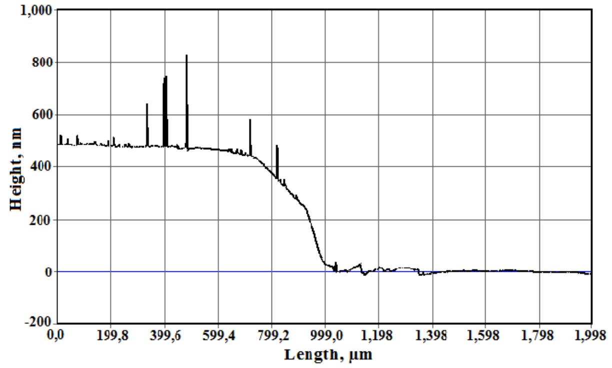

a) b)

Fig. 1. Surface height profiles of the Ti films: a) as-deposited,
b) plasma treated at 240 W, 0 V for 30 min.

Fig. 2 shows surface roughness (it is same sample as in Fig. 1). The studies revealed that the root mean square (RMS) of the as-deposited Ti film on the silicon substrate is equal to ~ 4.55 nm and it increases after the plasma treatment up to ~ 21.66 nm. The Ti film become significantly rougher after the water plasma treatment. Consequently, it can be said that the phase-structural transformations occurred on the surface of film and sufficiently smooth titanium were possibly oxidized to much rougher TiO_x.

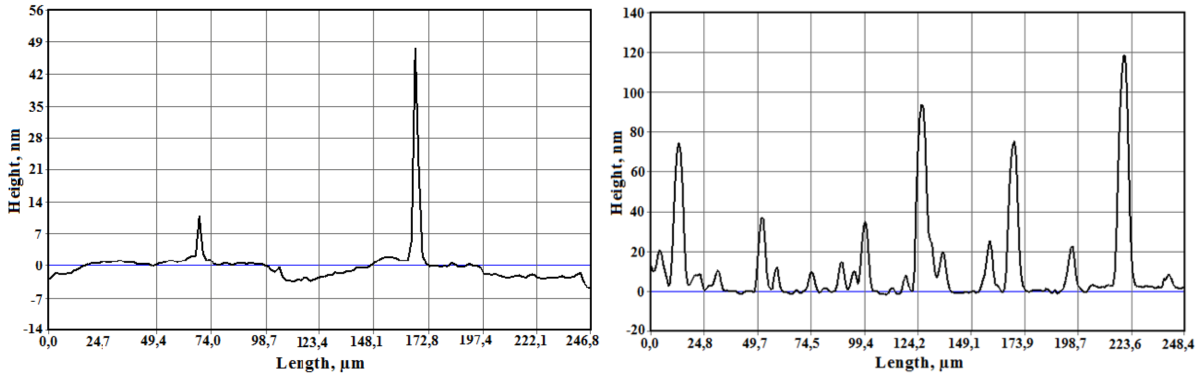

a) b)

Fig. 2.The profiles of surface roughness: a) as-deposited,
b) plasma treated at 240 W, 0 V for 30 min

Because the samples were formed at some different parameters the results will be discussed by grouping them according to the substrate bias voltage, film thickness and plasma treatment power.

3.1. Substrate bias voltage influence on the interaction between titanium films and water vapour plasma

Fig. 3 includes SEM surface views of plasma-treated, relatively thin (175–289 nm) Ti films: a) at bias voltage -200 V, b) at -100 V and c) at 0 V (grounded). It is seen that at -100 V (Fig. 3 b) were formed inconsiderable hydrogen bubbles, which at some place are exploded. While increasing the voltage up to -200 V (Fig. 3 a) the number of bubbles in the film increases and it's becoming more visible. It seems that at higher bias voltage film surface oxidation and hydrogen saturation into the bulk is more intensive. This could be explained by the fact that with increasing bias voltage increases the ion current dencity and ions energy. Thus, the film surface bombardment by ion flow becomes more active. The surface of titanium reacts with higher quantity of oxygen ions, thereby forming a thicker barrier layer of TiO_2. But due to the higher surface bombardment, stronger surface etching takes place. In this case the surface is saturated with hydrogen easier because the most active and fastest ions are the lightest ones that is why hydrogen moves into grain boundaries and penetrates deep into the Ti film.

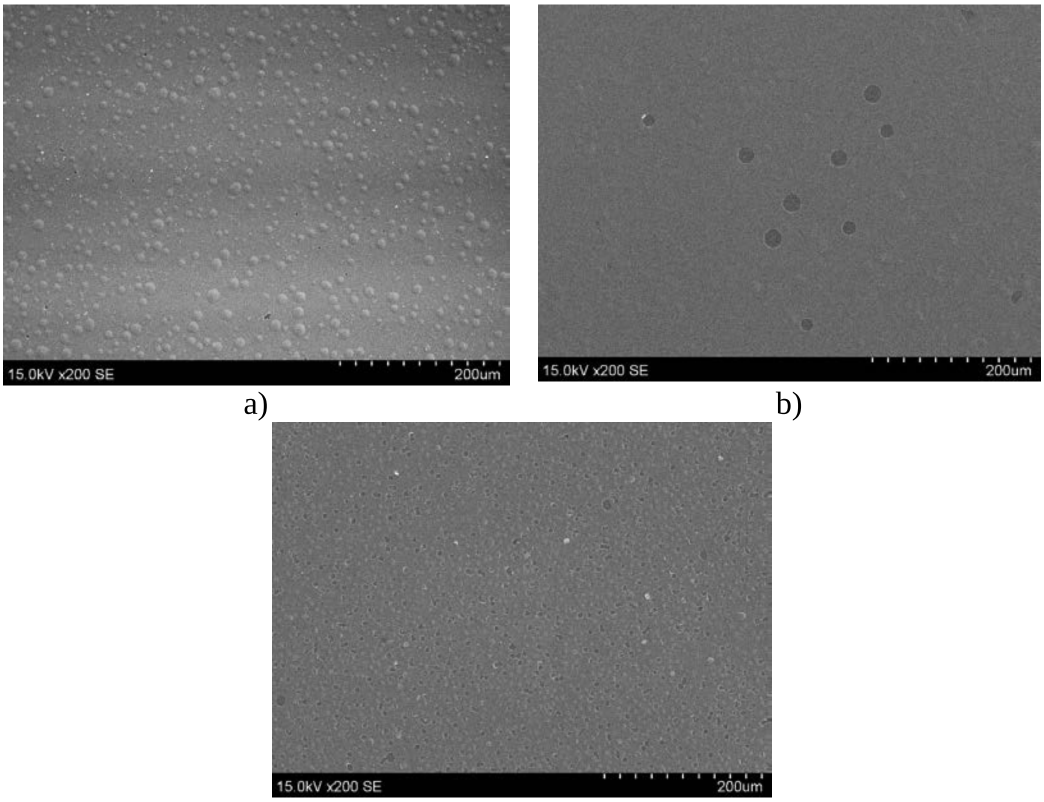

a) b)

c)

Fig. 3. SEM surface views of plasma-treated Ti films: a) -200 V (film thickness ~175 nm), b) at -100 V (film thickness ~192 nm) and c) at 0 V (film thickness ~289 nm). All samples treated at 270 W for 30 min

However, when the bias voltage is not used (Fig. 3 c) we can notice not only higher bubbles quantity in the film (what indicates that reaction occurs even faster than with -200V) but also higher burst of it. It is known that when reaction occurs using 0 V the film surface is attracted with lower ion flux and in this case barrier layer of TiO_2 is forming significantly slower. Based on previous research works [10, 11] it was shown that diffusion of hydrogen in TiO_2 is much slower than in Ti metal. The splitted atomic H wanders around in the oxide layer, until it is trapped or encounters another atomic H to recombine into H_2 and diffuses out of the oxide. As mentioned above hydrogen ion is lightest and fastest for this reason it penetrates easier into Ti film, especially when barrier layer is not thick. That is why, in this case, hydrogen saturation into film is faster.

It is also confirmed by the higher number of exploded hydrogen bubbles. Hydrogen atoms is diffusing deeper into the film, then react with each other and forms hydrogen molecules. Film volume increases and it becomes distended due to the formation of hydrogen and resulting micro strains. When concentration of H in the bulk exceeds the limit of solubility, formed bubbles explode following the release of hydrogen into the environment. The higher number of burst bubbles confirms that the reaction occurred faster and film was saturated with larger amount of hydrogen.

Fig. 4 shows the XRD patterns of the water vapour plasma treated Ti films at different bias voltage, which is equal to -200 V, -100 V, 0 V in curves 1–3, respectively (it is same samples as in Fig. 3). A comparison of the measured diffraction patterns of films revealed that there is no significant difference between the substrates which was treated at the bias votage -100 V and -200 V. In both cases, two wide peaks at 35.30° and 36.66°, which may be interpreted as superposition of TiO_2 peaks, were detected. TiO_2 is also identified at 42.42° and 61.88°. Whereas at 0 V measured diffraction pattern was different from the first two. It also established TiO_2 peaks which were found to be respectively at 25.5°, 35°, 37.7° and 42.5°. Based on the XRD results, titanium interaction with water vapour plasma led to intensive structural and compositional transformations of Ti films. Furthermore, X-ray diffraction indicates that film oxidation take place.

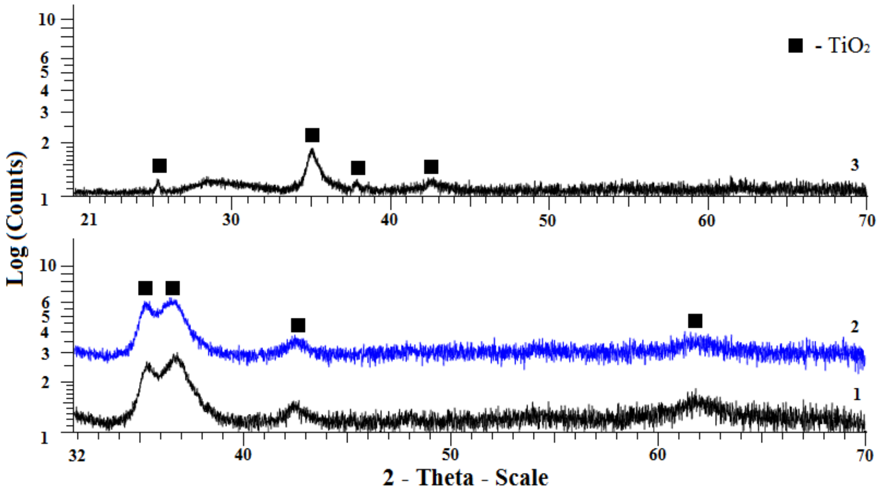

Fig. 4. The XRD patterns of Ti films after the water vapour exposure: curve 1 – Ubias = -200V; curve 2 – Ubias = -100V; curve 3 – Ubias = 0V

3.2 Film thickness influence on the interaction between titanium films and water vapour plasma

In order to determine whether the film thickness affects the reactions, Ti surface height profiles and surface roughness were measured using a nanoprofilometer. It was found that after interaction with water vapour plasma Ti films thickness and surface roughness increased. Fig. 5 shows surface roughness patterns. It is clear that the root mean square (RMS) of the as-deposited Ti film is equal to ~ 2.77 nm and it increased after the plasma treatment up to ~ 20.35 nm. Besides, thickness of untreated sample is equal to ~760 nm and after treatment it increases up to ~ 785 nm. On the basis of the obtained results it can be assumed that film oxidation and hydrogen saturation occurred.

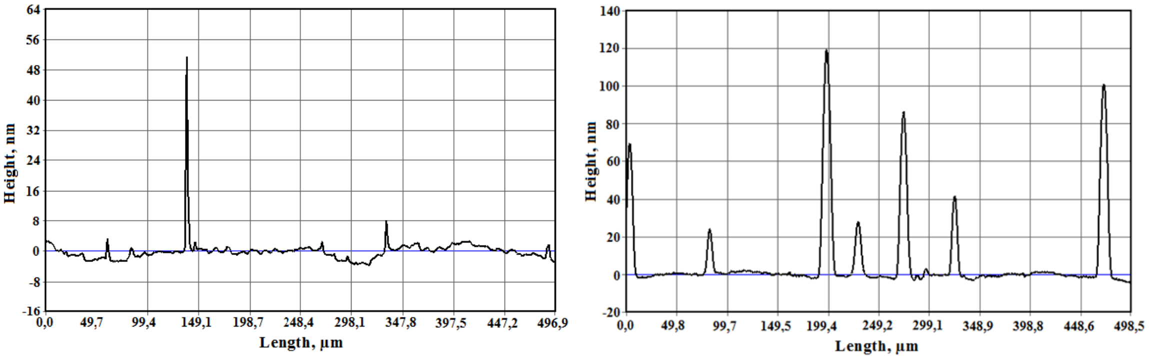

a) b)

Fig. 5. The profiles of surface roughness: a) untreated, b) plasma treated at 116 W, -200 V for 30 min

This is also can be seen from Fig. 6 which includes optical microscopy surface views of plasma treated Ti films. Reaction with a thin Ti film is more intensive (Fig.6 a)). The reason could be much easier saturation of the thin film with hydrogen than thick film. Consequently, the highest quantity of formed bubbles (which is approving the highest hydrogen concentration) is presented in thin film. On the other hand it is difficult for hydrogen atoms to diffuse deep into the thick film. From the previous studies [12] it is known that hydrogen (H_2) accommodates at film-substrate interface. It can be assumed that hydrogen atoms penetrates into thick film and accommodates only in certain parts of it. This explains why H_2 bubbles are less dispersed in the thick film (Fig. 6 b)).

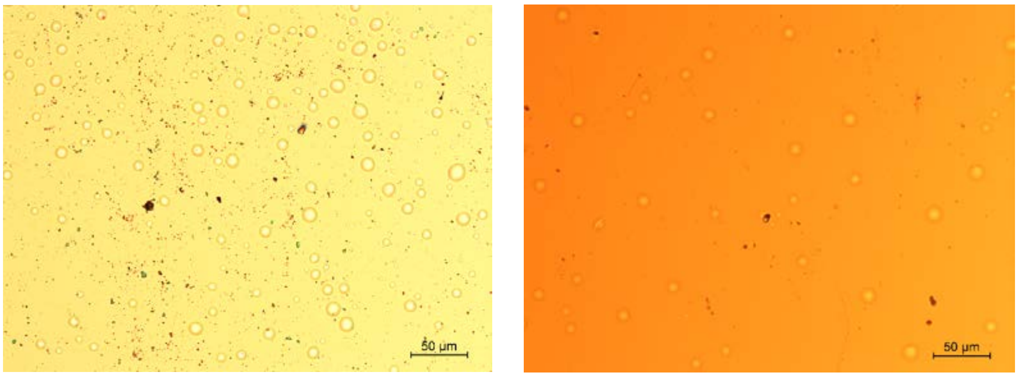

Fig. 6. The optical microscopy surface view of Ti films after plasma treatment at -200 V for 30 min: a) thin film (~175 nm), b) thick film (~785 nm)

In order to determine elemental composition of plasma treated Ti films, energy dispersive spectrometer (EDS) was used. Table 1 shows the constitution of the films - titanium, oxygen, silicon and carbon.

Table 1. Elemental composition of Ti films

	Concentration, at. %			
Sample	**Ti**	**Si**	**O**	**C**
Thin (~175 nm)	19.81	49.86	24.45	5.89
Thick (~785 nm)	74.41	4.67	18.74	2.18

EDS results show that none of the samples were oxidized to the stoichiometric TiO_2. Nevertheless, previously published article [13] noted that EDS analysis does not provide high degree of accuracy and gives complementary information about the average elemental concentration. This explanation correlates with our results obtained with X-ray photoelectron spectroscope (Fig. 7).

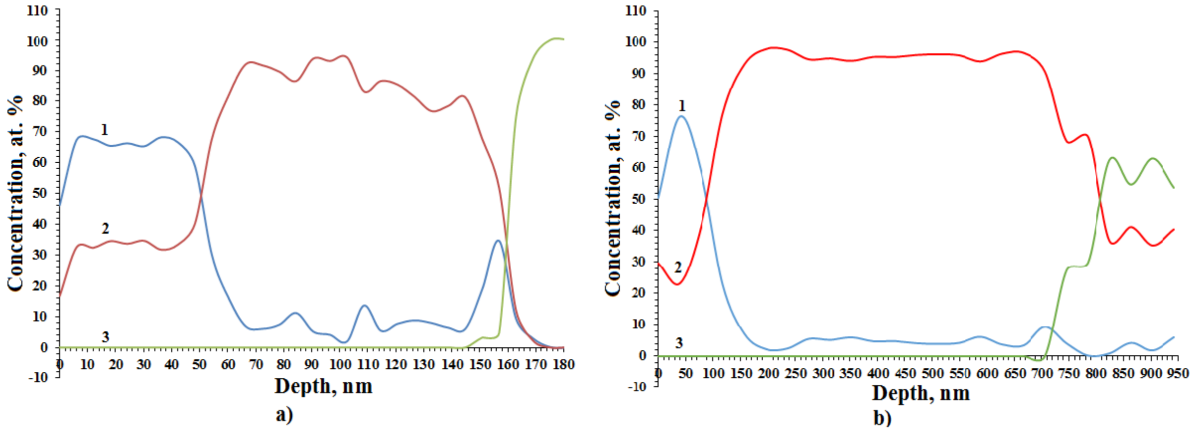

Fig. 7. XPS depth profiles of oxygen, titanium and silicon (curves 1-3 respectively) across Ti films: a) thin film (~175 nm), b) thick film (~785 nm)

Fig. 7 includes XPS profiles of the main elements (titanium, oxygen and silicon) across the thickness of Ti film treated using water vapour plasma. It is known that TiO_2 layer is formed on the top of the film. Fig. 7 a shows that the near-surface region of 42 nm thickness is oxidized stoichiometrically, as the O and Ti concentrations are distributed homogeneously and equals to 67 at.% and 33 at.%, respectively. Going deeper, O concentration drastically decreased and became variable from 13 at.% to 2 at.% meanwhile the concentration of titanium significantly increased (varied from 94 at. % to 78 at.%). Accordingly, titanium dominates at depths from 55 to 157 nm and at 175 nm it disappears because the silicon substrate is reached. While Fig. 7 b shows that the near-surface region of 39 nm thickness is also oxidized, as the O and Ti concentrations were equal to 76 at. % and 23 at. %, respectively. Beyond this layer, O concentration gradually decreased and became variable from 9 at. % to 2 at.% as well as the concentration of titanium increased and varied from 98 at. % to 69 at. %. Respectively, titanium dominated at depths from 118 to 706 nm and started to decrease until it reached a depth of 785 nm (Si substrate boundary). It can be concluded that oxidation fully succeeded to a depth of 42 nm in thin film and to a depth of 39 nm in thick film, whilst full oxidation did not occurred due to the lack of oxygen in the deeper layers of the films. Regardless of whether the film is thick or thin, the same thickness of the films was oxidized.

3.3 Plasma treatment power influence on the interaction between titanium films and water vapour plasma

Fig. 8 illustrates optical microscopy surface views of plasma treated Ti films: a) at 270 W, b) at 117 W. It is evident that at higher power (Fig. 8 a)) film oxidation and hydrogen saturation into the bulk occurs faster than at low powers (Fig. 8 b)).

At 270 W power we generated bigger, distinctly visible and more widespread hydrogen bubbles in the film. Reaction was faster because at higher power during the bombardment the higher ion flux reaches film surface. Higher plasma excitation power leads to a higher temperature of the material what determines that atoms of film surface layer become more active [14]. The results correlate with the measured diffraction pattern of samples (Fig. 9).

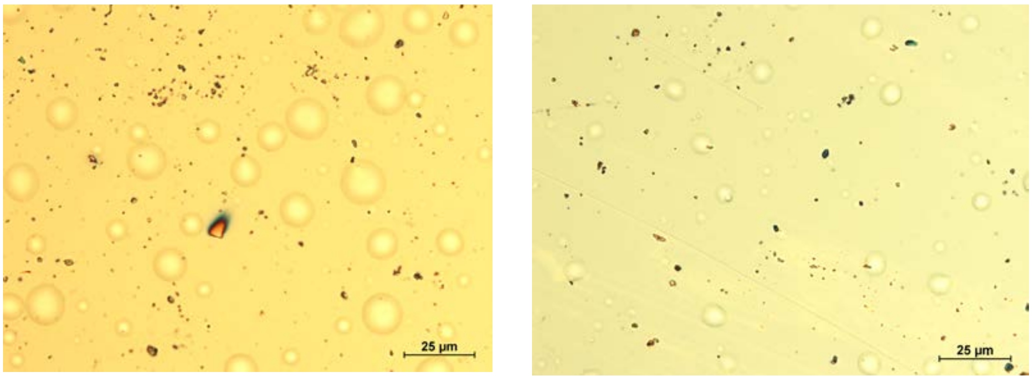

a) b)

Fig. 8. Optical microscopy surface views of plasma treated Ti films: a) at 270 W, -200 V (film initial thickness ~152 nm), and b) at 117 W, -100 V (film initial thickness ~ 273 nm)

TiO_2 phases were formed in both films (Fig. 9, 1 and 2 curves). Two wide peaks were identified at 35.30° and 36.66° in curve 1. It may be interpreted as a superposition of TiO_2 peaks, while curve 2 shows one wide, single peak of TiO_2 at 35.54° and only the rudiments of a small peak at 36.24°. In both curves small peaks of TiO_2 at 42.40° and 61.80° appeared. Diffraction difference suggests that due to the higher power the greater oxidation of the film and new phase formation occurred.

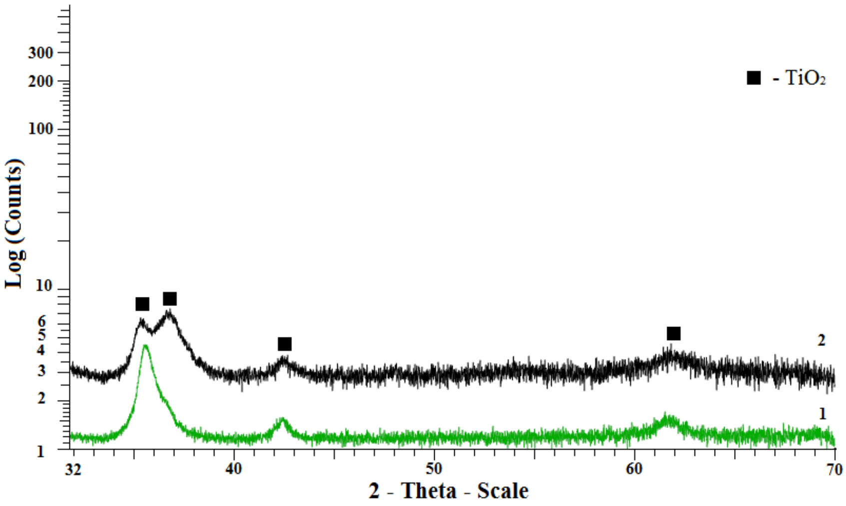

Fig. 9. The XRD patterns of Ti films after the water vapour exposure: curve 1 – P = 270 W; curve 2 – P = 117 W

Fig. 10 includes surface roughness after plasma treatment at different power. The studies revealed that at 270 W the root mean square (RMS) is equal to ~ 20.16 nm (Fig. 10 a)) and at lower power (117 W) it is significantly smaller and is equal to ~ 6.17 nm (Fig. 10 b)). Hence, the higher film roughness also confirms that the film better interacts with water vapour plasma at higher power.

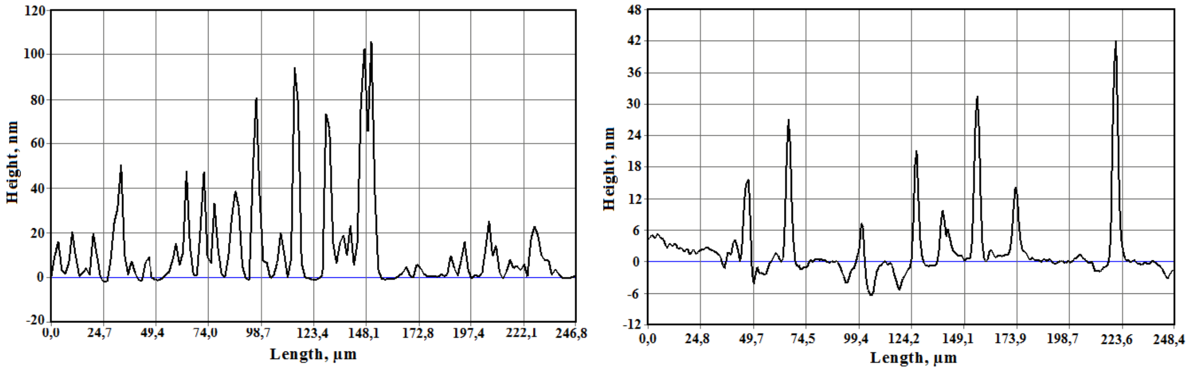

a) b)

Fig. 10. Ti films surface roughness after treatment with water vapour plasma:
a) 270 W, b) 117 W

4. CONCLUSIONS

Based on the nanoprofilometer results the films thickness (Fig. 1) and surface roughness (Fig. 2) increased after 30 minutes treatment with water vapour plasma. This results and the studies with XRD (Fig. 4) revealed that titanium interaction with water vapour plasma led to intensive structural and compositional transformations of Ti films. Furthermore, X-ray diffraction indicated that film oxidation took place and Ti were oxidized to TiO_2.

Results obtained with SEM clarified that at higher bias voltage film surface oxidation and hydrogen saturation into the bulk is more intensive (Fig. 3) because the film surface bombardment with ion flow becomes more active. However, when the bias voltage is not used, reaction occurs more intensive, because barrier layer of TiO_2 is forming significantly slower and leads to the more rapid hydrogen saturation into the film.

It was revealed that it is much easier to saturate the thin film (~175 nm) with hydrogen than the thick one (~ 785 nm) (Fig. 6). Moreover, due to the thin film it is easier to get close to the solubility limit of hydrogen.

Research with XPS (Fig. 7) established that regardless of the film thickness, mostly the same thickness of the films (~ 39–42 nm) were oxidized.

Last, but not least remark, higher plasma excitation power leads to a higher temperature of the material what determines that atoms of film surface layer becomes more active. That is why at higher power (270 W) films oxidation and hydrogen saturation into the bulk occurs more intensive than at lower powers (117 W) (Fig. 8, 9). Moreover X-ray diffraction (Fig. 9) revealed that due to the higher power new TiO_2 phase formation occurred.

5. ACKNOWLEDGEMENTS

The authors are grateful to prof. D. Milcius, the head of Hydrogen Technologies centre, for the experimental facilities used to perform this work, dr. S. Tuckute and dr. M. Lelis for the help to perform structural characterization of resultant materials. Research was supported by Lithuanian Energy Institute research fund and it was partly supported by project

“Promotion of Student Scientific Activities” (VP1-3.1-ŠMM-01-V-02-003) from the Research Council of Lithuania (D.G.). This project is funded by the Republic of Lithuania and European Social Fund under the 2007–2013 Human Resources Development Operational Programme’s priority 3.

6. REFERENCES

1. PARAMESHWARAN, R., KALAISELVAMB, S., HARIKRISHNANB, A., ELAYAPERUMALA, A. Sustainable thermal energy storage technologies for buildings: A review. *Renewable and Sustainable Energy Reviews,* 2012, 16, p. 2394–2433.
2. HULTMAN, N., REBOIS, D., SCHOLTEN, M., RAMING, C. The greenhouse impact of unconventional gas for electricity generation. *Environmental Research Letters,* 2011, 6, p. 1–9.
3. MA, Y., WANG, X., JIA, Y., CHEN, X., HAN, H., LI, C. Titanium Dioxide-Based Nanomaterials for Photocatalytic Fuel Generations. *Chemical Reviews,* 2014, 114, p. 9987–10043.
4. LIAO, C.H., HUANG, C.W., WU, J.C.S. Hydrogen Production from Semiconductor-based Photocatalysis via Water Splitting. Review. *Catalysts,* 2012, 2, p. 490–516.
5. LINSEBIGLER, A.L., LU, G.Q., YATES, J.T. Photocatalysis on TiO_2 surfaces: principles, mechanisms, and selected results. *Chemical Reviews,* 1995, 95, p. 735-758.
6. HOFFMANN, M.R., MARTIN, S.T., CHOI W.Y., BAHNEMANN D.W. Environmental applications of semiconductor photocatalysis. *Chemical Reviews,* 1995, 95, p. 69–96.
7. ZAHRAA, O., MAIRE, S., EVENOU, F., HACHEM, C., PONS, M.N., ALINSAFI, A., BOUCHY, M. Treatment of wastewater dyeing agent by photocatalytic process in solar reactor. *International Journal of Photoenergy,* 2006, p. 1–9.
8. ZHENG, Y., SHI, E., CHEN, Z., LI, W., HU. X. Influence of solution concentration on the hydrothermal preparation of titania crystallites. *Journal of Materials Chemistry,* 2001, 11, p. 1547-1551.
9. PRANEVIČIUS, L., URBONAVIČIUS, M., PRANEVIČIUS, L.L., TUČKUTĖ, S., GEDVILAS, K., RAJACKAS, T., GIRDZEVIČIUS, D. Study of Oxidation of Thin Ti Film Controlled by Reduction Processes in Water Vapor Plasma. *e-Journal of Surface Science and Nanotechnology,* 2012, 10, p. 613–618.
10. PEREZ, P. On the influence of water vapour on the oxidation behaviour of pure Ti. *Corrosion Science,* 2007, 49, p. 1172-1185.
11. LINSEBIGLER, A.L., LU, G., YATES, J.T. Photocatalysis on TiO_2 surface: principles, mechanisms, and selected results. *Chemical Reviews*, 1995, 95, p. 735–758.
12. TUČKUTĖ, S., PRANEVIČIUS, L.L. Separation of Hydrogen from Water Molecules by Ion Implantation into Thin Ti Films. Proceedings of the international conference nanomaterials: applications and properties 1 (4), 2012, p. 1–4.
13. PRANEVICIUS, L.L., TUCKUTE, S., MILCIUS, D., URBONAVICIUS, M. Investigation of hydrogenation of Ti films under ion irradiation from water plasma. *PRZEGLĄD ELEKTROTECHNICZNY (Electrical Review),* 2012. ISSN 0033-2097, R. 88 NR 11b.
14. TUČKUTĖ, S. *Investigation of simultaneous oxidation and hydriding of titanium films in water vapour:* Vytautas Magnus university, Doctoral dissertation, 2013, 147 p.

CYSENI 2015, May 27-28, Kaunas, Lithuania
ISSN 1822-7554, www.cyseni.com

IN-SITU LOW TEMPERATURE PLASMA HYDROGENATION OF PURE Mg THIN FILMS

D. Girdzevičius, S. Tučkutė, D. Milčius
Lithuanian Energy Institute
Breslaujos str. 3, LT-44403, Kaunas – Lithuania
Email: Dalius.Girdzevicius@lei.lt

ABSTRACT

MgH_2 can store essential amounts of hydrogen (up to 7.6 wt%) and can be used for direct hydrogen storage in solid state or as material for hydrogen production using $MgH_2 + 2H_2O \rightarrow Mg(OH)_2 + 2H_2 +$ 277 kJ reaction approach. Usually kinetics and thermodynamics of MgH_2 is enhanced by nanostructuring. We tried to apply in-situ low temperature plasma hydrogenation technologies in this work for direct hydrogenation of pure Mg thin films. SEM+EDS, XRD and high resolution profilometry applied for the received materials investigation. It is shown that plasma based hydrogenation approach leads to partial hydrogenation of pure Mg films and developed materials can serve as a basis for further hydrogen storage in solid state or production using $MgH_2 + 2H_2O \rightarrow Mg(OH)_2 + 2H_2 +$ 277 kJ reaction approach.

Keywords: hydrogen production, hydrogen storage, MgH_2, plasma hydrogenation

1. INTRODUCTION

Magnesium hydride (MgH_2) is well known as a promising candidate for hydrogen storage material because of its high capacity of hydrogen mass (7.6 wt%) and energy density (9 MJ/kg) [1, 2]. According to the MgH_2 reaction with water magnesium hydride can be used as material for hydrogen production purposes using $MgH_2 + 2H_2O \rightarrow Mg(OH)_2 + 2H_2 + \Delta H_r$ reaction, where $\Delta Hr = -277$ kJ/mole) [3].

Despite high gravimetric hydrogen density, application of MgH_2 is limited due to slow hydrogenation kinetics and high thermodynamic stability [4].

In order to become an effective and reliable energy storage solution or a source of hydrogen generation metal hydride must present high capacity, good reversibility, fast reactivity, sustainability and safety [5].

There are two different methods used for hydrogen storage in solid state. The first approach is related to H_2 dissociation and formation of H chemical bonds with the atoms of the material involved in the reaction. Such chemisorption takes place in metals and complex hydrides. The other approach describes physisorption process when hydrogen molecules are adsorbed onto the inner surface of porous solids [5].

Various techniques have been explored in order to enhance kinetics and thermodynamics for hydrogen absorption and desorption processes in magnesium hydrides, e.g. nanoconfinement, ball milling, utilization of catalytic additives or alloying with different metals [6]. Nanoconfinement technology is known as downsizing of metal particles and their confinement into nanoporous solids, e.g. MgH_2 can be embedded by porous carbon or polymer compounds [7]. Reactive ball milling is used to produce nanosized Mg/MgH_2 structures demonstrating enhanced storage properties due to increased surface area, decreased diffusion length, broken outer oxide layers, defects introduction and increase of interface contact between embedded catalyst and Mg/MgH_2. Ball milling is an effective way how activation energy can be reduced [7, 8]. Hydrogen absorbing alloys (e.g. Mg_2Ni, Mg_2Al, and Mg_2Si [7]) are called as promising functional materials used to improve thermodynamics and kinetics for hydrogen absorbtion/desorption reactions in metal hydrides [2]. Catalytic additives (e.g. transition metals, metal oxides, halides or different forms of carbons) are used to promote dissociation and recombination of hydrogen. Such reduction of activation energy is useful for absorption and desorption [8, 9].

Therefore, various attempts are carried out in order to improve operational characteristics of MgH_2.

According to majority of scientific works, palladium (Pd) is considered as one of the most appropriate and effective solutions to overcome such drawbacks as relatively high temperature and pressure required for Mg hydrogenation [1, 10, 11]. Time of hydrogenation process could be reduced three times by employing Pd as a catalyst [12]. However, using Pd as an additive interdiffusion of Mg/Pd and formation of $MgPd_x$ alloys cannot be avoided [13]. For example, increased activation energy is observed during formation of Mg_6Pd/MgH_2 interface compared to Mg/MgH_2 [10].

This work aims at in-situ hydrogenation of magnesium thin films and research of hydrogen sorption properties depending on synthesis parameters for fully hydrogenated MgH_2. Deposition of Mg thin films and further hydrogenation were carried out by using magnetrons sputtering technique. Synthesised samples were characterized using surface profilometry, SEM, EDX and XRD techniques.

2. EXPERIMENTAL TECHNIQUES

2.1. Deposition and hydrogenation of Mg thin films

Magnesium and magnesium hydride samples were prepared by a vacuum system consisting rotary and diffusion pumps. Magnetron sputtering technique was used to deposit thin layer structures on 0.5 mm thick fused silica substrates. DC power was supplied in order to generate plasma.

Samples were placed under Mg circular cathode (target) that was used as a source of plasma during sputtering process in argon (working gas). The power dissipated in plasma varied between 330÷350 W. Deposition of magnesium thin films was done under 4 mTorr ($5.3 \cdot 10^{-1}$Pa).

Samples were *in situ* hydrogenated for 4 hours under 20 mTorr and 100 mTorr respectively. The same DC current was maintained for both samples during sputtering (1.0 A) and hydrogenation (1.3 A) processes.

Sputtering and hydrogenation parameters for both samples are shown in Table 1.

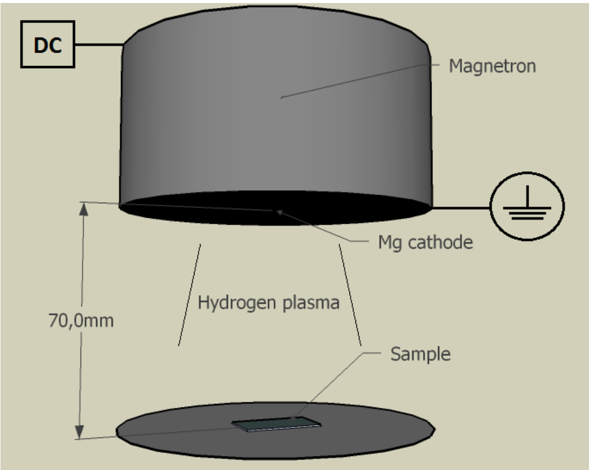

Fig. 1. An experimental scheme of hydrogenation process

Table 1. Sputtering and hydrogenation parameters for Mg films

	Mg-1	**Mg-2**	**Mg-1H**	**Mg-2H**
	Sputtering		Hydrogenation	
Target	Mg			
Substrate	Fused silica			
Target-substrate distance	70 mm			
Gas used	Ar		H_2	
Current / voltage	1.0 A / 340 V		1.3 A / 250 V	1.3 A / 200 V
Time	5 minutes		4 hours	
Pressure	4 mTorr ($5.30 \cdot 10^{-1}$ Pa)		100 mTorr ($1.33 \cdot 10^{1}$ Pa)	20 mTorr (2.67 Pa)

2.2. Characterization

The view of the surface and cross section of Mg thin films before and after hydrogenation was investigated by scanning electron microscope (SEM, Hittachi S-3400N).

Elemental composition of the samples was identified by energy dispersive X-ray spectroscopy (EDX, Bruker Quad 5040).

The room temperature X-ray diffraction measurements (Bruker diffractometer D8) were carried out in order to characterize microstructure of magnesium hydrides. Diffractometer was used for $20^{\circ} < 2\theta < 70^{\circ}$ using Cu Kα radiation in 0.01° steps. EVA Search Match software was used for identification of peaks.

Topographical information (thickness, roughness) of the samples was identified by high resolution profiler (AMBIOS XP 200).

3. RESULTS

Magnesium thin films were deposited in magnetron sputtering system. Hydrogenation was carried out without extraction of the samples to the atmosphere.

Thickness of magnesium samples after hydrogenation process was 1.5 µm for sample Mg-1H and 1.3 µm for sample Mg-2H. Roughness parameters of the analyzed samples are shown in Table 2.

Table 2. Roughness parameters of hydrogenated samples

Sample	**Average roughness Ra, nm**	**Root mean square roughness Rq, nm**
Mg-1H	43.70	75.87
Mg-2H	30.36	37.62

SEM images reveal surface structure of hydrogenated Mg (Fig. 2). Formation of columnar structures is observed when sample is hydrogenated at high pressure. As mentioned before, hydrogenation was carried out for 4 hours for both samples. The main difference of the samples is related to film thickness and hydrogenation pressure. Fig. 2 (a) and 2 (b) show sample Mg-1H (hydrogenation pressure 100 mTorr) and Fig. 2 (c) and (d) indicates sample Mg-2H (20 mTorr). Higher hydrogenation pressure level leads to the higher amount of hydrogen in a working chamber. Thus, increase of hydrogen content in the thin film causes changes in geometry and influences topographical alteration.

Consequently, it can be stated that pressure difference is the main reason, why surface of the thin film with lower hydrogenation pressure (sample Mg-2H) is relatively smoother compared to sample Mg-1H.

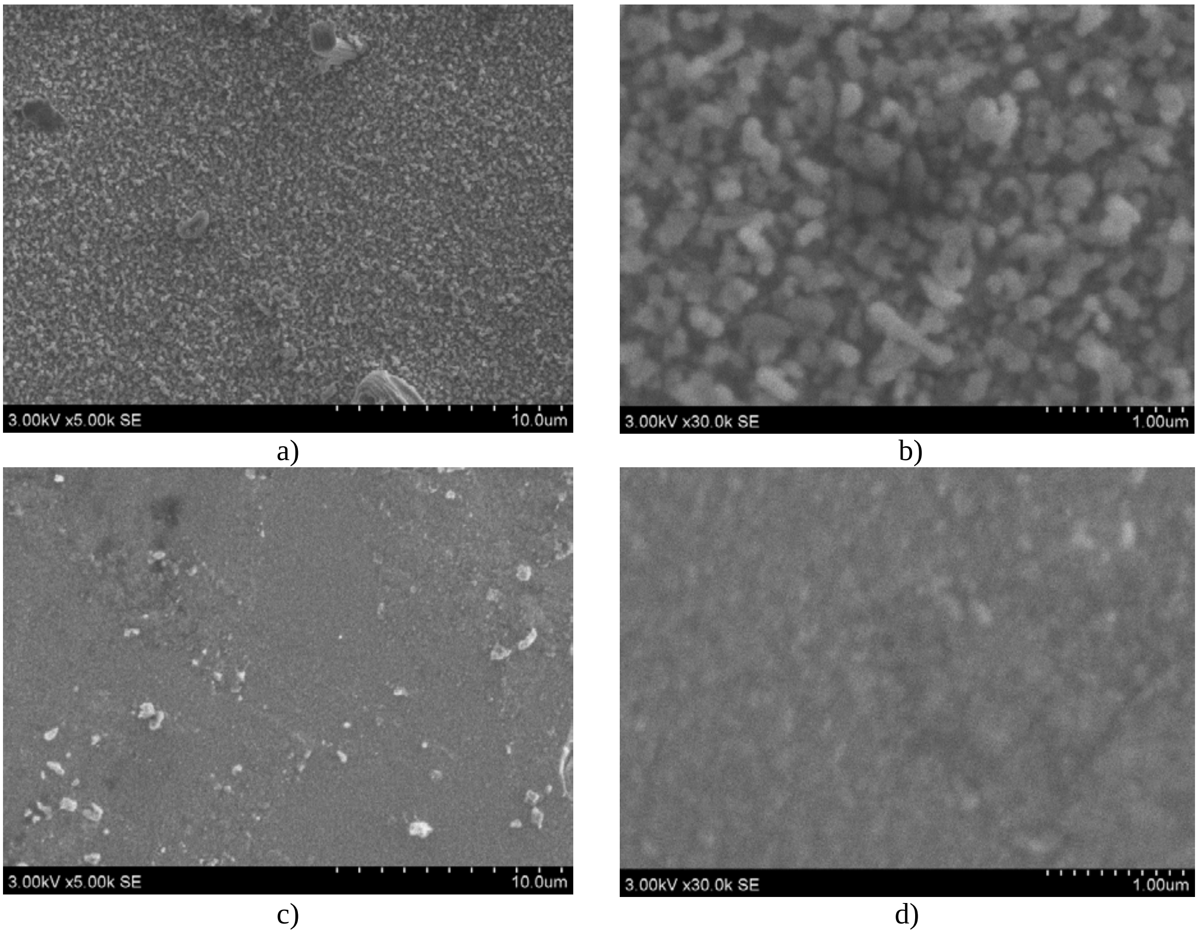

a) b)

c) d)

Fig. 2. SEM views of hydrogenated Mg samples with different hydrogenation pressure: a) and b) corresponds to sample Mg-1H with hydrogenation pressure 100 mTorr, c) and d) corresponds to sample Mg-2H with hydrogenation pressure 20 mTorr

Cross-section view was taken by SEM in order to identify what type of structure was formed in the bulk of the thin film (Fig. 3). The height of such columnar structure varies between 1.3 μm and 1.5 μm. It is important to mention, that sample Mg-2H did not have any prevailing structure that could be identified by this imaging technique.

EDX measurements were carried out for both samples in order to identify elemental composition. Except magnesium dominance, oxygen and silicon were also registered (Table 3). Silicon was registered mostly because of the thin film substrates. However, higher atomic concentration of oxygen was identified in sample Mg-1H. Despite influence of the substrate, increase of oxygen concentration can be explained because of the formation of columnar structure that leads to the larger effective surface area causing relatively higher rate of oxidation.

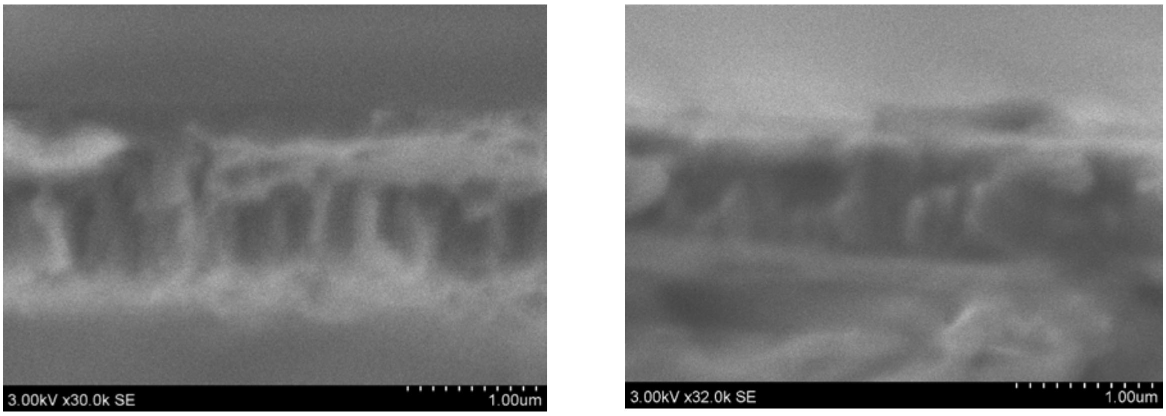

a) b)

Fig. 3. Cross-section view of sample Mg-1H (a) and sample Mg-2H (b)

Table 3. Elemental composition in all samples (at.%)

Sample	**Magnesium**	**Oxygen**
Mg-1H	70.74 %	22.08 %
Mg-2H	73.87 %	17.94 %

X-ray diffraction patterns of magnesium samples after hydrogenation at different pressure level are presented in Fig. 4.

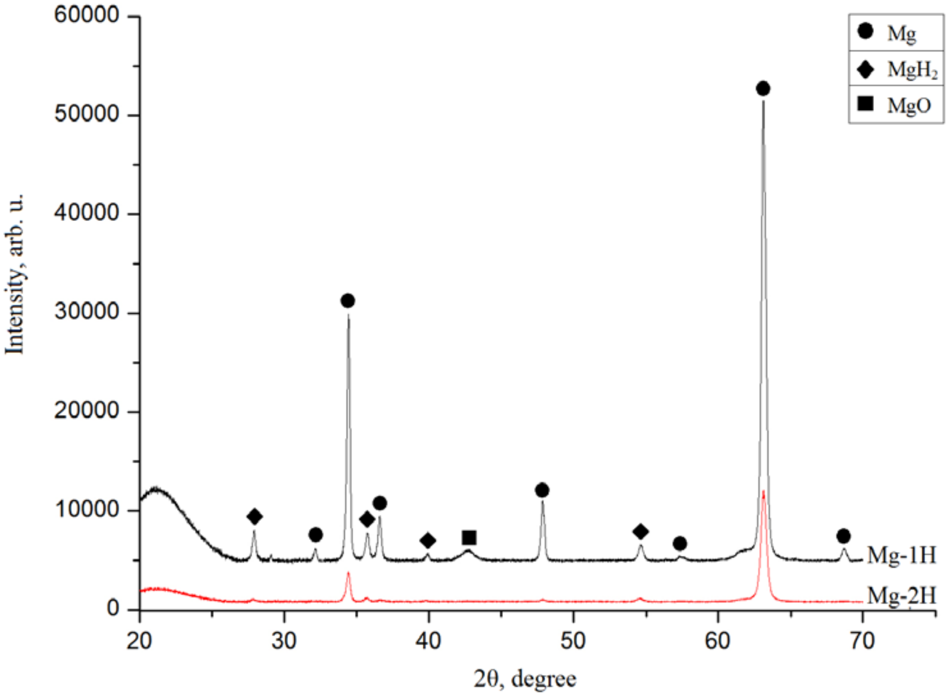

Fig. 4. XRD patterns of hydrogenated Mg thin films

Sample Mg-1H indicates increased intensity of Mg peak with hexagonal crystallographic structure, formation of MgO with cubic crystallographic structure and MgH_2 with tetragonal crystallographic structure. On the other hand, sample Mg-2H with lower hydrogenation pressure shows decreased intensity of Mg and MgH_2 peaks. It could be assumed that in sample Mg-2H Mg and H_2 forms solid solutions instead of chemical compounds due to the decrease of H_2 entering Mg film. Presence of MgO was not registered.

4. DISCUSSION

Pressure level applied during plasma hydrogenation process which directly corresponds to the amount of H_2 is one of the key factors influencing formation of magnesium hydride.

Topographical properties of *in situ* hydrogenated Mg thin films were identified by high accuracy surface profiler. Roughness parameters (Table 2) indicate noticeable surface changes when higher pressure is applied. Further surface investigation by scanning electron microscope demonstrates visible difference of the surface morphology between samples Mg-1H and Mg-2H. Cross-section views revealed formation of columnar structures in sample Mg-1H, when sample Mg-2H had a dense structure without any prevailing patterns. It is assumed that formation of columnar structure leads to the growth of surface roughness. According to XRD analysis sample Mg-1H with higher hydrogenation pressure indicates increased intensity of MgH_2 peaks and formation of MgO compared to sample Mg-2H demonstrating only MgH_2 peaks with lower intensities. These results are in good agreement with EDX analysis showing higher concentration of oxygen in sample Mg-1H. As mentioned previously, formation of MgO can be the reason due to the larger effective surface area causing relatively higher rate of oxidation.

Obviously, such physical characteristics as high rate of roughness (increased effective area), growth of columnar structures in the bulk of the thin film influence noticeably better hydrogenation process. This assumption is in agreement with experimental results indicated above and scientific literature stating that creation of grain boundaries enhance hydrogen diffusion and provide active nucleation sites in hydride formation [14].

5. CONCLUSIONS

Magnesium *in situ* hydrogenation was carried out without extraction of the samples to the atmosphere in order to avoid undesired oxidation reaction. Topographical and structural changes of the Mg thin films take place due to the difference of pressure used for hydrogenation. XRD analysis demonstrates an increase of MgH_2 peaks at higher hydrogenation pressure. This tendency is in good agreement with prior investigations showing increased surface roughness and formation of columnar structures in the bulk of the thin film synthesised when higher rate of hydrogen content is ensured.

Therefore, hydrogen sorption properties depend on plasma hydrogenation pressure that drastically influences physical characteristics of the sample.

This research will be continued in order to achieve an adequate repeatability of experimental results and identify the best synthesis conditions required for *in situ* hydrogenation.

REFERENCES

1. GAUTAM, Y.K., CHAWLA, A.K., KHAN S.A., AGRAWAL R.D., CHANDRA, R. Hydrogen absorption and optical properties of Pd/Mg thin films prepared by DC magnetron sputtering. *Hydrogen Energy*, 2012, Vol. 37, p. 3772–3778.
2. HIGUCHI, K., KAJIOKA, H., TOIYAMA, K., FUJII, H., ORIMO, S., KIKUCHI, Y. In situ study of hydriding–dehydriding properties in some Pd /Mg thin films with different degree of Mg crystallization. *Alloys and Compounds*, 1999, Vol. 293–295, p. 484–489.
3. HO, H.H. *Hydrogen Generation from Magnesium Hydride by Using Organic Acid*: University of Wisconsin-Milwaukee, Thesis and Dissertations, 2013 [referred on the 9th of February in 2015].

   Link to the internet < http://dc.uwm.edu/cgi/viewcontent.cgi?article=1291&context=etd >

4. KLIMKOWICZ, A., TAKASAKI, A., GONDEK, Ł., FIGIEL, H., ŚWIERCZEK, K. Hydrogen desorption properties of magnesium hydride catalyzed multiply with carbon and silicon. *Alloys and Compounds*, 2015, Article in Press, p. 1–4.
5. ZLOTEA, C., LATROCHE, M. Role of nanoconfinement on hydrogen sorption properties of metal nanoparticles hybrids. *Colloids and Surfaces A: Physicochemical and Engineering Aspects*, 2013, Vol. 439, p. 117–130.
6. LEY, M.B., JEPSEN, L.H., LEE, Y.S., CHO, Y.W., COLLBE, J.M.B., DORNHEIM, M., ROKNI, M., JENSEN, J.O., SLOTH, M., FILINCHUK, Y., JORGENSEN, J.E., BESENBACHER, F., JENSEN, T.R. Complex hydrides for hydrogen storage – new perspectives. *Materials today*, 2014, Vol. 17, No. 3, p. 122–128.
7. JIA, Y., SUN, C., SHEN, S., ZOU, J., MAO, S. S., YAO, X. Combination of nanosizing and interfacial effect: Future perspective for designing Mg-based nanomaterials for hydrogen storage. *Renewable and Sustainable Energy Reviews*, 2015, Vol. 44, p. 289–303.
8. WEBB, C.J. A review of catalyst-enhanced magnesium hydride as a hydrogen storage material. *Physics and Chemistry of Solids*, 2014, Article in Press, p. 1–11.
9. GASAN, H., CELIK, O.N., AYDINBEYLI, N., YAMAN, Y.M. Effect of V, Nb, Ti and graphite additions on the hydrogen desorption temperature of magnesium hydride. *Hydrogen energy*, 2012, Vol. 37, p. 1912–1918.
10. ARES, J.R., LEARDINI, F., DI´AZ-CHAO, P., FERRER, I.J., FERNANDEZ, J.F., SANCHEZ, C. Non-isothermal desorption process of hydrogenated nanocrystalline Pd-capped Mg films investigated by Ion Beam Techniques. *Hydrogen energy*, 2014, Vol. 39, p. 2587–2596.
11. YOSHIMURA, K., YAMADA, Y., OKADA, M., Hydrogenation of Pd capped Mg thin films at room temperature. *Surface science*, 2004, Vol. 566-568, p. 751–754.
12. ADAMS, B.D., CHEN, A. The role of palladium in a hydrogen economy. *Materials today*, 2011, Vol. 14, No. 6, p. 282–289.
13. LE-QUOC, H., LACOSTE, A., MIRAGLIA, S., ECHU, S.B, BES, A., LAVERSENNE, L. MgH_2 thin films deposited by one-step reactive plasma sputtering. *Hydrogen energy*, 2014, Vol. 39, p. 17718–17725.
14. SALAM, M.S., ABDULLAH, B., SUFIAN, S. Hydrogenated Microstructure and Its Hydrogenation Properties: A Density Functional Theory Study. *Nanomaterials*, 2014, Vol. 2014, p. 1–7.

CYSENI 2015, May 27-28, Kaunas, Lithuania
ISSN 1822-7554, www.cyseni.com

REACTION BETWEEN PLASMA ACTIVATED ALUMINUM POWDER AND WATER UNDER VARIOUS CONDITIONS

M. Urbonavičius, D. Milčius
Lithuanian Energy Institute
Breslaujos str. 3, LT-44403 Kaunas – Lithuania
Phone +370 643 63871
Email: Marius.Urbonavicius@lei.lt

ABSTRACT

In-situ hydrogen generation is a potential technology for pollution-free electronic gadgets and areas with no energy infrastructure. It could be used to provide hydrogen for fuel cells powered portable devices. Therefore, aluminum reaction with water becomes especially attractive. Approximately 1245 cm^3 of hydrogen could be generated after water reaction with 1 gram of aluminum and directly fed to fuel cell power system. However, a thin protective natural surface layer of alumina (Al_2O_3) inhibits the reaction. This research is focused on the formation of altered layer on the top of Al surface and activated aluminum powder reaction with water by changing reaction conditions.

Aluminum powder was treated and activated under hydrogen plasma at 200 W. Activated aluminum powder becomes hydrophilic and after immersion into the water goes to the bottom instantly. After certain time hydrogen production was observed. Some amount of sodium hydroxide was used as a promoter of aluminum-water reaction. The reaction (H_2 generation) was investigated under various conditions, such as: pH (different amount of NaOH); different amount of water and aluminum powder; temperature of water. Aluminum powder samples were characterized by scanning electron microscopy (SEM), energy dispersive X-ray spectroscopy (EDS) for elemental analysis and X-ray diffraction (XRD) for microstructure analysis. XRD analysis of reaction by-products (white color) which are stable and non-corrosive shows many peaks of aluminum oxides and hydroxides.

Keywords: aluminum powder, plasma, hydrogen generation, water

1. INTRODUCTION

Hydrogen fuel cells are considered as a promising power system for stationary and mobile applications in recent years [1]. Environmentally-friendly and cost-effective hydrogen generation and storage methods attracted much attention.

Progressive way to generate hydrogen is the reaction between metal and water. Therefore, in-situ hydrogen generation materials were extensively investigated [2]. Various expensive metal hydrides (LiH, NaH, $LiBH_4$, $NaBH_4$, etc.) are used for reaction with water. Among those metals aluminum and its reaction with water has received a lot of interest as an on-board hydrogen source for small portable power applications using PEM fuel cells [3].

Hydrogen is generated through the following possible aluminum reactions with water: (1) $2Al + 6H_2O \rightarrow 2Al(OH)_3 + 3H_2$; (2) $2Al + 4H_2O \rightarrow 2AlO(OH) + 3H_2$; (3) $2Al + 3H_2O \rightarrow Al_2O_3 + 3H_2$ [4]. All these reactions are highly exothermic. $Al(OH)_3$ is the most stable byproduct from room temperature up to 280 ^oC [4].

Theoretically 1245 cm^3 volume of hydrogen could be produced after complete reaction between 1 gram of aluminum and water [5]. Aluminum is relatively inexpensive, abundant, and lightweight metal.

However, a thin protective natural surface layer (5–10 nm) of alumina (Al_2O_3) leads to poor kinetics of Al-water system and prevents the reaction.

There are many methods to disrupt aluminum oxide layer. Ball milling of aluminum powder with salts (NaCl or KCl) was found as a way to rupture the layer [1]. Another widely used technique is alloying with some elements (Zn, Ga, Bi, In, Mg, Sn) [5].

Sodium hydroxide (NaOH) could be used as a promoter of Al-water reaction. Reaction kinetics can be controlled by altering several parameters such as amounts of aluminum and water, water temperature, alkali concentration and size of aluminum particles.

In the present study Al powder was activated in hydrogen plasma on purpose to disrupt or crack the surface layer and enhance aluminum reactivity. Yield of hydrogen production during the reaction between water and activated aluminum powder has been investigated. The influence of various parameters on hydrogen production (water and aluminum amount, concentration of NaOH, temperature of water) was studied experimentally. Furthermore structure of reaction byproduct was analyzed.

2. METHODOLOGY

2.1. Plasma treatment technique

Aluminum powder (size varies from 10 to 75 μm) was located in vacuum chamber under the circular magnetron on water-cooled pad (Fig. 1). Magnetron with Al cathode was used as a source of plasma. A vacuum system including rotary and diffusion pumps enabled a base pressure of 0.2 Pa. Plasma treatment was performed approximately at 13 Pa of hydrogen gas. DC power supply was used for plasma generation. Al powder was treated under hydrogen plasma at 200 W for 3 hours.

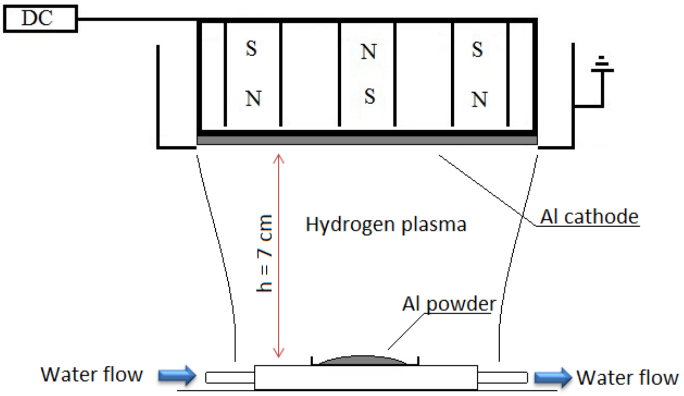

Fig. 1. The experimental scheme

2.2. Analysis methods

The microstructure of aluminum powder samples was characterized by X - ray diffraction (XRD) method using Bruker diffractometer (Bruker D8). The measurements were performed at 2θ angle in the range 20–70^o using Cu Kα radiation (λ = 0.15406 nm) in steps of 0.01^o. All X-ray diffraction peaks were identified using EVA *Search – Match* software. The powder views were investigated before and after hydrogen plasma treatment and after reaction with water by the scanning electron microscope (SEM, Hitachi S-3400N). Elemental composition of aluminum powder was analyzed by energy dispersive X-ray spectroscopy (EDS, Bruker Quad 5040).

Inverted burette filled with water was used to quantify hydrogen production volume where the quantity of H_2 gas was measured from water level change in the burette. More detailed scheme and equipment used in the hydrogen generation experiments is described in the study [6]. Hydrogen generation yield was defined by integrating the H_2 flow with time until the H_2 production flow dropped to practically zero.

3. RESULTS

3.1. SEM and EDS analysis of Al powder

Fig. 2 includes SEM views of untreated Al powder (a), hydrogen plasma activated Al powder at 200 W for 1 hour (b) and byproduct after Al powder reaction with water (c-d). Size of Al powder particles varies from 10 to 75 μm. Hydrogen production greatly depends on Al powder particle size [7]. Smaller particles with larger specific surface area produce hydrogen at higher rate. Surface area of plasma activated Al powder was measured 3.75 m^2/g. Meanwhile surface area of untreated Al powder was 3.51 m^2/g (Kelvin Sorptometer 1042 was used).

Morphology of Al powder has not changed significantly after plasma treatment. Surface seems to be relatively smooth in both cases (Fig. 2 (a-b)). Though higher charge accumulation at the edges of untreated Al powder was observed and some cracks were noticed after plasma activation.

Meanwhile views of byproduct powder (Fig. 2 (c-d)) after Al-water reaction drastically changed. Bulky solid structures were observed.

EDS elemental analysis of byproduct showed 10.7 at. % of aluminum, 72.4 at. % of oxygen, 11.1 at. % of sodium and 5.8 at. % of carbon. Whereas, elemental composition before the reaction with water was 95.9 at. % of Al and 4.1 at. % of O.

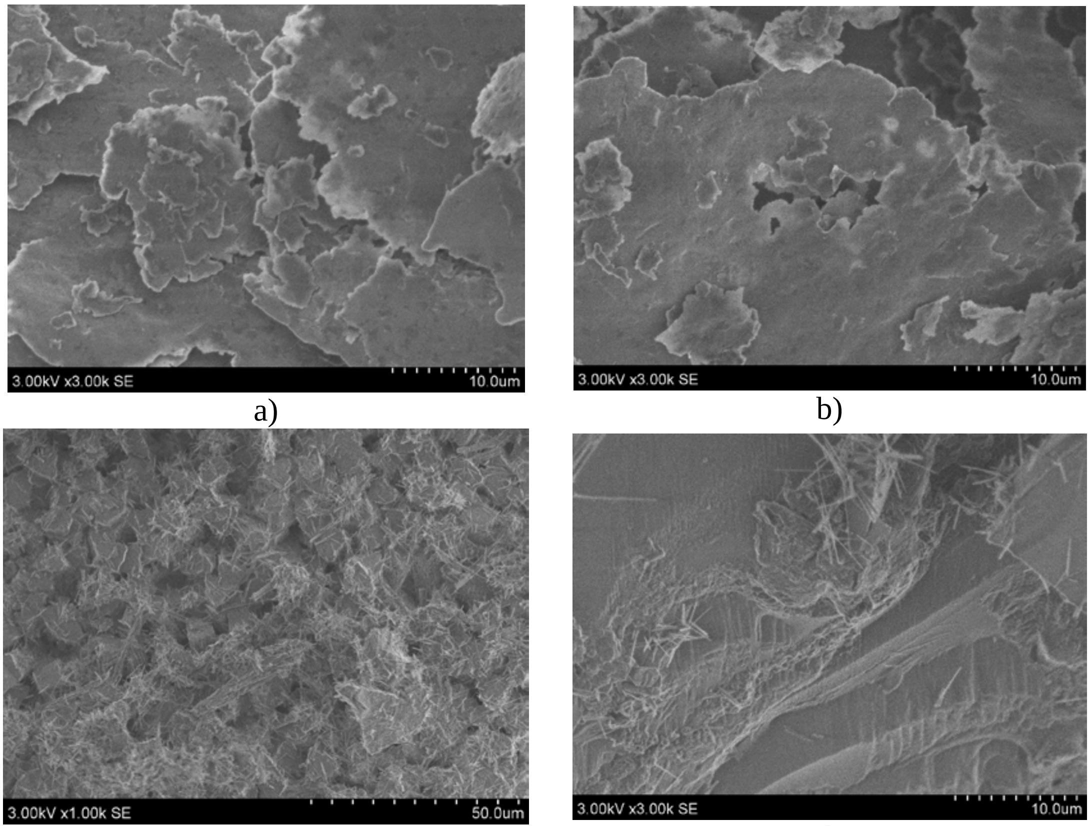

a) b)

c) d)

Fig. 2. SEM views of untreated Al powder (a), hydrogen plasma treated Al powder at 200 W for 1 hour (b) and Al powder after reaction with water (c-d)

3.2. XRD analysis of Al powder

Fig. 3 shows the X-ray diffraction patterns of untreated aluminum powder – curve 1, hydrogen plasma treated at 200 W for 1 hour – curve 2 and byproduct after Al-water reaction – curve 3. There were no significant structural changes identified after plasma treatment. Aluminum peaks with cubic crystallographic orientation were registered before and after plasma treatment at $2\theta = 38.3^\circ$, 44.6° and 65°, respectively (Fig. 3 (curve 1 and 2)). Very small peaks of tetragonal Al_2O_3 and orthorhombic hydroxides $Al(OH)_3$ and $AlO(OH)$ were identified at $2\theta = 34.5^\circ$, 41.8° and 43°, respectively. Moreover, the intensity of Al peak at $2\theta = 38.3^\circ$ increased after plasma treatment whereas intensity of other two Al peaks decreased.

Temperature of plasma treatment process was measured around 122 $^\circ$C. This could be the reason why aluminum hydride peaks were not registered at all. Decomposition temperature of AlH_3 varies from 60 to 100 $^\circ$C depending on structural phase [8].

White solid byproduct after Al-water reaction was dried and analyzed by XRD (Fig. 3 curve 3). The experiment was carried out using 0.1 g of Al powder in 50 ml volume of water and 0.2 g of NaOH solution. Results showed that byproduct is mainly composed by monoclinic aluminum hydroxide $Al(OH)_3$ and orthorhombic thermonatrite $Na_2CO_3 \cdot H_2O$. It is in agreement with EDS results.

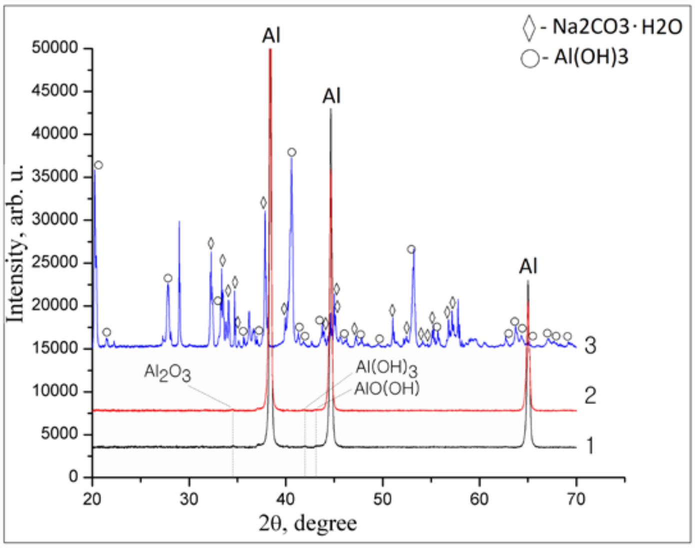

Fig. 3. XRD patterns of untreated Al powder (curve 1), after plasma treatment at 200 W for 1 hour (curve 2) and after Al powder reaction with water (curve 3)

3.3. Hydrogen generation analysis

Hydrogen production using reaction between plasma activated Al powder and water was investigated in 3 different cases: effect of water amount; influence of NaOH concentration; and influence of water temperature on the hydrogen generation. All these factors impact aluminum assisted water splitting reaction kinetics.

3.3.1. Effect of water/Al ratio

Activated Al powder (200 W, 1 hour) was immersed into the alkaline water. In this case, sodium hydroxide was used as the reaction promoter and 0.2 g of NaOH was dissolved in 100 ml volume of pure water resulting pH = 13.6. Plasma activated Al powder showed the increased hydrophilicity and sank in water.

Fig. 4 shows hydrogen production yield after reaction between 0.05 g of Al powder and different volume of alkaline water. Water temperature was 25.5 °C. The reaction started about 80 seconds after immersion, using 10 ml, 20 ml and 30 ml of alkaline water, whereas the process started after 55 s using 50 ml of water. Using different amount of water hydrogen production yield is 17 ml, 30 ml, 42 ml and 62 ml, respectively. Al reaction with 10 and 20 ml of water tend to be slow and passive. Aluminum powder completely reacted only with 50 ml of alkaline water.

Therefore hydrogen yield depends on water volume. More water with the same amount of Al powder means more OH groups which disrupt aluminum oxide layer and maintain the reaction.

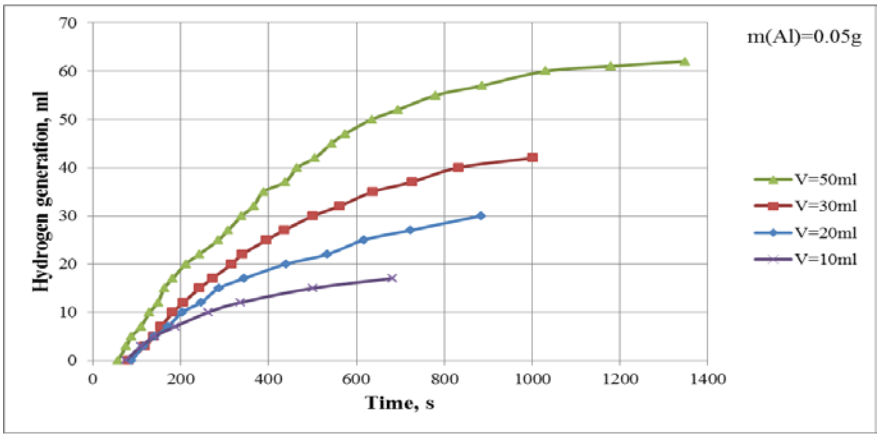

Fig. 4. Hydrogen evolution using 0.05 g of Al powder and different volume of water (10 ml, 20 ml, 30 ml and 50 ml)

Fig. 5 results obtained after 0.1 g of Al powder reaction with different volume of water under the same conditions as in Fig. 4. In this way Al-water reactions started faster than previous and the volume of hydrogen produced reached its maximum value faster as well. Reactions started after 50 s, 40 s, 44 s and 32 s using 10 ml, 20 ml, 30 ml and 50 ml of water respectively. Especially intensive hydrogen generation was measured using 50 ml of alkaline water where 95 ml volume of H_2 was reached after 1920 s. However, aluminum did not react completely. Presumably more water was needed to continue up to fully aluminum reaction.

More aluminum powder increases surface area which interacts with water and results hydrogen generation.

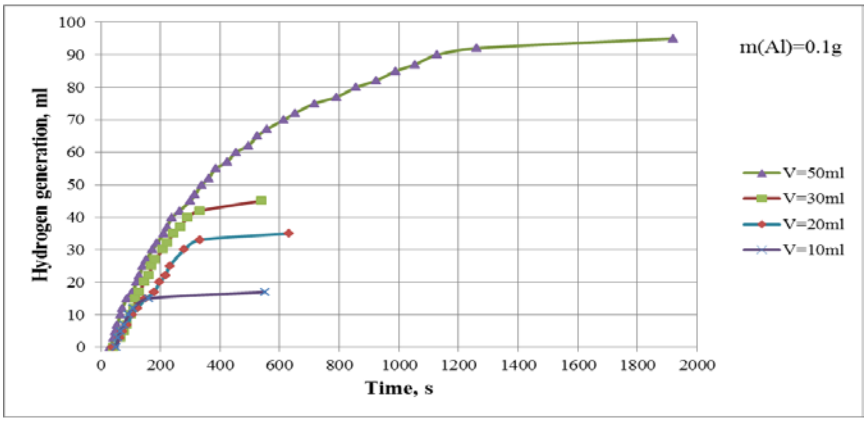

Fig. 5. Hydrogen evolution using 0.1 g of Al powder and different volume of water (10 ml, 20 ml, 30 ml and 50 ml)

3.3.2. *Influence of sodium hydroxide amount on hydrogen generation*

Hydrogen generation using 0.05 g of Al powder with different NaOH concentration (0.14 g, 0.24 g and 0.43 g) dissolved in 50 ml of pure water is presented in Fig. 6. Reactions started after 38 s, 35 s and 22 s using 0.14 g, 0.24 g and 0.43 g of NaOH respectively. Same volume of H_2 (65 ml) was generated in all cases. Reaction is accelerated and hydrogen production rate increased by increasing sodium hydroxide concentration.

Water type (tap water, sea water, pure water) is also important factor on hydrogen generation [9].

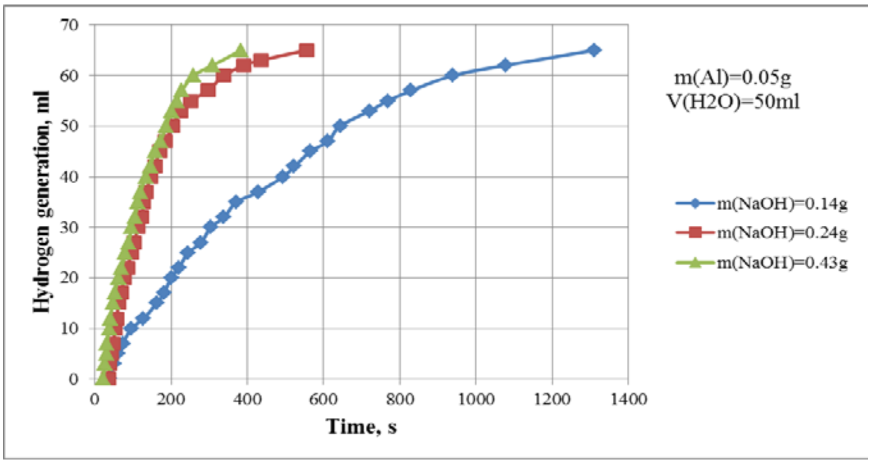

Fig. 6. Hydrogen evolution using 0.05 g of Al powder with different amount of sodium hydroxide (0.14 g, 0.24 g and 0.43 g) dissolved in 50 ml of water

3.3.3. *Effect of water temperature*

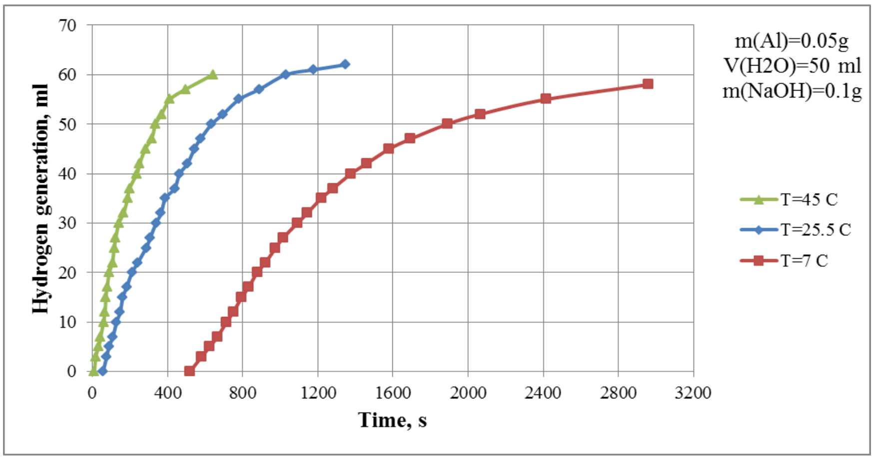

Fig. 7. Effect of water temperature on hydrogen generation using 0.05 g of Al powder with 0.1 g of NaOH dissolved in 50 ml of water

The volume of hydrogen generated from 0.05 g of Al powder at different water temperatures where 0.1 g of NaOH was dissolved in 50 ml of water is shown in Fig. 7.

After Al powder immersion in water cooled down up to 7 ^{o}C and reaction started only after 520 seconds (Fig. 7). During the experiment it was observed that higher NaOH concentration in water can start the reaction earlier and increase hydrogen yield.

The opposite process was observed after Al reaction with warm water (45^{o}C temperature measured after the reaction). Hydrogen generation rate increased with the increase of water temperature. Exothermic Al-water reaction increases temperature of water during the process as well. Similar results are published in references [9-11].

It is worth to mention that lowering the H_2 production temperature is important for portable fuel cell system designers [11].

4. DISCUSSIONS

Plasma activated aluminum powder becomes highly hydrophilic which means increased surface energy. SEM surface views (Fig. 2 (b)) of plasma treated aluminum did not show any significant changes except some small cracks. This could be the result of plasma bombardment with energetic ions. Although the XRD analysis did not show any new phases after plasma activation (Fig. 3, curve 2) it is possible that some part of hydrogen atoms could diffuse into the deep and form solid solution which is not registered by X-ray diffraction. Such effect also could lead to the higher surface energy and result some irregularities or defects of the near-surface area. Defects make easier to reach metal surface for water.

It is reported that Al-assisted water split reaction basically includes induction period – time from immersion moment to H_2 generation moment, which is followed by fast and after that slow reactions [12–13] (Fig. 9).

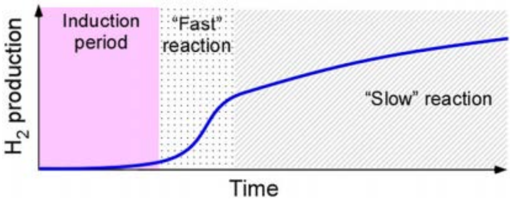

Fig. 9. Schematic diagram illustrating 3 stages [12]

Yield of hydrogen generation increased with the increase of water volume (Fig. 4 and 5). Also hydrogen volume and hydrogen production rate increased by increasing amount of aluminum powder. Therefore amount of hydrogen production mainly could be controlled by changing water/Al ratio.

Hydrogen production rate could be increased or decreased by controlling OH concentration dissolved in water (Fig. 6). Fig. 7 is an evident that water temperature plays an obvious role on the H_2 generation where time of induction period could be controlled by altering temperature. Further increasing temperature and NaOH amount can accelerate reaction and increase the yield of hydrogen (Fig. 7).

After full Al-water reaction, white, solid and bulky powder structures were obtained (Fig. 2 (c-d)). XRD analysis showed highly crystalline structures (Fig. 3, curve 3) mainly composed by $Al(OH)_3$ and $Na_2CO_3 \cdot H_2O$. It is in agreement with literature [14].

Reactions of Al powder with NaOH in water solution for hydrogen production: $2Al + 6H_2O + 2NaOH \rightarrow 2NaAl(OH)_4 + 3H_2$; $NaAl(OH)_4 \rightarrow NaOH + Al(OH)_3$. So, aluminum hydroxide was obtained as most stable byproduct from room temperature to 280 ^{o}C. Meanwhile some $Na_2CO_3 \cdot H_2O$ was formed due to CO_2 reaction with alkaline solution in contact with air and caused a reduction of OH concentration. Consequently, contact with air should be avoided.

5. CONCLUSIONS

Scanning electron microscope views and X-ray diffraction results did not show any significant morphologic (except a few small cracks) and structural changes of aluminum powder after plasma activation. Though plasma treated powder is active and hydrophilic in water. However, the plasma activation mechanism is insufficiently understood yet.

Investigation of hydrogen generation under various conditions has shown that yield of hydrogen production, hydrogen generation rate and time of induction period can be controlled by altering water/Al ratio, pH value and water temperature. Additionally, synergistic effect proceeded after increasing both water temperature and OH concentration.

REFERENCES

1. LI, F., SUN, L., ZHAO, J., XU, F., ZHOU, H., ZHANG, Q., HUANG, F. Mechanisms for H_2 generation for metal doped $Al_{16}M$ (M = Mg and Bi) clusters in water. *International Journal of Hydrogen Energy*, 2013, Vol. 38, p. 6930–6937.
2. GAI, W., LIU, W., DENG, Z., ZHOU, J. Reaction of Al powder with water for hydrogen generation under ambient condition. *International Journal of Hydrogen Energy*, 2012, Vol. 37, p. 13132-13140.
3. TEPROVICH, J., MOTYKA, T., ZIDAN, R. Hydrogen system using novel additives to catalyze hydrogen release from the hydrolysis of alone and activated aluminum. *International Journal of Hydrogen Energy*, 2012, Vol. 37, p. 1594–1603.
4. PETROVIC, J., THOMAS, G. Reaction of Aluminum with Water to Produce Hydrogen. *U.S. Department of Energy*, 2008, p. 1–26.
5. HUANG, X., GAO, T., PAN, X., WEI, D., L.V, CH., QIN, L., HUANG, Y. A review: Feasibility of hydrogen generation from the reaction between aluminum and water for fuel cell applications. *Journal of Power Sources*, 2013, Vol. 229, p. 133–140.
6. WANG, CH., CHOU, Y., YEN, CH. Hydrogen generation from aluminum and aluminum alloys powder. *Procedia Engineering*, 2012, Vol. 36, p. 105–113.
7. YAVOR, Y., GOROSHIN, S., BERGTHORSON, J.M., FROST, D., STOWE, R., RINGUETTE, S. Enhanced hydrogen generation from aluminum-water reactions. *International Journal of Hydrogen Energy*, 2013, Vol. 38 (35), p. 14992–15002.
8. GRAETZ, J., REILLY, J., SANDROCK, G., JOHNSON, J., ZHOU, W., WEGRZYN, J. Aluminum hydride, AlH3, as a hydrogen storage compound. *Advanced Materials for Energy Conversion III: A symposium in honor of Drs. Gary Sandrock, Louis Schlapbach, and Seijirau Suda*, 2006, p. 57–62.
9. ELITZUR, SH., ROSENBAND, V., GANY, A. Study of hydrogen production and storage based on aluminum-water reaction. *International Journal of Hydrogen Energy*, 2014, Vol. 39 (12), p. 6328–6334.
10. CZECH, E., TROCZYNSKI, T. Hydrogen generation through massive corrosion of deformed aluminum in water. *International Journal of Hydrogen Energy*, 2010, Vol. 35, p. 1029–1037.
11. HUANG, X., LU, CH., WANG, Y., SHEN, H., CHEN, D., HUANG, Y. Hydrogen generation from hydrolysis of aluminum/graphite composites with a core-shell structure. *International Journal of Hydrogen Energy*, 2012, Vol. 37, p. 7457–7463.
12. DUPIANO, P., STAMATIS, D., DREIZIN, E. Hydrogen production by reacting water with mechanically milled composite aluminum-metal oxide powders. *International Journal of Hydrogen Energy*, 2011, Vol. 36, p. 4781–4791.
13. NIE, H., SCHOENITZ, M., DREIZIN, E. Calorimetric investigation of the aluminum-water reaction. *International Journal of Hydrogen Energy*, 2012, Vol. 37, p. 11035–11045.
14. SOLER, L., MACANAS, J., MUNOZ, M., CASADO, J. Aluminum and aluminum alloys as source of hydrogen for fuel cell applications. *Journal of Power Sources*, 2007, Vol. 169, p. 144–149.

BARRIERS AND MARKET FAILURES THAT INFLUENCE THE DEVELOPMENT OF RENEWABLE ENERGY SOURCES

I. Ališauskaitė-Šeškienė
Lithuanian Energy Institute
Breslaujos str. 3, Kaunas, LT-44403 – Lithuania
Kaunas University of Technology
K. Donelaicio str. 20, Kaunas, LT-44239– Lithuania
Phone +370 699 07556
Email: seskiene@mail.lei.lt

ABSTRACT

While various military conflicts brewed across the world, energy has become the center of discussion. Back in the year 2000, United Nations and the World Energy Council published the survey named “Energy and the Challenge of Sustainability”, where it was observed that the key attribute of the modern energy system unsustainability – world's population unequal access to commercial energy and environmental, economic and geopolitical energy discontinuity results that will affect the future. Around that time, when the dispute between Russia and Ukraine arouse over natural gas, and the war in Iraq happened, it became clear that energy systems of different countries depend too heavily on other states, and that this is extremely dangerous.

The most important long-term scenario element of Lithuania and the EU, for the implementation of sustainable energy, is the replacement of the current energy to renewable energy sources. The benefits of renewable energy are obvious, so what prevents renewable energy to occupy dominant position? The paper aims to systematise, analyze and generalize market failures and barriers which impede the wider integration of RES in the general energy sector.

Keywords: renewable energy sources, RES technology, “green energy”, barriers and market failures

1. INTRODUCTION

Modern economies are closely linked with energy and depend on it, but still relatively recently, the main challenge faced by the state was to ensure adequate energy production and consumption [1]. In the pre-Kyoto period, energy policy mainly aimed at realising an affordable, reliable and secure energy system in order to maximally facilitate energy intensive industrial processes [2]. In 1997 the Kyoto protocol was adopted, in which countries committed themselves to the reduction of greenhouse gases [2]. In the survey "Energy and the Challenge of Sustainability", published in the year 2000 by United Nations and the World Energy Council, has been observed that the key to modern energy system unsustainable feature – unequal world's population access to commercial energy and environmental, economic and geopolitical energy discontinuity results that will also have an impact in the future. Around that time, in the event of war in Iraq, the energy crisis and the dispute between Russia and Ukraine over natural gas, it became clear how much the country's energy system is dependent on other countries and how it is dangerous. Thus, energy production and consumption is closely linked with all the global economic, social and environmental development [3]. It would appear, that the bigger part of all the mentioned problems would be solved with the global transition to renewable energy, which has obvious benefits, so what prevents renewable energy to occupy dominant position? In order to achieve the main task – answer this particular question, that is so important, taking into account the current economic and political situation in the world, the paper aims to analyse market failures and barriers which impede the wider integration of RES in the general energy sector. The remainder of this paper is organized as follows. Section 1 discusses the great importance of sustainable energy development and renewable sources in current political and economical context. After that, in section 2, market failures and other barriers are being presented. They are systematized and grouped in particular order. In this section it is also briefly referred to actions, the government should take in order to avoid interference of RES development. In the last section conclusions are being drawn.

2. THE IMPORTANCE OF SUSTAINABLE ENERGY DEVELOPMENT AND RENEWABLE ENERGY SOURCES

World countries, in order to realize sustainable development in the field of energy, usually faces three main challenges [4]:

1. Energy availability. Only 20 % the world's population consumes 80 % of energy produced in the world [5]. The fact, that around two billion people in developing countries do not use commercial energy, is a concern, since in the future, there will be rising social unrest and political instability in these countries, which can have a direct impact on the economic and social stability of global economy and transition countries [3]. It is necessary to establish the population support systems to ensure the availability of energy to low-income families. A well-functioning and commerce based global energy market would serve for all countries and people's interests [6].

2. Power supply. This is an opportunity to use various forms of energy, at any time and in sufficient quantities and at reasonable prices [3]. Energy security plays a decisive role in the economy of any country, because uneven distribution of fossil fuels, which in many countries is based on the energy system, determine development of economies and ensure the welfare of the population of individual countries [7].

3. The reduction of energy production and consumption negative impact on the environment or renewable energy. Continues use of fossil resources which cause environmental, ecological and technological problems. It is necessary to develop and implement technologies that reduce carbon dioxide emissions, as well as the implementation of economic measures for reducing pollution, for example: setting the pollution tax or emissions trading [7].

Thus, the main goal of sustainable energy development – to ensure that energy production and consumption would guarantee the long-term human development, economic growth and ecological sustainability, while maintaining stable institutions that will ensure global security [8]. Therefore, the objectives of sustainable energy policy, in order to achieve main sustainable energy development goals, is to ensure [9]:

- High-quality energy services accessible to every inhabitant of the world;
- The security of energy supply in the short, medium and long term;
- A well-balanced energy network systems that optimize the system's efficiency and cooperation;
- Increasing the efficiency of energy production and consumption, particularly in countries in transition;
- A permanent reduction of the environmental impact of energy, development and adaptation of green technology, moving from pollution-intensive technology (which governs greenhouse gas and other emissions) to less polluting technologies and more use of renewable energy resources.

It is also possible to define the core of the energy policy to help achieve a more sustainable energy future [6]:

1. Energy security and safety. Energy security and reliability by ensuring in particular the need to increase energy savings and efficiency, measures aimed at higher fuel mix diversity, diversification of energy supplies and maintaining strategic and commercial stocks, as well as promoting research and development of new technologies and renewable energy resources.

2. The energy production and efficiency. Energy efficiency policies can be based on direct and indirect price mechanisms (such as subsidies and the integration of external costs in energy prices), lowering the prices of consumer trends in sensitive sectors and applications. However, even without changing the pricing structures of energy efficiency policies can overcome market failure, such as the introduction of performance standards, equipment and product labeling, and legal norms properly inform users, planners and policy-makers and operators are well motivated and adequate payment for the energy system plays a crucial role in the successful the implementation of energy efficiency measures [6].

3. Cost-based pricing of energy, eliminating subsidies and the integration of external costs. Energy pricing is crucial in reducing the environmental impact of energy consumption and ensuring energy efficiency improvement measures, but the consideration of all the generation, transmission, distribution and consumption costs is needed in order to guarantee the total efficiency of the economy.

4. Energy market opening, liberalization and economic efficiency growth. The liberalization of the energy market ensures the efficiency of economic growth in the energy sector and contributes to the implementation of sustainable energy development goals [7].

5. The new technology research and development of cleaner fossil fuels, renewable energy resources. Research and development of renewable resources, plays a crucial role in ensuring sustainable energy development goals, but such research is necessary to implement institutional support [7].

Currently, the European Commission has set targets for the year 2020, 2030 and 2050 that should be achieved through sustainable energy policy [10]. The European Commission has developed the so-called climate and energy package. This is a binding set of laws aimed to ensure that European Union (EU) would fulfil its ambitious climate and energy targets for 2020. These targets, referred as the “20-20-20” targets, provides that in the year 2020 in the EU territory will be:

- 20% reduced greenhouse gas emissions (indicators compared with the ones of year 1990);
- 20% increased consumption of electricity produced from renewable sources, market share;
- 20% increased energy efficiency.

20-20-20 targets represent an integrated approach to climate and energy policy, which aims to combat climate change, improve the EU's energy security and to strengthen its competitiveness.

EU leaders are committed to the implementation of European Commission's proposal for 2030 – to reduce greenhouse gas emissions by 40% (indicators compared with the ones of year 1990). It is expected that in accordance with this agenda, in 2030 the EU's share of the energy produced from renewable resources, will be 27%, at the same time EU's economic and energy system will become more competitive, secure and sustainable. EU plans that by 2050 greenhouse gas emissions will be reduced to a large extent, but the implementation of this objective is a serious challenge for the existing energy systems, since the energy sector is responsible for about 80% of all EU emissions [11].

Lithuanian energy sector vision, goals and strategic initiatives match the guiding principles of the EU's energy policy – security of supply, competitiveness and sustainable development [12]. Lithuanian National Energy (Energy Independence) Strategy states that the country will increase energy efficiency. While technological developments increase so rapidly, by 2050 there will be significantly improved existing production and use patterns, and created an entirely new. In order to respond adequately to technological progress, the state will monitor and encourage the development of economically viable technologies in the energy sector. Lithuania will focus on the development of systematic capacity and competence management in the areas of nuclear energy management and energy production from renewable energy sources [11]. Lithuanian energy sector vision is based on three basic principles, each of which will take the highest priority the different periods of strategy implementation (until 2020, the year 2020–2030 and 2030–2050). By 2020, the country's highest priority is energy independence that will ensure the freedom to choose the type of energy resources and their supply sources (including domestic production) most relevant to the interests of consumers and the Lithuanian state energy security needs. The change of energy resources structure by gradually reducing dependence on fossil fuels and creating alternatives to the sole supplier of energy resources, will ensure the country's energy security and sustainable development in the energy sector. Strategic priority of the year 2020–2030 – a competitive and sustainable energy sector [11]. To achieve this, Lithuania will continue to build environmentally friendly energy sources in the framework of common fuels and improve energy infrastructure necessary for the potential of renewable energy resources to exploit. Lithuania by the year 2030 will have a competitive and environmentally friendly energy sector, where most of the energy will be produced from renewable energy sources and nuclear power. Strategic priority of the year 2030–2050 – further sustainable development of the energy sector. For this purpose there will be selectively adapted new technologies in Lithuania, with a particular emphasis on those technologies that contribute to environmentally friendly energy production and use of environmentally friendly development. In 2050 Lithuania will be independent from fossil fuel imports – all usable energy will be produced from nuclear power and renewable energy sources [11].

So, the most important element of Lithuania and EU’s long-term scenario, in order to implement sustainable energy, should be the change of current energy sources with RES, because it is impossible to ensure sustainable development without transfering the global energy system into a cohesive [8].

Renewable energy sources and technologies were identified as a means to reduce the impact of the energy system on the global climate and to reduce the dependence of national energy systems on foreign oil and gas [2]. RES accumulates the essential qualities inside itself for which these resources becomes the research center of attention of all sustainable energy development [3]:

- RES means the inexhaustibility of their use;
- Natural processes in terms of circulation, they mean that technological progress is oriented to human activities in harmony with the natural circulation of natural processes;
- Technical sense of progress has been immense, only because of high cost of electricity produced from RES they cannot go to the market on a larger scale.

RES development is an attractive alternative to traditional energy as fossil fuel burning significantly increases environmental pollution and global warming accelerates, causing more and more natural disasters. Economic theories emphasize the importance of renewable resources as growth without limits, compensating, most manoeuvrable type of capital [3]. It is important to note that the RES technology offers dual external benefits:

1. RES technologies not only helps to solve the problems of climate change, makes it possible to deal with the energy isolation and economic problems, but also indirectly reduce

poverty – a positive effect on the country's level of employment, create new jobs. These technologies promote industrial development, economic growth and development of new technologies [3].

2. The arising external costs while using RES technologies are significantly lower or absent compared with fossil energy. External costs or expenses referred to as external damage to the environment caused by burning traditional fuels (coal, oil, natural gas). Unfortunately, this damage is not reflected in the prices of these fuels, which also are unstable, and the resource of those technologies are finite and is running out [11]. Underestimating the external costs prevents the penetration of RES-efficient technologies into the market on a large scale [3].

So, although the environmental benefits of renewable energy are obvious, fossil fuel generated energy-efficient systems cheapness does not let to displace conventional energy kind from dominant positions [3].

In order to boost the popularity of renewable energy, the world's governments develop and implement a variety of mechanisms to promote new technology developers and manufacturers and investors to become involved in renewable energy generation market [3], but the universal energy RES support schemes available. Each EU country has its own system of incentives drawn up by its tasks, taking into account the situation of particular country, it [15]:

- Promote the tariffs or their accessories;
- Quota – certificates;
- Grants and targeted investments;
- Concessional loans;
- Tax cuts for the construction work;
- Exemption from tax for the sale of energy;
- Energy produced for own consumption.

The most popular and widely used methods of promotion is to encourage the setting of tariffs (support given to all energy producers using RES) and targeted investment (that is, one-time support).

RES technologies and their subsidies, as well as energy efficiency and conservation measures promotion, are the only ones justified in subsidizing energy [16]. As already mentioned, the external costs are not sufficiently integrated in energy prices, and therefore energy efficiency measures and renewable energy subsidies are justified in order to align with the environmental impact of different alternatives [8].

3. MARKET FAILURES AND OTHER BARRIERS THAT HAMPER RES

Renewable energy sources provide many additional advantages: allow to create new jobs in the production, transportation, construction and operation chain, reduce the cost of imported energy resources, reduce the country's energy independence [17]. Renewable energy sources and technologies are diverse and their future depends on a variety of circumstances [18]. Futhermore, they are not limited by the resources, but the technological, economic and political factors, so it is important to define each of these potential factors. According to the paper “Renewable energy costs, potentials, barriers: Conceptual issues” of Verbruggen et al. these potentials are defined as:

- Market potential: the amount of renewable energy output expected to occur under forecast market conditions that are shaped by private economic agents and are regulated by public authorities [18]. Market potentials are based on expected private revenues and expenditures, calculated at private prices (incorporating subsidies, levies, and rents) and with private discount rates. In reality, the private context is partly shaped by public authority policies [18]. Market potentials also are different by region or country. Since it is not possible to forecast the exact response to a certain policy instrument, as well as future costs, prices and consumer preferences, there is by default a level of uncertainty concerning the size of the market potential [18].

- Economic potential: the amount of renewable energy output projected when all – social and private–costs and benefits related to that output are included [18]. In realizing the economic potential, negative externalities and co-benefits of all energy uses and of other economic activities are priced, while social discount rates are used to balance the interests of consecutive human generations [18]. Steps in its direction are made by increasing internalization of externalities in the prices end-users face and by more focus on long-term interests [18]. In comparison to the market potential, the size of the economic potential is adding another layer of uncertainty, mainly due to limits in our knowledge of the extent of the external costs or how we should value identified externalities [18].
- Sustainable development potential: required amount of renewable energy produced when the implementation of sustainable development is being done in all three respects: environmental, economic and social. This contrasts with the market and economic potentials, which take only partial account of social and environmental issues in working towards sustainable development, issues of governance need to be addressed explicitly [18]. When public governance is more directed to developing RES, the environmental, economic and social interests can be better balanced and integrated.
- Technical potential: the amount of renewable energy output obtainable by full implementation of demonstrated and likely to develop technologies or practices.

Consequently, the existing technological, economic and political factors barriers of various RES technologies penetrate the market, and external costs are not the only obstacles to wider integration of RES in the total energy sector. There are two different scientific paradigms to explain the slow diffusion of RES technologies [2]. The first neo-classical economic paradigm argue that the reason – market failures. In order to encourage the development of RES, various tax incentives and encouraging tariffs (support given to all energy producers using RES) and targeted investment (that is, one-time support). Often, however, the market is not sufficiently analyzed in detail, and relief does not reach the target contact, but their scale is inaccurate [2]. The neoclassical approach challenges the second scientific paradigm, according to which emphasizes the importance of systematic innovation. In scholars view, the speed, direction and success of innovation processes are strongly influenced by the environment in which innovations are developed [2]. This environment is called the innovation system, technological innovation system or ecosystem. Innovation systems are socio-technological players, rules, and their communication systems [2]. Scientists supporting this approach argue that without market imperfections may exist and many other weaknesses in the system that hinder the rapid development and diffusion of innovation.

However, in most cases the main brake of the development of RES, economists identify the market barriers and market failures, which are divided into [19]:

- Commercial barriers as a result of new technologies competitive with conventional technologies;
- Market failures in terms of RES social benefits and negative external effects of traditional energy resources;
- Market barriers, such as inadequate information, access to capital constraints, change initiatives between home owners and tenants and high transaction rates by making small purchases, as well as institutional barriers.

To compete with traditional technologies, such as the use of nuclear and fossil fuel, RES has to overcome two major commercial barriers: poor infrastructure and lack of economies of scale in the production of the traditional technologies [19]. While developing new RES and their technologies, significant initial investment in order to form a new infrastructure becomes a necessity. However, this investment increases supply costs of electricity produced from RES, especially in the initial years [19].

Most of the benefits of RES consists of public goods, such as pollution reduction and environmental benefits to society. However, the user who buys “green energy” and pays for it has to breathe the same air as all consumers buying cheaper energy [19]. Here there lies a difficulty – not all the market participants, energy consumers, are willing to pay for such public goods, hence, wantonly heavier tax burden goes to consumers, who willingly pay for “green energy”.

RES technologies also face barriers in market transactions – consumers don’t have enough information, given by electricity supply companies, about energy sources and their emissions to the atmosphere. In addition, RES projects and their implementing firms are generally small, it has less resources compared to large companies [19]. Thus, both of these companies' ability to negotiate with customers, with large market participants, participate in lobbying and influence the market or procedures to participate in industry forums, which determine the rules of marketing, power is low.

The current energy system is strongly influenced by all economic processes, and therefore the aim to revolutionize the whole energy system, would cause the wave of changes in all other economic processes, while transitioning to “green energy” consumption. The transition from traditional energy to renewable energy consumption should be very gradual, and for every barrier to overcome different measures are being offered:

Table 1. Types of market barriers and measures that can alleviate them

Barrier	Key characteristics	Typical measures
Uncompetitive market price	Scale economies and learning benefits have not yet been realised	• Learning investments • Additional technical development
Price distortion	Costs associated with incumbent technologies may not be included in their prices; Incumbent technologies may be subsidised	• Regulation to internalise ‘externalities’ or remove • subsidies • Special offsetting taxes or levies • Removal of subsidies
Information	Availability and nature of a product must be understood at the time of investment	• Standardisation • Labelling • Reliable independent information sources • Convenient & transparent calculation methods for decision making
Transactions costs	Costs of administering a decision to purchase and use Equipment (overlaps with ‘‘Information’’ above)	
Buyer’s risk	• Perception of risk may differ from actual risk (e.g. ‘pay-back gap’) • Difficulty in forecasting over an appropriate time period	• Demonstration • Routines to make life-cycle cost calculations easy
Finance	• Initial cost may be high	• Third party financing

	threshold • Imperfections in market access to funds	options • Special funding • Adjust financial structure
Inefficient market organization in relation to new technologies	• Incentives inappropriately split—owner/designer/ user not the same • Traditional business boundaries may be inappropriate • Established companies may have market power to guard their positions	• Restructure markets • Market liberalization could force market participants to find new solutions
Excessive/inefficient regulation	Regulation based on industry tradition laid down in standards and codes not in pace with developments	• Regulatory reform • Performance based regulation
Capital stock turnover rates	Sunk costs, tax rules that require long depreciation & inertia	• Adjust tax rules • Capital subsidies
Technology-specific barriers	Often related to existing infrastructures in regard to hardware and the institutional skill to handle it	• Focus on system aspects in use of technology • Connect measures to other important business issues (productivity, environment)

Source: IEA 2003 [20]

However, sometimes barriers overlap, interact and influence the decision to invest in new technologies, that is why identifying and alleviating all barriers that hinder the development of RES is necessary to successful deployment of these technologies [21], e. g., technological barriers, production costs, and large-scale implementation limitations, are the main reasons for the small share of wind and tidal energies from the world's total energy mix [22].

In order to mitigate the barriers or circumvent them, the feasibility of energy alternatives in different regions should be taken into account, as not all energy sources are accessible in all regions due to different physical, technological, legal and institutional barriers [22].

4. CONCLUSIONS

1. Renewable energy sources and technologies are means to reduce the impact of the energy system on the global climate and to reduce the dependence of national energy systems on foreign oil and gas.
2. Existing technological, economic and political factors barriers of various RES technologies penetrate the market, and external costs are not the only obstacles to wider integration of RES in the total energy sector. In most cases the main brake of the development of RES are market barriers and market failures.
3. The transition from traditional energy to renewable energy consumption should be very gradual, i.e., for every barrier to overcome different measures are being offered,

nonetheless, sometimes barriers overlap, interact and influence the decision to invest in new technologies.

4. In order to mitigate the barriers or circumvent them, the feasibility of energy alternatives in different regions should be taken into account, as not all energy sources are accessible in all regions due to different physical, technological, legal and institutional barriers.

REFERENCES

1. REDDY, A.K.N.; WILLIAMS, R.H.; JOHANSSON, T.B. *Energy after Rio. Prospects and Challenges*. UNDP, 1997. 176 p. ISBN 92-1-12670-1.
2. NEGRO, S.O.; ALKEMADE, F.; HEKKERT, M.P. Why does renewable energy diffuse so slowly? A review of innovation system problems. *Renewable and Sustainable Energy Reviews*, 2012, No. 16, p. 3836–3846.
3. KLEVAS, V.; ŠTREIMIKIENĖ, D. *Lietuvos energetikos ekonomikos pagrindai.* Lietuvos energetikos institutas, 2006. 404 p. ISBN 9986-492-96-3.
4. United Nations initiated <http://www.se4all.org/>
5. *World energy assessment. Energy and the Challenge of Sustainability*. Overview, UNDP. 2000. 508 p. ISBN 92-1-126126-0.
6. ŠTREIMIKIENĖ, D. Tvari energetikos plėtra. *Aplinkos tyrimai, inžinerija ir vadyba*, 2002, Vol. 1, No. 19, p. 20–29.
7. ŠTREIMIKIENĖ, D. Vietiniai ir globaliniai darnios energetikos politikos plėtros įgyvendinimo Lietuvoje aspektai. *Energetika*, 2002, No. 1, p. 53–60.
8. ŠTREIMIKIENĖ, D.; ČIEGIS, R.; JANKAUSKAS, V. *Darnus energetikos vystymasis.* Vilniaus universitetas, 2007. 434 p. ISBN 9789986199922.
9. ČIEGIS, R. *Ekonomika ir aplinka: subalansuotos plėtros valdymas*. Vytauto Didžiojo universitetas, 2004. 552 p. ISBN 9955-530-11-1.
10. European Commission The 2020 climate and energy package <http://ec.europa.eu/clima/policies/package/index_en.htm>
11. Nacionalinis AEI veiksmų planas <http://www.ebb-eu.org/legis/ActionPlanDirective2009_28/national_renewable_energy_action_plan_lithuania_lt.pdf>
12. LR energetikos įstatymas <http://www3.lrs.lt/pls/inter3/dokpaieska.showdoc_l?p_id=415663>
13. LR Atsinaujinančių išteklių energetikos įstatymas <http://www3.lrs.lt/pls/inter3/dokpaieska.showdoc_l?p_id=398874>
14. LR Energetikos ministerija <http://www.enmin.lt/lt/activity/veiklos_kryptys/atsinaujantys_energijos_saltiniai/aei_more.php>
15. LR Valstybės kontrolė *Valstybinio audito ataskaita atsinaujinančių energijos išteklių potencialo naudojimas Lietuvoje* <www.vkontrole.lt/failas_senas.aspx?id=4007>
16. MOUNTFORD, H. Experiences with Reforming Energy Subsidies. Proceedings of International Conference Enhancing the Environment by Reforming Energy Prices. Pruhonice, Czech Republic. 2000 June 14–16.

17. GALINIS, A.; LEKAVIČIUS, V.; MIŠKINIS, V. Atsinaujinančių energijos išteklių platesnio naudojimo kryptys. *Mokslas ir technika,* 2010, 6, p. 4–6.
18. VERBRUGGEN, A., et al. Renewable energy costs, potentials, barriers: Conceptual issues. *Energy Policy,* 2010, No. 38, p. 850–861.
19. ŠTREIMIKIENĖ, D.; PAREIGIS, R. Atsinaujinančių energijos išteklių naudojimo skatinimas Lietuvoje. *Ūkio technologinis ir ekonominis vystymas*, 2007, Vol. 13, No. 2, p. 159–169.
20. *Creating markets for energy technology*. International Energy Agency. 2003. 170 p. ISBN 92-64-09963-8.
21. ELEFTHERIADIS, I.M.; ANAGNOSTOPOULOU, E.G. Identifying barriers in the diffusion of renewable energy sources. *Energy Policy,* 2015, 80, p. 153–164.
22. HADIAN, S., MADANI, K.A. system of systems approach to energy sustainability assessment: Are all renewables really green? *Ecological indicators*, 2015, 52, p. 194–206.

CYSENI 2015, May 27–28, Kaunas, Lithuania
ISSN 1822-7554, www.cyseni.com

PRODUCTION OF PRODUCER GAS FROM BIOMASS IN GASIFIER OF DOWNDRAFT TYPE

T. Antoshchuk
The Gas Institute of National Academy of Sciences of Ukraine
Degtjarivska str. 39, 03113, Kyiv-113, Ukraine
Phone: (m) +38 099 224 32 65
(w) +38 044 453 31 32
Email: taras-ant@i.ua

ABSTRACT

It is known that Ukraine has one of the highest potential among European countries in amounts of alternative solid biofuels that in quantitative equivalent makes around 25 million tons of standard coal. So it is obvious that in Ukraine implementation of energy technologies with use of named solid biofuels are more preferable compared with other types of alternative energy sources, such as solar, wind, etc. Gasification is one of popular type of technologies producing energy from alternative solid fuels. In this work we considered gasification of different types of alternative solid biofuels (biomass) in gasifier of downdraft type. As the fuels there were considered local species of biomass, namely wood chips, wood pellets, sunflower and rice husk, sunflower husk pellets. Gasification was carried out with the aim of producer gas production as alternative gaseous fuel, which was subsequently burned in industrial water steam boiler in admixture with natural gas. During the experiments and laboratory tests the following parameters of gasifier were under control: fuel load capacity, operating temperature of the gasifier, indicators of consumed air and gas, air pressure and producer gas pressure, also there were taken gas samples for composition analysis. During experiments different operational modes of gasifier were determined, depending on the kind of initial fuel, the given results had led to changes in the whole operation rules of the gasifier complex. Also advantages of producer gas were determined, and eliminated some shortcomings of previous complex maintenance. As a conclusion it is possible to point out that described gasification technology with downdraft gasifier allows substituting of 30% of natural gas, which confirms the efficiency of technology.

Keywords: gasifier, downdraft type, biomass, gasification, producer gas

1. INTRODUCTION

It is a fact that nowadays Ukraine faces acute need in reducing of consumption of natural gas, especially in industrial sector as well as in municipal economy. The most probable and real solution of this problem is transition to local kinds of fuels, that should involve technologies of direct fuel combustion and fuel gasification.

The biomass potential of Ukraine is about 25 million ton of standard coal that makes equivalent to about 20 billion m^3 of natural gas. It is necessary to point out that not all kinds of biomass can be utilized as alternative fuel, because each of it has its own characteristics and requires individual approach to its use; though practically all kinds of local fuels can be used for direct combustion and some can be gasified into producer gas [1, 2].

The most common types of biomass in Ukraine are: wastes from woodworking industry – wood chips and sawdust (also in form of pellets and briquettes); wastes from agricultural grain-crops, such as sunflower husk, rice husk, and cereal straw.

Biomass quantity from woodworking industry in Ukraine makes about 15–20% of the total amount of biomass in the country. This fact proves enormous potential of using of these products in direct combustion and gasification processes.

Now the most widespread technology of biomass gasification is process of air gasification, due to simplicity of process and servicing, as well as the low investment in equipment. In this type of gasification are mostly used the low cost biomass, as a rule its non-processed wood chips, sawdust and husks. Producer gas - result of solid fuel gasification, can be widely used as alternative to natural gas in fuel consuming units designed for gaseous fuels.

In view of above mentioned fact Gas Institute of National Academy of Sciences of Ukraine has developed, tested and put into operation gasifiers specially designed for gasification of coal, processed biofuels and wastes [3]. The projects were implemented both as a laboratory stands and industrial units with permanent operation processes.

Thus gasifiers of periodic action (GPD gasifier) are equipment with periodic action type (Fig. 1), they use downdraft technology and have single-pass periodic fuel load that occupy total volume of the reactor. Air flow is organized bottom-up (upward), producer gas flows in the same direction, the output of produced gas is organized through the upper lid. Combustion of the fuel bed is arranged downward.

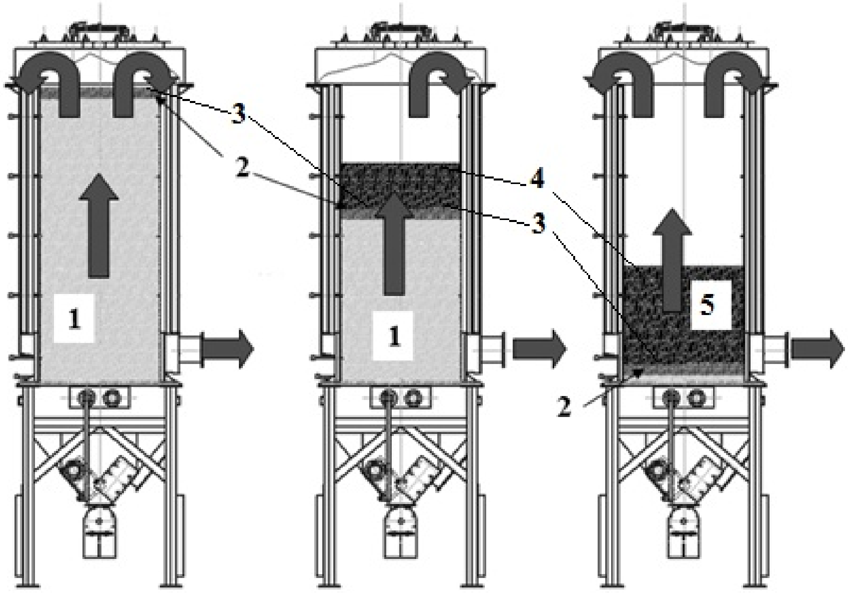

Fig. 1. Schematic diagram of the gasifier of periodic action
Legend: 1 – fuel stock zone; 2 – heating zone; 3 – oxidation zone; 4 – reduction zone;
5 – zone of coke-ash residuum Arrows – direction of the producer gas

This described technology resembles the Lurgi gasification (Lurgi) [4], but it has several advantages, as it is designed to operate on fuels with high content of volatiles. All produced gas passes through high temperature zone, in which all the hydrocarbon compounds are combusted.

2. DESIGN AND OPERATION OF GDP GASIFIERS

Operation of gasifiers is following: solid fuel (biomass, coal) is loaded into chamber of gas generator through the upper lid, and then the lid is closed. The tube space of heat exchanger, that is located between the inner and outer cylinders of generator’s frame, is filled through the water inlets. Then electric heater or other ignition device, located on the upper lid, heats solid fuel and there starts gasification process. Air, that is necessary for the gasification of solid fuels, is transferred through the grate and air jet located in the bottom of the gasifier. When the fuel starts to burn up, the nominal operation of gasifier starts in few minutes.

Producer gas is collected into upper manifold in upper chamber of the gasifier and then distributes in pipes of the heat exchanger. Producer gas, moving downward, releases the heat to water filling the tube space, gradually cools down and descends to the lower gas gathering manifold. This gas is ready product to be burnt in gas-burning units. For its turn, the heated water in tube space can be used as heat-carrying agent for drying of biofuels or for own needs or complex.

The ashes residues received after gasification of solid biofuels is collected in lower chamber of gasifier and then is moved out.

Chemical and physical reactions during operation of the GPD gasifier passes in five relative zone:

Fuel stock zone – it is zone located below the combustion level, not affected by reactions. During operation of the gasifier combustion front moves down and fuel decreases. When fuel is consumend, gasifier stops its operation for cooling up the coke-ash residuum and recharging.

Function of the zone: providing prolonged operation of the gasifier.

Heating zone – it is thin zone whose thickness is close to the linear dimensions of solid fuel particles, zone is located below the combustion front. The layer consists of particles that are heated under the radiation influence of oxidation zone and heat conductivity. Under heating of fuel there goes process of sequential liberation of water vapor and volatiles. Escaping substances are transferred to the combustion zone by air supplied from the bottom zone of fuel stock.

Function of the zone: preparation of the fuel before it enters the oxidation zone.

Oxidation zone – it is burning zone. In this zone goes combustion reaction with heating of all depth of fuel particles and accompanied by liberation and combustion of volatiles. The thickness of oxidation layer and its temperature is determined by the intensity of fuel consumption and fuel properties. The temperature of the combustion products in the layer operating in normal mode makes 750–1300 °C.

Functions of the zone:

– production of high-temperature flow of combustion products, consisting of CO_2, nitrogen and water vapor;

– heating of fuel;

– formation of carbon based high-temperature layer.

Reduction zone – it is zone in which forms producer gas. Temperature of gas at the zone outlet not exceeds 800 °C. Here go several interrelated processes that ensure generation of gaseous fuel from the heated carbon dioxide and water vapor.

Functions of the zone:

– reduction of CO_2 to CO under reaction which goes with heat absorption;

– receiving of molecular hydrogen by decomposition of water vapor under reaction [5], which goes with heat absorption;

– gradual cooling of the layer due to reduction reactions;

– decomposition of volatiles into simpler components under influence of high temperatures.

Zone of coke-ash residuum – it is zone with decreased reaction rate due to substantial temperature pull-down. Here goes purification of received producer gas from tars and fine particles of ash, the process occurs owning to the gradual reduction of gas velocity under sufficiently high temperatures.

Function of the zone: gas purification.

3. EXPERIMENT

The experiments with biofuels processed in gasifiers of GPD model were conducted in following way:

- weighing the original fuel. Prior to testing there was analysis of fuel composition and determination of its energy characteristics;
- inflammation of the gasifier. Measurements of air supply and consumption, temperature measurement;
- registration expenses of water flow in the cooling system and the temperature at inlet and outlet of the gasifier;
- measurement of the temperature in the gasifier and the temperature of gas at the output of gasifier.
- periodic extraction of producer gas and determination of its composition;
- combustion of producer gas in boiler with the determination of composition of combustion products;
- stoppage of air supply after reaching the lower level of reaction zone (grate).
- cooling of coke-ash residuum, its following discharging and determination of its composition.

During the research work there were carried out tests with gasifiers working with next kinds of biofuels:

- Wood chip;
- Rice husk;
- Wood pellets
- Sunflower husk pellets;
- Lignite:
- Brown coal.

The initial compositions of fuels are presented in table.

Table 1. Composition of the initial fuel

Components	**Wood chips**	**Rice husk**	**Wood pellets**	**Pellets of sunflower husk**	**Lignite**	**Brown Coal**
C, %	50.0	50.3	51.0	51.5	57.0	60.0
H_2, %	6.0	6.1	6.0	5.9	6.0	5.0
O_2, %	43.45	42.8	42.0	41.9	35.0	34.0
N_2, %	0.5	0.7	0.95	0.5	1.0	0.0
S, %	0.05	0.1	0.05	0.2	1.0	1.0
Ash value, %	2.0	20.5	2.0	2.8	6.38	23.5
Moisture ,%	15.0	10.0	10.0	15.0	15.0	19.5
Low heat value , MJ/kg	19.0	18.68	19.2	19.1	16.78	17.8

The main purposes of the tests with laboratory gasifier enabled to obtain information about abilities of stand (Fig. 2), also gave opportunity to compile heat balance, determine efficiency factor of gasification and also define optimal temperature conditions (load) in operation of gasifier.

Indication of the scheme:

T_1 – T_5 – thermocouples TCA. Working temperature up to 1100 °C. Task – temperature measuring in reacting zone.

T_6, T_7 – thermocouple TCC (Chromel-Copel). Working temperature – up to 100 °C. Task – water temperature measuring in cooling circuit of the gasifier.

T_{gas} – thermocouple TCA. Working temperature up to 1100 °C. Task – measuring of gas temperature at the outlet of the gasifier.

G_1 – gas-meter. Flow range 10 - 40 m^3/h. Task – measurement of air flow supplied to the gasifier.

G_2 – water meter. Flow range 0 - 1.5 m^3/h. Task - measuring water flow for cooling of gasifier.

P_1, P_2 – manometer. Measured pressure – 4 kPa. Task – measuring the differential pressure in gasifier.

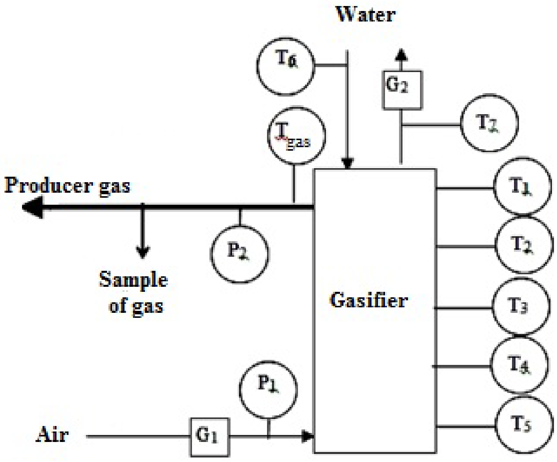

Fig. 2. Schematic view of the experimental installation

The results of tests showed high energy efficiency of the GPD gasifier while working on all above mentioned types of solid fuel. But it is worth to present more detailed results for prepared fuel - wood pellets, as this type of fuel is main for receiving producer gas intended for replacement of natural gas in boilers.

For permanent receiving of high characteristics of producer gas (quantity and quality) it is necessary to keep up steady velocity of gasification process, which depends on adjustment of air consumption and gasifier design.

Design of GPD gasifier gives opportunity for easy operation over gasification process due to installation of control equipment, it is carried out by using of five thermocouples.

Also according to the marking on the scheme of installation, parameters were fixed at the moment when fuel was passing thermocouples zone. Each biofuel received its own results. The received results were averaged, the error indication does not exceed 10% (Table. 2).

Table 2. Indexes of laboratory experimental installation

Zone of front passage	**T_1, ^0C**	**T_2, ^0C**	**T_3, ^0C**	**T_4, ^0C**	**T_5, ^0C**	**T_6, ^0C**	**T_7, ^0C**	**T_{gas}, ^0C**	**P_1, mm water eq**	**P_2, kPa**	**G_1, m^3/h**	**G_2, m^3/h**
1	669	100	102	99	94	66	121	103	430	0.18	367	583
2	267	617	98	93	81	60	102	95	480	0.16	361	583
3	215	285	692	68	66	50	84	95	520	0.1	325	545
4	203	219	286	620	68	55	89	98	680	0.1	352	537
5	211	201	248	308	625	59	97	98	700	0.06	350	628

4. RESULTS OF EXPERIMENTS

As it was found out during the tests, GPD gasifier of the given design obtains distinctive peculiarity, as after gasification process there remains ash-coke residuum, which contains high percentage of carbon. By gasification of biomass with low ash content there was received ash-coke residuum that meets definition of "charcoal" [6]. This “charcoal” has high energy indexes and can be further used in biofuel plants, designed for direct burning of solid fuels.

The chemical energy of the fuel during gasification is distributed in such processes:

- Conversion of solid fuel into producer gas. At that, the energy potential of producer gas consists of its energy potential as fuel and heat of the gas;
- Heating of water in cooling system of the gasifier;
- Formation of coke-ash residuum, which in its turn also performs as potential fuel.
- Heat losses during operation of the installation.

Analysis of all components of the energy balance of the gasifier has shown that its efficiency can reach 97 %, on condition that there will be used all advantages of the installation, e.g. heat of received producer gas and water in cooling system, and also energy potential of coke-ash residuum. At that, the potential of initial fuel is taken as 100%, and distributed as follows:

- Energy potential of producer gas – 74%
- Heat capacity of cooling system – 10%
- Energy potential of coke-ash residuum – 13%
- Heat losses – 3%

Average composition of producer gas, its energy indexes and also unit consumption of fuel for natural gas substitution are shown in Table 3 [7].

Table 3. Producer gas received from solid fuels, its composition and replacement indexes

Parameters	**Solid fuels for gasification**					
	Wood chips	**Rice husk**	**Pellets**		**Lignite**	**Brown coal**
			Sunflower husk	**Wood**		
Composition of the producer gas,%						
H_2	13.35	11.36	16.86	11.3	12.24	20.01
N_2	48.83	54.8	44.92	49.45	55.24	49.27
CO	16.03	15.69	19.51	12.59	11.88	14.10
CH_4	5.57	4.72	5.81	6.71	4.24	3.32
CO2	12.49	10.55	9.15	15.84	12.87	11.14
C_2H_4	0.77	0.55	0.71	0.95	0.98	0.13
C_2H_2	0.16	0.02	0.0	0.34	0.0	0.0
C_2H_6	0.11	0.07	0.18	0.21	0.0	0.11
C_3H_8	0.07	0.03	0.1	0.13	0.0	0.04
H_2O	2.62	2.21	2.69	2.49	2.34	1.88
$\sum$	100	100	100	100	100	100
Indicators of substitution and energy indexes						
low heat value, MJ/m^3 (kKal/m^3)	6.13 (1464)	5.24 (1251)	6.97 (1664)	6.77 (1617)	4.92 (1175)	5.32 (1270)
Amount of solid fuel necessary for the substitution of 1 m^3 natural gas, kg	3.7	3.3	2.5	2.6	3.2	2.8

Taking into consideration that given gasifier has non-standard downdraft design and operates in periodic regime one of the tasks of investigation was to determine changes in component composition of producer gas. Composition of gas in each corresponding zone of the thermocouple was collected with subsequent laboratory analysis. Next graphs (Fig. 3 – Fig. 8) are showing changes in amount of main components of producer gas received from different types of initial fuel. During tacking of gas samples there was fixed temperature not higher than 700 ^{o}C.

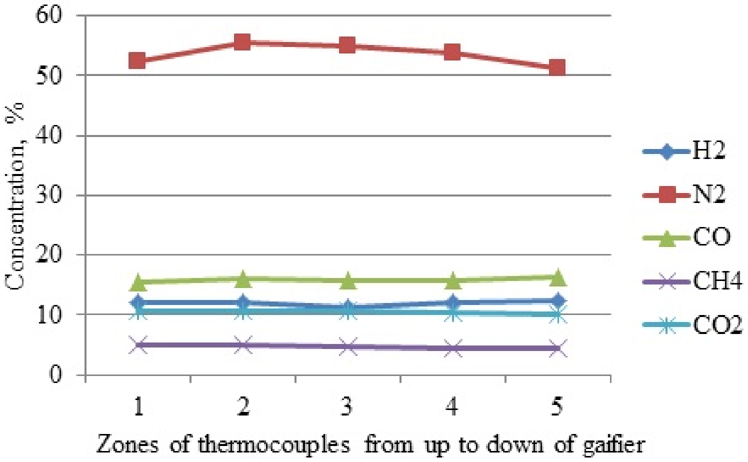

Fig. 3. Concentration of main components of producer gas from rise husk

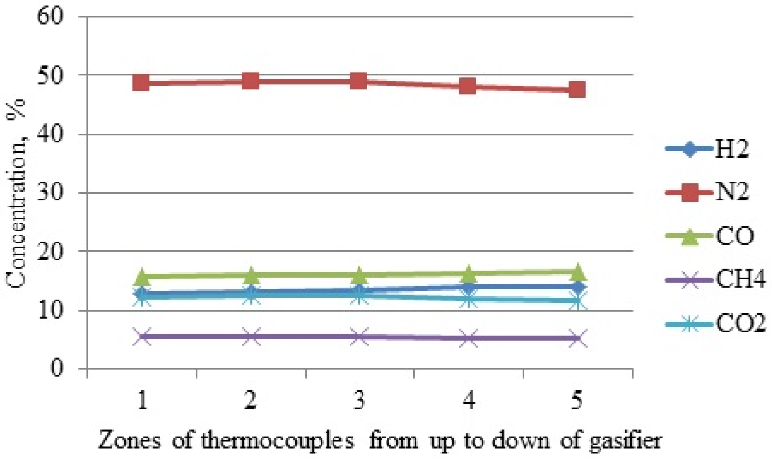

Fig. 4. Concentration of main components of producer gas from wood chips

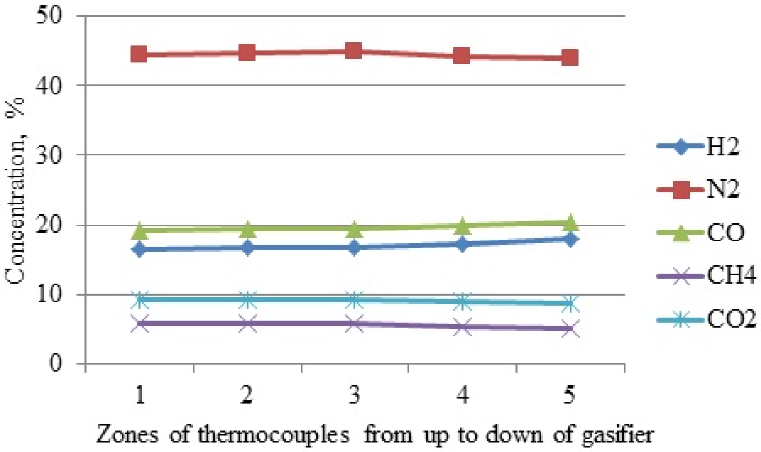

Fig. 5. Concentration of main components of producer gas from pellets of sunflower husk

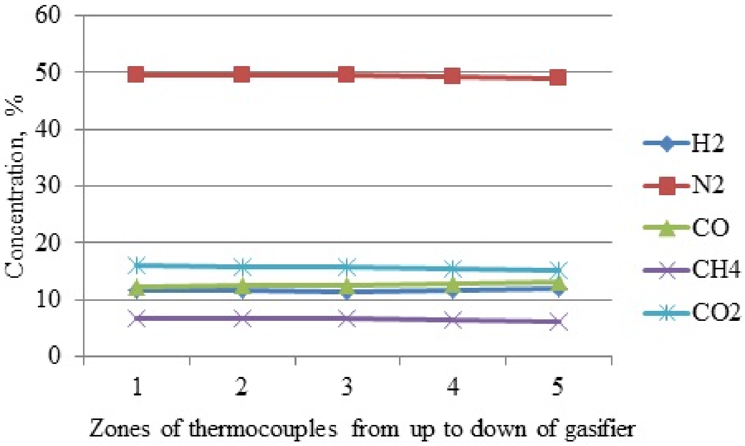

Fig. 6. Concentration of main components of producer gas from wood pellets

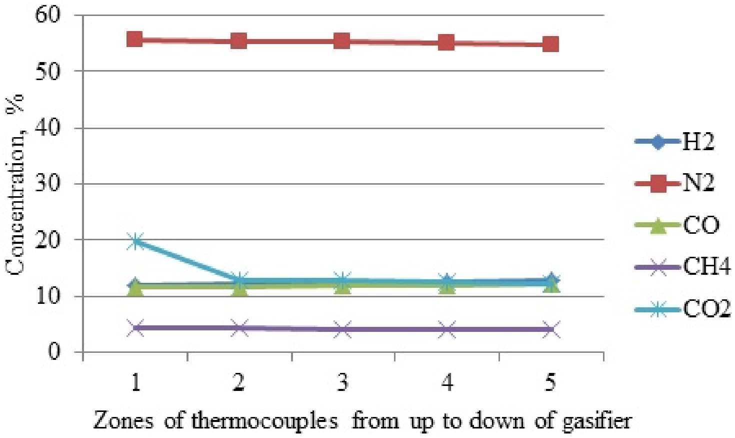

Fig. 7. Concentration of main components of producer gas from lignite

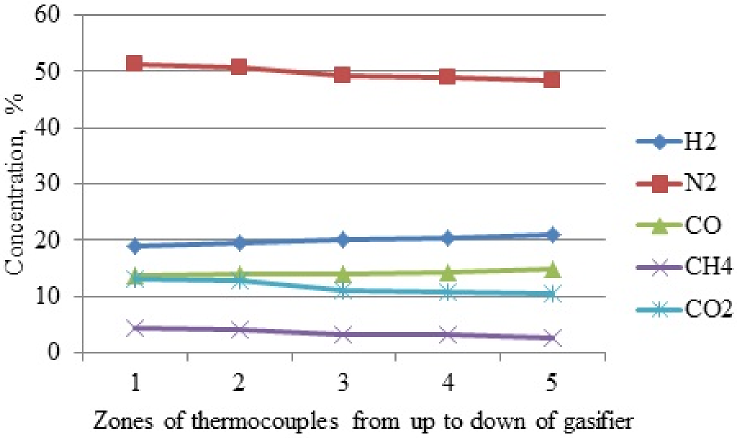

Fig. 8. Concentration of main components of producer gas from brown coal

5. CONCLUSIONS

During realization of experiments there were determined temperature regimes of GPD gasifier operational modes, duration of its operation on one load working on different kinds of biomass, and also component composition of producer gases received. There was defined heat balance of named gasifier, that produces not only gaseous mixture but also residuum product that can be used a charcoal. The heat exchanger, that is present in design, gives opportunity to receive hot water that is possible to use for needs of the installation or for host enterprise of the installation.

During the experiments versatility in usage of different biofuels in this type of gasifier was proved. It was defined that constructional disadvantages of the installation are graded by technological features of gasifier operation, namely air consumption during gasification and water consumption in the heat exchanger depending on biomass kind.

Also simplicity and universality of gasifier design give opportunity to exploit this gasifier quite a long period, and the main existing disadvantage is periodicity of operation. This disadvantage can be eliminated by installation of several gasifiers with periodical work, but permanent joint operation of the gasifier complex.

REFERENCES

1. Geletukha G.G., Zhelyezna T.A., Zhovmir M.M., Matveev Yu.B., Drozdova E.I. “Assessment of potential of biomass energy in Ukraine - PART 1: Agricultural waste and wood biomass”. ISSN 0204-3602. *Prom. thermo*, 2010,Vol. 32, No. 6, p. 58–65. (translated from Ukrainian).
2. Geletukha G.G., Zhelyezna T.A., Zhovmir M.M., Matveev Yu.B. and Drozdova E.I., “Assessment of potential of biomass energy in Ukraine-Part 2: Energy crops, liquid biofuels”. ISSN 0204-3602. *Prom. thermo*, 2011, Vol. 33, No. 1, p. 57–64. (translated from Ukrainian).
3. Karp I., Pyanykh K., Yudin A. Combustion and Gasification for Substitution of natural gas *Industrial Heating* June 2013, p. 39–42.
4. КОПЫТОВ, Вадим В. *Газификация конденсированных топлив: ретроспективный обзор, современное состояние дел и перспективы развития.* Москва:Агрорус, 2012. 509 с.

5. DESHALIT, G.I. *Calculation of fuel gasification processes.* Kharkov: Publisher Kharkov Red Banner of Labor State University A.M. Gorky, 1959. 284 p. (translated from Russian).
6. ANTOSHCHUK, T., PYANYKH, K. Comparison of the technological characteristics of gasifiers of air gasification as a result of industrial exploitation. Energy Efficiency – 2013. International Scientific and Technical Conference. [CD] Kyiv. 2013 October 14–16 (translated from Russian)ю
7. ANTOSHCHUK, T., PYANYKH, K. Experience in development and industrial exploitation of gasifiers series GPD. Energy Efficiency – 2014. International Scientific and Technical Conference. [CD] Minsk. 2014 October 14–16 (translated from Russian).

CYSENI 2015, May 27–28, Kaunas, Lithuania
ISSN 1822-7554, www.cyseni.com

INVESTIGATION OF WIND SPEED FORECASTS ERRORS FOR WIND POWER GENERATION

G. Gecevicius, M. Marciukaitis
Lithuanian Energy Institute
Breslaujos str. 3, LT-44403 Kaunas – Lithuania
Phone +370 37 401 846
Email: Giedrius.Gecevicius@lei.lt, Mantas.Marciukaitis@lei.lt

ABSTRACT

Installed wind power capacity reached 282 MW in Lithuania in 2014. Recent study prepared by researchers suggests ambitious targets - to have installed wind power capacity of 840 MW by 2030. To achieve this target it is very important to analyze the impact of wind power integration in Lithuanian power system. It is necessary to decrease negative impact of wind turbines on the grid reducing wind forecasts errors as much as possible.

The paper analyses seasonal, diurnal and hourly wind speed forecasts errors and discusses main obstacles for wind speed and wind power prediction. Research was carried out by using Microsoft Excel and Matlab 13 software. The data were provided from LITGRID (*Lithuanian Electricity Transmission System Operator*), HIRLAM (*High Resolution Limited Area Model*) run in Lithuanian Hydrometeorological Service and wind turbines operating in Lithuanian coastal region and mast located in Mazeikiai region.

Results indicate that wind prediction errors for the first 24 hours remain stable and tend to increase for longer prediction horizons (24-48 h). Analysis of seasonal indicators presents large scale error dependence on temperature volatility, and the largest deviation exists in winter. Diurnal prediction errors depend on local conditions, mostly on the frequency of weather changes.

Keywords: wind speed and power prediction, wind turbines

1. INTRODUCTION

In recent years, wind power was one of the fastest growing renewable electricity generation technology in the world. The worldwide wind capacity reached 318 GW by the end of 2013, out of which more than 35 GW were added in 2013. During this period the biggest added value was China (16.1 GW), Germany (3 GW) and United States (1.1 GW) [1].

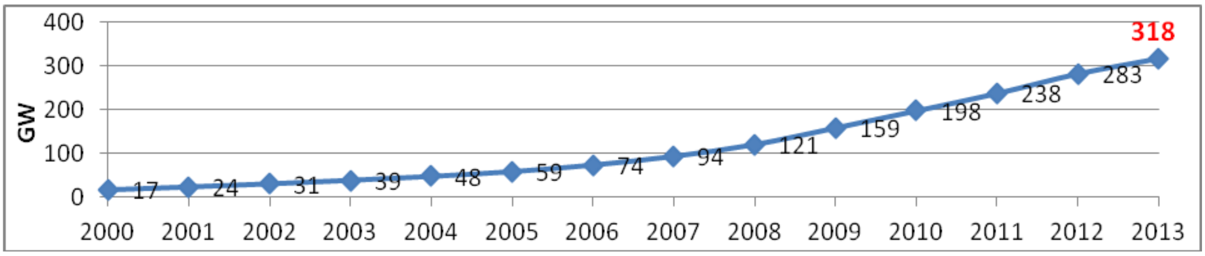

Fig. 1. Wind power total world capacity, 2000–2013 (GW) [1]

To compare installed wind power capacity in Lithuania reached 282 MW and by 2013 it was already well developed renewable source for electric power generation [2]. Despite the environmental benefits of wind power, it has an interference [3], which could affect power systems security and reliability [4].

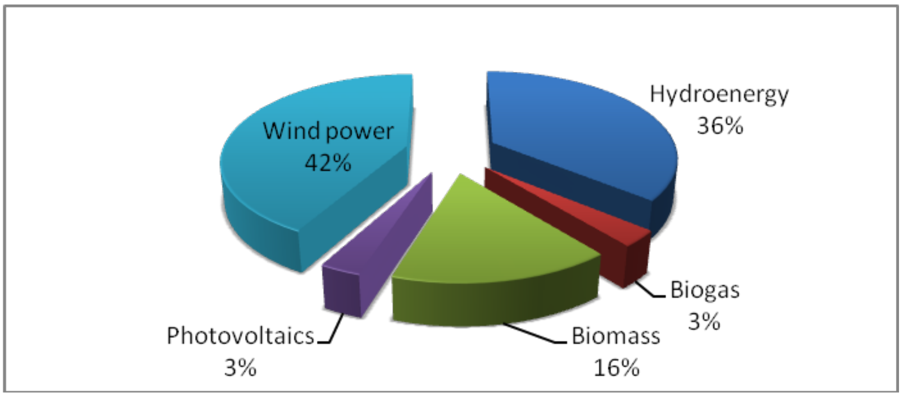

Fig. 2. Annual electric energy yield from renewable energy sources (percents) (2013)

In order to have secure and reliable system it is very important to control flexibility of wind power generation [5]. One of the most important aspects – is wind power prediction errors. There are main wind power forecast models: time series, statistic, physical and artificial neural networks [6-7]. Also, there is combined hybrid model with the best forecast results [5]. These models and those forecasts are used to predict the wind power output of a wind turbine or a wind farm and they use wind turbine or wind farm production curves [8]. Three time scales of wind speed are typically analysed: short-, medium-, and long-term. [9]. Short- term prediction aims at estimating wind speed at time intervals such as 10-sec or 10 min. Medium-term wind speed prediction usually focuses on intraday timescale, and long-term wind speed prediction extends up to several days ahead. Short- term wind speed prediction is important to the control of wind turbines. Long-term wind speed prediction is used in determining generation mix and scheduled maintenance of power systems [10].

On a global scale, wind power generation is influenced by topographical and metrological conditions. Spatial variability is attributed to the fact that there are different climate regions on the world affected by the altitude and solar insulation. On a regional scale, wind speed varies according to the geographical location depending on the sizes of land and sea, and the presence of mountains and plain areas [8]. Moreover, wind power prediction errors depend on variability of temperature processes, pressure changes, size of wind farms.

Hence, despite improvements in wind power forecasting methods, evaluation of topographical and metrological wind power forecasts still suffer from relatively high errors, ranging from 8% to 22% depending on several factors, such as, forecasting horizon, type of forecasting model, size of wind farm and geographic location [5, 11, 12]. As a result of that it is very important to analyse correlation of seasonal, diurnal, hourly forecast errors and wind speed, temperature inversion and air flows' vertical and horizontal stratification [13].

2. OBJECTS OF INVESTIGATION AND METHODOLOGY

Annual wind power prediction error (WPPE) variability is attributed to seasonal and hourly variations. To analyze relative annual, seasonal and hourly wind power forecast errors there are evaluated installed wind power capacity and WPPE by equation 1,

$$f = \frac{x}{c} 100\%, \tag{1}$$

where

f – wind power prediction error (percents);
x – hourly wind power generation prediction error (MW);

c – installed wind power capacity (MW).

For the estimation of RMSE (root mean squared error) equation 2 is used,

$$RMSE = \sqrt{\sum_{i=1}^{n}(x_i - y_i)^2}, \tag{2}$$

where

RMSE – root mean squared error;
x_i –hourly wind power generation prediction error (MW);
y_i – hourly energy power (MW).

For the estimation of correlation coefficient between wind speed and wind power forecast errors Equation 3 is used

$$\mathrm{r} = \frac{\sum_{i=1}^{n}(xx_i - \bar{x})(yy_i - \bar{y})}{\sqrt{\sum_{i=1}^{n}(xx_i - \bar{x})^2 \sum_{i=1}^{n}(yy_i - \bar{y})^2}} \tag{3}$$

where

r – correlation coefficient;
xx_i – hourly wind power generation prediction error (percents);
$\bar{x}$ – average of hourly wind power generation forecast error (percents);
yy_i – hourly wind speed (m/s);
$\bar{y}$ – average of hourly wind speed (m/s).

In this work WPPE are presented by annual, seasonal and hourly intervals. Seasonal evaluation involves last five years (2010, 2011, 2012, 2013, 2014) of WPPE variations. Hourly variations include analyses by 3 hours intervals from 00 to 24 hour in last five years. Correlation between wind speed and WPPE is also evaluated. Wind speed measurement mast is located in Mazeikiai, height of anemometer is 100 m. WPPE were calculated based on Lithuanian Electricity Transmission System Operator (Litgrid AB) data.

3. INVESTIGATION OF WIND POWER PREDICTION ERRORS

The main changes of installed wind power capacity occurred in 2012, when 73 MW of wind power were added. Later installed capacity changed slightly from 275 to 282 MW in 2014. Although the RMSE and total installed power capacity increased from 2010 to 2012, but relative wind power prediction errors decrease from 2010 to 2014. One of the main reasons of that could be historical wind power and speed data analyses and interpretation for hybrid prediction model (Fig. 3). It means last five years wind power predictions were analysed and data adopted for model.

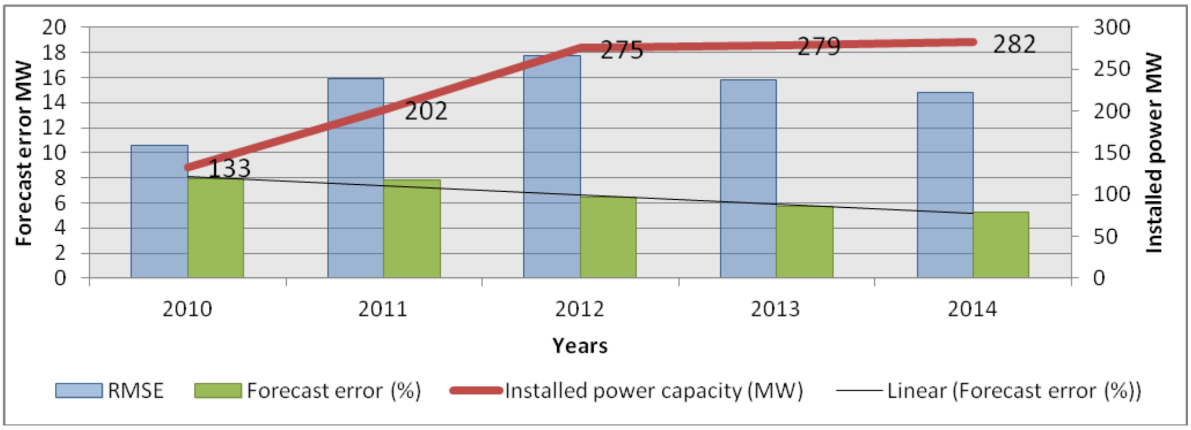

Fig. 3. Installed wind power capacity and power prediction errors

3.1 Analysis of seasonal wind power prediction errors

The analysis of seasonal components provides detailed variation of wind power yield [11]. As was mentioned before, wind power prediction is getting more accurate from 2010 to 2014 years. To compare there was a 5% difference between summer (4.79%) and autumn (9.87%) WPPE in 2010, and only 1.33% between summer (4.72 %) and winter (6.06%) in 2014. It means, seasonal impact for prediction decreased. Also wind power forecast model – Aiolos – could be changed, but there is no clear information. On the other hand it is very important to minimize errors. The largest prediction error values were found in winter (9.87%) and the smallest in summer (4.72%) (Fig. 4).

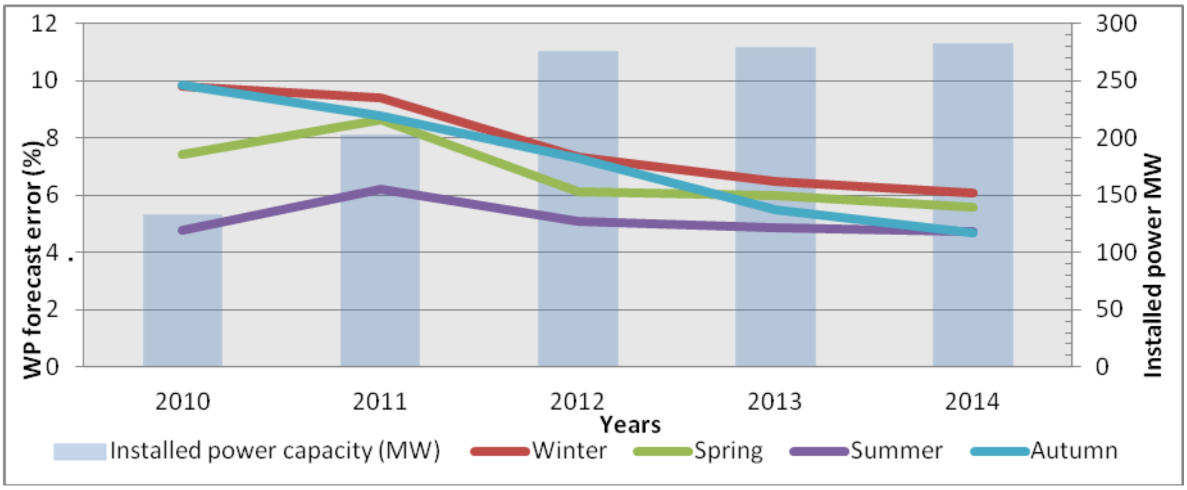

Fig. 4. Installed wind power capacity and seasonal WPPE

There are several reasons which could explain the difference in the seasonal errors. One of them is thermal stratification of the atmosphere. It means in winter and autumn, when temperature changes gain significant values, they give huge variations for wind speed, and in summer when the land and sea surface have constant temperature it gives constant wind speed [15]. Another explanation could be global processes. The reason is atmospheric pressure and air temperature differences between north pole and tropics, because pressure gradient and temperature changes are main wind formation source [14].

3.2 Analysis of hourly wind power prediction errors

Diurnal wind power prediction error variation is presented in Figure 5. The lowest error values exist at 3, 6 and 9 (average respectively 5.83%, 6.17%, 6.27%) o'clock in the morning and the biggest at 18 and 21 o'clock (average respectively 8.55% and 9.12%).

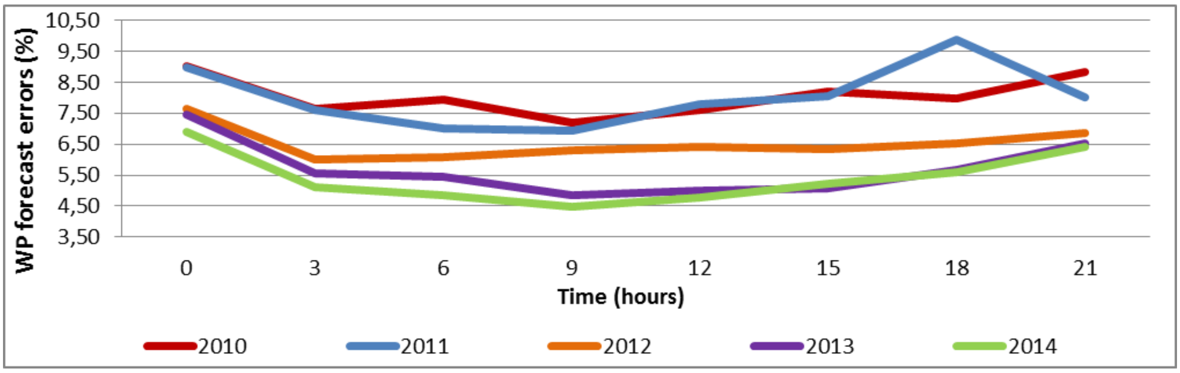

Fig. 5. Hourly WPPE variation

The explanation of that is diurnal wind variations regarding temperature inversion. At night, motion of turbulent intensity and thermal inversion values is very weak. In the morning, when the sun is rising, turbulence increases between lower and higher layers. Later wind speeds up in boundary layers and reaches maximum values at noon [15]. After sunset, due to decreased layers' friction minimum wind speed values are reached.

As was mentioned before, wind speed variations depend on topographical and meteorological conditions. Wind speed data were carried out from Mazeikiai mast by 100 m height (2011) and WPPE (2011) analysed method of correlation. Analysed results present relation of wind speed and wind power prediction errors. Correlation coefficient between these variables is 0.64 (medium range correlation). Result indicates that there is nonlinear relation (r = 0.64), and it means, impact of indicators variability is attributed to various conditions, but impact of wind speed for power prediction is the bigger than other conditions (Fig. 6).

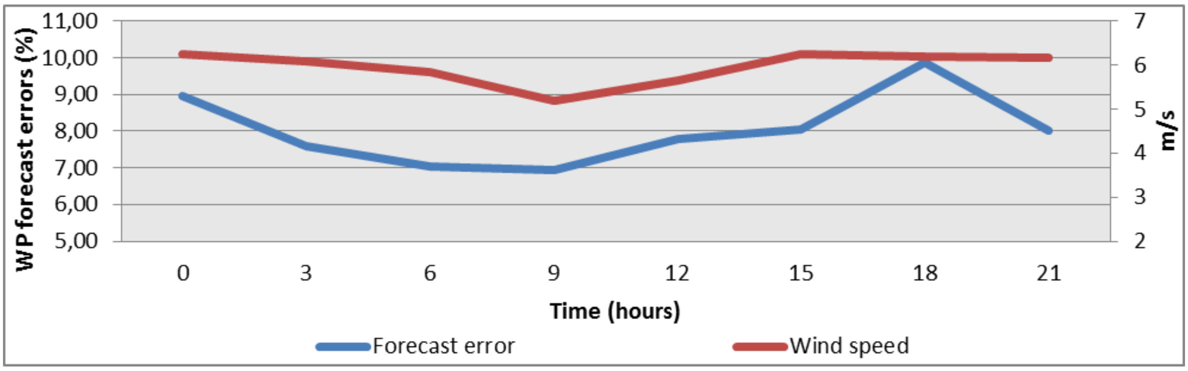

Fig. 6. Hourly WPPE and wind speed in 2011

To explain influence of other topographical factors for WPPE, need to analyse boundary layer. Wind flows are resulted topographical conditions as a surface, buildings, forest and etc., make turbulence[15]. Moreover thermal friction between boundary and higher atmospheric layers also generates turbulence. As a result of that there is no linear relation between wind speed and power prediction errors.

Relation between seasonal and hourly WPPE makes easier to understand the synergetic effect. Synergetic effect means impact meteorological and topographical conditions together. The lowest WPPE is in summer (Fig. 4) and at 3 o'clock at night (Fig. 5). Influence of synergetic effects has shown lowest values in summer 6, autumn 9, winter 9, spring 12 o'clock (Fig. 7). The biggest values were for all seasons from 21 to 00 o'clock and it confirms that there is no linear relation between meteorological conditions.

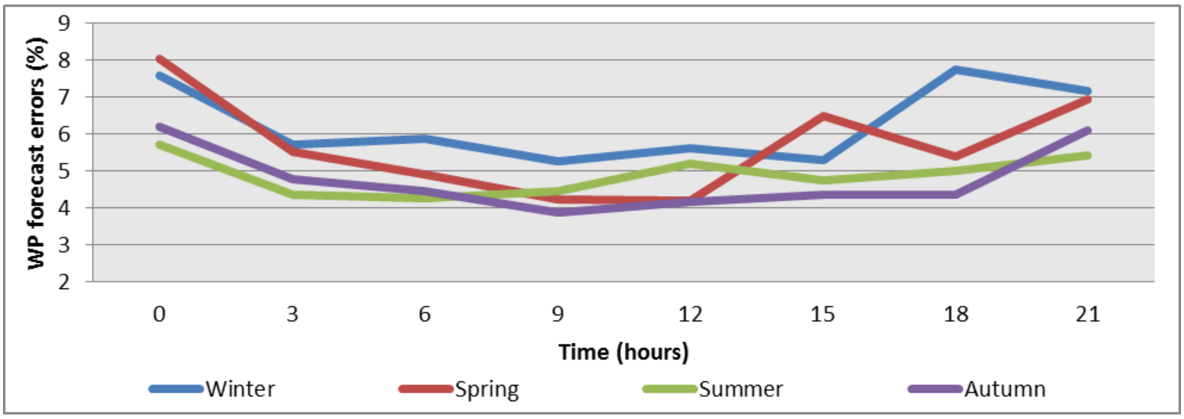

Fig. 7. Hourly and seasonal WPPE in 2014

The main reasons of seasonal and hourly WPPE relation could be Baltic Sea and land surface thermal inertia. Also wind power forecast accuracy could be improved by historical data, and general result of that is small WPPE variation between seasons and hourly wind power prediction.

4. CONCLUSIONS

Despite the fact installed power capacity increased 2010-2014 years, but relative wind power prediction errors all this period were significant decreased.

The same period seasonal WPPE errors decreased and the difference between winter in summer was 5% in 2010 and 1.33% the same period in 2014. The largest prediction error values were found in winter (9.87%) and the smallest in summer (4.72%).

Diurnal wind power prediction errors present the lowest values at 3, 6 and 9 (average respectively 5.83%, 6.17%, 6.27%) o'clock in the morning and the biggest at 18 and 21 o'clock (average respectively 8.55% and 9.12%).

Correlation coefficient between wind speed and WPPE is 0.64 (medium range correlation) and it indicates that there is nonlinear relation and it proves wind power predictions errors depend not only on wind speed variation.

REFERENCES

1. REN21. *Renewables 2014 Global Status Report*, 2014. ISBN 978-3-9815934-2-6.
2. GECEVIČIUS, G., MARČIUKAITIS, M. Technical and economic evaluation of wind turbines in different regions of Lithuania. CYSENI 2014. Proceedings of annual conference of young scientists on energy issues. [CD]. Kaunas: Lithuanian Energy Institute. 2014 May 29–30.

3. ALBADI, M., H., EL-SAADANY, E., F. Overview of wind power intermittency impacts on power systems. *Electric Power Systems Research*, 2010, Vol. 80, No. 6, p. 627–632.
4. STRBAC, G., SHAKOOR, A., BLACK, M., PUDJIANTO, D., BOPP, T. Impact of wind generation on the operation and development of the UK electricity systems. *Electric Power Systems Research*, 2007, Vol. 77, p. 1214–1227.
5. FOLEY, A., M., LEAHY, P., G, MARVUGLIA, A., MCKEOGH, E., J. Current methods and advances in forecasting of wind power generation. *Renewable Energy*, 2012, Vol. 37, No. 1, p. 1–8.
6. BROWN, B.G., KATZ, R.,W., MURPHY, A., H. Time Series Models to Simulate and Forecast Wind Speeds and Power. *Journal of Climate and Applied Meteorology*, 1984, Vol. 23. p. 1184–1195.
7. LEI, M., SHIYAN, L., CHUANWEN, J., HONGLING, L.,A., YAN, Z. A review on the forecasting of wind speed and generated power. *Renewable and Sustainable Energy Reviews*, 2009, Vol. 13, p. 915–920.
8. HU, J.,WANG, J., ZENG, G. A hybrid forecasting approach applied to wind speed time series. *Renewable Energy*, 2013, Vol. 60, p. 185–194.
9. BLONBOU, R., MONJOLY, S., DORVILLE, J.F. An adaptive short-term prediction scheme for wind energy storage management. *Energy Conversion and Management*, 2011, Vol. 52, No. 6, p. 2412–2416.
10. KUSIAK, A., ZHANG, Z., VERMA, A. Prediction, operations, and condition monitoring in wind energy. *Energy*, 2013, Vol. 60, p. 1–12.
11. ZHANG, W., WU, J., WANG, J., ZHAO, W., SHEN, L. Performance analysis of four modified approaches for wind speed forecasting. *Applied Energy*, 2012, Vol. 99, p. 324–333.
12. ROY, S. Performance prediction of active pitch-regulated wind turbine with short duration variations in source wind. *Applied Energy*, 2014, Vol. 114, p. 700–708.
13. HAMEED, Z., AHN, S., H., CHO, M.Y. Practical aspects of a condition monitoring system for a wind turbine with emphasis on its design, system architecture, testing and installation. *Renewable Energy*, 2010, Vol. 35, No. 5, p. 879–894.
14. CHENG, M., ZHU, Y. The state of the art of wind energy conversion systems and technologies: A review. *Energy Conversion and Management*, 2014, Vol. 88, p. 332–347.
15. BURTON, T., SHARPE, D., JENKINS, N., BOSSANYI, E. *Wind Energy Handbook*. West Sussex: John Wiley & Sons, 2001, p. 617. ISBN 0-471-48997-2.

CYSENI 2015, May 27–28, Kaunas, Lithuania
ISSN 1822-7554, www.cyseni.com

PECULIARITIES OF SMALL SCALE WIND TURBINES USE IN URBAN AREAS

G. Kondrataviciene
Lithuanian Energy Institute
Breslaujos str. 3, LT-44403 Kaunas – Lithuania
Phone +370 37 401 856
Email: Gabija.Kondrataviciene@lei.lt

ABSTRACT

Environmental degradation at the global scale encourages integration and development of renewable energy sources, as well as new research areas and technological innovations in the world. Recently wind power has been among the fastest growing energy industry sectors. Due to the technical and social conditions only a small part of wind energy resources can be exploited, however, this part would be sufficient to cover most of the world's energy needs. Therefore, wind energy is considered to be a perfect alternative to fossil fuel power. Nowadays small scale wind turbines are gaining increasing popularity as they are able to cover a part of the energy demand in urban territories. These turbines are intended for private and public buildings local energy supply and for street lighting.

Urban wind conditions are specific, because buildings and differences of their height lead to formation of gusts and cause higher turbulence. In addition to this, mean wind speed in urban areas is lower comparing to open areas, therefore wind turbines must be adapted for local wind conditions and their location must be selected with care. In this paper, the experience of small scale wind turbines use is reviewed, statistical analysis of wind characteristics in urban areas is provided, methodologies of wind flows modelling and efficiency calculations are analyzed. It was determined that efficiency coefficient of small scale wind turbine depends on wind speed and reaches the value of 0.16 on average.

Keywords: small scale wind turbine, wind conditions, energy efficiency coefficient

1. INTRODUCTION

Nowadays, due to technical and social conditions wind power can be used in all the land, but it is sufficient that wind energy could cover a large part of current electricity needs for humans.

Wind turbines built in the city allow generating green electricity from the wind. In-depth investigations showed improvement in the efficiency of small wind power plant. Most of these plants are working efficiently at low wind speed of 2–3 m/s. Wind turbulence does not have a significant impact on the wind-driven power plants in cities. The three bladed horizontal axis design solution for large wind turbines operating in rural areas is not an obvious choice for the built environment, where wind is highly turbulent. Small wind turbines are less noisy than the high-power plants and do not affect the birds. Their dimensions are around 10 to 20% of the characteristic building height. Small plants are mostly built on multi-storey buildings and their technical potential is enormous [1].

World Wind Energy Association collected the data on the use of small wind turbines in the world and presented them in Small wind world report, in 2013. Since not all countries of the world collect data on the built small power plants and provide them for the World Wind Energy Association, these figures presented in Fig. 1 and Table 1 are preliminary. However, only at the end of 2011 small wind power development in the world began to increase intensively. Since 2011, end of period a cumulative total of at least 730'000 small wind turbines have been installed worldwide with the exception of India and Italy, where there were 74'000 power plants newly built that year. During 2011, small wind power construction increased by 11% [2].

In 2011, the newly built small wind power capacity increased by 27%. Average installed power of small scale wind turbines increased from 0.66 kW to 0.77 kW respectively in 2010 and 2011 [2].

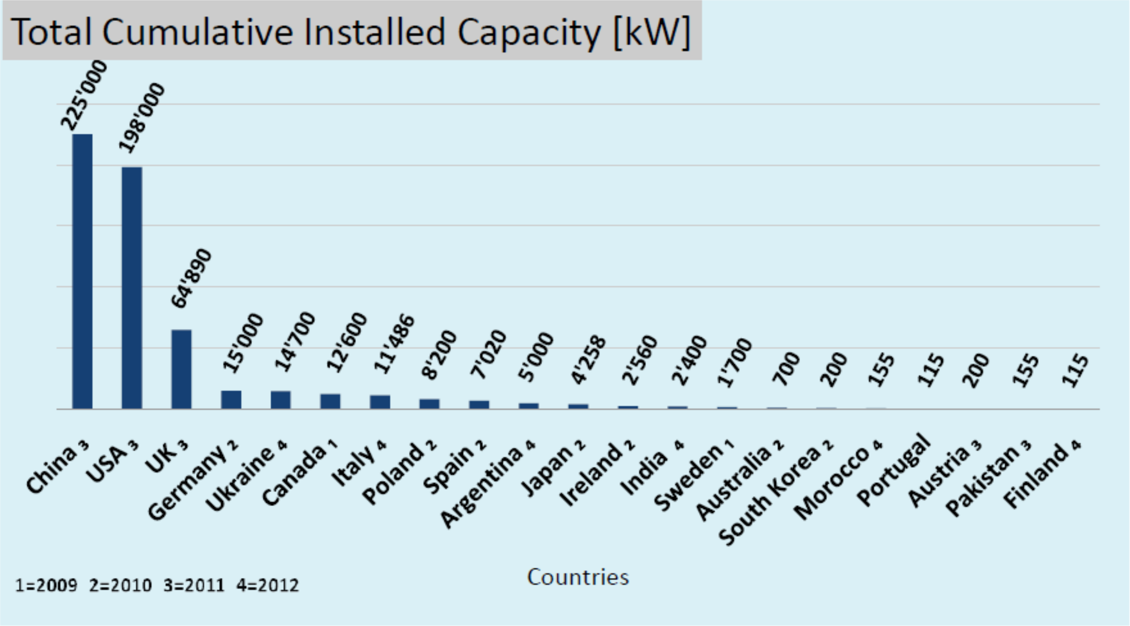

Fig. 1. Total cumulative installed small wind capacity [kW] in the World [2]

Horizontal-axis wind turbine (HAWT) technology has dominated for over 30 years. Total HAWT manufactures are 242 numbers and vertical-axis wind turbines (VAWT) manufactures are 60 numbers in 2011. Therefore there is a need for detailed scientific research of VAWT small wind power technology (Table 1).

Table 1. VAWT and HAWT 2011 Statistics [2]

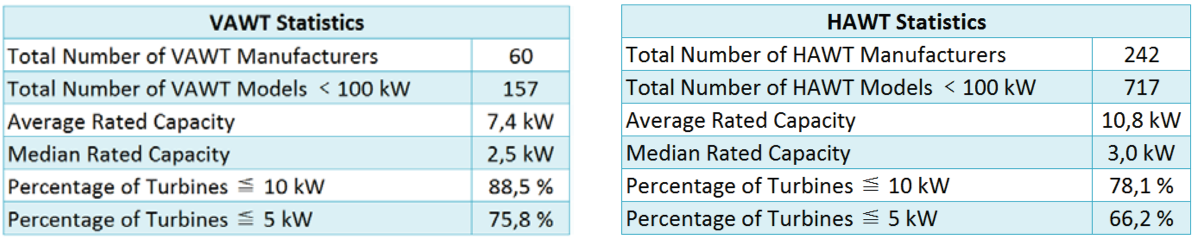

VAWT Statistics	
Total Number of VAWT Manufacturers	60
Total Number of VAWT Models < 100 kW	157
Average Rated Capacity	7,4 kW
Median Rated Capacity	2,5 kW
Percentage of Turbines ≦ 10 kW	88,5 %
Percentage of Turbines ≦ 5 kW	75,8 %

HAWT Statistics	
Total Number of HAWT Manufacturers	242
Total Number of HAWT Models < 100 kW	717
Average Rated Capacity	10,8 kW
Median Rated Capacity	3,0 kW
Percentage of Turbines ≦ 10 kW	78,1 %
Percentage of Turbines ≦ 5 kW	66,2 %

1.1 Small wind power in Lithuania

Lithuanian accession to the EU has become a very important issue of energy independence: a concern for energy self-sufficiency and effective use of energy. The EU acts ensure the development of renewable energy sources and energy independence. In terms of wind power stations, the financial EU support is provided, procedures for issuing building permits are simplified, as well as the terms of buying electricity are changed. In the period of 2011, the European Wind Energy Association of Lithuania installed 16 MW power of wind energy. At the end of 2011, in total there were 179 MW of wind energy installed [3, 4].

Performed comprehensive metrological studies have shown that the best Lithuanian region in order to build wind power is coastal zone, where the prevailing average annual wind speeds are the highest – 5–6 m/s (Fig. 2) [5]. Most high power horizontal axis wind turbines and parks are built in the Lithuanian coastal zone, as well as the north and the south Lithuania regions. In other regions of Lithuania, the average annual wind speed is about 4 m/s. Small wind power plants are more economical and effective according to such a wind resource comparing to high power horizontal axis wind turbines.

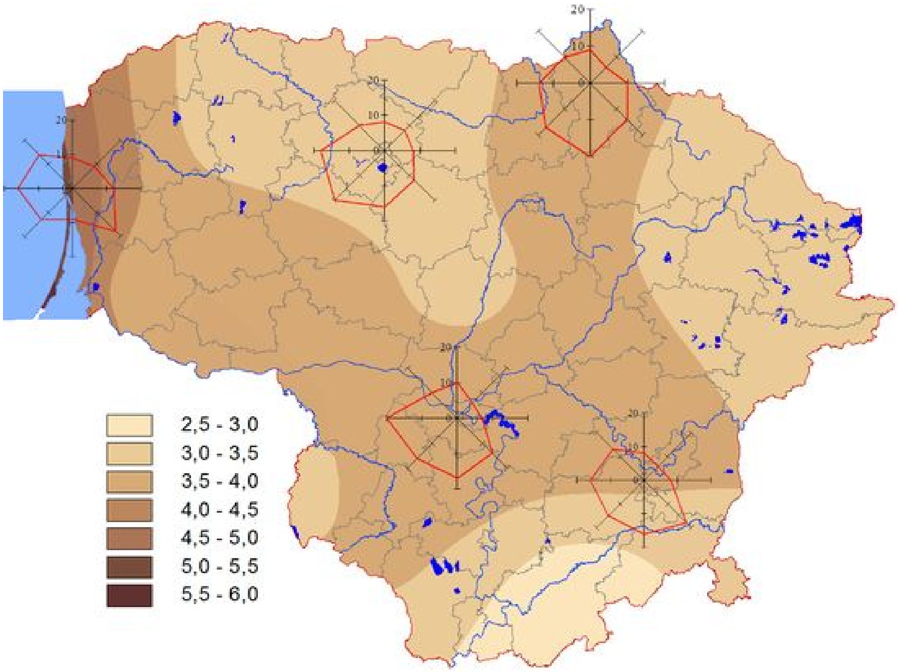

Fig. 2. Winds map of Lithuania. The average annual wind speed and dominant wind directions [5]

There are a lot of small pilot wind turbines built in various regions of Lithuania. Small Wind turbines can be used for different purposes: only light or electricity production, as well as the electric energy and heat. Currently in Lithuania there are built 17 pilot plants with 4 wind turbines and 13 hybrid solar-wind power plants. They are designed for scientific and educational purposes and activities. Most small wind power turbines are adapted to individual needs in farmsteads, small farms and residential homes. Due to wind variability and seasonality, various hybrid systems are widely used, including the most common solar-wind power, often adapted in remote areas where there is no electric power supply or power supply is irregular. Small wind power turbines can also be connected to the electricity grid, and are obliged to purchase the electricity at a fixed rate, but only in 2013, three small power plants were connected to the electricity grid. There is no accurate data on the number of low-power wind turbines built which are not connected to the electricity grid, and use electricity for their own use. According to the data collected from the Lithuanian companies, which produce and supply wind turbines to manufacturers from other countries, the total installed power capacity for its own use is about 321.4 kW.

Currently, horizontal axis wind turbines are the most common in both the world and Lithuania. Large horizontal axis wind turbines are cost-effective work in comparison to the vertical axis wind turbines. Small capacity wind turbines can be effective in both the vertical axis and horizontal axis and therefore can be used over Lithuania cities. Small capacity wind turbines will start at low wind 2.5–3 m/s.

Small capacity wind turbines can be used for streets, parks, lighting, parking machines, to satisfy the needs of individual houses and apartment houses, thus, research is the needed for further development.

2 OBJECTS OF INVESTIGATION AND METHODOLOGY

As technology has evolved and primary (fossil) energy sources have become more expensive, the need to use renewable energy source is increasing. There is a new conceptual plant which conducts research and development in technology.

One of the main components of the wind turbine energy is to calculate the wind speed. Wind energy is proportional to the cube of wind speed.

Wind turbine air passing through it slowed the flow rate and changes its direction. According to Betz's law (principle), ideally 2/3 wind kinetic energy can be converted into a wind turbine mechanical power. Therefore, the aerodynamic properties of rotor impact energy are extremely important.

There are two main types of wind turbines: horizontal axis and vertical axis. They are sought as technical solutions to increase the mechanical efficiency, aerodynamics by changing the impeller shape, weight and volume.

2.1 Types of wind turbines

Wind flow passing through HAWT consists of turbulence, so the construction of more turbines needs to properly calculate the distance between turbines that is not affected by turbulence near stationary turbine Fig. 3. The construction HAWT necessary to calculate turbulent flow and power plant set over them Fig. 4.

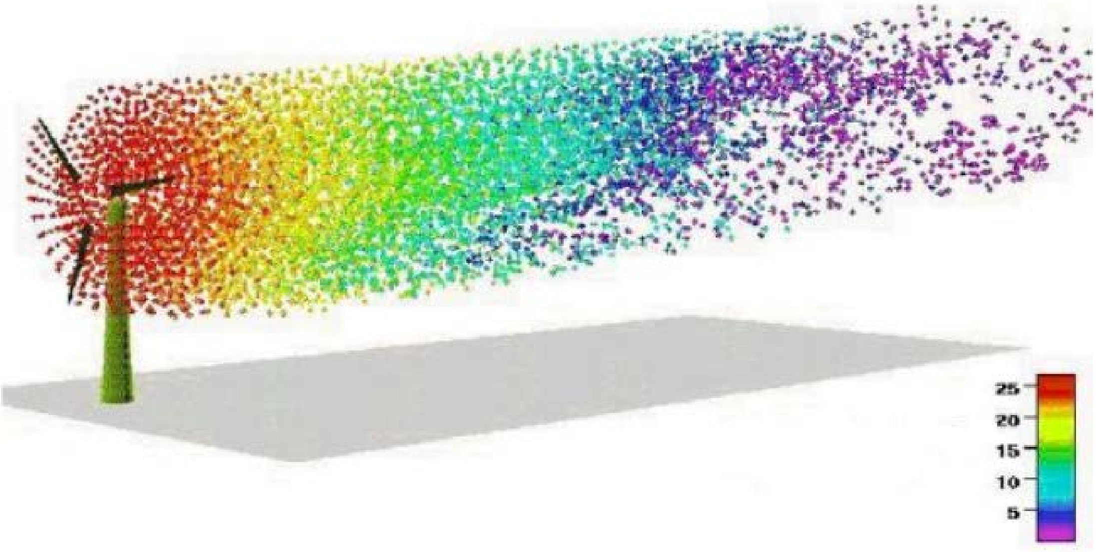

Fig. 3. The duration of the extinction turbulence (seconds) [6]

The American study also showed that each VAWT rotated in the opposite direction than standing next to, they all rotate together quickly, because the opposite rotation reduces the resistance of each power plant tance and thus increases the efficiency. Less noise, lower wind and a better functioning air turbulence conditions – the three key advantages over VAWT – HAWT. Unlike than HAWT, VAWT can operate effectively without being directly facing the wind. For this reason, the vertical axis is especially suitable to install in areas of volatile wind direction, such as between buildings.

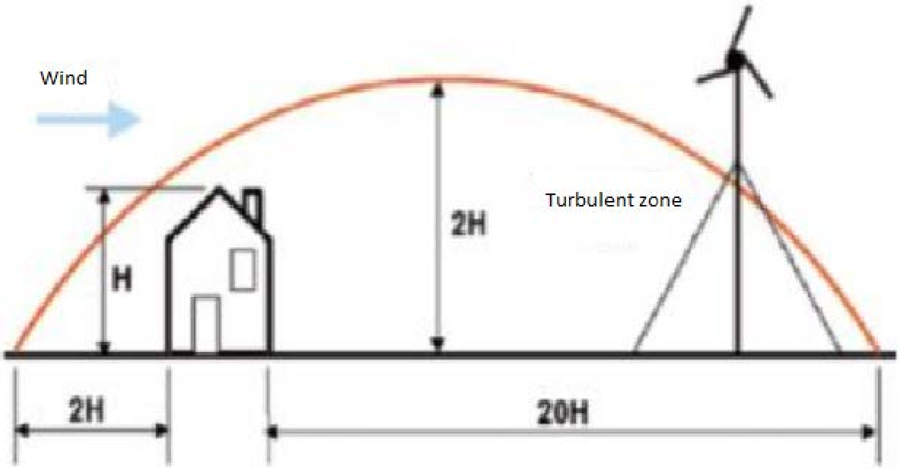

Fig. 4. Turbulent zone [6]

Small wind power turbine has simple construction, high starting torque and low noise level. Savonius vertical axis turbine can be successfully operated in urban areas. Efficiency of the turbine depends not only on the weather conditions, but also on the geometrical parameters of the turbine: the ratio the overlap and the separation spaces between the blades and the number, the profile and the step ratio. Savonius wind turbine has a lower power factor (CP = 0.15) than the wind turbine with the horizontal axis (CP = 0.45) or Darieus type of wind turbine with a vertical axis (CP = 0.35) defined by mathematical modelling and experimental studies [7]. The researchers studied various designs Savonius type wind turbine structures, their geometry parameters on its effectiveness, such as blades, number of sections, wings the overlap ratio, end plate on the presence or absence of wings winder, etc. Collated power factor and a high speed wind turbine rotor efficiency divorced his addiction helical vertical axis wind turbine. Its results were compared with the traditional Savonius vertical axis wind turbine. Collated power factor and in a high speed wind turbine rotor efficiency divorced his addiction helical vertical axis wind turbine.

A number of scholars have researched various designs of Savonius type wind turbine structures, their geometry parameters on its effectiveness, such as blades, number of sections, wings overlap ratio, rear. The presence or absence of the plate, and the twisting of the wings, etc. comparing the power factor and the wind turbine rotor its dependence on a high speed efficiency divorced helical vertical axis wind turbine.

Its results were compared with the traditional Savonius vertical axis wind turbine. It was found that the same wind turbine rotor in a high speed coefficients (0.4), helical vertical axis wind turbine power coefficient higher (more than 0.2) than conventional Savonius wind turbines (about 0.15). A more detailed analysis was carried out with helical Savonius wind turbine with wings attached to the shaft to rotate relative to each other at an angle of 180 degrees, and the divide between the axis of the rotor wing is equal to 0 (Fig. 5). Power plant height to diameter ratio of 0.52 [8].

Fig. 5. Pilot small wind turbine [8]

Wind velocities distributed according to the distribution function using the Weibull and in most cases dominant from 3 to 5 m/s of wind set, the of environmental parameter data. The power dependence on the wind speed distribution by the power function. Power values are signs of growth start when the wind speed reaches 3 m/s value. The wind velocity varies from 1.8 to 17.9 m/s^2, the wind flow power per square meter was in the range of 7.5 to 3775 W/m^2. Evaluating the wind turbine rotor revolutions to a given wind speed, it was found that the exploitation of wind energy by 48% [8].

Turby® is a conceptual small wind power turbine designed for the use in urban areas. It is created using the principle of the well-known Darrieus design. Studies show that compared to other wind turbines of similar size, Turby® shows good aerodynamic and electric performance. This conceptual small wind power plant is not fully investigated yet [9].

Wind tree (Fig. 6.) idea was presented by Michaud-Lariviere. He a realised that energy had to come from somewhere, and that it must be able to be transferred into watts. Wind tree is 11 meters high and 8 meters in diameter with 72 artificial leaves. The wind tree is completely silent as the leaves turn in the wind. Micro - generators are integrated into the leaves and the cables are integrated into the branches. Micro-generators ensure production virtually throughout the year with a production threshold lowered to winds of less than 2 m/s. The wind tree can function around 320 days of the year – almost double traditional machines. The tree is profitable after two years with winds of 3.5m/s [10]. Wind tree turbines were built in December 2014, in the French cities.

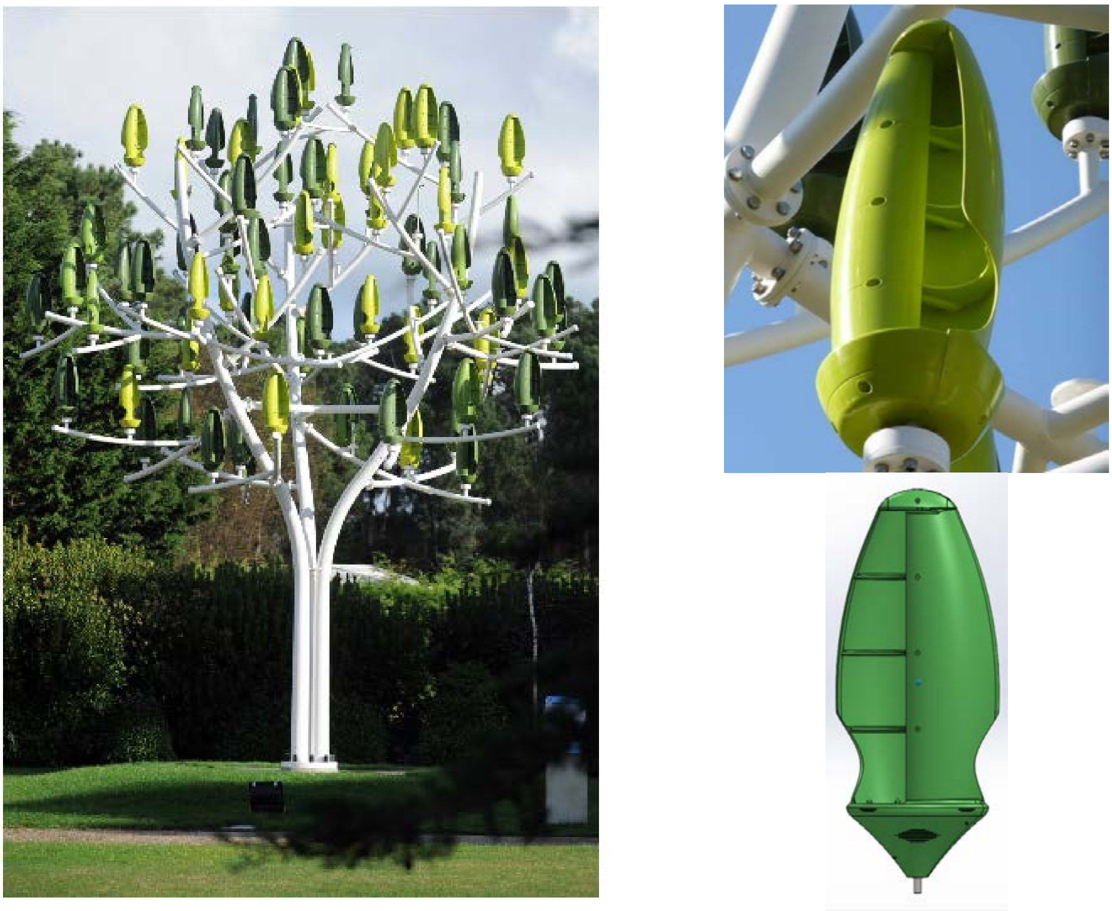

Fig. 6. 'Wind trees'– small wind power

3. CONCLUSIONS

1. In Lithuania average wind speed is 4 m/s. This resource is sufficient for the small wind power turbines in order to work efficiently.
2. Due to the high turbulence in urban areas small wind vertical axis turbines are more suitable than the horizontal axis high-power wind turbines.
3. New aerodynamic solutions can increase the work of vertical axis turbines, as well as use turbulence in more applicable way.
4. Certain small wind turbine models are adapted to the cities so further investigations and improved technology are needed.
5. Recently, scientific research has focused on the mechanical power turbines and the main control methods of rotational speed, the aerodynamic shapes and noise reduction.
6. Exploitation of turbulent flow in vertical axis turbines requires further scientific research.
7. Small capacity wind turbines can be effective in both the vertical axis and horizontal axis and therefore can be used over Lithuania cities. Small capacity wind turbines will start at low wind 2.5–3 m/s.

REFERENCES

1. BUSSEL G.J.W., MERTENS S.M. Small wind turbines for the built environment. *EACWE4 — The Fourth European & African Conference on Wind Engineering*. ITAM AS CR, Prague, 2005 July 11–15.
2. Small wind world report 2013.World Wind Energy Association. [Referred on the 3th of March in 2000 y.]. Link to the internet <www.wwindea.org>.
3. Wind in power 2011 European statistics. The European Wind energy association. [Referred on the 5th of January in 2015 y]. Link to the internet <http://www.ewea.org/fileadmin/ewea_documents/documents/publications/statistics/Stats_2011.pdf>.
4. The Lithuanian Wind Power Association. Statistics. [Referred on the 7th of January in 2015 y]. Link to the internet <http://www.lvea.lt/index.php/lt/p/vejo-energetika/statistika>.
5. Lithuanian Hidrometeorological Service under the Ministry of Environment. [Referred on the 3th of December in 2014 y.]. Link to the internet <http://www.meteo.lt/klim_lt_klimatas.php?tipas=vejas>.
6. Dinsmonas D. Vertical axis wind turbine wings simulation. Vilnius 2013, p. 57.
7. GUPTA R., DEB B., MISRA R. D. Performance Analysis of a Helical Savonius Rotor with Shaft at 45° Twist Angle Using CFD Mechanical Engineering Research; Journal of Urban and Environmental Engineering (JUEE), 2013, Vol. 7, No. 1, p.126–133.
8. GEDRIMAITĖ K., GRIGONIENĖ J., RAZMAS S. Low vertical axis wind power mechanical powers of investigation. Technology research papers west Lithuania IX Klaipeda, 2014, p.74–77**.**
9. BUSSEL G.J.W.; MERTENS S.M. The development of *Turby*®, a small VAWT for built environment. Global Wind Energy Conference 2004.
10. Osborne H. 'Wind trees' could replace controversial giant turbines in race for sustainable energy. [Referred on the 1th of *December* in 2014 y]. Link to the internet http://www.ibtimes.co.uk/wind-trees-could-replace-controversial-giant-turbines-race-sustainable-energy-1477461.

CYSENI 2015, May 27–28, Kaunas, Lithuania
ISSN 1822-7554, www.cyseni.com

SUPPORT MEASURES FOR RENEWABLE ENERGY ASSESSING THE DEVELOPMENT EFFECTIVENESS

M. Krečius
Lithuanian Energy Institute
Breslaujos str. 3, LT-44403, Lithuania
Phone +370 (37) 401801
Fax +370 (37) 351271

ABSTRACT

Currently there are many discussions related to renewable energy (RE) not only among to scholars, but also includes others stakeholders – enterprises, residents, policy makers. However, the main topics of many discussions of RES are the following: sustainability, price and energy independence. Lithuania as well as other EU states have to achieve energy targets defined by European Parliament until 2020. Therefore, Lithuanian energy strategy related to RE shall be clearly understandable in accordance with successful practices of RE strategy from developed countries, but also pay attention for a long time period benchmarking of energy sustainability indicators that are as follow: *economy*, *energy security*, *climate change*, *energy efficiency*. In general, RE technologies satisfy a strict energy targets, but also covers environmental compliance, economy growth and is mainly driver for sustainability. Eventually, by doing this in successful way it is necessary to involve one more thing – support measures.

This paper analyses different support measures for RE such as: *regulations*, *feed-in tariff*, *investment subsidies*, *taxation and regulation*, not only in Lithuania but also covering neighbour states as well. Effectiveness of support measures for developing RE technologies' is a vital that brings a huge impact on the above mentioned sustainable indicators.

Keywords: Renewable energy, sustainability, support measures

1. INTRODUCTION

The government engagement is significant so as to assure the development of renewable energy technologies and protect them from main competitors − conventional technologies However, there are some positive things of renewable energies in comparison with conventional energy such as climate change mitigation and energy supply stability (Menanteau at al. 2003). Additionally, support measures for renewable energies is essential for several purposes: energy security, energy resource diversification (Valente at all. 2011). Besides the mentioned facts, renewable energy meets sustainability criteria: economics, social and environmental. The European Union (EN) have decided with it's member states to move a further steps – Low carbon economy. The following ambitious steps require additional targets by diminishing by 20% greenhouse gas emissions till 2020 compared to 1990, by increasing 20% energy efficiency and by providing 20% final energy consumption from renewable energy sources and complying with the Kyoto protocol (European Parliament, 2009). It is assumed that energy consumption will constitute an increasing share of the global energy demand over the next of several decades. However, there are key points of concerns such as: political instability, climate change and rising price of fossil fuels (before conflict among Russia and Ukraine) that leads to wider energy contribution and consumption from renewable energy perspective point of view (Abolhosseini S., Heshmati A., 2014). Besides the following facts, renewable energy has become a challenging policy target for the major part of the states in the world. Notwithstanding many affirmative aspects there is a huge gap (barriers and market failure) by renewable energy in the market since a major part of investment is still directed to traditional energy technologies. In additional, Gutermuth, P. G. (1998) claims that renewable energy technologies comprise a small part by fulfilling usage an optimal level of total commercial energy demand (either economically or/and ecologically) that comprise a gap of the following aspect. In general, it‘s accounts for financial barriers where it have to be identified and solved on purpose to shape financial energy policy approaches for renewable energy technologies‘ not only locally but internationally as well. Hence, in order to reach EU targets for sustainable growth, there are two options: 1) *Investments in renewable energy production* 2) *Energy efficiency improvements*. In fact, appropriate distributions of investments for RET’s is significant from policies point of view where legal and regulatory systems provide access to investments of capital market for small scale RET’s (Wohlgemuth N., Madlener R., 2000). It should be stressed that capital market are frequently discriminated from investments to small scales renewable energy technologies. This paper analyse the most frequently applied renewable energy support measures in an international context and Lithuania. Support measures will be analysed and described affirmatives and negatives consequences for economic, sustainability.

The aim of this paper is to estimate the most efficiency renewable energy support measures in Lithuania. The main objectives of the following information analysis are:

- to analyze renewable energy support measures existing in Europe,
- to examine different applied renewable energy support measures in Lithuania,
- to explore renewable energy support measures effectiveness indicators,
- to suggest the most commonly applicable effectiveness indicators of renewable energy support measures in Lithuanian energy sector.

Data collection of this study will be applicable in accordance with the following method:

- Statistical data analysis.

It should be pointed out that status of the following paper − objectives and methodology adjustment, information analysis that leads to dissertation status.

2. ENERGY SUPPORT MEASURES

It is assumed that there are in total 582 support measures have been indentified in 32 EEA (European Environment Agency) countries. Distribution of all energy support measures are presented in Table 1. As can be seen from the table the vast part of energy support measures 310 comprise fossil fuel and the rest 236 constitute renewable energy support measures. In addition, fiscal measures are the most widespread form of energy support measures that link more with conventional energy (fossils fuels), meanwhile, renewable energy to be mostly supported by direct subsidy (monetary transfer).

Table 1. Energy support measures, by energy carrier and technology, 2012, EEA-32 (European Environment Agency, 2014)

	Fossil fuels	Nuclear	Renewables	Electricity and heat	Biofuels	**Total**
Direct Subsidy	47	3	111	14	3	**178**
Fiscal exemption	245	0	28	17	28	**318**
Non-financial measures	4.5	0	34	2	22.5	**63**
Non-financial measures	1.5	1	8	2.5	0	**13**
Transfer or risk to government	3	5	2	0	0	**10**
Total	**301**	**9**	**183**	**36**	**53**	**582**

Hence, renewable energy still cannot compete with conventional energy sources, therefore support measures schemes is necessary to stimulate the investment in renewable energy and get over the market barriers and failures. In this case, the absence of appropriate management of support measures may be able to distort the energy market functioning that causes additional consequences as higher cost for business and households. However, one of the main driving force for renewable energy penetration in the market is government policies that ought to be supportive. Notwithstanding many negative factors as fast changing governments, energy policies and targets, still there are four key reasons why governments supports renewables energy: 1) Energy sources diversification 2) Stimulation domestic economy 3) Oil & Gas imports reduction 4) Dependence reduction on fossil fuel. For these reasons, there are various market mechanisms that are being employed for purpose to promote renewable energy technologies. Hence, deployment policies are most frequently categorized into four parts: ***public finance***, ***access policies***, ***fiscal incentives*** and ***regulations*** (Mitchell C. et al., 2011). Nevertheless, according to organization IRENA (2012) deployment policies shows each countries targets, ambitions and particular barriers.

2.1. Public finance

There are still a commercial financing restrictions for many renewable energy projects, especially in developing states because of weak and insufficiency institutions that are not able to increase the participants (private sector) involvement in such process. According to Mitchell (2011) the objectives of public finance are the following:

1) *Direct* – such subsidies are the most attractive incentive system for simplicity, however for appropriate functioning it has to be monitored by institutions to ensure whether the cost of projects are not being artificially enlarged (Wohlgemuth N. at al., 2000).
2) *Indirect* – usually it helps to shape and create sustainable market for renewable energy sector.

Nevertheless, the following deployment policy (public finance) constitute these commonly applied support measures:

- **Investment** – use by sector (*Electricity, Heat and Transport*).

For the most part that a government or funder (privately)-managed funds by directly investing equity in renewable energy projects and companies.

- **Public procurement** – use by sector (*Electricity, Heat and Transport*).

The preference for public entities to purchase renewable energy services (electricity or equipment).

- **Loan** – use by sector (*Electricity, Heat and Transport*).

The most frequently loans are provided by development bank or government on preferential terms (lower interest rates) in return for debt obligations.

- **Guarantee** – use by sector (*Electricity, Heat and Transport*).

There is allocated risks among commercial bank and renewable energy company by existing a high credit risk. In principal a guarantee shows that there will be covering a portion of the outstanding loan.

2.2. Access policies

Many of renewable energy projects need a huge money for infrastructure (connection to networks) development in order sell heat or electricity. However, it is necessary to point out that there are different requirements for networks connections and sales for renewable energy generation products (electricity, heat or fuels). Moreover, in order to ensure and improve the RE access policies, in most cases are categorized in such options:

Net metering – use by sector (*Electricity*)

Net metering is one of energy policy options that seek to increase the deployment of renewable energy sources. Yet, net metering is one of access instrument that enables small scales electricity producer (wind and solar photovoltaic (PV)) to connect to the grid and the same time sell the product (electricity). However, Net metering is a policy where consumers make an agreement for purpose to apply of its own generated electricity and use two flow electricity meter: take from the grid and by existing excess take back to the grid.

Priority or guaranteed access to network – use by sector (*Electricity*, *Heat*)

According to EU Directive 2001/77EC all EU states have to ensure that all operators that are accountable for transmission and distributions will be able to guarantee a a grid access for electricity generated by RE (European Parliament and of the Council, 2009). Moreover, European Union countries that use FIT (Feed – in tariff) have launched the regulations requirements that means that electricity generated by RE have priority access to network.

Priority dispatch – use by sector (*Electricity*, *Heat*)

Authorization that supply of renewable energy, despite others sources that are incorporated within energy systems.

2.3 Fiscal incentives

Fiscal incentive mechanism aim to promote renewable energy by grant, energy production payment, rebate, tax credit, tax reduction/exemption, variable or accelerated depreciation. Wohlgemuth (2000) claims that Fiscal incentive policy is one of the simplest policy to implement, as all states have budget and tax policies. According to IEA (2008) there is a great importance of fiscal incentives for RE projects during the initial phase of the market introduction, when funds are restricted or limited. Despite the great importance of RE there are some shortage as well: this mechanism largely depends on government budget that leads to unstable yearly budget; policy changes closely related to enlarged risks of RE projects (Jager D. & Rathmann M., 2008).

Grant – use by sector (*Energy, Heat and Transport*)

IEA (International Energy Agency, 2008) claims that grants diminish capital cost for RE projects. Furthermore, Grant mechanism helps to reduce a risk by investing in RE projects that linked by cutting down early investment in installation and diminishing cost for RE production. In general, grant mechanism based on money that is receiving before investment to RE projects.

Energy production payment – use by sector (*Energy, Heat and Transport*)

This is also linked to government support mechanism (direct) per unit of renewable energy generation.

Rebate – use by sector (*Energy, Heat and Transport*)

Rebate is closely related to Grant system. Both mechanisms (grant & rebate) contribute to RE project directly from the government point of view. Usually, rebate mechanism is based on finished RE projects, where refund for some percentage of total investment or particular installed capacity (megawatt). Rebate and Grant mechanisms take place in small scale RE projects as solar thermal to large scale project as combined electricity and heater biomass plant.

Tax credit (*production or investment*) – use by sector (*Energy, Heat and Transport*)

All tax policies can greatly influence Renewable energy demand and supply. For instance, tax credit for production – increase RE production in the market. Overall, tax credits enable RE investors to be deducted from income or taxes (fully or partially).

Tax reduction/exemption – use by sector (*Energy, Heat and Transport*)

Tax reduction or exemption model can be successfully efficient in these countries, where taxes in energy sector quite high (Scandinavian countries). All in all, the following support instrument apply as extra support mechanism (IEA, 2008). It is worth to pay attention that this support mechanism is not sufficient with low level tax system policies, therefore it necessary to take into account another support measures.

Variable or accelerated depreciation – use by sector (*Energy, Heat and Transport*)

Such support instrument can be mostly commonly used as the reduction of taxable income for the first year that scale up the investment to RE projects. This mechanism was successful in Sweden and Denmark supporting small scales wind development (Mitchell C. et al., 2011).

Regulations

Regulations can be distinguished into smaller and different policies forms such as: *Quantity*, *Price* and *Quality* based policies.

Price and Quantity based policies

Price (*Fixed payment Feed in tariff, Premium payment*) an quantity (*Tenderring*/*Bidding* or *Renewable portfolio standard*/*Quata obligation or mandate*)policies highly linked to each other, where targets are the same – market regulations and management. In fact, price incentive program clearly determine a price where the market by itself define the quantity whereas quantity based policy clearly determine the quantity where the market by itself determine the price.

Fixed payment Feed in tariff (FIT) – use by sector *(Electricity and Heat)*

The following incentive program based typically on obligation to purchase the electricity generated by renewable energy producers in such tariff that is set by the public authorities and ensure for a certain time of period (roughly 15 years) (Menanteau at al. 2003). This system is widely used in highly effective countries such as: Germany, Denmark, Portugal and Spain on purpose to deploy RE (wind power). Notwithstanding, according to (IEA, 2008) Feed-in tariffs mechanism with respect to long term is not effective, it is more valuable in initial phases of RE deployment (IEA, 2008). Also the feed-in tariff scheme is considered as subsidy appointed to RE producers.

Premium payment – use by sector *(Electricity and Heat)*

Usually, such system guarantee additional payment for RE producers. The main differences among *Feed in tariff* and *Premium payment* that the letter brings competitiveness in electricity market.

Tendering/Bidding – use by sector *(Electricity)*

Tendering is allocated as alternative resource to price or quota based mechanisms (Mitchell C. 2011). Yet, this system based on a fixed amount of energy from renewable energy producer and the bidding have to ensure that the cheapest price is accepted (IEA, 2008). This system is integrated as gradual incentive diminishing.

Quota obligation or mandate – use by sector *(Electricity, Heat and Transport)*

Under mandate, authority set a clear defined targets for RE by pointing out the obligations: suppliers or consumers to source a certain percentage of their energy from renewable sources (IEA, 2008).

Quality based policies

Quality based policy is determined by two additional elements such as *green energy purchasing* and *green labelling* that gives the whole information for customers (consumers) related to quality of energy that allows for customers to promote RE demand (IEA, 2008).

green energy purchasing – use by sector *(Electricity, Heat and Transport)*

Adjust voluntary supply purchases of RE by consumers, beyond existing RE obligations.

green labelling – use by sector *(Electricity, Heat and Transport)*

Government (encompassing private sector) labelling ensure that energy products meet certain sustainability criteria on purpose to facilitate voluntary green energy purchasing.

3. SUPPORT MEASURES IN LITHUANIA

Support measures for the most part are appointed to renewable energy production sector in European Union. Lithuania as Belgium, Netherlands, Italy are considered as the most having support measures for renewable energy (EEA, 2014). Hence, in Lithuania support measures relate mostly to Electricity and Heat (Transport support measures will not be considered in this paper) that are the following:

Electricity

Feed-in tariff

Electricity is mainly supported by feed-in tariff mechanism. The tarrifs one time per quarter is set by The National Control Commission for Prices and Energy for RES plants with capacity up to 10 kW, whereas the tariff is provided through tenders mechanism if generated capacity is exceeded 10 kW.

Loan

In essence, there is designed a fund that is intended to be used for the purpose to support RE project that might be able to decrease greenhouse gases. In general, this support mechanism is focused on environmentally friendly technologies. Although the funds are applied as a loan form, however, it is supported as subsidies form as well.

Subsidy

RE projects are supported by The Lithuanian Environmental Investment Fund (LEIF). The following fund is accountable for reduction of environmental damage in long term. Such mechanism is applied for all RES-E project apart from geothermal energy.

Subsidy – (The Fund of the Special Programme for Climate Change Mitigation)

The fund of Special Programme for Climate Change Mitigation is designed for RE projects, where the goal - decrease greenhouse gases. More than 40% of this funds investments are going to be applied to stimulate the RE usage and focus on environmentally friendly technologies.

Tax regulation mechanism

Tax regulations mechanism is based on *Law on Excise Taxes.* It is necessary to pay an excise taxes on electricity for the following reasons (Kelpšaitė J. 2014):

1) it is sold or otherwise transmitted to a person who has no business licence,
2) it is received by an unlicensed person from another EU member state,
3) it is imported by an unlicensed person .

Heating

In Lithuania, there are a few support schemes based on RE deployment: *price-based mechanism, subsidy* and *tax regulation* (Kelpšaitė J. 2014).

Price-based mechanism

Heat suppliers are committed to purchase heat energy that is being generated by independent heat producers from RES that is cheaper than the heat produced by the heat supplier himself and meets corresponding requirements: security, quality and environmental conditions.

Tax regulation mechanism

All operators with fuel burning installations have to pay environmental pollution taxes where thermal capacity exceeds 50 MW. Nevertheless, such taxes shall be paid by operators that operate at least one solid fuel boiler, whose nominal thermal capacity exceeds 0.5 MW. On the other hand, all operators using RES (solid/liquid biomass and biogas) shall be dismissed from pollutions taxes.

Subsidy

The Lithuanian Environmental Investment Fund (LEIF) plays a crucial role by supporting projects for purpose to diminish environmental damage in the long term. This mechanism includes heating plants in order to change from solid fuels to liquid biomass and geothermal resources.

4. SUPPORT MEASURES EFFECTIVENESS

Renewable support application is a challenge for each country since it is require commitment from authority point of view, applicable support policy design and it's implementation. Therefore, the authority have to respond to the main questions: How to accelerate the deployment of RE support measures in the most effective and cost-efficient way (IEA, 2008). It should be stressed that many scientific articles point out that *effectiveness* and *efficiency* are closely related. Nevertheless, these two (efficiency & effectiveness) also has separate definitions. According to Ragvidz (2012) ***Efficiency*** is based on *support paid compared to generation cost*, whereas ***effectiveness*** is based on *realised growth*. Moreover, effectiveness and efficiency shows that might be able to impact on the market growth (IEA, 2008). For this reason, in this paper efficiency indicators will be combined to effectiveness indicators. Hence, there are number indicators that can be used to measure support measures effectiveness:

- **Average Annual growth rates**

$$G_n^i = \left(\frac{G_n^i}{G_{n-t}^i}\right)^{\frac{1}{t}} - 1 \tag{1}$$

G_n^i = Average Annual growth rates

- **Absolute annual growth**

$$a_n^i = \frac{(G_n^i - G_{n-1}^i) - 1}{n} \tag{2}$$

a_n^i = Absolute annual growth rate

- **Effectiveness indicator**

$$E_n^i = \frac{(G_n^i - G_{n-1}^i)}{ADDPOT_n^i} \tag{3}$$

E_n^i = Effectiveness indicator for RES technology i for the year n.
$ADDPOT_n^i$ = Additional generation potential of RES technology i in year n until 2020

- **Total cost indicator (TCI)**

TCI – how much a country spends in addition to the market price for energy to get an x amount of additional generation from a renewable technology

- **Policy impact indicator (PII)**

PII – additional generation in a given year divided by the difference between the generation in 2005 and the potential defined by the policy target.

- **Employment**

  Employment estimation generated by Renewable Energy Sector

Yet, some indicators (*Average annual growth rate*, *Absolute annual growth rate*, *Effectiveness indicator*) show political objectives– policy success on growth market, whereas the rest part of indicators (TCI, PII) indicate cost − efficiency. Nevertheless, all efficiency and effectiveness support measures indicators might be distinguished to positive and negative features (Table 2).

Table 2. Effectiveness and efficiency indicators advantages and disadvantages

Effectiveness Indicator	**Advantage**	**Disadvantage**
Average Annual growth rate	Based on empirical value	No consideration of country specific factor
Absolute annual growth rate	Based on empirical value	No consideration of country specific factor
Effectiveness indicator	Country-specific factors taken into consideration	Difficult to identify additional mid-term potential
Efficiency Indicators	**Advantage**	**Disadvantage**
TCI (Total cost indicator)	The total wholesale value of a country's power generation is used as a benchmark for comparison.	TCI does not take into account the lowering of wholesale prices that occur due to higher penetration
PII (Policy impact indicator)	The indicator enable to compare policy effectiveness in different countries by stimulating deployment for different technologies.	It does not measure the impact of individual policies or insights into why a particular national policy is effective or ineffective linked to performance in other sectors or countries
Employment	Significantly contribute to regional development and focus on positive employment effects	Others industry sectors are able to lack human resource because of migration to RE sector

There is no so much calculations concerned with Lithuanian efficiency and effectiveness indicators for support measures. However, by comparing policy effectiveness indicator for onshore wind in 2009 (Figure 1.) it can be seen that highest policy effectiveness indicators with acceptable profit for investors have the following countries − Hungary, Spain, Germany. It should be stressed that the following countries use Feed-in system. In addition, countries such as (Italy, Belgium, Sweden) use quota obligation support system, where policy effectiveness indicator is a little bit less than previous mentioned countries that apply feed-in system. On the other hand, potential profit range for investors by using quota obligation support system is higher than feed-in tariff. Countries such as Latvia, Poland have very low policy effectiveness indicator despite high profit for investors. As can be seen from (Fig. 1) Lithuanian policy effectiveness indicator is higher by comparing with countries such as Latvia, Poland. Nevertheless, Lithuanian feed-in tariff too low for investors to accelerate onshore wind penetration.

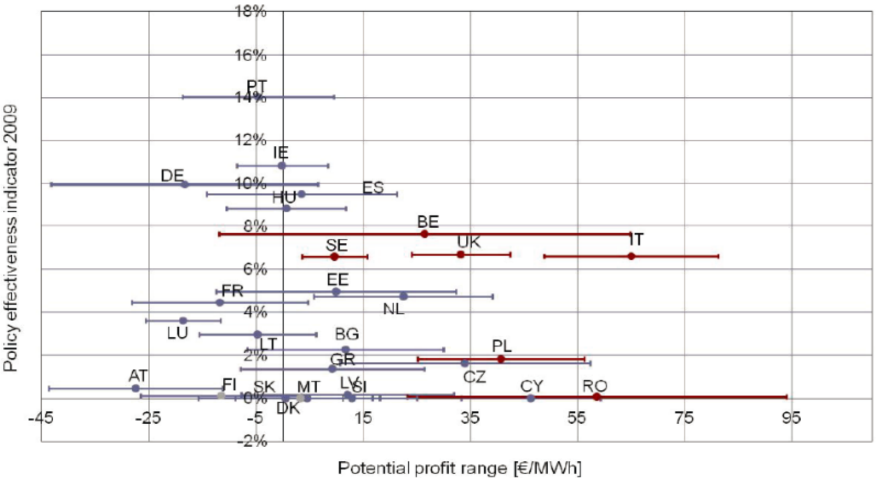

Fig. 1. Policy Effectiveness Indicator for onshore wind in 2009 and potential profit ranges for investors (Ragvidz M., 2012)

It should be pointed out that different kind of support schemes have different levels of maturity in particular some countries that use quota obligation systems are still in a transitional phase.

5. CONCLUSIONS

In Lithuania, renewable energy support measures effectiveness still has not been assessed. In order to estimate the most effective support measures in Lithuania context it is necessary deeper analysis including all above mentioned indicators. There are a wide range of support schemes that can be successfully and effectively applied relying on technology and country. However, some successful incentive schemes in one country will not necessarily be acceptable in another country (Manecon Consulting, 2013). Despite the following fact, there are a key aspects of renewable energy policy design (IEA, 2008):

- By removing non-markets barriers *(Unclear, non-transparent new legislation*; *Poor status of the infrastructure in some areas; High connection cost; Procedure for the adoption of the new law not transparent)* for the purpose to improve policy and market function:
- By increasing support framework transparency and predictability in order to attract investors.
- By fostering and monitoring technological innovation and moving technologies quickly towards market competitiveness through the introduction of transitional incentives.
- By developing and implementing of appropriate incentives guaranteeing a specific level of support to different technologies based on their degree of technology maturity, in order to exploit the significant potential of the large basket of renewable energy technologies over time.
- By taking the impact into consideration of the large-scale penetration of renewable energy technologies on the overall energy system, especially in liberalized energy markets, with regard to overall cost efficiency and system reliability.

Moreover, Mitchell (2011) claims that it has to be explicitly considered for defining support measures implementation effectiveness and efficiency. There is no systematic monitoring support policy effectiveness. Most indicators refer to general policy indicators, not particular measures. In additional, International Energy Agency (IEA, 2008) claims that administrative obstacles (non-economic barriers) such as: lack of mutual coordination among different authorities, long term period by getting authorization) also information gap and inappropriate social acceptance that leads to poor support measures policies effectiveness in many countries. Hence, support measures effectiveness highly rely on policy framework where each country have a different attitude and targets on renewable energy sector.

REFERENCES

1. ABOLHOSSEINI S., HESHMATI A. The Main Support Mechanisms to Finance Renewable Energy Development. Discussion Paper No. 8182. Germany. 2014 of May.
2. GUTERMUTH, P.G. Financial measures by the state for the enhanced deployment of renewable energies. (1998). *Solar Energy, 64*(1–3), 67–78. doi: 10.1016/s0038-092x(98)00066-
3. WOHLGEMUTH N., MADLENER R., Financial support of renewable energy systems: investments vs operating cost subsidies. Proceedings of the Norwegian Association for Energy Economics (NAEE) Conference „Towards an Integrated European Energy Market“, Bergen/Norway, 31 Aug. – 2 Sep. 2000
4. The European Parliament and the Council of the European Union. Decision No 406/2009/EC of the European Parliament and of the Council of 23 April 2009
5. European Environment Agency (EEA). Energy support measures and their impact on innovation in the renewable energy sector in Europe (2014) [referred on the 16th of February in 2015 y.]. Link to the internet <http://www.eea.europa.eu/publications/energy-support-measures>
6. MANECON CONSULTING. Assessing the effectiveness of policies to support renewable energy (2013) [referred on the 16th of February in 2015 y.]. Link to the internet <http://orbit.dtu.dk/ws/files/69996503/Assessing_the_effectiveness.pdf>
7. MENANTEAU P., FINON D., LAMY M.L. Prices versus quantities: choosing policies for promoting the development of renewable energy. *Energy Policy* 31 (2003) Institut d’Economie et de Politique de l’Energie, CNRS/Universite Pierre Mendes-France, BP 47, 38040 Grenoble Cedex 9, France. 799–812
8. VALENTE C., SPINELLI R., HILLRING G.B. LCA of environmental and socio-economic impacts related to wood energy production in alpine conditions: Valle di Fiemme (Italy). *Journal of Cleaner Production* 19 (2011). 1931–1938
9. MITCHELL C., et al. *Chapter 11: Policy, Financing and Implementation”, in IPCC Special Report on Renewable Energy Sources and Climate Change Mitigation,* Cambridge University Press, Cambridge and New York, p. 865–950. (2011).
10. European Commission (2009a). Directive 2009/28/EC of the European Parliament and of the Council of 23 April 2009 on the promotion of the use of energy from renewable sources and amending and subsequently repealing Directives 2001/77/EC and 2003/30/EC (2009). *Official Journal of the European Union*, p. 16–61.
11. IRENA (International Renewable Energy Agency). Evaluating policies in support of the deployment of renewable power. 2012.
12. IEA (International Energy Agency). Deploying renewables. Principles for effecting policies. 2008 [referred on the 22th of February in 2015 y]. Link to the internet <http://www.iea.org/publications/freepublications/publication/deploying-renewables-principles-for-effective-policies.html>
13. JAGER D., RATHMANN M. Policy instrument design to reduce financing costs in renewable energy technology projects. 2008 – [Referred on the 22th of February in 2015 y].

Link to the internet <http://iea-retd.org/wp-content/uploads/2011/10/Policy_Main-Report.pdf>

14. KELPŠAITĖ J.T. Legal sources on renewable energy. 2014- [referred on the 25th of February in 2015 y]. Link to the internet http://www.res-legal.eu/search-by-country/lithuania/single/s/res-hc/t/promotion/aid/price-based-mechanisms-purchase-of-heat-produced-from-res/lastp/159/
15. RAGVIDZ M. STEINHILBER S. RE-Shaping: Shaping an effective and efficient European renewable energy market (2012). [Referred on the 26th of February in 2015 y]. Link to the internet www.reshaping-res-policy.eu

CYSENI 2015, May 27–28, Kaunas, Lithuania
ISSN 1822-7554, www.cyseni.com

COHERENT POLICY OF RENEWABLE ENERGY SOURCES SUPPORT IN LITHUANIAN DISTRICT HEATING SECTOR

L. Murauskaitė
Lithuanian Energy Institute
Breslaujos str. 3, LT-44403 Kaunas – Lithuania
Phone +370 37 401982
Email: Lina.Murauskaite@lei.lt

ABSTRACT

European Union 20-20-20 goals have made a significant influence for the changes in national Member States' energy policy. Renewable energy sources (RES) will have to play the main role for the movement towards sustainable development in all energy sectors. Implementation of RES technologies is restricted by slow demand rates that are mainly influenced by underestimated externalities of fossil fuels. District heating may be appropriate infrastructure for the implementation of RES technologies on the production and demand sides. Therefore this paper aims at coherent policy of RES methodology formation, based on analysis of Scandinavian experience and application of the possible support measures on the territorial aspects. After comparative analysis of Scandinavian countries and Lithuanian energy strategies influence for district heating sector, scenario method was used to justify the possibility for the use of diversified RES, such as solar collectors and heat pumps, on district heating system's demand and supply sides. The calculations were done by the use of EnergyPro modelling tool and levelised cost of energy method. The results have showed that coherent energy policy is a key aspect that influences the preeminent position of different types of fuels, and after evaluation of externalities in fossil fuel costs RES might become the attractive technology for the generation of energy.

Keywords: district heating, renewable energy sources, energy policy

1. INTRODUCTION

European Union 20-20-20 goals on increasing renewable energy, energy efficiency, and decreasing greenhouse gas emissions were enacted through the climate and energy package in 2009. Later Renewable Energy Directive [1] set binding national targets for each member state to raise the share of renewable energy sources (RES) in their final energy consumption by 2020. Lithuania as well as others EU members in National Action Plans explained how to reach these goals in electricity, heating, and transport sectors. Renewable Energy Directive was the first legal driver from EU level for recognising district heating as important infrastructure to reach the goals of RES and to integrate large biomass, solar, and geothermal facilities.

Lithuania enacted the Law on Renewable Energy in 2011 with legally binding targets for RES, which were mainly driven by Renewable Energy Directive. During EU Structural Funds period support was given mainly for biomass boilers on the district heating supply side. The installation of solar collectors and heat pumps on the demand side of district heating were also supported, mainly in multifamily buildings, and some public and private buildings. Nevertheless, implementation of RES technologies is still restricted by slow demand rates that are mainly influenced by underestimated externalities of fossil fuels. Externalities encompass greenhouse gas emissions (mainly from fossil fuel), air quality impacts, land impacts, and other environmental impacts.

The previous researches mainly looked more into detailed about externalities in the electricity sector, for example [2], [3]. Only few researches are available on the externalities or social costs in the district heating sector, and mainly from Scandinavian countries [4], [5]. Therefore this paper firstly takes analysis of the Scandinavian district heating sector development and searches for threshold of RES in the fuel mix that was made in the last century.

The aim of this paper is coherent policy of RES methodology formation, based on analysis of Scandinavian experience and application of the possible support measures on the territorial aspects. Comparative analysis of Scandinavian countries and Lithuanian energy strategies influence for district heating sector was done; scenario method was used to justify the possibility for the use of diversified RES, such as solar collectors and heat pumps, on district heating system’s demand and supply sides. Methods of the research are scientific literature analysis, based on comparative and summarization method, descriptive analysis, also logic and synthesis. The calculations were done by using scenario method, with EnergyPro modelling tool database and levelised cost of energy method.

The next chapter provide short economical point of view to district heating infrastructure as a natural monopoly. Then examples of Scandinavian countries experience in the development of RES in district heating sector, main challenges and achievements. Later the methods used for scenarios are briefly defined. In the last chapter long-term coherent policy of RES formation is presented.

2. DISTRICT HEATING INFRASTRUCTURE AS A NATURAL MONOPOLY

Scientific approach to district heating infrastructure as a natural monopoly is twofold. Some would presume that the whole district heating production system is to be considered a natural monopoly, while others would limit the monopoly to the distribution grids. The conception of natural monopoly represents a challenging regulation dilemma. A traditional definition, as it is defined in [6], is that natural monopoly was considered to occur in cases where economies of scale exist. This means that a single company can supply the market at the lowest cost, compare with several companies. Scale economies are considered as a barrier to entry the market; due to the monopoly power, natural monopoly is seen as a market failure, therefore intervention of the government is required (in the forms of nationalization, regulation, or antitrust). District heating is one example of public utility that is usually characterised by having substantial sunk costs due to large infrastructures [7].

The traditional (economist) way of understanding the nature of a public utility is that the operation can be divided into three different components: production, transmission and distribution (sales). If there is a natural monopoly present, the market is best served if only one firm supplies the total market demand, at least according to neo-classical economics. For many public utilities the firms are vertically integrated and a recent issue has been the unbundling of these different components into competitive elements and “natural” monopolies.

As noted by [7], district heating are not considered by none of the EU directives on liberalisation, such as the electricity and gas markets. Nonetheless, the district heating as a system offers the possibility for competition between fuels and technologies on the market for space heating and hot water. Author agrees with [8] opinion, that one of the main advantages of large district heating system is environmental benefits from the perspective of industry, government, and society.

The next chapter will look more into details about competition of fuels and technologies in Scandinavian countries (Denmark, Sweden, and Finland). The Scandinavian countries, as well as Lithuania, have a well-developed district heating infrastructure and long-term experience of planning and legal regulation.

3. RES DEVELOPMENT IN DISTRICT HEATING OF SCANDINAVIAN COUNTRIES

Lithuanian district heating sector has challenges in recent years. After the adoption of the Law on Renewable Energy and EU Structural Support period 2007–2013, there was no stable state policy on district heating. Support was given for small scale biomass boilers up to 5 MW capacity and competition on the production side of district heating was encouraged by Law on Heat. On the other side, pricing was not favourable for municipalities' producers, especially in largest Lithuanian cities; therefore many small private investors started business at producing heat in small biomass boilers. An example of successful energy policy and strategic planning could be Denmark.

According [9] the transition period of energy system based on fossil fuel technologies and centralisation in Denmark started since the 1970 s. One of the main results was long-term energy planning, which had been influenced by an open and flexible political process. The introduction and dissemination of cogeneration (CHP) technology, as well as district heating, wind energy, and biogas were priorities for support from targeted programmes. Denmark's first overall energy plan "Danish energy plan" was enacted in 1976. The plan was intended to lay the basis for a long-term energy policy. The public policy in Denmark has a regulatory approach with a specific heating law, including tariff regulation, zoning etc. District heating has a strong position in the Danish heat market. As demonstrate [10], two major issues in the Danish law (Act on heat supply) have large effects in the market. First, since 1982 there is an obligation to connect new and existing buildings to public supply. Second, there is since 1988 a ban on installing electrical heating in new buildings and since 1994 there is ban on installing electrical heat systems in existing buildings with water based central heating. In comparison to Lithuania, there is no existing ban for electric heating or the use of natural gas in buildings; therefore district heating should compete with alternatives on the market conditions.

Important role is given to municipalities in Denmark. As stated in [11], heat planning was introduced in 1979, and it was mandatory for municipalities to establish a heat plan in accordance with specific rules given by the Ministry of Energy. Strategic municipal heat planning was successful in the 1980s, but became less effective after the revision of the Heat Supply Act in 1990, as argue [12]. The first Danish Heat Supply Act of 1979 had the requirement to designate geographical heat supply areas; responsibility was given to the municipalities together with counties, and local utility companies. As a result, heat supply made a transition from individual forms of heating, such as oil boilers or electric heating, to more efficient and collective forms, such as district heating and natural gas. After the establishment of well-defined heat supply areas, most municipalities restricted themselves to acting as project authorities that would approve single heat supply projects without having long-term aspects in mind. Municipalities still have the authority to devise heat plans, which nowadays mainly contain general objectives and can be the basis for initiating specific heat supply projects. In general, overall municipal heat planning has been given a lower priority in many municipalities during the last two decades. In Lithuania, municipality role in district heating sector usually is defined by the decision of district heating price in small municipalities for a 3-5 years period. Zoning of district heating areas in cities/towns of Lithuania is still seldom. Decisions, however, also requires clear support and guidelines from the central level, which should set the frame for strategic municipal energy planning in general, and municipal heat supply and demand planning in particular.

Other authors [13] state that since the late 1970s Danish energy administration has been using a geographical database for heat demand and supply. Authors express the opinion that geographical database could be a base for a future stabilisation of state policy for district heating. After each change of government there is a tradition in Lithuania to change National Strategy, there is no available geographical database. A lack of stable strategic planning and more active role of municipalities are the key elements that should be improved in the nearest future.

Denmark's price regulation on district heating was introduced with the Heat Supply Act of 1979. The fact that district heating in Denmark supplies a large number of individual houses, together with the option of mandatory connection, gives it a dominating position in the heat market and a natural monopoly. Therefore the act specifies that district heating must be operated as a non-profit activity, with cost-based pricing. Nowadays in Denmark district heating is owned by consumer cooperatives or municipal utilities. On contrary, in Lithuanian district heating companies are mainly owned by municipalities or private investors.

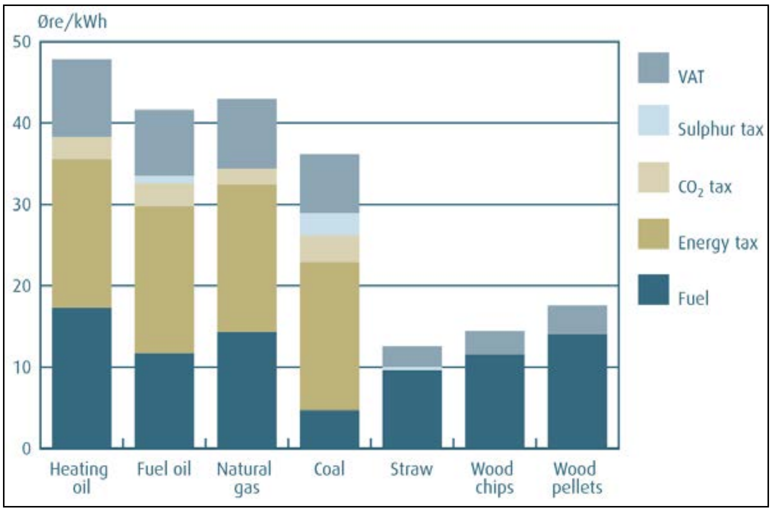

Fig. 1. Fuel costs for district heating production in Denmark in 2002

Successful example of energy strategy implementation was pricing of fuel policy in Denmark. During the 1970s and 1980s, taxes were applied to fuels used in heat generation with the objective of encouraging the use of environmentally friendly energy and efficient energy utilisation. Biomass and biogas were exempted from taxes. As could be seen from the Figure 1, variable part of district heating price was depending on taxes of fuel types. According Danish energy planning and state policy, oil and natural gas had a high taxes, because the Danish government supported production in CHP instead of boilers and encouraged people not to use natural gas for individual heating, but connect to district heating network. Therefore the competitive price of district heating occurred. The main reason was that fuel, used for the production of electricity, did not have the taxes on natural gas. Denmark continues high environmental and CO_2 taxes nowadays. In Lithuania, there are no high taxes for fossil fuel; therefore diversification of fuel sources in district heating requires additional support from the state budget or EU funds.

Concerning support measures [14], they appear as burden measures, financial support, market control, and planning mandates. Burden measures include fiscal and carbon taxes for fossil fuels, giving better opportunities for district heating to compete with other heating alternatives. Financial support is mainly investment grants supporting expansion. Market control and supervision may decrease the risk for market abuse, giving customers more confidence to use the technology. Planning mandates can reduce the capacity risk by harmonised extensions, since capacity in both supply and distribution must be available before connection of new customers.

Some policy support for district heating also exists in EU legislation. The purpose of the Waste directive, with the waste hierarchy and the ambition of diverting waste from land-fills, give an indirect support for other waste management activities such as waste incineration. The Industrial Emissions directive, and its core best available techniques approach, is also an indirect support for district heating. Energy Efficiency directive contains ideas for realising the district heating potential.

Sweden has an extensive district heating sector. District heating accounts for about 40 % of the heating market in Sweden. The change in the fuel mix has been impressive: compared to 1970, when oil was the main fuel, oil accounts for only a few percent today. More than 62 % of district heating fuel today is biomass [15]. The main key forces for the transition from oil to biomass are favourable public policies such as the introduction of a carbon tax in 1991 and the Tradable Renewable Electricity Certificates scheme in 2003. Compare to Lithuania, the main force to make transition from natural gas based district heating to biomass based district heating is support from EU funds and requirements of RES Directive. The lack of long-term energy policy creates the situation when support is concentrated only till 2020 in Lithuania.

The Swedish district heating market is already deregulated in the sense that companies may charge the price they see fit (unless they are municipal administrations). It is also deregulated in the meaning that any company wishing to enter the market by starting a district heating business may do so, provided relevant permits etc. can be granted by the authorities. On the other hand, district heating is not deregulated since all companies are vertically integrated and when a local de-facto monopoly for district heating has been established no competition exist in that specific district heating market [16]. In Lithuania, district heating production should work on market conditions, but is still regulated by National Commission for Energy Control and Prices.

Denmark and Sweden are small and have a well-developed district heating infrastructure. Lithuania was a part of Soviet Union, and district heating was monopoly during that times. Nowadays a competitive market in district heating sector is encouraged by Law on Heat and support is given mainly from EU Structural funds.

Environmental benefits of district heating are integrated as a part of public policy in Denmark and Sweden. On the other hand, Finland has chosen less sustainable development of district heating.

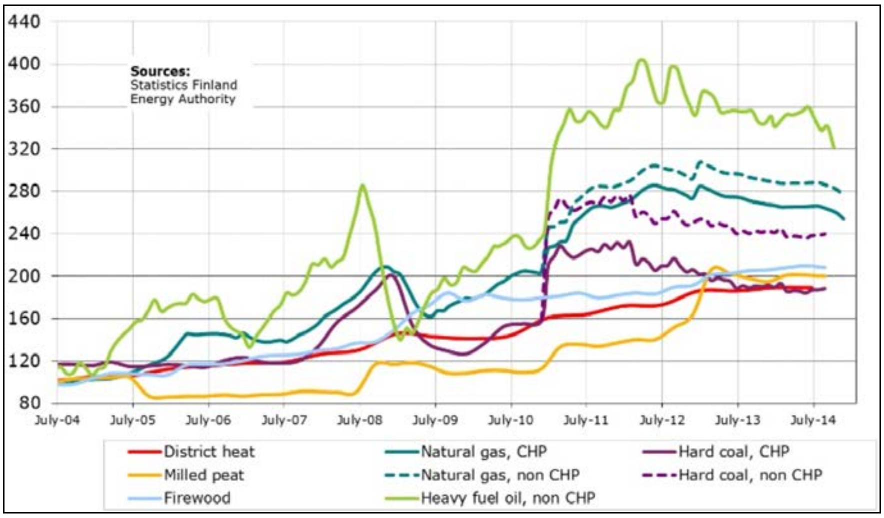

Fig. 2. Prices of district heating and fuels in heat production of Finland, 2004–2014

District heating has a stable pricing policy in Finland. Most fuel prices have risen steeper than the price of district heating since 2004. One reason why the DH sector has managed this well is the diversified use of fuels, another is the increase in the use of peat and waste wood and a third is the wide spread use of coal [17]. Fig. 2 shows prices of district heating and fuels in heat production of Finland during the last decade. The prices of fossil fuels increased after 2011 due to implemented environmental taxes. Finland, as well as Denmark and Sweden, use high environmental taxes for fossil fuel with exception for CHP. Lithuania is not going the same direction at the moment; on the contrary, feed-in tariff for electricity from CHP has decreased during recent years.

As reported by [18], district heating production originated in Finland in the 1950s. Following, the initiative, integrated heat and power production has become a significant element of energy production in Finland. Centralised heat production using water boilers started simultaneously with the integrated production. District heating almost became a fashion in Finnish municipalities during the 1970s after the oil crisis. From the policy perspective of market deregulation and industry restructuring, the results are encouraging. The electricity market restructuring, which started in 1999 and affects district heating markets only indirectly, has lowered district heating prices [19]. In Lithuania, lower feed-in tariff for electricity from CHP also had indirect effect to district heating prices, but negative.

To summarise, Denmark has a heat zoning, many decentralised district heating plants, and working on non-profit basis. RES integration is based on taxation of fossil fuels; therefore, preeminent position of RES is even without the support for investment or operation. Sweden has chosen deregulated market of district heating, but has influence for the market by taxation for fossil fuel. Finland has chosen less sustainable district heating sector, which is based on diversification (both RES and fossil fuel). Preeminent position has lower price. All three countries have high energy and environmental taxes.

4. METHODS FOR SCENARIOS

Analysis of Scandinavian countries development of district heating from fossil fuel based to renewable based system revealed that state policy provides a key role towards sustainable development. The case of Lithuania is in transition period from natural gas based district heating system to biomass based. The main problem is concentration on only one fuel resource (biomass) and lack of diversification in fuel sources. Possibility of different options for more diversified fuel sources, as well as multifamily building renovation, and comparison of different options at unified basis is analysed in this paper. Scenario method was used to justify the possibility for the use of diversified RES, such as solar collectors and heat pumps, on district heating system's demand and supply sides. EnergyPRO modelling tool provides an extensive database of hourly solar radiation and outdoor temperature, also basic economic indicators for calculations; LCoE method lets to compare different options at unified basis with existing district heating price.

EnergyPRO by EMD [20] modelling tool database and evaluation of the production of heat by solar collectors has been used. Software allows carrying out comprehensive and detailed analyses of energy projects. EnergyPRO in scientific papers is used for techno-economic analysis of simulating CHP plants and district heating systems with multiple energy producers [21], [22], [23]. Within the software other types of projects, e.g. geothermal, solar collectors, can also be analysed and detailed [24]. EnergyPRO has been chosen for the reason to model production of solar thermal, as well as to connect district heating network. EnergyPRO has very good database of solar radiation and outdoor temperatures in different parts of Lithuania, therefore it was used to evaluate the production of heat from solar collectors during the whole life time.

EnergyPRO evaluates characteristics of solar collector and its inclination and orientation to the sun, accurately models hourly amount of produced heat. The formula for a solar collector is as follow:

$$Y = A \cdot \left(\left(I_{beam} \cdot K_{\theta} + \left(I_{diffuse} \right) \cdot K_{60^0} \right) \cdot \eta_0 - a_1 \cdot \left(T_m - T_a \right) - a_2 \cdot \left(T_m - T_a \right)^2 \right) \tag{1}$$

where: Y – heat production, [W]; A – solar collector area [m^2]; I_{beam} – beam radiation on a horizontal plane, [W/m^2]; K_{θ} – incidence angle modifier; $I_{diffuse}$ – diffuse radiation on an inclined plane, [W/m^2]; T_m – solar collectors average temperature, [^{o}C], that is an average between the temperature of the cold water entering the collector and the hot water leaving the collector; T_a – ambient temperature, [^{o}C].

The efficiency of the solar collector is defined by three parameters: η_o – intercept (maximum) of the collector efficiency, [-]; a_1 – the first-order coefficient in collector efficiency equation, [W/(m^2 ^{o}C)]; a_2 – the second-order coefficient in collector efficiency equation, [W/(m^2 ^{o}C)]. The radiation is split into beam radiation and diffuse radiation. Since the diffuse radiation per definition has no incidence angel is used the incidence angle modifier or K_{θ} at 60^o.

The user of energyPRO is provided with a detailed financial plan that presents monthly cash flows, the operating results for the project, and key investment figures such as Net Present Value (NPV), Internal Rate of Return (IRR) and Payback Time [20]. The economic feasibility analysis of the chosen solar collectors in Varėna town for district heating purposes in EnergyPRO is based on mentioned traditional key investment figures.

Levelised cost of energy (LCoE) is widely used approach for comparison of different energy generation alternatives, especially in electricity sector, but scarcely used for district heating. Method is based on the principle that present value of total life cycle costs is calculated considering stated discount rate and then allocated per one unit of energy. LCoE is the price of energy, which has to be set that at the stated discount rate, which is equal to capital price, all discounted expenditures are equal to income, and the net present value equals zero. Excel based calculator was used for the comparison of the price of heat that is produced by solar collectors, heat pumps, and district heating. Also effect of multifamily building renovation was included with different support levels. Calculator was developed by the group of energy economists from the Lithuanian energy institute under the research that was supported by Research Council of Lithuania (IEP-01/2012). Calculator was adapted for the evaluation of alternatives in district heating sector on Varėna town case.

LCoE method is appropriate, because all main criteria can be concentrated in it, such as NPV (equal to 0) and IRR. The main advantage of this indicator is possibility of comparison to the competitive price of energy in the market. LCoE shows that the project will have, for example, 10 % IRR (that is determined), if the price of district heating (or any other producer/supplier) is not lower than the price that is calculated by the formula.

The calculation of LCOE is based on an extended LCOE approach, which is described:

$$LCOE = \frac{\sum_{t=0}^{T} \frac{I_t + O\&M_t + F_t - PTC_t - ITC_t - ATL_t}{(1+d)^t} - \frac{RV}{(1+d)^T}}{\sum_{t=0}^{T} \frac{C_I \cdot 8760 \cdot LF \cdot (1-DR)^t}{(1+d)^t}}, \tag{2}$$

where: I_t – investment cost at time step t, EUR; $O\&M_t$ – operation and maintenance cost at time step t, EUR; F_t – fuel cost at time step t, EUR (zero for solar collectors); PTC_t – subsidy for energy production, EUR; ITC_t – investment subsidy, EUR; ATL_t – income / cost for emission allowances, EUR; RV – residual value, EUR; C_I – installed capacity, kW (MW); LF – load factor, %; d – discount rate, %; t – life time, years; DR – degradation rate of technology, %.

The advantage of the extended LCOE approach is that it allows assessing the effect of different RES support schemes on energy cost, as well it takes into account both environmental constrains and technological limitations. LCoE method is suitable for the evaluation of a wide spectrum of different options. The result obtained, for example, 1 kWh levelised cost of heat, can be compared to official district heating price, and the feasibility of a project can be decided. Therefore LCoE has been used for the evaluation of different scenarios for the comparative analysis of different options: renovation of multifamily building, installation of solar collectors and heat pumps, solar collectors field connected directly to district heating network. The application of LCoE method allows estimation of technical aspects and economic projections to the levelised cost of the heat unit.

5. COHERENT POLICY OF RES METHODOLOGY FORMATION IN LITHUANIA

Coherent policy of RES methodology formation in Lithuania is primarily based on analysis of Scandinavian experience. Comparison of three Scandinavian countries (Denmark, Sweden and Finland) showed that the main driver of changes in all three countries was diversification of fuels. Each country has chosen different pathway to changes. Denmark has a long term strategy and local district heating planning; together with Sweden aims at high energy taxes for fossil fuels and CO_2. Since 2011 Finland also increased energy taxes for fossil fuels, with reduced tariff for CHP plants. Such examples show that Scandinavian countries are trying to estimate externalities of fossil fuels by environmental taxes. Simultaneously with environmental taxes countries implemented different programs of support measures. For example, tax incentives on the production of district heating through cogeneration exist in all three analysed countries.

Implementation of RES technologies in Lithuania is restricted by slow demand rates that are mainly influenced by underestimated externalities of fossil fuels. Application of the possible support measures in case of Lithuania should be based on unified comparative basis. Scenario method was used to justify the possibility for the use of diversified RES, such as solar collectors and heat pumps, on district heating system’s demand and supply sides. EnergyPRO modelling tool database was used for hourly solar radiation and outdoor temperature estimation. Extended LCoE approach was used for comparison of different options in district heating system in case of Varėna town in Lithuania.

Author’s previously published research [25] presented the results of modelling large scale solar collectors’ field on the supply side of district heating in Varėna town. Scenarios were presented that all/half/minority hot water demand during summer time could be covered by solar collectors’ field. The payback time, calculated with energyPRO, was longer than 10 years; therefore this time extended LCoE based calculation has been used for the evaluation process.

Three basic scenarios have been calculated for solar collectors’ field on supply side of district heating system (DH_SOL): no subsidy, 30 percent, and 50 percent subsidy for investments of solar collectors’ field, and soft loan with 3 percent fixed interest rate for 20 years period. Scenarios resulted in LCoE for produced heat around 4-6 euro cent per kilowatt hour (average district heating price from biomass is 5.8 €ct/kWh in Varėna town in 2014). This result revealed that state support, such as investment subsidies with soft loan, could create a competitive source for biomass boiler during summer time in Varėna town, which already had subsidy from Lithuanian Environmental Investment Fund. The advantage of solar collectors’ field is stable price for district heating in long-term period, because no fuel is required. The disadvantage is high investment costs and intermittent production of heat. Therefore solar collectors’ field could not be estimated as the alternative for biomass boiler, but only as complementary installation that enables to fix price for the long-term period, when price for biomass is expected to increase due to raise in demand.

Calculations of extended LCoE approach have also been applied for the multifamily building in Varėna town, which has already installed solar collectors for the preparation of hot water and heat pumps for the space heating. This five floors multifamily building with 40 apartments is the only one in Lithuania that uses both types of RES technology for heating purposes already. Figure 3 shows LCoE analysis of RES scenarios in district heating sector on the supply and demand sides, and renovation of multifamily building. Three main scenarios of renovation (REN) were calculated: no subsidy, 30 and 50 percent intensity of subsidy. Furthermore, three additional scenarios were calculated of solar collectors and heat pump (SOL_HP) in multifamily building without subsidy, with 30 and 50 percent intensity of subsidy. Comparison of LCoE with various intensity of subsidy reveals that in the case of complete renovation of multifamily building even with fifty percent intensity of subsidy savings in heating cost is higher than average existing district heating price (5.8 €ct/kWh) in Varėna town. Moreover, complete renovation requires large investments. This problem could be solved by separate effective elements of renovation, such as renovation of heating system, replacement of windows, etc. On the other hand, RES on the demand side, such as solar collectors and heat pump, could compete with district heating price without any subsidy in Varėna town. It should be noted, that even high investment costs in renovation of multifamily buildings in Lithuania is necessary due to very inefficient use of heat energy in multifamily buildings that was built more that 30–40 years ago.

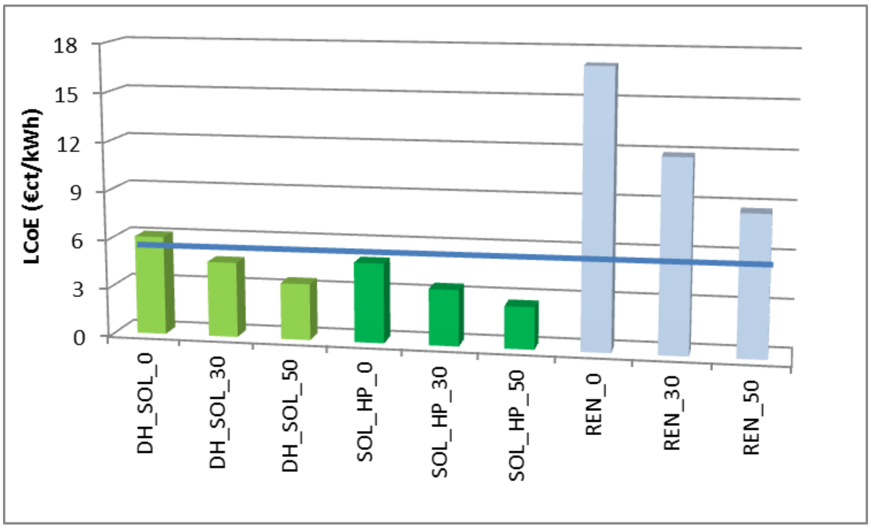

Fig. 3. LCoE analysis of RES scenarios in district heating sector on the supply and demand sides, and renovation of multifamily building (€ct/kWh, excl. VAT)

Estimation of local and foreign capital investments of solar collectors has also been done. The results showed that only less than 25 percent of local capital could be used for the installation of solar collectors. Therefore country should take into consideration this drawback and encourage research and development in the field of RES in local scale. Integrated territorial investments could promote the concept of sustainable cities as well as regional growth and development.

Although traditional LCoE is a simplified indicator of the price consumers will pay for generating heat unit from different fuel sources at a given point in time, it could account for externalities in the calculations presented above. An externality is a consequence of an economic activity that is not reflected in the price of that activity. It is important to look at the entire life cycle of a fuel source or generation technology when considering externalities. Different district heating generating technologies also have a number of benefits that may not be reflected in the LCOE. These include energy security, job creation, and long-term price stability. Furthermore, after reliable methodological evaluation of positive impact, integration of RES could be more successful for solving economic, social, rural development problems in regional development context. Integrated Resources Planning approach, which allows avoiding partial optimization, could be used for the future evaluation of how to implement the objectives of the state programs.

Responsibility for fulfilling the Renewable Energy Directive goals lies at the national level, while responsibility for district heating is often split between national, regional, and local bodies. Principal scheme of coherent policy of RES formation is shown in Fig. 4.

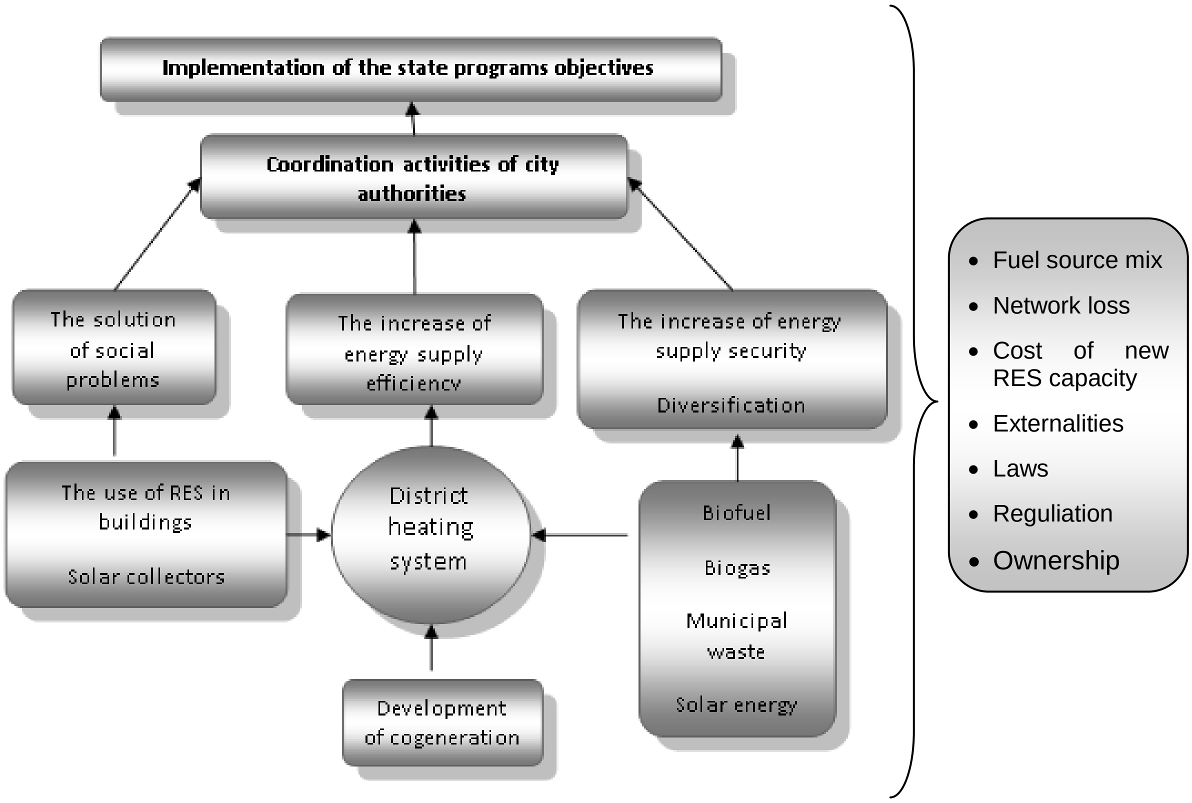

Fig. 4. Principal scheme of coherent policy of RES formation

Principal scheme represents district heating as the central infrastructure. Integration of RES on the demand and supply sides of district heating may help to reach the state's long-term goal of energy security, energy efficiency, and social problems. Important criteria that must be taken in the long-term energy planning is shown on the right. Incorporating externalities into long-term RES energy policy that should be based on continuing researches and development could increase the possibility of developing the economical and sustainable district heating system from a societal perspective.

6. CONCLUSIONS

The results have showed that coherent energy policy is a key aspect that influences the preeminent position of different types of fuels, and after evaluation of externalities in fossil fuel costs RES might become the attractive technology for the generation of energy. Externality is a consequence of an economic activity that is not reflected in the price of that activity Analysis of Scandinavian countries experience on district heating development revealed that incorporating externalities into long-term RES energy policy could increase the possibility of developing the economical and sustainable district heating system from a societal perspective. Diversification of fuel sources and environmental taxes could help to solve market failures, which requires coherent energy policy in Lithuania.

Comparison of LCoE of diversified RES on district heating system's demand and supply sides with various intensity of subsidy reveals that in the case of complete renovation of multifamily building even with fifty percent intensity of subsidy savings in heating cost is higher than average existing district heating price in Varėna town. On the other hand, RES on the demand side, such as solar collectors and heat pump, could compete with district heating price without any subsidy. Solar collectors' field on the supply side could not be estimated as the alternative for biomass boiler, but only as complementary installation that enables to fix price for the long-term period, when price for biomass is expected to increase due to raise in demand.

Meeting demand for a future district heating in a responsible and cost-effective manner requires highly sophisticated analysis of different variables including current and possible fuel source mix, network loss, the cost of adding new capacity of RES, consideration of externalities, current and anticipated law and regulation considering RES, and meeting the expectations of ownership. The incorporation for these variables in long-term RES energy policy requires integrated resource planning.

Different fuel sources offer different advantages and disadvantages. Any deep transformation of the district heating sector in Lithuania and elsewhere will require a tremendous amount of foresight, focus, and partnerships, as well as continued research and development.

REFERENCES

1. Directive 2009/28/EC of the European Parliament and of the Council on the promotion of the use of energy from renewable sources and amending and subsequently repealing Directives 2001/77/EC and 2003/30/EC. Official Journal of the European Communities, 5.6.2009.
2. ROTH, I.F., LAWRENCE, A.L. Incorporating externalities into a full cost approach to electric power generation life-cycle costing. *Energy*, 2004, Vol. 29, No. 12–15, p. 2125–2144.
3. NEUHOFF, K. Large-Scale Deployment of Renewables for Electricity Generation. *Oxford Review of Economic Policy*, 2005, Vol. 21, No. 1, p. 88–110.
4. FAHLÉN, E., AHLGREN, E.O. Accounting for external environmental costs in a study of a Swedish district-heating system – an assessment of simplified approaches. *Journal of Cleaner Production*, 2012, Vol. 27 p. 165–176.
5. BOWITZ, E., DANG TRONG, M. The social cost of district heating in a sparsely populated country. *Energy Policy*, 2001, Vol. 29, No. 13, p. 1163–1173.
6. MOSCA, M. On the origins of the concept of natural monopoly: Economies of scale and competition. *The European Journal of the History of Economic Thought*, 2008, Vol. 15 p. 317–353.
7. GROHNHEIT, P.E., GRAM MORTENSEN, B.O. Competition in the market for space heating. District heating as the infrastructure for competition among fuels and technologies. *Energy Policy*, 2003, Vol. 31, No. 9, p. 817–826.
8. REZAIE, B., ROSEN, M.A. District heating and cooling: Review of technology and potential enhancements. *Applied Energy*, 2012, Vol. 93 p. 2–10.

9. SPERLING, K., HVELPLUND, F., MATHIESEN, B.V. Centralisation and decentralisation in strategic municipal energy planning in Denmark. *Energy Policy*, 2011, Vol. 39, No. 3, p. 1338–1351.
10. DANISH ENERGY AGENCY. Heat supply in Denmark, Who, What, Where, and Why. *Copenhagen*, 2005.
11. NIELS I. MEYER, B.V.M. AND F.H. Barriers and Potential Solutions for Energy Renovation of Buildings in Denmark. *International journal of Sustainable Energy Planning and Management*, 2014, Vol. 01, p. 59–66.
12. SPERLING, K., MÖLLER, B. End-use energy savings and district heating expansion in a local renewable energy system - A short-term perspective. *Applied Energy*, 2012, Vol. 92, p. 831–842.
13. NIELSEN, S., MÖLLER, B. GIS based analysis of future district heating potential in Denmark. *Energy*, 2013, Vol. 57, p. 458–468.
14. PERSSON, U., WERNER, S. District heating in sequential energy supply. *Applied Energy*, 2012, Vol. 95, p. 123–131.
15. DI, L., ERICSSON, K. Low-carbon district heating in Sweden – Examining a successful energy transition. *Energy Research & Social Science*, 2014, Vol. 4, p. 10–20.
16. WESTIN, P., LAGERGREN, F. Re-regulating district heating in Sweden. *Energy Policy*, 2002, Vol. 30, No. 7, p. 583–596.
17. HAVSKJOLD, M., SKÖLDBERG, H. The future of the Nordic district heating. *Nordic Energy Perspectives*, 2009, p. 9–51
18. WESSBERG, N. Local decisions in the Finnish energy production network - A socio-technical perspective. *Landscape and Urban Planning*, 2002, Vol. 61, p. 137–146.
19. LINDEN, M., PELTOLA-OJALA, P. The deregulation effects of Finnish electricity markets on district heating prices. *Energy Economics*, 2010, Vol. 32, No. 5, p. 1191–1198.
20. EMD International. EnergyPRO user's guide. Aalbor, 2011.
21. FRAGAKI, A., ANDERSEN, A.N. Conditions for aggregation of CHP plants in the UK electricity market and exploration of plant size. *Applied Energy*, 2011, Vol. 88, No. 11, p. 3930–3940.
22. STRECKIENĖ, G., MARTINAITIS, V., ANDERSEN, A.N., KATZ, J. Feasibility of CHP-plants with thermal stores in the German spot market. *Applied Energy*, 2009, Vol. 86, No. 11, p. 2308–2316.
23. RASBURSKIS, N., LUND, H. Optimization methodologies for national small-scale CHP strategies (the case of Lithuania). *Energetika*, 2007, Vol. 53, No. 3, p. 16–23.
24. NIELSEN, S., MÖLLER, B. Excess heat production of future net zero energy buildings within district heating areas in Denmark. *Energy*, 2012, Vol. 48, No. 1, p. 23–31.
25. MURAUSKAITE, L. Presumptions for Increasing the Use of Renewable Energy Sources in Large Scale in District Heating. *Digital proceedings: 8th conference SDEWES, Dubrovnik, Croatia, September 22-27, 2013. Croatia, 2013. ISSN 1847-7178*, 2013, p. 1–9.

CYSENI 2015, May 27–28, Kaunas, Lithuania
ISSN 1822-7554, www.cyseni.com

NATIONAL RENEWABLE ENERGY SUPPORT SCHEMES IN THE EU LEGAL FRAMEWORK

J. Paškevičius
Vytautas Magnus University
Jonavos str. 66, Kaunas, Lithuania
Phone +370 69812393
Email:Julius.paskevicius@gmail.com

ABSTRACT

Currently renewable energy gains more and more attention from the energy policy perspective. Since the EU policies moves towards internal energy market, the rules of renewable energy sector sustain convergence in terms of common objectives and common instruments. Support schemes as instruments for promotion of renewable energy raise a lot of questions with regard to their design and application. Therefore legal framework of the EU law establishes guidance for design and application of support schemes. This paper examines whether support schemes do not contradict to the principle of free movement of goods. For that purpose the pattern of principles established by the case-law are applied to different support schemes with the aim to examine each of them.

Keywords: support schemes, renewable energy, free movement of goods, internal energy market

1. INTRODUCTION

These days economic growth faces new challenges. Therefore energy being as a foundation for every economic activity attains more and more attention. From Lithuania perspective the development of gas sector and electricity sector including renewable energy is of huge importance not just in the light of energy security, but also due to the new nature of free energy market. Since renewable energy falls under priorities for further development of energy sector, it is important to determine how electricity from renewable energy resources is promoted in the framework of free market. Lithuania is obligated to pursue free energy market on the national level and in the EU framework. Despite different directions of policies they are inevitably interconnected. For the purpose of renewable energy, the EU policies set the framework for support schemes that should be implemented on the national level.

The renewable energy sector received more and more attention in the past years. The main focus was on the functioning of support schemes from the technical point of view. In addition, there were a number of articles by scholars examining the support schemes in order to determine which support schemes works the best. Unfortunately, there is a shortage of legal literature regarding support schemes compatibility to the EU law.

The energy sector faces many legal challenges in its alteration into the internal energy market, especially, incorporation of promotion tools taking into account the EU objectives. On the national level Member States design their support schemes in accordance to their internal economic and political situation. Though, national rules determine the structure and conditions for actors to benefit from the support scheme. This stands insecure in the context of EU fundamental freedoms. Interestingly, it seems that any national renewable energy policy that deviate from the compliance to the fundamental freedoms may be justified, since the TFEU grants states an exclusive right to determine the conditions to exploit its energy resources. These conditions may be in a form of the support schemes where every design of support scheme mismatches with one another. The vagueness of the rights allocation to set the frameworks of support schemes leads to promiscuity in the policies of different authorities.

On the other hand, the EU law in the form of directives establishes objectives for the support schemes that have to be in accordance to the fundamental principal of the EU. Since currently no internal electricity market exists and policies with regard to the support schemes vary between member States, it is likely that separate policies in Member States lead to impediments for foreign actors to participate in the national support schemes. The EU objective to pursue for the internal electricity market based on the principle of the free movement of goods may be obstructed. Consequently, the collision between different objectives appears to exist. Then the question should be whether different framework of support schemes is in compliance to the EU objectives.

D. Fouquet and T.B. Johansson examine support schemes from the national and EU perspectives [3]. A. Campoccia & etc. examine the main support policies for PV with the purpose of highlighting the differences in implementation of the FIT [1]. R. Fagiani & etc. compare FIT mechanism with the certificate market system [2].

The objective of the article is to determine whether the support schemes of renewable energy do not contradict to the principle of free movement of goods.

The article explores questions: (i) whether the nature of internal electricity market have implications on the renewable energy policies regarding support schemes; (ii) whether harmonisation of support schemes on the EU level contribute to the free movement of goods; (iii) what concepts stand behind the principle of free movement of goods; (iv) whether the support schemes are designed in conformity with the principle of free movement of goods.

In the article comparative and analogy methods were used to apply the legal framework for support schemes of renewable energy in order to determine their compatibility to the principle of free movement of goods.

2. INTERNAL ELECTRICITY MARKET AND RES SUPPORT SCHEMES

In comparison to gas or biofuels market the electricity market has some specifics in terms of its object, objective and features. Therefore, understanding the context of electricity market where the supports schemes have to operate is of highly importance. Firstly, electricity properties differ from other goods while it is intangible in nature. So pursuing to determine its legal definition will enable to examine support schemes of electricity compatibility to the principle of free movement of goods. Secondly, the creation of internal electricity market aims for objectives that other tools that are applied in the market have to be in accordance. In this case, the support schemes may be identified as such tools that have to be design to favour internal electricity market development and its objectives. Lastly, the elaboration of impediments for internal market in electricity development provides a similar view of the issues with regard to the support schemes development.

The importance of electricity in modern day society cannot be argued. Businesses use electricity in their everyday operations and any shortage or instability of supply threatens economic growth. Furthermore, every appliance needs electricity that is used by the households. Consequently, a considerable proportion of expenditure is spent for electricity. Last but not least, the concerns are growing regarding environmental protection. The need was apparent to create tools to mitigate these risks. On the one hand, there was a wide spread urgency in the European Community (now – European Union) to obtain the proper level of energy security and environment protection, on the other hand, the cost of energy prices had to be reduced in order to stay competitive in the global market and safeguard households well-being. These were the primary factors contributing to legal development in the integration of the electricity market.

In order to address these issues, it was suggested to establish a framework at EC level. Consequently, the idea of internal electricity market (IEM) was proposed in the White Paper that mainly focused the attention on harmonisation of taxation and standards as well as liberalization of the equipment procurement [4]. Since Commission proposal do not oblige states, but highlights the issues that must be addressed, some agreement on EC level was needed. Though, the Single European Act followed to establish legal background for the IEM. Mainly, these were the documents to commence the development of convergence in the energy market as a whole.

Even though the EU legislature aims to establish internal electricity market in pursuant earlier mentioned objectives, the technical and legal hindrances exist. One of the most important is the lack of interconnections between Member States that is essential for enhancement of cross-border trade. In comparison to other issues, it required most financial resources and political will. Some countries find themselves bound to invest in infrastructure of collateral importance, since being a transit country. For this reason the infrastructure projects of the EU importance had to be distinguished and the most appropriate way to do it was in the framework of the internal electricity market where all countries contribute their fair share and gain accordingly. National measures regulating third party access was the next legal challenge. Member States had long lasting monopoly over energy sector with no or very small number of private actors participating in the market. Such conditions were adverse to free trade on the national and the EU level.

On the other hand, the number of positive outcomes may be identified. The inter-Member States trade began to emerge with an increase in production capacity. The creation of the economy of scale which enable to have more efficient production of electricity serve to influence the price reduction. While some states had significant capacity leading to lower price, others felt scarcity of both of them. Furthermore, it is much more efficient in terms of investment management. A level playing field for all players stimulate investments in those areas of energy industry whose had been unprofitable due to the small scale. The free market approach will benefit consumers granting them an opportunity to choose. For the purpose of renewable energy, the internal electricity market enables to create common support instruments through EU. Currently, every state has distinct support instrument in terms of its structural features, but common legal framework in general. The elimination of divergences would have effect not only on the occurrence of the internal electricity market, but also foster inter-state trade. In addition, the growth of the competition between producers and suppliers has positive affect. This should lead to higher standards of service for consumers and businesses. Since the number of beneficial outcomes may be identified, the convergence may be seen as a positive outcome.

Especially, uncertainty exists in the electricity sector due to the nature of electricity. Electricity is not a material object or a substance as such. Also you cannot identify electricity once it is supplied into the grid and it must be used immediately as it cannot be stored. These characteristics do not correspond to the ordinary features of `goods`. However, the case-law dealt with this question quite early and determined that electricity is a `good` in the sense of the free movement of goods [5]. While electricity is defined as a `good`, the EU law obliges Member States to withdraw any possible obstruction to the free trade in electricity. As far as free trade concerns, the free movement of goods is best achieved in the free market environment [6], where consumers can freely choose their suppliers and all suppliers freely deliver their goods to their customers [7]. The concept of a ‘good’ and nature of electricity will be examined below.

Though, the support schemes legal framework objectives in essence correspond to the internal electricity market objectives to protect environment and to ensure security of supply.

However, internal electricity market encompasses in its framework renewable energy policies, but the application aiming for these objectives differ. While internal electricity market is implemented on the EU level, support schemes more concerns national policies.

3. HARMONISATION OF SUPPORT SCHEMES

The idea of internal market is based on the premise that each Member States regulate national market in accordance to the common principles and objectives of the EU law. Such general application of principles and objectives in the national law inevitably fosters convergence in rules of the separate economic areas. It may be suggested that internal electricity market and harmonisation of support schemes go hand-in-hand in the way that harmonisation is at the core of the market concept. For the purpose of renewable energy, the convergence of support schemes would diminish the possibility to design support scheme incompliance to the principle of free movement of goods as the common legal framework is applied. The common legal framework should be understood in terms of common objectives, structure and applicability. Though, the view from the policy perspective may enable to identify whether convergence is possible of the support schemes so that the principle of the free movement of goods will not be infringed.

In terms of renewable energy sector, in particular, support schemes, convergence removes any possible obstructions for every person to participate in any support scheme and consequently to the free movement of goods. However, the Member States are granted exclusive rights with regard to renewable energy that have dual effect. On the one hand, the granted rights to design taking into account internal situation may possibly obstruct the free movement of goods, on the other hand, Members States pursuance of the best design of support schemes leads to their convergence.

There are two possible ways to pursue convergence of support schemes: top down and bottom up. In the top down approach a fully harmonised system is created, where the support schemes are decided top-down and implemented alike in all member states, and as currently exist the bottom up approach where all states have an independent choice of support schemes and the best practise will emerge [8]. This distinction between approaches serves as a guideline for further examination.

However, it is also important to ascertain whether the situation is such that convergence is possible in renewable energy sector. The Commission thinks that it is currently not the time to follow full harmonization [9]. Firstly, harmonization would have an opposite effect on renewable energy support instruments as there is no model of best working measures. Secondly, difficulties arise to establish common support instrument due to different cost of different installation across EU. The similar opinion follows scholars suggested that currently a fully European-wide harmonised scheme cannot be recommended by any means [10]. It must be acknowledge that a number of more obstructions must be mitigated in order to establish the common framework of support scheme. At present, hindrances to converge separate energy island into one are scarcity of adequate connections between Member States [11], access to the network, tarification issues and different degrees of market opening between Member States [12]. There are significant challenges for full harmonisation, therefore, different legal frameworks will exist for the time being.

In addition, since energy issues are highly regarded of national importance, Member States are unwilling to give up much of their influence in the energy sector. It may be suggested that states are awarded exclusive rights. For example, in renewable energy sector Member States are granted a right to control the effect and costs of their national support schemes according to their different potentials [13]. However, a legal framework is enacted to mitigate the obstructions by giving up some of the exclusive rights, even though national policies have considerable impact on the further development of the framework of support schemes.

The energy sector is one of those areas that lack full harmonisation, but as the internal electricity market develops, renewable energy sector is affected as well. Since the frameworks of support schemes lack full harmonisation, national measures must be examined not only in accordance to directives, but also in the light of the primary law [14]. This principle enables to examine whether national support measures are design in conformity with the principle of the free movement of goods, because otherwise in the EU law full harmonisation is followed by the secondary law that encompass all principles and objectives setting the necessary legal background.

Currently, bottom up and top down convergence do not reach the threshold of full harmonisation. However, EU and national policies with respect to support schemes let reasonable to believe that not far from now common support scheme will be applied across EU. The reason for this suggestion is inherent in the fundamental principle of the free movement of goods. In order to foster free trade convergence of rules and regulations is a must, because otherwise no one can expect faster growth in the number of installations and capacity to produce more and cheaper electricity from renewable energy resources. In addition, other objectives such as environment protection and energy security can my ensured. On the other hand, bottom up convergence is obstructed due to economic disparities between Member States. This situation also raises question whether poorer countries will be able from national budgets to finance renewable energy development in the form of support schemes in the same manner as richer countries. One of the ways to address this issue is to finance renewable energy from EU budget or to establish common fond that distributes money in accordance to production efficiency of installations and meeting EU objectives of environment protection and energy security. Though, taking everything into consideration it may be reasonable to suggest that even though bottom up and top down convergence is still in the process, however, in a quick future common support scheme will not be an issue to the free movement of goods.

4. THE PRINCIPLE OF FREE MOVEMENT OF GOODS

The free movement of goods is one of the fundamental principles of European Union. This provision define general legal framework in terms of trade in goods between Member States [15]. However, very often national legislature establishes legal hindrances obstructing free movement of goods in the Member States practice dealing with trade in goods. In order to mitigate this impediment special provision addresses this issue [16]. The issue aroused with regard to two definitions - the quantitative restrictions and measures having equivalent effect to quantity restriction (MEQR) – that were not elaborated in the Treaty. Though, due to its vagueness it has been followed by numerous case-laws.

The scope of the MEQR was determined by the Court of Justice (ECJ) in the case-law. The rules regarded as MEQR can fall under the three different considerations. The first was introduced in *Dassonville* case [17]. The definition was quite vague which led to a lot of room for interpretation. The second landmark case in the development of MEQR case-law was *Cassis de Dijon*, which established the principle of mutual recognition [18]. Consequently, rules regulating package, labelling, composition and quality of goods have mutual recognition between Member States. This principle of `mutual recognition` is applied also in other areas of EU law. The third important case introduced the concept of selling arrangement [19]. The selling arrangement concerns how the products were marketed and do not determine a physical outlook of the product.

However, the ECJ provided justified derogations in pursuance of EU objectives. There are two possible justifications to challenge these concepts. It may be either the Treaty derogations which are in article 30 EC or either overriding requirements developed in the case-law. Article 30 EC sets out public interest grounds that have a priority against other EU values [20]. A restrictive measure can be regarded as suitable for securing the attainment of the objective pursued only if it genuinely reflects a concern to attain that objective in a consistent and systematic manner [21]. On the other hand, the concept of mandatory requirements enable Member States to deviate from MEQR insofar as those provisions may be recognized as being necessary in order to satisfy mandatory requirements relating in particular to the effectiveness of fiscal supervision, the protection of public health, the fairness of commercial transactions and the defence of the consumer [22]. The list of mandatory requirements is open ended therefore additional areas may be added to the list that help to achieve EU objectives. For the purpose of support schemes, it is essential to note that the ECJ set out the protection of the environment as essential to the list [23].

In addition, the MEQR must be proportionate to the objective pursued and non-discriminative between national and foreign actors. Whether the measure is proportionate the court determines on the case by case basis. In essence, the principle of non-discrimination is one of the core features of the MEQR. With regard to renewable energy promotion schemes, the principle of non-discrimination raises the issue if national and foreign actors can acquire the same financial and other benefits. Since the form of discrimination can be any measure or act, support scheme may be identified as constituting the hindrance to free movement of goods.

The MEQR have some limitations in its application. Firstly, national rules are prohibited which actually affect more imported then domestic goods [24], imposing an unreasonable cost on the sale or merely diminish sales [25]. Secondly, measure to be regarded as the hindrance can be slight or mitigated [26] and whose effect is too `uncertain and indirect` [27]. Lastly, a person that create MEQR has to carry out a public duty on behalf of the state, or that it is controlled by state [28], private law bodies are subject to Article 34 whenever they restrict free movement `in the same manner as do measures imposed by the state` [29] and the state does not actively support market-closing measures, but simply refrains from taking actions against them [30].

The EU law prohibits not only obstacles to imports, but exports likewise [31]. As a condition for the article to be applicable, the measures have to have direct effect. Furthermore, provided that the measure had not directly imposed quantitative restrictions on exports, it would not be regarded as constituting a MEQR on exports [32]. However, justifications are provided on the grounds in Article 30 EC or overriding requirements, in compliance with the principle of proportionality in pursuance of legitimate objective [33].

5. SUPPORT SCHEMES

In the light of the EU law, the elaboration of the main properties of support schemes is crucial in order to identify possible failures in their frameworks with regard to the compliance with the principle of free movement of goods. The EU law provide legal framework to support renewable energy, but Member States design support schemes corresponding to internal situation, for instance, geographical factors or the market share of renewable energy. Member States has a right to choose support scheme that they think is most suitable in pursuance of national targets. Even though common frameworks of support schemes may be identified, their design varies. However, some convergence features such as application terms do not play the vital role distinguishing them. Hence, all designs of support schemes do not have to be examined in order to find out if any particular framework of support scheme hinders free movement of goods.

Due to their application in the installation phase, they can be separated into few groups. One group subsidizes investments and another operation costs. Operational support measures can be divided into instruments which fix a quantity of renewable energy to be produced and instruments that fix a price to be paid for renewable energy [34]. This approach for the distinction is the most widely accepted among scholars. However, another approach is to make a distinction between market-based and regulated instruments. Even though they have some similarities, the former approach is more concerned with the framework of support schemes, while the latter to the characteristics of the existing energy supply system, structure of the political system and the EU membership [35]. This type of approach for analyses will not be used owing to the lack of acceptance in the legal literature.

The support scheme Tradable Green Certificate is the second most popular instrument in EU. It is structured that free market powers would be unleashed and the benefit of free market would be shared among the significant number of people. The producers of renewable energy participating in the support schemes of Tradable Green Certificate receive a certificate for electricity they produce and later sell them to the suppliers of electricity - on the market or bilateral contracts - or to the Distribution System Operator at a pre-determined price. The suppliers of electricity are obliged to buy the specific number of certificates every year and at the end of the year present to National Regulatory Authority. The number is determined by taking into account the percentage of the total amount of electricity supplied to consumers. Failing to do that, suppliers are penalized for every certificate which is absent. This system makes a distinction between electricity which is sold on the electricity market and certificates that are sold on a Tradable Green Certificate’s market. Since electricity produced from renewable energy resources is tradable separately from certificates themselves, the certificates can be defined as a security which is traded on the special market in accordance to supply and demand interaction. On the other hand, electricity and certificates can be sold together on the contract bases.

The price based instruments are Feed-in tariff and Premium. On the whole, the most common used support scheme is Feed-in tariff, because it seems that a well-designed FIT system can be deployed in the shortest time and at the lowest cost for society [36]. The few properties that can be indicated in the design between all Member States that is priority dispatch to eligible generation, long-term perspective, guaranteed prices for a specific period or for a pre-determined amount of production [37]. The price is established prior to the construction of installation and will vary according to the type of installation. This instrument enables investors better to foresee the return of their investment and to secure the stable income for a defined period. On the other hand, the support measure Premium is more market orientated which enables producer to sell electricity on the spot market. Income is received from two sources: stable premium tariff determined by National Regulatory Authority and the electricity market price. This type of instrument encourages competition between producers as they sell produced physical electricity on the spot market.

However, few hindrances prevail which must be mitigated. The creation of the level playing field required the withdrawal of national measures that can be justified on overriding requirements of general interest [38] and they must be compatible with Community law [39]. Despite that some derogations from free market principles are inevitable, for instance, a Member State's right to determine the conditions for exploiting its energy resources, its choice between different energy sources and the general structure of its energy supply [40]. These rights of the Member States may seem to be not related to internal electricity market, however, different preferences for energy sources in each state may create situation where one state promote renewable energy while other states gas or nuclear energy. Similar situation can be seen with regard to the national targets of renewable energy in energy mix, as some states strive for 10 percent others four times as much [41]. Consequently, the result is that different financial resources are designated in Member States leading to legal obstructions to protect national market. While there are many divergences between Member States in their national policies in energy sector, free inter-state trade is highly questionable. Legal and economic reasons appear to be at the heart of the debate pursuing internal electricity market.

6. TRADABLE GREEN CERTIFICATES

There are two approaches to the obstruction of the TGC to the principle of the free movement of goods. One may suggest that strictly national application of the TGC is legally justified under the EU law. Since this area lacks full harmonisation, Member States has a right to choose the instruments taking into account internal situation. Another one suggests that it potentially obstruct free movement of goods and it can only be justified provided that few conditions are fulfilled – the national measures must be appropriate and has to be proportionate to the objective pursued [42].

The EU policy is to promote the use of renewable resources in Member States in accordance with the national potentials. In the context of the EU primary law and secondary law objectives, the full harmonisation of support schemes do not exist currently. So it may be suggested that no contradiction between strictly national nature of the TGC and impediments for producers to gain benefits from the foreign TGC appears to exist, irrespective of their nationality [43]. However, this reasoning has some drawbacks due to identified pattern of convergence in all energy sectors in pursuance of the free market.

In order to determine whether the TGC do not obstruct free movement of goods the ECJ set out legal framework. This logic of the possible indirect effect to inter-state trade in electricity follows from the case-law. On the condition that foreign producers do not receive the TGC or count the TGC towards host quota obligation, it is possible to name the TGC as an obstruction to trade in electricity. Consequently, strictly national application may be regarded as measures having equivalent effect to quantity restriction (MEQR). Since electricity is a `good` and the TGC possibly hinders trade in electricity, therefore a national legislation establishing the TGC must be objectively justified in order to succeed [44]. Some doubts may exist whether this support scheme is about trade in electricity or obtainment and trade in the `certificates` of the TGC. Provided that the TGC in essence dealt with the `certificates`, the suggestion will have been different due to the lack of definition of the `certificates` as a `good` and with no limitation to use it in trade as a security.

Since national support schemes possibly may hinder free movement of goods, a number of derogations are established. While some are covered under Article 36 TFEU, others called overriding requirements are established by case-law. The Article 36 TFEU is the list of values of public interest such as public morality, public policy, public security and etc. For the purpose of the free movement of goods, the TGC does not have any correlation with the TFEU stated derogations. On the other hand, the overriding requirements are an open ended list of justifications that can be applied. Also overriding requirements encompass the protection of the environment issue [45]. Promotion of the renewable energy and environmental protection in the EU policy goes hand-in-hand in terms of their objectives.

Though, to justify national legislation it must be taken into account the objective pursued. In the context of all EU objectives, environmental protection falls under the overriding requirements. Even though it is not in the Article of 36 TFEU, the environment protection is also assigned to the section of energy in TFEU. Though, this value is reiterated in different contexts with the possible goal to highlight the importance in the EU.

Furthermore, the legitimate objective of the protection of the environment helps to reduce greenhouse gas emissions that the EU pledged to combat [46]. It may be suggested that the public interest to have protected environment is much more valuable objective than free trade which merely serves economic gains. In addition, the TGC belong to the group of operational support schemes and this link between environmental protection and support measure is direct. While the goal to reduce greenhouse gases can be most effectively achieved in where the electricity is produced [47], environmental protection is definitely a justifiable objective.

Lastly, the promotion schemes should be in accordance with the principle of proportionality. In other words, there should be no encumbrance to obtain and trade in the TGC. The requirement for suppliers to obtain the TGC under free market conditions that would not be detrimental to any of them is essential part of this principle, on the other hand, the penalties for the failure to fulfil quota obligation due to possible market imperfections should not be in an excessive manner [48]. The right to obtain should be granted irrespective of nationality, but taking into account the place of the production of renewable energy. Different approach in terms of trade should be taken. Since the TGC is a financial instrument, the trade in them should not be impeded. Any person can trade them and use for any legal purpose, except for fulfilment of quota obligation with foreign certificates. Overall, the principle of proportionality should be examined on case-by-case bases and solely the elaboration of some of the attributes may be distinguished.

7. FEED-IN TARIFF

As mentioned before Member States use different support schemes, but the FIT is the most widely used instrument [49]. However, some similarities and disparities may be identified. In comparison with the TGC, they diverge in means that are used for the same objective. The FIT is a price based instrument, where production is directly linked to the stable price and free market principles are abandoned. The producers of the renewable energy receive pre-determined price for every MWh that was produced. This is one of the advantages that the FIT possess, since all produced electricity is bought directly by the DSO and producers of the renewable energy can sell them as much electricity as they are able to produce. In short, the FIT obliges DSO to buy electricity from the producers of the renewable energy on the pre-determined price by the NRA for a specific period of time [50]. In addition, this type of support measure is the significant advantage for investors, because they can calculate their return margin in advance. Therefore due to the stability and predictability using the FIT the Member States attain the most attention from investors. On the other hand, Member States become vulnerable to their obligation to reach national target goal, since price based mechanism can cause high uncertainty owing to the failure to anticipate future production level [51].

Despite being the most popular support scheme, there was no case-law regarding the FIT compliance with the principle of the free movement of goods. In fact, it did not raise any issues to the design in any of the Member States or application in general. Therefore only possible theoretical situations can be simulated and examined where established legal principles can be applied.

The FIT possible obstruction to the free movement of goods may exist when foreign producers attempt to receive the FIT for the electricity produced from renewable energy resources. In this case, the produced electricity and an `award` are so interconnected that possession of one without the other is not possible. The national DSO is not obliged to buy electricity from foreign producer of renewable energy even though interconnection between Member States enables to do so. Of course this does not concern trade on the spot market. However, the failure to be eligible to obtain predetermined price by foreign producers may possibly obstruct the supply of foreign electricity to the grid not only from renewable energy resources, but electricity in general. Provided that foreign producers of renewable energy do not derive any benefit from national FIT, the barriers would be unacceptable for the free trade. Though, territorial limitation following the ECJ logic can be a MQER as far as the FIT concerns.

With regard to justification, the FIT the same as the TGC may be justified by one of the overriding requirements. They aim the same objective to reduce greenhouse gas emissions and consequently to protect environment. Since all support schemes are designed for the same objectives, the environment protection as the ground for justification should be reiterated in all cases.

Lastly, the FIT design should be in accordance to the principle of proportionality. Although all support schemes share the same justification, the question whether they are proportionate should be examined on the case by case bases. It may be assumed that some features can be taken from the TGC framework. Firstly, despite of nationality all producers of renewable energy located in national territory should be eligible to participate in the FIT support scheme. The principle of non-discrimination is interconnected with the principle of proportionality in a sense that former encompass some specific provision of the latter. Furthermore, the amount awarded to the producers of the renewable energy should be proportionate and not exceed what is reasonable, otherwise new installations will not be built and fair participation for all actors may be obstructed. On the condition that too low tariffs for FIT support schemes were established, participation for smaller actors would have been difficult to adapt to such small threshold in terms of financial capability. Consequently, some actors could gain benefits while others do not.

8. PREMIUM

The last support scheme is a Premium. It was developed quite late as new forms of support schemes were examined. The peculiarity of the Premium that it has some attributes from both the TGC and the FIT. One of the reasons why it was established is that there was a need to support free market forces in the functioning of the support schemes and in particular the FIT.

In general, the Premium enables producers of RES to sell electricity on the market and in addition to receive a fixed amount of financial support for a definite period. It seems like the FIT and the TGC was merged into one. Since the electricity is sold on the spot market, the price is determined by the interaction of supply and demand. This part of income is volatile due to the competition between the market actors. The second part of income is the predetermined amount of money that does not change. In comparison with the FIT, in Premium the trade between Member States is possible.

Using the same framework for the Premium as for the TGC and the FIT, it may be possible to determine whether the Premium is in accordance to the principle of free movement of goods. Currently, no case-law was published regarding the Premium therefore just theoretical situations may be constructed.

Foreign producers of electricity from RES cannot claim benefit from the national Premium. The same as in before examined cases this is possibly the MEQR for the purpose of the principle of free movement of goods. After that there should be used the same derogation of environment protection to be able to justify possible MEQR. Finally, the issue of proportionality should be studied. Since the Premium is divided into two portions, it should be looked separately to each of them. One portion consists of income received from government for a specified in advance time period. In order for the Premium to be in accordance to the principle of proportionality, the sum should be proportionate to the required investment in renewable energy installation taking into account that another portion of income is volatile. In most cases the second portion functions fully by the free market principles, therefore no additional requirement can be distinguished.

9. CONCLUSIONS

1. Due to the specific nature of the electricity, internal electricity market and renewable energy support schemes have substantial links with regard to objectives and object. Therefore, pursuant to establish internal electricity market inevitably affects how electricity from renewable resources will be produced and sold. These two factors reflects in the design of support schemes as they try to regulate production in terms of where to produce, how much to produce and sale in terms of cost and in some cases buyers. Against this background it may be suggested that while they share the same object – electricity – and the same objectives – environment protection and energy security – the support schemes will be more and more incorporated into the internal electricity market possibly leading to full convergence.
2. Support schemes convergence possibly removes any possible obstructions for every person to participate in any support scheme and consequently to the free movement of goods. There are two ways to achieve this convergence is top down and bottom up. Currently, no new proposals were made by legislature to foster top down convergence. However, bottom up convergence despite obstructions due to economic disparities between Member States develops quite substantially. One of the ways to address this issue is to finance renewable energy from EU budget or to establish common fond that distributes money in accordance to production efficiency of installations.
3. The general legal pattern of support schemes laid by ECJ is based on the notion that TGC, FIT and Premium have to be designed without disproportionate restrictive measures. These support schemes were chosen for examinations since they are most widely used by Member States. As the issue of proportionality is determined on the case-by-case basis, the answer to the question whether any of the mentioned support scheme contradict to the principle of free movement of goods can only be made on the theoretical level. Applying the legal pattern of ECJ, all examined support schemes are in accordance to the free movement of goods despite restrictive measures inherent in their design. For the purpose of future of support schemes development it may be suggested that a number of restrictive measures should deplete affected by more joint support schemes or other mechanisms leading to common support in the EU and free trade.

REFERENCES

1. CAMPOCCIA A., DUSONCHET L., TELARETTI E., ZIZZO G. An analysis on feed-in tariffs for solar PV in six representative countries of the European Union, Solar Energy 107, (2014) 530–542, 531 p.
2. FAGIANI R., BARQUIN J., HAKVOORT R. Risk-based assessment of the cost-efficiency and the effectivity of renewable energy support schemes: certificate markets versus feed-in tariffs, Energy Policy 55, (2013), 648-661, 659 p.
3. FOUQUET D., JOHANSSON T.B. European renewable energy policy at crossroads – focus on electricity support mechanisms, Energy Policy 36, (2008), 4079-4092, 4086 p.
4. White Paper, Completing the Internal Market, 14 June 1985.
5. Case 6/64, Costa v ENEL [1964] ECR 585.

6. Directive 2009/72 of the European Parliament and of the Council of 13 July 2009 concerning common rules for the internal market in electricity and repealing Directive 2003/54/EC, OJ L211 2009.08.14, Recital 3.
7. Directive 2003/54 of the European Parliament and of the Council of 26 June 2003 concerning common rules for the internal market in electricity and repealing Directive 96/92/EC, OJ L 176 2003.07.15, recital 4.
8. KITZING L., MITCHELL C., MORTHORST P.E. Renewable energy policies in Europe: Converging or diverging? Energy policy 51 (2012) P. 193.
9. Angus Johnston, Guy Block. EU Energy Law, 2012, p.339.
10. Communication from the Commission to the Council and the European Parliament - Report on progress in creating the internal gas and electricity market {SEC(2009) 287} 3 p.
11. Directive 2003/54 of the European Parliament and of the Council of 26 June 2003 concerning common rules for the internal market in electricity and repealing Directive 96/92/EC, OJ L 176 2003.07.15, recital 5.
12. Directive 2009/28 of the European Parliament and of the Council of 23 April 2009 on the promotion of the use of energy from renewable sources and amending and subsequently repealing Directives 2001/77/EC and 2003/30/EC, OJ L 140/16, 2009.06.05, Recital 25.
13. C-573/12 – Ålands Vindkraft Para. 57.
14. Treaty on the Functioning of the European Union, Article 28.
15. Treaty on the Functioning of the European Union, Article 34.
16. Case 8/74, Dassonville, para. 5.
17. Case 120/78, Cassis de Dijon, para. 14.
18. Joined cases C-267/91 and C-268/91, Keck and Mithouard para.16.
19. Mickelsson and Roos, Commission v Portugal, Commission v Italy.
20. Case C‑28/09 Commission v Austria para. 126.
21. Case C-309/02 Radlberger Getränkegesellschaft mbH & Co. and S. Spitz KG v Land Baden-Württemberg para. 75.
22. Case C‑28/09 Commission v Austria para. 120.
23. Case C-309/02 Radlberger Getränkegesellschaft mbH & Co. and S. Spitz KG v Land Baden-Württemberg para. 75.
24. Joined cases C-158/04 and C-159/04 Alfa Vita Vassilopoulos AE and Carrefour Marinopoulos AE v Elliniko Dimosio and Nomarchiaki Aftodioikisi Ioanninon.
25. Joined cases 177/82 and 178/82 Van de Haar [1894] ECR 1797.
26. European Union Law.
27. Case 102/86 Apple and Pear Development Council v Commissioners of Customs and Excise.
28. Case C-171/11 Fra.bo SpA v Deutsche Vereinigung des Gas- und Wasserfaches eV (DVGW) - Technisch-Wissenschaftlicher Verein Para. 25 and 26.
29. Case C-265/95 Commission v. France.
30. Case C‑161/09 Kakavetsos-Fragkopoulos Para. 22.
31. Case C‑161/09 Kakavetsos-Fragkopoulos para. 26.
32. Case C‑161/09 Kakavetsos-Fragkopoulos para. 51.
33. Angus Johnston, Guy Block. EU Energy Law, 2012, 332 p.
34. HAAS R., PANZER C., RESCH G., RAGWITZ M., REECE G., HELD A. A historical review of promotion strategies for electricity from renewable energy sources in EU countries, Renewable and Sustainable Energy Reviews 15 (2011) 1033 p.
35. KITZING L., MITCHELL C., MORTHORST P.E. Renewable energy policies in Europe: Converging or diverging? Energy policy 51 (2012) 194 p.

36. Directive 2009/72 of the European Parliament and of the Council of 13 July 2009 concerning common rules for the internal market in electricity and repealing Directive 2003/54/EC, OJ L211 2009.08.14, Recital 22.
37. Directive 2009/72 of the European Parliament and of the Council of 13 July 2009 concerning common rules for the internal market in electricity and repealing Directive 2003/54/EC, OJ L211 2009.08.14, article 43 section 1.
38. Treaty on the Functioning of the European Union, Article 194 section 2.
39. National overall targets for the share of energy from renewable sources in gross.
10. Final consumption of energy in 2020 Directive 2009/28 annex 1.
40. Joined Cases C‑204/12 to C‑208/12 Essent Belgium Para. 73.
41. Case C-573/12 - Ålands Vindkraft Para. 76.
42. Joined Cases C‑204/12 to C‑208/12 Essent Belgium Para. 121.
43. Joined Cases C‑204/12 to C‑208/12 Essent Belgium Para. 88.
44. Case C-573/12 - Ålands Vindkraft Para. 77.
45. Joined Cases C‑204/12 to C‑208/12 Essent Belgium Para. 91.
46. Joined Cases C‑204/12 to C‑208/12 Essent Belgium Para. 98.
47. Directive 90/377/EEC (price transparency) [1990] OJ L185/16; Directive 90/547/EEC (transit) [1990] OJ L313/30.
48. D. Fouquet, T. B. Johansson, European renewable energy policy at crossroads – focus on electricity support mechanisms, Energy Policy 36, (2008), 4079-4092, 4086 p.
49. CAMPOCCIA A., DUSONCHET L., TELARETTI E., ZIZZO G. An analysis on feed-in tariffs for solar PV in six representative countries of the European Union, Solar Energy 107, (2014) 530-542, 531 p.
50. FAGIANI R., BARQUIN J., HAKVOORT R. Risk-based assessment of the cost-efficiency and the effectivity of renewable energy support schemes: certificate markets versus feed-in tariffs, Energy Policy 55, (2013), 648-661, 659 p.

CYSENI 2015, May 27–28, Kaunas, Lithuania
ISSN 1822-7554, www.cyseni.com

EXPERIMENTAL RESEARCH ON SWELLING AND SHRINKING OF WOOD AND STRAW PELLETS DURING PYROLYSIS

R. Paulauskas, A. Džiugys, N. Striūgas
Lithuanian Energy Institute
Breslaujos str. 3, LT-44403 Kaunas – Lithuania
Phone +370 37 401875
Email: Rolandas.Paulauskas@lei.lt

ABSTRACT

Nowadays renewable energy sources are widely used for electricity and heat production. The growing demand for these stocks and their price results in searching for ways how to use low-quality biofuels. Gasification is one of the options to turn low-quality biofuel into higher quality gas, which is used to generate heat or electricity. However, use of granulated biofuel for the gasification results in fuel agglomeration that stops the entire process. It occurs when the biofuel pellets are moving from the pyrolysis zone to the oxidation zone and pellets stick together in lumps, which disrupts the movement of fuel. In order to investigate the cause and regularities of fuel agglomeration, experimental research of wood and straw pellets thermal deformations during pyrolysis was performed.

Experimental studies were performed in an electrically heated tubular furnace from 300 °C to 1000 °C temperature in an inert atmosphere capturing biofuel pellet thermal deformations by a digital camera. During investigation, the centre temperature of the pellet was also measured. Analysed results showed that biofuel pellet final diameter decreased when the heating temperature increased, but wood pellet diameter shrank 10 % more than straw pellet diameter. It was also established that the wood pellet expanded from 400 °C to 900 °C while straw pellet expanded from 300 °C to 900 °C heating temperature at the beginning of pyrolysis process. The maximum swelling effect was reached at 550°C temperature for wood pellet and at 650 °C for straw pellets and after it, swelling intensity was decreasing till 900 °C temperature for both particles. Overheating temperature of 900 °C, the expansion phenomenon was no longer visible. The obtained results explain the reason for agglomeration of biofuel pellets in the gasifier and reveal regularity of biofuel pellet size changes with increasing heating temperature.

Keywords: pyrolysis, wood pellet, straw pellet, shrinking, swelling

1. INTRODUCTION

Renewable fuel resources are increasingly used for electricity and heat production. The growing demand for these stocks and their price results in searching for ways to use low-quality biofuels. One of the ways – gasification [1]. During this process, obtained a higher quality gaseous fuel from low-quality solid biofuels can be used in industry. Using granulated fuel for gasification process, there are created conditions in which the wood pellets clump together and stop further process. The fuel bridging problem can occur in hoppers [2], oxidation zone due to a high ash continent in fuel [3] and in the pyrolysis reactor zone where fuel drops to the gasification zone. One of the reasons influencing adhesive bond of the fuel particles are changes of wood pellets at high temperatures when the fuel particle expands and shrinks due to the chemical reactions taking place inside, caused by high temperatures. Thermal deformations of the wood pellets affect the fuel movement and mixing. In order to avoid clogging of the reactor, the regularities of this phenomenon are investigated by experimental study on the fuel particles changes at high temperatures during pyrolysis.

Several researchers investigated thermal deformations of wood particles during pyrolysis at 700 ºC temperature [4]. The cylindrical particles with a diameter of 25 mm, length of 300 mm was inserted in an electrically heated vertical furnace where was created an inert environment. The temperature was measured by five thermocouples installed at the sample surface and by one seated in the center of the sample. The results showed that wood particle heated up to 700 ºC during 800 s and shrank till 20 mm in the radial direction.

Scientist group from Sweden [5] researched swelling and shrinking of recovered solid waste pellets (8 mm diameter) during pyrolysis in 500–900 ºC temperature range. The sample was placed on a holder in the horizontal pyrolysis reactor, where the constant temperature and nitrogen flow were maintained. The holder was connected to the digital scales for pellet mass change recording and the pellet surface and center temperature was measured by K-type thermocouples during the pyrolysis process. The change in the size of the pellet was captured by the CCD camera and the collected data analysed using the Image software. Obtained results showed that the recovered solid waste pellets expanded to 54% of the initial volume per 70 s at 550 C heating temperature and after that the particle shrank to the initial volume value per 80 s. The swelling of the pellet reached 58% of the initial volume per 40 s at higher heating temperature (660 ºC). For comparison purposes, the authors repeated the experimental investigation with the straw pellets. The tendency of the straw pellet swelling and shrinking was different: the pellet expanded to 18% of the initial volume at 660 ºC heating temperature and after that began to shrink till 44% of the initial volume [5].

In order to determine the origin of the adhesion of biomass pellets due the expansion and find possible solutions to decrease the risk of the bridging, it is necessary to investigate size changes of biomass pellets at high temperatures. According to this, experimental investigations were performed in the electrically heated horizontal furnace from 300 ºC to 1000 ºC temperature at an inert environment. The wood and straw pellet with 8 mm diameter was captured by the digital camera during the pyrolysis process and the obtained results are presented in this paper.

2. RESEARCH METHODOLOGY

Experimental research of wood and straw pellets swelling and shrinking was carried out using the electrically heated horizontal tubular furnace Nabertherm RS 80/500/13. A scheme of this experimental rig is shown in Fig. 1.

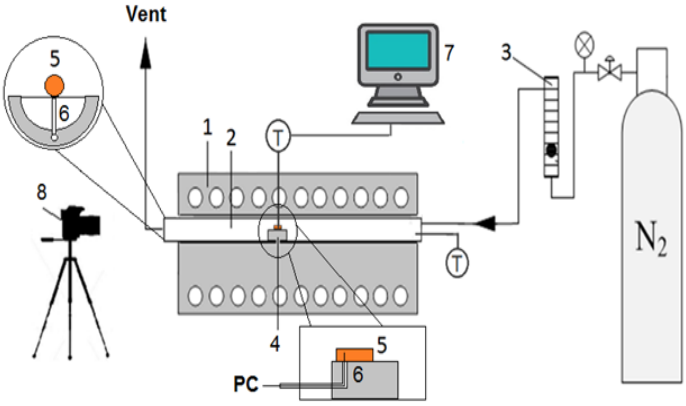

Fig. 1. Scheme of the experimental rig: 1 – electrical furnace RS 80/500/13;
2 – heating tube; 3 – nitrogen flow meter; 4 – sample holder with thermocouple;
5 – wood pellet; 6 – K-type thermocouple; 7 – computer; 8 – digital camera Fuji HS25 EXR

A heating tube (2) with outer diameter of 80 mm and length of 850 mm was mounted inside the furnace (1) and heated on both sides. One end of the tube was supplied by a nitrogen flow, which temperature was measured by an installed K-type thermocouple. The other end of the tube was left open for placement of a special pad with pelletized fuel particle and for capturing the sample size changes. The nitrogen flow of 8 l/min controlled by the flow meter (3) was fed into the furnace when the temperature reached the desired level. The special pad (4) with the sample (5) was inserted in the middle of the working tube through the open end. K-type thermocouple (6) was installed in the pad for sample centre temperature measurement during the pyrolysis process. The measured center temperature values were collected by data logger PICO TC-08 and sent to the computer (7). The pelletized fuel particle was captured with the digital camera Fuji HS25 EXR (8) through the open end of the tube during the pyrolysis process until the pellet stopped shrinking. The digital camera has integrated wide-angle (24–840 mm) lens, and the distance between the camera and the sample was 700 mm. The initial diameter of the sample was measured with a varnier caliper, which provided precision to 0.05 mm before the sample load. The measurements were performed with wood and straw pellets at constant heating temperature from 300 °C to 1000 °C by 50 °C step repeating 5 times. The high-resolution (1920 x 1080 pixels) recorded videos of pelletized fuel particles changes were analysed using GIMP software. Each 150th recorded video frame was converted into a photo and the pelletized fuel particle diameter was measured with a digital ruler in pixels with 0.5 pixel accuracy. The measured sample diameter in pixels was expressed as the relative units. In order to reduce errors due to occurrence of digital processing, the measurements of the wood pellet diameter were repeated 3 times in GIMP program.

3. RESULTS AND DISCUSSIONS

The biomass pellets diameter changes and center temperature profile at 300 °C pyrolysis temperature are presented in Fig. 2.

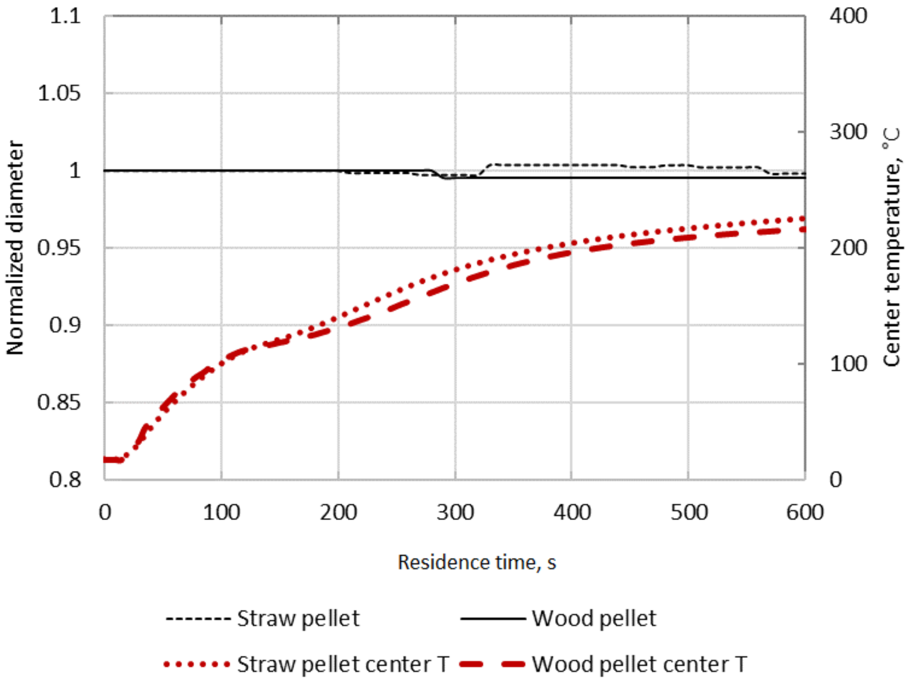

Fig. 2. Biomass pellets diameter changes and center temperature profile at 300 °C heating temperature

At low heating temperature the biomass pellets slowly overheat due to the small amount of heat from ambient causing barely noticeable diameter changes: wood pellet loses 0.5 % of the initial diameter while straw pellet expands 0.3 % of the initial diameter and after 220 s shrinks to original size. The center temperature of both pellets rises till 220 °C (see Fig. 2.). Further increase of the heating temperature to 400 °C, the samples diameter changes became more intensive. When the center of the pellets heats up to 130 C, the swelling phenomenon occurs in both pellets at the same time. Wood pellet expands 0.9% of the original diameter while straw pellet expands 1.5 % of initial diameter. The swelling phenomenon lasts 90 s till the pellets center temperature reaches about 200 °C value (see Fig. 3). After that the expanded pellets starts to shrink. Wood pellet diameter loses 7% of the initial diameter and straw pellet – 8 % of the initial diameter at the end of the pyrolysis process. At the end of the contraction process, the straw pellet center temperature increases from 280 °C to 340 °C which indicates a partial decomposition of pellet when tars are released (see Fig. 3). Due to different structure of samples, temperature peak at wood pellet center is not observed. Both pellets center temperature reaches 305 °C at the end of pyrolysis process.

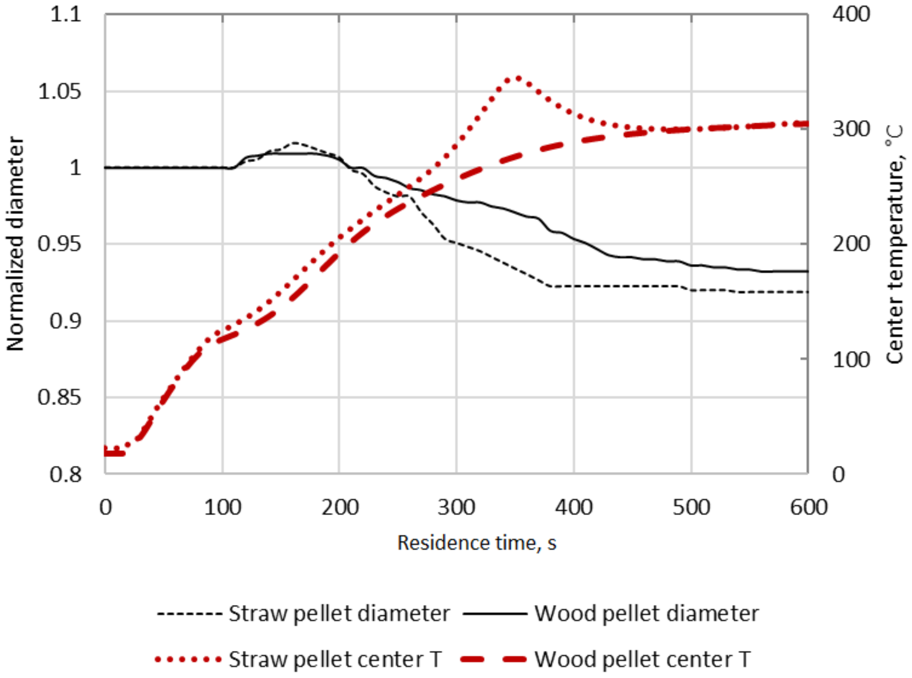

Fig. 3. Biomass pellets diameter changes and center temperature profile at 400 °C heating temperature

The most intensive swelling effect is observed at 600 °C heating temperature. The expansion of both samples is similar: wood pellet expands in the radial direction 3.25% of the initial diameter, straw pellet – 3.5 % (see Fig. 4.). During pyrolysis of the pellets, the center temperature curves are different: straw pellet overheats 120 s quicker then wood pellet what indicates faster decomposition of straw pellet. After the expansion, the pellets shrinks for 180 s and straw pellet loses 15% of the initial diameter, wood pellet – 24%.

At higher temperature (1000 °C) only the shrinkage of pellets is detected. The straw pellet shrinks in radial direction by 16% of the initial diameter, wood pellet – 22 % of the initial diameter (see Fig. 5). The center temperature profile shows that straw pellet overheats faster than wood pellet till the shrinking of the pellets stops.

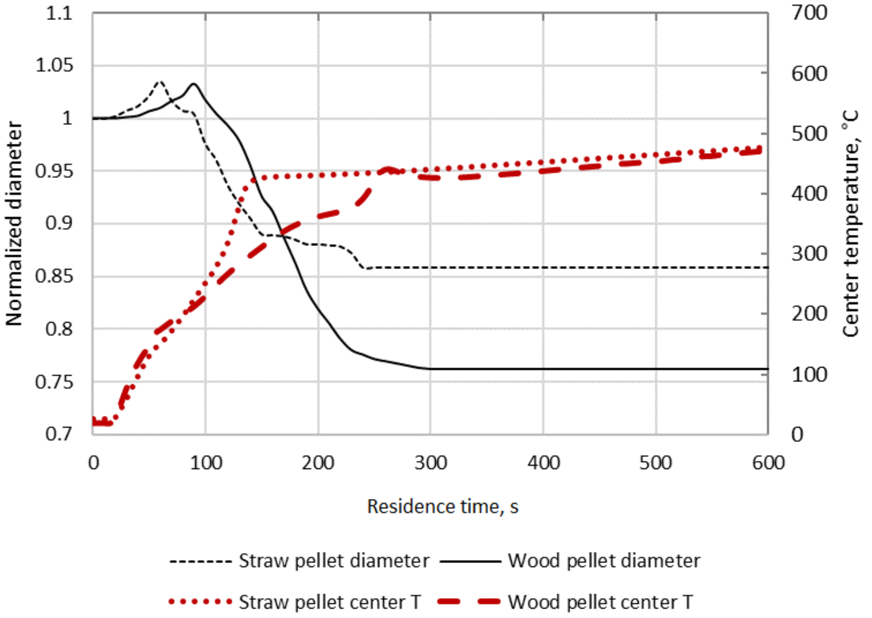

Fig. 4. Biomass pellets diameter changes and center temperature profile at 600 °C heating temperature

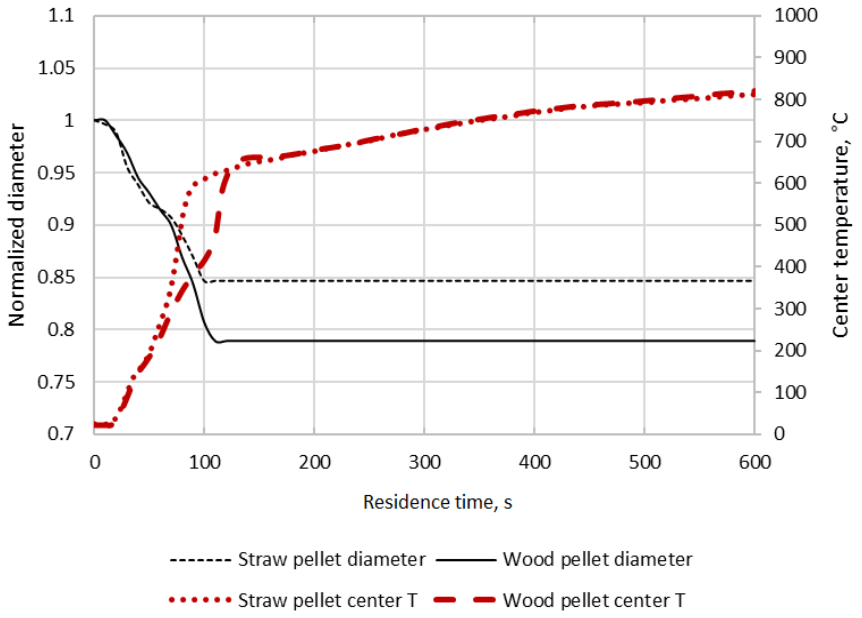

Fig. 5. Biomass pellets diameter changes and center temperature profile at 1000 °C heating temperature

The results show that the pellet diameter changes depend on the pyrolysis temperature and heat transfer in the particles. The heat flow is higher from the reactor environment to the particle and volatile release mechanism also is different at higher temperatures. The expansion of the pellets is due to a slow heat transfer which influences volatiles release from pellets. When the particle heats evenly at low temperatures (till 300 °C), the pressure of water vapour and volatiles compounds do not reach a critical value inside the particles and the pellets surface is not destructed by water and volatile diffusion from it. The higher heating temperature (from 300 °C to 700 °C) causes the pellets quickly overheat resulting in failure of water and volatiles diffusion from pellet. In this way, water vapour and volatiles accumulate inside the pellet and internal pressure is growing near the pellet surface. When the internal pressure is too high, it destroys the surface structure of the pellets by expanding pellet and freeing accumulated water vapour and volatiles. Shrinkage of pellets begins after volatiles evaporation.

However, the pellets expansion decreases above 700 °C temperature, what maybe it is due to the faster particle heating. The particle overheats so quickly that emitted compounds from the surface layer decompose by high temperatures and the way for volatiles evaporation is open from the deeper layers. The expansion phenomenon is no longer detected over 900 °C temperature.

4. CONCLUSIONS

Experimental investigation of wood and straw pellet shrinkage and swelling during pyrolysis process can be summarized in few statements. The observed changes of biomass pellets diameter and the center temperature variation reveal that when increasing the heating temperature from 300 C to 1000 C, the wood pellet loses from 0.5% to 24% of the initial diameter respectively while straw pellet loses from 0.2% to 16%. This is due to a higher ash content in straw pellets (straw pellet ~ 7%, wood pellet ~0.4%). At low temperatures (up to 400 C), the center of the biomass pellets heats evenly up to 230 C temperature and only water evaporation and negligible fuel decomposition occur; the latter process influences the pellet shrinking only by 0.1–0.5% of the initial diameter. At higher 400 C heating temperature, the decomposition process is more intensive due to the higher amount of heat what causes the pellets expansion approximately till 1.5% of the initial diameter. The swelling phenomenon intensifies with the heating temperature increase up to 600 C causing maximum expansion: wood pellet by 3.25%, straw pellet 3.5% of the initial diameter. When the heating temperature is higher than 600 C, expansion of pellets starts decreasing and disappears when the temperature is higher than 900 C due to the intensive biomass decomposition which causes full release of volatiles and char formation. The expansion phenomenon is no longer observed at 1000 °C temperature.

According to the obtained results it can be stated that the fuel agglomeration in the gasifier using biomass pellets occurs due to the pellet expansion in pyrolysis zone between 400 and 900 C temperatures. In order to avoid the bridging problem it is necessary to maintain 900 C temperature at the end of the pyrolysis zone of gasifier.

REFERENCES

1. STRIŪGAS, N., ZAKARAUSKAS, K., DŽIUGYS, A., NAVAKAS, R., PAULAUSKAS, R. An evaluation of performance of automatically operated multi-fuel downdraft gasifier for energy production. *Applied Thermal Engineering*, 2014, Vol. 73, Issue 1, p. 1149–1157.
2. HAMEL, S., HASSELBACH, H., WEIL, S., KRUMM, W. Autothermal two stage gasification of low density waste derived fuels. *Energy*, 2007, Vol. 32, p. 95–107.
3. PATERSON, N., ZHOU, Y., DUGWELL, DR., KANDIYOTI, R. Investigation of ammonia formation during gasification in an air blown spouted bed: reactor design and initial tests. *Energy Fuels*, 2002, Vol. 16, p. 127–35.
4. LARFELDT, J., LECKNER, B., MALAAEN, M.C. Modelling and measurements of the pyrolysis of large wood particles. *Fuel*, 2000, Vol. 79, p. 1637–43.
5. ZHOU, C., ZHANG, Q., ARNOLD, L., YANG, W., BLASIAK, W. A study of the pyrolysis behaviors of pelletized recovered municipal solid waste fuels. *Appl Energy*, 2013, Vol. 107, p. 173–82.

CYSENI 2015, May 27–28, Kaunas, Lithuania
ISSN 1822-7554, www.cyseni.com

BIOMASS QUALITY OF TALL FESCUE GRASS UNDER DIFFERENT FERTILIZATION AND IN-FIELD LEACHING SYSTEMS

L. Pocienė, V. Tilvikienė, S. Lazauskas, Ž. Kadžiulienė
Institute of Agriculture, Lithuanian Research Centre for Agriculture and Forestry
Instituto al. 1, Akademija, Kėdainiai distr., LT-58344 – Lithuania
Phone+37065420788
Email:linapociene1@gmail.com

ABSTRACT

Utilization of bio-based resources to replace fossil fuels has the potential to make progress because of their variable composition and properties which depend on the systems applied. Tall fescue grass (TFG) was investigated in an experiment conducted on an *Endocalcari-Epihypogleyic Cambisol*. The study was aimed to determine the gross calorific value and ash content of biomass as influenced by different fertilization and in-field leaching systems. The composition of the biomass in per cent weight of silicon (Si) and potassium (K), which are the major components of ash, was established. Gross calorific value was a measure of the energy content of biomass samples expressed in MJ kg^{-1}. Energy content was measured with a colorimeter IKA C200. The data suggest that non fertilization and fertilization of plants and in-field leaching 2 weeks with additional precipitation and without them substantially increased the calorific value of TFG compared with fertilized and non fertilized samples and in-field leaching for one week. The highest gross calorific value (almost 19 MJ kg^{-1}) was obtained from tall fescue grass fertilized with N_{90} with the application of a two-week in-field leaching system with additional precipitation imitation. The biomass of grass fertilized with N_{90} and N_0 and exposed to in-field leaching for one week contained the lowest concentration of ash, which is a desirable feature for combustion process. In this experiment, Si reduction occurred only in in-field leaching and non-leaching systems with mineral and digestate fertilization. A significant difference of fertilization and in-field leaching reduction of the concentration of potassium in ash were founded especially in fertilized with digestate and non fertilized samples with one week in-field leaching system with and without additional precipitation level.

Keywords: Tall fescue grass, biomass, fertilization, in-field leaching

1. INTRODUCTION

Developments in modern eco-energy production system is widely analyzed in all countries of the world, especially those that are not having fossil fuels resources [1–4]. The interest in the use of biomass on agricultural lands for solid bio fuels in Europe, North America, and Asia has been increasing for the last several years [5].

Lithuania has a vast capacity for energy production. Properly trimmed available biomass sector, from its own resources, could make even the 70 percent of current energy demand and thus not only meet the EU Directive that are complied for Lithuania, but also greatly exceed them.

The one of most suitable source for bio energy in agriculture are perennial grasses [3, 4]. Perennials can be grown in one place without reseeding more than 10 years; they do not require a lot of fertilizer and their quality can be managed by the cutting frequency, fertilization or by choosing the most suitable variety of grasses [5–8]. Different requirements of biomass quality are for biogas production and for solid fuels, but there is one, which is the same for all bio energy sources – it is biomass yield [9, 10].

The aim of supplying biomass for combustion is to achieve high energy yield per unit area (GJ ha^{-1}) and best possible fuel quality. The energy yield comprises the biomass yield

(t_{DM} ha^{-1}) and the energy content of the biomass (MJ t_{DM}^{-1}). Fuel quality is determined by the physical and chemical properties and influences the entire process of thermal utilization [6].

This study investigated the variability in herbaceous biomass quality for combustion fuel characteristics due to the direct effect of selected agronomic treatments, precisely crop species, nitrogen fertilizer application rate and origin (mineral or organic), harvest time and in-field leaching. The fuel characteristics floated by using proximate and ultimate analyses, energy content (gross caloric value) and ash composition. The composition of the biomass in per cent weight of silicon (Si) and potassium (K), which are the major components of ash, was established.

2. METHODOLOGY

Samples of tall fescue grass biomass for this study were collected from experimental field plots located at the Institute of Agriculture, Lithuanian Research Centre for Agriculture and Forestry (lat. (55° 40′ N, 23° 87′ E)). The soil at this site is a Endocalcari-Epihypogleyic Cambisol with loam texture. The experiment was designed as randomized complete block with three replicates. Plot size was 3x10 m. Harvested plot size – 25 m^2.

P and K fertilization was applied on all the area before sowing grasses to average nutrition rate. In the first year, N_{45} was applied as a started to stimulate growth. In the second year, nitrogen fertilization scheme N_0, N_{90} – mineral and organic (digestate) was developed. Nitrogen fertilization was continued each year after resumption of vegetation. Perennial grasses were cut one times per year on fall (October).

Ultimate analysis provided the composition of the biomass in percent weight of the major components for ash and slag forming elements Potassium (K) and silicon (Si). Gross calorific value was a measure of the energy content of biomass samples expressed in MJ kg^{-1}. Individual plant species biomass chemical composition analyzes were conducted to evaluate in LRCAF agronomy institute analytical laboratory. Gross calorific value was measured with a colorimeter IKA C200.

Statistical analyses were performed on the measured data as well as computed indices to determine the averages and standard errors of all the data.

3. RESULTS

Proximate analysis was used to determine content of ash. In our research ash content varied with the agronomic treatment too.

Tall fescue grass was affected to the fertilization with organic nitrogen (digestate). Before in-field leaching system applying the average ash content are located as fallow (from highest to lowest) 7.09% on non fertilized 7.05 % on fertilized with N90 (mineral) and 6.36% on fertilized with digestate (N90 organic). In-field leaching, as agricultural treatment, show highest effect on samples which were left for self leaching for one week in field after harvesting and which got additional water (precipitation imitation) for 25mm of water (Fig. 1).

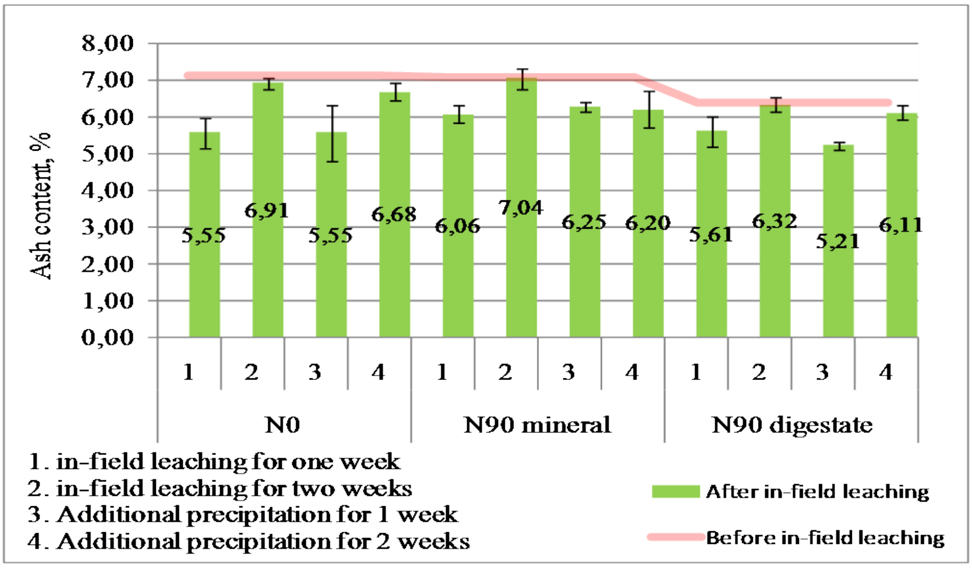

Fig. 1. Ash content in tall fescue grasland before in-field leaching and after

In our experiment silicon content in tall fescue biomass strongly depends from fertilization and in-field leaching system applying. (Fig.2.) Higher Si content were reached on non-fertilized samples before applying in-field leaching and there amount of silicon was 0.67%. Fertilization with mineral and organic N_{90} reduced silicon level to 0.44% and 0.50 % in mineral and digestate as follows. In-field leaching shows promising results especially in fertilized samples. Lowest average level of silicon was reached on samples with fertilization of mineral N_{90} and all in-field leaching systems.

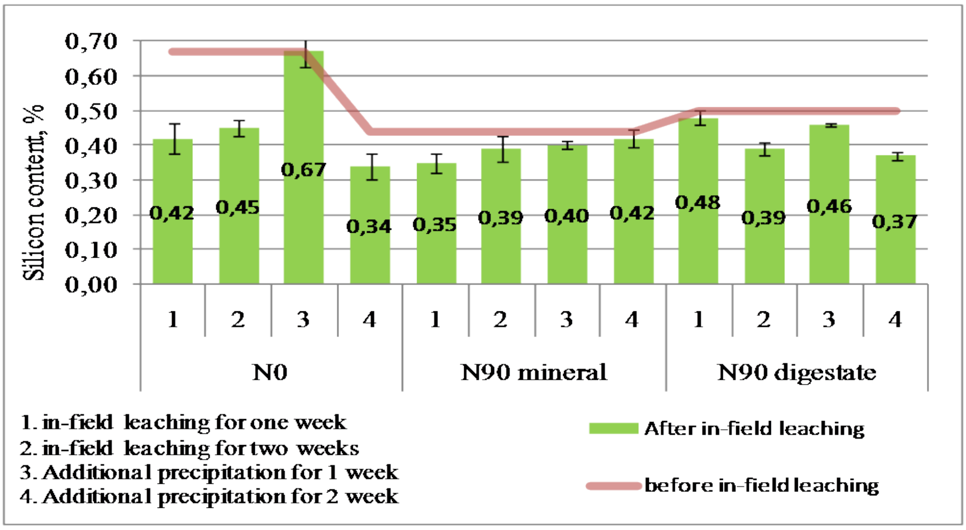

Fig. 2. Silicon in the ashes of tall fescue before in-field leaching and after

Level of potassium in this experiment was always opposite to level of silicon (Fig. 3). As columns 3; 9; 11 in silicon chart shows biggest level of silicon as same columns in K chart are smallest. As data suggested there is high difference in non leached and leached samples. Non leached samples of non-fertilized, fertilized with mineral and fertilized with digestate were distributed as follows: 1.51; 1.49; 1.57 % of K in dry matter. After application of in-field leaching data have changed to lowest side in all samples, especially in those which were left in field for one week with additional precipitation and without.

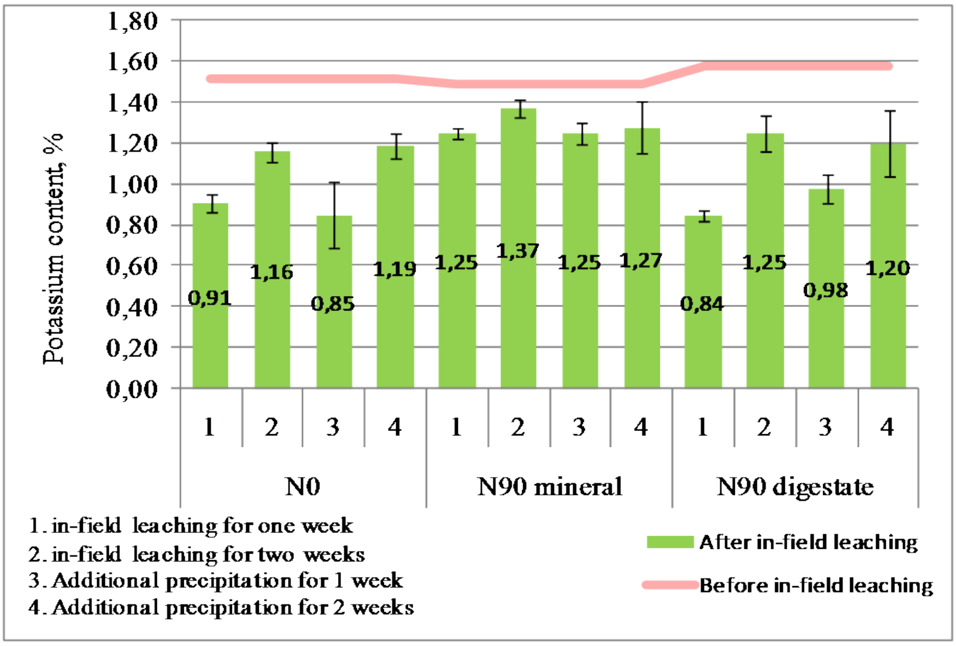

Fig. 3. Potassium in the ashes of tall fescue before in-field leaching and after

Highest calorific values were achieved after applying the in-field leaching for two weeks without precipitation imitation. Overall, management measures to improve fuel quality such as delaying harvest and reducing level of fertilization [11]. Without application of leaching our research shows exactly the same result.

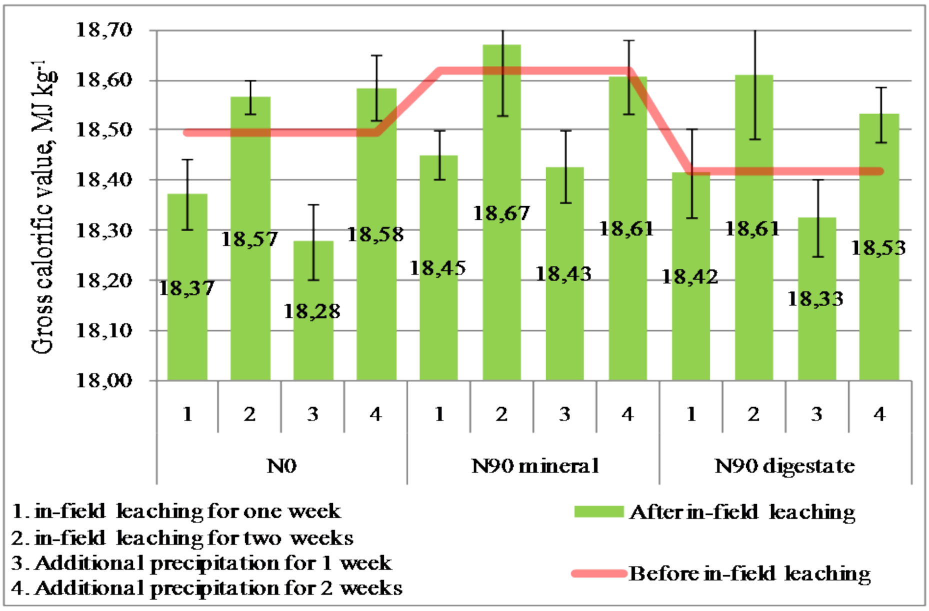

Fig. 4. Gross calorific value of tall fescue under different agronomical treatment

4. DISCUSSION

Ash content in the herbaceous energy crop biomass depends on a large number of factors including plant type, plant fraction, growing conditions, fertilization, harvest date, harvest techniques, and conversion systems. In this research the fertilization and in-field leaching as agronomical treatment were analyzed. Some doubts emerged, for example, why ash content is higher in those data columns where it should be lower because of lower Silicon amount in them. Only one answer is possible to this question – the reason is soil structure, Si could be higher in soils with much clay in them. And of course bigger ash content means lower heating value [12]. Chemical composition of grass biomass can be extremely variable, depending on soil fertility, and harvest management. This confirmed the results of research, by A. Prochnow and others [13, 14], that the extensive grassland management system with one late cut and low level of fertilization (better organic) is favoured for grass as a solid bio fuel especially tall fescue grass. Soil type and inherent soil fertility can strongly impact mineral uptake, which is very important for grass chemical characteristics [15]. In general, approximately one half of the total ash content of grass is silicon. Silicon, especially in combination with K and other elements (not so powerful as K), affect the ash melting behaviour in grasses. High total Si content result in lower energy content [16]. The same results have been gotten in our research too. Harvest management can have a major impact on grass composition, particularly for water soluble components such as K [16]. Potassium level in the research was similar to Ogden at.al.[17] and Kludze at.al.[18] studies in which a reduction of K is a result of field leaching in relation to harvest time. Highest calorific values were got after applying the in-field leaching for two weeks without precipitation imitation. Overall, management measures to improve fuel quality such as delaying harvest and reducing level of fertilization [13].

5. CONCLUSION

Low level of fertilization (better organic) is favoured for grass as a solid bio fuel. Hence, grassland management for solid biofuel production has to be directed primarily at raw material quality and in second instance at biomass yields. Applying an in-field leaching shows promising results in all (ash, Si and K) elements reducing data. But optimum gross calorific value was reached after in-field leaching with additional two weeks (50mm) of precipitation was added. The selected traditional energy crop showed the promising results of it productivity for combustion in the first year of sward use, however for more accurate material more studies are needed.

ACKNOWLEDGEMENTS

This work was part of ESF project “Scientific validation of C3 and C4 herbaceous plants’ multi-functionality for innovative technologies: phyto-raw materials – bio-products – environmental effects” (VP1-3.1-ŠMM-08-K-01-023).

REFERENCES

1. ASKEW M.F. In.: Grassland: a global resource. By: D.A. McGilloway. p. 179–187.
2. HEATON E., VOIGT T., LONG S. A quantitative review comparing the yields of two candidate C_4 perennial biomass crops in relation to nitrogen, temperature and water. *Bioresource Technology*, 2004, Vol. 27, Nr.1. p. 21–30.
3. WELTZIN J.F., LOIK M.E., SCHWINNING S. *et al*. Assessing the response of terrestrial ecosystems to potential chantes in precipitation. *BioScience*, 2003, Vol. 53, No. 10. p. 941–952.
4. LEWANDOWSKI I., SCURLOCK J.M.O, LINDWAL E., CHRISTOU M. The development and current status of perennial rhizomatous grasses as energy crops in the US and Europe. *Biomass and Bioenergy*, 2003, Vol. 25, Iss. 4, p. 335–361.

5. MUSSHOFF O. Growing short rotation coppice on agricultural land in Germany: a real options approach. *Biomass and Bioenergy*, 2012, Vol. 41, p. 73–85.
6. CEOTTO, E. Grasslands for bioenergy production. A review. *Agronomy for Sustainable Development*, 2008, Vol. *28(1)*, p. 47–55.
7. GUNASEELAN, V.N. Anaerobic digestion of biomass for methane production: a review. *Biomass and Bioenergy*, 1997, Vol. 13, p. 83–114.
8. HEJDUK, S., HRABĚ, F. Influence of different systems of grazing, type of swards and fertilizing on underground phytomass of pastures. *Plant, Soil and Environment*, 2003, Vol. 49, p. 18–23.
9. KANAPECKAS J., LEMEŽIENĖ N., TARAKANOVAS P., NEKROŠAS S., PAPLAUSKIENĖ V. Dependence of the productivity and qualityof perennial grasses on time of heading. *Agricultural Sciences* 1999, Vol. 1, p. 10–16.
10. KANAPECKAS J., LEMEŽIENĖ N., BUTKUTĖ B., STUKONIS V. Evaluation of tall fescue (*Festuca arundinace* Scherb.) varieties and wild ecotypes as feedstock for biogas production. *Žemdirbystė=Agriculture*, 2011, Vol. 98, No. 2, p. 149–156.
11. LEMEŽIENĖ, N., KANAPECKAS, J., BUTKUTE, B. Varieties, breeding lines and ecotypes of cocksfoot (*Dactylis glomerata* L.) that are the most suitable for biogas production. *Žemdirbystė=Agriculture*, 2009, Vol. 96, p. 36–46.
12. JENKINS B.M., BAKER R.R., WEI J.B. On the properties of washed straw.*Biomass and Bioenergy*, 1996, Vol. 10, p. 17–46.
13. PROCHNOW, A., HEIERMANN, M., PLÖCHL, M., LINKE, B., IDLER, C., AMON, T., HOBBS, P. Bioenergy from Permanent Grassland – A Review: 1. Biogas. *Bioresource Technology*, 2009, Vol. 100, p. 4931–4944.
14. PROCHNOW A., HEIERMANN M., PLOCHL M., LINKE E.B., IDLER C., AMON T., HOBBS P.J. Bioenergy from Permanent Grassland – A Review: 2. Combustion. *Bioresource Technology*, 2009, Vol. *100*, p. 4945–4954.
15. BURVALL J. Influence of harvest time and soil type on fuel quality in reed canary grass. *Biomass Bioenergy*, 1997, Vol. 12, p. 149–154.
16. CHERNEY H.J., VERMA K.V. Grass pellet Quality Index: A tool to evaluate suitability of grass pellets for small scale combustion systems. *Applied Energy*, 2013, Vol. 103, p. 679–684.
17. OGDEN C., ILELEJI K., JOHNSON K., WANG Q. In-field direct combustion fuel property changes of switchgrass harvested from summer to fall. *Fuel Processing Technology*, 2010, Vol. 91, p. 266–271.
18. KLUDZE H., DEEN B., DUTTA A. Impact of agronomic treatments on fuel characteristics of herbaceous biomass for combustion. *Fuel Processing Technology*, 2013, Vol. 109, p. 96–102.

CYSENI 2015, May 27–28, Kaunas, Lithuania
ISSN 1822-7554, www.cyseni.com

HEAVY METALS CONCENTRATION IN STEMWOOD OF ENERGETIC TREES FERTILIZED WITH SEWAGE SLUDGE

M. Praspaliauskas, N. Pedišius
Lithuanian Energy Institute
Breslaujos str. 3, LT-44403 Kaunas, Lithuania
Phone+37062251687
Email: Marius.Praspaliauskas@lei.lt

A. Gradeckas
Institute of Forestry, Lithuanian Research Centre for Agriculture and Forestry
Liepų Str. 1, Girionys, LT-53101 Kaunas distr., Lithuania
Phone *+370 37 547221*
Email: a.gradeckas@gmail.com

ABSTRACT

Energetic trees have been grown in the areas fertilized with different amount of sewage sludge: 180, 360, 720 t/ha, and in a not-fertilized area (Ežerėlis peatbog). Hybrid poplar (*Populus tremula x Populus tremuloides*), developed for energetic plants, three local trees species: *Alnus incana* (L.) Moench, *Betula pendula* Roth, *Picea abies* (L.) H.Karst., potentially promising for energetic plantations, and one introduced species (*Acer negundo* L.) have been investigated. These plantations were established by Lithuanian Forests Research Institute (now Institute of Forestry, Lithuanian Research Centre for Agriculture and Forestry) in 1993.

During the investigation period, the concentrations of heavy metals (Cd, Cr, Cu, Ni, Pb and Zn) in the stemwood of trees grown in fertilized and not-fertilized plots were determined. Cd and Cr were found only in some wood samples and their concentration was close to the limits of detection. Consequently, more detail analyses of these metals was not carried out.

The study findings showed that significantly high amounts of Zn, Cu and Cr but lower amounts of Pb, Ni entered the soil with sludge and their high level concentrations remained for two decades. During 20-year period, total concentration of these metals in the soil decreased by 17, 26 and 40 % when they were fertilized by 180, 360 and 720 t/ha of sludge, respectively. However, trees accumulated very limited amount of heavy metals in their stemwood regardless of fertilization intensity. The following sequence of heavy metals accumulation factor in the analyzed trees stemwood was found: Zn > Pb > Ni > Cu > (Cr, Cd).

Keywords: sewage sludge, heavy metals, soil, energetic trees, stemwood, accumulation factor, saturation limit

1. INTRODUCTION

Cultivation of energetic trees plantations for energetic purpose becomes particularly important due to the permanent decrease of the fossil energy resources (oil, coal, natural gas, etc.) and fast increase of its price, as well as of the continued growth of greenhouse gas emissions. On the basis of the survey results and the assessment of the subsidies needed for replacement of fossil fuel by alternative fuel from biomass, short rotation trees plantations have been recognized as the promising alternative for energy production compared to other types of biomass. Therefore the development of such trees plantations for energetic purposes becomes one of the public policy objectives for each country that engaged to follow International conventions for environment protection [1].

Recently, the growing demand for wood fuel and the increasing quantities of sewage sludge force to develop integrated solutions. One of such solutions is the cultivation of energetic trees in plantations being fertilized with sewage sludge. However, such utilization of sewage sludge still remains under discussion, because it contains high levels of pollutants accumulated, for example heavy metals (hereinafter referred to as HM) that cause groundwater pollution. HM are also accumulated in trees that have recently been increasingly used for energy production. Studies show that the concentration of HM is distributed within stemwood in the following sequence: Zn > Cu > Cd > Ni > Pb > Cr [2]. When energetic trees plantations are fertilized with sewage sludge, the HM accumulation within stem, branches and leaves of trees is not-homogeneous. Long-term observations and studies [3, 4] show that within the stemwood of *Larix decidua and Populus trichocarpa x P. deltoides* HM have a tendency to be accumulated in a constant manner as they do not participate in the decomposition cycle.

2. MATERIALS AND METHODS

2.1 Plantation establishment and initial evaluation

Five tree species (Table 1) and their hybrids had been chosen for the tests. Plots were established with four replicates by 30 two-five years old trees, planted in rows (1×3 m), planting density was 3300 unit/ha, height of saplings was 0.5–1.0 m [5].

The studied plantations were established by Lithuanian Forests Research Institute (now Institute of Forestry, Lithuanian Research Centre for Agriculture and Forestry) in 1993 Ežerėlis peatbog Kaunas district [5].

Fig. 1. View of energetic trees plantation after 20 years: ○ – sampling locations

In November 2013, samples of 20-year old trees and soil of the plantation were collected. The analysed tree species were as follows:

- Grey alder (*Alnus incana* (L.) Moench);
- Silver birch (*Betula pendula* Roth);
- Common aspen x American aspen (*Populus tremula* L. x *P. tremuloides* Michx.);
- Norway spruce (*Picea abies* (L.) H.Karst.);
- Box elder (*Acer negundo* L.).

170 stemwood samples were taken at 1.3 meters above-ground using a Pressler drill.

In each treatment, five samples of mineral soil were randomly taken using a soil-scoop. Upper 0–6 cm depth soil layer was sampled in not-fertilised plantation. Soil samples in fertilised plantations were sampled as follows: at 8 cm depth – in the fertilised with 180 t/ha plantation, at 16 cm – in the 360 t/ha, at 24 cm – in the 720 t/ha (totally there were 20 soil samples). The wastewater sludge in 1993 have been spreaded entirely on surface with three layers of different thickness 8, 12, 24 and 6 cm. In that way there have been four variants of experiment: minimal dose – 180 t/ha, middle – 360 t/ha, maximal – 720 t/ha of dry matter and not fertilized variant.

Table 1. Total number of tree stemwood and soil samples taken from the plantations in 2013

Fertilization doses **Tree species**	**0 t/ha**	**180 t/ha**	**360 t/ha**	**720 t/ha**
Grey alder (*Alnus incana* (L.) Moench)	9	6	6	6
Silver birch (*Betula pendula* Roth)	10	12	10	10
Common Aspen x American Aspen (*Populus tremula* L. x *P. tremuloides* Michx.)	5	8	9	10
Norway spruce (*Picea abies* (L.) H.Karst.)	8	9	9	9
Box elder (*Acer negundo* L.)	9	9	7	9
Soil samples	5	5	5	5

2.2 Laboratory analysis

In the laboratory the stemwood and soil samples were dried for 18 hours within a laboratory low temperature electrical furnace SNOL60/300 LFN at 105 ºC. The dried stemwood samples were retained in a desiccator to the room temperature and then mechanically chopped into (3–4) mm chips.

The samples of soil and stemwood chips (approx. 0.4 g) were placed into 100 ml inert test-tubes designed for mineralization and flooded with 8 ml of concentrated nitric acid (HNO_3 Supra-quality ROTIPURAN Supra 69 %). After that the samples were placed into a mineralizer Multiwave 3000 (8 samples per one cycle) and mineralized for 1 hour 15 minutes (at 750 W power, p_{Lim}: 60 bar, p_{Rate}: 0.3 bar/s), from which 15 minutes were allocated for heating, 45 minutes for mineralization in accordance with the established parameters and 15 minutes for cooling.

After the mineralization, the solution was poured into 50 ml flasks and diluted with deionized water to 50 ml. The analysis of the solutions prepared from the different stemwood and soil samples was performed using an inductively coupled plasma optical emission spectrometer ICP-OES. The analytical wavelengths were 288.802 nm for Cd, 267.716 nm for Cr, 327.393 nm for Cu, 231.604 nm for Ni, 220.353 nm for Pb and 206.2 nm for Zn.

2.3 Statistics and calculations

The data was statistically analysed using STATISTICA 7 software. Mean values with standard error (SE) and standard deviation (SD) were calculated for each species at each fertilization plot from results of chemical analysis.

Bioconcentration factor or accumulation factor (AF) was calculated in percent according to the following equation [6]:

$$Accumulation\ \ factor\ \ (AF) = \frac{C_{wood}}{C_{soil}} \times 100\,; \tag{1}$$

here AF – accumulation factor %; C_{wood} – metal concentration in plant tissue; C_{soil} – metal concentration in soil.

To ascertain the significance of differences of metal accumulation between different fertilization and different tree species, the mean values were further statistically evaluated with a one-way analysis of variance (ANOVA) F-test, followed by Tukey lines method and calculate regression (95% confidence) for a p = 0.05 significance level and r – the coefficient of correlation. In order to demonstrate relation between two variables, the relation was described as a linear function (2) or a second degree polynomial (3) in the most cases:

$$C_{HM} = A \pm B \times I\,, \tag{2}$$

$$C_{HM} = A - B \times I + C \times I^2; \tag{3}$$

here C_{HM} – cumulate metal concentration in stems; A, B and C – coefficients; I – intensity of sludge fertilization.

3. RESULT AND DISCUSSION

3.1 Metals concentration in soil after fertilization in 1993 and 2013

Table 2 shows the initial HM concentrations in the soil after sewage sludge fertilization of the plantation in 1993, [5] and their concentrations in the soil after 20 years, in 2013.

Table 2. HM concentrations in the plantation soil in 1993 [5] and 2013

Fertilization doses, t/ha	**HM, mg/kg**											
	Cd		**Cr**		**Cu**		**Ni**		**Pb**		**Zn**	
	1993	**2013**	**1993**	**2013**	**1993**	**2013**	**1993**	**2013**	**1993**	**2013**	**1993**	**2013**
0	-	<0.19	20.6	52.4	8.6	5.10	6.9	14.1	10.3	2.6	75.8	12.3
180	-	0.34	73.1	171.6	121.8	97.8	32.2	49.2	72.5	26.2	362.3	204.5
360	-	1.38	89.3	217.9	459.0	134.7	45.9	84.0	57.8	37.0	357.3	270.5
720	-	1.71	100.6	244.5	845.3	184.9	61.2	86.6	80.0	50.4	417.6	329.9

In spite of the facts that sewage sludge was taken from the storage, where it was saved for several years. Initial analysis of fertilized and reference non-fertilized soil was carried out before 20 years. Applied analysis methods and instruments in 1993 were different from those used in 2013. Plantation was established in few acid high-moor peatland, it is possible to make up some concluding remarks, especially taking into account the variation of total HM concentration.

After 20 years, the total HM concentration in the soil decreased in proportion to its initial concentration. Compared to the initial concentration values in 1993, the total concentration in 2013 decreased by 17, 26 and 40% correspondingly to earlier indicated concentrations of fertilization but remained high even after 20 years. Such decrease was caused by various factors, the most probable of which were leaching to the ground-water under acid conditions and tree uptake – roots, stemwood, bark, leaves [7].

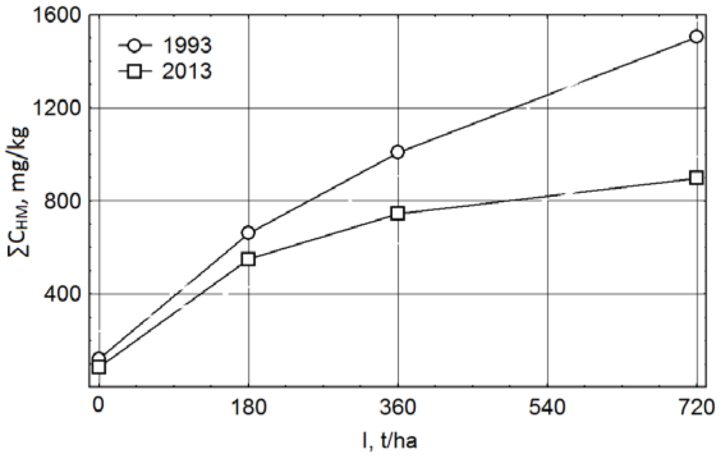

Fig. 2. Dependence of total Cr, Cu, Ni, Pb and Zn concentration in the soil on the intensity of fertilization in 1993 [5] and after 20 years in 2013

3.2 Metals accumulation in the tree stemwood

Table 3 shows the concentrations of individual metals (Cu, Ni, Pb and Zn) that were measured in stemwood of all investigated tree species. Cd and Cr were found only in some wood samples and their concentrations were close to the limits of detection or qualification. Analysis of these elements results are not presented in the discussion section.

The results demonstrate that during 20 years the trees accumulated a small HM amount from the sewage sludge with which the soil was being fertilized. Various hypotheses are made about soil acidity, composition, parameters of materials used for fertilization and even dilution. According to literature concentrations of the elements are "diluted" in the case of wood biomass increase [8].

Table 3. Cu, Ni, Pb and Zn concentration (mean value, mg/kg ± SD) in stemwood of various tree species after the soil fertilization with different amount of sewage sludge

Tree species HM in plots		**Grey alder**	**Silver birch**	**Common aspen x American aspen**	**Norway spruce**	**Box elder**
0 t/ha	Zn	33.56±1.04	24.4±13.22	32.77±7.71	32.44±4.53	10.44±1.17
	Pb	6.26±1.42	8.43±0.06	4.62±0.42	5.65±0.59	5.98±1.50
	Ni	2.37±0.40	2.5±0.33	1.12±0.09	2.24±0.40	2.14±0.52
	Cu	1.99±0.59	0.75±0.02	0.66±0.2	1.44±0.27	4.6±1.86
180 t/ha	Zn	34.48±1.55	43.45±10.94	49.20±6.93	25.29±4.99	4.74±1.0
	Pb	5.75±0.83	7.00±1.02	5.00±0.46	5.29±0.61	4.74±1.0
	Ni	2.25±0.12	2.26±0.36	1.51±0.25	1.65±0.15	1.97±02
	Cu	2.9±0.37	0.65±0.09	1.26±0.22	1.35±0.32	1.39±1.14
360 t/ha	Zn	34.20±1.58	35.05±11.59	50.25±8.9	17.93±4.0	4.6±3.04
	Pb	5.85±1.39	6.12±0.81	5.27±0.55	5.72±0.65	5.23±0.95
	Ni	1.66±0.27	2.06±0.28	1.58±0.26	1.62±0.16	1.73±0.43
	Cu	3.24±0.45	0.67±0.05	1.2±0.23	0.52±0.27	0.89±0.7
720 t/ha	Zn	34.79±1.4	31.61±9.43	34.70±4.96	18.03±2.74	5.54±1.49
	Pb	5.72±0.72	5.72±0.65	5.56±0.42	5.17±0.72	4.77±1.3
	Ni	2.18±018	1.86±0.22	1.60±0.22	1.74±0.24	1.43±0.48
	Cu	2.95±0.35	0.49±0.22	0.75±0.37	0.42±0.18	0.6±0.21

With regards to the individual metal, the accumulated HM content in the stemwood sampled from the fertilized trees maintain the same stable trend as from the not-fertilized area: Zn > Pb > Ni > Cu. However, the cumulative quantities are not statistically significant than ones in the control trees.

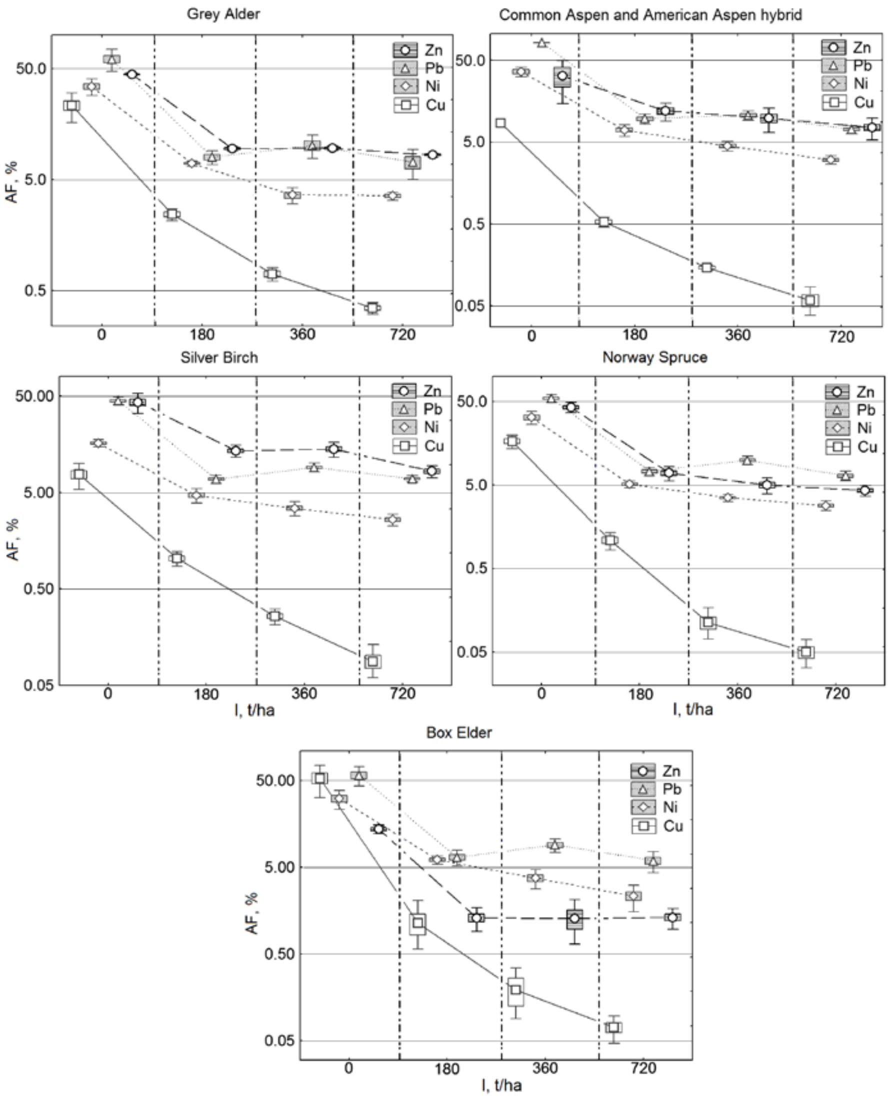

Fig. 3. Dependence of Cu, Ni, Pb and Zn accumulation factors (mean values ± SE and SD) in all tree species on the intensity of fertilization

Fig. 3 shows that mean values of accumulation factor for all metals are maximal for the trees grown in the non-fertilized plot as the difference between soil HM concentrations and trees stemwood is insignificant.

Some studies also show that wood accumulates only a certain quantity of HM’s, which remains stable regardless the HM concentrations in soil [9, 10]. Even at a constant HM concentration in soil, the HM accumulation in trees does not follow stable sequences.

Since the trees have accumulated significantly lower amount of HM than it has been inserted into the soil in all cases accumulating factor decreases with increasing intensity of fertilization. However, the assessment of certain metals accumulation shows that Cu accumulation factor curves are the most characteristic (outstanding) confirming the low level of this metal accumulation. Although change of Zn, Pb and Ni accumulation factors in fertilized plots are declining, but are less dependent on the intensity of fertilization and tree species.

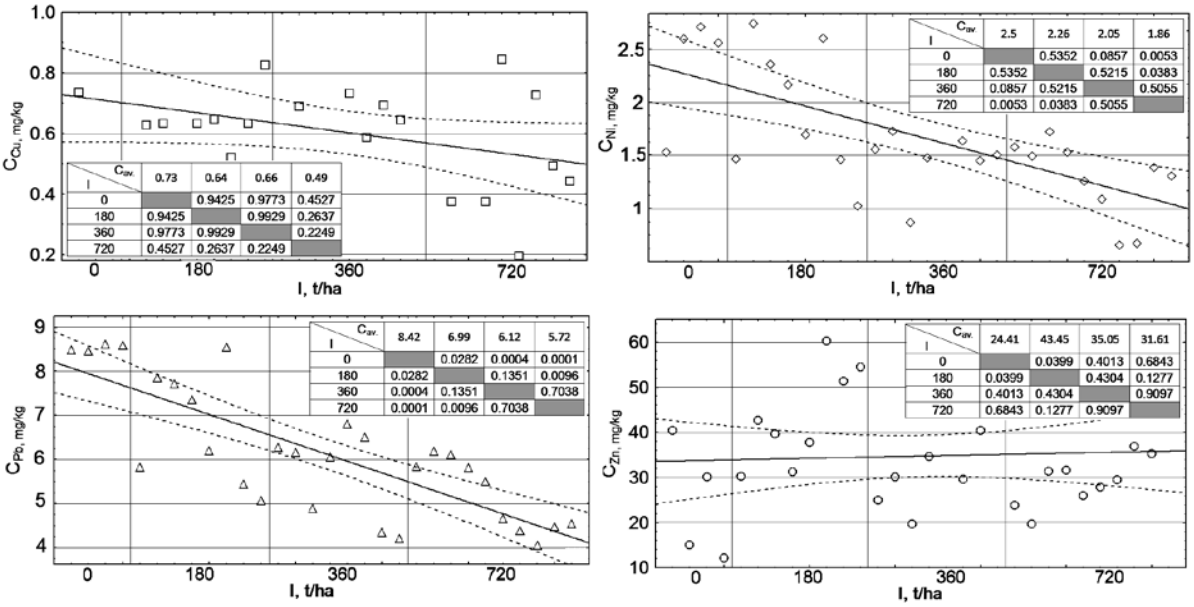

Fig. 4. Regression analysis of Cu, Ni, Pb and Zn concentrations in stemwood of Common aspen and American aspen hybrid dependence on the intensity of fertilization

In the wood of aspen hybrid, Cu, Ni and Pb concentrations decrease with the increase of the amount of the sewage sludge (Fig. 4). Significant decrease was determined only for Pb (C_{Pb} = 24.68 – 0.10*I; $p < 0.05$, r = – 0.7) and Ni (C_{Ni} = 6.62 – 0.02*I; p = 0.0001, r = – 0.6). Decrease of Cu concentration with the increase of the sludge amount is unreliable (C_{Cu} = 1.88 –0.007*I; p = 0.07, r = – 0.4). Significant increase of Zn concentration in the stemwood of Common and American aspen hybrids was also not determined (C_{Zn} = 21.76 + 0.075*I; p = 0.77, r = 0.05). Significant difference in the concentrations in the stemwood depending on the fertilization rate was determined for Pb when compared the unfertilized and all fertilized plots, as well as between fertilized 180 t/ha and 720 t/ha plots. The same difference was determined for Ni between unfertilized and fertilized with 720 t/ha of sludge, as well as with 180 t/ha and 720 t/ha fertilized plots; for Zn the difference was determined only between unfertilized and 180 t/ha fertilized plots. Significant decrease of concentrations for Cu under different intensities of fertilization was not determined.

4. CONCLUSIONS

- When compared the sludge fertilization effect during the 20-year period, it was determined that significantly high amounts of Zn, Cu and Cd as well as the lower amounts of Pb, Ni and (Cd, Cr) enter the soil with sludge and their high level concentration remains for 20 years.
- During 20 years, total concentration of Zn, Pb, Ni, Cu metals in the soil decreased only by 17, 26 and 40 % when intensity of fertilization was 180, 360 and 720 t/ha, respectively.
- Trees accumulated very limited amount of heavy metals in their stemwood regardless of intensity of fertilization. The following sequence of accumulation factor of heavy metals in the analyzed trees stemwood was found: Zn > Pb > Ni > Cu > (Cr, Cd).

REFERENCES

1. RIEPŠAS E., ŽALKAUSKAS R., PRANSKŪNAS R. Plantacinių želdinių įveisimo ir auginimo teisinio reglamentavimo tobulinimas. Mokslinio – taikomojo darbo Nr. SBMŪRP5 5–39 ataskaita, 2005, LŽŪU, Kaunas (in Lithuanian).
2. LAUREYSENS, I., BLUSTB, R., TEMMERMAN, DE L., LEMMENS, C., CEULEMANS, R. Clonal variation in heavy metal accumulation and biomass production in a poplar coppice culture. *Pollution*, 2004, Vol. 131, p. 485–494.
3. ORLANDIA, M., PELFINIB, M., PAVANA, M., SANTILLIB, M., COLOMBINIA, M.P. Heavy metals variations in some conifers in Valle d'Aosta (Western Italian Alps) from 1930 to 2000. *Microchemical Journal*, 2002, Vol. 73, p. 237–244.
4. LETTENS, S., VANDECASTEELE, B., DEVOS B., VANSTEENKISTE, D., VERSCHELDE, P. Intra- and inter annual variation of Cd, Zn, Mn and Cu in foliage of poplars on contaminated soil. *Science of the Total Environment*, 2011, Vol. 409, p. 2306–2316.
5. GRADECKAS, A., DILIŪNAS, J., GRADECKAS, A. Heavy metal accumulation in willow biomass and its evaluation from a nature conservation standpoint. *Geology,* 1999 (in Lithuanian).
6. WILSON, B., PYATT, F.B. Heavy metal bioaccumulation by the important food plant, Olea europaea L., in an ancient metalliferous polluted area of Cyprus. *Bull. Environ. Contamin. Toxicol,* 2007, Vol. 78, p. 390–394.
7. UNTERBRUNNER, R., PUSCHENREITER, M., SOMMER, P., WIESHAMMER, G., TLUSTOS, P., ZUPAN, M., WENZEL, W.W. Heavy metal accumulation in trees growing on contaminated sites in Central Europe. *Environmental Pollution,* 2007, Vol. 148, p. 107–114.
8. MORIN, M.D. Heavy metal concentrations in three-year old trees grown on sludge-amended surface mine spoil, in: PULFORD I.D, WATSON C. Phytoremediation of heavy metal-contaminated land by trees – a review. *Environment International*, 2003, Vol. 29, p. 529–540.
9. VANDECASTEELE, B., MEERS, E., VERVAEKE, P., DE VOS B., QUATAERT, P., M.G. TACK, F. Growth and trace metal accumulation of two Salix clones on sediment-derived soils with increasing contamination levels. *Chemosphere*, 2005, Vol. 58, p. 995–1002.
10. REIMANN, C., ARNOLDUSSEN, A., FINNE, T.E., NORDGULEN, F.K.U., ENGLMAIER. P. Element contents in mountain birch leaves, bark and wood under different anthropogenic and geogenic conditions. *Applied Geochemistry*, 2007, Vol. 22, p. 1549–1566.

CYSENI 2015, May 27–28, Kaunas, Lithuania
ISSN 1822-7554, www.cyseni.com

INVESTIGATIONS OF NOISE GENERATED BY SMALL WIND POWER PLANTS

Donatas Sankauskas, Vladislovas Katinas
Lithuanian Energy Institute
Breslaujos str. 3, 44403Kaunas – Lithuania
Phone +370 616 25100
Email: d.sankauskas@gmail.com

ABSTRACT

Investigations of small wind power plants for wind speed varying from 4 m/s to 10 m/s show that the intensity of noise generated by wind power plants depend on absorption of sound pressure pulsations in atmosphere and land surface, reflection, topographic land surface effect, meteorological conditions and many other determinants and factors. Data of the investigation show that small as well as large wind power plants generate some noise. When distance from the power plant increases, noise intensity decreases. Noise is absorbed better in soft land surface than hard surface. Also, absorption in the surface substantially depends on the frequency of noise. In the frequency range from 100 Hz to 1000 Hz the best noise absorption is observed. Noise reduction is carried out by reducing the noise at its generation source, and also, using architectic constructional means, also sprouts.
An analysis of data found in the literature shows that a noise level above 40 dB(A) can be irritating for some people. Limitations for construction of wind power plants near residential houses and public buildings are set due to noise generated by operating wind power plants.

Keywords: wind power plants, acoustic noise

1. INTRODUCTION

The use of alternative energy resources is expanded in the world and Lithuania, in order to reach energy independence. Wind power is expanded very intensively. In 2013, total capacity of wind power plants (WPPs) was 318488 MW, and 117289 MW of these were operating in EU countries [1]. In the end of 2014, total installed capacity of WPPs in Lithuania was more than 279 MW and generated 5.6% of electricity used in the country. However, WPPs, as other energy objects, have negative environmental impacts as they generate acoustic noise. It is known that noise above 32 dB(A) is a strong irritator of a nervous system for some people, and noise of 40 dB(A) and above creates a strong discomfort for most people [2].

It is determined that human ear, in average, can hear sounds in the frequency range from 16 Hz to 20 kHz. Sounds below 16 Hz are referred to as an infrasound, and above 20 kHz – an ultrasound [3]. Human hearing cannot perceive them, however, higher levels of infrasound or ultrasound generate feeling of discomfort and can damage human hearing [4–6]. Human hearing is more sensitive to relative changes of sound pressure than for absolute changes, therefore, sound pressure is expressed in a logarithmic scale as a level of sound pressure Lp in decibels (dB). For human hearing, limits of sound pressure variation intensity are in the range between 0 and 140 dB. Noise above sound levels of 140 dB produces pain and can damage hearing organs [5, 6]. Investigations show that noise generated by WPPs and background noise of the environment is a function of the wind speed. Aerodynamic processes of noise management are quite difficult. Processes of the mechanical noise of WPPs and means for mitigation are less problematic than in the case of the aerodynamic noise.

Data of acoustic noise of WPPs show that noise they generate can be split into two main sources, namely, mechanical and aerodynamic noise. The mechanic noise is generated by moving parts of the rotor, redactor, nacelle rotation mechanism, etc. the aerodynamic noise appears due to variations of air flow flowing round wings. These are turbulent pulsations generated at the air attack point, and also changes of boundary layer flow at a wing surface, etc. [7-9]. Also, aerodynamic pulsations are generated due to an interaction of rotating wings and constructive elements of the WPP tower. Beside the aerodynamic and mechanical noise, an environmental noise always exists, which is generated by wind flows, and also vehicles, birds, production plants, etc. background noise is more intensive at the daytime, and becomes less intensive at the night time due to lower wind speeds as well as external impacts.

Energy of sound pressure pulsations, if there is no interference, decreases with decreasing distance from the source. A human ear distinguishes sound variation when this difference is above 3 dB(A), if the distance from the source doubles, with a spatial energy dispersion, the level of sound level pulsations decreases around 6 dB(A), investigations show that there is almost no influence if the noise level increases at 1 dB(A), there is conceivable influence with increase at 3 dB(A), a clearly felt influence – at 6dB(A), and a strongly felt influence- at 10 dB(A). WPPs usually are installed in an open place, therefore, good conditions for acoustic noise dispersion are created [13]. With relief obstacles or buildings, noise dispersion is oscillated by these elements.

In order to prevent negative noise impacts, it is important to understand its physical origin, dispersion regularities, and to find noise mitigation means. Investigations of WPP noise emission dispersion in natural conditions were performed in this work, as well as a mathematic modelling in order to find means to mitigate negative environmental impacts.

2. INVESTIGATION METHODOLOGY

WPP acoustic noise is characterized by intensity and a frequency of noise pressure pulsations. Intensity of noise pressure pulsations is expressed in decibels, using this formula:

$$L_I = 10\lg(I/I_0)\,, \tag{1}$$

where I – measured sound intensity, W/m^2; I_0 – marginal intensity of an audible sound, ($I_0 = 10^{-12}$ W/m^2).

For theoretical evaluation of the noise level generated by an object, in decibels, the following formula can be used [10-13]:

$$L_{pj} = L_w - 10\lg(2\pi R^2) - \alpha R + L_g\,, \tag{2}$$

where L_{pj} — noise level generated by a WPP, in decibels, dB(A); L_w — the level of noise generated by the WPP rotor; R — distance from the WPP rotor axis to the measurement device; α — an atmospheric absorption coefficient; L_g – a correction of noise level due to reflection of sound pressure pulsations from the earth surface.

The meaning of the atmospheric absorption coefficient α depends on the temperature and humidity of the environment and the frequency of the acoustic noise. If the temperature or frequency increases, the acoustic absorption in the atmosphere increases [8, 9]. The speed of sound wave spreading depends on characteristics of the environment it spreads in, and increases with increased density of the environment.

Theoretical calculations of noise level depending on the distance from the WPP with different atmosphere absorption coefficients show that the influence of the atmosphere absorption coefficient α on the level of the noise generated by a WPP is expressed more intensely in a larger distance from a WPP. An earth surface correction L_g for power plants installed in the mainland is presumed as 1,5 dBA, and in the sea – 3dBA. However, it must be considered that a background noise exists in any traditional environment, and its impact must be evaluated when determining the noise of WPP .

The total noise level generated by a WPP (L_{pj}) and background noise (LpA) is calculated using the formula [7-9]:

$$L_{ps} = 10\lg\left[10^{(0,1LpA)} + 10^{(0,1Lpj)}\right], \tag{3}$$

where LpA – background environment noise, dB(A); L_{pj} – noise generated by a WPP, dB(A).

Experiments were performed as measurements of noise generated by small WPP (up to 250 kW) “Vestas 34” operated by UAB “Kamris” in Kalvarija municipality, Akmenų dist., Girkantai village. It is in a quite large distance from a habituated territory (more than 500 m) and its tower height is 50 m. The WPP is surrounded by an agricultural land. There are no high trees nearby the WPP, but there are small bushes at one side. Also, a noise level was investigated for a WPP “Enercon E33” operated by UAB “Vėjo trauka” which is installed near a settlement, and there are large trees a one side. The tower height of the WPP is 50 m., its installed capacity is 350 kW.

Investigations were performed at a wind speed of 6 m/s, at the tower level a noise analyzer 2250 manufactured by Bruel and Kjaer, Denmark, was used. Following spectrum parameters were determined with the spectrum analyzer, together with spectrum statistics: LXeq, LXFmax, LXSmax, LXFmin, LXSmin. Here, X is weighting filters of frequency, A, B, C and Z. Spectrum statistics were reviewed as a percentage spectrum of the LXYN where Y is time load F or S, and N is one of percentage parameters.

3. RESULTS OF THE INVESTIGATION AND ANALYSIS

Calculations performed according to Formulas (1)–(3) show that it is purposeful to evaluate the impact of the background noise LpA on the total noise generated by a WPP and an environment Lp only in the case when level of these noises are close to each other. When levels of these noises are approximately equal, then the total noise increases in 3 dB(A), and when their difference is 10 dB(A), the total noise level increases only in 0,4 dB(A). In this case, the total noise level is almost equal for the noise level calculated according to the Formula (2).

Data of the numerical modelling show that with high wind speed (v = 12 m/s) and a small distance (100 m) from the WPP tower, noise generated by a WPP has a low impact on the total noise level, as the background environmental noise dominates. With decreasing wind speed, noise levels of the WPP and environment also decrease.

The level of the WPP noise at the level of rotor axis at the wind speed v = 6 m/s, compared to wind speed v = 12 m/s, has decreased from 107 dBA to 96 dBA, and the environmental background noise – from 53 dB(A) to 40 dB(A). Experimental and theoretical calculation data in the Fig.1 show that in a small distance (100 m) from the WPP and at a wind speed of 6 m/s the level of the environmental noise level is much lower than the noise generated by a WPP.

Investigations performed with different type WPP show that noise generated by WPPs can be evaluated quite accurately using the (2) Equation (shown in Figures 1 and 2).

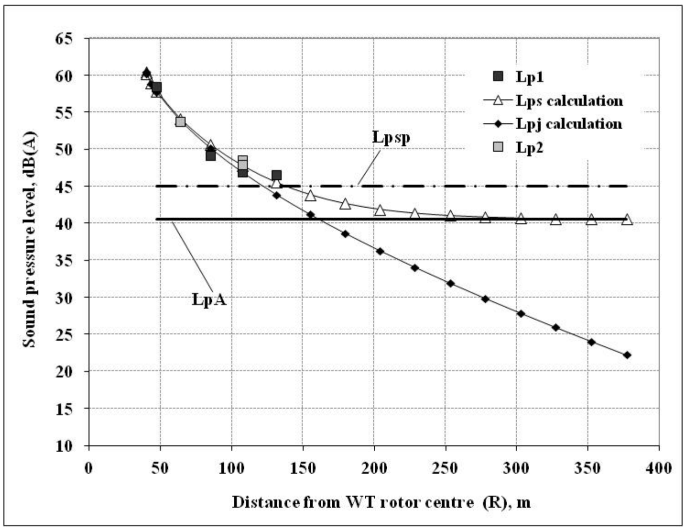

Fig.1. Variation of statistic indicators of the acoustic noise *Lp* of the wind power plant “Vestas 34” at a level of the rotor axis, at a wind speed ~ 6 m/s, *Lps* – total WPP noise level calculation using the (3) Equation; *Lpj* – theoretical calculation using the (2) Equation; *Lp1* and *Lp2* – experimental data; *Lpsp* – maximum level in the hygiene norm (45 dB(A)) [11]; *LpA* – level of the background environmental noise (40 dB(A)). Level of the noise generated at the level of the WPP rotor axis *Lw* ≈ 96 dB(A)

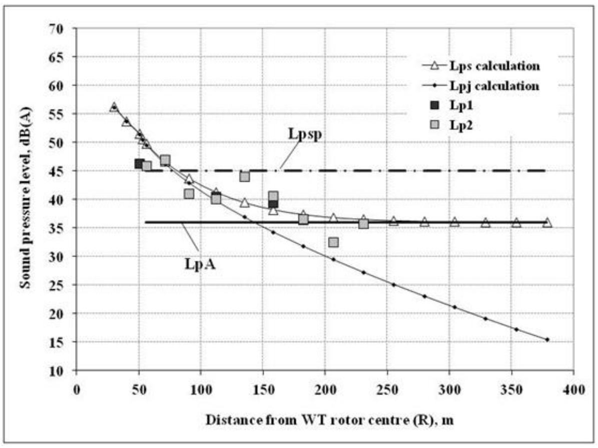

Fig. 2. Variation of statistic indicators of the acoustic noise *Lp* ow the wind power plant “Enercon E33” at a level of the rotor axis, at a wind speed ~ 6 m/s. *Lps* – total WPP noise level calculation using the (3) Equation; *Lpj* – theoretical calculation using the (2) Equation; *Lp1* and *Lp2* – experimental data; *Lpsp* – maximum level in the hygiene norm (45 dB(A)) [11]; *LpA* – level of the background environmental noise (36 dB(A)). Level of the noise generated at the level of the WPP rotor axis *Lw* ≈ 96 dB(A)

Investigations and the literature review show that at higher wind speeds noise generated by WPPs is masked by the background environmental noise generated by wind.

4. CONCLUSIONS

1. The literature review shows that even a noise level of 32 dB(A) can be a strong irritator of the nervous system, and a level of 40 dB(A) is a strong nervous irritator for some people. In most cases, noise generated by wind power plants is broadband, without expressed peaks in infrasound, audible sound and ultrasound.

2. Noise generated by wind power plants can be split into two groups: mechanical noise and aerodynamic noise. Mechanical noise is generated by moving parts, aerodynamic noise is generated by a wind flow flowing round rotor wings. Wings of the wind power plant moving near tower construction elements create aerodynamic pulsations that can generate acoustic noise in characteristic frequencies.
3. Beside the mechanical and aerodynamic noise generated by wind power plants, a background environmental noise exist that is generated by wind flows flowing round relief inequalities, vehicles, animals etc. the background environmental noise is more intense at the daytime, and decreases at the nighttimes due to decreased wind speeds and lower intensity of economic activities.
4. Using the fast Fourier transformation algorithm, it has been determined that in the acoustic noise spectrum from 200 Hz to 3 kHz generated by wind power plants, an increase of sound pulsation intensity is observed. Human hearing is most sensitive in this frequency range.
5. A theoretical model for calculation of wind power plant noise energy dissipation in a decreasing distance from the wind power plant is provided.

REFERENCES

1. 2014 Half – year Report. *The World Wind Energy Association. WWEA* 2014, 17 p.
2. TAYLOR J., EASTWICK C., LAWRENCE C., WILSON R. Noise levels and noise perception from small and micro wind turbines. *Renewable Energy*. 2013, 55, p. 120–127.
3. Lietuvos higienos norma HN 30:2009. Infragarsas ir žemo dažnio garsai: Ribiniai dydžiai gyvenamuose ir visuomeninės paskirties pastatuose.
4. KNOPPER L.D.A., OLLSON C. Health effects and wind turbines: a review of the literature. *Environmental Health* 2011; 10:78.
5. ALBERTS D.J. *Addressing Wind Turbine Noise*. Lawrence Technological University. 2006. 19 p. Inter. access: *http://www.maine.gov/doc/mfs/windpower/pubs/pdf/AddressingWindTurbineNoise.pdf*
6. VAN DEN BERG G. P. Effects of the wind profile at night on wind turbine sound. *Journal of Sound and Vibration*, 2004, 277, p. 955–970.
7. ROGERS T., OMER S. The effect of turbulence on noise emissions from a micro-scale horizontal axis wind turbine. *Renewable Energy*. 2012, 41, p. 180–184.
8. Intern. Standard IEC 61400-11. Wind turbine systems. Part 11: Acoustic noise measurement techniques.
9. Calculation methods in the Danish Statutory Order on wind turbine noise. Inter.access: http://www.es.aau.dk/?id=1132
10. Lietuvos higienos norma HN 33:2011. 2011. Triukšmo ribiniai dydžiai gyvenamuosiuose ir visuomeninės paskirties pastatuose bei jų aplinkoje.
11. Environmental Noise Booklet. Inter. access: *http://www.nonoise.org/library/envnoise/index.htm*

CYSENI 2015, May 27–28, Kaunas, Lithuania
ISSN 1822-7554, www.cyseni.com

KEY MODEL OF PV SOLAR COOLING

A. Snegirjovs, P. Gantenbein, M. Rommel
University of Applied Sciences Rapperswil
Oberseestr. 10, CH-8640 Rapperswil – Switzerland
Phone +41 55 222 48 27
Email: andrejs.snegirjovs@spf.ch

P. Shipkovs
Institute of Physical Energetics
Aizkraukles 21, LV-1006 Riga – Latvia
Phone +371 67 553 537
Email: shipkovs@edi.lv

ABSTRACT

Widespread installations of solar energy systems and price reduction of solar energy absorbing equipment opens new opportunities for solar energy application. Solar radiation is available at the same time as cooling demand is needed in buildings. In this case solar cooling of buildings is a reasonable energetic and economic solution. Solar cooling systems have their main tasks of reducing peak electricity power demand and in general is an environmentally friendly – nature protecting – energy conversion method. In the current market situation Photo-Voltaic (PV)-electric driven compression chillers are favourable compared to solar thermal driven sorption cooling because some of the system components like the compressor and heat rejection subsystem have a smaller footprint. A solar cooling concept with Photo-Voltaic electric energy and compression chiller (PVSC) is developed. The definition, analysis of the working parameters and system yield are described.

The system was developed and optimised by assessing results of pre-simulations of a solar PV-electric driven compression chillers system. The PVSC contains a cold tank to bridge the gap between solar energy gain and cooling demand. The energy from the heat rejection sub-system is used to pre-heat the domestic hot water. This concept has two advantages, on one hand it increases the heat rejection efficiency because of lower temperatures, and on the other hand it allows the use of indoor heat for hot water preparation. In addition, for a higher efficiency of the heat rejection subsystem during night time, a sensible hot storage tank was implemented in the system. To fulfil the domestic hot water demand in the non-cooling season the system will be operated in the reversed mode for pre-heating.

The cooling load of the solar cooling system was adequate to the cooling loads of buildings in certain climatic conditions. The investigations include the analysis of a reference system and the working parameters in cold and hot temperate as well as in the Mediterranean climatic zone. In the simulation template three types of buildings are used for a comparison of the cooling loads. After definition of the simulation template a validation will be done to assess the influence of the components on the system yield.

Keywords: renewable energy, solar energy, solar cooling, photo voltaic

1. INTRODUCTION

To reduce the CO_2 emission of private houses and office buildings alternatives to conventional energy sources are required to fulfil the expected increase of cooling needs. Solar energy – as a renewable energy source - is available at the same time as room cooling is needed, and in this case a solar cooling system can be a reasonable alternative. Reduction of component costs and innovative solutions in the area of solar energy technologies opens wider opportunities for their application in different building sectors. Authors [9] report about the increase of the number of solar cooling systems in the last decade of close to hundred systems per year and most of them are installed in Europe.

Solar cooling components convert the solar radiation into cold that may be done in several ways. Today the most popular technologies are thermal driven ab- and adsorption chillers in combination with solar thermal collectors. However, the numbers of sorption machines and collectors are growing very slow because of the high market prices. In contrary, the photo-voltaic (PV) market developments is fast with a continuing PV module price reduction. This economic reason increase the attractiveness of solar-electrical driven systems. Hence, the coupling of PV modules with an electrically driven air condition system is the concept of PV-based air-conditioning. For a PV electric driven cooling system all components are commercially available.

Electrically driven heating and cooling equipment such as vapour compression heat pumps (HP), chillers or reversible heat pumps in connection with heat and/or cold storages are attractive options for the energy supply in buildings. However, except of some European regions, today only a few complete system solutions use photovoltaics for energy supply in buildings that are available in the market. Therefore, a lack information on overall cost and performance of such systems is identified [1].

Existing pilot-systems and research activities [2, 3, 4, 6, 8] show that there are several options to install and use PV-driven cooling systems:

- Grid connected system with PV electric power being feed to the public grid and a standard grid-powered air-conditioner [7].
- Grid-independent system (stand-alone) with electrical energy storage to bridge PV converted solar radiation and cooling needs [5].

The objective of this study is to determine the potential of an enhanced grid connected PV system. The investigations of the PVSC are based on two parts: 1st a dynamic simulation of a system model in the Polysun® program software – presented in this paper, and 2nd a real system driven in a moderate climatic zone weather conditions, which will be presented in future publication. The system will also be compared with sorption-type solar cooling technology.

2. SYSTEM DESIGN AND METHODS

The assessment of a solar cooling system is done in this study. The system consists of a photo-voltaic electric energy driven compression chiller with cold and hot sensible thermal storages and the use of the rejected energy to preheat the Domestic Hot Water (DHW). In the frame of these requirements a design study was done with the Polysun® (Version 7.1) simulation program.

A simplified schematic of the analysed system is shown in Fig. 1.

The electricity for the compression chiller is produced by a grid connected (crystalline Si) PV module field, which has an area of A_{PV}=17.5m^2, is south orientated and has a tilted angle of 15° to the horizontal. The PV nominal power is 2.43kW$_n$. The direct current (DC) from the PV field is converted to AC by using a 2.5kW inverter with a European weighted efficiency of η_{EU}=95.8%. The PV inverter is installed in a technical room. Surplus PV electricity is feed to the electricity grid via the PV inverter, and in case of lack of electricity the compression chiller runs with grid power. Additional electricity consumers in the PVSC are a heat rejection unit (HRU), pumps and a system control including switching valves. The Additional electricity consumers of the PVSC are included in energy flow analysis.

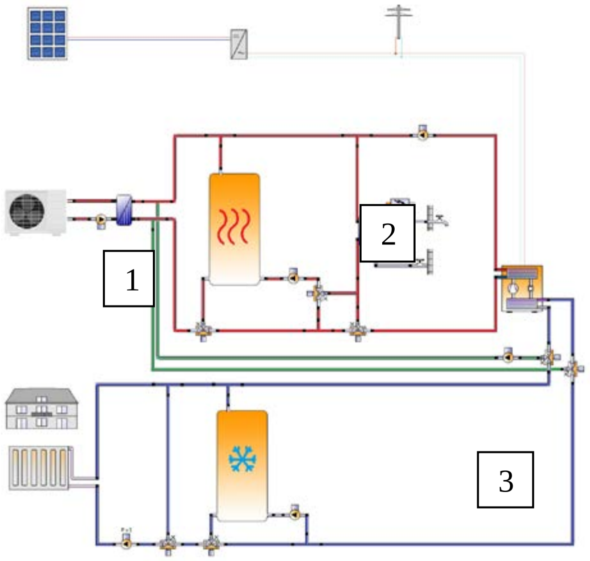

Fig. 1. Simplified, merged schematic of the photo voltaic solar electric cooling system. The simulation were done with three sub-system templates

A heat pump (HP) with vapour compressor is used as cooling machine. The nominal cooling power of the HP is P_{cool}=4.98 kWp at a rejected heat fluid temperature of T=24°C and an outlet-inlet temperature difference of ΔT=5°C. At these parameters the coefficient of performance of the HP is COP =5.81. The COP of the HP is decreasing to COP=4.32 at a cold loop output temperature of 10°C and heat rejection loop temperature 35°C. Thermal part of the system has three fluid loops, see Figure 1. The heat rejected loop is split into an indoor (2) and an outdoor (1) part, and is connected by 5kW/K medium heat exchanger. The cold loop (3) has a tube length of L(3)=29 m, the indoor heat rejected loop is L(2)=38 m, and outdoor heat rejected loop is L(1)=4m. All tubes have a diameter of D=25mm and are insulated, while the thermal conductivity of insulation is λ=0.045 W/m/K. As a heat transport fluid technical water is used in the indoor heat rejection and in the cooling loops. For freeze protection a 20vol% mixture of the ethanol-water is in the outdoor loop. In the whole system for the heat carrying fluid transport six pumps are installed. All pumps are variable-flow regulated, and the pumps maximal power are according with flow rates and pressure drops in loops. Cold ceilings are used for the cold distribution to reduce high indoor air mass flow and thus a higher comfort standard is reached. However, the temperature can’t be decreased lower in the cold ceilings than the dew point to prevent condensation. The cold ceilings power corresponds to HP cooling power. In case of no or partly coincidence of the solar energy gain and the cooling demand a cold storage tank of V=490 l, installed in the cold fluid loop, can bridge the gap. The cold tank is overall insulated with d=30mm ethylene propylene diene monomer (EPDM) rubber. The heat rejection operates with a dry heat rejection outdoor unit. The design cooling capacity of this unit is almost P_{th}=8 kW at a maximum air flow of 1.14m^3/s. The two stage electric power consumption of the outdoor unit ventilator is $P_{el.}$=195 W and $P_{el.}$=325 W.

The heat rejected is used for DHW preheating. With this concept it is possible to convert “waste heat” from indoor to useful thermal energy for DHW preparation. A benefit is the increase of the heat rejection efficiency because of the generally lower temperature of the tap water feed than the outdoor air temperature in the cooling season. DHW preheating can only be done in DHW consumption time. Therefore, a hot (warm) water storage tank is installed in the heat rejection loop. This tank has two advantages. On one hand it bridges the operation gap of HP and the need of DHW. And on the other hand it increases the heat rejection performance, through the possibility of heat rejection during night times (free-cooling), when the outdoor temperature is lower than the storage tank temperature. The volume of the hot storage tank is V=490 l and the glass-wool insulation has a thickness of d=100 mm. As a consequence of techno-economic reasons the bottom surface of the hot tank has a thinner thermal insulation of d=50 mm glass-wool. The DHW preparation (preheating of tap water) has a second priority in this study. Nevertheless, to reach the DHW temperatures of T>50°C an electric flow heater is installed.

The reference building is a single family house with heated/air-conditioned living area of A=100 m^2 and room height of H=2.5 m. The overall heat loss coefficient (U-value) of the building is 0.5 W/K/m^2 and the heat capacity is 500 kJ/K/m^2, it corresponds to an average insulated light construction building. The ratio of windows glazing to the building wall area is 25%, and is constant for all building sides. The solar radiation transmittance of the windows is τ_{sol}=0.82. The natural ventilation produces an exchange rate of 0.3 $h^{-1}$and infiltration is 0.2 h^{-1}. Internal heat gains are Q=0.44 kW. The ON of the cooling machine is at room temperatures of T_{room}>22°C, and shading will become active at T_{room}>25°C.

In the non-cooling season it is possible to run the part of the system in the reverse mode for DHW production. In this mode the ambient air is used as a heat source. In this case, the cold ceilings and the cold storage tank are switch-off from the system. In place of these components the cold side of the HP is connected the outdoor unit by using three-way controlling valves, see Fig. 1. In this reverse mode the hot water storage tank still takes its function and the HP runs in the same way, but most of the time at a higher temperature range as in the cooling season.

The system simulation and the energy analysis was done for three climatic zones with reference cities:

- Cold Temperate, seaside – Riga (Latvia), 57° Northern latitude;
- Hot Temperate, continental – Rapperswil (Switzerland), 47° Northern latitude;
- Mediterranean, seaside – Almeria (Spain), 37° Northern latitude.

In the simulation software the Meteonorm 6.1 weather data are implemented.

3. RESULTS AND DISCUSSION

The system of located in Rapperswil (Switzerland) stays as the reference system. The global solar irradiation on a horizontal surface is Gh=1100 kWh/m^2/a. The irradiation on the PV modules plane with south orientation and a tilted angle of 15° is G=1205 kWh/m^2/a.

Specific annual DC yield of the PV modules is almost 900kWh /kWn/a, and overall AC energy production of PV array is 2 060 kWh/a. 58% of the PV produced electricity is in cooling season. The overall inverter efficiency during the year is 94.6%. And the DC electric energy losses of the DC lines is in the range of 30 kWh/a.

The cooling season (room temperature requirements) is in the time range of middle May until beginning of October.

The specific cooling energy demand is Q_{cool}=57.5 kWh/m^2/a. In the cooling season the building heat gain approx. 10.4MWh, where the solar gain through the windows is 74.8%, 22.7% stems from heat flow through the building envelope and 1.7% heat gain from natural ventilation and infiltration. In short times when the outdoor air temperature is higher than indoor air a total of 0.7% of heat energy flows via building envelope, ventilation and infiltration into the cooled building. In turn, when the outdoor temperature is lower than the indoor air temperature, a high part of energy is rejected via building envelope, natural ventilation and infiltration. The cooling system rejects 55% of the building heat gain, 31% is rejected by the building envelope and 14% is rejected by natural ventilation and infiltration.

The building indoor average temperature during cooling season is slightly lower than 22°C, and it varies in the range of T_{room}=19.3°C to T_{room}=23.0°C.

Electricity is consumed to drive the heat pump, heat rejection unit and fluid pumps. The total electricity consumption in the cooling season is 1420 kWh where 77% is used to run the heat pump, 19% for the heat rejection unit and 4% for the pumps. Because of a very low electricity consumption the system control is neglected.

An average of 49% of the PV produced electricity is used by the HP for cold production. This value counts for 47% of all electricity consuming components of the system. As mentioned previously, the PVSC system produced 1.19 MWh/a with the PV array, and 1.42 MWh/a are consumed by all systems electricity consumers in the cooling season. In this case the PVSC can theoretically provide itself up to 83% of the necessary electricity consumptions. This means that a high potential of optimization exists in the availability of the PV array electricity and the electric energy consumption for the cold production.

A part of the waste energy from the HP is redirected to the “water tank” for DHW preheating. Although DHW preheating has not the first priority for the PVSC in the cooling season the systems overall performance is increased by using this heat energy. The redirected heat for DHW needs is 370 kWh/a. This energy amount is 26.4% of the necessary heat energy needed for DHW preparation. In average the DHW temperature is increased by ΔT=11.4°C, and in case of good conditions the water is even preheated up to T=39°C. Fig. 2 shows the yearly HP operation temperatures of the cold (chilled) and of the hot (heat rejection) sides.

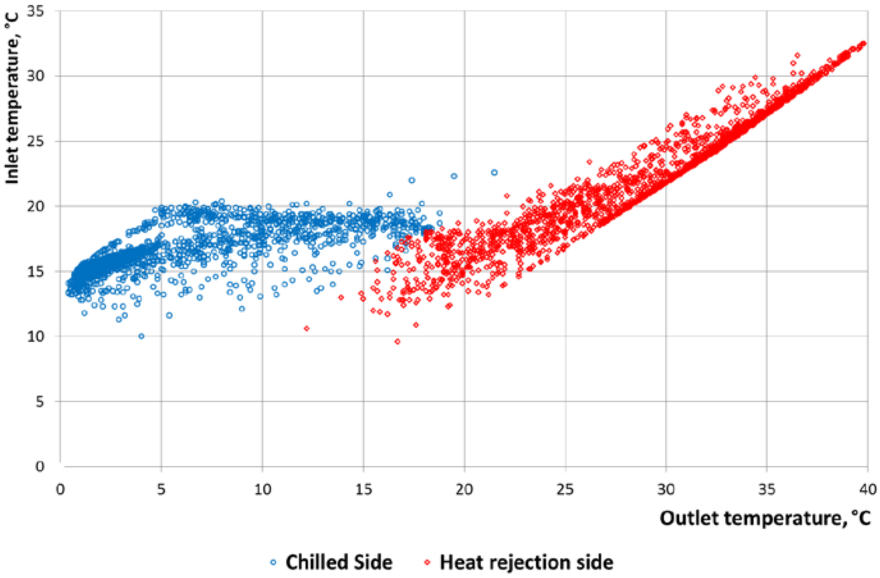

Fig. 2. Heat pump fluid working temperatures. Read: Fluid inlet temperature on the left vertical axis and fluid outlet temperature on the horizontal axis for the cold (blue circles) and the hot (red diamonds) side of the heat pump

The efficiency of the whole system significantly decreases by a rising heat rejection loop temperature. The fluid flow rates in the cold loop is lower than half of the flow rate in the heat rejection loop. Consequently, ΔT of cold loop fluid temperature is higher than the ΔT of heat rejection loop. At some short periods the temperature difference increases to ΔT=15.4°.

The cooling Seasonal Energy Efficiency Ratio (SEER) of HP is 5.65. This value of the whole system over the total year is reduced to 4.32, including taking in to account energy supplied for DHW preheating.

In the non-cooling season a part of the PVSC system is running for DHW preheating with the outdoor heat rejection unit as heat source. In this time the PV array total produced electricity is 42%. In the non-cooling season the heat pump output temperature for the DHW reaches T=55°C. Therefore, the electricity consumption of the heat pump, the heat rejection unit and the pumps is 365 kWh/a for DHW preheating. 82% of this electric energy is used for the heat pump, 16% for the heat rejection unit (source), and 2% for the pumps. In this mode and period the system takes 1.16MWh energy from outdoor air. Moreover, 77.3 % of HP produced heat is transferred to DHW needs, and the rest is heat loses into technical rooms. The DHW preheating in the non-cooling season is a less energy efficient process than in the cooling season. The SEER of this process is only 3.14.

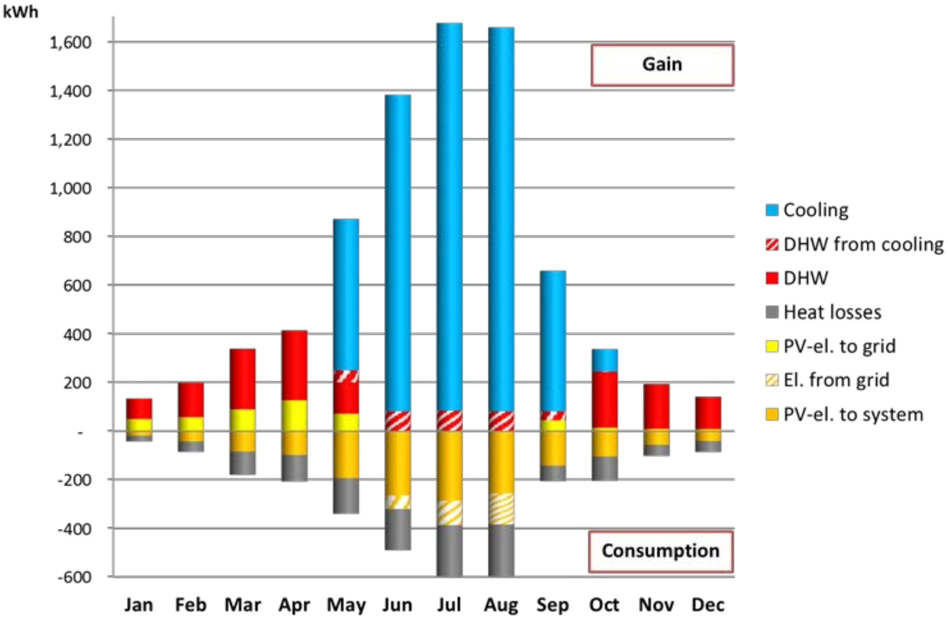

Fig. 3. Monthly energy flows at the reference location of Rapperswil

A ratio of the consumed electricity and the gains of the driving PVSC system is shown in Fig. 3. The system has room cooling as priority and DHW preheating decreases in the cooling season. Because of a freezing protection in at low outdoor temperature conditions the outdoor air heat used is limited. Therefore, DHW preheating decreases in the months November until March. Fig. 3 shows that the electricity energy flow is divided in three parts: the PV-el. to system – is the PV electricity gain used for cooling system needs; the PV-el. to grid – is surplus PV electricity that is feed to the public grid; and El. from grid –additional electricity demand used from grid. The annual electricity balance has an excess of almost 280kWh/a. All the equipment, except the heat rejection unit, is installed in a technical room, and heat losses from this component should not affect cooling or heating demands of the heated / chilled rooms. It could be possible to equalize the energy balance by adding heat rejection/heat absorption energy flows via HRU, and by excluding PV impact.

The reference system is simulated for 3 climatic zones and the performance is determined: cold temperate (Riga, Latvia); hot temperate (Rapperswil, Switzerland); and Mediterranean (Almeria, Spain). The results are presented in table 1

Table 1. System performance in different climatic zones

Location (-)	PV yield (kWh/a)	Electricity consumption (kWh/a)	Cooling demand (kWh/m^2/a)	Cover of cooling demand (%)	DHW (kWh/a)	Annual SEER of Cooling/ DHW
57° north, Riga,	1 910	1 960	56.3	100.0	2 190	3.99
47° north, Rapperswil	2 060	1 780	57.5	100.0	1 520	4.08
37° north, Almeria	3 420	4 980	200.4	99.2	570	4.14

For the two climatic zones, cold and hot temperate, the main result parameters of the cooling system performance are in a +/-10% range. A higher energy supply to DHW preheating in Riga corresponds to a longer non-cooling season. The difference of the time length for the cooling seasons in Riga and Rapperswil is almost one week.

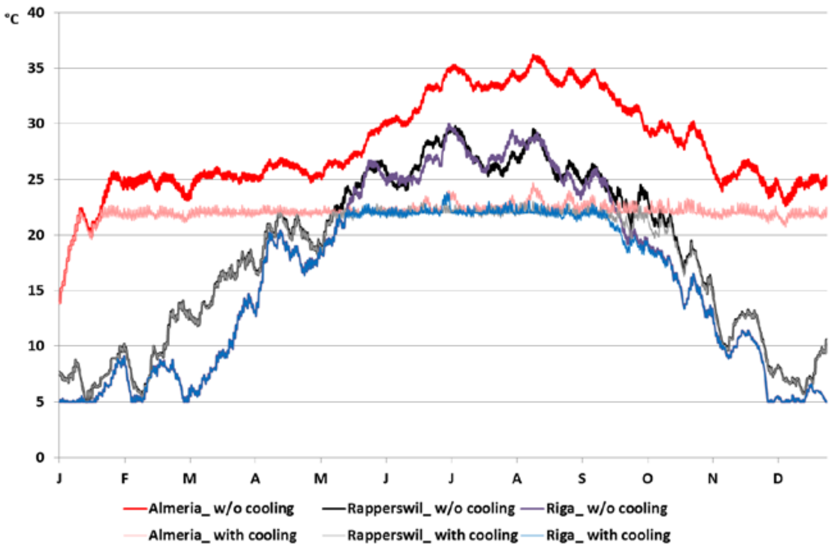

Fig. 4. Temperatures in the building with and without cooling in cold temperate (Riga), hot temperate (Rapperswil), and Mediterranean climatic (Almeria) zones

Fig. 4 shows the indoor temperatures of buildings in the three different climatic zones. Furthermore, the graph shows that the cooling demand in the Mediterranean climate is much higher than in the cold and hot temperate climates. The systems reverse operation mode is almost not used in Almeria. The Fig. 4 shows that in Almeria cooling is needed in all moths of the year, otherwise the temperature in the living rooms of the building will be no longer in the comfort zone range. As mentioned previously, driving the system in the non-cooling season is a process of lower efficiency, because of the unfavourable temperature levels. A system verification in the Mediterranean climate shows, that the nominal power per square meter is at its limit. In case of higher internal loads and external heat gains (solar; high outdoor temperatures) this slightly too small designed system will let rise the room temperatures out of the comfort zone range. This will even aggravate the situation in a wet climate condition.

In the frame of the work to the system analysis the extension by system parts (adding sub-system components) were investigated in relation of their effect on the system performance in total. But in all cases the requirement was that the cooling demand had to be covered in all system types. The base cooling system (schematic) consists of a heat pump (cooling machine), cold ceilings and a heat rejection unit. All other (relevant) components are added one by one until the reference system is reached. Table 2 presents the simulation results of all the different system versions.

Table 2. Results of the system type variation – base system + extension

System & extension	**DHW**	**HT**	**CT**	**Reverse mode**	**Electricity consumption (kWh/a)**	**Cooling supply (kWh/m^2/a)**	**DHW (kWh/a)**	**Annual SEER**
Base system (BS)	-	-	-	-	1 410	58.6	0	4.16
BS + DHW	X	-	-	-	1 400	58.7	290	4.40
BS + Hot tank (HT)	X	X	-	-	1 430	58.0	370	4.31
BS + Cold tank (CT)	X	X	X	-	1 400	57.5	340	4.35
BS + Reverse mode, DHW in non-cooling season (building with normal insulation)	X	X	X	X	1 780	57.5	1520	4.08
Building with low efficient insulation	X	X	X	X	1 630	43.9	1970	3.91
Building with high efficient insulation	X	X	X	X	2 360	88.6	1230	4.28

The implementation of heat rejection via domestic hot water preheating redirects / reuses 5% of the rejected heat. The implementation of a hot water tank increases the amount of redirected heat to 6.4%. The electricity consumption is also increased because additional pumps have to be used in these cases. On the other hand it is possible to reduce the electricity consumption by increasing the time of heat rejection into the hot water tank and release it during night time in a free cooling mode. This is reached because the outdoor temperature is decreased during the night, therefore the ΔT is increased between rejecting liquid and outdoor air. The reuse of the rejected heat for DHW preheating is increasing the system efficiency. However, electric driven components running during night time suffer power while they are coupled to a PV array, and the concept of a PV solar cooling system only can be kept by an additional electric energy storage.

In our system the main target of the cold storage tank is to reduce peak cold demand. With the insertion of a cold storage tank the HP operation is closer to the optimum diving temperature range, which slightly increases the HP seasonal efficiency. In the non-cooling season the HP with the heat rejection unit is used as heat source for DHW preheating and for this purpose a total of 1180 kWh/a is used. Because the non-cooling season SEER is 3.14 the annual SEER of cooling/DHW preheating system decreases down to 4.08.

The building envelope insulation, the proportion of window area to wall area, the amount of natural ventilation and infiltration are affecting the cooling demand of the building. The effect of the cooling demand on the cooling system is shown by the system located in Rapperswil. The buildings with a low U-value of 0.8 W/K/m^2 are according the single-family detached house built in the years 1982–1995 or older and buildings with U-value of 0.2 W/K/m^2 are according to passive multi-family detached houses. The use of materials of lower thermal conductivity means higher investment costs and can lead to higher cooling power needs in the cooling season. The influence on the annual SEER depending of the driving proportion in the cooling and the non-cooling season can be seen.

A further extension or upgrade of the PV solar cooling system could be with a free-cooling and a "free heating" mode.

4. SUMMARY

A Solar Cooling concept with Photo-Voltaic electric energy and compression chiller is developed. The definition and the analysis of the working parameters and the system yield are described. The performance of a reference system is defined for: cold Temperate; hot Temperate (reference); and Mediterranean climate zones.

The system was developed and optimised by assessing results of pre-simulations of a solar PV-electric driven compression chillers system.

The PV array of the PV solar cooling system produces 2.06 MWh/a. 58% of the PV produced electricity stems from the cooling season.

The cooling demand of the reference system is 57.5 kWh/m^2/a, and it can be fully covered by a 5kW$_p$ compression cooling machine. The PVSC can provide up to 83% of necessary electricity consumption for the cooling needs. In the cooling season 6.4% of rejected heat is reused for hot water preheating.

A reverse mode of the system is used to preheat DHW from heat rejection unit in the non-cooling season. In this time 1.15 MWh/a of thermal energy is supplied to DHW preparation needs.

The investigations include the analysis of the effect of sub-system parts on the system performance.

In European climatic zones the annual SEER of Cooling/DHW range from 3.9 to 4.4, depending of the application of the system versions.

The annual electricity balance in the reference climatic zone has a surplus of +280 kWh/a.

ACKNOWLEDGEMENTS

Financial support by the Swiss Sciex Program is gratefully acknowledged. Further we gratefully acknowledge financial support of HSR University of Applied Sciences Rapperswil.

REFERENCES

1. HENNING, HANS-MARTIN; MOTTA, MARIO; MUGNIER, DANIEL. *Solar Cooling Handbook*. Ambra; 3rd Revised & enlarged edition, September 2013. 368 p. ISBN: 3990434381.
2. KOHLENBACH, PAUL; JAKOB, ULI. *Solar Cooling: The Earthscan Expert Guide to Solar Cooling Systems*. Routledge, August 2014. 224 p. ISBN: 0415639751.
3. FRANCISCO, J.; AGUILAR. Operation and energy efficiency of a hybrid air conditioner simultaneously connected to the grid and to photovoltaic panels. *Energy Procedia*, Vol. 48, 2012, p. 768-777.
4. HA, Q.P. Modelling and optimal control of an energy-efficient hybrid solar air conditioning system. *Procedia Engineering*, Vol. 49, 2012, p. 116–123.
5. BAN-WEISS, G. Electricity production and cooling energy savings from installation of a building-integrated photovoltaic roof on an office building, *Energy and Buildings*, Vol. 56, January 2013, p. 210–220.
6. TAGLIABUE, LAVINIA C.; MAISTRELLO M., DEL, PERO C. Solar heating and air-conditioning by GSHP coupled to PV system for a cost effective high energy performance building. *Energy Procedia*, Vol. 30, 2012, p. 683–692.

7. SHAHSAVAR, A. Energy saving in buildings by using the exhaust and ventilation air for cooling of photovoltaic panels. *Energy and Buildings*. Vol. 43, Issue 9. September 2011, p. 2219–2226.
8. CULLHED, P. The Almedalen Library – an energy low-cost solution. World Library and Information Congress: 71th IFLA General Conference and Council "Libraries – A voyage of discovery". Oslo: Norway. 2005 August 14–18. 4 p.
9. MAUTHNER, FRANZ; WEISS, WERNER. *IEA Solar Heating & Cooling Programme*. AEE INTEC, AEE – Institute for Sustainable Technologies. Gleisdorf, Austria. June 2014. [Referred on the 15th of January in 2015 y] Link to the internet http://www.nachhaltigwirtschaften.at/iea_pdf/solar_heat_worldwide_2014.pdf.
10. MUGNIER, DANIEL. *New Generation solar cooling & heating systems (PV or solar thermal driven systems)*. IEA Solar Heating & Cooling Programme Work plan for Task 53. Task description and Work plan November 2013. [Referred on the 14th of January in 2015 y] Link to the internet http://task53.iea-shc.org/data/sites/1/publications/Task 53-Work-Plan.pdf

CYSENI 2015, May 27–28, Kaunas, Lithuania
ISSN 1822-7554, www.cyseni.com

DEVELOPMENT OF A RISK MATRIX CONSIDERING SPECIFIC FEATURES OF THE POWER TRANSFORMER PARK OF LATVIA

G. Poiss
Riga Technical University
12/1 Azenes str., Riga, LV-1048 – Latvia
Phone +371 28289322
Email: gints.poiss@rtu.lv

ABSTRACT

The power transformer is an important element of the power system on a national as well as international level. The different structures and features of the transformer park create the necessity for individual risk assessment to increase the reliability of the power system. This paper presents the early stages of the development of a power transformer technical condition index using the risk matrix method for the power transformer park of Latvia. Power transformer park of Latvia has a large reserve base but it is noticeably aged. The age, regularity of replacement, diagnostic periodicity and other specific features of the power transformer park have to be taken into account during the development of a risk matrix with a suitable mathematical model.

Keywords: risk matrix, diagnostic methods, life cycle, power transformer

1. INTRODUCTION

The transformer is an important component of any power transmission system. Its function is to transfer electrical power to different voltage levels and it is the most expensive component in the substation.

There are fifteen 330 kV substations and one hundred twenty two 110 kV substations under the management of the Latvian transmission system operator „Augstsprieguma Tīkls" JSC. The company is responsible for all of the power transformers in the transmission system of Latvia and it determines all the diagnostic methods, periodicity, condition assessments and maintenance schedules.

The power transformer park of Latvia consists of 246 power transformers and 23 autotransformers [11]. Depending on the substation, one, two or three transformers or autotransformers have been installed.

The analysis of the power transformer park of Latvia reveals the actual situation - the transformer park is noticeably aged and has a large reserve base. Power transformer reserve (backup) consists of transformers which are possible to switch in operation condition immediately in case of the main transformer being shut down by protection or it is shut down due to maintenance or diagnostic measurements [7].

The objective of the paper is to determine suitable indicators for the development of technical condition index risk assessment. The risk matrix is selected considering its illustrative and understandable pattern where the results will show the overall condition of the particular transformer of power transformer park of Latvia.

Proposed condition assessment in its early stages excludes transformer parts like bushings, conservator tank, radiator and cooling system and on-line tap-changer.

2. RISK MATRIX DEVELOPMENT

The majority of power transformers in the power transmission system of Latvia have been in exploitation for more than 20 years [10]. Due to this situation it is highly recommended to use both short and long-term risk assessments that suit the particular power transformer park.

The short-term risk assessment comprises of biannual power transformer condition assessment of DGA (dissolved gas analysis) and oil analysis. The technical assessment is conducted without taking into account the rest of the useful information about the power transformer.

Review of scientific literature [2], [5], allows concluding that the risk matrix method can be applied for any transmission system, but its mathematical model depends on specific features of particular transformer park and periodicity of diagnostic methods.

Results provided by risk matrix are illustrative yet and based on the results and trends of various diagnostic tests considering maintenance history as well thus suitable for long-term risk assessment.

The 5x5 risk matrix shown in Fig. 1 is proposed for early stages of this research since it provides a conventional scale (5 tiers) for gradation of the likelihood of the occurrence and the consequence of an event. The likelihood is scaled from 1 as the least likely event, to 5 as a highly possible event and the consequence is scaled from A – minor effects, to E – huge, possibly disastrous effects [4]. Size of the risk matrix for the power transformers of Latvia is variable that can be changed considering results of the condition index method and from data about failures over long period of time.

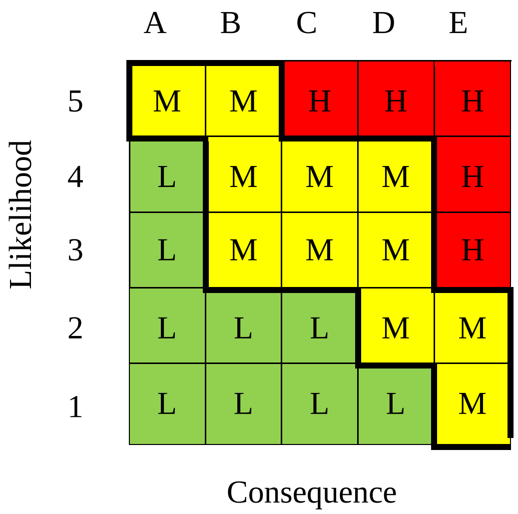

	A	B	C	D	E
5	M	M	H	H	H
4	L	M	M	M	H
3	L	M	M	M	H
2	L	L	L	M	M
1	L	L	L	L	M

Fig. 1. A conventional pattern of a risk matrix

3. TRANSFORMER TECHNICAL CONDITION INDEX

3.1. Condition indicators

It is necessary to evaluate the full spectrum of results and create a condition index – a tool which suits best for the overall condition assessment and combines the results of each inspection, test, operation and scheduled maintenance [1]. It is important to decide what information is necessary to be included in the technical condition index, and it mainly depends on the individual transmission system and the specific features of the power transformer park.

Three main condition indicators are proposed for the technical condition index development of the power transformer park of Latvia. Each of the condition indicators covers different important sections of the power transformer (Table 1). Indicators are selected based on available diagnostic tools in power transformer park of Latvia [7].

The condition indicators:

- Operation and maintenance;
- Transformer oil;
- Electrical measurements.

The technical condition index method consists of parameters that have scoring and which make up the individual indicator that will have it‘s own weight. All of the parameters are included in the creation of the final technical condition index, which in turn will be inserted into the risk matrix.

The key of this method is to properly work out the condition scoring and the weight for indicators [1]. Weights for indicators will determined after full condition scoring development.

During the early stages of the condition index development, the parameter condition scoring system is derived on a scale of 1 to 5, where parameters are evaluated from 1 (good condition) to 5 (very poor condition).

To understand the development of the technical condition index, an example of the rating table (Table 2, Table 3, Table 4) is given in every section.

Table 1. Proposed condition indicators and their parameters

Operation and Maintenance	**Transformer oil**		**Electrical measurements**
	Oil analysis	**DGA**	
Age	Dielectric strength	H_2, CH_4	Insulation resistance
Loading	Moisture content	CO, CO_2	Tanδ
Tripping per year	Acidity	C_2H_4, C_2H_6, C_2H_2	No-load loss
Importance in the system	Dissipation factor	C_3H_6, C_3H_8	Winding resistance
Maintenance history	Mechanical particles		Short-circuit impedance
	Fire point		

3.1.1. Operation and maintenance

The operation and maintenance section contains information about the transformer’s:

- Age;
- Loading;
- Tripping per year;
- Importance in the transmission system;
- Maintenance history.

These parameters complement the following indicators with significant information. The age of the power transformer and loading can aid in explaining the electrical measurements and oil diagnostic results; importance of the transformer in the system and average tripping per year can be used to assess the degree of urgency for maintenance of each individual transformer or autotransformer. Maintenance history is an important parameter which provides useful information about the reason and time of the extra measurements or oil analysis, and it may indicate failures or problems of equipment of similar design and construction [9].

The scoring table for transformer age (Table 2) has been created based on the analysis of the available data about the age of the power transformer. The majority of power transformers of the transformer park of Latvia is above the useful lifetime the age group of 26-40 years, but the age group of 41 up to 50 years is the second largest. Other groups have been created deriving from the periodicity of changed transformers [7].

Table 2. Scoring table for transformer age

Age (years)	**Condition Score**
0–2	1
3–10	2
11–25	3
26–40	4
>41	5

3.1.2. Transformer oil

The life of the transformer massively depends on the lifespan of the insulation paper, and the lifespan of the paper can be extended by maintaining the best possible oil quality and carefully monitoring gases and moisture content [9]. The section Transformer oil covers two of the most exploited diagnostic methods in the world – DGA and oil analysis, which are used as indicators.

Using the analysis of DGA, the type of the fault can be determined. Within the power transformer park of Latvia, eleven gases (including O_2 and N_2) are regularly monitored (Table 1). Latvian Energy Standard LEK 118 is used for the interpretation and evaluation of the results. The standard determines the periodicity of the DGA 6 months and oil analysis – 4 years for 110 kV transformers and 2 years for 330 kV autotransformers [8].

All of the gas ratings in the oil are important and show the ongoing processes in the power transformer. For example, age-related gases and their concentration affect the electrical characteristics and oxidation of the insulating oil.

Oil analysis helps to evaluate the state of the transformer in regard to the degree of degradation of insulation materials as well as possible internal electrical and thermal faults [6]. The test results should be examined carefully to determine whether the moisture content is increasing and if the moisture content is doubled in a power transformer, the lifespan of the paper insulation is cut by a half [9]. During the creation of the scoring table for moisture content, the provided thresholds for transformers with various rated power in LEK 118 were used (Table 3).

Table 3. Scoring table for moisture content in power transformer oil

Moisture content (ppm)		**Condition Score**
LEK 118 (A,T)	LEK 118 (T)	
<5	<5	1
≤10	≤15	3
>10	>15	5

A – 330 kV autotransformers and 110 kV transformers with rated power >63 MVA
T – 110 kV transformer with rated power ≤63 MVA [8]

3.1.3. Electrical measurements

The most important and frequently used electrical measurements utilized in the power transformer park of Latvia for technical condition index model development are proposed as follows:

- Insulation resistance;
- Measurement of tanδ;
- No-load loss;
- Winding resistance;
- Short-circuit impedance.

For these electric measurements covers insulation in power transformer, iron core, winding and connection conditions.

The insulation resistance, through the absorption coefficient (Kabs) R60/R15 allows the estimation of the degree of moistness of the insulation of transformer [3].

Condition score and absorption coefficient values (Table 4) and periodicity – for electrical measurements has been created based on the national normative base of the Latvian transmission system operator through guides to electrical insulation testing and IEC standards.

Periodicity – for electrical measurements is 8 years for 110 kV transformers and 330 kV autotransformers.

Table 4. Scoring table for power transformer insulation resistance

K_{abs}	Condition Score
>1.6	1
1.25 ÷ 1.6	2
1 ÷ 1.25	4
<1.0	5

4. SUMMARY AND FUTURE WORK

The structure and features of the transformer park create the necessity for individual risk assessment development to increase the reliability of the power system. Specific features such as the large reserve, noticeably aged transformers, regularity of replacement, diagnostic periodicity and loading of the power transformer park provide useful processable condition parameters which provide the basis for the creation of the technical condition index.

The proposed risk matrix with the condition index method are suitable for the power transformer park of Latvia and will be develop further.

Further agenda:

- A condition score for each parameter will be derived, based on the standards and technical literature;
- Each indicator will be provided with its weight;
- The numerical value of the technical condition index will be obtained, which in turn will be incorporated within the risk matrix;
- This is the very beginning of the development of the risk matrix;
- The scores and weights are in the process of development.

REFERENCES

1. YOUNG, J., LIN, M., LIYUAN, W., JIAN, T., LIN, H. A new method to determine condition index for equipment condition assessment, In Proc. Prognost, Health Manage. Conf., 2010 Jan, p. 1–6.
2. XIE, Q., LI, Y., LIU, Y., LI, Y., LV, F. Research on Failure Risk Assessment and Maintenance Tactics of Transformer based on the Extension Engineering Method and IAHP, International Conference on High Voltage Engineering and Application, Chongqing, China, November 9–13, 2008, p. 705–709.
3. POPESCU, CONSTANTIN M.; POPESCU, C. Digital Moulding of the Solicitations within the Dielectric of the Transformers and the Evaluation of Life Cycle of the Insulation Systems, Ozean Journal of Applied Sciences, 2010, Vol. 3(1), p. 39–60.
4. SMOLARKIEWICZ, M. SMOLARKIEWICZ, MIECZYSLAW M.; BIEDUGNIS, S., PODWÓJCI, P., CZAPCZUK, A. Matrix methods for risk management – Associated Matrices Theory, Annual Set The Environment Protection, 2011, Vol. 13, p. 241–252.
5. TAENGKO, K., DAMRONGKULKAMJORN, P. Risk Assessment for Power Transformers in PEA Substations using Health Index, 10th International Conference on Electrical Engineering/Electronics, Computer, Telecommunications and Information Technology, Krabi, 2013, 15-17 May, p. 1–6.
6. GRADNIK, Maja K. Physical-Chemical Oil Tests, Monitoring and Diagnostic of Oil-filled Transformers, Proceedings of 14th International Conference on Dielectric Liquids, Austria, 2002 July.
7. POISS, G., VITOLINA, S. Overview of the power transformer park and diagnostic methods in Latvia, Powereng 2015, 5th Int. Conf. on Power Engineering, Energy and Electrical Drives, Riga, 2015, 11–13 May, [Manuscript accepted for publication].
8. Latvian Energy Standard LEK 118. *Transformer oil testing*, Latvia, 2014, 45 p. (in Latvian)
9. Facilities, Instructions, Standards and Techniques. *Transformer Diagnostics*, United States Department of the Interior Bureau of Reclamation, 2003, Vol. 3-31, 63 p.
10. BRENERS, N. Technical and Economic Estimation of Measures to Increase Reliability of Transformer Base Functioning, 2011, Riga Technical University, Doctoral dissertation.
11. *Development plan of transmission power system – 2014*, „Augstsprieguma tīkls“ JSC, Riga, 2014. Link to the internet <http://www.ast.lv/eng/par_ast/public_reports>

CYSENI 2015, May 27–28, Kaunas, Lithuania
ISSN 1822-7554, www.cyseni.com

IMPROVED THERMO-ELECTRICAL ANALOGY MODEL FOR PELTIER ELEMENTS

V. Jurkans
Riga Technical University
Azenes 12, LV-1048 Riga – Latvia
Phone +371 26077479
Email: vilnis.jurkans@gmail.com

J. Blums
Riga Technical University
Azenes 14, LV-1048 Riga – Latvia
Phone +371 29774351
Email: blum@latnet.lv

ABSTRACT

Thermo-Electrical analogy method is very powerful instrument for transient heat-flow simulation and analysis. Therefore, to analyze Peltier element as a part of cooling or heating system it is necessary to evaluate thermo-electrical analogy model that would describe Peltier element as close as possible. There are various successful approaches developed for the moment however most of them tend to ignore various properties of Peltier elements due to little impact on final results or to maintain simplicity. This paper attempts to develop model that would include specific, previously ignored thermal and electrical effects to describe Peltier element more precisely. Although these effects have small impact on conventional operation of Peltier element, one can find certain conditions or applications that should not ignore them. The model can also serve as educational material that helps to understand Peltier elements or thermoelectric effects better or serves as base in other research. Developed model is compared to other thermo-electrical analogy models for Peltier coolers.

Keywords: Peltier element, thermoelectric effect, Thermo-Electrical analogy, modeling, heat flow simulation

1. INTRODUCTION

Peltier element is a semiconductor device that can be used as a heat pump or electrical generator. Because of its ease of use it is gaining more and more interest in various appliances that is increasing constantly. Starting with household applications and moving towards to high speed supercomputers and measuring equipment.

Nowadays a lot of device development processes involve computer simulation of whole or certain parts of the final system. Simulation can increase development speed and precision as well. Electronic circuit simulation using SPICE models in certain CAD software to see the exact behavior of circuits seem to be most popular in development of electronic systems.

The same software can be used to simulate heat processes in thermal circuit using thermo-electrical analogy. Therefor thermo-electrical analogy models need to be comprehended if one is planning to simulate such devices as Peltier elements.

There are many thermo-electrical analogy models provided nowadays, however they can be improved by adding effects normally occur during operation of Peltier element.

2. PREVIOUSLY DEVELOPED THERMO-ELECTRICAL ANALOGY MODELS

A lot of scientists have described their models according to different considerations and different needs.

In work [1], researcher describes model for thermal and electrical part of Peltier element:

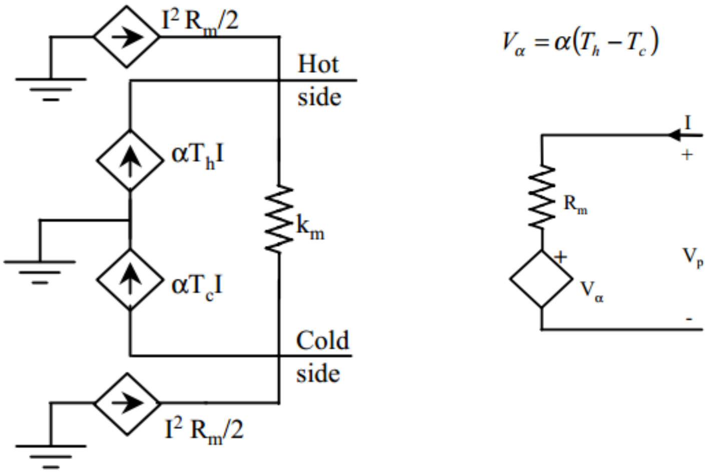

Fig. 1. Equivalent Peltier model from [1]

Circuit on the left side is thermal part which consists of Joule heat divided in two parts using current sources ($I^2 R_m / 2$) and Peltier effect, which is divided in two parts using current sources (αTI) as well. Resistance k_m represents thermal resistance between hot and cold side of Peltier element.

Circuit on the right side represents electrical part of Peltier element and consists of voltage source V_α that represents voltage that is created by Seebeck effect and resistance R_m which is electrical resistance of Peltier element.

It is able to simulate influence of 4 main phenomena of Peltier element:

1. Joule heat
2. Peltier effect
3. Seebeck effect
4. Heat flow / backflow through the Peltier element

These are the main effects that occur in Peltier element and thus model is able to describeand simulate processes with decent precision.

After few considerations in [1], model is improved by adding thermal masses as capacitances and uniting current sources to combine the effects:

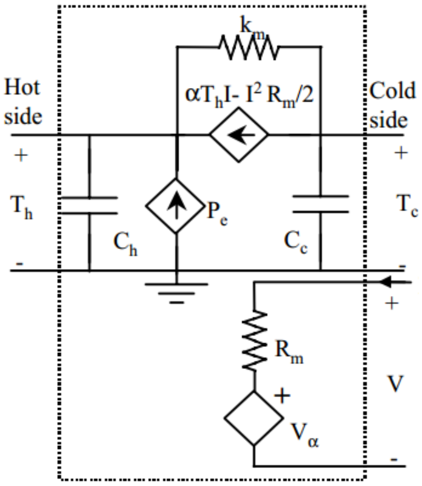

Fig. 2. Equivalent Peltier model from [1]

Similar model is suggested by [2] where one of the current sources is replaced by voltage source:

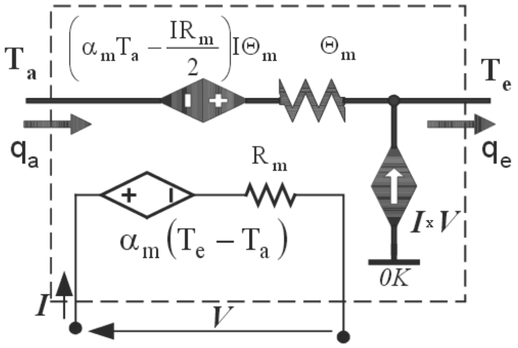

Fig. 3. Equivalent Peltier model from [2]

In [3] previously used $I \cdot U$ or Pe is separated using two different current sources – one for describing heat produced at Ohmic resistance and other for heat transported by thermoelectric effect.

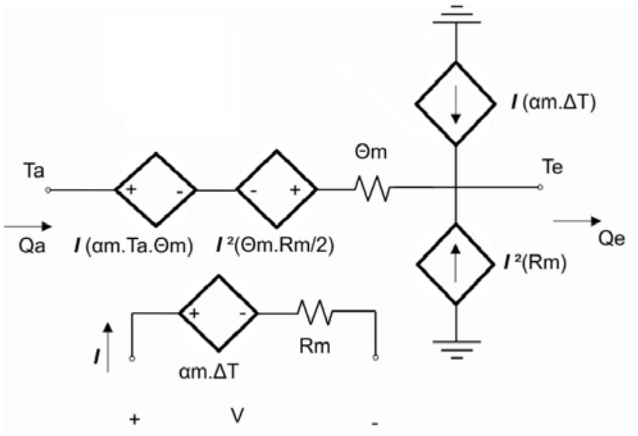

Fig. 4. Equivalent Peltier model from [3]

These models are meant to simulate Peltier element at decent level. However, if higher precision is needed or system is working at some specific mode then there are more properties to be aware of.

3. IMPROVEMENT OF THERMO-ELECTRICAL ANALOGY MODEL

3.1. Expressions for the heat fluxes on both sides of Peltier element

Thermal fluxes for cold and hot sides of Peltier element in cooling/heating mode for simple model are following:

$$Q_H = \alpha \cdot I \cdot T_H - \frac{\Delta T}{\Theta} + \frac{1}{2} \cdot R \cdot I^2, \tag{1}$$

$$Q_C = \alpha \cdot I \cdot T_C - \frac{\Delta T}{\Theta} - \frac{1}{2} \cdot R \cdot I^2, \tag{2}$$

where Q_H and Q_C are heat balance on hot and cold side of Peltier element, α – Seebeck coefficient, I – electrical current that flows through Peltier element, T_H and T_C – temperatures on both sides of Peltier element, $\Delta T = T_H - T_C$, Θ – thermal resistance of Peltier element, R – electric resistance of Peltier element.

3.2. Electrical resistance of Peltier element

All semiconductors change their resistance depending on their temperature. Peltier as semiconductor device is no exception. Peltier device unfortunately is complex system and consists of different semiconductors and metal. Therefor the temperature coefficient should be searched in technical information for certain Peltier element or defined experimentally. In Peltier element working temperature range this dependence can be approximated with linear function.

Curve for Peltier element resistance temperature dependence can be measured following way:

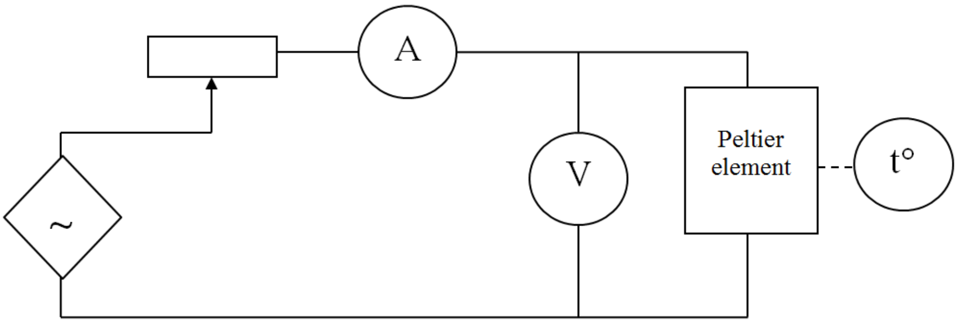

Fig. 5. Setup for measuring Peltier resistance dependence from temperature

Setup should be used to heat Peltier element by supplying Alternating current to it, thus eliminating voltage generated by Seebeck effect. Dependence curve can be built by registering voltage and current at different temperatures and calculating resistance using Ohm’s law.

Now thermal fluxes for cold and hot sides of Peltier element cooling/heating mode are:

$$Q_H = \alpha \cdot I \cdot T_H - \frac{\Delta T}{\Theta} + \frac{1}{2} \cdot R(t^\circ) \cdot I^2 \tag{3}$$

$$Q_C = \alpha \cdot I \cdot T_C - \frac{\Delta T}{\Theta} - \frac{1}{2} \cdot R(t^\circ) \cdot I^2 \tag{4}$$

3.3. Thomson effect and Seebeck coefficients thermal dependence

It is one of the most abandoned effects for Peltier element. It is mostly considered as negligible and therefore is ignored for simplicity of calculations and simulation. However research [5] has shown the benefits of using Thomson effect.

Thomson effect tends to counter[1] the Joule effect. Consequently, the Thomson effect is advantageous in cooling mode, whereas it is disadvantageous in heating mode. Thomson effect contribution as an additive term is only valid if a thermal dependence of the value of the Seebeck coefficient is considered. [4]

Therefore, Peltier cold and hot side heat balance is described by the expressions:

$$Q_H = \alpha_H(t^\circ) \cdot I \cdot T_H - \frac{\Delta T}{\Theta} + \frac{1}{2} \cdot R(t^\circ) \cdot I^2 - \frac{1}{2} \cdot \tau \cdot I \cdot \Delta T\ , \tag{5}$$

$$Q_C = \alpha_C(t^\circ) \cdot I \cdot T_C - \frac{\Delta T}{\Theta} - \frac{1}{2} \cdot R(t^\circ) \cdot I^2 + \frac{1}{2} \cdot \tau \cdot I \cdot \Delta T\ , \tag{6}$$

where τ is Thomson coefficient, α_C and α_H – separate Seeback coefficients for cold and hot side of Peltier element.

Electrical power that is supplied to or generated by Peltier element is described by the expression:

$$P = (\alpha_H(t^\circ) \cdot T_H - \alpha_C(t^\circ) \cdot T_C) \cdot I + R(t^\circ) \cdot I^2 - \tau \cdot I \cdot \Delta T\ . \tag{7}$$

Seebeck coefficient should be calculated from data that is given by manufacturer either measured experimentally. Thomson coefficient can be derived from Seebeck coefficient by equation:

$$\tau = T \cdot \frac{d\alpha}{dT}\ . \tag{8}$$

4. IMPROVED THERMO-ELECTRICAL ANALOGY MODEL

Using equations (5), (6) and (7) the thermo-electrical analogy model that consist of both thermal and electrical parts can be composed (see Fig. 6).

---

[1] Thomson effect absorbs heat that is generated by Joule effect.

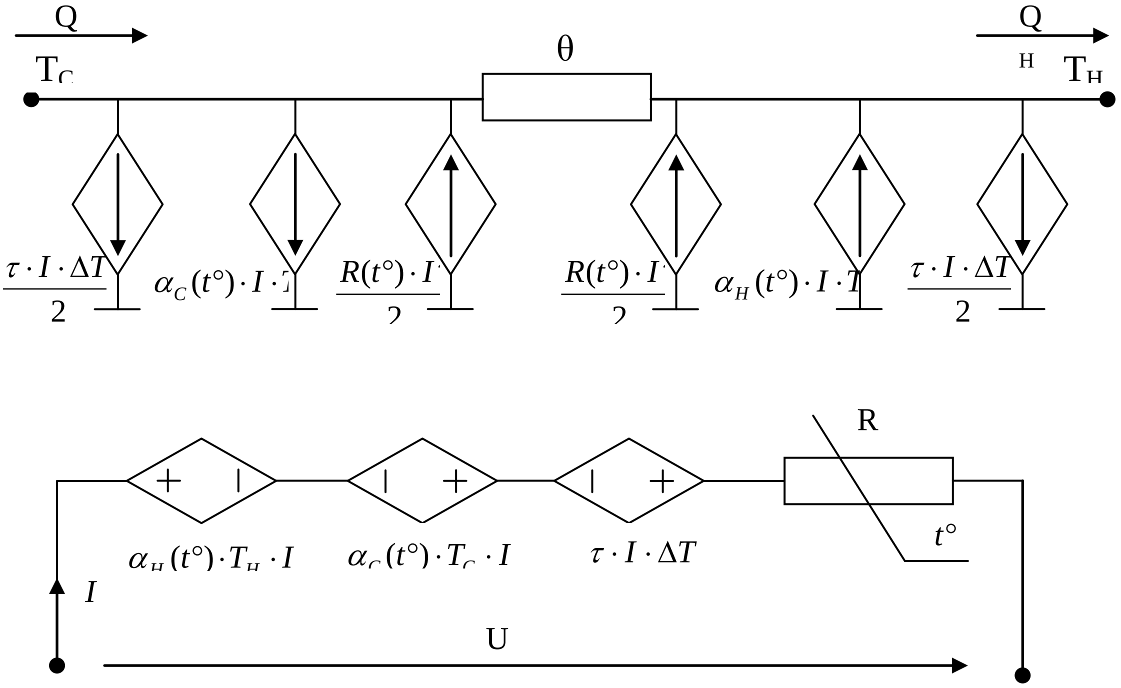

Fig. 6. Thermo-electrical analogy model with advanced parameters. Upper diagram describes thermal processes, lower diagram – electrical processes

Electrical part consists of two counteracting voltage sources for both side Seebeck effect generated voltage, voltage source for Thomson effect created voltage and temperature dependent resistance R that describes Ohmic resistance of Peltier element.

Thermal part has thermal resistance θ, which is surrounded by 6 current sources. On the cold side there is a half of heat flux created by Thomson effect which transports heat away from the cold side together with Peltier effect for cold side. These two fluxes are represented by the half of overall Joule heat. On the hot side of Peltier element same fluxes are valid with exception of Peltier effect that adds to Joule heat and is calculated by its own Seebeck coefficient.

5. SIMULATION OF IMPROVED THERMO-ELECTRICAL ANALOGY MODEL

Following model was created and simulated in SPICE software to estimate the difference between the simulation results of simple and advanced model:

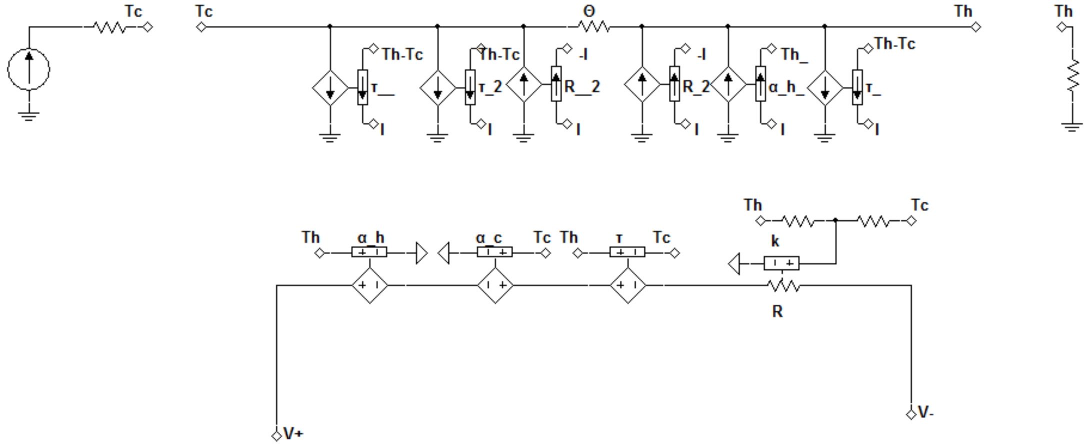

Fig. 7. SPICE model for thermo-electrical analogy model with advanced parameters

Heat source and heat sink is added to model on terminals T_c and T_h.

Simulation was done using settings listed in Table 1. Simple model simulation is made with constant values and Thomson coefficient is 0.

Table 1. Thermoelectric parameters for the simulation

	Advanced model	Simple model
Thermal resistance	0.16 K/W (K/W)	0.16 (K/W)
Electrical resistance	(3.4+0.00052*T) (Ω)	0.29 (Ω)
Seebeck coefficient	0.018+0.000012*T (V/K)	0.024 (V/K)
Thomson coefficient	0.000012*T (V/K)	0 (V/K)

Temperatures of hot and cold side were observed. Difference between both models is shown in Fig. 8.

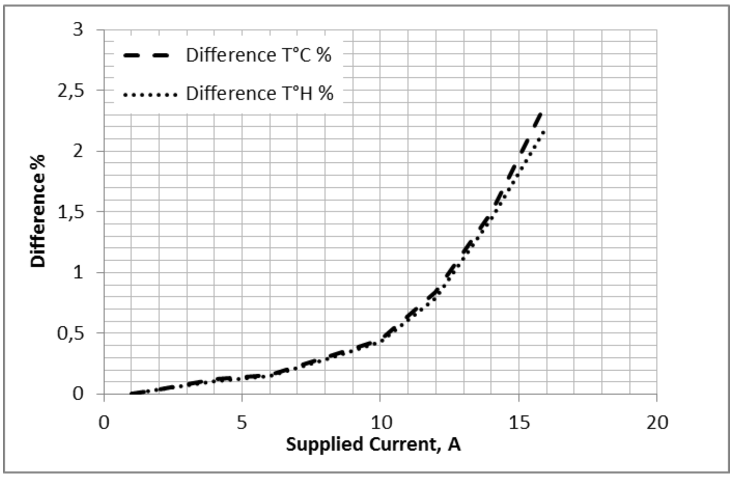

Fig. 8. Differnce between results of simulation

6. CONCLUSIONS

In this study improvements for existing Peltier thermo-electrical analogy models were suggested. Advanced model was constructed taking into account properties of Peltier elements that are usually ignored for the simplicity and small impact in overall results.

Study show that improved model is constructible using SPICE software, however model is more complicated. Difficulties could occur when obtaining thermoelectric parameters for specific Peltier element.

Simulation results show 2.5% difference in results when high current is supplied to Peltier element, though these numbers could be higher if Peltier element with other parameters would be used.

REFERENCES

1. CHAVEZ, J. A., et al. SPICE model of thermoelectric elements including thermal effects. In: *Instrumentation and Measurement Technology Conference, 2000. IMTC 2000. Proceedings of the 17th IEEE*. IEEE, 2000. p. 1019–1023.
2. LINEYKIN, Simon; BEN-YAAKOV, Sam. SPICE compatible equivalent circuit of the energy conversion processes in thermoelectric modules. In: *Electrical and Electronics*

Engineers in Israel, 2004. Proceedings. 2004 23rd IEEE Convention of. IEEE, 2004. p. 346–349.

3. ALAOUI, Chakib. Peltier thermoelectric modules modeling and evaluation. *International Journal of Engineering (IJE)*, 2011, 5.1: 114.
4. FRAISSE, G., et al. Comparison of different modeling approaches for thermoelectric elements. *Energy Conversion and Management*, 2013, 65: 351–356.
5. MITRANI, D., et al. Lumped and distributed parameter SPICE models of TE devices considering temperature dependent material properties. In: Thermal Investigation of ICs and Systems, 2007. THERMINIC 2007. 13th International Workshop on. IEEE, 2007. p. 202–207.

CYSENI 2015, May 27–28, Kaunas, Lithuania
ISSN 1822-7554, www.cyseni.com

HEAT TRANSFER ENHANCEMENT IN SHELL-AND-COIL HEAT EXCHANGER

T. Muszyński, R. Andrzejczyk, P. Kozak
Gdansk University of Technology
Narutowicza 11/12, 80-233 – Gdansk, Poland
Phone 58 347 24-22
Email: tomasz.muszynski@pg.gda.pl, rafal.andrzejczyk@pg.gda.pl,
przemyslaw.kozak@pg.gda.pl

ABSTRACT

In the paper authors presented their own constructions of shell and tube heat exchangers with intensified heat transfer. The shell-and-coil heat exchangers are in common use in heat ventilations and air conditioning systems. Those types of recuperators are quite simple constructions, the low value of pressure drops and good conditions of heat transfer. The present study shows an experimental investigation of the heat transfer in a shell-and-coil heat exchanger. Data are reported for various Reynolds numbers and various surface modifications as in Fig 1. The purpose of this article is to assess the influence of the surface modification over the performance coefficient and modified effectiveness of vertical helical coiled tube heat exchangers. The calculations have been performed for the steady conditions and the experiments were conducted for both laminar and turbulent flow inside coil. Gathered experimental data are compared with correlations from literature.

Keywords: heat transfer enhancement, shell-and-coil heat exchanger

1. INTRODUCTION

The advent of the twenty-first century has brought increased interest in miniaturization and nanotechnology in almost all branches of technology. Reduction of the adverse impact of industry on the environment, as well as the reduction of energy and material usage. In addition, if you realize that the heat exchangers and heat recovery units are especially 25 to 30% of energy conversion devices, and therefore their correct design and manufacture is the key to high thermal efficiency, reducing investment and energy savings. One way of reducing the size and increasing the efficiency of these devices is to increase the heat load heat exchange surface. Unfortunately, increasing the amount and density of energy processed in the equipment causes an increase inmaterial requirements to reduce the cost of the manufactured product it is necessary to know the precise value of the local flowresistance and the heat transfer coefficient. Heat transfer intensification of the given surface at a predetermined temperature drop is achieved, i.e. by the increase in heat transfer coefficient by turbulization, destabilization of flow or by other kind of interaction with the boundary layer. The benefits of higher heat transfer coefficient and consequently heat transfer directly translate into savings of primary and secondary sources of energy, reducing the size of the heat exchange apparatus, operational and investment costs. In the longer term, this leads to a reduction in harmful emissions into the atmosphere of carbon, sulfur and nitrogen (CO, CO_2, SO_2, NO_x).

Heat exchangers are used in a wide variety of applications including power plants, nuclear reactors, refrigeration and airconditioning systems, automotive industries, heat recovery systems, chemical processing, and food industries [1–4].

Several studies have indicated that helically coiled tubes are superior to straight tubes when employed in heat transfer applications [5–6]. The centrifugal force due to the curvature of the tube results in the secondary flow development which enhances the heat transfer rate. This phenomenon can be beneficial especially in laminar flow regime.

2. GEOMETRY OF SHELL AND COIL HEAT EXCHANGER

The investigated shell and coiled tube heat exchanger is shown in Fig. 1 and Fig. 2. Fig. 1 shows the inner coil of heat exchanger with and without surface intensification.

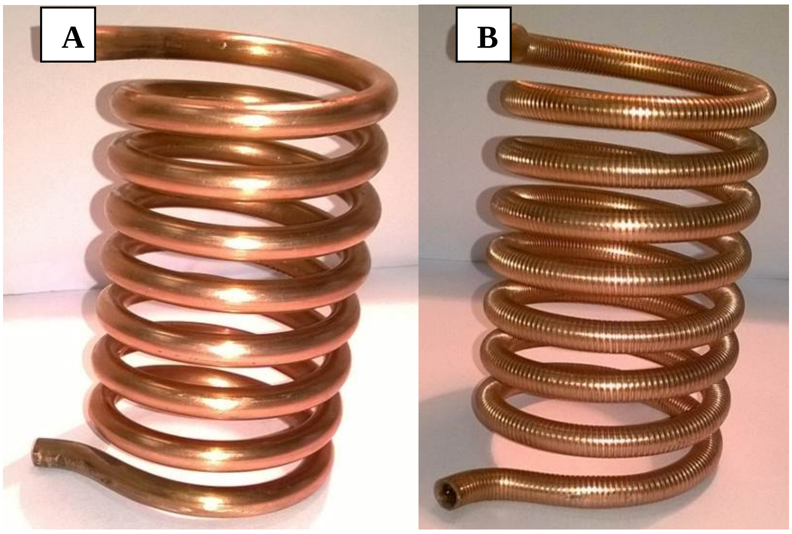

Fig. 1. The different coils surfaces: A – smooth pipe, B – modified coil

In Fig. 2, D is the diameter of the coiled tube, r is the curvature radius of the coil, C is the inner diameter of shell, and the coil pitch is 1.5 D. The important dimensionless parameters of coiled tube namely, Reynolds number (Re), Nusselt number (Nu), Dean number (De), and Helical number (He) are defined for inner tube and for outer shell of heat exchanger. Relevant geometrical parameters are listed in Table 1.

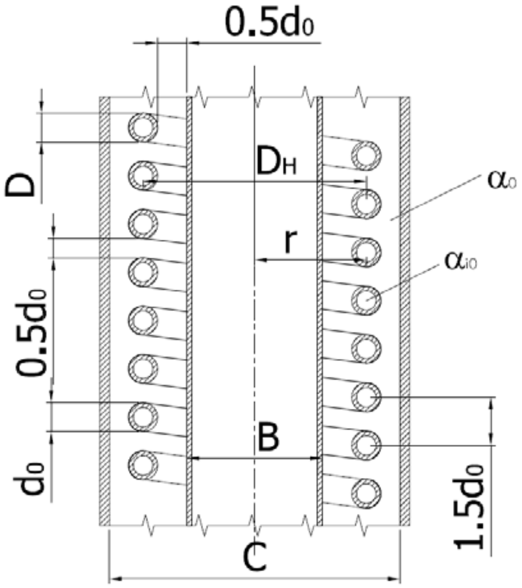

Fig. 2. Dimensions of internal coil of heat exchanger

Table 1. Geometrical dimensions of heat exchanger

Symbol	Dimension	Value
r	m	0.02
p	m	0.02
C	m	0.06
d_0	m	0.006
d_1	m	0.004
D	m	0.006
D_H	m	0.040
B	m	0.022

3. EXPERIMENTAL RIG SET-UP

The schematic diagram of experimental set-up is shown in Fig. 3. The set-up is a well instrumented single-phase heat exchanging system in which a hot water stream flowing inside the tube-side is cooled by a cold water stream flowing in the shell-side. The main parts of the cycle are coiled tube heat exchanger, pump, tank and heater.

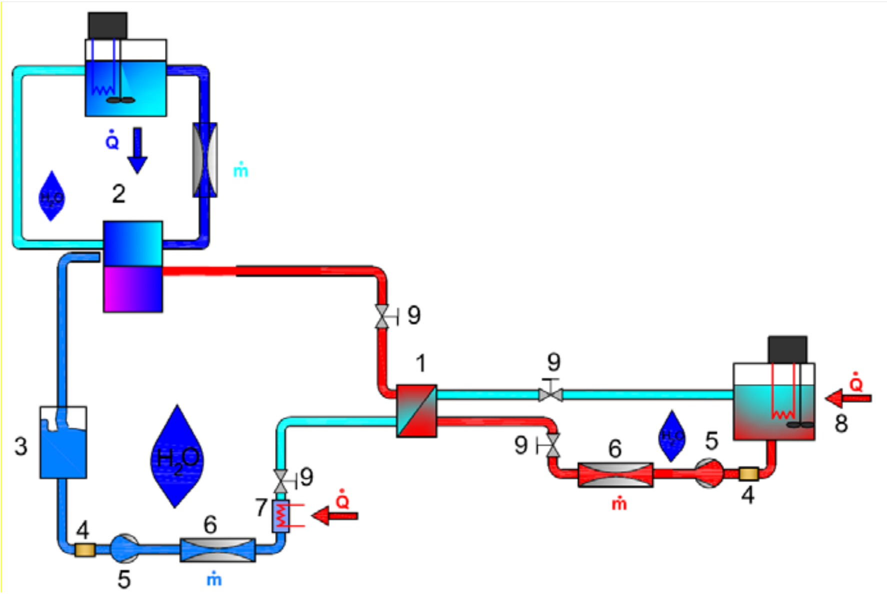

Fig. 3 The schematic diagram of experimental rig

The heat exchanger include a copper coiled tube and an insulated shell. The dimensions of the heat exchangers are depicted in Table 1. The water storage tank is heated using an thermostatic bath. Reaching to a prescribed temperature, pump is started to circulate the hot water in the loop. A set of valves are used to control the flow rate of coolant water and hot water, respectively. To measure the flow rate of the cold stream a Promass 63 mass flow meter is installed upstream of the heat exchanger while for the hot stream a measuring pot with the accuracy of 0.3 g/s is used. The inlet and outlet temperatures of hot and cold water were recorded using 4 T-type thermocouples inserted in the small holes made in the inlet and outlet tubes of each heat exchanger and sealed to prevent any leakage. Also, all the pipes and connections between the temperature measuring stations and heat exchanger were duly insulated. All the temperatures were measured three times with accuracy of 0.5 C in the time steps of 20 min, and the average values were used for further analysis. Appropriate arrangements were provided to measure the pressure loss of both tube-side and shell-side streams. All the tube- and shell-side fluids properties were assessed at the mean temperature of the fluids (average of inlet and outlet temperatures).

A shell and coiled tube heat exchanger cross section is shown in Fig. 4 with two investigated flow arrangements.

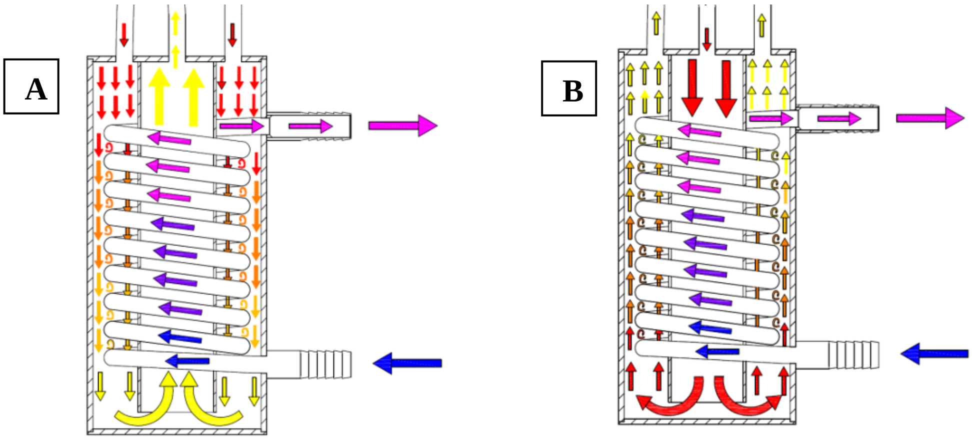

Fig. 4. Two cases of flow arrangement in heat exchanger: A) counter current B) concurrent

4. EXPERIMENTAL RESULTS

Fig. 5 shows the experimental results of pressure drop in heat exchanger shell. In case of enhanced surface, higher fluid inlet velocity resulted in increase of pressure drop. But still lower than in reference type heat exchanger

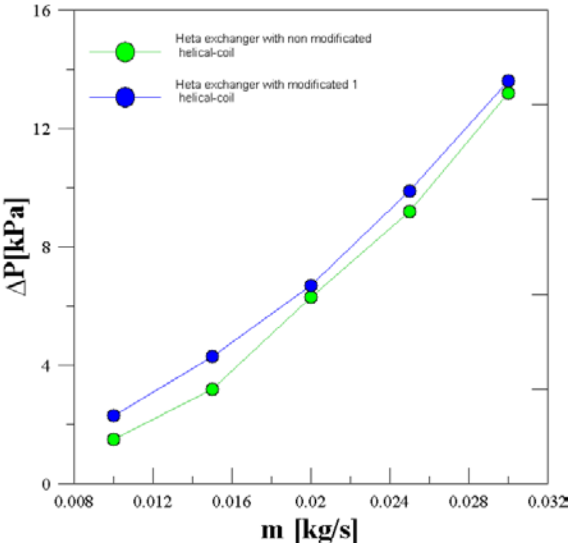

Fig. 5. The experimental results of pressure drop in heat exchanger shell

The analysis of the Fig. 6 and 7 indicates that, heat exchanger efficiency slightly increases with increase of NTU. This indicates that, as flow rate inside shell increases the velocity increases, which increases the heat transfer but for enhanced surface increase of effectiveness is smaller than in reference type heat exchanger.

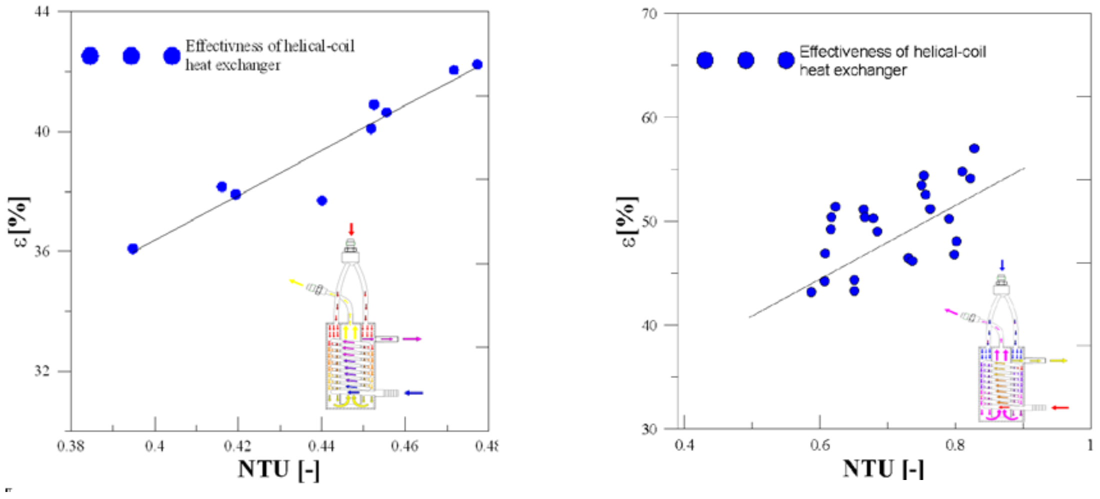

Fig. 6. The experimentally obtained effectiveness of reference type heat exchanger for counter current (left) and concurrent flow arrangement

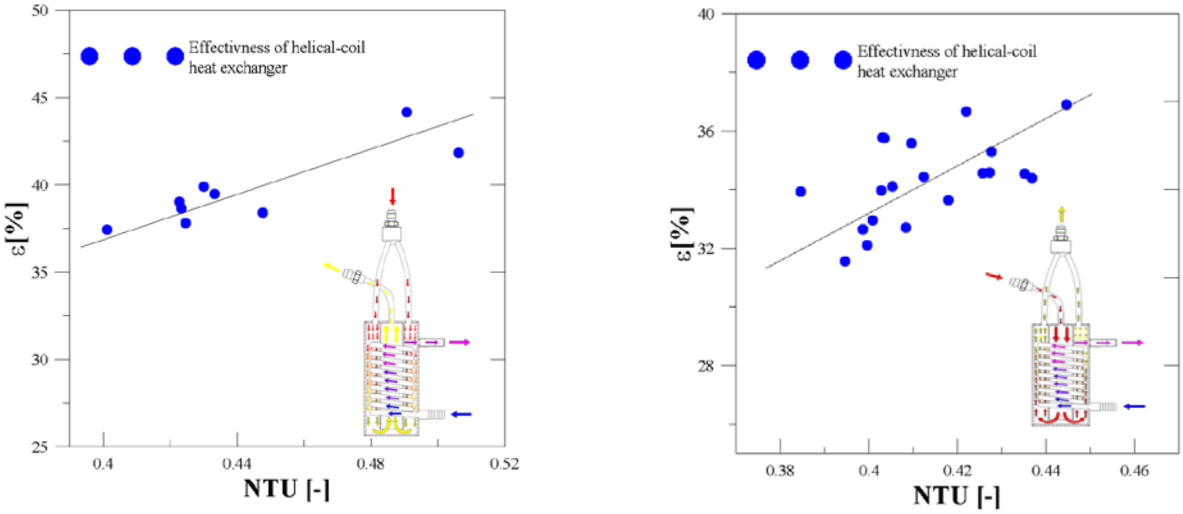

Fig. 7. The experimentally obtained effectiveness of enhanced type heat exchanger for counter current (left) and concurrent flow arrangement

5. CONCLUSIONS

An experimental investigation was carried out to study heat transfer coefficients of the shell and coil heat exchangers. Heat exchangers with two different coils were tested for counter and concurrent flow configuration. Further investigations are needed in order to develop correlations to predict the inner and outer heat transfer coefficients of the coiled tube heat exchangers.

REFERENCES

1. ROHSENOW, WARREN M.; HARTNETT, JAMES P.; GANIC, EJUP N. Handbook of heat transfer applications. New York, McGraw-Hill Book Co., 1985, 973.
2. CENGEL, YUNUS A., MICHAEL A. BOLES. Thermodynamics: an engineering approach. Vol. 5. New York: McGraw-Hill, 2011.
3. KANDLIKAR, S.G. Two-phase flow patterns, pressure drop, and heat transfer during boiling in minichannel flow passages of compact evaporators. Heat Transfer Engineering, 2002, 23.1: 5–23.
4. RUGH J.P., PEARSON J.T., RAMADHYANI S. A study of a very compact heat exchanger used for passenger compartment heating in automobiles Compact Heat Exchangers for Power and Process Industries, ASME Symp. Ser. (2nd edn), HTD – Vol. 201, ASME, New York (1992), p. 15–24
5. NAPHON, P., WONGWISES, S., A review of flow and heat transfer characteristics in curved tubes, Renewable Sustainable Energy, Rev 10 (2006) p. 463–490.
6. P. NAPHON, Thermal performance and pressure drop of the helical-coil heat exchangers with and without helically crimped fins, Int. Commun. Heat Mass Tran. 34 (3) (2007) 321–330.

CYSENI 2015, May 27–28, Kaunas, Lithuania
ISSN 1822-7554, www.cyseni.com

AIR FLOWRATE AND TEMPERATURE CONSIDERATIONS FOR EFFICIENT WARM AIR SUPPLY INTO SINGLE OFFICE ROOM

A. Prozuments, A. Zajacs
Riga Technical University
Kalku str. 1, LV-1658 Riga – Latvia
Phone +371 2919 0871
Email: aleksejs.prozuments@rtu.lv

ABSTRACT

In mixing ventilation systems indoor air quality is highly dependent on air mixing effectiveness. However, it is necessary to control air distribution in order to prevent excessive air velocity and draught rate occurrence in human's occupancy zone. With warm air supply systems, there is a risk of air stratification in the room, when a layer of fresh and warm air mass builds up right below the ceiling, whereas layer of stuffy and relatively cooler air mass stays in human's occupancy zone.

Most often there are convectors, radiators or space heaters used for heating the office rooms, instead of airborne heating via air terminal devices. In this study, a research on air stratification was carried out and possible ways to prevent it were analyzed, when warm air is supplied via air supply diffusers from the ceiling.

Supply air flowrate and supply air temperature can be varied to maintain room temperature set point according to the air temperature conditions outdoors and heating loads indoors. Increasing the supply air temperature and decreasing supply air flowrate can save energy, but it causes reduced air circulation and thus leads to low indoor air quality risk. Increasing the supply airflow will improve air circulation and mixing effectiveness within the room, but it will increase energy consumption.

The objective of this study was to identify the correlation between the minimum airflow and supply air temperature that would maintain a satisfactory thermal comfort in the human's occupancy zone when introducing warm air into the room. The study was conducted in the full-scale test chamber that represents a typical single office room. 24 air velocity and temperature measuring probes were positioned in different levels and locations of human's occupancy zone. Supply air diffuser prototype with a perforated faceplate was integrated into the ceiling and tested to see how the warm air is distributed within the test chamber. Numerous different supply air temperature and flowrate variations were analysed during the study and 6 scenarios are presented in this paper.

Keywords: energy efficiency, ventilation, heating, air mixing, air stratification, temperature gradient

1. INTRODUCTION

Supplying a warm air from the ceiling into the room is accompanied by numerous factors that can compromise occupants' comfort. Such factors are:

- air mass stratification;
- insufficient air mixing effectiveness;
- short-circuiting.

Air mass stratification occurs when there is not sufficient airflow that forces the supply air to reach humans' occupancy zone and thus to ensure a good mixing effectiveness within the space. Due to the buoyancy effect the layer of warm air[1] builds up in the upper part of the room and sticks to the ceiling, whereas in the humans' occupancy zone air temperature doesn't change considerably. This is particularly common in traditional heating ventilation systems that are not designed properly. What's more important, that the air stratification doesn't only dissatisfy human's comfort, it is also a significant drawback in the indoor air

---

[1] An air layer or air mass with the temperature above the room's ambient temperature.

quality. Air supplied via ceiling integrated air terminal device has also a function to deliver fresh air and replace stuffy air via mixing. The mixing air distribution aims to dilute the pollution generated in the ventilated space [1]. If supply air temperature is above room's ambient air temperature, than air mass stratification inevitably leads to insufficient air mixing effectiveness, thus compromising the indoor air quality.

Given that in traditional ventilation systems exhaust terminal devices and exhaust grilles are placed in the upper part of the room, the risk of short-circuiting adds up, when supply air is flowing directly to the exhaust unit.

In heating ventilation systems preheated air is supplied because it is necessary to compensate for the most part of heat losses of the building. Such systems can be effectively used as an air heating system and in this way, eliminate the need for other heating sources. The air heating system will be effective only if heat losses of the building are compensated by supplying the minimum amount of fresh air required for building ventilation, and the temperature of the supplied air is not higher than 50°C. If the supply temperature exceeds 50°C dust combustion process begins in the air ducts and the supplied air no longer satisfy the hygiene requirements [2].

Supply air flowrate and supply air temperature can be varied to maintain room temperature set point according to the air temperature conditions outdoors and heating loads indoors. Increasing the supply air temperature and decreasing supply air flowrate can save energy, but it causes reduced air circulation as supply air temperature rises above the space temperature and leads to above-mentioned risks. On the other hand, increasing airflow will improve air circulation; however, it will increase energy consumption [3].

Air mixing effectiveness also depends on the design of the air terminal devices or diffusers. In traditional applications (offices, hotels, classrooms, restaurants etc.) air supply diffusers are designed to maintain Coanda effect, which is not a major concern when supplying warm air into the room, however in cooling or isothermal conditions it is a prerequisite.

Air supply diffusers are designed to discharge a preconditioned air into the space, so that occupant comfort criteria are met. Supply diffusers may cause occupant discomfort if the airflow and supply air temperature are not suitable. During the winter period, stratification and short-circuiting can cause thermal discomfort [1]. Studies have shown, that for warm air supply diffusers with a perforated faceplate are more effective.

Thermal comfort is defined as that condition of mind which expresses satisfaction with the thermal environment. Dissatisfaction may be caused by warm or cool discomfort of the body. Thermal dissatisfaction may also be caused by an unwanted cooling (or heating) of one particular part of the body. Local discomfort may also be caused by an abnormally high vertical temperature difference between head and ankles, by too warm or cool a floor or by too high radiant temperature asymmetry. Discomfort may also be caused by too high a metabolic rate, or by heavy clothing [4].

The objective of this study was to identify the correlation between the minimum airflow and supply air temperature that would maintain a satisfactory thermal comfort in the human's occupancy zone when introducing warm air into the room. The study was conducted in the full-scale test chamber that respresented a typical single office room.

2. METHODOLOGY

2.1. Full-scale testing concept

Designers of supply air diffusers recognised the importance of maintaining the Coanda effect with turndown and achieved it using a slot geometry diffuser that created good room air circulation and reduced the airflow [3]. Researchers have worked to improve air circulation by studying the distribution and movement of air. Studies include air distribution tests of variable air volume air-conditioning systems that use various types of supply outlets [4, 5].

Studies on air movement and distribution within the enclosed spaces are conducted using full-scale test methodology. Full-scale test rooms are used for identification of diffusers with regard to the flow they generate. Detailed temperature and velocity measurements are performed close to the diffuser to identify the characteristics of the generated pattern, including throw length of the jet[2], jet drop (when cold air is supplied) and jet rise (when warm air is supplied) of the flow from the diffuser, spread of the supplied flow, etc. [1].

For the purpose of room airflow modeling, the air distribution in the flow at the vicinity of the diffuser can be identified. In this case measurements can be performed with special probes connected to a multichannel low velocity anemometer. A set of omnidirectional transducers placed vertically is used to measure the air distribution across the wall jet generated by a ceiling air terminal device. The transducers are attached on device that makes it possible to change the distance between the transducers in vertical direction as well as to place the transducers at different distance from the diffuser. In this way several air temperature and velocity profiles can be measured.

2.2. Test chamber

In this study the tests were performed in a specially designed test chamber which represented a typical single office room (Fig. 1). The floor area of the test chamber was 24.35 m^2 (width = 4500 mm, length = 5410 mm) and height was 2580 mm.

Detailed dimensions and parameters set for the test chamber are given in Table 1.

Table 1. Test chamber set parameters and dimensions

Width of the test chamber, mm	4500
Length of the test chamber, mm	5410
Height of the test chamber, mm	2580
Ambient air temperature (outside the test chamber) , °C	22.0±1.0
Air set temperature, °C	24.0±0.5
Internal heat loads, W	240
Number of measuring probes, total	24
Number of measuring probes, at 200 mm above the floor	2
Number of measuring probes, at 1100 mm above the floor	11
Number of measuring probes, at 1800 mm above the floor	11

---

[2] Distance from the diffuser where velocity becomes equal to 0.2 m/s.

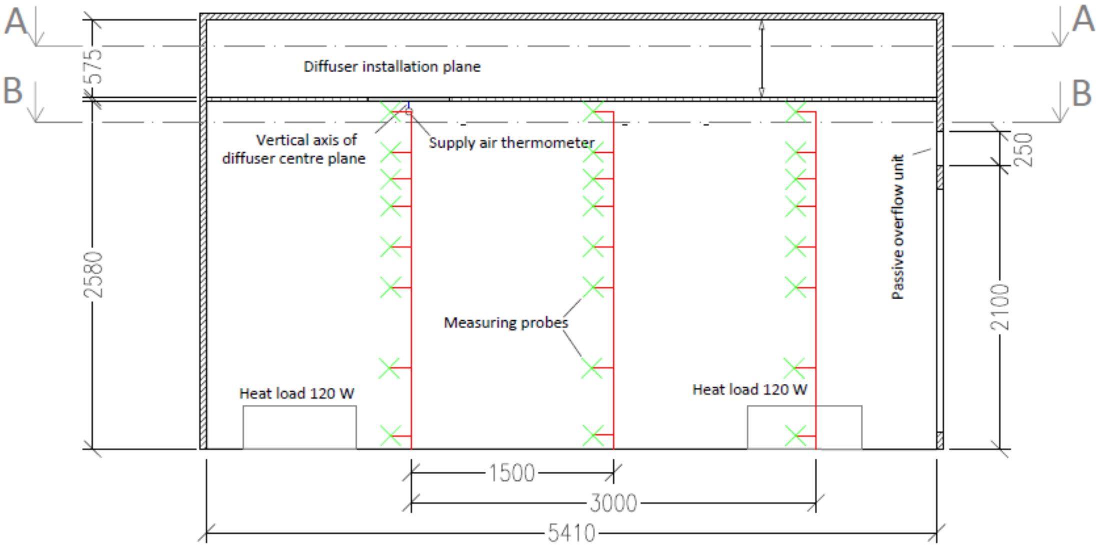

Fig. 1. Test chamber's layout

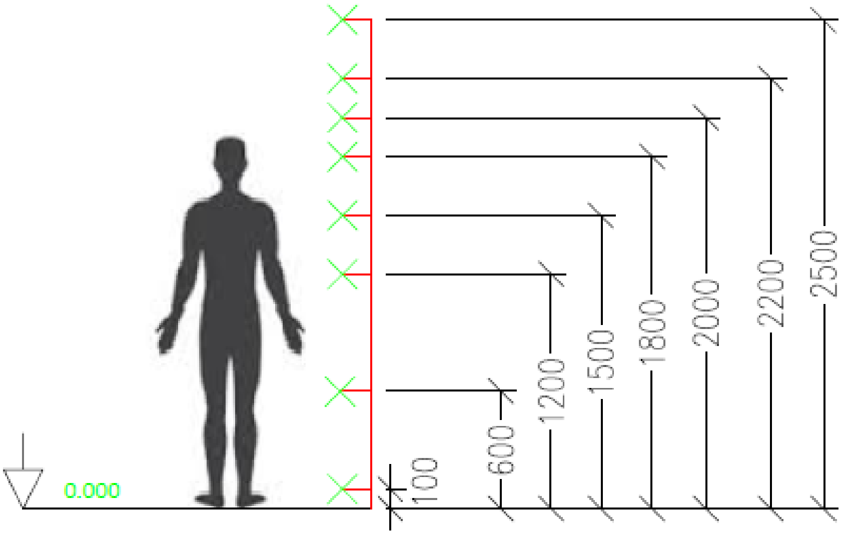

Fig. 2. Vertical profile of the measurement points
(human's silhouette is added as a height level reference)

24 measuring probes were installed at 8 height levels covering human's occupancy zone and the zone under the ceiling (Fig. 2). At each of 24 points air temperature and velocity were measured.

The point of reference for the disposition of the probes was the vertical axis of the diffuser installation plane. The measuring probes were attached to 3 support bars that were placed in three horizontal offsets (x_1= 0 mm, x_2 = 1500 mm, x_3 = 3000 mm) from the vertical axis of the diffuser installation plane (Fig. 1).

The test chamber was maintained to allow the heat transfer between the test chamber and surroundings. A passive overflow grill was integrated on the backside of the test chamber to eliminate the occurrence of overpressure and overheating. Room set temperature was 24,0±0,5°C, surrounding temperature outside the test chamber was kept at 22,0±1°C. All measurements were carried out by gradually increasing supply air temperature, whilst tracking the minimum supply air flowrate for acceptable air mixing effectiveness (t↑, q↓).

Several different t↑, q↓ patterns were analyzed for this particular study to find the best matching correlation between the supply airflow decrease against the increase of supply air temperature.

Throughout the study the supply air temperature was being preheated by the heating coil installed in the air duct system prior to the plenum box. The air temperature and air movement velocity data were registered every 20 seconds so that any fluctuations or deviations were excluded.

3. RESULTS AND DISCUSSIONS

Fig. 3 shows the relationship between the supply air temperature and the airflow at heating load conditions of 240 W and at room set temperature of 24.0±0.5^{o}C. The airflow rate and supply air temperature can be adjusted to maintain the room temperature set point based on the heating load. If there is a low supply air temperature, a relatively high airflow is necessary to satisfy the room temperature requirements. This will improve overall air circulation and ensure good air mixing effectiveness; however, it will also increase the energy consumption. Increasing supply air temperature and decreasing the airflow can save fan power energy, but it will reduce the rate of air circulation.

In this particular case the supply airflow and supply air temperature were being constantly adjusted to maintain the room temperature level at the 24.0±0.5^{o}C set point.

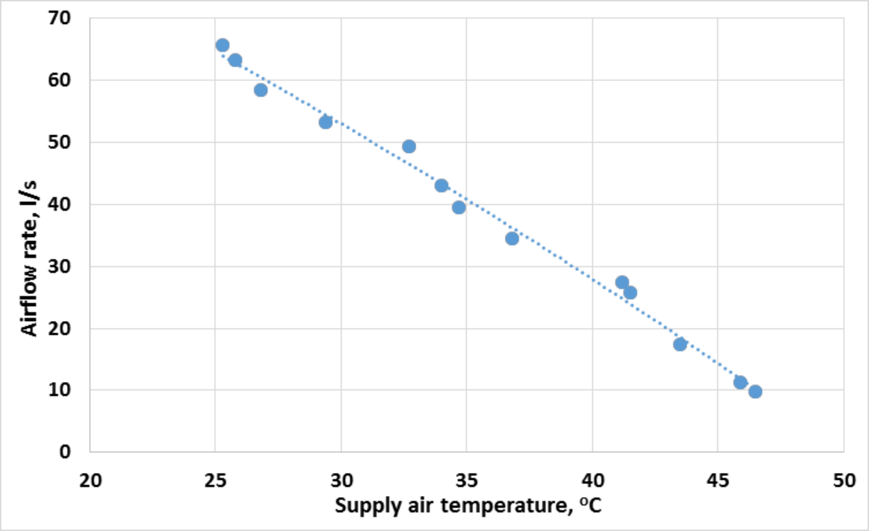

Fig. 3. Relationship between the supply air temperature and supply airflow at 240 W heating load and 24,0±0,5^{o}C room set point condition

From the graph (Fig. 3) it is seen that the decrease of the air flowrate requires supply air temperature to be increased quite significantly. The points on the graph are scattered quite evenly, and mathematically this relation can be described as follows:

$$y = -0{,}0133 \cdot x^2 - 1{,}5801 \cdot x + 112{,}38\,. \qquad (1)$$

Where:

y – supply airflow rate, l/s;

x – supply air temperature, ^{o}C.

However, it is important to note that any external variations may disrupt the effectiveness of such mathematical interpretation, therefore Equation (1) in this study was applied only to show the predicted trendline.

Table 2. Measured air temperature profile (x_1=0; x_2=1500; x_3=3000), perforated diffuser prototype

Height, m	**Air temperature, °C, x_1=0 mm**	**Air temperature, °C, x_2 = 1500 mm**	**Air temperature, °C, x_3 = 3000 mm**
2.5	26.6	26.8	26.9
2.2	26.3	26.2	26.0
2.0	25.7	25.8	25.8
1.8	24.3	24.6	24.5
1.5	23.8	23.8	24.1
1.2	23.5	23.2	23.3
0.6	23.4	23.4	23.6
0.1	22.8	22.8	22.9

In residential ventilation systems occupant thermal comfort can be achieved if a vertical room air temperature difference is low. ASHRAE 55 Standard requires that the vertical temperature gradient in the room is less than 3°C. However, ensuring a low temperature gradient can compromise energy efficiency of the household. Therefore, the near-optimal supply air temperature and airflow rate should be determined using a minimal amount of energy under conditions of good air circulation in occupied areas.

Table 3 provides a more detailed picture of temperature profile. Vertical air temperature gradient in all three cases is below ASHRAE's recommended threshold, however, above the height level of 1.5 m ATG[3] temperature varies substantially, resulting in the vertical temperature gradient close to 3°C/m. The average room temperature in the human's occupancy zone (below 1.8 m ATG) throughout the test was about 23.5±0.5°C whereas the average temperature above the human's occupancy zone was about 25.5±0.5°C, that is close to the supply air temperature. This indicates the occurrence of intense air stratification due to insufficient air mixing.

If the airflow is increased, it will result in better air mixing and thus temperature profiles will be smoother. Moreover, in such case the supply air temperature may be lowered to some extent.

Table 3. Vertical air temperature gradients (x_1=0; x_2=1500; x_3=3000), perforated diffuser prototype

Parameter	x_1=0 mm	x_2 = 1500 mm	x_3 = 3000 mm
Temperature gradient 0.1÷2.5 m ATG, °C/m	**1.58(3)**	**1.66(6)**	**1.66(6)**
Temperature gradient 0.1÷1.5 m ATG, °C/m	0.714	0.714	0.857
Temperature gradient 1.5÷2.5 m ATG, °C/m	2.80	3.00	2.80
Average temperature below 1.8 m, °C	23.55	23.70	23.70
Average temperature above 1.8 m, °C	25.45	25.70	25.70

To analyze how an air distribution pattern varies under different supply air temperature and flowrate arrangements, 6 different scenarios were run.

---

[3] ATG – above the ground level.

Test chamber's set temperature was 24°C±0.5°C at a level of 1.5 m ATG. Two flowrate values were set for the particular perforated diffuser prototype based on the following criteria;

- 35 l/s – to ensure a sufficient supply of fresh air according to CR:1752 requirements for B category office space;
- 45 l/s – a forced flowrate to ensure better air circulation.

Supply air temperature ranged from 25°C to 30°C to track the correlation of supply air temperature increase and flowrate adjustment.

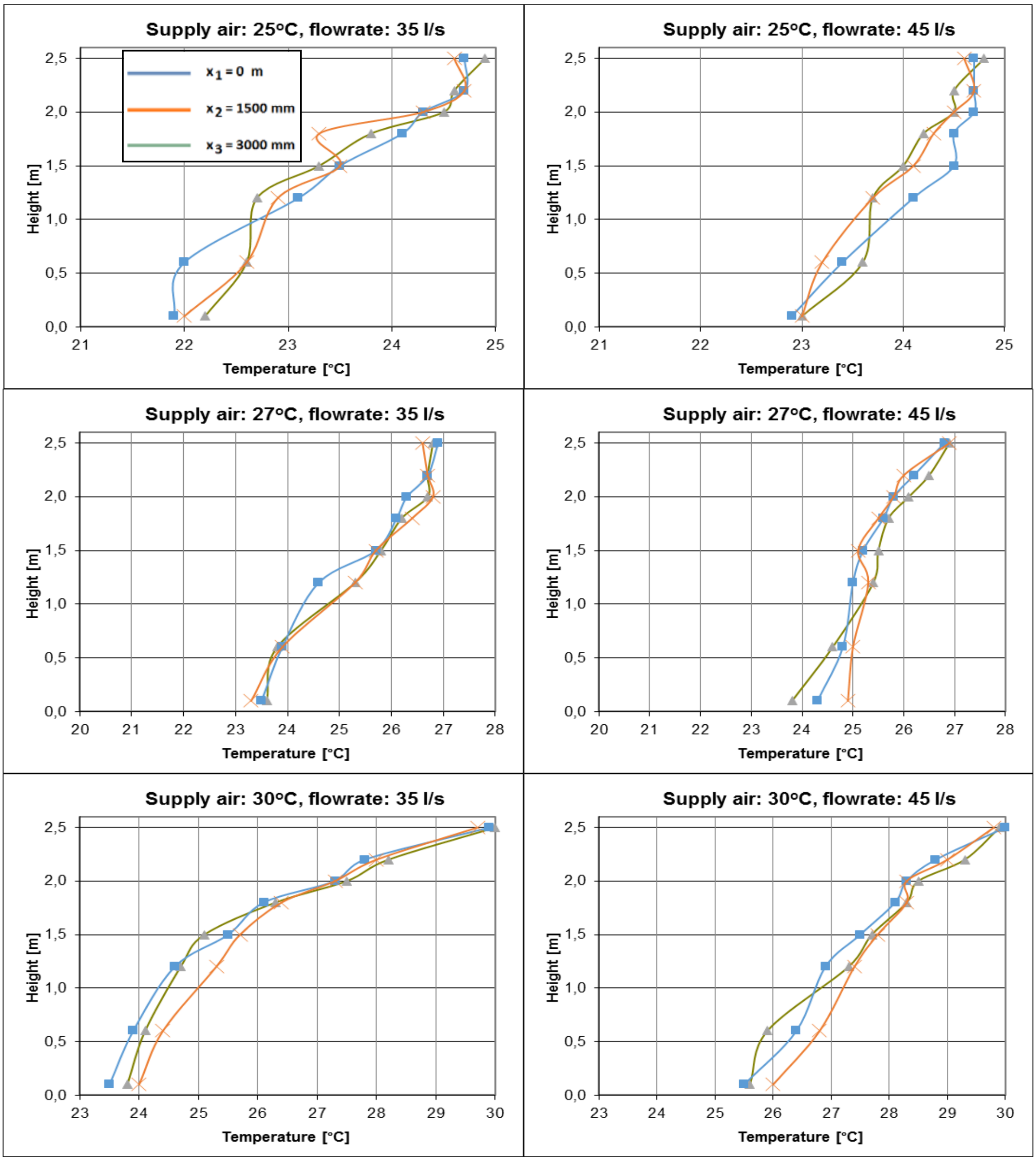

Fig. 4. Temperature profiles under varying temperature and flow rate set arrangements

Fig. 4 encompasses all 6 scenarios: blue curve represents the measuring section at x_1 = 0 mm distance, orange curve – at x_2 = 1500 mm, green curve – at x_3 = 3000 mm. At lower supply air flowrate (35 l/s, graphs on the left) the vertical temperature gradient is evident. As the supply air temperature is raised, so does the vertical temperature gradient – at 25^{o}C the vertical temperature difference is 3^{o}C, whereas at 30^{o}C it reaches 6.6^{o}C. This indicates, that supply air temperature rise alone will not ensure the desired temperature level at the human's occupancy zone. Even if the supply air is heated up from 25^{o}C to 30^{o}C, human's occupancy zone expierences only $\Delta t=2.5^oC$ increase. Further supply air temperature increase to 35^{o}C resulted in just $\Delta t=2^oC$ increase in human's occupancy zone compared to 30^{o}C levels (not shown in the graphs).

Air velocity values are not presented in the grpahs as in all cases air velocity measurements were significantly below the critical value of 0.2 m/s. For this reason, air velocity analysis is disregarded in the discussion.

Given that supply air temperature increase in these conditions doesn't provide the needed temperature rise in human's occupancy zone, and rather causes the discomfort due to the high temperature gradient, the supply air flowrate was increased to 45 l/s.

At 45 l/s the temperature profiles in all three cases are substantially smoother (graphs on the right). It is better described by the temperature gradients that are considerably lower at higher flowrate (1.9, 3.1 and 4.2 accordingly). Further increase in the airflow rate resulted in even smoother temperature profiles, however, was not considered as a reasonable and efficient solution with regards to the increase in energy consumption.

4. CONCLUSIONS

If building envelope is tight enough and outdoor air infiltration risk is prevented, airborne heating via ceiling integrated diffuser is an effective way to heat single office type rooms and to reduce costs for radiators and convectors. Good air mixing can be reached and thus, air stratification can be prevented, by using diffusers with a specific face plate pattern that are specifically designed for cooling and heating purposes.

The airflow rate and supply air temperature can be adjusted to maintain the room temperature set point based on the heating load. If there is a low supply air temperature, a relatively high airflow is necessary to satisfy the room temperature requirements. This will improve overall air circulation and ensure good air mixing effectiveness; however, it will also increase the energy consumption. Increasing supply air temperature and decreasing the airflow can save fan power energy, but it will reduce the rate of air circulation.

The graphs in Fig. 5 describe the basic concept of the efficient warm air supply into the office space – a slight increase in supply air temperature and flowrate results in satisfactory indoor climate conditions and at the same time keeps the building's energy consumption at acceptable levels. Even though the energy consumption will go up, good indoor air quality and thermal comfort will be maintained in the human's occupancy zone eliminating the need for additional heating sources.

This study was solely focused on air temperature pattern in the test chamber and other parameters like air velocity, turbulence and draft rate were disregarded. In airborne heating systems air velocity in the human occupancy remains low and is usually not a cause for concern, while the air temperature gradient and air mixing are subjected to be thoroughly analyzed.

REFERENCES

1. MULLER D., KANDZIA C., KOSONEN R., MELIKOV A. K., NIELSEN P.V. Mixing ventilation. Guide on mixing air distribution design. *REHVA guidebook*, 2013, Vol. 19, 114 p.
2. PODERYTĖ J., BLIŪDŽIUS R., BANIONIS K., BLAŽEVIČIUS E., BURLINGIS A. The research of supplied air flow parameters in air heated buildings. *MECHANIKA*, 2013, Vol. 19 (4), p. 410–416.
3. CHOA YOUNG-HUM, LIUB M. Correlation between minimum airflow and discharge air temperature. *Building and Environment*, July 2010, Vol. 45, Iss. 7, p. 1601–1611.
4. ASHRAE, ASHRAE standard 62-2004. Ventilation for acceptable Indoor Air Quality (IAQ); 2004.
5. PROZUMENTS A., BORODINECS A., ZEMITIS J. The Optimal Operating Range of VAV Supply Units. *Cold Climate Conference*, July 2012, 7 p.

CRITICAL FLOW VELOCITY DETERMINATION FOR TUBE-BUNDLE WITH APPLICATION OF NUMERICAL EXPERIMENT METHOD

A. Samolysov, S. Kaplunov, N. Valles,
O. Marchevskaya, E. Dronova
IMASH RAS
Maliy Haritonievskiy line 4, 101990 Moscow – Russia
Phone 8(499)1353514
Email: kaplunov@imash.ru, klevdr54@mail.ru

ABSTRACT

The work is devoted to creation and application of mathematical models for the most dangerous oscillations excitation mechanisms of tubes and cylindrical form bluff structures in liquid or gas flow, as well as to creation of efficient computational methods for description of these models.

Numerical investigation method of hydrodynamic forces arising from separated flow, and tube bundles oscillations excited by these forces was worked out by authors.

Method is based on application of created original tube-bundles hydroelastic oscillations excitation in cross flow mathematical model. Hydroelastic excitation problem is reduced to the stability analysis of elastic tubes undisturbed state. Analysis is conducted with the assumption of linearity of the destabilizing forces. On basis of mathematical model theoretical studies of necessary and sufficient condition for the stability, expressed through the dimensionless system parameters (mass, damping, velocity), was obtained.

Numerical identification of the linear hydrodynamic connection matrix algorithm for particular tube-bundles was elaborated. Algorithm and based on it programs verification were performed by results of test computations and bank of available experimental data correlation.

Method for determination of linear hydrodynamic connection matrix for tube-bundles with cross section regular arranging was offered. It is based on computation of relatively small, but sufficient for reliable results, part of tube-bundle.

Keywords: tube-bundle**,** numerical experiment, hydroelastic excitation, separated flow, linear hydrodynamic connection matrix

1. PROBLEM STATEMENT

The work is devoted to creation and application of mathematical models for the most dangerous oscillations excitation mechanisms for tubes and cylindrical form bluff structures in liquid or gas flow, as well as for creation of efficient computational methods for description of these models. Combined approach based on correlation of numerical experiment and nature objects investigation is necessary for our problem solution.

Work objective is creation and implementation of viscous fluid and gas flow effective modeling methods in form of program complexes for investigation of aerodynamic loads on bodies, performing voluntary movements including change in shape for solution of conjugate bodies motion problems under action of aerodynamic forces.

2. APPLIED METHODS

Caring out this work, the following methods were applied: modernized method of discrete vortices (MMDV), conformal transformation method, collocation method, multicomponent system estimation with application of linear hydrodynamic connection matrix, multicomponent system stability analysis with Lyapunov criterion, decomposition of a potential function by small parameter method, finite-difference methods, statistical modeling and optimization method, similarity and dimensional analysis theory.

The main method applied in our work is the original and efficient modernized method of discrete vortices (created in IMASH RAS) [1–4], makes it possible to solve a wide range of tasks for flow of stiff and flexible bodies of different configuration of cross-section in a specified range of Reynolds numbers during numerical experiment (Fig. 1).This method application was approved by known physical experimental data. Under this method, determination of aerodynamic forces acting on the moving parts and multicomponent infrastructure systems constructions (bridges, pedestrian bridges, tube constructions and elastic station constructions), as well as the calculation of constructions self-oscillations with the passage of high-speed trains in 2D statement were worked out.

Existing software systems of computational fluid dynamics applying grid methods are not sufficiently effective for structures with variable geometry analysis. Calculation time is very long. Therefore application of vortex methods (MMDV) applying environmental models seems to be relevant because it allows obtain non-stationary loading at substantially lower computational time. Accuracy is reasonable for engineering calculation.

The developed method significantly expands possibilities of vortex formation mechanism numerical investigation, as well as non-stationary separated flows structure under arbitrary motions and shape change of streamlined bodies numerical investigation. Also, this method is relevant for problems of optimal cross section parameters choice solving.

Here fluid is believed to be incompressible. The flow rate is in range Re = 10^3-10^5, typical for real heat exchangers. For such flows the viscosity renders essential influence on fluid in thin boundary layers, which are formed on streamlined profiles. The flow is divided into two areas: the area of flow of viscous liquid in thin boundary layers and area of external flow, where fluid is necessary inviscid, and flow is potential. The vortex wake formed behind structure as a result of separated flow, is simulated by a set of discrete vortexes, which are brought into external current from disruption points of a boundary layer in the definite moments of time. In such a way calculation of the continuous process of flow development is replaced by discrete one, occurring in design moments of time. Sequentially, in each instant the parameters of an inviscid flow are counted in turn.

Model for calculation of a separated flow of a tube allows to account influence of Re-number by a choice of the position of disruption points of boundary layer from a surface of a tube on the basis of experimental dependence for viscous liquid. Numerous calculations show, that the design quantitative performances of flow, obtained at such approach (frequency of variation of a lift force, values of drag and lift coefficients and parameters of Karman vortex street) are well compounded with known experimental data in a practically relevant range of Re – numbers from Re = 10^3 up to 10^6.

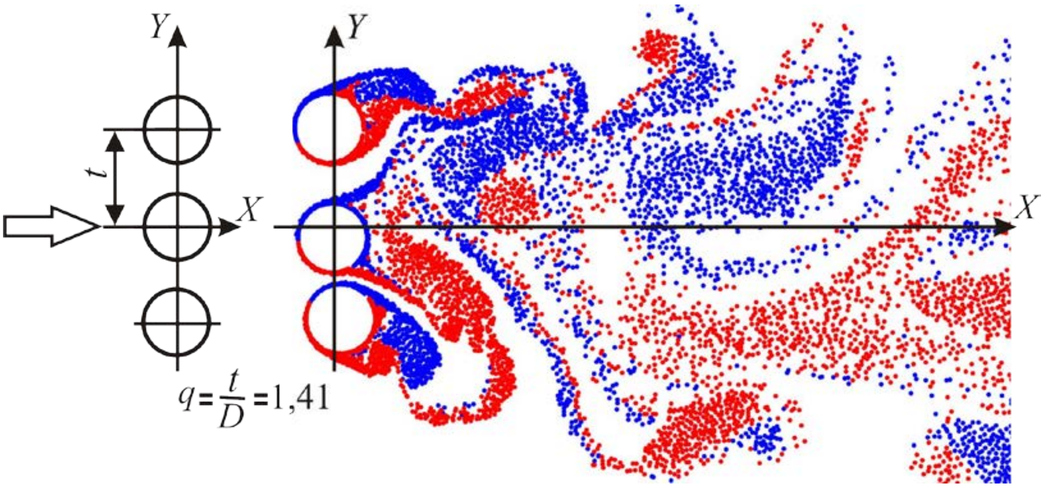

Fig. 1. Numerical experiment setup example applying numerical method

3. EXCITATION MECHANISMS

Basing on experimental data there are several specific mechanisms of excitation: turbulent buffeting, periodic vortex separation, hydroelastic excitation.

It is shown, that possibility of hydroelastic excitation is the spoilage warning for tube bundle.

Primarily during development engineering it is essential to appraise the possibility of tube bundle hydroelastic excitation and only after its exclusion oscillations amplitudes, caused by hydroelastic excitation calculation makes sense.

4. OBTAINED MODELS HIERARCHY

As shown by long experience modeling with method of discrete vortices created model possesses the following advantages. On a consolidated mathematic and computational basis you can create a hierarchy of software covering a wide range of applications. On this base in combination with the physical experiment accumulation of an important cognitive experiment the limits of schemes and models applicability are set. This establishes a transition from individual tasks to creation of complex tasks on a regular basis. It was turned out that addition of discrete vortices method with boundary layer model (to determine its separation) allows you to make a new step in discrete vortices method empowering (expanding opportunities). Change in vortices separation angle enables you to simulate the impact of Re number on the hydrodynamic forces and vortices separation arrangement consequently discrete vortices method was extended to the Re-numbers area from 10^2 to 10^6. In the computations effect of resistance C_x, C_y crisis was reproduced for Re-numbers Re > $2{\cdot}10^5$.

Original boundary problem solution allowed to apply combined method to extend discrete vortices method to calculation of bodies with arbitrary (non-circle) cross-section flow.

Joint equations system solution describing the body oscillations and defining corresponding hydrodynamic forces at each step of calculation allowed to apply modernized discrete vortices method for different constructions self-oscillations calculation.

5. HYDROELASTIC EXCITATION

Mathematical model of the hydroelastic interaction, where interaction between oscillating tubes is taken into account in the most common form (in framework of destabilizing forces linearity hypothesis) is given in [5, 6]. Model describes hydroelastic excitation mechanism as instability of elastic tubes unperturbed state development.

Mathematic model for elastic tubes bundle hydroelastic excitation by external cross flow was worked out. Hydroelastic excitation task is reduced to unperturbed state of elastic tubes stability analysis. Based on theoretical investigation of this model the necessary and sufficient stability conditions expressed through the dimensionless system parameters was received.

Received by mathematical model analysis necessary and sufficient stability condition was recorded in visual form through the dimensionless system parameters. Condition allows reasonably carry out available experimental critical parameters data generalization. Included in stability condition dimensionless parameters determine similarity criteria for hydroelastic excitation which is necessary for experimental (and numerical) process in tube bundle modeling.

6. NUMERICAL EXPERIMENT SETTING

Methodology and design scheme of the numerical experiment are similar to those presented in [7] for costly and laborious physical experiment.

1. One cylinder is oscillating, other is stationary. This is repeated 2N times separately in X and Y directions, so we receive $\hat{V}(\tau)$ hydrodynamic connection matrix (Program 1) (Fig. 1, 2).

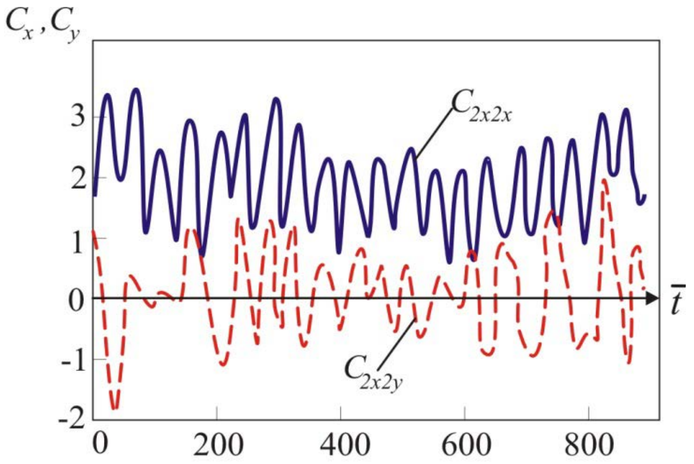

Fig. 2. Hydrodynamic interaction matrix elements (dimension [6ˣ6]) for three tube row. Hydrodynamic force C_{2x2y} – force acting on the second cylinder in the direction of axis X from fluctuations of the second cylinder in the direction of Y-axis. Hydrodynamic force C_{2x2x} force acting on the second cylinder in the direction of axis X from the fluctuations of the second cylinder in the direction of X axis

2. Receive linear hydrodynamic connection matrix $\hat{S}(p)$ which represents Laplace image of matrix (Program 2).

3. Find $\lambda_j(p)$ the eigenvalues of matrix $\hat{S}(p)$ (Program 3). Out of all eigenvalues we find one λ with the maximum imaginary part. On stability region border $p=i\omega$ – imaginary value. Accounting parameters ξ and μ_1 values not higher than first order of smallness we receive critical parameter value $(2\xi/\mu_1)_{cr}$:

$$\left(\frac{2\xi}{\mu_1}\right)_{cr} = \frac{\mathrm{Im}[\lambda(p)]}{\omega_1^2} \tag{1}$$

4. Repeat all points at a different flow velocity and receive stability boundary for tube bundle.

7. RESULTS

1. Method of discrete vortices, was developed and modernized. Method allows to visualize picture (animation) of separated cross flow over complex configuration cylinder in real time (Fig. 1).
2. According to developed algorithm programs were written for hydrodynamic non-stationary forces estimation under separated flow around stationary circular and non-circular profiles oscillating over a given law, profiles self-oscillations. Calculation reliability was checked by obtained results comparison with available experimental data (Fig. 2).
3. Critical velocity values of the flow as a function of dimensionless parameter (including value of logarithmic oscillations decrement and dimensionless bundle mass parameter), was defined, it allows instantly troubleshoot inadmissibility of hydroelastic excitation of already commissioned heat exchanger (Fig. 3).

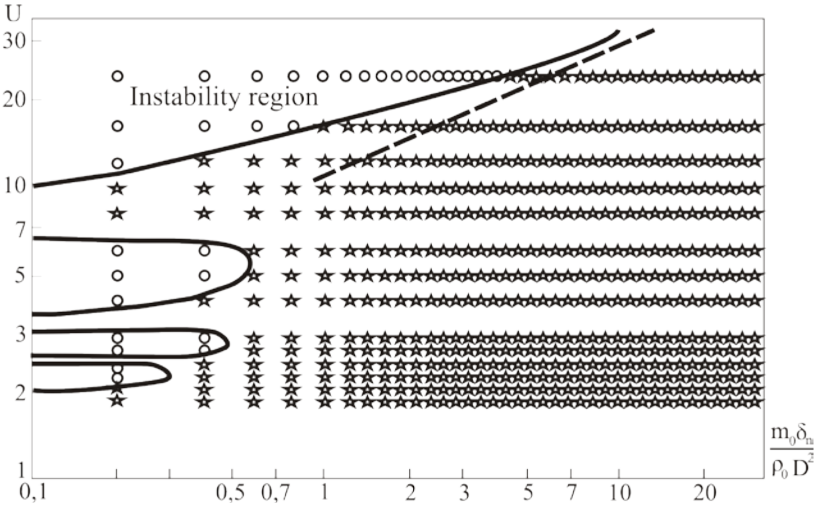

Fig. 3. Stability region boundary for a number of tubes *(q=t/D=1.41):*
solid line – authors calculation for three tubes series dashed line – experiment for infinite number of tubes [8]

4. Mathematic model of hydroelastic oscillations excitation for elastic tube bundle in cross flow was worked out. Task of hydroelastic excitation investigation is reduced to stability analysis of undisturbed elastic tubes. Based on theoretical investigation of this mathematic model necessary and sufficient stability condition expressed through the dimensionless system parameters was received.
5. Method for hydrodynamic forces determining in bundles consist of great tubes number with regular layout cross section was proposed.
6. Developed numerical method for hydrodynamic forces and excited tube bundle oscillations can partly replace or expend costly and time-consuming experimental investigations.

REFERENCES

1. KAPLUNOV, S., VALLES, N., GORELOV, E., SHITOVA, L. Metod of Hydrodynamic Oscillation Exciting Mechanism of Heat Exchanges Tube Bundles Mathematical Modelling // *Problems of Mechanical Engineering and Reliability*, 2008, No. 3, p. 107–112.
2. KAPLUNOV, S., VALLES, N., SHITOVA, L. Discrete Vortexes Method Application for Tube in Liquid Flow Self-Oscillations // *Problems of Mechanical Engineering and Reliability*, 2009, No. 4, p. 13–18.
3. VALLES, N., MASEVICH, A., SAMOLYSOV, A. Application of discrete vortices method for separated flow calculation of one- and double-component constructions // *Problems of mechanical engineering and automation*, 2013, No. 3, p. 42–45.
4. VALLES, N., MASEVICH, A., SAMOLYSOV, A. Vortex flow past a stationary and oscillating cylindrical bodies calculation applying method of discrete vortices // *Bulletin of the scientific-technical development*. 2014, No. 6, p. 31–37.
5. SMIRNOV, L., NIKOLAEV, N. Tube bundles of heat exchangers vibration // *Hydrodynamics and convective heat transfer in heat exchangers: Proceedings of the international school – seminar*, Vilnius, 1981, p. 60–71.
6. KAPLUNOV, S., VALLES, N., CHENTSOVA, N., FURSOV, V. Mathematical Model for the Fluidelastic Mechanism Exciting Vibrations in System of Blunt Bodies Placed in Cross Flow of Liquid // *Thermal Engineering*, 2012, No. 6, p. 462–467.
7. TANAKA, H., TAKAHARA, S. Unsteady Fluid Dynamic Force on Tube Bundle and its Dynamic Effects on Vibration // *PVP-Vol. 41*, *New York: ASME*, 1980, p. 77–92.
8. CONNORS, H. Fluidelastic vibration of tube bundles of heat exchangers // *Engineering Design and Technology*, 1978, No. 2, p. 95–102.

CYSENI 2015, May 27–28, Kaunas, Lithuania
ISSN 1822-7554, www.cyseni.com

ACHIEVING ENERGY EFFICIENCY IN THE BUILDING SECTOR IN SELECTED CEE COUNTRIES: POLICY BASED ENERGY DEMAND SCENARIOS UNTIL 2030

A. Toleikyte, L. Kranzl, A. Müller
Vienna University of Technology
Gusshausstraße 25-29, A-1040 Vienna, Austria
Phone +43 (0) 1 58801 370337
Email: toleikyte@eeg.tuwien.ac.at, kranzl@eeg.tuwien.ac.at, mueller@eeg.tuwien.ac.at

ABSTRACT

To achieve energy savings in the European building sector the Energy Performance of Buildings Directive 2010/31/EU (EPBD, recast of 2002/91/EC) was established. The directive has to be implemented on the national level setting up policy instruments to trigger investments in energy efficiency measures. In this paper, policy instruments to achieve energy efficiency in the building sector will be analysed in Bulgaria, Czech Republic and Romania. Moreover, the impact of the existing policy instruments on the final energy demand until 2030 is modelled. The following steps are carried out: (I) data on the building stock, renovation solutions, prices and policies are collected (II) current energy demand for space heating and hot water in the whole building sector are calculated (III) scenarios until 2030 are modelled implementing existing national policy instruments and ambitious policy instruments. The scenarios are modelled by using a bottom-up, techno-socio-economic approach in Invert/EE-Lab model. Invert/EE-Lab is a dynamic building simulation tool that evaluates effects of economic and regulatory incentives on the energy demand in the whole building sector in a country. The final energy demand for space heating and hot water in the residential and service buildings in 2008 was 27 TWh in Bulgaria, 88 TWh in Czech Republic and 82 TWh in Romania. The implementation of existing policy measures shows energy demand reduction of 7%, 20% and 26% from 2008 to 2030 in Bulgaria, Czech Republic and Romania respectively. The results show different energy saving potentials among the countries. These differences are due to different policy instruments, different climate conditions, energy prices and costs of investments which have an impact on the effectiveness of renovation measures and the corresponding renovation rate of the building stock, which is often considered as the main indicator for an effective policy.

Keywords: Energy efficiency, building sector, energy modelling, EPBD, policy instruments

1. INTRODUCTION

The European residential sector (EU-28) was responsible for 27% of the total final energy demand in 2013 [1]. In Bulgaria, Czech Republic and Romania, the share of energy demand in the residential sector on the total final energy demand is 26, 27%, 35% respectively. The number varies between the countries due to the building renovation activities recently and thus different energy efficiency of the building as well as climate conditions.

Following the European energy strategy 20/20/20 and corresponding national strategies which are defined in national energy efficiency action plans (NEAP), energy efficiency in the building sector plays an important role in helping to meet these targets. On the European level, the Energy Performance of Buildings Directive was established (EPBD 2002, EPBD recast). Following this directive, the European member states have to define policy instruments to trigger investments in energy efficiency in the building sector.

The main question of this paper is as follows: What is the impact of the policy instruments on the final energy demand by 2030 in Czech Republic, Romania and Bulgaria?

In order to analyse effect of the policy instruments on the final energy demand in the building sector a bottom-up approach is applied. The bottom-up approach enables to analyse the building sector based on disaggregated data. That means that the building technical characteristics, specific climate conditions, energy performance of the building by applying different energy efficiency measures can be analysed. This also enables to investigate future energy demand by manipulating building energy performance while applying different depth of renovation measures. This allows us to show the importance of the depth of building renovation on the reduction of energy demand for space heating for a particular building and for the whole building stock.

There are numerous studies which model energy demand of the building sector in different countries or regions by applying the bottom-up approach [2], [3], [4], [5]. Almost all papers show total final energy demand reduction for space heating in the building sector and investigates the impact of the climate change and policy measures.

2. METHOD

2.1. Data collection and definition of the building segments

The scenario modelling is based on the disaggregated building stock data. The disaggregated data of the building stock in one country can be clustered to the following data categories: building types, building periods, building geometry, building envelope quality, heating supply systems, user profiles etc. These data were collected in the project ENTRANZE for all EU-28 and between them for the three investigated countries [6], [7], [8]. Further, to model the energy demand, climate data is used, namely monthly temperature and solar irradiation. Data on temperature and solar irradiation is based on three defined climate regions. The climate regions are Prague, Bucharest and Sofia. Data on monthly temperature and solar irradiation in Prague, Bucharest and Sofia come from IWEC[1] database. For the techno-economic calculation, energy fuel prices, renovation solutions and their investment costs were collected in the frame of the abovementioned project [9]. In order to investigate the impact of the policy instruments, data on policy measures were taken into account [10], [11].

The building sector is divided into the building segments which have to be arranged for the calculation in the bottom-up building simulation tool Invert-EE/Lab [12], [13], [14], [15]. A building segment characterises building category (e.g. single family detached house, apartment), building period, user profile, climate region and heating supply type. For all investigated countries, these parameters were defined country specific.

2.2. Modelling of the energy demand for space heating and hot water

To model final energy demand for space heating and hot water in the whole building sector, a bottom-up approach is applied. To model the current and future final energy demand, building simulation tool Invert-EE/Lab is applied. Invert/EE-Lab is a dynamic bottom-up techno-socio-economic simulation tool that evaluates the effects of different policy packages on the total energy demand, energy carrier mix and CO_2-emission reduction [12], [13], [14].

The calculation is carried out by the following steps which are also described in the subsector below: (II) calculation of the final energy demand for space heating and hot water (III) calculation of the buildings and building components to be renovated or demolished (III) determination of the renovation measures to be installed.

---

[1] The International Weather for Energy Calculations (IWEC) data files are 'typical' weather files suitable for use with building energy simulation programs, derived from up to 18 years of DATSAV3 hourly weather data.

2.2.1. Calculation of the final energy demand for space heating and hot water

Energy need for space heating and hot water is modelled on a monthly basis. The energy need is calculated by using a monthly energy balance approach, quasi-steady-method, according to the following literature, Austrian, German and EU standards: Pöhn Christian: "Bauphysik. Erweiterung 1, Energieeinsparung und Wärmeschutz, Energieausweis – Gesamtenergieeffizienz” and the following standards ÖNORM B 8110-5, ÖNORM H 8055, DIN V 4108-6, DIN V 4701-10, EN ISO 13790: 2008. Final energy demand is calculated by using energy performance coefficient of the heating systems. To be in line with the statistical data on the final total energy demand in the building sector, calculated total final energy demand was compared with the statistical total final energy demand and calibrated. The calibration was carried out by adjusting the following parameters: coefficient of heating systems and energy related used behaviour. The data was also validated by comparing the calculated specific energy demand for space heating for specific building with data given in project TABULA [17] and BPIE report [18].

2.2.2. Scenario modelling

The scenario modelling is derived by the two following components of the model. In the first component, the number of buildings to be demolished or renovated is calculated. The calculation is carried out by the Weibull-distribution. In the second component, so called decision component, it is decided what kind of renovation measure is applied. The investment decision is driven by techno-economic assessment of the renovation measures. The model assigns the highest market share to the most cost effective measures. Thus, not only the most cost-effective option of the measures is taken into account but also the market share of less attractive options which is modelled with the nested logit approach.

Different types of policy instruments are implemented in the model as follows:

– Economic incentives change the economic effectiveness of different options and thus lead to investment decisions. This change leads to higher market share of the supported technology in the Invert/EE-Lab (via the nested logit approach).

– Regulatory instruments (e.g. building codes) restrict the technological options that decision makers have.

– Information and qualification instruments: information campaigns lead to willingness to invest in high energy performance renovation. Qualification instruments are implemented due to the higher quality of renovation activities which are stipulated with the lower U-values in the model.

3. RESULTS

3.1. Input data

Total floor area of the building stock in 2008 was 261 Mm², 400 Mm², 516 Mm² in Bulgaria, Czech Republic and Romania, respectively [6], [8], [7]. The highest share of the building floor area makes up the apartment building stock in all countries. In Czech Republic, 71% of the residential building floor area were built before 1970 [8]. In Romania, 64% of the residential building floor area were built before 1980 [7]. The share of the residential buildings built before 1980 is 62% in Bulgaria. Energy performance of these buildings due to the construction standard the construction time are very poor. These buildings provide a huge energy saving potential as a huge number of these buildings are still not renovated.

In Czech Republic, 55% of the apartment buildings are connected to district heating, followed by natural gas heating (35%) [8]. In Bulgaria, 23% of the residential buildings are connected to district heating, 47% of the buildings use biomass heating system and 27% coal heating system [6]. In Romania, 23% of residential buildings are supplied by district heating, 47% of residential buildings use biomass and 28% are heated with natural gas [7].

Four following types of renovation measure were determined and implemented in the model: maintenance renovation, standard renovation, good renovation and ambitious renovation. These renovation measures differ in technical parameters and corresponding investment costs (see Table 1). Maintenance renovation measure is a renovation undertaken for esthetic reasons and is not related to energy performance achievement. The other three renovation sets, standard, good and ambitious, are renovation measures improving the U-value of the roof, external wall and windows.

Table 1. Renovation measure package description and specific initial costs for Czech Republic, Bulgaria and Romania [9]

Renovation measure	**Description**	**Initial costs, €/m² *** CZE/BGR/ROU		
Maintenance	Renovation of the building elements for aesthetic reasons (e.g. façade painting)	28	14	13
Standard	Roof insulation – 15 cm of thermal insulation, External wall insulation – 10 cm, Window replacement – Double glass with air cavity, U_g= 1.7 W/m²K	100	74	61
Good renovation	Roof insulation – 20 cm of thermal insulation, External wall insulation – 15 cm, Window replacement - Triple glass with argon cavity, U_g= 1.0 W/m²K	106	90	73
Ambitious renovation	Roof insulation – 30 cm of thermal insulation, External wall insulation – 20 cm, Window replacement – Triple glass with argon cavity, U_g= 1.0 W/m²K	140	97	79

* These costs present the average cost of big size building renovation (apartment buildings and service buildings).

3.2. Scenario framework

3.2.1. Economic parameters

Table 2 shows energy fuel prices for households for 2008 and 2030 for Czech Republic, Bulgaria and Romania. Reference scenario derived by POLES model of Enerdata is taken in this paper [19]. In this scenario, oil energy price is expected to increase by 6.5%/year, gas price by 7.6%/year and biomass price development varies strongly from country to country (see Table 2).

Table 2**.** Energy fuel prices for households for 2008 and for 2030 in Czech Republic, Bulgaria and Romania

	Price for households for 2008, €/MWh				**Price for households for 2030, €/MWh**			
	Oil	**Gas**	**DH**	**Biomass**	**Oil**	**Gas**	**DH**	**Biomass**
CZE	63.8	39.5	63.3	57.9	99.2	62.1	81.6	60.8
BGR	96.3	38.9	38.4	23.9	159.0	64.1	58.9	32.9
ROU	96.6	27.8	38.4	39.4	183.2	60.1	55.3	39.1

To calculate cost-effectiveness of the renovation measures, interest rate of 4% for residential buildings and 7.5% for service buildings were taken into account. Depreciation time is 20 years.

3.2.2. Policy instruments

To assess the impact of different policy settings, policy packages, i.e. bundles of instruments were defined. Two different scenarios were investigated, business as usual (BAU) and ambitious scenario. The first scenario, called BAU reflexes existing policy instruments which were analysed and defined for each country separately. This scenario aims to investigate the impact of the existing policy measures on the energy savings for the long-term perspective.

The second scenario, ambitious scenario, is defined in order to show the potential of energy savings by implementing ambitious policy instruments. In this scenario, the same policy instruments were defined for three investigated countries which also let us to compare the countries in terms of the building age structure, climate condition, investment costs and energy prices. This is possible due to the impact of these parameters on the cost-effectiveness of renovation actions which is the basis of the techno-economic modelling (see 2.2.2).

There are four major policy instruments implemented in the assessment, namely the building codes, renovation obligation, financial instrument in the form of investment subsidies and information instruments. Following the implementation of EED, the member states have to renovate 3% of floor area of central governmental buildings annually [20]. Further, according to the EPBD-recast, the member states have to make sure that all new buildings constructed after 2020 are nZEB buildings [21]. These two obligations are taken into the modelling for all investigated countries in both, BAU and ambitious scenarios. The national legislation differs in the financial instruments which are implemented in the BAU scenario. While in Czech Republic and Romania, there are relatively high investment subsidies for building renovation with the focus on the apartment buildings from 60´s, in Bulgaria, there is no budget for building renovation (see Table 3). Existing policy instruments are the input for the BAU scenario. In the ambitious scenario, the financial policy instruments are intensified. In the ambitious scenario, investment subsidies were defined very high for all building categories.

To sum up, the BAU scenario reflexes the existing policy measures in three countries. The ambitious scenario, additionally to the BAU scenario, provides intensified investment subsidies for deep renovation.

Table 3**.** Policy instrument description used in the BAU and Ambitious scenarios

Country	Scenario	Policy description
All	BAU & Ambitious	(1) 3% of floor area of central governmental buildings renovated annually (2) nZEB implementation (according to national definition) for new public buildings from 2018 and 2020 for private buildings
BGR	BAU	(1) Building performance requirements from 2009 (2) no financial resources for building renovation
CZE	BAU	(1) Green Investment Scheme PANEL 2013+ : investment subsidies of 21% for good and ambitious renovation for MFH (2) Investment subsidies of 30% and 33% for single family houses and service buildings, respectively
ROU	BAU	(1) Building performance requirements from 2009 (2) Investment subsidies of 6%, 50% and 40% for single family houses, apartment buildings built between 1945 and 1990 and public buildings, respectively
All	Ambitious	(1) Investment subsidy for good and ambitious renovation: 50% for single family houses, public buildings and service buildings and 60% for apartment buildings (2) Information instruments: due to the information campaigns, willingness to invest in the maintenance renovation is low, while in the good and ambitious renovation – high

3.3. BAU scenario

Final energy demand for space heating and hot water in 2008 is 88 TWh, 82 TWh and 27 TWh in Czech Republic, Romania and Bulgaria, respectively (Fig. 1). Final energy demand was calculated by using Invert-EE/Lab and calibrated according to Odyssee-database. Final energy demand in the buiding sector decreases over the period 2008 and 2030 in all investigated countries. In the Czech Republic, final energy demand for space heating and hot water is reduced by 14% by 2020 and by 20% by 2030. In Romania, final energy demand is calculated to go down by 20% in 2020 and by 26% in 2030. In Bulgaria, final energy demand decreases by 1% by 2020 and by 7% by 2030. It has to be mentioned, that the energy demand reduction is a result of the energy efficiency achievement by building stock renovation and of to the replacement of the heating system. In Romania, the heating system replacement rate is high which leads to high energy reduction. The energy savings in BAU scenario is not a result of the building renovation in Romania.

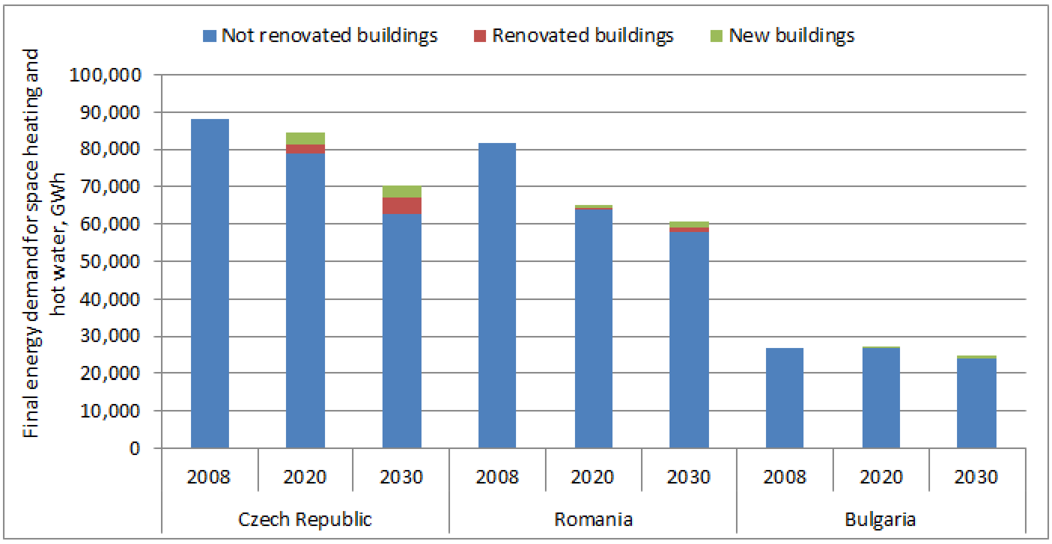

Fig. 1. Final energy demand for space heating and hot water in 2008, 2020 and 2030 in Czech Republic, Romania and Bulgaria building sector, BAU scenario

Fig. 2, Fig. 3 and Fig. 4 show the share of gross floor area of the new buildings, not renovated buildings, buildings with maintenance renovation, good renovation and ambitious renovation (for detailed definition of these renovation levels, see 3.1).

In Czech Republic, the share of renovated buildings is 8%. More than 50% of the renovated buildings are renovated by a using maintenance renovation. The new buildings make up 11% of the total floor area in 2030.

In Bulgaria, the share of the buildings with maintenance renovation on the total renovated building stock is more than 90% in 2030. Only a small part of the renovated buildings are being renovated with ambitious or good renovation. The share of the buildings with a thermal renovation is 2% in 2030. The new buildings make up the share of 5% in 2030.

In Romania, the share of renovated buildings on the total building stock in 2030 is 7%. 68% of the buildings are renovated using maintenance renovation, 21% ambitious renovation and 8% good and 3% standard renovation.

The results of the renovation rate and renovation depth show differences between three countries. In the Czech Republic, existing financial subsidies for building renovation lead to the higher share of the ambitious building renovation. Since the calculation is based on the cost effectiveness of the renovation packages, high fuel energy price compared to other countries, lied to the investment decision in ambitious and good renovation packages in Czech Republic. In Bulgaria, due to the relatively low energy prices and lack of the policy instruments supporting renovation activities, only a small share of the buildings undertakes good or ambitious renovation. Although, there are financial subsidies for building renovation in Romania, only a small part of the buildings are renovated by using a thermal renovation. The barrier of this, again, is relatively low energy fuel prices.

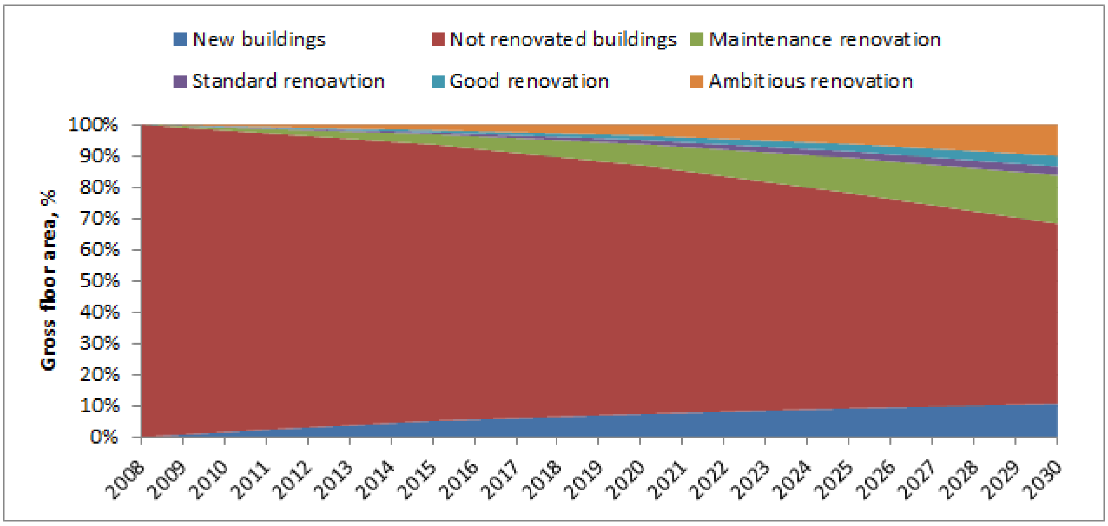

Fig. 2. Czech Republic: Share of the floor area of not renovated buildings, renovated buildings and new buildings on the total gross floor area: BAU scenario

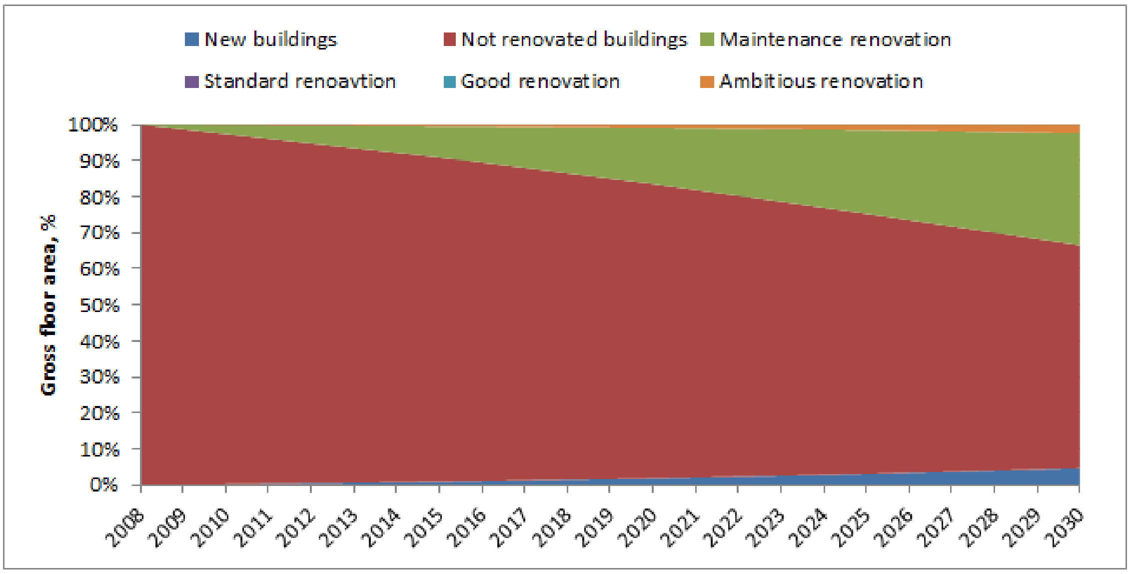

Fig. 3. Bulgaria: Share of the floor area of not renovated buildings, renovated buildings and new buildings on the total gross floor area: BAU scenario

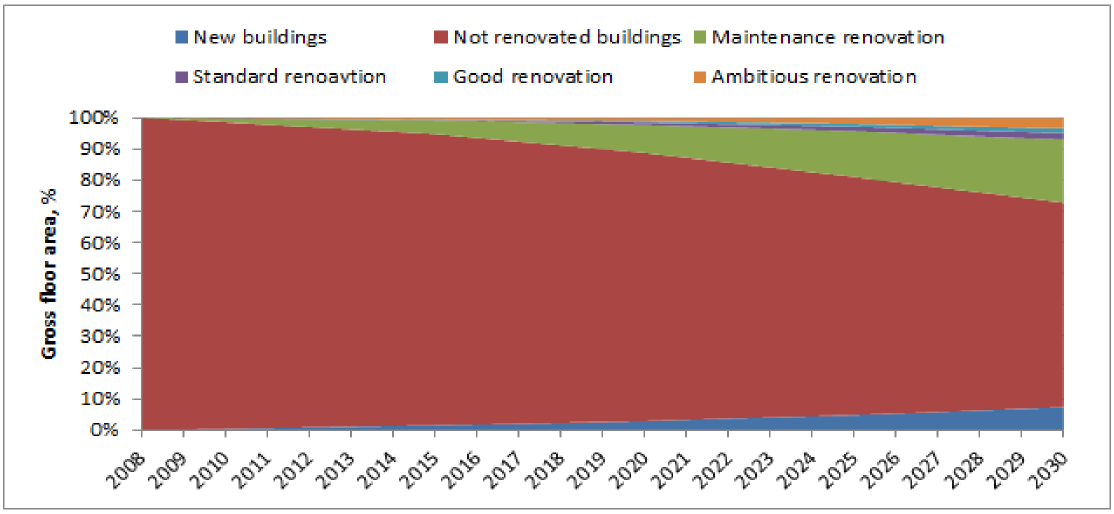

Fig. 4. Romania: Share of the floor area of not renovated buildings, renovated buildings and new buildings on the total gross floor area: BAU scenario

3.4. Ambitious scenario

Final energy demand in the building sector in ambitious scenario decreases over the period 2008 and 2030 in all investigated countries. In the Czech Republic, final energy demand for space heating and hot water is reduced by 9% by 2020 and by 27% by 2030. In Romania, final energy demand is calculated to go down by 19% in 2020 and by 33% in 2030. In Bulgaria, final energy demand decreases by 10% by 2020 and by 27% by 2030.

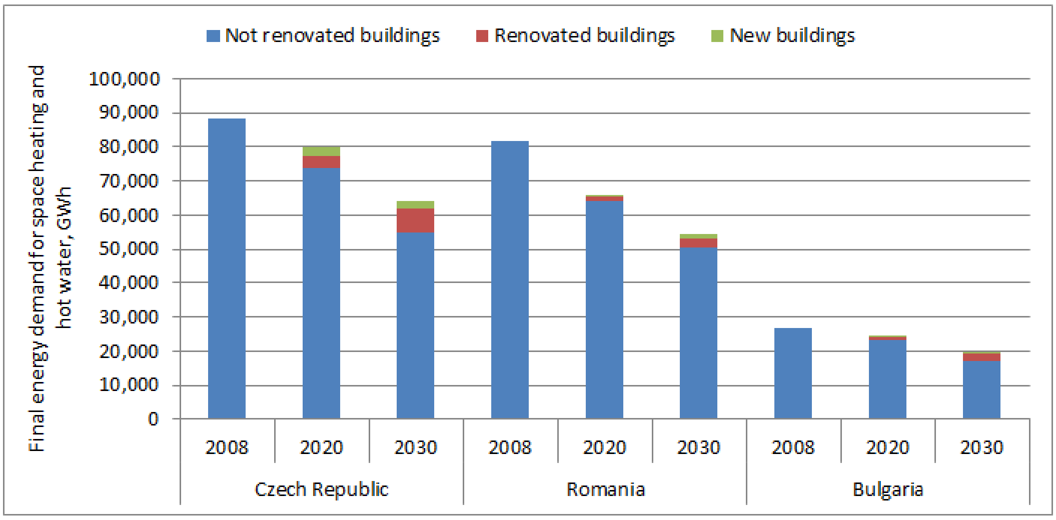

Fig. 5. Final energy demand for space heating and hot water in 2008, 2020 and 2030 in Czech Republic, Romania and Bulgaria building sector, Ambitious scenario

Due to the high financial subsidy for building renovation, the share of the renovated buildings by using a thermal renovation is high compared to the BAU scenario. In the Czech Republic, 28% of the total building stock in 2030 is expected to be renovated by using a standard, good or ambitious renovation. In Bulgaria, 32% of the total building stock in 2030 is renovated by using a standard, good or ambitious renovation. In Romania, 16% of the total building stock is being renovated in 2030. Different energy fuel prices, initial investment costs and climate conditions in the investigated countries lead to different composition of the renovation depth.

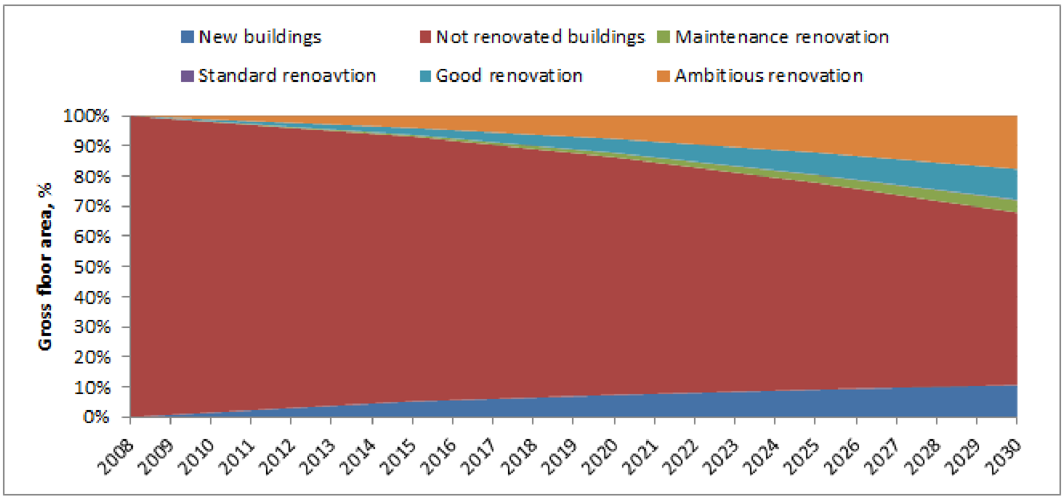

Fig. 6. Czech Republic: Share of the floor area of not renovated buildings, renovated buildings and new buildings on the total gross floor area: Ambitious scenario

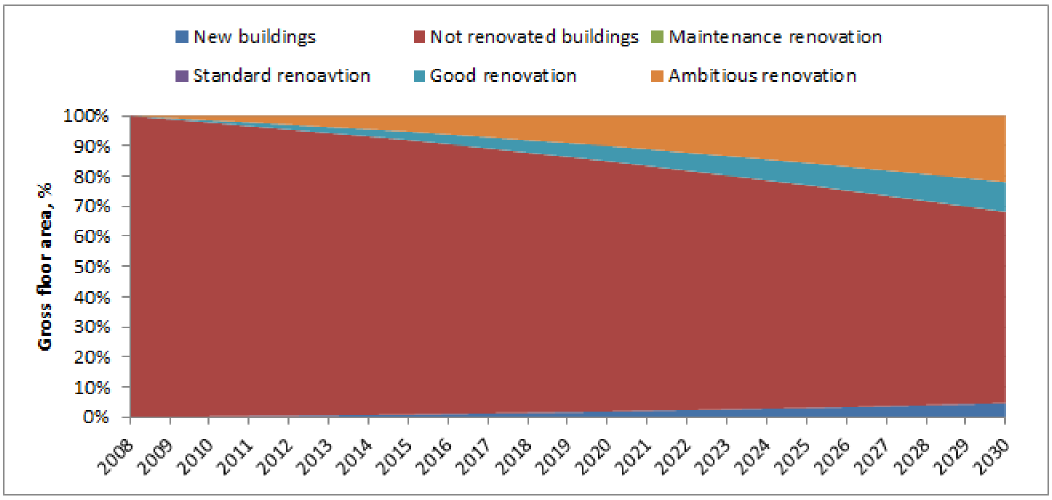

Fig. 7. Bulgaria: Share of the floor area of not renovated buildings, renovated buildings and new buildings on the total gross floor area: Ambitious scenario

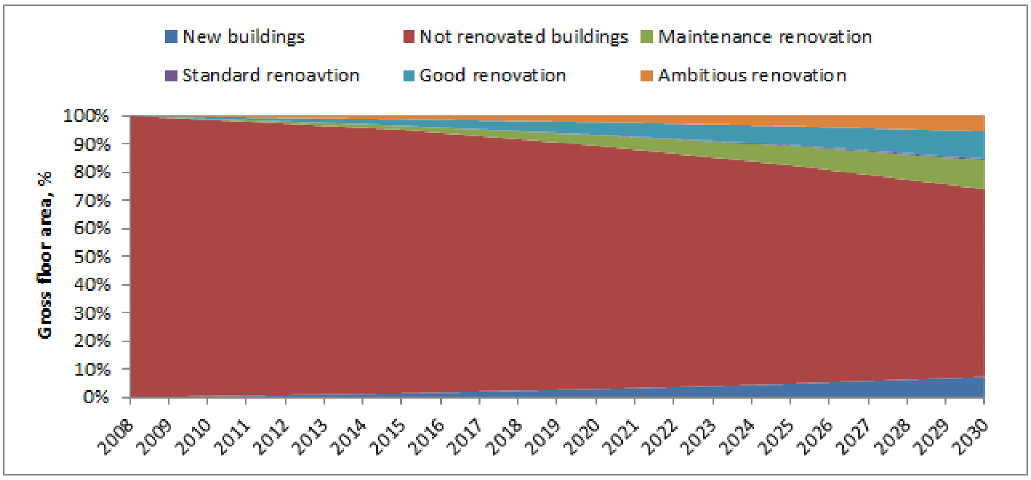

Fig. 8. Romania: Share of the floor area of not renovated buildings, renovated buildings and new buildings on the total gross floor area: Ambitious scenario

4. CONCLUSIONS

In this paper, final energy demand in the whole building sector for three selected EU countries was calculated. Two different energy demand scenarios were estimated. The first scenario shows energy demand development by implementing existing policy measures. The second scenario is calculated by implementing ambitious policy measures. Different policy measures have an impact on the cost effectiveness of the renovation activities and thus lead to the energy savings in the total building stock.

By considering building construction periods and building thermal characteristics, energy saving potential is shown. The calculation showed that in 2030, 36% in Czech Republic, 35% in Bulgaria and 28% in Romania of the total building stock can be renovated as a results of the life time of the buildings. However, what saving potential can be achieved depends on the renovation depth. In the BAU scenario, in the Czech Republic due to the existing financial support measures and relatively high energy fuel prices, 15% of the buildings are being renovated by using good and ambitious renovation. In Bulgaria, on the other hand, only 3% of the total buildings are being renovated by using good and ambitious renovation. For the rest of the buildings which should be renovated based on their life time, the maintenance renovation are being applied. This leads to the lock-in effect.

To show energy saving potential, the ambitious scenario was calculated. In this scenario, in Bulgaria, 33% of the buildings are being renovated by using good and ambitious renovation. This leads to the energy savings of 27% by 2030.

REFERENCES

1. Eurostat, „Final energy consumption, by sector“, 2014. [Online]. Verfügbar unter: http://epp.eurostat.ec.europa.eu/portal/page/portal/statistics/search_database. [Zugegriffen: 27–Mai-2014].
2. McKENNA R., MERKEL E., FEHRENBACH D., MEHNE S., FICHTNER W. „Energy efficiency in the German residential sector: A bottom-up building-stock-model-based analysis in the context of energy-political targets“, *Build. Environ.*, Bd. 62, S. 77–88, Apr. 2013.
3. BROIN E.Ó, MATA É., GÖRANSSON A., JOHNSSON F. „The effect of improved efficiency on energy savings in EU-27 buildings“, *Energy*, Bd. 57, S. 134–148, Aug. 2013.
4. AMSTALDEN R.W., KOST M., NATHANI C., IMBODEN D.M. „Economic potential of energy-efficient retrofitting in the Swiss residential building sector: The effects of policy instruments and energy price expectations“, *Energy Policy*, Bd. 35, Nr. 3, S. 1819–1829, März 2007.
5. OLONSCHECK M. Corresponding author contact information, HOLSTEN A., KROPP J.P. „Heating and cooling energy demand and related emissions of the German residential building stock under climate change“, *Energy Policy*, 2011.
6. GEORGIEV Z., SHICHKOV I., PAUNOVA-GALEVA D. „The challenges, dynamics and activities in the building sector and its energy demand in Bulgaria. D2 .1 of WP 2 from Entranze Project“.
7. ATANASIU B., ECONOMIDOU, MAIO J. „The challenges, dynamics and activities in the building sector and its energy M. demand in Romania. D2 .1 of WP 2 from Entranze Project“.
8. ZAHRADNIK P., KARASEK J., SESTAKOVA Z. „The challenges, dynamics and activities in the building sector and its energy demand in the Czech Republic. D2 .1 of WP 2 from Entranze Project“.
9. BONETA M.F. „Cost of energy efficiency measures in buildings refurbishment: a summary report on target countries. D3.1 of WP3 from Entranze Project“, CENER.
10. BÜRGER V. „Overview and assessment of new and innovative integrated policy sets that aim at the nZEB standard“, Report.

11. ATANASIU B., MAIO J., KOULOUMPI II., KENKMANN T. „Overview of the EU-27 building policies and programs. Factsheets on the nine Entranze target countries. Cross-analysis on member-states´ plans to develop their building regulations towards the nZEB standard“, Report.
12. STADLER M., KRANZL L., HUBER C., HAAS R., TSIOLIARIDOU E. „Policy strategies and paths to promote sustainable energy systems—The dynamic Invert simulation tool“, *Energy Policy*, Bd. 35, No. 1, S. 597–608, Jan. 2007.
13. KRANZL L., HUMMEL M., MÜLLER A., STEINBACH J. „Renewable heating: Perspectives and the impact of policy instruments“, *Energy Policy*, Bd. 59, S. 44–58, Aug. 2013.
14. KRANZL L., STADLER M., HUBER C., HAAS R., RAGWITZ M., BRAKHAGE A., GULA A., FIGORSKI A. „Deriving efficient policy portfolios promoting sustainable energy systems—Case studies applying Invert simulation tool“, *Renew. Energy*, Bd. 31, Nr. 15, S. 2393–2410, Dez. 2006.
15. MÜLLER A. „The development of the built environment and its energy demand. A model based scenario analysis“, Dissertation, Vienna University of Technology, 2015.
16. KRANZL L., MÜLLER A., TOLEIKYTE A., HUMMEL M., STEINBACH J., KOCKAT J., ROHDE C., SEBI C., KERAMIDAS K., LAPILLONE B. „Policy pathways for reducing energy demand and carbon emissions of the EU building stock until 2030“, Report.
17. The TABULA Project, „National building typologies“. [Online]. Verfügbar unter: http://episcope.eu/building-typology/. [Zugegriffen: 05-März-2015].
18. STANIASZEK D., ANAGNOSTOPOULOS F., ATANASIU B., DANCIU S. „Renovating Romania: A Strategy for the energy renovation of Romania’s building stock“.
19. SEBI C., LAPILLONE B., KERAMIDAS K. „Exogeneous framework conditions for Entranze scenarios“.
20. *Directive 2009/28/EC of the European Parliament and of the Council of 23 April 2009 on the promotion of the use of energy from renewable sources and amending and subsequently repealing Directives 2001/77/EC and 2003/30/EC. .*
21. *Directive 2010/31/EU of the European Parliament and of the Council of 19 May 2010 on the energy performance of buildings – LexUriServ.do.*

CYSENI 2015, May 27–28, Kaunas, Lithuania
ISSN 1822-7554, www.cyseni.com

USE OF ENERGY SOURCES IN THE RESIDENTIAL SECTOR IN THE DEVELOPING COUNTRIES OF CENTRAL EU AND SWEDEN

G. Venzhego, Tord af Klintberg, F. Björk
Royal Institute of Technology
Brinellvägen 23, SE-100 44 – Sweden
Phone +46 9 7906000
Email: venzhego@kth.se, tord.klintberg@byv.kth.se

ABSTRACT

A comparative analysis of energy consumption in the residential sector has been done for 11 countries: Bulgaria, Estonia, Croatia, Hungary, Lithuania, Latvia, Romania, Slovenia, Slovakia, Sweden and Ukraine. The analysis was carried out using the following criteria: total primary energy consumption, taxes on and prices of gas and electricity, type of energy sources, energy consumption in district heating, CO_2-emissions, population and climate. Data for the analysis was taken from the official databases of international organizations. Energy consumption by energy sources was analysed based on the energy balance tables of the International Energy Agency (IEA), France, and on statistical data of the U.S. Energy Information Administration (EIA), Washington. Statistical information for district heating was taken from EUROHEAT & POWER Association, Belgium, and information on prices for electricity and gas was obtained from Eurostat, the statistics office of the European Union. Results of the research show that the dependence on fossil fuels such as coal, oil and natural gas of many European countries, except Sweden, is very high. From the investigation, Sweden was determined to be one of the leading countries actively using alternative energy sources.

Keywords: energy consumption, energy sources, carbon dioxide emissions, climate, comparative analysis, residential sectors, Sweden, EU countries

1. INTRODUCTION

There is a great need for energy saving measures within the residential sector in central Europe, both regarding CO_2-emissions and dependence on oil and gas. The environmental situation in many central European countries can be compared with the situation in Sweden during the 20th century, when most of the heating was performed in small stoves and with fossil fuels, often oil. The housing sector in Sweden has, during the last 20 years, succeeded in saving a significant amount of energy and the energy consumption per square meter continues to drop. Sweden has also managed to move the heating of apartment buildings to a district heating system fuelled by biomass, waste and waste heat. Only a small fraction of fuel now comes from fossil fuels such as coal and oil. Small houses in Sweden are mostly heated by ground source heat pumps or by modern biomass pellet stoves.

According to the European Union's '20-20-20' objectives, both energy consumption of primary energy and greenhouse gas (GHG) emissions have to be reduced by 20% by 2020. Within the same period of time, energy consumption produced from renewable resources have to be increased by 20% compared with the figures for 2005 [1–3].

This paper provides a comparative analysis of energy consumption in the residential sector for the following European countries: Bulgaria (BG), Estonia (EE), Croatia (HR), Hungary (HU), Lithuania (LT), Latvia (LV), Romania (RO), Slovenia (Sl), Slovakia (SK), Sweden (SE) and Ukraine (Ukr) are based on the statistical information of 1993–2012 years. Most of these countries joined EU during last 10 years with the exception of Sweden and Ukraine. Sweden is represented as a long-time-experience and new-technology-use country, Ukraine as a country which is in a process of preparing their systems to European level of efficiency. The aim of this work is to review energy consumption, and, in particular, energy consumption for heating, in the residential sector. Evaluation of the energy consumption by the countries will show the level of energy efficiency technologies implementation and alternative source use. In publications sources the statistical information is given separately for the OECD and non-OECD countries. Estonia, Hungary, Slovenia, Slovakia and Sweden are all members of the Organization for Economic Co-operation and Development (OECD), while the rest of the reviewed countries are non-OECD countries.

The reviewed European countries are considered to have different climates. As a result, calculations of each country's energy needs for heating were performed using Heating Degree Days.

Indicator of Heating Degree Days for the considered countries varies from 1500 in Croatia to 7000 in northern Sweden. For a comparative analysis of energy consumption for heating it is important to take into account the climate condition (Fig. 1) of each country. According to Eurostat calculation principles, the heating threshold is a mean daily outdoor temperature lower than 15°C.

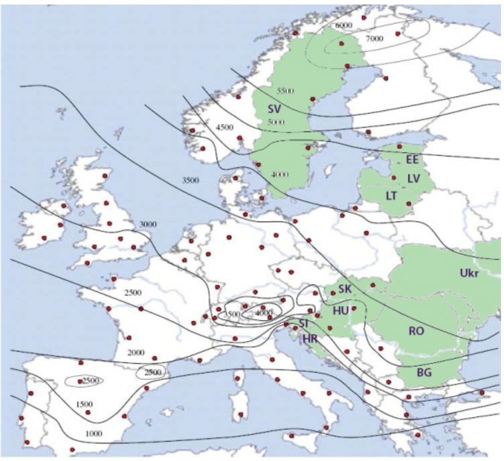

Fig. 1. Map of Europe and distribution of the Heating Degree Days. Source: EEA [4]
(Countries reviewed in this paper are marked in green)

2. METHODOLOGY

The comparative analysis of energy consumption in the residential sector was made using balance tables of the International Energy Agency (IEA), France (http://www.iea.org/statistics/), and statistical data of the U.S. Energy Information Administration (EIA), Washington (http://www.eia.gov/countries/). Statistical information for district heating is taken from EUROHEAT & POWER Association, Belgium (http://www.euroheat.org/Comparison-164.aspx), and information on prices for electricity and gas was obtained from Eurostat, the statistics office of the European Union (http://epp.eurostat.ec.europa.eu). The analysis was carried out taking into account the main principles used in reports by the IEA [5–10], the European Commission [11] and other institutions [4, 12].

3. ENERGY CONSUMPTION

The energy consumption of a country means the energy required for the functioning of all industrial and consumer sectors. The present comparative analysis of energy consumption was carried out in terms of total primary energy supply (TPES) and total final consumption, using the normalized unit of energy in tons of oil equivalent (toe), which allows to compare the energy that was received in a result of various resources use.

Major international agencies involved in the collection of statistical data of energy consumption are the International Energy Agency (IEA), the U.S. Energy Information Administration (EIA), and the European Environment Agency (EEA).

The main sectors of a country's energy consumption are industry, transport, households and other sectors. According to the average data for EU-28 countries for 2012, final energy consumption by sectors was distributed in the following proportions from total: industry – 25.3%, transport – 31.8%, households – 25.2%, and all other sectors – 16.3%.

3.1. Primary energy consumption

Data of total primary energy supply (1993–2011) of the selected countries, according to the EIA, is collected in Table 1. According to this data, Ukraine has the highest consumption, and it is many times higher compared to other reviewed countries and 2.5 higher than Sweden. The differences in consumption are partly due to the size of the country and its population. For most of the countries, energy consumption does not change significantly over the years. The largest countries by population (Table 1) are Ukraine, with around 45 million people, and Romania, with around 21 million people.

Table 1. Total primary energy supply (consumption) TPES and population, in millions of people, according to year. Source: EIA (Note: Quadrillion is 10^{15})

Country	1993		2000		2005		2011	
	TPES 10^{15}Btu (MToe)	million people	TPES 10^{15}Btu (MToe)	million people	TPES 10^{15}Btu (MToe)	million people	TPES 10^{15}Btu (MToe)	million people
Bulgaria	0.80(20.3)	8.4	0.87(21.9)	7.8	0.92(23.2)	7.5	0.78(19.6)	7.1
Croatia	0.30(7.6)	4.5	0.38(9.5)	4.4	0.40(10.2)	4.5	0.35(8.7)	4.5
Estonia	0.09(2.4)	1.5	0.08(2.1)	1.4	0.08(2.1)	1.3	0.08(1.9)	1.3
Hungary	1.02(25.8)	10.3	1.02(25.8)	10.2	1.16(29.1)	10.1	1.03(25.9)	10.0
Latvia	0.16(4.1)	2.6	0.15(3.9)	2.4	0.19(4.7)	2.3	0.16(4.1)	2.1
Lithuania	0.38(9.5)	3.7	0.30(7.5)	3.7	0.35(8.9)	3.6	0.28(7.2)	3.0
Romania	1.87(47.1)	22.8	1.59(40.0)	22.5	1.66(41.9)	22.2	1.51(38.1)	21.9
Slovakia	0.78(19.6)	5.3	0.79(19.8)	5.4	0.82(20.6)	5.4	0.74(18.5)	5.5
Slovenia	0.24(6.0)	2.0	0.29(7.3)	2.0	0.32(8.0)	2.0	0.31(7.7)	2.0
Sweden	2.24(56.6)	8.8	2.27(57.2)	8.9	2.34(59.0)	9.0	2.18(54.8)	9.1
Ukraine	8.09	51.9	5.75(144.9)	49.0	6.33(159.4)	47.0	5.40(136.0)	45.1

The economic activity of a country is better evaluated by looking at the distribution of the Total Primary Energy Consumption per capita. Thus, using the population, set out in Table 1, and the total primary energy supply, one can calculate the total primary energy consumption per capita during the period (Table 2).

By looking at the distribution of the TPEC per capita, it can be seen that Sweden is first among the reviewed countries, although we can also see that overall consumption in Sweden decreased slightly between 2005 and 2011.

Table 2. Total Primary Energy Consumption per Capita, in tons of oil equivalent (toe)

Country	**1993**	**2000**	**2005**	**2011**
Bulgaria	2.4	2.8	3.1	2.8
Croatia	1.7	2.2	2.3	1.9
Estonia	1.6	1.5	1.6	1.5
Hungary	2.5	2.5	2.9	2.6
Latvia	1.6	1.6	2.0	1.9
Lithuania	2.6	2.1	2.5	2.0
Romania	2.1	1.8	1.9	1.7
Slovakia	3.7	3.7	3.8	3.4
Slovenia	3.0	3.6	4.0	3.9
Sweden	6.5	6.4	6.6	6.0
Ukraine	4.0	3.0	3.4	3.0

It is important to consider energy consumption per capita (per person) and also per Gross Domestic Product (GDP) when comparing energy consumption from an economic point of view and for evaluation of efficiency of energy sources. For evaluation of efficiency use of energy sources, the primary energy consumption per GDP is considered and represented in Fig. 2. All countries have reduced their energy use per GDP over time. The largest reduction has been in Ukraine.

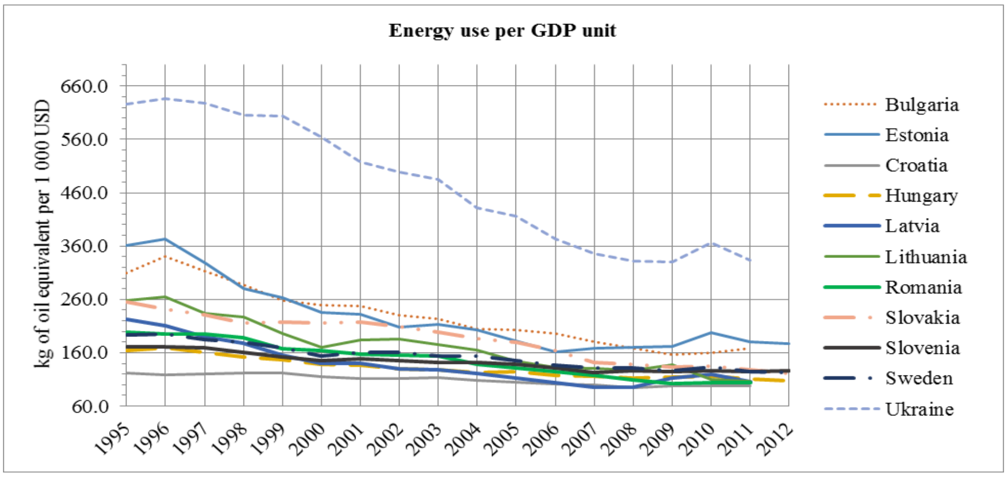

Fig. 2. Primary energy consumption per GDP. Source: Bluenomics

3.2. Energy consumption in the residential sector

The study of energy consumption in the selected countries was carried out using statistical data of several international organizations, as mentioned previously. The energy balance was used as an important tool for making a comparative analysis between different sources and countries. The evaluation of energy consumption in the residential sector was done using tables of the energy balance from the International Energy Agency.

3.2.1. Final energy consumption in the residential sector

Total final energy consumption in the residential sector is used for: space and tap water heating, cooking, lighting, appliances and other equipment use. The amount of total final energy consumption in the residential sector depends on the efficiency of buildings and on the use of all service components.

Tables 3 and 4 present the final energy consumption in the residential sector by the sources in ktoe and in kgoe (kilogram of oil equivalent) per capita, respectively. In this study, the analyses are made by looking at seven groups of primary and secondary energy sources: coal and peat; oil products; natural gas; geoth., sol.; bio/waste (biofuels and waste); electricity; and heat. The highest total final energy consumption in the residential sector, as well as total primary consumption for all needs of the country, are in Ukraine (23604 ktoe), followed by Romania (7848 ktoe), Sweden (6956 ktoe) and Hungary (5448 ktoe). This is partly due to the population and economic activities of the different countries.

Table 3. Final energy consumption in the residential sector by source, (ktoe) 2011
Source: (http://www.iea.org/) International Energy Agency (IEA)

Country	Coal and peat	Oil products	Natural gas	Geoth., sol.	Bio/waste	Electricity	Heat	**Total**
Bulgaria	238	27	56	8	747	938	359	**2374**
Croatia	6	206	544	6	387	561	147	**1857**
Hungary	172	115	2966	6	724	973	529	**5484**
Romania	19	223	2331	12	3146	996	1120	**7848**
Slovakia	48	7	1172	4	44	387	458	**2121**
Slovenia	0	252	113	27	415	276	89	**1173**
Sweden	4	52	69	11	1183	3133	2504	**6956**
Estonia	11	9	52	0	364	166	333	**935**
Latvia	26	54	107	0	624	152	354	**1318**
Lithuania	68	41	145	0	558	225	485	**1522**
Ukraine	708	84	14060	0	937	3308	4507	**23604**

Table 4. Final energy consumption in the residential sector, in kgoe per capita, 2011

Country	Coal and peat	Oil products	Natural gas	Geoth., sol.	Bio/waste	Electricity	Heat	Total
Bulgaria	33.6	3.8	7.9	1.1	105.3	132.2	50.6	334.7
Croatia	1.3	45.9	121.3	1.3	86.3	125.1	32.8	414.2
Hungary	17.2	11.5	297.3	0.6	72.6	97.5	53.0	549.7
Romania	0.9	10.2	106.4	0.6	143.6	45.5	51.1	358.3
Slovakia	8.8	1.3	214	0.7	8.0	70.7	83.6	387.3
Slovenia	0.00	126.0	56.5	13.5	207.5	138	44.5	586.5
Sweden	0.4	5.7	7.6	1.2	130.2	344.7	275.5	765.3
Estonia	8.6	7.0	40.5	0.0	283.7	129.4	259.6	728.8
Latvia	11.8	24.5	48.5	0.0	283.0	68.9	160.7	597.8
Lithuania	19.2	11.6	41.0	0.0	157.8	63.6	137.2	430.5
Ukraine	15.7	1.9	311.5	0.0	20.8	73.3	99.9	523

When considering the source consumption by countries, it was noted that the main user of electricity, calculated using consumption per capita, is Sweden (344.7 kgoe), of bio and waste is Estonia and Latvia (each around 283 kgoe), of natural gas is Ukraine and Hungary (311.5 and 297.3 kgoe, respectively), of oil products is Slovenia (126 kgoe) and of coal/peat is Bulgaria (33.6 kgoe).

The highest consumption of energy per capita for the residential sector is found in Sweden (765.3 kgoe), followed by Estonia (728.8 kgoe). Fossil fuels play an important role in most of the investigated countries. For Croatia, Hungary, Latvia, Lithuania and Ukraine, the main fuel used in district heating is natural gas, making up 60% of all resources in Bulgaria, and Estonia, and around 30% in Romania, but just 6% in Slovakia, Slovenia and Sweden. Sweden used mainly alternative sources of energy in district heating, such as bio/waste (68%). In Slovakia, 30 % of heat for district heating was produced by nuclear power plants. In Bulgaria, Romania and Slovenia, heat was produced mainly by thermal plants burning coal and peat.

3.2.2 Heat consumption in residential sector

The heat consumption is shown with additional information by type of energy source. Heat consumption by source for heating in the residential sector is based on data for heat consumption by source in all sectors combined with the amount of heat sold to the final customers in the residential sector. In Fig. 3 shown a part of energy balance tables of International Energy Agency by data for 2011 year for Sweden. In table the energy in thousand tonnes of oil equivalent (ktoe).

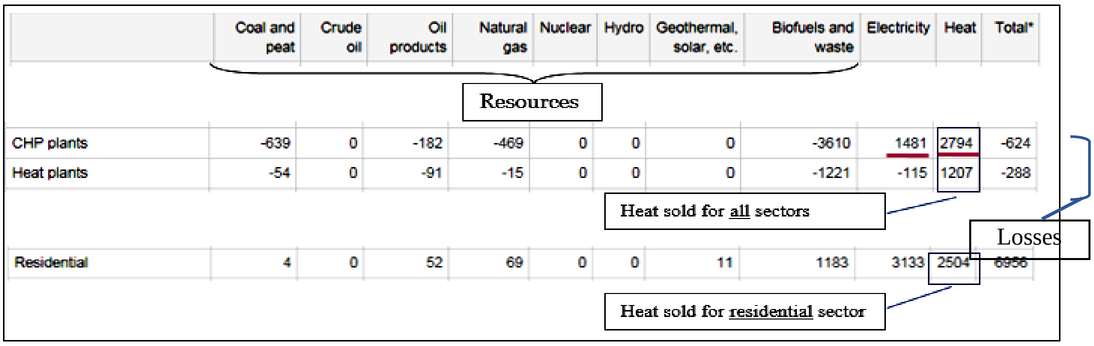

	Coal and peat	Crude oil	Oil products	Natural gas	Nuclear	Hydro	Geothermal, solar, etc.	Biofuels and waste	Electricity	Heat	Total*
CHP plants	-639	0	-182	-469	0	0	0	-3610	1481	2794	-624
Heat plants	-54	0	-91	-15	0	0	0	-1221	-115	1207	-288
Residential	4	0	52	69	0	0	11	1183	3133	2504	6956

Fig. 3. Part of the energy balance table included information of heat production and consumption

Here “heat” is considered to be the quantity of fuel burned to generate heat that is sold to a consumer under a contract. It includes heat that is generated and sold by combined heat and power plants and by community heating networks (also known as *district heating*).

Determination of the resources amount used for production the heat for residential sector calculated by follows algorithm:

1) According to data for CHP stations, the amount of resources used for producing the heat is determined proportionally as ktoe total energy consumption subtracting the energy for electricity production:

$$\text{Resourse}_{\text{CHP without elctr}}=\text{Resourse}_{\text{CHP}}–(\text{Electr}_{\text{CHP}}\cdot\text{Resourse}_{\text{sum CHP}})/(\text{Electr}_{\text{CHP}}+\text{Heat}_{\text{CHP}}))$$

2) Summarizing the obtained part of the resources used for producing the heat from the cogeneration plants with thermal plants get the amount of resources used for heat in all spheres of final consumption:

$$\text{Resourse}_{\text{sum Heat}} = \text{Resourse}_{\text{CHP without elctr}} + \text{Resourse}_{\text{Heat}}$$

3) The amount of resources used in the residential sector for heating is determined proportionally:

$$\text{Sources}_{\text{Heat res}} = \text{Source}_{\text{sum Heat}} \cdot \text{Heat}_{\text{resid}} / \text{Heat}_{\text{sum}}$$

Results for each country are summarized in Table 5 below.

Table 5. Energy consumption in the residential sector for district heating by energy source, in ktoe 2011

Country	Coal and peat	Oil products	Natural gas	Nuclear	Geoth., sol.	Bio/waste	Losses*
Bulgaria	224	21	214	4	0	3	-106
Croatia	1	42	165	0	0	6	-67
Estonia	103	22	163	0	0	131	-87
Hungary	85	3	563	3	3	51	-180
Latvia	5	8	331	0	0	90	-79
Lithuania	3	26	467	0	0	125	-139
Romania	739	130	784	0	0	38	-571
Slovakia	166	35	208	387	2	73	-414
Slovenia	130	2	30	0	1	11	-84
Sweden	295	131	201	0	0	2241	-435
Ukraine	811	59	4341	35	0	101	-839

Losses* – the losses during heat production.

The percentage distributions for different fuels in each country are shown in Fig. 4 below, showing a high dependence on natural gas for the majority of the countries. In the same time natural gas use give the minimum losses compared to another sources. Thermal and especial nuclear plants have highest losses.

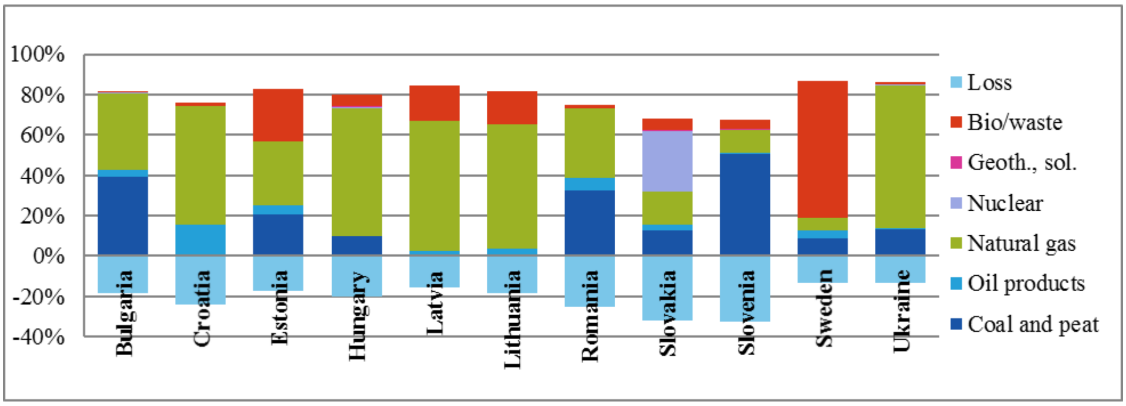

Fig. 4. Share of energy consumption for heating by fuels in the residential sector, by country in 2011

In this context, it is worth mentioning that in Scandinavian countries the average living space per person is 40–50 square meters, while in Central Europe it is 20–30 square meters (National Statistical Office 2014). Considering the data for district heating floor space from the EUROHEAT & POWER Association, as set out in Table 3 (final energy consumption in the residential sector for heating), it is possible to determine heating consumption per square meter in order to describe the energy efficiency of buildings (Fig. 5). Analysis of energy consumption per square meter shows the low efficiency of houses in Romania, which has energy consumption for heating four times higher than that in Sweden. Consumption of energy for heating in the Baltic countries are about the same level, i.e., around 11–14 kgoe/sqm.

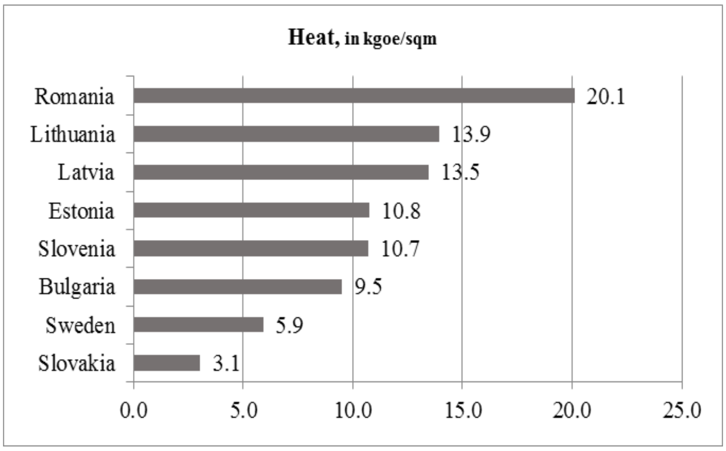

Fig. 5. Heat consumption per square meter for eight different countries

3.2.3 CO_2 Emissions from fuel combustion in the residential sector

The energy sources needed for the residential sector result in CO_2-emissions per capita that are very different in the selected countries, with Ukraine as the highest emitter and Sweden as the lowest, see Fig. 6 [11]. Ukraine emits five times more per capita in the residential sector when compared to Sweden. All these countries, except Sweden, use coal as one of the main fuels for electricity production.

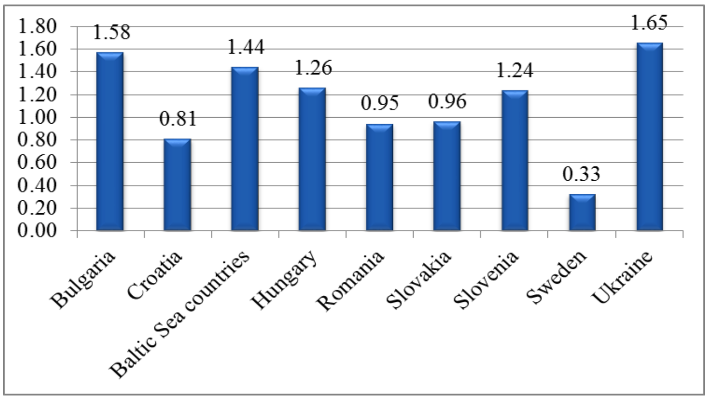

Fig. 6. CO_2 emissions from electricity and heating in the residential sector in 2012, in million tonnes of CO_2 per capita. Source: IEA

The burning of fossil fuels such as coal, oil and natural gas is the main cause of anthropogenic emission of CO_2. One of the ways to reduce the amount of CO_2 emitted is to increase the use of alternative energy sources which do not produce this gas. Switching quickly from fossil fuel sources to alternative energy sources, however, is very difficult and demands a substantial investment of both knowledge and time.

4. ENERGY TAXES AND PRICES

The determination of prices for gas and electricity in each country is a complicated economic and political process that is dependent on many factors. Even from a brief analysis of Eurostat's data for gas and electricity prices and taxes by country [12], as set out in Fig. 7, it is easy to see that Sweden has one of the highest taxes for electricity and gas. High taxes are one of the main reasons for the use of alternative energy sources.

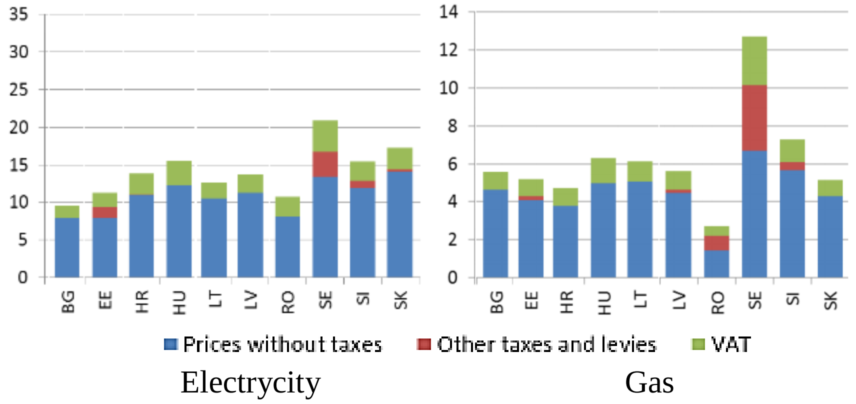

Fig. 7. Retail prices, taxes and VAT for Electricity (2500 kWh<Consumption<5000 kWh) and Nat. gas (20GJ<Consumption<200GJ) for domestic consumers in cent/kWh (2nd half of 2012)

5. CONCLUSION

This study highlights energy consumption in 10 countries in central Europe, and compares this with energy consumption in Sweden.

By the average data for EU-28 countries the primary energy consumption used for household need is around 26% of total primary energy consumption.

Total primary energy consumption in Sweden per capita is two to four times higher than that in any of the central European countries considered in this study.

District heating in the residential sector is widely used in countries with a cold climate, such as Estonia, Latvia, Lithuania, Slovakia, Sweden and Ukraine. The percentage of the population served by district heating in such countries is 35–67%. The share of final energy consumption for district heating in the residential sector of these countries is 35–40% of total consumption for all household needs. In countries with a warmer climate, such as Croatia, Bulgaria, Romania, Hungary, and Slovenia, the percentage of the population served by district heating is just 11–19%, and the share of final energy consumption for district heating in the residential sector is just 11–20% of total consumption for all household needs.

A comparison of countries by efficiency of district heating shows that Sweden has energy consumption for residential heating on the same level as countries with a warmer climate and two to four times less when compared with other cold climate countries. This fact illustrates the high level of thermal insulation of external constructions and energy-saving technologies used in the residential sector in Sweden.

The types of energy sources used for household needs, such as space heating, water heating, cooking, space cooling, lighting and electrical appliances, are different in the selected countries and are dependent on many factors, both economic and political. In Sweden, taxes on gas are the highest in Europe and 10–20 times those in other considered countries. The policy of high taxation on gas, especially for households, has led to the use of renewable energy sources such as biofuel and waste for heating and to a high rate of energy efficiency of buildings. So, in Sweden, the average consumption of energy per year for heating of one square meter of dwelling space is 5.9 kgoe, which is at the same level as countries with a much warmer climate, such as Slovakia (3.1 kgoe/sqm), and two to three times less when compared to other countries with a cold climate, such as Latvia (13.5 kgoe/sqm).

In countries such as Ukraine, Slovakia and Hungary, the main source of energy is natural gas (more than 50%), while in Romania and Croatia it is around 30%.

The data compiled in this study shows a big dependence on fossil fuels, such as coal, oil and gas, in central Europe. It also shows that Sweden has experience in and knowledge about energy saving and that it can contribute to a process of more efficient use of energy and a transition towards the use of renewable resources.

REFERENCES

1. Directive 2005/32/EC of the European Parliament and of the Council on establishing a framework for the setting of ecodesign requirements for energy-using products.
2. Directive 2002/91/EC of the European Parliament and of the Council on the energy performance of buildings.
3. Directive 2006/32/EC of the European Parliament and of the Council on energy end-use efficiency and energy services.
4. EEA Report No 6/2008 “Energy and environment”.
5. IEA Statistics. Energy balances of OECD countries (2014 edition) OECD/IEA, 2014.
6. IEA Statistics. Energy balances of non-OECD countries (2012 edition) OECD/IEA, 2012.
7. World energy balances: beyond 2020 documentation (2014 edition) OECD/IEA, 2014 http://www.iea.org/statistics/topics/energybalances/.
8. Energy Efficiency Indicators: Fundamentals on Statistics. OECD/IEA, 2014.
9. Energy statistics manual. OECD/IEA, 2005.
10. Combined heat and power. OECD/IEA, 2008.
11. CO_2 emissions from fuel combustion. OECD/IEA, 2014.
12. European commission. Commission staff working document. Energy prices and costs report. Brussels, 17.3.2014 SWD (2014) 20.

APPENDIX

Main international statistical sources

EEA European Environment Agency

EIA U.S. Energy Information Administration

Total primary energy supply (consumption) changes with years –

http://www.eia.gov/countries/

Population, in millions people – http://www.eia.gov/countries/data.cfm

Final energy consumption in residential sector by the sources – http://www.iea.org/

European Commission

Prices for electricity and gas – Report “Energy prices and costs in Europe” of European commission, 2014.

http://ec.europa.eu/taxation_customs/resources/documents/taxation/excise_duties/energy_products/rates/excise_duties-part_ii_energy_products_en.pdf

Euroheat & Power International association representing the District Heating and Cooling (DHC) and Combined Heat and Power (CHP) sector in Europe and beyond.

Statistics overview of district heating – http://www.euroheat.org/Statistics-69.aspx
http://www.euroheat.org/Comparison-164.aspx

Eurostat statistical office of the European Union situated in Luxembourg.

Yearly electricity and gas prices –
http://epp.eurostat.ec.europa.eu/statistics_explained/index.php/Energy_price_statistics

Bluenomics

Primary energy consumption per GDP –
http://www.bluenomics.com/#!data/energy/energy_1/energy_use_per_gdp_unit|chart/line

IEA International Energy Agency

Energy balances –
http://www.iea.org/statistics/statisticssearch/report/?country=SWEDEN&product=balances&year=2012

OECD The Organisation for Economic Co-operation and Development

Definitions – http://stats.oecd.org/glossary/detail.asp?ID=1163

CYSENI 2015, May 27–28, Kaunas, Lithuania
ISSN 1822-7554, www.cyseni.com

COMPREHENSIVE APPROACH TO THE EVALUATION OF THERMAL INSULATION PROPERTIES OF THE VENTILATED FACADES

G. Venzhego
Royal Institute of Technology
Brinellvägen 23, SE-100 44 – Sweden
Phone +46 9 7906000
Email: venzhego@kth.se

ABSTRACT

Ventilated facade of buildings is a complex structural system with ventilated air layer along the facade surface. Because of the wide variety of ventilated facade systems, the common methodology for all systems does not exist. In this article it was proposed to carry out the evaluation of systems divided them by structure of external cladding into three groups: I - the constructions with solid external cladding, II - the constructions that have breaks in external cladding, III - the constructions with evenly air-permeable external cladding. Such factors like thermal heterogeneity and air infiltration are the main factors that decrease thermal insulation properties of wall systems. The influences of these factors are analysed and discussed considering to the construction group of external cladding.

Keywords: ventilated facade, external cladding, thermal insulation properties, air infiltration, thermal heterogeneity

1. INTRODUCTION

The increase of requirements to the thermal insulation of external walls led to the necessity of multi-layered structures use. To ensure the architectural appeal of complex multi-layered structures and protect the structures against the effects of precipitation and wind, the various external systems that differ significantly in design are used. Taking into account complexity of the constructions, the problem of the comprehensive evaluation of thermal insulation properties of multilayer constructions arises.

The composition of external wall constructions with ventilated air gap assumes consist of the following layers: inner base layer, insulation layer, air layer and external curtain layer. The external curtain layer is attached to metal bars and beams, which, in their turn, are attached to the wall inner layer by brackets. Metallic elements in thermal terms are heat-conducting inclusions, which reduce heat uniformity of construction and reduce thermal resistance.

If the thermal heterogeneity of a construction is considered as the first important factor influencing its insulation characteristics, then the effect of air filtration through construction is the second factor, not less important, but less investigated.

The external wall constructions hereinafter mean the facade system with insulation and ventilated air gap. In compliance with DSTU B V.2.6-35:2008 [1], facade systems with ventilated air gap and external cladding are classified into subclasses according to their finishing layer material. After the classification of existent facade systems has been analysed the author proposed to divide these subclasses by external cladding structures into three main groups (Fig. 1) as follows: I – the constructions with solid screen, II – the constructions with break in screen, III – the constructions with solid air-permeable material.

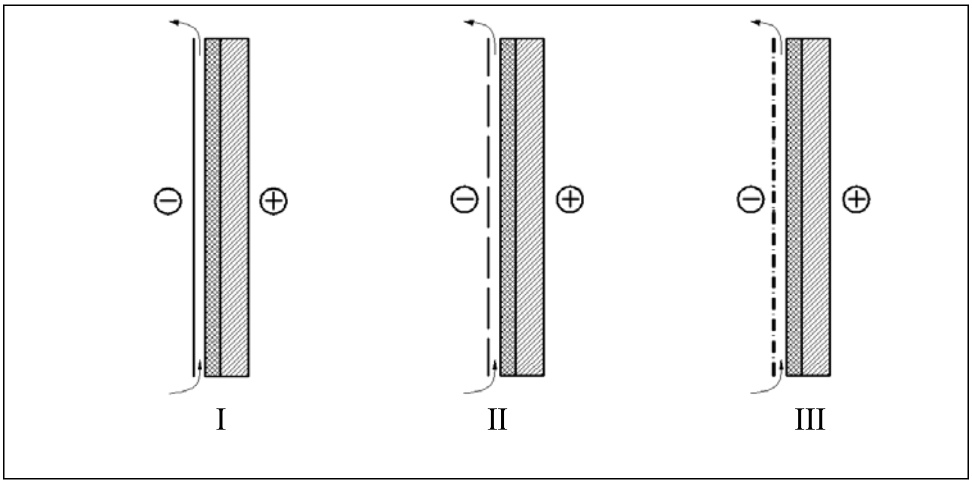

Fig. 1. Construction groups of external cladding of walls with thermal insulation and ventilated air gap

The paper is aimed at developing the algorithm for the complex approach to the thermal characteristics calculation for multi-layered constructions with ventilated air gap**.**

2. THERMAL HETEROGENEITY OF FACADE SYSTEMS

Influence of thermal heterogeneity on thermal insulation property of constructions are actively investigated. At present, a series of computational and experimental works have been carried out for the determination of the reduction factors of thermal resistance for constructions [2–4]. The thermal engineering uniformity coefficient, r, is determined as a ratio of the reduced thermal resistance of a structure with heat-conducting inclusions, R_{inc}, to the thermal resistance of a uniform structure, $R_{0,}$ $r = R_{inc}/R_0$ and is 0.83÷0.99 depending on the thickness and type of a thermal insulation, quantity of brackets and material of the internal bearing layer of a wall.

Fox example below represented calculation results of typical part of the ventilated facade (Fig. 2). The methods based on mathematical modelling of temperature fields were used.

The model of facade shown in Fig. 2 is consists of a base layer (variants: masonry wall – brick with a thermal conductivity 0.81 W/(m·^{o}C), density 1800 kg/m^3; reinforced concrete with a thermal conductivity of 2.04 W/(m·^{o}C), density 2500 kg/m3; foam concrete with a coefficient of thermal conductivity of 0.37 W/(m·^{o}C), density 800 kg/m^3), a insulation layer, heat-conducting inclusions (metal dowels, bracket and anchor made of galvanized steel with a coefficient of thermal conductivity of 58.0 W/(m·^{o}C). Between the bracket and the bearing wall is installed gasket, which reduces the influence of heat loss through the bracket and increasing the thermal engineering uniformity coefficient r. Boundary conditions were taken as follows: external environment with temperature minus 22 ^{o}C and the heat transfer coefficient 23 W/(m^{2}·^{o}C); internal environment with temperature 18 ^{o}C and the heat transfer coefficient 8.7 W/(m^{2}·^{o}C).

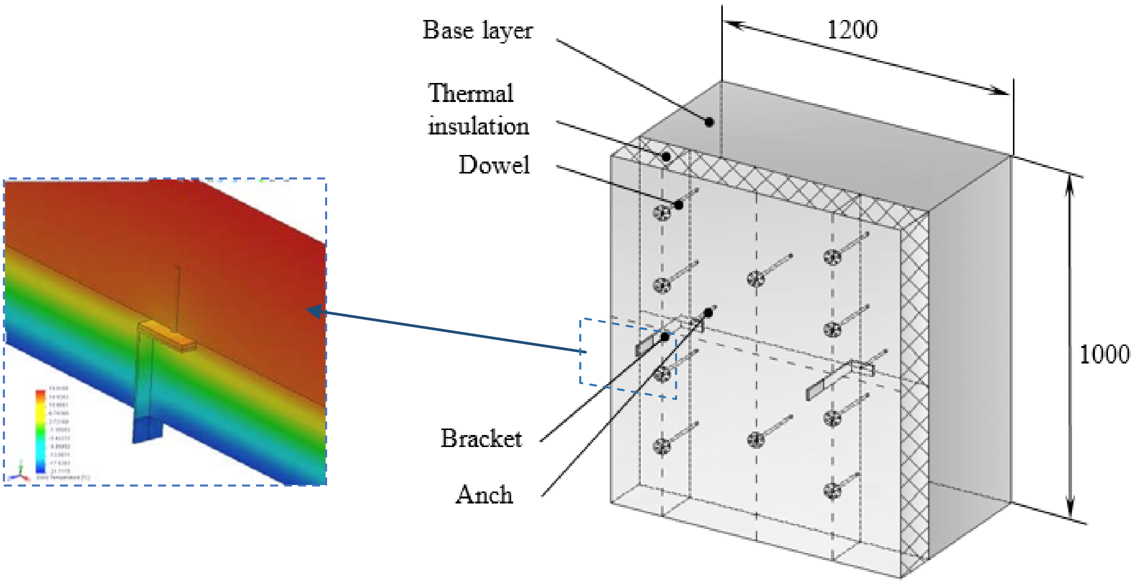

Fig. 2. Model of typical part of the ventilated facade with example of thermal field simulation result

By the calculation results represented in the table 1 was defined the change of the thermal engineering uniformity coefficient from the thickness of insulation (Fig. 3) and the thermal conductivity of insulation material (Fig. 4). The results are shows the decrease of the thermal engineering uniformity coefficient r with insulation thickness increase and increase of the thermal engineering uniformity coefficient r with increasing of the thermal conductivity of insulation layer but these dependences are not directly proportional as for single layer thermally homogeneous structures.

Table 1. Thermal engineering uniformity coefficient **r** for different constructions

Thickness and material of base layer	**Thickness of thermal insulation, m**	**Thermal engineering uniformity coefficient r**		
		λ = 0,04 W/(m·°C)	**λ = 0,05 W/(m·°C)**	**λ = 0,08 W/(m·°C)**
0,38 m Masonry wall	0,1 0,15 0,2	0,9 0,9 0,91	0,91 0,92 0,93	0,95 0,95 0,96
0,51 m Masonry wall	0,1 0,15 0,2	0,86 0,87 0,88	0,88 0,89 0,9	0,93 0,93 0,94
0,64 m Masonry wall	0,1 0,15 0,2	0,83 0,84 0,85	0,86 0,87 0,87	0,91 0,92 0,92
0,38 m Reinforced concrete	0,15	0,86	0,88	0,92
0,38 m Foam concrete	0,15	0,89	0,91	0,94

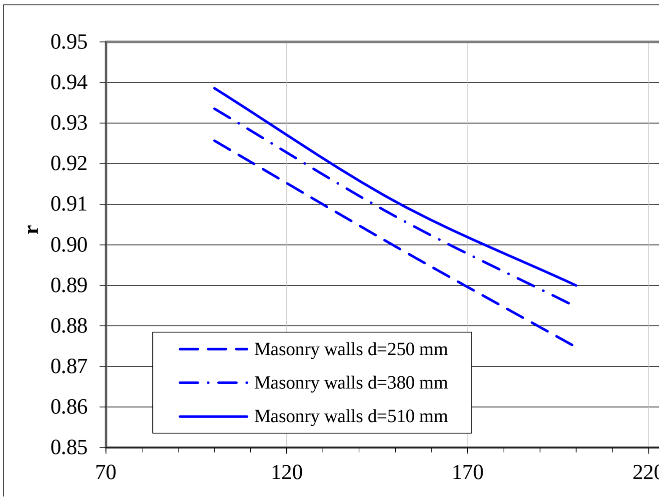

Fig. 3. The changes of thermal engineering uniformity coefficient **r** from the insulation layer thermal conductivity (accounting that thickness is 150 mm)

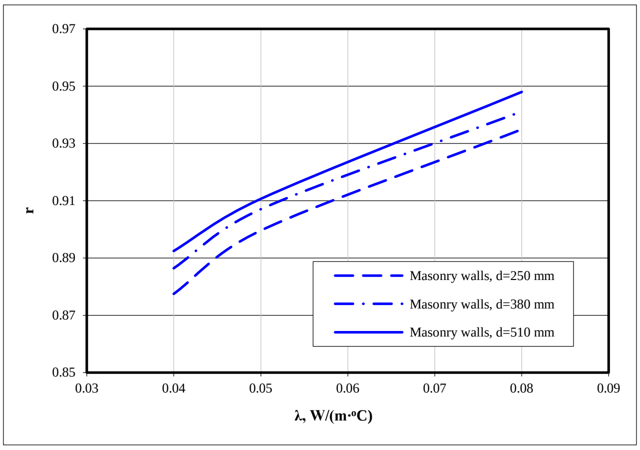

Fig. 4. The changes of thermal engineering uniformity coefficient **r** from the insulation layer thickness (accounting that thermal conductivity is 0.05 W/(m·°C))

Thermal properties evaluation of modern external walls with thermal insulation facade systems should be carried out by the thermal field simulations with accounting of thermal inhomogeneity influence of thermal bridges. The easy engineering calculations do not give real characteristics of multilayer systems with thermal heterogeneity.

Such factors like geometric characteristics of the inclusions, their number, thermal conductivity of the insulation materials and thickness affect thermal engineering uniformity coefficient significantly.

Represented results in table 1 shown influence of thermal heterogeneity on thermal insulating properties of ventilated facades. Thermal resistance decrease makes 5-13% for structures with minimum amount of fastening elements.

3. AIR FILTRATION THROUGH FACADE SYSTEM

It is known that such phenomenon as air filtration through walls occurs because of the difference of air pressures on the opposite sides of the external walls, which causes the infiltration or exfiltration of air to the building premises. Pressure difference occurs due to wind (stack effect) and difference temperature effect. The outside air inflow is positive for the hygienic characteristics of air regime in a premise, but has a considerably negative effect on the insulation characteristics of constructions in the case of infiltration into insulation layers or penetration between insulation layer and inside base layer. The amount of infiltrated or exfiltrated air depends on the air permeability of facade system layers. In the case of air infiltration the displacements of temperature fields and decreases of structure thermal resistance are observed, which is reported in works by R. Briling, K. Fokin and V. Bohoslovskii [5–8]. The character of the displacements of temperature fields and variations of thermal flow resistance is schematically shown in Figures 5 and 6, respectively. The reduction of thermal insulation characteristics can be explained by the heat losses for air heating during its penetration into the pores of a material. The phenomenon of air penetration into material pores and its movement within them is called a longitudinal or transversal filtration. The longitudinal filtration means the movement of air, which enters because the airtight external layer leakage and moves in the depth of the structure along it. In the case of the transversal filtration an air enters into the layer depth through its external surface perpendicularly to the construction depth.

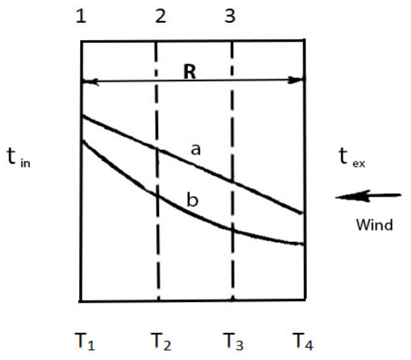

a – temperature distribution curve not considering the air infiltration

б – temperature distribution curve considering the air infiltration

Fig. 5. Schematic view of the thermal field displacements in a construction layer

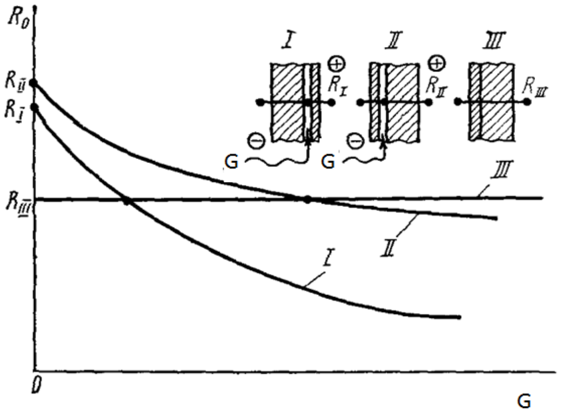

I – location of an air gap near the construction internal layer

II – location of an air gap near the construction external layer

III – an air space is absent

Fig. 6. Schematic view of the structure thermal resistance variations depending on the air losses, existence and location of ventilated air gap

In works of Uvslokk, Yarbrough, Straube [9, 10, 11] the results of the investigations of wind impact on thermal performance of the insulation products demonstrated that heat loss can reach 10–30%.

There are several calculation methods, which take into account the air permeability influence on the structure thermal regime. It is possible to determine the temperatures distribution by F. Ushakov's formula [5]:

$$\tau_x = t_{ex} + (t_{in} - t_{ex}) \cdot \left[(e^{cWRx} - 1)/(e^{cWRo} - 1) \right],$$

where τ_x is a temperature in any plane of the enclosure, t_{in} and t_{ex} are the temperatures of internal and external air, ^{0}C, e is a base of natural logarithms, R_x is an enclosure thermal resistance from the external air up to examined plane in the absence of infiltration, m^2 ·K/W, R_o is a thermal resistance of the entire enclosure in the absence of infiltration, m^2 ·K/W, W is an amount of air passing through the structure, kg/m^2·h.

With such approach the determination of temperatures and pressures in air gap becomes the main task. So, for the first group (I) of the constructions the average air temperature in the space should be determined by formula [7]:

$$t_{av} = t_o - (t_0 - t_{ex}) \cdot (X_o / L) \cdot \left[1 - e^{-L/Xo} \right],$$

where t_o is a temperature of the air in air gap, ^{0}C, X_o is a conditional height where the air temperature in the air gap differs from the temperature t_o by e times (e ≈2,7) less than at the entrance into the space, m, L is a height of a continuous air gap, m.

For the second group (II) of the constructions in literature [12] there is an analytical method for the calculation of air movement in a space described by the system of equations, the solution which of requires some revision and verification based on the results of full scale investigations.

4. CONCLUSIONS

The developed algorithm for the calculation of facade systems with ventilated air gap has a following structure:

1. The determination of a construction group for the industrial finishing.
2. Calculations for the determination of temperature and pressure in the ventilated air gap using the method according to the construction group of external cladding.
3. Calculation of temperature fields taking into account the air infiltration.
4. Calculation of temperature fields taking into account the construction thermal heterogeneity.
5. The determination of the thermal resistance taking into account the air infiltration and heating engineering heterogeneity of the construction.

The further researches goal shall envisage the comparison of the results of experimental investigation of external wall construction thermal characteristics obtained in laboratory conditions and during field tests with the computational ones.

REFERENCES

1. DSTU B V.2.6-35: 2008 Construction of buildings and structures. Constructions of outward walls with facade heat-insulation and finishing industrial lagging wits ventilated air layer General technical condition.
2. GAGARIN V.G., KOZLOV V.V., TSYKANOVSKY E.Y. “Thermal protection of facades with ventilated air gap”, AVOK. 2004 No. 2, 3.
3. PODLASOVA I.A., CHERTNETA V.Y., KOPANITSA N.O., SOLODNIKOV E.V., “Thermal resistance of walls with hinged facade thermal insulation”, AVOK. 2005, No 3.

4. FARENYUK G.G., VENZHEGO G.S., “Thermal resistance determination of the curtain walls with ventilated air gap with constructions inhomogeneity account”, Rekonstruktsiya Zhytla. – No. 8, 2007.
5. BOHOSLOVSKII V.N. “Building thermal physics”, "High School", 1982.
6. FOKIN K.F. “Building envelopes thermal engineering”, “Gosstroiizdat”, 1973.
7. BRILING R.E. “Air permeability of the walls and materials”, “Stroyizdat”, 1949.
8. POWELL F., KRARTI M., TULUCA A. Air movement influence on the effective thermal resistance of porous insulations: A literature survey. Journal of building physics 1989 12: 239. http://jen.sagepub.com/content/12/3/239
9. UVSLOKK, S., “The Importance of Wind Barriers for Insulated Timber Frame Constructions,” J. Thermal Insul. & Building Envelopes, Vol. 20, July 1996.
10. YARBROUGH, D.W. AND GRAVES, R.S. The Effect of Airflow on Measured Heat Transport Through Wall Cavity Insulation, ASTM Symposium on Heat, Air, and Moisture Transport in Buildings, Toronto, Canada, 2006.
11. STRAUBE J. Thermal metrics for high performance enclosure walls: the limitations of R-value. Building science press 2009. Research report – 0901, 2007.
12. KOZLOV V.V. “Analytical method for calculating the air movement in the air gap ventilated facades cladding which containing periodical breaks”, NIISF – 50, 2006.

CYSENI 2015, May 27–28, Kaunas, Lithuania
ISSN 1822-7554, www.cyseni.com

METHODOLOGICAL AND PRACTICAL ASPECTS OF THE ADEQUACY ASSESSMENT METHODOLOGY FOR ENTSO-E SYSTEMS

E. Grigonytė
Lithuanian Energy Institute
Breslaujos str. 3, LT-44403 Kaunas – Lithuania
Phone +370 37 401939
Email: Ernesta.Grigonyte@lei.lt

ABSTRACT

To ensure the sustainable development of power systems, ENTSO-E is increasingly concerned with security of energy supply and, in particular, the adequacy of system generation and demand in ENTSO-E member countries. Each member country develops its adequacy outlook reports, consisting of questionnaires in spreadsheet forms, and submits them to the ENTSO-E, separately for summer and winter periods. The ENTSO-E processes the received country adequacy outlooks using the *Adequacy Assessment Methodology* and releases the Outlook Reports.

The paper aims at analyzes the methodological and practical application aspects of the Methodology, with regard to the Guidelines for Completing the Country Spreadsheets. Also, the review of Lithuania – case from the ENTSO-E Summer Outlook reports is presented.

Keywords: ENTSO-E, Adequacy Assessment, electrical power system, generating capacities, renewable, country cases

1. INTRODUCTION

On 21 May 2014, the European Network of Transmission System Operators for Electricity (ENTSO-E), represented by the 41 electricity transmission system operators (TSOs) from 34 countries across Europe [1], submitted its annual summer generation adequacy outlook report for 2014 ENTSO-E receives and publishes on an annual basis the “Summer Outlook and Winter Review” as required by Article 8 of the EC Regulation n. 714/2009 [2]. It does not clearly indicates to the summer and winter reviews. However, such reviews are of utmost relevance for the preparation of future outlooks and, alike, created by a long-standing practice of the associations of TSOs.

The ENTSO-E Outlook Report presents the views of Europe's electricity TSOs about national or regional security of supply for the summer or winter periods. The aim is to provide the opportunity to share information and gives impetus to further studies on a bilateral or multilateral basis and underlines possibilities for neighbouring countries to contribute to the generation / demand balance in critical situations if required [3].

National Generating Capacity (NGC): The Net Generating Capacity of a power station is the maximum electrical net Active Power it can produce continuously throughout a long period of operation in normal conditions. The National Generating Capacity of a country is the sum of the individual Net Generating Capacity of all power stations connected to either the transmission grid or the distribution grid [4] .

Net Transfer Capacity (NTC): The Net transfer capacity is the maximum total exchange program between two adjacent control areas compatible with security standards applicable in all control areas of the synchronous area, and taking into account the technical uncertainties on future network conditions [4];

Reference Points: Reference points are the dates and times data are collected for:

- Sundays of Summer on the 5th hour (05:00 CET) and on the 11th hour (11:00 CET);
- Wednesday of Summer on the 12th hour (12:00 CET) [4].

Remaining capacity (RC): The RC on a power system is the difference between the RAC and the Load. The RC is the part of the NGC left on the system to cover any programmed exports, unexpected load variation and unplanned outages at a reference point [4];

Severe conditions are related to what each TSO would expect under a 1 in a 10 year scenario. For example, the demand will be higher than under normal conditions and in certain regions, the output from generating units (e.g. wind) may be very low or there may be restrictions in thermal plants which operate at a reduced output under very low or high temperatures [4].

2. METHODOLOGY: SCOPE OF APPLICATION AND INPUT DATA

2.1. Scope of Application

This methodologies aim is to present TSOs' views on any matters concerning security of supply for the forthcoming summer period and it also seeks to identify the risks and the countermeasures proposed by the TSOs in cooperation with neighbouring countries, whilst also assessing the possibility for neighbouring countries to contribute to the generation/demand balance if required.

The Methodology is based on structuring the National Generating Capacity to a number of components. Special focus is given to the structure of generating capacities and their relation with cross-border exchanges, to the load factors for renewable in-feed and to the differences between normal and severe conditions, between "downward" and "upward" adequacies.

2.2. Stakeholder Consultation Process on future ENTSO-E Adequacy Assessment

The European electricity industry is facing significant changes, such as the integration of large amounts of renewable energy sources, new storage technologies, the creation of the Internal Electricity Market (IEM), demand side response and evolving policies all these factors require an improvement of the adequacy assessment methodologies.

ENTSO-E is developing its existing European methodology with a special attention on harmonised inputs, system flexibility and interconnected assessments. It is important that stakeholders are involved in the process of developing a new methodology for system adequacy from the outset. The most important aim is to become aware of expectations, concerns and requirements of stakeholders and interested parties with regards to the adequacy methodology [3].

2.3. Data for power balances and upward/downward adequacy analysis

The ENTSO-E Summer Outlook 2014 reports on the expectations of the regional and national power balances between forecast generation and load at reference points on a weekly basis for the upcoming summer period, from 1 June (week 22) to 17 September 2014 (week 38) [4].

An extensive regional analysis was added to per-country analysis in the methodology of seasonal outlooks. The aim of this investigation whether the electrical energy will be available at certain points in time to allow the countries with a generation deficit to import the electric power needed from the surrounding countries and European scale have to be taken into account [4].

It was used a synchronous point in time for all countries to allow for a meaningful analysis when determining the feasibility of cross border flows. Before starting the data collection, and using European historical load data, a study was conducted to identify the most representative synchronous time for covering the global European peak load in summer. It was concluded that Wednesday, 12:00 CET most closely represents this situation, and therefore data was requested from TSOs for this time point. With regards to the regional analysis, the values which were actually used from the data collection spreadsheet:

- The Remaining Capacity for normal and severe conditions;
- Simultaneous importing and exporting capacity;
- A best estimate of the minimum Net Transfer Capacity (NTC) values towards and from individual neighbouring countries [4].

Also, across the period of assessment for the next summer, any European "downward regulation" issues where excess inflexible generator output exceeds demand are investigated. It provides an indication which countries require exports to manage inflexible generation, it is necessary to analyze of their ability to export this energy to neighbouring regions that are not in a similar situation. This analysis is required to the fact that a number of TSOs expressed that they are experiencing growing problems for system operation (mainly) due to the increase of intermittent generation on the system (wind and solar) and the lack of more flexible generation means [4].

To carry out a regional downward analysis, a synchronous point in time was used for all countries in order to allow for meaningful analyses when identify cross border flows. The same European load study mentioned before concluded that minimal demand conditions generally take place around 05:00 CET on Sunday morning. It was concluded that these issues with inflexible generation are not only possibility to happen during the night, but also during daytime when the energy production of solar panels nears its maximum. To cope with this effect, an additional synchronous time point was added for Sunday 11:00 CET, when a combination of potentially high photo-voltaic in-feed and reduced demand levels exist. Quantitative data for this point in time was therefore also requested from all TSOs to allow for a meaningful regional analysis [4].

For the regional downward analysis, the values which were actually used from the data collection spreadsheet can be summarized as:

- The expected inflexible generation surplus at Sunday 05:00 and 11:00 CET;
- Sum of the inflexible and must-run generation;
- Simultaneous importing and exporting capacity;
- A best estimate of the minimum NTC values towards and from individual neighbouring countries can see in Fig. 1 [4].

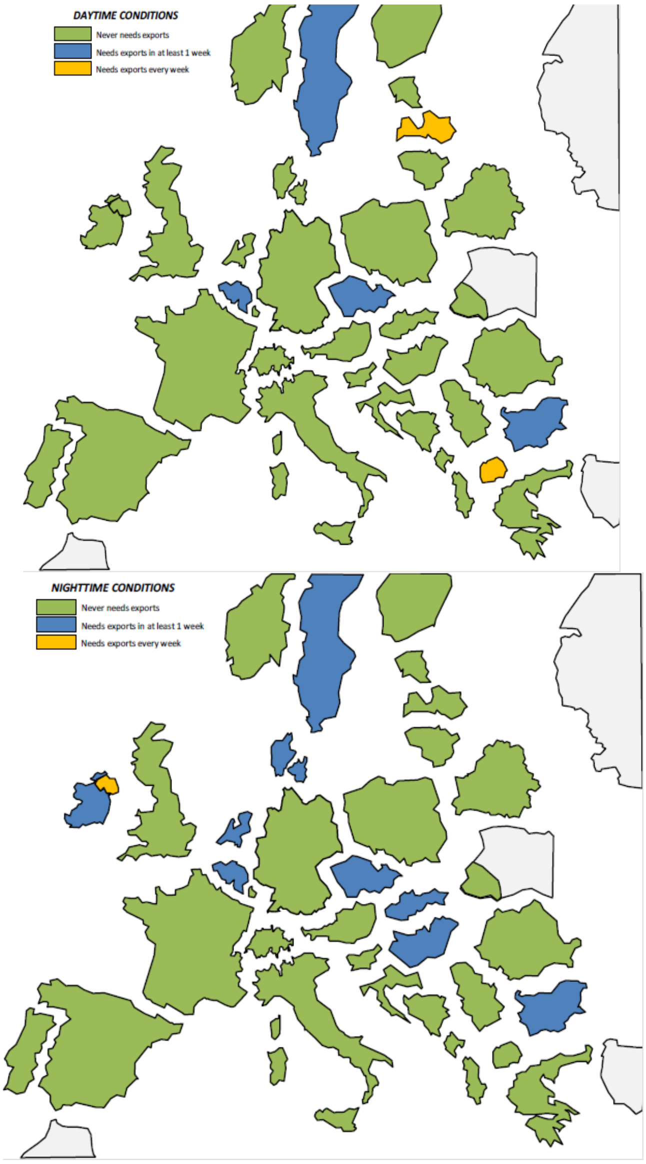

Fig. 1. Overview of the export needs for the daytime nighttime scenario [4]

2.4. Renewables in-feed data

For the per-country analysis, each TSO gave an estimation of the highest expected proportion of installed solar, onshore wind and offshore wind capacity to be taken into account for the downward analysis. Default values of 65% for wind and 95% for solar were presented, allowing for every country to enter its best estimate. For the generation adequacy analysis the renewables in-feed is handled through an estimate of the non-usable capacity in normal and severe conditions by each TSO. For the regional analysis though, a Pan-European Climatic Database used containing per-country load factors for solar, onshore wind and offshore wind per hour for a ten-year period [4].

To achieve per-country representative load factors for the generation adequacy analysis, the 50th and 10th percentile respectively for normal and severe conditions of the load factors per country and for solar, wind onshore and wind offshore separately are calculated considering historical values, per month, and for the suitable time period. A renewable in-feed scenario is created which is a corresponds to worst-case scenario over the different countries and for the different primary energy sources [4].

The methodology for the downward analysis is very similar to the one above, with the difference that the 90th percentile is used. It is envisioned for the future outlooks to use the experience gained on this matter and further refine the applied methodologies [4].

3. METHODOLOGY: UPWARD AND DOWNWARDS ADEQUACIES

3.1. Upward adequacy

The methodology consists of identifying the ability of generation to meet the demand by calculating the so called “remaining capacity” under two scenarios: normal and severe weather conditions. The methodology is schematically depicted on the Fig. 2 [4]:

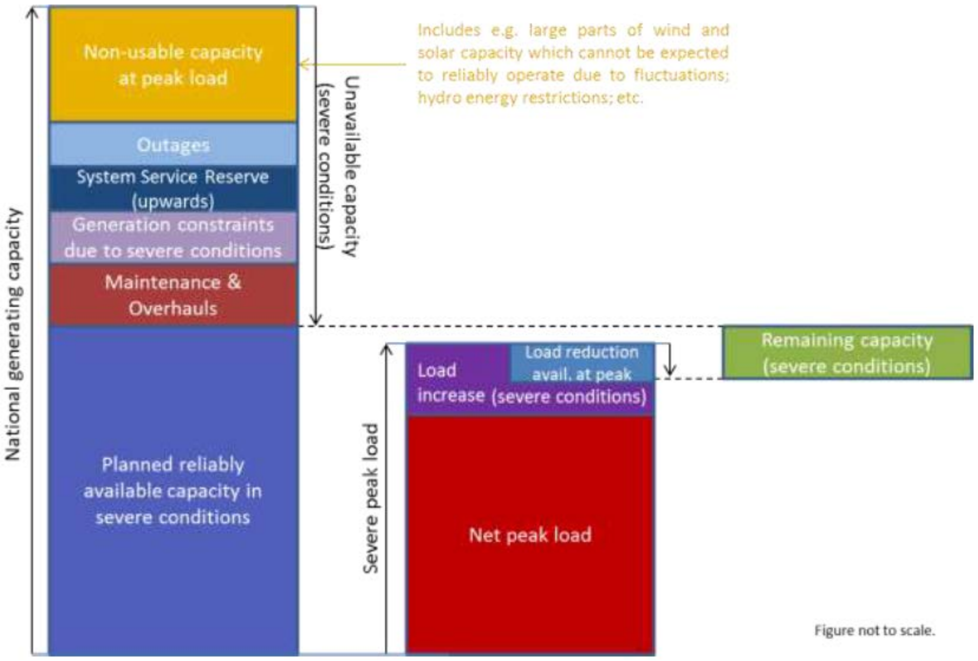

Fig. 2. Summary of upward adequacy methodology [4]

The basis of the analysis is the situation called “normal conditions” it is conditions that correspond to normal demand on the system (i.e. normal weather conditions resulting in normal wind or hydro output and an average outage level). A “severe conditions” scenario shows the sensitivity of the generation-load balance to high temperature and extreme weather conditions. The severe conditions are related to what each TSO would expect in terms of demand which will be higher than in normal conditions and in terms of generation output which is reduced (i.e. severe conditions resulting on lower wind or restrictions in generation power plants due to extended drought) [4].

The basis of the regional analysis is a constrained linear optimization problem. The target is to detect if problems can arise on a pan-European scale due to a lack of available capacity. No market simulation or grid model simulation whatsoever is taken into account. The goal is to provide an indication whether countries requiring imports will be able to source these across neighbouring regions under normal and severe conditions, it means that the investigation carried out is purely a “feasibility” analysis. [4]

The first element that is checked is whether in a “copperplate” scenario there is enough power capacity to cover the demand. A second, more precise approach modelled as a linear optimization with the following constraints:

- Bilateral exchanges between countries should be lower or equal to the given NTC values;
- Total simultaneous imports and exports should be lower or equal to the given limits.

Based on this methodology, it was calculated which groups of countries would have a generation deficit for a certain week due to saturated cross-border exchanges [4].

3.2. Downward adequacy

Under minimum demand conditions, there is a potential for countries to have an excess of inflexible generation running. Every TSO is likely to have varying levels of "must-run" generation Fig. 3. This may generators that are required to run to maintain dynamic voltage support etc. In addition there will be renewable generation such as run of river, solar and wind whose output is inflexible and variable. At times of high renewable output e.g. wind, the combination can result in generation exceeding demand and the pumped storage capacity of the country. In that case, the "excess" generation is either exported to a neighbouring region or curtailed [4].

The analysis will highlight periods where groups of countries cannot export all of their excess generation. It should be again stressed that this analysis is not a market simulation. Rather, it conducts a feasibility analysis to indicate countries which may be required to curtail excess generation due to limited cross border export capacity [4]

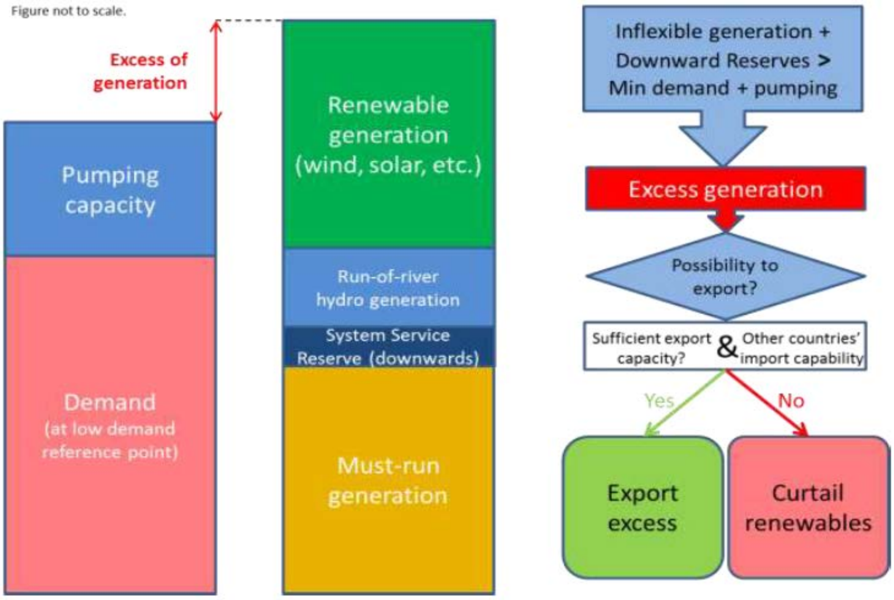

Fig. 3. Summary of downward adequacy methodology [4]

The downward adequacy assessment involves cases when due to low overnight demands, an excess of generation can be present in the system, especially when changeable renewable generation and inflexible classical generation are at high output levels. This could also appear on weekend days (characterised by low load and possibly high PV generation output). In seasonal outlooks, two different reference points, one overnight and one daytime, are examined for downward adequacy. Assumptions provided these downward assessments are based on different transmission conditions and may require specific means of action [4].

In such cases, there could be used an excess of inflexible generation which would be need to exported or curtailed. And when in a country generation exceeds demand, due to one of the above reasons, cross border flows will occur in regions which can be imported the excess generation, when the cross border capacities are fully exploit, curtailment of renewables (or other inflexible generation) will occur due to the lack of suitable infrastructure, including storage facilities, which may be used to balance the inflexible generation [4].

In order to harmonise as far as practicable the preconditions on intermittent energy sources, considering the inherent differences between countries, two different approaches are applied: the Pan European Assessments include a harmonised probabilistic approach using a Pan European Climate database (PECD), data from Technical University of Denmark, meanwhile the individual country analysis includes the data provided by the TSOs in order to take into account each country specificities. For being able to conduct a Worst-case analysis necessary to use the best estimate of the minimum NTC values [4].

4. GENERAL OVERVIEW OF SUMMER OUTLOOK – 2014

4.1. General overview

The coordination team which developed the regional analysis methodology is comprised of very experienced experts from various TSOs across Europe. The data submitted has been inspected by team members with a focus on those regions on which they have extensive knowledge and have confirmed that the main conclusions from the analysis are valid. It should be noted that the analysis was based on data submitted by each TSO. A synchronous point in time was requested for all data in order to allow for a comparison between regions. Hence, a feasibility test to determine that there is enough generation to meet demand under normal and severe scenarios was enabled [4].

Based on the data submitted by each TSO, Europe as a whole should have over 155 GW of spare capacity to meet demand and reserves under normal conditions in the ideal case of unlimited interconnection capacity. Taking into account the cross border capacities, the analysis indicated that there is sufficient interconnection capacity between countries to take full advantage of this excess of generation capacity to cover the demand in all countries [4].

Taking into account the reported interconnection capacities and using a consistent scenario for the renewables in-feed, the analysis revealed that under the considered circumstances sufficient means should be available to export energy out of the countries which expect an excess of inflexible generation. The ENTSO-E Summer Outlook 2014 highlights the fact that during certain weeks over the summer, it may be necessary to reduce excess generation in various countries as a result of insufficient cross border export capability [4], for example, the combination of high renewables in-feed and inflexible generation.

4.2. Country overview (Lithuania)

In Fig. 4 below can be observed potentially stressed situation in certain periods for the Lithuania system.

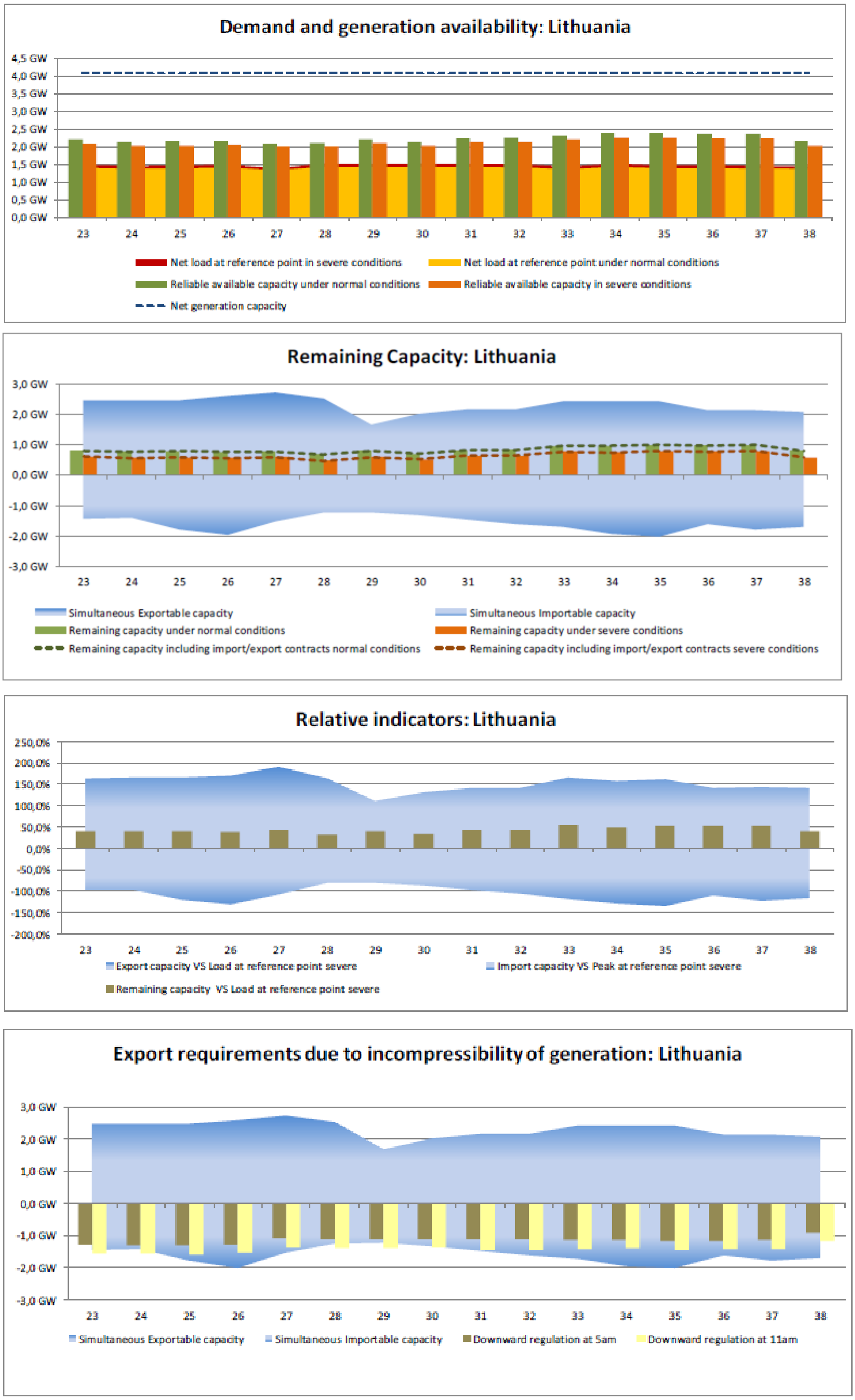

Fig. 4. Adequacy characteristics for Lithuanian power system's Summer-2014 Outlook [4]

The Lithuanian adequacy is in general good NGC is much higher than the system load and the reliable available capacity but it means that a large part of NGC is unreliable (see 1st panel of the Fig. 4).

On 1 December 2014, ENTSO-E submitted its annual winter generation adequacy outlook report for 2014/15 the “Winter Outlook report 2014/15 and Summer review 2014” [5] in overall the majority of countries reported an average or milder summer compared to previous years.

5. CONCLUSIONS

Methodology is being prepared each time is improved. ENTSO-E is taken into account recommendations from ACER’s opinion on the previous Summer Outlook report by providing the evolution of the main results and values compared to those of the previous year. Also improvements on spare capacity and data due to export capacities for downward regulation analysis.

Outlook report underline possibilities for neighbouring countries to contribute to the generation / demand balance in critical situations. It provides possibility to share information and gives signal to further studies on a bilateral or multilateral basis.

A number of countries reported congestion issues on parts of the network including some interconnector sites. A small number of countries reported high precipitation and flooding [5]. Peak demand was generally lower than what was predicted in the Summer Outlook Report and there were no reports of unusually high demand. And the majority of countries did not report any system adequacy issues over the summer.

Lithuania seems to have better adequacy than Poland, but worse than Norway.

REFERENCES

1. European Network of Transmission System Operators for Electricity, 2014 [referred on the 3th of March in 2015 y]. Link to the internet <https://www.entsoe.eu/about-entso-e/Pages/default.aspx>
2. European Network of Transmission System Operators for Electricity, 2014 [referred on the 3th of March in 2015 y.]. Link to the internet <https://www.energy-community.org/portal/page/portal/ENC_HOME/DOCS/3528173/20141217_1st_SoS_CG_SG-E_ENTSO-E_Winter_Outlook_Schroeder.pdf>
3. European Network of Transmission System Operators for Electricity, 2014 [referred on the 3th of March in 2015 y.]. Link to the internet < https://www.entsoe.eu/publications/system-development-reports/outlook-reports/Pages/default.aspx>. The same as [1]
4. European Network of Transmission System Operators for Electricity, Summer outlook report 2014 and winter review 2013/14, 2014, p. 1–62.
5. European Network of Transmission System Operators for Electricity, Winter outlook report 2014/15 and summer review 2014, 2014, p. 15.

REVIEW OF METHODS FOR MEASURING SUSTAINABLE DEVELOPMENT

A.E. Lutynska
Vytautas Magnus University
Vileikos str. 8, LT-44404 Kaunas – Lithuania
Phone +370 37 327898
Email: a.lutynska@if.vdu.lt

ABSTRACT

Sustainable development is a popular and important concept, which can be understood as meeting the needs of present generations without compromising the ability of future generations to meet their needs. But it is the one that is difficult to define with precision and, therefore also difficult to measure. The last two decades have seen a proliferation of methods and indicators to measure sustainable development. An indicator is a special index, which provides numerical values to important factors of the investigated sector. The emphasis on sustainability indicators has multiple motivations, which include decision making and management, advocacy, participation and consensus building, also research and analysis. The aim of this paper is to review the methods for measuring sustainable development. There are presented two multi-purpose methods: barometer of sustainability and integrated sustainability indicator.

Also, it is advisable to have tools to predict sustainable development. In this article is proposed to use dynamic model. However, it is appropriate to analyse all sustainability indicators together, including investigation and determination of their interdependence. Furthermore created dynamic model enables us to forecast the dynamics of the indicators according to new factors.

Keywords: sustainable development, sustainability indicators

1. INTRODUCTION

There is no doubt that nowadays many societies are concern with their ability to satisfy the needs of present generation without jeopardizing the possibility of doing so for future generation, thus sustainable development becomes an important issue. The concept of sustainable development has helped scientists and practitioners to understand not only the environmental impacts but also the social and economic effects of projects as the human race interact with the surrounding. But the concept is difficult to define with precision and, therefore, difficult to measure. The last two decades have seen a proliferation of methods and indicators to measure sustainable development. An indicator is a special index, which provides numerical values to important factors of the investigated sector. A single sustainability indicator defines a key issue, which characterizes a certain aspect of sustainability in the observed system. It is therefore necessary to produce meaningful measures capable to effectively monitor the current progress of sustainable development.

The aim of the paper is to analyze various sustainability assessment approaches and review the methods and tools for measuring sustainable development. Nowadays, there are different ways of measuring sustainable development, which basically depend on the specified objectives of the study (see table 1). There are also developed methods for multi-purpose measuring of sustainability. One of them is barometer of sustainability. The barometer of sustainability measure a society’s well-being and progress toward sustainability, sustainability depend on improving and maintaining the well-being of people and their ecosystem. Another tool is integrated sustainability development indicator. Integrated sustainability assessment indicators are being developed for monitoring progress of implementing the Sustainable Development Strategy. Indicator acquire the form of scores making it possible to analyze the trends of an integrated indicator and assess progress of the sustainable development.

Many of research analyzed only sustainable development monitoring. Policymakers need methods for measuring and assessing the current and future effects of processes on human health, human society, air, soil and water. So, it is advisable to develop method for sustainability assessment forecasting. This article proposes to use a dynamic model.

2. CONCEPTS OF SUSTAINABLE DEVELOPMENT

The most widely accepted definition is creatively ambiguous: “Humanity has the ability to make development sustainable – to ensure that it meets the needs of the present without compromising the ability of future generations to meet their own needs” [1]. This is the standard definition when judged by its widespread use and frequency of citation. The use of this definition has led many to see sustainable development as having major focus on intergenerational equity [2]. It is also definition for sustainability that „challenged the traditional ways of doing business, changed the interpretation of the world development, and helped scientists and practitioners to understand not only the environmental impacts but also the social and economic effects of projects as the human race interact with the surrounding” [3]. The Brundtland report also contains two key concepts: the concept of “needs”, in particular the essential needs of the world’s poor, to which overriding priority should be given; and the idea of limitations imposed by the state of technology and social organizations on the environment’s ability to meet present and future needs [3].

The 2002 World Summit on Sustainable Development marked a further expansion of the standard definition with the widely used three pillars of sustainable development: economic, social and environmental [4]. These pillars posed by three characteristics: independency, inter-relation/inter-connection, and equality (see Fig. 1). Based on these characteristics, an alternative definition of sustainable development is stated as the path to balance social, economic, and environmental needs. Principles, which underlining that developing in a sustainable manner goes beyond environmental aspects, are: equity, futurity, environment, and public participation [3]. “The protection of the environment is at the forefront of sustainable development, and this can be accomplished only through collaborative decisions, increased regulation, and each individual becoming a steward of the environment on a personal and global level”[4], which implies that a sustainable future is in the hands of all of us, and the responsibility is shared, not to be left to politicians and policy decision makers.

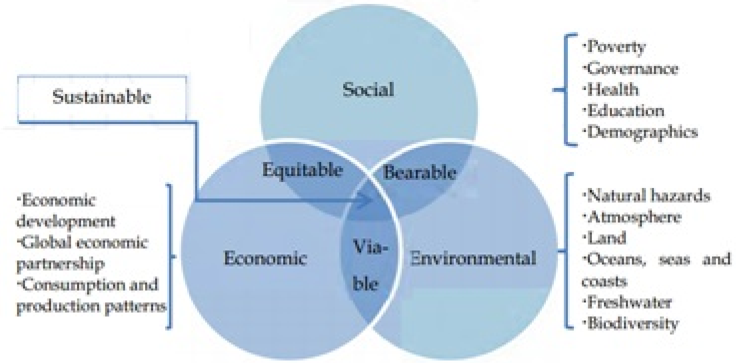

Fig. 1. Three pillars of sustainable development

2.1. Indicators

Another way to define sustainable development is in how it is measured. Despite sustainable development's creative ambiguity, the most serious efforts to define it, albeit implicit in many cases, come in the form of indicators [6]. Indicators are variables. A variable is an operational representation of an attribute or characteristic of a system; it can convey information on the condition and/or trend of an attribute of the considered system. Sustainability indicators define characteristics that are important for sustainable development. A single sustainability indicator defines a key issue, which characterizes a certain aspect of sustainability in the observed system. Sustainability indicator systems capture the complexity and order of the systems, and they offer new knowledge about the system that can be communicated to the general public [7]. The emphasis on sustainability indicators has multiple motivations, which include decision making and management, advocacy, participation and consensus building, also research and analysis.

Taken together, the indicators give a clear picture of the whole system, including interlinkages and trade-offs among various dimensions of sustainable development and long-term implications of current decisions and behaviour. Changes in the indicator values overtime mark progress or lack of it towards sustainable development [8].

According to article [8], the recommendations to define the set of sustainable indicators are: representativeness (to represent the relevance of the product or process identified), comparability (to be comparable in both space and time), data collection (there must be reliable source to supply the data), clarity and synthesis (to transmit information in a simple synthesis being indentified), forecast and targets (to anticipate problems and seeking solutions being instrumental in setting targets).

2.2. Measuring sustainable development

The discussion on sustainability is part of the process of working towards sustainable development. However, we do not know if we are becoming more sustainable without finding a way to measure it. Measuring sustainability is a major issue as well as driving force for the discussion on sustainable development. Developing tools that reliably measure sustainability is a prerequisite for identifying non-sustainable processes informing design-makers of products' quality and monitoring impacts on the social environment. Policymakers need methods for measuring and assessing the current and future effects of processes on human health, human society, air, soil and water. The need is to determine whether the current actions are sustainable and, if not, how to change them in order to make sustainable [8].

The number of methodologies, models, approaches, and appraisals for assessing sustainability has dramatically increased since the concept of sustainable development was recognized as separate from economic wealth creation and environmental degradation in the 1960 s.

Nowadays, there are different ways of measuring sustainable development which basically depend on the specified objectives of the study. Sustainability assessment practitioners have developed an increasing variety of tools [9]. Table 1 presents selected efforts to measure sustainable development. Each of them describe some sustainable development aspects, which are focused on environment, economic or social performance. But we are looking for versatile method, which can be used for multi-purpose measuring of sustainability. There are selected and widely presented two of them: barometer of sustainability and integrated sustainability indicator.

Table 1. Definitions and motivations for measuring sustainable development

Indicator initiative	What is to be sustained?	What is to be developed?	Motivation
United Nations Commissions on Sustainable Development	Climate, clear air, land productivity, ocean productivity, fresh water, biodiversity	Equity, health, education, housing, security, stabilized population	“Indicators can provide crucial guidance for decision-making in a variety of ways”
Wellbeing Index	“A condition in which the ecosystem maintains its diversity and quality – and thus its capacity to support people and the rest of life – and its potential to adapt to change and provide a wide change of choices and opportunities for the future”	“A condition in which all members of society are able to determine and meet their needs and have a large range of choices to meet their potential”	Provide : “a way of measuring progress toward the goal”, “an analytical tool for deciding priority actions”, “a process to keep the goal constantly in mind and to help people learn how to reach it”
Environmental Sustainability Index	“Vital environmental systems are maintained at healthy levels, and to the extent to which levels are improving rather than deteriorating” and “levels of anthropogenic stress are low enough to engender no demonstrable harm to its environmental systems”	“People and social systems are not vulnerable to environmental disturbances; becoming less vulnerable is a sign that society is on a track to greater sustainability”	“Assist the move toward a more analytically rigorous and data driven approach to environmental decision making”, “identification of issues where national performance is above or below expectations”, “tracking of environmental trends”
Genuine Progress Indicator	Clean air, land and water	Economic performance, families and security	To replace GDP as the primary scorecard of the nation’s well-being for the general public, policymakers
Ecological Footprint	“The area of biologically productive land and water requires to produce the resources consumed and to assimilate the wastes produced by humanity”	–	“Help inform production choices”, “keep the market on an efficient Path over time”, adjust market prices to include the cost borne by third parties

2.2.1. Barometer of Sustainability

To obtain a clearer understanding of the overall situation when dealing with multiple criteria and indicators, one might use the barometer of sustainability that Robert Prescott-Allen developed for IUCN to measure a society’s well-being and progress toward sustainability [10]. The barometer organizes and combines indicators from a wide range of issues or criteria into a two-dimensional index. The *y*-axis represents a combined index score for human well-being; the *x*-axis – a combined index score for ecosystem well-being (see Fig. 2). This two-dimensional index treats people and the environment as equally important [11].

With the barometer, each indicator is associated with its own performance scale using values appropriate to the issue or criterion. Only those indicators with values that can be interpreted as bad or good with respect to well-being can be used. A simple calculation is used to convert each indicator measurement into one of the five sectors of the 100-point scale: good, OK, medium, poor, or bad.

The barometer can accommodate any hierarchical arrangement of criteria. (see Fig. 3). It does not matter how many levels make up the hierarchy, as long as the subsystems are ecosystem and people. Individual scores for the indicators are combined up the hierarchy, from indicator, to criteria, to category, to sub-system, resulting in an index for people and an index for the ecosystem. The indicators on a particular level are combined — they are averaged when they are equally important, and they are weighted if they vary in importance [11].

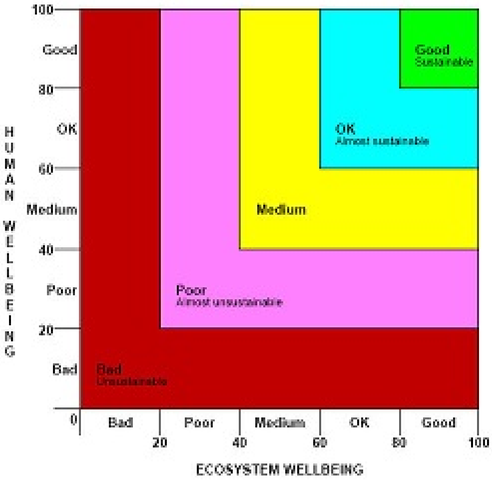

Fig. 2. Barometer of Sustainability

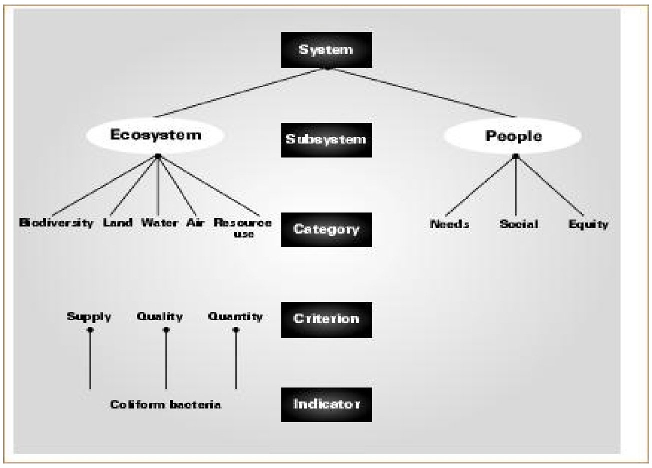

Fig. 3. Hierarchy of indicators

The barometer results, along with an analysis of the key issues, will enable participants to draw conclusions about the conditions of people and their ecosystem in relation to the system under study. Sustainability will depend on improving and maintaining the well-being of people and their ecosystem.

2.2.2. *Integrated Sustainability Indicator*

Integrated sustainability assessment indicator are being developed for monitoring progress of implementing the Sustainable Development Strategy and sustainability assessment of policies and measures seeking to reflect the main issues of sustainable development set in the National Sustainable Development Strategy. Such indicators constructed from a wide range of specific structural social, economic and environmental indicators aim to evaluate important features of the investigated social, economic and environmental issues addressed in National Sustainable Development Strategy and the same time they indicate how the changes of structural indicators influence dynamics of an integrated indicator. Therefore, integrated indicator represent:

- static characteristics of structural indicators forming integrated and their dynamics;
- weights of structural indicators and their importance in tracking dynamics of integrated indicator;
- forecast of structural indicators changes;

- correlation of structural indicators;
- static characteristics of an integrated indicator, its dynamics and forecast.

Integrated sustainability indicator can be calculated by summing the weighted indices of all indicators [12]:

$$I_n = \sum w_i I_{in}, \tag{1}$$

here I_n – integrated indicator for sustainability assessment at time moment n; I_{in} – index of indicator i at time moment n; w_i – weight of indicator i in the integrated indicator.

Indices of indicators are derived by the following formula:

$$I_{in} = q_{in}/q_{i0} \tag{2}$$

q_{in} – value of indicator i at time moment n; q_{i0} – value of indicator i for base year (the first year of monitoring).

If indicator decrease (e.g. external costs or private cost) is positive in terms of sustainability assessment, the indices of such indicators are integrated as inverted indices:

$$I_{in} = 1/I_{in} \tag{3}$$

In this way, indicators acquire the form of scores making it possible to analyze the trends of an integrated indicator and assess progress of the sustainable development path in the country.

3. PREDICTING SUSTAINABILITY

In many areas models of different processes take into account various factors that are time-dependent and dependent on each other. Thus, it is advisable to construct dynamic model in order to describe these dependences. In dynamic model we use indicators. An indicator is a special index, which provides numerical values to important factors for the investigated sector.

Let us construct a homogeneous differential equations system, according to the interdependencies between indicators

$$\begin{cases} \dfrac{\mathrm{d}I_1(t)}{\mathrm{d}t} = a_{11}I_1(t) + a_{12}I_2(t) + \cdots + a_{1N}I_N(t), \\ \vdots \\ \dfrac{\mathrm{d}I_N(t)}{\mathrm{d}t} = a_{N1}I_1(t) + a_{N2}I_2(t) + \cdots + a_{NN}I_N(t), \end{cases} \tag{4}$$

here a_{ij}, $i,j=1,\ldots, N$ are coefficients, I_i, $i=1,\ldots, N$ – indicators, describing factors of different areas.

Coefficients a_{ij}, $i,j=1,\ldots,N$ in formula (4) may be calculated using different methods: algebraic, statistical, etc. In [13] is presented limitations of algebraic method: the matrices should be square. So, the number of indicators and the number of time moments (when factual values of indicators are observed) must be the same. So, it is better to use the least square method (LSM) for calculation of coefficients [13]. For the application of LSM number of observed factual values of indicators $n: n \geq N-1$.

Let us give the variation for each indicator $\Delta I_i(t) = (I_i(t+\Delta t) - I_i(t))/\Delta t,\ i=1,\ldots,N$ and construct system of algebraic Equations

$$\begin{cases} \Delta I_1(t) = a_{11}I_1(t) + a_{12}I_2(t) + \cdots + a_{1N}I_N(t), \\ \vdots \\ \Delta I_N(t) = a_{N1}I_1(t) + a_{N2}I_2(t) + \cdots + a_{NN}I_N(t), \end{cases} \tag{5}$$

We take values of each indicator in time moments t_k, k=1,.., n and define $I_{ik}=I_i(t_k)$, i=1,…, N, k=1,…, n. So, we have N algebraic systems of N Equations with N^2 unknowns

$$\Delta I_{ik} = a_{i1}I_{1k} + a_{12}I_{2k} + \cdots + a_{1N}I_{Nk}, \ \ i = 1,\ldots,N, \ k = 1,\ldots,n. \tag{6}$$

The solution of differential Equations system (4) is obtained from the formula (7) [14].

$$\mathrm{I}(t) = \sum_{j=1}^{N} C_j B_j \mathrm{e}^{\lambda_j t}, \tag{7}$$

here $\mathrm{I}(t)=(I_1(t), I_2(t),\ldots, I_N(t))^{\mathrm{T}}$, $B=(b_1,\ldots, b_n)^{\mathrm{T}}$ – vector of constants, C_j – constants. Eigenvalues of matrix A $\lambda_j, j = 1.2,\ldots,n$ of the system (4) can be real and/or complex $\lambda_j = \alpha_j + \mathrm{i}\beta_j$ and $\lambda_{j+1} = \alpha_j - \mathrm{i}\beta_j$. In the latter case constant $C_j = \tilde{C}_j + \mathrm{i}\tilde{\tilde{C}}_j$

Aiming to find a particular solution for differential Equations system (4), i.e. particular expression of each indicator as on time dependent function, we need to formulate initial conditions for differential equations system. Constants C_i, i=1,…,N of general solution may be found by solving system of differential Equations (4) in time moment t_0

$$I_1(t_0) = I_1^0, \ldots, I_N(t_0) = I_N^0, \tag{8}$$

here I_{i}^0, i=1,…, N – normalized factual value of indicator in time moment t_0.

Created dynamic model will enable us to forecast alternation of different systems factors, such integrated sustainability indicators according to introducing new objects. In this case we should correct the initial conditions (8) of differential equations system. Since parameters of new objects are not exactly known, these uncertainties should be reflected in the initial conditions. Thus, in such conditions, the values of indicators are random variables [15].

In mathematical statistics theory it is well known that Bayesian method allows a combination of two kinds of information: prior (for instance, generic statistic data, subjective option of experts) and measurements or observations [16]. Bayesian method allows updating estimates of all parameters in the model with a single new obtained observation, i.e. Bayesian method does not require to have new information on the values of all factors involved in the created model.

Bayesian method also allows taking into account the experts' opinion, i.e. when instead of real data we have experts' opinion about factors behaviour in the future. Expert judgment – probable mean values of indicators time t^*: $I(t^*) = (I_1^*, \ldots, I_N^*)$, with standard deviations σ_i, $i = 1, \ldots, N$, that represent uncertainties. C_i , $i = 1, \ldots, N$, in (7) solution of differential equations system (4) are independent random variables, with prior probability density functions (pdfs) $p_i(x_i)$, $i = 1, \ldots, N$ [15].

Non-stationary processes are analyzed, i.e. the values of factors depend on time t. Classical application of Bayesian method is not correct in this case, because observations obtained in different time moments represent the other state of the indicators. The modified application of Bayesian method for the calculation estimates of parameters of non-stationary process mathematical models is presented in research papers [15], [17].

3.1. Example of calculation

An integrated indicators approach was constructed for monitoring implementation of sustainable development strategy in Lithuania in [12]. For practical demonstration of the proposed forecasting method the example of 8 structural indicators have been selected (see Table 2), using the statistical data collected in [12].

Table 2. Dynamics of integrated sustainability indicators for Lithuania

	2000	2001	2002	2003	2004	2005	2006	Weight
Average real wage	1.00	0.98	0.99	1.03	1.09	1.29	1.51	0.1
Share of enterprises using computers	1.00	1.05	1.06	1.12	1.14	1.14	1.13	0.1
Labour productivity, value added per working hour	1.00	1.11	1.17	1.27	1.39	1.50	1.71	0.2
Share of high technology sector value added in total value added	1.00	0.94	1.02	1.01	1.06	1.06	1.09	0.2
GHG emissions	1.00	0.95	0.94	0.92	0.89	0.85	0.83	0.1
Emigration	1.00	0.97	0.99	0.63	0.46	0.45	0.56	0.1
Human development index	1.00	1.02	1.02	1.04	1.07	1.08	1.09	0.1
Employment	1.00	0.97	1.02	1.04	1.04	1.07	1.08	0.1
Integrated weighted sustainability assessment indicator	1.000	1.006	1.039	1.035	1.060	1.101	1.181	

LSM is applied to calculate estimates of unknown coefficients of Equation (6) with assumption that $a_{ii}=0$, $i=1,\dots,N$. The separate solution of differential equations system (4) was obtained using data of year 2005 in initial condition (8). Further this dynamic model was used for forecasting values of indicators. The obtained values were compared with the factual values of indicators in that year (see Table 3).

Table 3. Comparison of indicators values

	Factual	Dynamic model	Error
Average real wage	1.51	1.33	0.19
Share of enterprises using computers	1.13	1.14	0.01
Labour productivity, value added per working hour	1.71	1.53	0.17
Share of high technology sector value added in total value added	1.09	1.07	0.03
GHG emissions	0.83	0.84	0.01
Emigration	0.56	0.47	0.08
Human development index	1.09	1.08	0.01
Employment	1.08	1.07	0.01
		mean of error	0.06

As we can notice, the mean of error is quite small. So, we can use dynamic model for forecasting integrated indicators values. The forecast of indicators is being obtained by applying differential equations system (4) with data of year 2006 in initial condition (8). Integrated sustainability indicator (1) was calculated by summing the weighted predicted values of all indicators.

In Fig. 4 dynamics of monitored and forecasted integrated sustainability assessment indicator of Lithuania is presented. In all analyzed period an increase in this indicator is showing the positive trends toward sustainable development. Long – term forecasting for integrated sustainable development indicator could loses the sense. Over the time surroundings are changing, new factors and characteristics can appear. Then we should correct the initial conditions (8) of differential equations system. For long – term prediction we can involve experts' judgment. We could do that applying modified Bayesian method [15].

In this paper suitability of using dynamic model for integrated sustainable assessment indicator forecasting is shown.

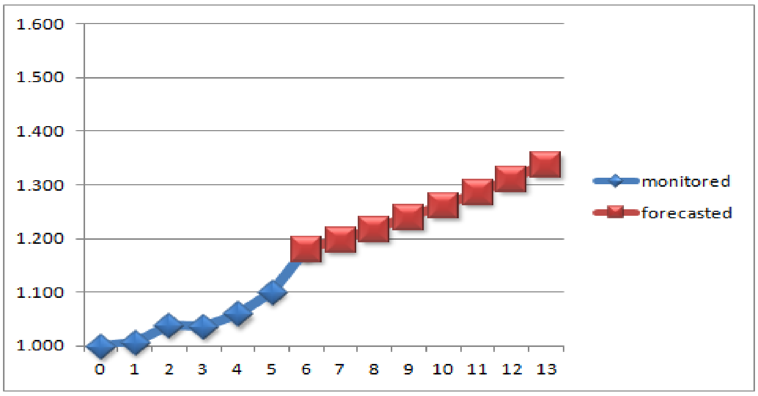

Fig. 4. Integrated weighted sustainability assessment indicator

4. CONCLUSIONS

One of the most important concerns of society is a decision making especially on sustainable development issues. However, we do not know if we are becoming more sustainable without finding a way to measure it. There are many methodologies, models, approaches, and appraisals for assessing sustainability. They basically depend on the specified objectives of the study. But sustainability is a complex and multi-dimensional area. Therefore, we looking for versatile method. There are presented two multi-purpose methods: barometer of sustainability and integrated sustainability indicator. Barometer of sustainability is two-dimensional index and includes the well-being of people and their ecosystem. Integrated sustainability indicator acquire the form of scores and can be used the most widely. It is possible to analyze the trends of an integrated sustainability indicator and assess progress of the sustainable development path.

Many of research analyzed only sustainable development monitoring. In a monitoring process, calculations of the sustainable indicators help us to understand where political action is needed. The next question is how to evaluate the consequences of this interaction? It is advisable to have forecasting methods for sustainable development. In this article is proposed to use dynamic model. As an example, dynamic model was used to forecast integrated sustainability assessment indicator for Lithuania. In analyzed period an increase in this indicator is showing the positive trends toward sustainable development.

REFERENCES

1. World Commission on Environment and Development (WCED), *Our Common Future*, New York: Oxford University Press, 1987, 8 p.
2. National Research Council, Policy Division, Board on Sustainable Development, *Our Common Journey: A Transition toward Sustainability*, Washington, DC: National Academy Press, 1999, 22 p.
3. POVEDA, C.A., LIPSETT, M.G. A Review of Sustainability Assessment an Sustainability/Environmental Rating Systems and Credit Weighting Tools. *Journal of Sustainable Development*, 2001, Vol. 4, No. 6, p. 36–55. <http://dx.doi.org/10.5539/jsd.v4n6p36>
4. *The Johannesburg Declaration on Sustainable Development*. New York: NGO Committee on Education, 2002. Link to the internet <http://www.un-documents.net/jburgdec.htm>.
5. COLLIN, R.M., COLLIN, R.W. Encyclopaedia of Sustainability. Santa Barbara: ABC-CLIO, LLC, 2010.
6. KATES, R.W., PARRIS, T.M., LEISEROWITZ, A.A. What is Sustainable Development? Goals, indicators, values, and practice. April 2005 Issue of Environment: Science and Policy for Sustainable Development, 2005, Vol. 47, No. 3, p. 8–21.
7. SCHLOR, H., FISCHER, W., HAKE, J.-F. Methods of measuring sustainable development of the German energy sector. *Applied Energy*, 2013, Vol. 101, p. 172–181. <http://dx.doi.org/10.1016/j.apenergy.2012.05.010>
8. ZEN, A.C., LIMA, A., BIANCHI, A.L. BABOT, L. Sustainability, Energy and development: A Proposal of Indicator. *International Journal for Infonomics*, 2012, Vol. 5, Issue 1/2, p. 537–541.
9. KATES, R.W., PARRIS, T.M. Characterizing and Measuring Sustainable Development. *Annual Review of Environment and Resources*, 2003, Vol. 28, p. 559–586.
10. GRENIER, L. *IUCN's Barometer of Sustainability*. International Development Research Centre, 1998- [referred on the 3th of December in 2014 y.]. Link to the internet: <http://web.idrc.ca/openebooks/847-3/#page_79>
11. GAIGALIENĖ, R., PETKEVIČIENĖ, V. Pabaltijo šalių darnaus vystymosi įvertinimas. Šiaulių universitetas, 2011 – [Referred on the 3th of December in 2014 y.]. Link to the internet: <http://webcache.googleusercontent.com/search?q=cache:AZFRnwAClnwJ:www.slk.lt/studentu-konferencijos/2011/articles/DOC/8_Gaigaliene_Petkeviciene_SU.doc+&cd=1&hl=en&ct=clnk&gl=lt>
12. ŠTREIMIKIENĖ, D., GIRDZIJAUSKAS, S., STOŠKUS, L. Sustainability Assessment Methods and Their Application to Harmonization of Policies and Sustainability Monitoring. *Environmental Research, Engineering and Management*, 2009, Vol. 48, No. 2, p. 51–62.
13. AUGUTIS, J., KRIKŠTOLAITIS, R., LUTYNSKA, A.E., PEČIULYTĖ, S., ŽUTAUTAITĖ, I. Evaluation of Coefficients for Energy Security Indicators System. SAFE – 2013. Proceedings of the 5th international conference on safety and security engineering. Rome. 2013 September 17–19.
14. GOLOKVOSČIUS P. *Diferencialinės lygtys*. Vilnius, TEV, 2000.
15. KRIKŠTOLAITIS, R., LUTYNSKA, A.E., PEČIULYTĖ, S., ŽUTAUTAITĖ, I. Involvement of expert judgement in dynamic model. ESREL 2014. Proceedings of the European Safety and Reliability Conference. Wroclaw. 2014 September 14–18.
16. BERNARDO, J.M., SMITH, A.F.M. *Bayesian theory* New York: John Willey & Sons, 2003.
17. ŽUTAUTAITĖ-ŠEPUTIENĖ, I, AUGUTIS, J., TELKSNYS, L. Parameters estimation in modelling of gas-gap in RBMK type reactor using Bayesian approach. *Informatica*. Vol. 21, No. 2, p. 295–306.

CYSENI 2015, May 27–28, Kaunas, Lithuania
ISSN 1822-7554, www.cyseni.com

THE ENTSO-E CENTRAL INFORMATION TRANSPARENCY PLATFORM (REGULATION (EU) NO. 543/2013). MILESTONE FOR THE IMPLEMENTATION OF THE EU INTERNAL ENERGY MARKET

A. Ļvovs
Institute of Physical Energetics
Aizkraukles str. 21, LV-1006, Riga, Latvia
Phone +371 259 700 20
Email: aleksandrs.lvovs@inbox.lv

ABSTRACT

The paper deals with the ENTSO-E Central Information Transparency Platform (further – the Platform) – the Platform created according to Regulation (EU) No. 543/2013 to provide market participants and Transmission System Operators (further – TSOs) with timely information on the expected consumption and generation, power transmission lines and power generators outages, physical and commercial power flows, balancing and countertrade data, etc. in order to create more transparent, liquid and well functioning power marked as well as to increase security of power supplies and give TSOs possibility to control their networks in a better way.

The paper gives in-depth overview of the Platform from the perspective of data provider (mainly – from Transmission System Operator perspective) as the author of the paper was the main manager of the Platform's go-live preparation works in Latvia – in Latvian TSO "Augstsprieguma tikls".

Taking into account that before the Platform's go-live date (on January 5th, 2015) several local transparency platforms have already been in operation, in the paper there is also given comparison of the Platform with other existing Transparency platforms and the web-sites with Power market data.

And mainly – overall analysis of The Platform, it's Benefits and drawbacks for Power Market participants, EU Internal energy market, and power sector researchers and analysts is given in the paper.

Keywords: Central Information Transparency Platform, ENTSO-E, Power market

1. INTRODUCTION

Liberalization process of electricity market in Europe started with adaptation of Directive 96/92/EC concerning common rules for the internal market in electricity in December 1996 [1]. Entering into force in 1997, Directive 96/92/EC was the first step for transformation of vertically integrated electricity enterprises (monopolies) – separation of electricity generation and trading functions from transmission functions – in order to create well functioning electricity market that would have competition among electricity producers. After almost 20 years electricity market in Europe is almost fully liberalized. Transmission system operators (further – TSOs) are separated from electricity producers and trades and several organized market places, e.g. APX, Belpex, EPEX SPOT, GME, Nord Pool Spot, OMIE and OTE, etc., have been created and are well functioning. But nowadays electricity market to some extent is fragmented and has uncertainties for market participants.

The ENTSO-E(European network of transmission system operators for electricity) Central Information Transparency Platform (further – the Platform) created according to Regulation (EU) No. 543/2013 to provide market participants and Transmission System Operators (further – TSOs) with a lot of information describing electrical power systems and information from power markets [2]. Such information availability in one place and in harmonized, coordinated and standardized format shall increase transparency and liquidity of power markets, as well as decrease uncertainties for market participants. Creation of such

Platform can be treated as important step towards creation of common European electricity market, that requires aforementioned standardization [3].

Preparatory work for Platform's go-live lasted for several years with extra intensive work during year 2014, when wide-scale tests of the Platform have been performed by ENTSO-E and data providers. TSOs – members of ENTSO-E – through participation in ENTSO-E working groups and developing local transparency projects played main role in the process of the Platform creation and launching. Besides ENTSO-E, as the main developer of the Platform, TSOs are the main competence centers on the Platform operation.

Starting form 5 January 2015 Platform is officially functioning and market participants, as well as other interested parties, like scientific institutes, researchers, economists, etc., can access all data published at the Platform. While a number of energy players, including ENTSO-E and its Members, already voluntarily publish some market data, this is the first time that such an extensive range of over 60 different data items, from the Member States and other ENTSO-E Member countries, has been integrated to a single platform and made freely available using following web-address: https://transparency.entsoe.eu [4].

2. THE ENTSO-E CENTRAL INFORMATION TRANSPARENCY PLATFORM OVERVIEW

According to ENTSO-E estimation, the Platform displays around 6 million separate data values, if operates as required. Data publication timeframes depends on the data item and market setup and vary from 15 minutes through to yearly. All the data presented in the platform arranged in 6 major categories [5]:

- Load;
- Generation;
- Transmission;
- Balancing;
- Outages;
- Congestion Management.

Data published at the Platform comes from data providers, who in their turn collect and process data from primary data owners, as well process and send their own data if data provider is also being considered as primary owner of data (typical situation for TSO and Power exchanges). The data journey form primary data owners to market participants is illustrated at Fig. 1 (Figure taken from ENTSO-E Transparency Info Sheet [17]).

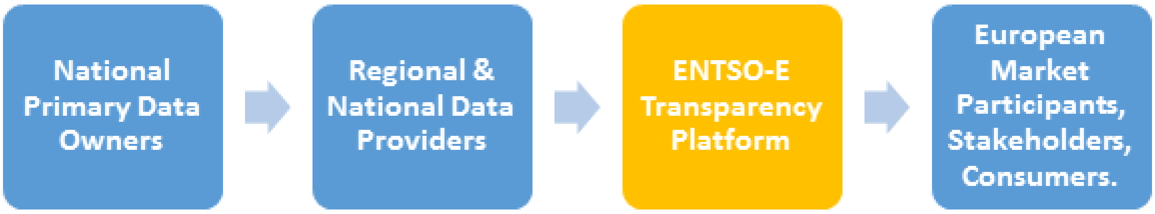

Fig. 1. Data journey form primary data owners to market participants

2.1. Preparation work for data providers

To ensure data sending to the platform, extensive preparation work shall be performed on TSO and data provider side.

At the first step there shall be identified so called Reference data - information on Bidding zones, Control areas, Countries and Cross borders (cross-border areas) that are related with TSO. EIC codes shall be assigned for aforementioned zones and areas [6]. There shall also be identified Master data – all data on equipment of power system: a) transmission assets (transmission lines and equipment that affects cross-border capacities for at least 100MW); b) production units – separately with power more than 100MW and more than 1MW; and c) consumption units with power more than 100MW. EIC codes shall be assigned also for these elements.

Despite the fact that according to Regulation 543/2013, primary data owners shall inform TSOs on required information by themselves and National regulatory authorities shall ensure that the primary owners of the data, TSOs and data providers comply with their obligations under the Regulation, in reality TSOs had to solve almost all issues and find all information by themselves, because primary data owners haven’t been aware of such regulation existence.

The second preparation step is gathering all information from SCADA system (applicable for TSO) and other sources (from data provider’s own sources as well as primary data owners) and creation of data processing rules on Data provider’s side. At this step requirements of Regulation, as well as Platform’s documentation, has been studied deeply in order to ensure the right process of data aggregation, processing and publication timing. On the basis of analysis of data amount, aggregation necessity and sending frequency to the Platform, decision on the automatical data submission mode or manual data submission mode was made.

Work on the third step – Platform configuration – starts almost in parallel with the second step. During the third step platform is configured in order to accept data from data provider. Reference and Master data are being configured first giving the base for further configuration and tests performing. Platform is also configured in order to identify information (data) that shall be expected from data provider when data provider will start data submission.

Attention shall be paid to relations between Country area, Control area and Bidding zone (Reference data) in order to have proper representation of data on all levels. In Baltic States aforementioned is not big issue and configuration of interdependencies between aforementioned reference data can be configured easily, because Country area, Control area and Bidding zone represent the same area, but, for example, in Germany there are 1 Country area, that consists of 4 Control areas and is related with 2 Bidding zones. One more example is Italy, that has one Country and Control areas, but has more than 15 Bidding zones. After proper configuration of Reference data, data provider will have to send data only to one level, but the Platform will process data as configured and they will appear also on the other levels. For example, if data provider configured data submission on Control area level and attached configuration links from Country level and from Bidding zone level to Control area level, for this data provider it is necessary to send data only on Control area level – on the other areas data will appear automatically.

When configuring Master data it is important to make configuration checking in order to be sure that all Transmission, production and consumption units have been configured correctly. This can be done using special window with list of configured Master data. Fig. 2 illustrates configured master data for production units for Lithuania country area.

Configuration of data expected from data provider allows Platform to accept data and properly process them. For each data item there shall be made separate configuration. During configuration there has to be chosen type of Aggregation of SubAreas/SubBorders (data from Reference data configuration used), Aggregation of several Data Providers and Time zone of submitted data. For some data items there could be several data providers – like for physical flows between control areas or forecasted transfer capacities. For each data provider it is allowed its own data submission resolution. When configuring several data providers for one data items, the Platform requires setting priority to each data provider and aggregation of data provider's information in order to define who's data or what data to be published at the Platform.

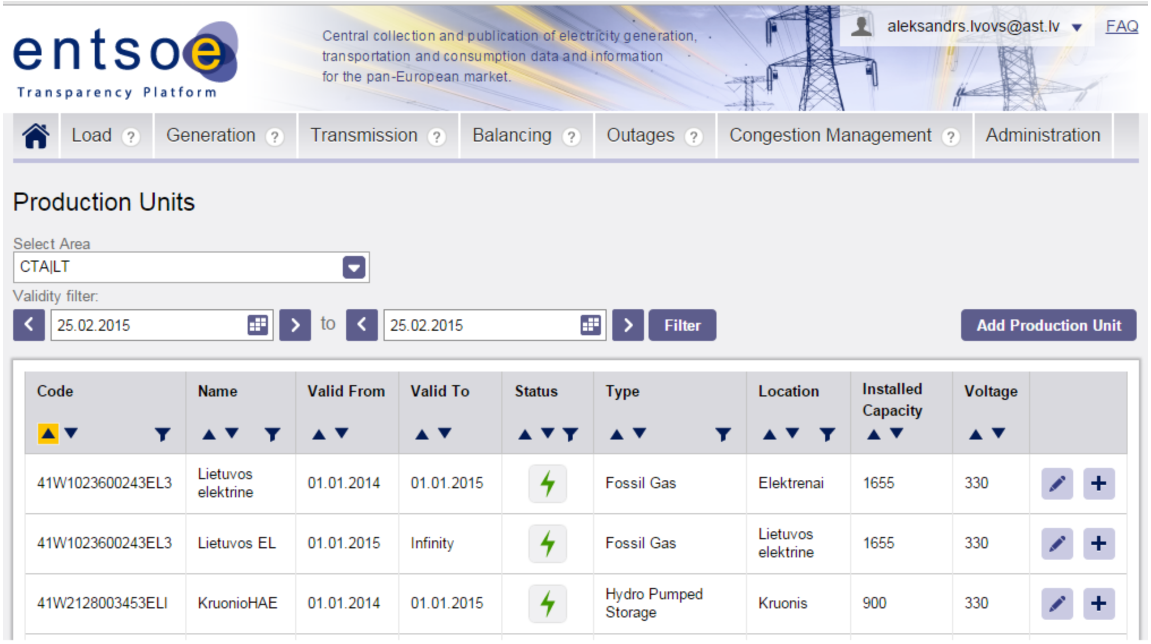

Production Units

Select Area: CTA|LT

Validity filter: 25.02.2015 to 25.02.2015

Code	Name	Valid From	Valid To	Status	Type	Location	Installed Capacity	Voltage
41W1023600243EL3	Lietuvos elektrine	01.01.2014	01.01.2015	⚡	Fossil Gas	Elektrenai	1655	330
41W1023600243EL3	Lietuvos EL	01.01.2015	Infinity	⚡	Fossil Gas	Lietuvos elektrine	1655	330
41W2128003453ELI	KruonioHAE	01.01.2014	01.01.2015	⚡	Hydro Pumped Storage	Kruonis	900	330

Fig. 2. Configured master data for production units. Lithuania country area

As an example, configuration and the Platform's behaviour on data publication can be given for Regulation 543/2013 Article 12.1.G (Physical flows) for Latvia-Lithuania cross-border. According to the Platform's "Business requirements specification": "" … the Platform shall publish the value available from the party with the highest priority. If, for a given market time unit period, data is missing from the provider with the highest priority, then the value from the data provider with the inferior priority shall be displayed if available…" [7]. Such Platform's activity is expected if No aggregation of data providers is set. In case Latvia-Lithuania cross-border physical flows, the Platform is configured to represent average value of data provided by both data providers (see Fig. 3). In this case (when aggregation of data providers is set to "Average"), the Platform will not publish any data if only one data provider provided data and will wait for data from both data providers. In case if data is available from both data provider, the Platform will calculate average value of provided data. Example of data processing by the Platform can be seen at Fig. 4, where Lithuanian TSO (Litgrid AB) provided value "511", Latvian TSO (AS "Augstsprieguma tikls") provided value "514", but the Platform calculated average value of flow – "513" (average value – "512.5" is rounded up to integer value "513").

It should be mentioned, that for some data items there could be only one data provider – like for offered day-ahead or intraday transfer capacities. In order to avoid information duplication, TSOs shall also decide on who will publish data on cross-border lines' outages as soon as both TSOs are responsible for this data item submission. There also exist some other data items that require close cooperation and information coordination between TSOs, e.g. data publishing according to Articles 9.1 and 11.4 of the Regulation 543/2013. Due to the fact

TSOs shall closely coordinate their activities in order to fully comply with Regulation 543/2013 requirements.

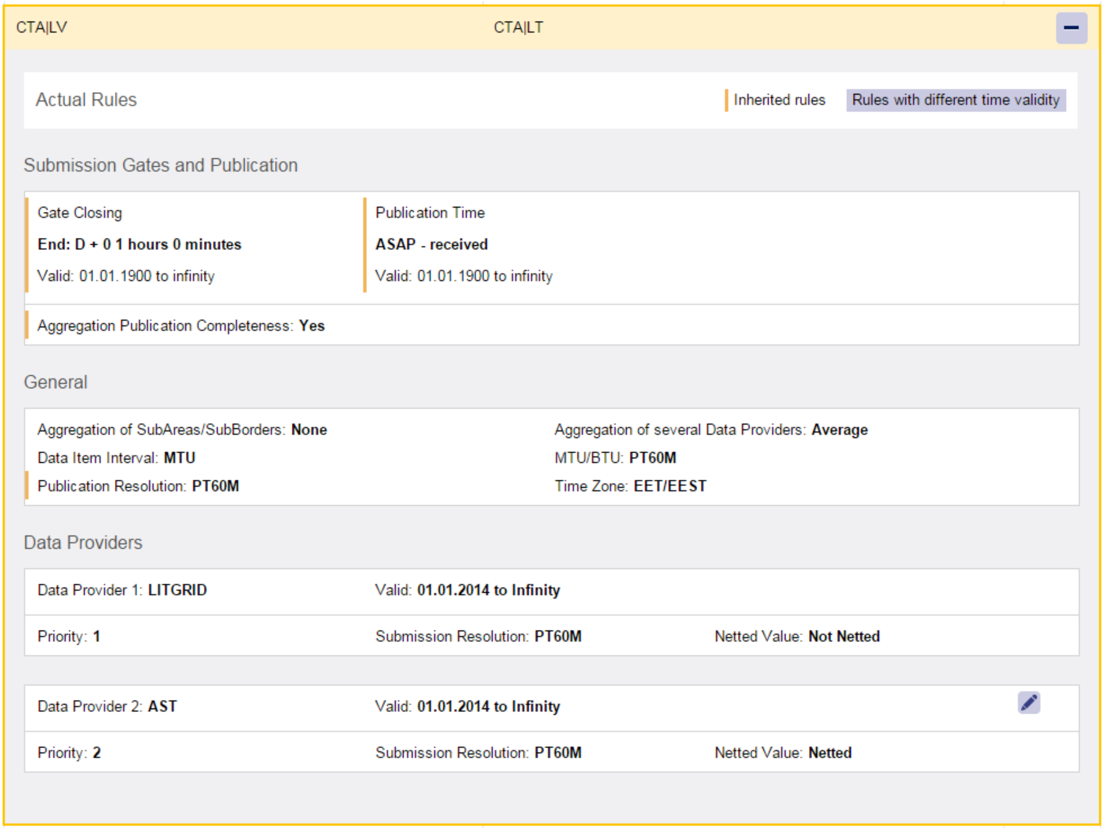

CTA|LV CTA|LT

Actual Rules

Submission Gates and Publication

Gate Closing
End: D + 0 1 hours 0 minutes
Valid: 01.01.1900 to infinity

Publication Time
ASAP - received
Valid: 01.01.1900 to infinity

Aggregation Publication Completeness: **Yes**

General

Aggregation of SubAreas/SubBorders: **None**
Aggregation of several Data Providers: **Average**
Data Item Interval: **MTU**
MTU/BTU: **PT60M**
Publication Resolution: **PT60M**
Time Zone: **EET/EEST**

Data Providers

Data Provider 1: **LITGRID**
Valid: **01.01.2014 to Infinity**
Priority: **1**
Submission Resolution: **PT60M**
Netted Value: **Not Netted**

Data Provider 2: **AST**
Valid: **01.01.2014 to Infinity**
Priority: **2**
Submission Resolution: **PT60M**
Netted Value: **Netted**

Fig. 3. Platform’s configuration for receiving and publishing data on Physical flows

When all configuration activities have been performed, testing period starts, that is the fourth step of preparation work for data publication. During the testing period data provider sends data to Platform’s test environment and only after successful tests it is allowed to start data submission to Platforms production environment.

In total there are over 60 data items that could be sent to the Platform. Not all data items shall be sent from each data provider or even from a country. Number of data to be send to platform depends on different factors, like electricity market setup, availability of transmission and production assets (e.g. offshore wind power plants or DC cables, that don’t exist in every country or TSO’s control area), etc. For Latvia there are 45 data items to be reported. 35 data items go through Latvian TSO AS “Augstsprieguma tikls” (further – AST) where AST is considered as Data provider. The rest 10 data items are being provided to the Platform by power market operator in Latvia – Nord Pool Spot AS (further – NPS). AST as well as NPS are data providers of their own data (they are considered as primary data owners of the data), as well as providers of data from other primary data owners. AST managed to develop all solutions for data submission to the Platform using only their own human resources (Electrical engineers and IT specialists), while majority of other TSOs, in addition to their own human resources, used services of external IT companies. According to the author thoughts this fact can be explained by following main reasons – big amount of data to be send to the platform, complexity of the data aggregation and submission process to the Platform, and finally lack of experienced personnel that could work on the project of such level.

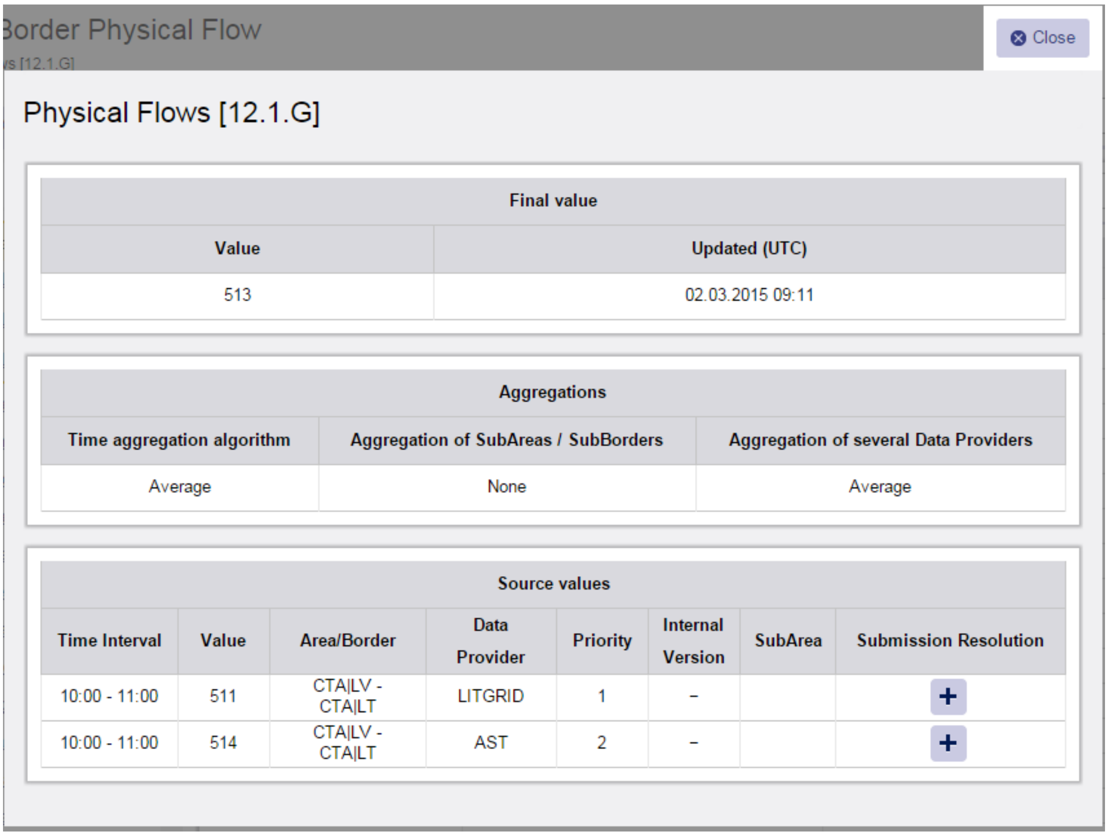

Physical Flows [12.1.G]

Final value	
Value	Updated (UTC)
513	02.03.2015 09:11

Aggregations		
Time aggregation algorithm	Aggregation of SubAreas / SubBorders	Aggregation of several Data Providers
Average	None	Average

Source values							
Time Interval	Value	Area/Border	Data Provider	Priority	Internal Version	SubArea	Submission Resolution
10:00 - 11:00	511	CTA|LV - CTA|LT	LITGRID	1	-		+
10:00 - 11:00	514	CTA|LV - CTA|LT	AST	2	-		+

Fig. 4. Data submission by TSOs and processing by the Platform (LV-LT physical flow)

2.2. Daily routines

Due to the fact that some data items shall be reported rarely (once per year, month or week) and include small amount of data, there is no intention to create IT solution for these data, that would ensure data sending in automatic mode. Such data shall be send manually and in AST are being send using 2 information delivering channels: a) data sending to the platform through specially developed web-interface (developed by AST IT specialists); b) data sending by direct input at the Platform (via XML file input or using graphical user interface – GUI). Other data are being sent in automatic mode.

Daily routines include manual data sending on time specified by Regulation (EU) No. 543/2013 and checking for automatic data publication and errors on the Platform. At the moment checking for errors and data publication takes quite long time as at the moment Platform is not equipped with efficient tool to overview data sending and publication.

2.3. Platform usage

Platform's main mission is to provide high quality data on transmission power systems and market in a timely manner and standardized way in order to improve transparency of European power markets. As previously mentioned, all the data presented in the platform arranged in 6 major categories. Names of categories located at the top line of the Platform's interface (see Fig. 5). Below the categories line Dashboard appears representing random information from the platform in map view and five column chart views. When logging into the Platform there is possibility to set exactly what information shall be represented at the dashboard.

Further there is given brief description of information available at the Platform.

2.3.1. Load

Under the section “Load” there is available information on the year-ahead, month-ahead, week-ahead and day-ahead load forecasts, as well as information on actual load and year ahead forecast margin that represents the difference between yearly forecast of available generation capacity and yearly forecast of total load, evaluated at local market time unit of annual maximum load.

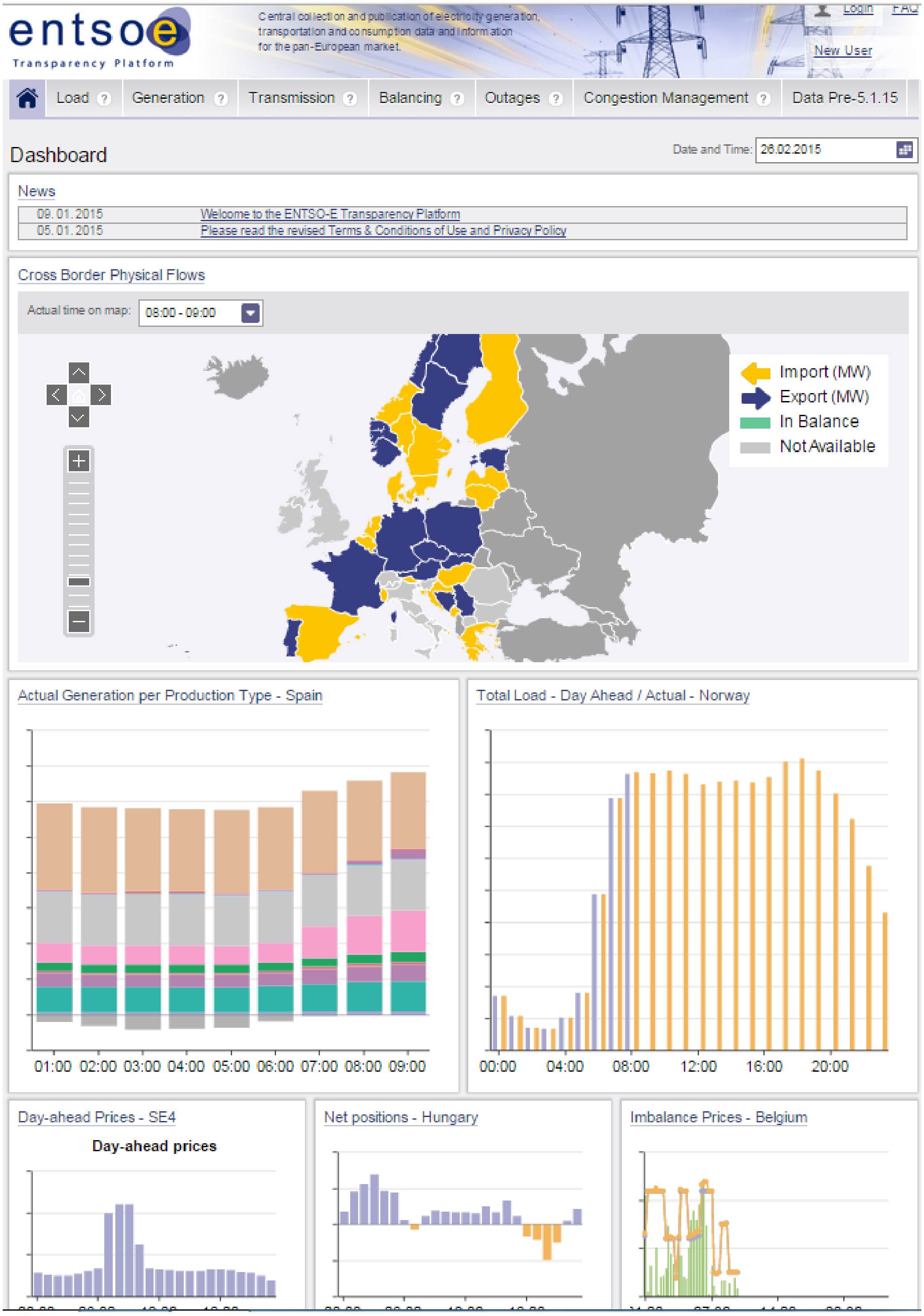

Central collection and publication of electricity generation, transportation and consumption data and information for the pan-European market.

Dashboard

Date and Time: 26.02.2015

News

09. 01. 2015	Welcome to the ENTSO-E Transparency Platform
05. 01. 2015	Please read the revised Terms & Conditions of Use and Privacy Policy

Cross Border Physical Flows

Actual time on map: 08:00 - 09:00

Fig. 5. Start page of The ENTSO-E Central Information Transparency Platform

2.3.2. *Generation*

Under the section "Generation" there is available information on the installed capacity per production type, installed capacity per production unit (power plant), aggregate filling rate of water reservoirs and hydro storage plants (amount of energy stored in water reservoirs during week – in MWh), actual generation per production type, actual generation per generation unit, day-ahead generation forecast, day-ahead generation forecasts for wind and solar.

2.3.3. *Transmission*

Under the section "Transmission" there is available information on the forecasted, offered and allocated transmission capacities for different timeframes, scheduled commercial exchanges, cross-border physical flows, day-ahead prices, explicit allocation revenues, transfer capacities allocated with third countries, congestion incomes on day0ahead and intraday markets, ramping restrictions and intraday transfer limits of DC lines, information on expansion and dismantling projects for the following three years, as well as information (reports) on critical network elements limiting transfer capacity.

2.3.4. *Balancing*

Under the section "Balancing" there is available information on the rules on balancing applicable in the control area of TSO, volumes of offers for balancing reserves (include offers from local area traders, as well as may include offers from foreign areas traders. in addition amount of activated balancing reserves and price is shown), balancing volumes reservation and balancing volumes reservation price (in case if balancing energy is reserved for some period in the future), imbalance (absolute volume of imbalance), cross-border balancing (volumes of offers for balancing reserves from traders of foreign areas. amount of activated balancing reserves from only foreign areas and price is shown), financial expenses and income for balancing.

2.3.5. *Outages*

Under the section "Outages" there is available information on the transmission network planned and unplanned outages (information on elements' outages that reduce cross-border transmission capacity (NTC) by at least 100MW), information on the offshore grid planned and unplanned outages, information on the production and generation units' unavailability, as well as information on consumption unit unavailability.

2.3.6. *Congestion management*

Under the section "Congestion management" there is available information on the countertrades, redispatching, as well as costs of aforementioned activities.

2.3.7. *Administration*

"Administration" section allows user see configuration of the platform for his organization (if user is from any data provider) and make some changes in configuration. It is also possible to manually submit data in XML file format through the section, as well as monitor data submission and processing process at the Platform. The last mentioned option allows identify errors in send data and make correction in the file submission system or in the Platform.

Large amount of useful information available at the Platform for all European power systems/market bidding zones/counties and considering the fact that information is available in the standardised form and appears almost simultaneously (according to the timeframes described in Regulation 542/2013 [2]), makes the Platform an irreplaceable tool for research, planning and other possible activities for market analysis in order to move forward toward common European energy market in a more faster and efficient way.

One of the possible applications of the platform in practical research could be usage of detailed information on generation by types and it's changes from hour to hour, changes of loads, balances and imbalances of countries, cross-border physical power flows, existing NTCs on the cross-borders, electricity prices, etc. information for development and testing of flow-based capacity calculation methodologies. Already nowadays researchers use publicly available information on power systems and markets [8]. The reason of usage publicly available information is hard communication with TSOs and local Regulatory authority on the access to power system's and power market's information and inability to reach information on foreign power systems and markets, if research organization is not involved in international research activity/project that is initiated at high level.

3. THE ENTSO-E CENTRAL INFORMATION TRANSPARENCY PLATFORM VS OTHER EXISTING INFORMATION SOURCES

One could argue that quite big (if not the biggest) part of the information published at the Platform could be accessible also previously through TSOs' web pages (where information on generation, load, net transfer capacities (NTCs), physical flows is available), Power Exchanges' web pages (where information on commercial exchanges (flows), electricity prices, outages in the power grid, and other market information is available) and other web pages, like "Nordic Power System Map", that provides various information on the power grid [9–14]. Fig. 6 gives an illustration of consumption, production and physical flows information at Estonian TSO's (Elering) web page.

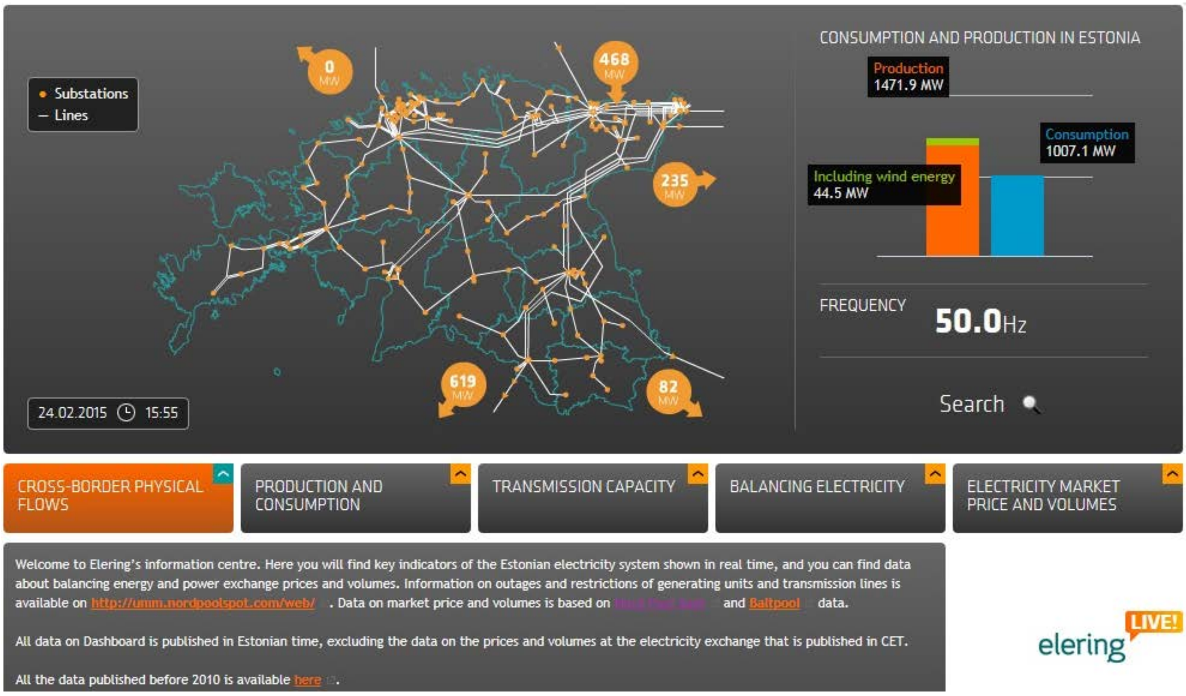

Welcome to Elering's information centre. Here you will find key indicators of the Estonian electricity system shown in real time, and you can find data about balancing energy and power exchange prices and volumes. Information on outages and restrictions of generating units and transmission lines is available on http://umm.nordpoolspot.com/web/ . Data on market price and volumes is based on Nord Pool Spot and Baltpool data.

All data on Dashboard is published in Estonian time, excluding the data on the prices and volumes at the electricity exchange that is published in CET.

All the data published before 2010 is available here .

Fig. 6. Information on consumption, production and physical flows at Elering's web page

But the main added value of Transparency platform is in data aggregation from all over Europe and in data standardization. The Platform gives easy access to data and gives possibility to automatize data receiving. Standardization and automatization functionality makes it possible to perform analysis of power market and situation in grid faster, more reliable and in a new scale that was hard to imagine previously.

4. THE ENTSO-E CENTRAL INFORMATION TRANSPARENCY PLATFORM GO-LIVE AND FURTHER DEVELOPMENT

On the 5th of January 2015 the Platform was successfully launched and is operating. Every day more and more information is published and gathered at the Platform. All data providers do their best to publish all the data required by the Regulation 543/2013 and in the best quality. But taking into account that this is the first such scale project towards common European electricity market, it is possible that in future there will be need in some minor changes in the platform or even Regulation 543/2013 in order to meet make the Platform more informative, useful and easy understandable.

Further development is possible also in the purely technical things, like development of some tools allowing TSOs and other data providers better supervise their data submissions, or make data download more easy.

Taking into account increased level of transparency and possibility to compare data from all over the Europe in easy way, improvement of communication could be expected between all market participants.

On the basis of REMIT regulation (Article 8(5)), as well as REMIT Implementing acts, further development of the Platform includes activities related with Fundamental data submission to ACER (The Agency for the Cooperation of Energy Regulators) in order to avoid double reporting from TSOs and other market participants [15, 16].

5. CONCLUSIONS

The ENTSO-E Central Information Transparency Platform has been developed by ENTSO-E and launched on 5th of January 2015 with the common efforts of ENTSO-E and European TSOs. Platform’s go-live was preceded by extensive development activities both on the Platform’s (ENTSO-E) side and TSOs’ side.

Bearing in mind that creation of well-functioning Common European internal electricity market needs a lot of research activities and studies, the Platform can be treated as the milestone for the Common European internal energy market - the Platform provides market participants, European commission, ACER, economists and scientists with detailed information on electricity market and power grid functioning data. Of course, implementation of Common European internal electricity market will require research with exact case studies and deep detailing, but existence of the transparency Platform will definitely help to perform large scale research all over the Europe, that, in its turn help to find the right direction for the way forward of the market development and more detailed studies initiated by European Commission in future.

REFERENCES

1. Directive 96/92/EC of the European Parliament and of the Council of 19 December 1996 concerning common rules for the internal market in electricity. Official Journal of the European Union L 027, 30/01/1997 P. 0020 – 0029. [Referred on the 25th of February in 2015 y.]. Link to the internet: http://eur-lex.europa.eu/LexUriServ/LexUriServ.do?uri=CELEX:31996L0092:EN:HTML
2. Commission Regulation (EU) No 543/2013 of 14 June 2013 on submission and publication of data in electricity markets and amending Annex I to Regulation (EC) No 714/2009 of the European Parliament and of the Council Text with EEA relevance. Official Journal of the European Union L 163/1, 15/06/2013. [Referred on the 25th of February in 2015 y.]. Link to the internet: http://eur-lex.europa.eu/legal-content/EN/TXT/?uri=CELEX:32013R0543
3. BOISSELEAU, F.H. The Role of Electricity Trading and Power Exchanges for the Construction of a Common European Electricity Market. Transmission and Distribution Conference and Exhibition 2002: Asia Pacific. IEEE/PES. Vol. 2. p. 728–732, 2002 October 6–10.
4. Press release of ENTSO-E. [Referred on the 25th of February in 2015 y]. Link to the internet: https://www.entsoe.eu/news-events/announcements/announcements-archive/Pages/News/Transparency-Towards-Open-Competitive-Internal-Energy-Market.aspx
5. The ENTSO-E Central Information Transparency Platform. [Referred on the 25th of February in 2015 y.]. Link to the internet: https://transparency.entsoe.eu/
6. ENTSO-E web page for EIC codes. [Referred on the 25th of February in 2015 y]. Link to the internet: https://www.entsoe.eu/data/energy-identification-codes-eic/Pages/default.aspx
7. “Business requirements specification”. Referenced document for Manual of procedures of the ENTSO-E Central Information Transparency Platform. [Referred on the 2nd of March in 2015 y]. Link to the internet: https://www.entsoe.eu/major-projects/central-information-transparency-platform/manual-of-procedures/Pages/default.aspx
8. SORES, P., DIVENYI, D., RAISZ, D. "Flow-based Capacity Calculation Method Used in Electricity Market Coupling", 10th International Conference on the European Energy Market (EEM), 2013, p. 1–7.
9. Latvian TSO AS “Augstsprieguma tikls” web page with information on power system. [Referred on the 24th of February in 2015 y]. Link to the internet: http://www.ast.lv/eng/power_system/current_situation_in_power_system/planned_and_actual_demand__net_exchange_and_production/
10. Estonian TSO “Elering” Dashboard with information on power system. [Referred on the 27th of February in 2015 y]. Link to the internet: http://elering.ee/dashboard/
11. Lithuanian TSO “Litgrid AB” Dashboard with information on power system. [Referred on the 27th of February in 2015 y]. Link to the internet: http://www.litgrid.eu/index.php/dashboard/630
12. Nordic Power System Map. [Referred on the 27th of February in 2015 y]. Link to the internet: http://www.statnett.no/en/Market-and-operations/Data-from-the-power-system/Nordic-power-flow/
13. Nord Pool Spot AS power exchange’s web page. [Referred on the 27th of February in 2015 y]. Link to the internet: http://www.nordpoolspot.com/Market-data1/Elspot/Area-Prices/ALL1/Hourly/?view=table

14. OMIE power exchange's web page. [Referred on the 27th of February in 2015 y]. Link to the internet: http://www.omie.es/en/inicio
15. REGULATION (EU) No 1227/2011 OF THE EUROPEAN PARLIAMENT AND OF THE COUNCIL of 25 October 2011 on wholesale energy market integrity and transparency. [Referred on the 2nd of March in 2015 y]. Link to the internet: http://eur-lex.europa.eu/LexUriServ/LexUriServ.do?uri=OJ:L:2011:326:0001:0016:en:PDF
16. COMMISSION IMPLEMENTING REGULATION (EU) No 1348/2014 of 17 December 2014 on data reporting implementing Article 8(2) and Article 8(6) of Regulation (EU) No 1227/2011 of the European Parliament and of the Council on wholesale energy market integrity and transparency. [Referred on the 2nd of March in 2015 y]. Link to the internet: http://eur-lex.europa.eu/legal-content/EN/TXT/PDF/?uri=OJ:JOL_2014_363_R_0009&from=EN
17. ENTSO-E Transparency Info Sheet. [Referred on the 13th of April in 2015 y]. Link to the internet:https://www.entsoe.eu/Documents/MC%20documents/Transparency%20Platform/ENTSO-E%20Transparency%20Info%20Sheet.pdf.

CYSENI 2015, May 27–28, Kaunas, Lithuania
ISSN 1822-7554, www.cyseni.com

WILL IMPROVED PALM OIL YIELDS SUFFICE TO THE DEVELOPMENT OF SUSTAINABLE BIODIESEL FEEDSTOCK IN INDONESIA?

C. Palmén, S. Silveira & Dilip Khatiwada
Division of Energy and Climate Studies
Royal Institute of Technology (KTH)
Brinellvägen 68, SE - 100 44, Stockholm – Sweden
Phone +46-8-790 74 65
Email: cpalmen@kth.se

ABSTRACT

By the expansion of oil palm plantations, Indonesia has become a world leading producer of crude palm oil. However, Indonesia has also been largely criticized due to issues of land use change and deforestation. The country now promotes the use of palm oil for biodiesel production as part of policies to achieve renewable energy targets. Currently yields on palm oil plantations are far from optimal. Do new policies promoting biodiesel production address the issue of yields properly? This study analyses the driving forces for the expansion of palm oil plantations in Indonesia and the palm oil yields obtained in the country. Data is collected through a multi-disciplinary structured literature review of relevant palm oil publications from the last 15 years. We identify the policies that have been put in place and the strategies used to establish palm oil plantations in the past years. We look at the newly defined policies of the Indonesian government towards renewables and climate mitigation, in particular, targets for biodiesel production and fuel substitution. The idea is to verify whether the new policy will address the low yield issue. Presently, palm oil yields are much lower in Indonesia than in neighbouring Malaysia, also a major producer. Particularly, smallholders have lower yields than private and government estate plantations. Expanding production has been focused on covering new areas with palm oil plantations and less on developing farming methods. In earlier stages, the establishment of plantations included proper education of farmers and incentives to maintain production. Smallholders nowadays start palm oil production with little or no previous experience; still they favour oil palm over traditional crops. New policies have to address farming improvements to guarantee sustainable feedstock for biodiesel.

Keywords: Palm Oil, Oil Palm Plantations, Biofuel, Policy

1. INTRODUCTION

Palm oil has become an important crop globally not only for cooking but increasingly also for biofuel production. In fact, palm oil is one of the most interesting feedstocks for biodiesel production due to the high yields that can be achieved per hectare (ha) compared to other oil-crops [3]. In addition, palm oil production generates employment in rural areas. In 2011, the palm oil industry employed 3.7 million workers in Indonesia alone, and contributed to about 7% of the country's GDP [30]. In 2012, Indonesia produced 26 million tonne of crude palm oil[1] of which 20 million tonne were exported [25]. However, they only achieved a yield of 3.7 tonne per ha [25], compared to Malaysia's 4.4 tonne per ha [35], and a maximum 6 tonne per ha [8].

---

[1] Regarding palm oil in biodiesel production: Fresh fruit bunches (FFB) are harvested from oil palm trees from the age 2 to 4 years. These bunches contain the palm fruit from where the oil is extracted. The mesocarp in the palm fruit contains the oil from which crude palm oil (CPO) is derived using milling. The palm fruit kernel also contains a smaller amount of extractable oil. These two oils are then the basis for any further refined oil products. For producing fuel the refined oils are put in a process of esterification in which methanol is used to produce biodiesel and glycerol.

Indonesia now has plans to expand the use of renewable energy in the country. As part of this effort, the government aims at developing the biodiesel industry and has set 30% biodiesel blending targets for 2020: the public service obligations (public transport), industry and for power generation. Biodiesel production was for 2012 2.2 million kilolitre in Indonesia of which 1.05 was domestically used, amounting to four percent of total diesel use [31]. If the targets are to be reached with domestically produced biodiesel without competing with current exports and food supply, an increase in palm oil production is required.

Palm oil production in Indonesia has been highly criticised in past years, and identified as a significant cause of land conversion and deforestation in the country [5, 11, 14]. Therefore, it is essential that measures are taken to make sure the development of the biodiesel industry and the shift towards bioenergy are achieved in a sustainable way. In this context, measures for increasing palm oil yields may constitute an important step. This paper addresses the conditions for improving the sustainability of palm oil production in Indonesia looking at the historic expansion, the issues with yield and role of policy in dealing with issues concerning lower yields.

2. METHODOLOGY

A literature search was carried out in 2015 between January the 15th through the 19th on the scientific databases Science direct and Wiley Online Library. Using a full text search for journals and books published between 2000 and 2015, by combination of keywords found in the appendix. Resulting in a total of 16054 non-unique hits of which 514 were relevant. Of these 106 sources were chosen as relevant to the topics: strategy, yield or policy, another 17 were collected by reference review. Policy documents from the official biofuel policy and the ISPO guidelines were then analysed against findings in literature for correlation or contradiction. Statistical data gathered from official documents released by the Indonesian Ministry of Agriculture [25].

3. INDONESIAN PALM OIL DEVELOPMENT STRATEGIES

Indonesian palm oil plantations have grown at an average rate of over 10 percent per year between 1967 and 1997, reaching 2.5 million ha. Though the increase per year decreases both palm oil, biodiesel production and plantation area are growing Fig. 1 and Fig. 2, adapted from [25].

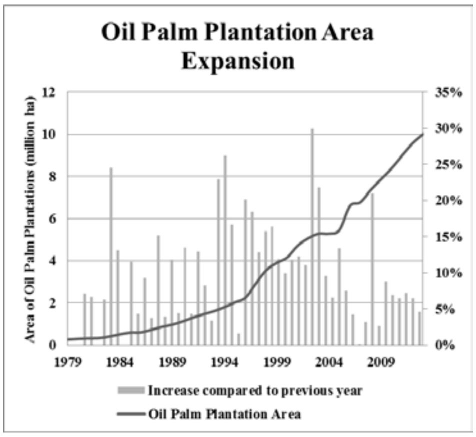

Fig. 1. Oil Palm plantation area development and yearly percentage increases in Indonesia, 1979 to 2013

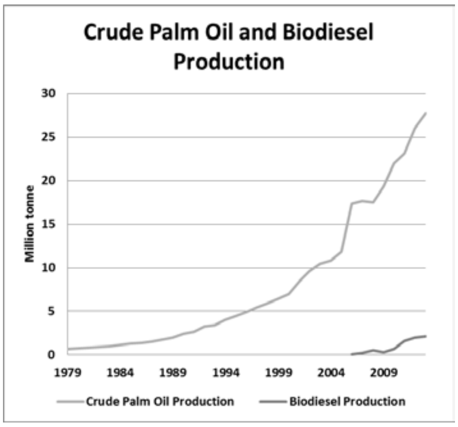

Fig. 2. CPO and Biodiesel production development in Indonesia, 1979 to 2013

3.1. Structure of the Indonesian Palm Oil Sector

There are typically three types of plantation owners in Indonesia: government estates, private estates, and smallholders. For distribution of land and production share Fig. 3 [25]. Higher return on the land and increased profit per worker are the main financial appeals for farmers. The land return for palm oil is 10 times higher than rice per cycle; an oil palm plantation generates €2100 per hectare compared to €200 for rice paddy [11]. Together with the lower demand for workers compared to traditional crops, has been driving the expansion of palm oil plantations [6,28].

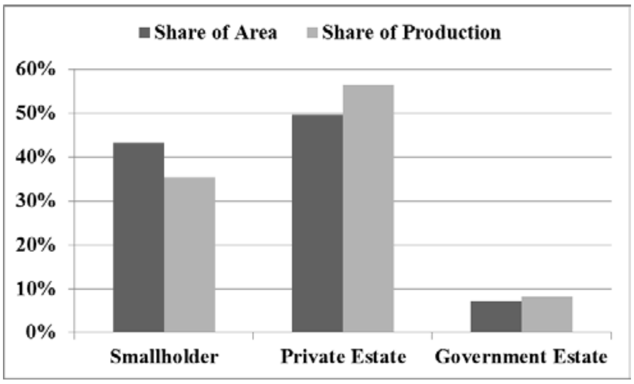

Fig. 4. Distribution of occupied land for oil palm and production of CPO in Indonesia

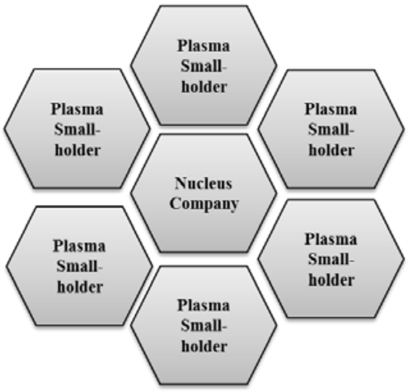

Fig. 3. Schematic diagram of the NES-scheme

With a rural structure composed of many smallholders and in face of high initial investment requirements, various schemes, financial models and strategies have been employed to enable smallholders and companies to establish palm oil plantations. The initial capital requirements for palm oil production are large this includes the costs of labour to clear and plant the new crop, and fertilizers, herb- and pesticide application where the application of fertilizer and herb- and pesticide amount to over 60% of the initial cost [28]. The oil palm trees then start producing fruit around the third year after plantation at the earliest.

Smallholders are responsible for plantations below 50 ha [17] which, in turn, can be classified in: NES-smallholders (Nucleus Estate and Smallholder Scheme – NES, or Perkebunan Inti Rakyat – PIR in Bahasa Indonesia), and independent smallholders [9] who operate independently and sell their product to mills. The NES-type schemes offer financial and technological support to smallholders who want to enter the palm oil sector, schematic diagram in Figure 4. In the NES-schemes, an assigned agent, usually a private company prepares the land by clearing and planting trees, once it matures, hands it over to the smallholder. The name derives from a cell analogy, the estate company represents the nucleus and the smallholders constitute the surrounding plasma. By securing FFB delivery from the nucleus smallholders to the estate, palm oil investors were able to achieve the economies of scale required for the palm oil business. However, this also puts the smallholders in the hands of only one buyer for their product [21]. More companies in the same area would allow NES farmers to make use of the competition to negotiate more favourable deals for their FFB [11].

The plantations had since Indonesia's independence been nationalized and a first phase of the palm oil expansion was started in 1968 when the government, backed up by the World Bank, invested in state-owned plantation companies. In 1979, the first NES-scheme was launched, the plantations would be developed by private actors (the Nucleus) who would transfer a percentage of the developed plantations and technical information to the smallholders after the plantation had matured [12]. Each plot was 2 ha and had access to a central processing facility for the fresh fruit bunch (FFB) [2]. The World Bank had been promoting these types of NES schemes elsewhere since the 1960's [9]. A bank was usually financing the cost of land clearing, land preparation, planting and applying fertilizers. This was a loan that would later have to be paid by the landholder. The Plasma would continue the development under direction of the Nucleus.

This type of scheme was carried on into new similar programs, the PIR-trans 1986–1994 and Koperasi Kredit Primer untuk Anggota (KKPA) 1995–2000. For financing the expansion in the 1980s, policy was implemented to attract foreign capital by granting private companies concessions to develop oil palm plantations [21]. The PIR-trans scheme was run similar to the previous NES scheme, where a company instead represented the Nucleus and a bank or the state was financing the land preparation. In the PIR-trans scheme, many migrants (trans refers to transmigration) from more populous areas of Indonesia became smallholders and provided a cheap workforce in the new palm oil business [7, 21]. The KKPA scheme remained in the eastern parts of Indonesia where large areas were being dedicated to oil palm plantations. In the KKPA scheme it was a local land owners instead of migrants would have their land converted into oil palm plantations in an agreement that they transferred one third of their land to the nucleus company.

3.2. Indonesian Financial Crisis

Companies were until the financial crisis in Indonesia of 1997 making large profits as a result of beneficial loans for establishing plantations, cheap workforce; high cost for CPO and windfall profits. Though Indonesia was going through an economic crisis, the palm oil sector was still profitable in 1997 and the government was encouraging foreign investors to invest in the business. As companies watched the Rupiah collapse they sought to sell their products outside the country, which led to high earnings, but reduced supply and increased prices for palm oil within Indonesia. Eventually, this led to an export ban as a way to protect domestic food supply, later replaced with high export taxes. Palm oil companies were eventually starting to report losses, which eventually slowed down the palm oil expansion in the country, Figure 1. The new government issued new policies for the palm oil sector at the end of the 1990's. The export tax was kept to protect the declining domestic supply, despite complaints from companies. Concession permits were withdrawn from estate companies that were not developing the plantation business. Maximum development area per company became limited to 20 thousand ha per lot, up to a total of 100 thousand ha in the whole country for one single company. This was meant to prevent the formation of monopolies. However, no limit was set for the total area used by conglomerates.

3.3. Post Crisis 2000's

Following the crisis, the government introduced five new schemes to encourage investor-farmer-cooperation. Since no financial support was provided, these schemes were less successful [21], and the expansion continued to slowdown Figure 1. Lower palm oil prices, changed market conditions, and reduced state support, reduced the investors interest to develop Indonesian palm oil [7]. A new governmental program was started 2005 and initiated in 2007, the Plantation Revitalization Program, it aimed at the development of 1.5 million ha of land. The program applied an organization similar to the previous nucleus model, developing smallholder plantations with the help of estate companies. Three banks are financing the program through the Credit Loan Program for Bio Energy Development and Plantation Revitalization (KPEN RP). This program has been criticized for not analysing and improving the situation for local landowners who had their land converted often based on informal agreements and without any clear jurisdiction, or local governmental oversight [21].

More recently a movement of independent farmers has started opening up new plantations with the help of loans from local traders, often leading to the clearing of forested areas. Forest jurisdiction in Indonesia is not sufficiently clear on the rights to the forest on local level and there have been no sanctions for violations of the law. With a local interpretation of the forest belonging to the local community this is leading to conversion of forest into plantations, both by local farmers and migrants who want to cease the chance for a better life [1]. New migrants often clear the forested land before requesting a permit from the local village head, but this permit is not recognized by the local government. Land conversion that cannot easily be controlled by policy measures and the increasing employment in the sector, are threatening the long term sustainability of the palm oil business [4].

These strategies have resulted in large portion of independent and plasma smallholders but also a large amount of foreign owned companies with private estates. Malaysian private ownership and influence over Indonesian palm oil is especially strong [37].

4. INDONESIAN PALM OIL YIELDS

In 1997 the CPO yield in Indonesia was at 3.37 tonne per ha, as reported by Oil World via [7], for 2012 this number was 3.72 tonne per ha. In best conditions the FFB yield can reach 30 tonne per ha and year [8], this is equal to 6 tonne CPO per ha (low estimate of 20% CPO in FFB).

Fig. 4 shows the trend of the last 5 years and the difference in yields among different owner types. The graph displays CPO yield and not FFB yield, as some factors described below will have an effect on the amount of extractable oil and also the available data presents CPO yield. Smallholders are even in the best performing regions producing a ton less per ha than the private estates [25]. If the smallholder yields were to reach the 4 tonne per ha equal to that of private estates it would have meant a production increase of 2 million tonne of CPO in 2012. This makes it not only of interest to biofuel development but to the economy of smallholders.

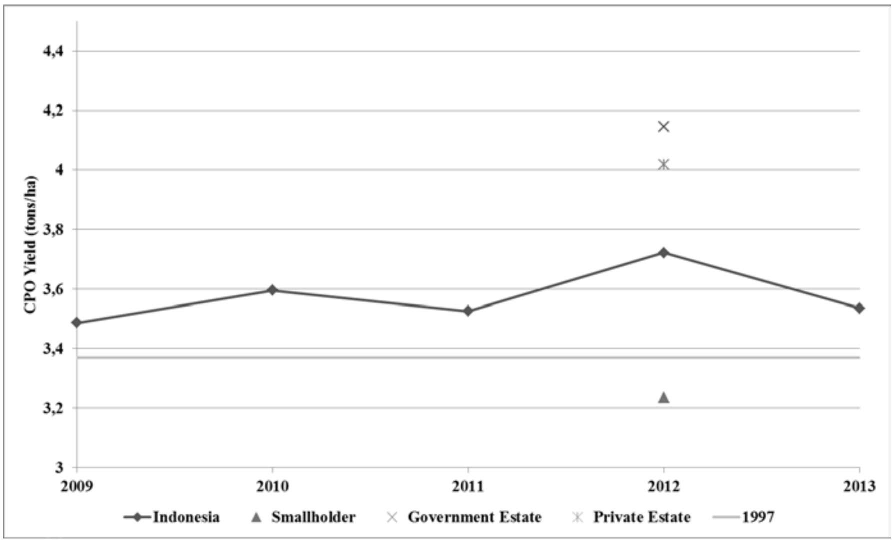

Fig. 5. Average yield for recent years, 2009 to 2013 reported by Directorate General of Estate Crops [26, 27], 1997 reported by Oil World [7]

The Indonesia Energy Outlook 2014 [31] suggests conversion of another 10 million ha of land for palm oil production, 7.3 million ha from undeveloped palm oil concessions and the remaining 3.7 million ha from conversion of wetlands. The area occupied for palm oil production in 2012 was 9.6 million ha with 7 million ha of mature plantations [25]. Indonesia converted eight percent of their CPO into 2163 million litre biodiesel in 2012 [36]. Fig. 5 display the potential increase of 18% more biodiesel if neighbouring Malaysia's 4.4 tonne per ha [35] were achieved, maintaining the use of 8% of the CPO production.

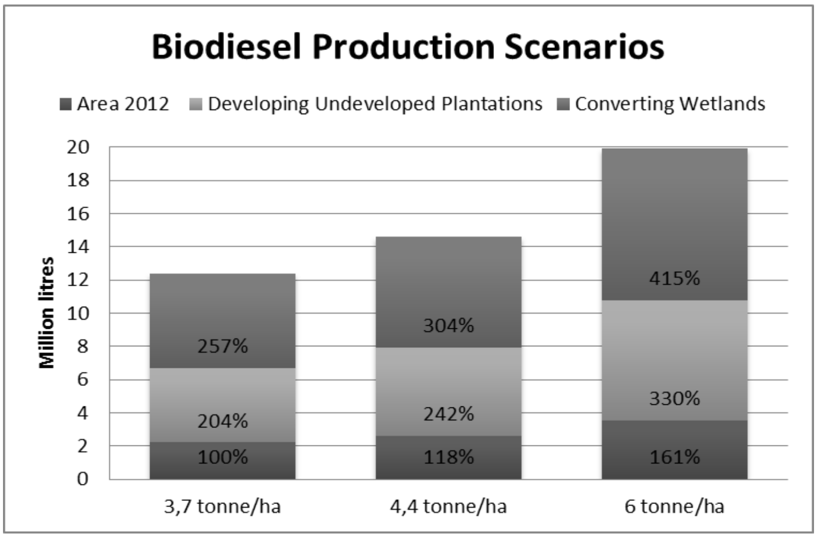

Fig. 6. Potential Biodiesel production increase from yield increase and land expansion considering a maintained use of 8% of produced CPO

4.1. Limiting Factors for Palm Oil Yield in Indonesia

Several factors have been identified and described below which influence the CPO yield of an oil palm plantation run by smallholders. These are identified from literature of Indonesian cases or general to plant growth. Smallholders outside the estate-like nucleus schemes may struggle to find adequate financing leading sometimes to the purchase of lower quality, locally produced, seedlings which results in lower yield and quality of the FFB [2, 13]. The seedlings and the technical advice from a NES type system are advantageous for the smallholders, but seedlings may be unobtainable for them as companies reserve the supply for many years to come [11]. An incorrect or less than optimal planting pattern will affect the yield that can be obtained from each tree. During its life-time, the tree may be affected by factors which are maintenance related, such as pruning and pest or weed control and use of fertilizer. Smallholders may have difficulties in obtaining fertilizers due to the price or do not know where to obtain good planting material [29]. Noteworthy is that fertilizer and certified oil palm seedlings were an integral part of the agricultural policies during schemes prior to the financial crisis [29].

Palm oil has been a major contributor to farmers converting from rice [32] tempted by the higher profitability in palm oil. As the rice farmers converts from rice they lack the necessary skill in oil palm cultivation and some reported cases used fertilizer dedicated to food production in palm oil production [1]. Law No. 41 in 2009 state that land for food production may not be converted and should be conserved to protect food supply. Longer experience in cultivating oil palm has been seen as beneficial to achieve higher yields [6].

There are links between the government's performance and approaches for increased production, increasing plantation area as opposed to intensification. Higher quality government focuses on intensifying production and lower quality focuses on expanding the plantation area [19]. The expansion of palm oil has been increasingly aided by the decentralization of administration and the decision making following the years after the financial crisis [20]. In Indonesia the expansion of production has led to land and forest being converted into oil palm plantations [11]. There is also an idea that increasing production by expanding the land can be done through family labour and as so requires no outside support [1].

The FFB trading system can be a reason for the yields [1]. Smallholders are granted favourable loans by local traders in exchange for their FFB deliveries. The local traders in turn get their money in loans from holders of district orders (traders with rights and a quota to sell to the mill). In turn they accept lesser quality FFB to make sure they fill their quota; this is disguised by either mixing the fruit or bribing the quality controller at the mill. Low quality and productivity stem from a lack in capital, knowledge and information among smallholders, as well as little interest from the farmers themselves in increasing the quality or productivity. With more mills and higher palm oil demand this is leading to a drop in FFB quality delivered to the mill.

4.2. Improvement Actions

The use of high quality seedling would improve yields by 47% from 2009's level [22]. Smallholders outside the estate-like nucleus schemes may struggle to find adequate financing leading sometimes to the purchase of lower quality, locally produced, seedlings which results in lower yield and quality of the FFB [2,13]. The seedlings and the technical advice from a NES type system are advantageous for the smallholders, but seedlings may be unobtainable for them as companies reserve the supply for many years to come [11]. During its life-time, a tree may be negatively affected by factors which are maintenance related, such as pruning and pest or weed control and use of fertilizer. Management and fertilization are issues that can be corrected on active producing plantations. By implementing best management practices (BMP) and a short harvest interval the FFB production could be improved in Indonesia [16].

Fertilizer cost is large part of the initial cost and around one third of the running costs for plantations until ten years of age and about half of the running cost for older plantations [18]. Compared to Malaysia, Indonesian labour cost is lower, whereas machine and building value depreciation is higher but the fertilizer costs are similar in the two countries [2].

Palm oil has been a major contributor to farmers converting from rice [32] tempted by the higher profitability in palm oil. As the rice farmers convert from rice they lack the necessary skill in oil palm cultivation and some reported cases used fertilizer dedicated to food production in palm oil production [1]. Law No. 41 in 2009 state that land for food production may not be converted and should be conserved to protect food supply. Longer experience of cultivating oil palm has been seen as beneficial to achieve higher yields [6].

Implementing sustainable practices as the Roundtable for Sustainable Oil Palm (RSPO) can be beneficial to yield and could possibly be a 'low hanging fruit' for many. But it adds a cost that not all are willing to pay, especially smallholders [17]. Another obstacle is that as a large part of the market for palm oil, largely China and India may not be interested in the environmental benefits of certified plantations [15]. Indonesia is in these countries promoting the estate mandatory ISPO, while similar to RSPO certification, no results on improved yields have been presented yet.

Increasing yields can also be achieved by more modern mills and by quality control of the FFB [2]. To increase FFB quality a suggested solution is less mills that would increase competition among farmers to deliver higher quality FFB [1]. In contrast independent smallholders may require the opposite in regions where they instead have problems in accessing the oil palm mills and often receive a lower price for their FFB.

5. INDONESIAN BIOFUEL POLICIES

The Biofuels Integrated Policy is published by the Indonesian Department of Energy and Mineral Resources. It contains laws, regulations, decrees and policies related to biofuels in Indonesia. Three laws, in particular, affect plantation factors that could in turn influence yields. These are summarized below with relevant information to the topic. The relevant laws are Law Number 12 of 1992 Concerning Plant Cultivation System [33], Law Number 18 Concerning Plantation [34], and Law of the Republic of Indonesia Number 39 2014 about Plantations [23]. Only the articles and paragraphs within the law that are relevant to this topic of policy and yield have been reviewed. The law on plantations was updated in 2014 and therefore the newer version is also included. Indonesia has its own certification scheme, Indonesian Sustainable Palm Oil (ISPO), which is mandatory from the end of 2014 for all estate companies.

Law no. 12 1992 concerning plant cultivation system states that anyone can breed plants in order to achieve a better producing plant, and can even be rewarded for doing so, but the seedling must be approved by the government to secure quality standard and to be certified. Planting should be performed in a way to maximize growth and productivity by using appropriate planting techniques and seeds and maintenance should be performed to optimize growth and productivity. The government supervises distribution of fertilizer and tools to be used for cultivation, and is obliged to offer services regarding information that can aid in the development of cultivation.

In the recently updated law on plantations, law no. 39 from 2014 (as in the law of Plantations no. 18 from 2004) the core idea of plantations are: provide income, for the state and for the people, to provide work opportunities, fulfil the demands and to improve productivity and added value. Capacity building shall be provided officially, local, regional or national, for increasing the added value on plantations. Stricter rules are put in development of granted lands, at least 30% must be developed within 6 years of being granted the land or the state will recall the permit. The search for, or breeding of, improved seeds can now only be carried out by a legal person with the consent from the Minister of Agriculture. Priorities for crops are first to meet the domestic supply and raw materials for the industry before other demands. Mixing and falsifying quality that leads to unfair competition, in the steps of processing, distribution or marketing, is now not allowed and punishable. R&D shall respect local knowledge while also producing scientific knowledge and developing technology. Development of human resources has been targeted and is to be performed by a local or national authority; in order to develop and/or increase knowledge, skills, professionalism, independence and dedication of farmers.

As ISPO certification has become mandatory for estates in Indonesia, a summary of the relevant principles and criteria in the audit process [24] will be presented. The standards are based on Technical Guidelines Development Gardens Palm Oil (Pedoman Teknis Pembangunan Kebun Kelapa Sawit). The seeds have to be recognized by the government, certified and age and quality is monitored or the estate will be reported. Planting layout regarding amount of trees, distance and pattern should be according to best practice standards. Maintenance should be according to standard operating procedure for water use and weeding, and fertilization by analysis of soil and leaves. Pest control performed using a variety of techniques. Harvest according to standard operating procedure, including determining ripeness and crop rotation. In transportation protect the FFB from damage, contamination and fermentation, and timeliness to reach treatment facility. At the treatment facility there must be criteria for accepted FFB, the criteria must be open and rejection of non-complying. In the mill the machinery should be controlled and maintained to ensure that the FFB treatment will meet the expected quality. An ISPO certification that focuses on plasma farmers is being developed and contains a lot of the same criteria's.

6. DISCUSSION

Indonesia has had strategies that promoted company estate involvement with farmers but this has in many instances failed to produce high yielding plantations. As the involvement after the initial handover is not clearly described in literature there is a chance companies are only interested in payback of the loans handed out. Instead of focus should be placed on further developing their own and their plasma smallholders' plantations. This will be of importance if the country wants to avoid further deforestation or land conversion due to increased demand for palm oil from biodiesel production. As seen in Figure 5 the potential increase for biodiesel production by increased yield and even more so if further expansion is decided.

Phases of the palm oil production have factors which may be controlled and/or improved to achieve a higher yield, displayed in the improvement actions are marked as either addressed or not, the effectiveness of the policy is not evaluated. Many of the issues have been noted and have been included in the ISPO certification requirement, although fewer in related laws regarding plantations. Showing there are still many improvements that can be further explored and that deserve attention.

Table 1. Factors limiting in Indonesia palm oil yield, related policy and improvement actions, underlined actions are proposed in the policies

Parameter Group	**Identified factors limiting yield in Indonesia**	**Source**	**Related Indonesian Policy**	**Actions for improvement (Addressed)**
Agricultural Practices	Wrong planting pattern or distance between trees. Both low and high tree density reduce FFB output per ha.	[28]	ISPO	SOP (standard operating procedure) for planting.
	Use of uncertified seed or seed of lower quality. Due to availability, lack of knowledge or financial constraints	[2, 11, 28]	Law no. 12 1992 Article 11, 12, 13. Law no. 39 2014 Article 26, 27. ISPO	Stricter breeding control. Increase certified seedling supply.
	Improper fertilizer application due to knowledge or financial constraints. Affect tree and fruit growth.	[1, 28, 29]	ISPO	Capacity building for benefit of fertilizer. Policy development for oil palm fertilizer.
	Pesticide: Pests and diseases affect leaf area, root and stem and can decrease growth or kill the tree	[8]	ISPO	Pesticide. GMO.
	Lack of experience and knowledge in oil palm cultivation.	[1,6]	Law no. 39 2014 Article 88, 89.	Knowledge transfer from authorities and estates.
Management Practices	Management practices for cultivation; harvesting, pruning and maintenance.	[10, 16, 28]	ISPO	Training in BMP. Applying BMP.

	Behaviour of farmers and decentralized administration; focus on land expansion rather than intensification for increased production.	[1, 19, 20]	-	Central directions for expansion and focus on developing concessions.
	Poor quality of FFB delivered to palm oil mills. Due to high demand for FFB, lack of or indulgent quality control and/or poor farming practices.	[1]	Law no. 39 2014 Article 77. ISPO	BMP for harvest. Quality monitoring and control at mill.
	Long transportation or retention time of FFB causing free fatty acid build up and reduced oil yield.	[22]	ISPO	Infrastructure development. SOP for harvest and transportation. Decrease retention time.
Environmental Factors	Natural environment: Light, carbon dioxide, temperature. Affect tree and fruit growth.	[8]	-	-
	Local environment: soil type, nutrient and water availability. Affect tree and fruit growth.	[8]	ISPO	Choice of location. Fertilizer application. GMO.

Agricultural practices related to start up such the planting pattern and seedlings are of little issue in estate companies and plasma smallholders but especially quality seedling for independent smallholders need improvement. Only increasing quality control may affect the demand side therefore increasing the supply of seedlings could ensure that more plantations acquire quality trees.

Fertilizers are one of the most important and costly factors for oil palm cultivation. Easier access would most likely be beneficial to yields in Indonesia but as recognized in the ISPO certification, the application procedure of fertilizer is important. It can be damaging to soils which in turn affect the sustainability for biofuels, as fertilizer production has a high environmental and energy impact. This makes a subsidies policy volatile regarding risk and benefit. In order to make fertilization an effective measure, farmers need to understand the benefits of applying it and the proper application of fertilizers to not damage the soils. As of now little is done toward fertilizers and smallholders who cultivate a large portion of the land, intensification will benefit these farmers' income and change their behavior method towards increasing production. For example there is a policy regarding rice fertilizer in Indonesia and a similar one could be developed for palm oil production.

In terms of FFB quality delivered to mills better management may improve harvesting timing leading to better fruit and less retention time which causes deterioration of the oil. BMP bring several benefits to a plantation and should be an integral part of biofuel policies to ensure good practices and reducing the loss of potential palm oil.

The ISPO certification is a good step for securing more sustainable feedstock for the biodiesel production in Indonesia. It targets many problem areas regarding yield and with similar measures that have been suggested in the literature. As ISPO became mandatory further steps should be taken to ensure that biodiesel is produced from sources holding the certification and those criteria is upheld. But it must also be redirected toward smallholders who hold a great part of the land but with a low output Fig. 3 and Fig. 5, which require a different approach then estate companies.

7. CONCLUSION

As Indonesia targets higher biofuel blending targets the potential benefits of increasing the yield for the main biodiesel feedstock cannot be overlooked. Not only does it provide significant potential on current land, it can also reduce the requirement on converting additional land by intensifying on currently occupied land and if expanding there are advantages in terms of biodiesel potential if aiming for high yielding plantations. The biofuel policy will need to target fertilizer especially among smallholders and the use of best management practices in all plantations to realize the potential in current and future plantations. Strengthen the knowledge exchange and focus on capacity building between estate companies and research institutions with each other and other farmers. Higher yields are possible and if achieved it will be a step towards a more sustainable biodiesel feedstock as the Indonesian oil palm plantations realize their true potential.

REFERENCES

1. ANGGRAINI, E., GRUNDMANN, P. Transactions in the Supply Chain of Oil Palm Fruits and Their Relevance for Land Conversion in Smallholdings in Indonesia. In *The Journal of Environment & Development*. 2013. Vol. 22, No. 4, p. 391–410. [Referred on the 9th December 2014]. Link to the internet <http://jed.sagepub.com/cgi/doi/10.1177/1070496513506225>
2. BARLOW, C. et al. The Indonesian oil palm industry. In *Oil Palm Industry Economic Journal*. 2003. Vol. 3, No. 1, p. 8–15. [Referred on the 21st January 2015]. Link to the internet <http://fic.nfi.or.th/vfc/pdffile/Palmoil/ID1.pdf>
3. BART, J.C.J. et al. *Biodiesel Science and Technology*. [s.l.]: Elsevier, 2010. ISBN 9781845695910.
4. BUDIDARSONO, S. et al. Oil palm plantations in Indonesia: The implications for migration, settlement/resettlement and local economic development. In *Biofuels - Economy, Environment and Sustainability*. 2013, p. 173–193. [Referred on the 16th December 2014]. Link to the internet <http://www.intechopen.com/books/biofuels-economy-environment-and-sustainability/oil-palm-plantations-in-indonesia-the-implications-for-migration-settlement-resettlement-and-local-e>
5. BUTLER, R. a. et al. REDD in the red: palm oil could undermine carbon payment schemes. In *Conservation Letters*. 2009. Vol. 2, No. 2, p. 67–73. [Referred on the 10th December 2014]. Link to the internet <http://doi.wiley.com/10.1111/j.1755-263X.2009.00047.x>
6. CACHO, O.J. et al. Benefits and costs of deforestation by smallholders: Implications for forest conservation and climate policy. In *Ecological Economics*. 2014. Vol. 107, p. 321–332. [Referred on the 11th December 2014]. Link to the internet <http://www.sciencedirect.com/science/article/pii/S0921800914002821>
7. CASSON, A. Bogor, Indonesia: CIFOR, 2000. [Referred on the 21st January 2015]. Link to the internet <http://www.cifor.org/publications/pdf_files/casson.pdf>
8. CORLEY, R., TINKER, P. Growth, flowering and yield. In *The oil palm*. 4th. Ed.Oxford, 2003. p. 89–131. [referred on the 10th February 2015]. Link to the internet <http://onlinelibrary.wiley.com/doi/10.1002/9780470750971.ch4/summary>
9. CRAMB, R., CURRY, G.N. Oil palm and rural livelihoods in the Asia-Pacific region: An overview. In *Asia Pacific Viewpoint*. 2012. Vol. 53, No. 3, p. 223–239. [Referred on the 16th January 2015]. Link to the internet <http://doi.wiley.com/10.1111/j.1467-8373.2012.01495.x>
10. DONOUGH, C. et al. Penang, Malaysia, 2010. [Referred on the 26th January 2015]. Link to the internet <http://www.tropcropconsult.com/downloads_files/Donough2010.pdf>

11. FEINTRENIE, L. et al. Why do farmers prefer oil palm? Lessons learnt from Bungo district, Indonesia. In *Small-scale forestry*. 2010. Vol. 9, No. 3, p. 379–396. [Referred on the 2nd February 2015]. Link to the internet <http://link.springer.com/10.1007/s11842-010-9122-2>
12. FLEMING, E., COELLI, T. Assessing the performance of a nucleus estate and smallholder scheme for oil palm production in West Sumatra: a stochastic frontier analysis. In *Agricultural Systems*. 2004. Vol. 79, No. 1, p. 17–30. [Referred on the 15th January 2015]. Link to the internet <http://www.sciencedirect.com/science/article/pii/S0308521X0300043X>
13. HARSONO, S.S. et al. Energy balances and greenhouse gas emissions of palm oil biodiesel in Indonesia. In *GCB Bioenergy*. 2012. Vol. 4, No. 2, p. 213–228. [Referred on the 27th November 2014]. Link to the internet <http://doi.wiley.com/10.1111/j.1757-1707.2011.01118.x>
14. KOH, L.P., WILCOVE, D.S. Is oil palm agriculture really destroying tropical biodiversity? In *Conservation Letters*. 2008. Vol. 1, No. 2, p. 60–64. [Referred on the 12th July 2014]. Link to the internet <http://doi.wiley.com/10.1111/j.1755-263X.2008.00011.x>
15. LAMBIN, E.F. et al. Effectiveness and synergies of policy instruments for land use governance in tropical regions. In *Global Environmental Change*. 2014. Vol. 28, p. 129–140. [Referred on the 21st July 2014]. Link to the internet <http://www.sciencedirect.com/science/article/pii/S0959378014001125>
16. LEE, J.S.H. et al. Oil palm smallholder yields and incomes constrained by harvesting practices and type of smallholder management in Indonesia. In *Agronomy for Sustainable Development*. 2013. Vol. 34, no. 2, p. 501–513. [referred on the 29th October 2014]. Link to the internet <http://link.springer.com/10.1007/s13593-013-0159-4>
17. LEVIN, J. 2012. start here tomorrow 28/1.
18. LIFIANTHI, L.H. Productivity And Income Peformance Comparison of Smallholder Oil Palm Plantation at Dry Land and Wet Land of South Sumatra Indonesia. In *APCBEE Procedia*. 2012. Vol. 3, p. 270–275. [Referred on the 15th January 2015]. Link to the internet <http://www.sciencedirect.com/science/article/pii/S2212670812001522>
19. MANDEMAKER, M. The role of governance in agricultural expansion and intensification: a global study of arable agriculture. In *Ecology and Society*. 2011. Vol. 16, No. 2. [Referred on the 6th February 2015]. Link to the internet <http://www.ecologyandsociety.org/vol16/iss2/art8/ES-2011-4142.pdf>
20. MCCARTHY, J.F. et al. Swimming Upstream: Local Indonesian Production Networks in “Globalized” Palm Oil Production. In *World Development*. 2012. Vol. 40, No. 3, p. 555–569. [Referred on the 15th January 2015]. Link to the internet <http://www.sciencedirect.com/science/article/pii/S0305750X11001872>
21. MCCARTHY, J.F., CRAMB, R. A Policy narratives, landholder engagement, and oil palm expansion on the Malaysian and Indonesian frontiers. In *Geographical Journal*. 2009. Vol. 175, No. 2, p. 112–123. [Referred on the 19th January 2015]. Link to the internet <http://doi.wiley.com/10.1111/j.1475-4959.2009.00322.x>
22. MINISTRY FOR ECONOMIC AFFAIRS *Master Plan for Acceleration and Expansion of Indonesia Economic Development 2011–2025*. Jakarta: Coordinating Ministry for Economic Affairs, 2011. ISBN 9789793754147.
23. MINISTRY OF AGRICULTURE Law of the Republic of Indonesia Number 39 2014 About Plantations. In. 2014. [Referred on the 4th February 2015]. Link to the internet <http://www.indolaw.org/UU/Law No. 39 of 2014 on Plantations.pdf>
24. MINISTRY OF AGRICULTURE PEDOMAN PERKEBUNAN KELAPA SAWIT BERKELANJUTAN INDONESIA. In. 2011. [Referred on the 2nd March 2015]. Link to the internet <http://www.ispo-org.or.id/images/lamp_sk19.pdf>

25. MINISTRY OF AGRICULTURE Statistik Perkebunan Indonesia Tree Crop Estate Statistics of Indonesia 2012-2014 Kelapa Sawit Palm Oil. In. 2013.
26. MINISTRY OF AGRICULTURE OF INDONESIA Produktivitas Kelapa Sawit Menurut Provinsi di Indonesia, 2009 - 2013. In. 2013. [Referred on the 6th February 2015]. Link to the internet <http://www.pertanian.go.id/IP_ASEM_BUN_2013/Prodtv-KelapaSawit.pdf>
27. MINISTRY OF AGRICULTURE OF INDONESIA Produktivitas Kelapa Sawit Menurut Provinsi di Indonesia, 2010–2014. In. 2014. [Referred on the 6th February 2015]. Link to the internet <http://www.pertanian.go.id/IP_ASEM_BUN_2014/Prodtv-KelapaSawit.pdf>
28. PAPENFUS, M. 2000. [Referred on the 21st January 2015]. Link to the internet <http://www.worldagroforestrycentre.net/sea/publications/files/workingpaper/wp0033-04.pdf>
29. POTTER, L., BADCOCK, S. Tree crop smallholders, capitalism, and adat: Studies in Riau Province1, Indonesia. In *Asia Pacific Viewpoint*. 2004. Vol. 45, no. 3, p. 341–356. [Referred on the 21st January 2015]. Link to the internet <http://onlinelibrary.wiley.com/doi/10.1111/j.1467-8373.2004.00245.x/full>
30. RSPO [s.l.]: Round Table of Sustainable Oil Palm, 2012. start here tomorrow 28/1.
31. SUGIYONO, A. et al.Eds. *INDONESIA ENERGY OUTLOOK 2014*. Jakarta: Badan Pengkajian dan Penerapan Teknologi (BPPT), 2014. ISBN 9786021328026.
32. SUSANTI, A., BURGERS, P. Chapter 19 Oil palm expansion: competing claim of lands for food, biofuels and conservation. In BEHNASSI, M. et al.Eds. *Sustainable Food Security in the Era of Local and Global Environmental Change*. Dordrecht: Springer Netherlands, 2013. p. 301–320. [Referred on the 5th November 2014]. ISBN 978-94-007-6718-8Link to the internet <http://link.springer.com/10.1007/978-94-007-6719-5>
33. THE DEPARTMENT ENERGY AND MINERAL RESOURCES Law No. 12 of 1992 Concerning Plant Cultivation System. In *Biofuel Integrated Policies*. 1992. [Referred on the 4th February 2015]. Link to the internet <http://en.calameo.com/read/00082252855a8a671c721>
34. THE DEPARTMENT ENERGY AND MINERAL RESOURCES Law No. 18 Concerning Plantation. In *Biofuel Integrated Policies*. 2004. [Referred on the 4th February 2015]. Link to the internet <http://en.calameo.com/read/00082252855a8a671c721>
35. USDA Southeast Asia: Post-2020 Palm Oil Outlook Questionable. In *Commodity Intelligence Report*. 2014. [Referred on the 11th February 2015]. Link to the internet <http://pecad.fas.usda.gov/highlights/2014/09/SEAsia/index.htm>
36. USDA FOREIGN AGRICULTURAL SERVICE 2014. [Referred on the 5th November 2014]. Link to the internet <http://scholar.google.com/scholar?hl=en&btnG=Search&q=intitle:Indonesia+Biofuels+Annual#5>
37. VARKKEY, H. Malaysian investors in the Indonesian oil palm plantation sector: home state facilitation and transboundary haze. In *Asia Pacific Business Review*. 2013. Vol. 19, no. 3, p. 381–401. [Referred on the 26th February 2015]. Link to the internet <http://www.tandfonline.com/doi/abs/10.1080/13602381.2012.748262>

Appendix

Keyword 1	Keyword 2	Keyword 3	Keyword 4	Keyword 5
Indonesia	Oil Palm	Estate	Development	Driver
Indonesia	Oil Palm	Estate	Expansion	Driver
Indonesia	Oil Palm	Plantation	Development	Driver

CYSENI 2015, May 27–28, Kaunas, Lithuania
ISSN 1822-7554, www.cyseni.com

AN EXPERIMENTAL STUDY ON THE PERFORMANCE OF THE AIR SOURCE HEAT PUMP IN CENTRAL EUROPE’S WORKING CONDITIONS

R. Andrzejczyk, T. Muszyński

Gdansk University of Technology
Narutowicza 11/12, 80-233 – Gdansk, Poland
Phone 58 347 24-22
Email: rafal.andrzejczyk@pg.gda.pl, tomasz.muszynski@pg.gda.pl

ABSTRACT

Great advancements have been made in air source heat pumps due to concerns for water and consciousness of sustainable development; however there is still a serious shortcoming that limits their widespread applications, especially in sub-zero regions. The working parameters of an air source heat pump water? (ASHP) in Central Europe is considered and the influence of the heat source air on the heating efficiency of the heat pump is investigated. In addition, the impacts of frosting on the operational performance of an ASHP unit was also evaluated. The ASHP was validated and ran a whole winter in Gdansk, Poland. The relevant dynamic-performance functions were tested and the outcomes show that this new kind of ASHP can work very well under ambient temperatures as low as -9 °C.

Keywords: heating, air source heat pump, renewable energy

1. INTRODUCTION

For a long time the coal-fired boilers and coal-fired domestic stoves were the primary heating sources for people of central Europe [1–3]. Unfortunately, with the development of society, the cities in these regions have grown, and these conventional heating methods do not meet the requirements of sustainable development since they contribute to severe environmental problems such as atmospheric pollution. Great efforts have been made to control the air-pollution level in these regions and seek sustainable alternative heating methods. Efficiency of the improved ASHP under all circumstances is addressed and the improved system's increased efficiency can save energy. In this way the application scope of ASHP has enlarged and a simple and feasible alternative heating service was developed for heat in central Europe, which can also partly solve the atmosphere pollution problem.

Many studies on the performance of the ASHP system were made. Ma Guoyuan et al. [4] developed an improved ASHP system for cold regions, in which system employing scroll compressor with supplementary inlet was used. Yi-guang Chen et al. [5] experimentally investigated of a split-type ASHP system effects of the outdoor air parameters on defrosting cycle performance and dynamic defrosting characteristics of the ASHP unitare discussed. Roth et al. described the strategies used to improve ASHP performance [6], including increasing outdoor coil capacities, the use of carbon dioxide for refrigerant, and the use of multiple or modulating compressors, among others.

Morrison et al. [7] presented an ASHP water heater seasonal performance assessment method based on experimental results. They indicated the effect of surrounding air temperature on the system performance is more significantly than the effect of initial water temperature during the heating process. Mei et al. [8] investigated the difference of R22 and R407C in the practical ASHP water heat system. They also studied the effect of different style natural convection immersed condensers to the heat pump water heater [9]. Rankin et al. [10] presented a study about demand side management for commercial building using an inline air-source heat pump water heater methodology.

2. EXPERIMENTAL SETUP

The experimental implementation of ASHP system is intended to perform a quantitative assessment of the operational costs. An air source heat pump was chosen as system since it is widely used in commercial applications in the South European region. An 7 kW heating power (ambient temperature 0 °C and water temperature of 35 °C) heat pump was implemented and instrumented. Heat pump was supplying heat to house with 3 kW of heat loses. Fig. 1 presents view of internal parts of heat pump and the view of an evaporator, Table 1 presented the basic operation conditions of pump. Heat pump evaporator is made from straight copper tubes with aluminum wavy fins covered with hydrophobic layer.

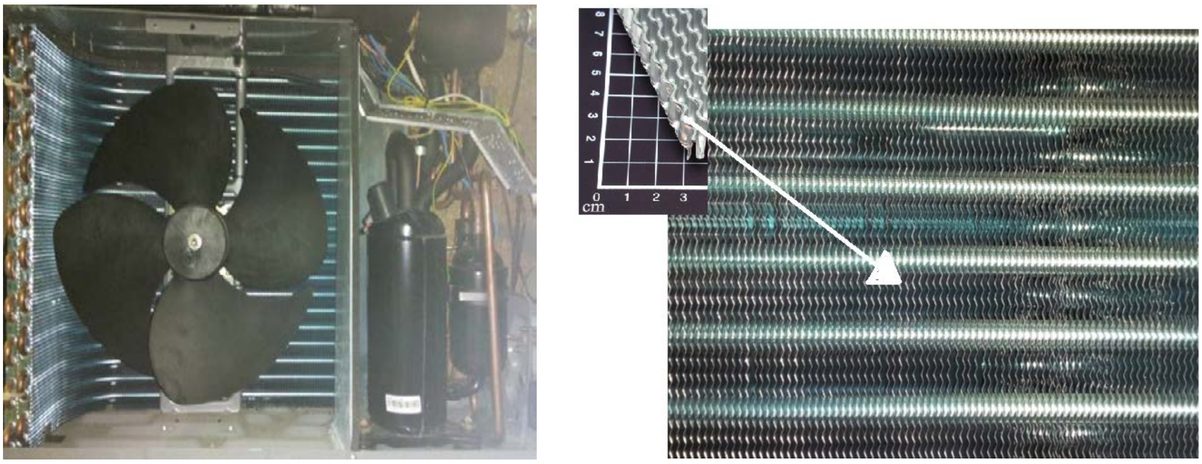

Fig. 1. Investigated heat pump and air source heat pump: evaporator with geometry of wavy fin (right) and unit view (left)

Table 1. Characteristic operation conditions of ASHP

Heating Capacity	6790 W
Power input	1920 W
Refrigerant	R410A
Water flow volume	150 l/h
IV	-22
V	-24

3. EXPERIMENTAL RESULTS

ASHP was installed and ran a whole winter in Gdansk, Poland. The Table 2 presents average temperatures for all climates zones in Poland. Fig. 2 shows map of Poland with matched climate zones for winter conditions, authors singled geographic positions of Gdansk. The ASHP performance was tested and the outcomes show that new kind of heat pump can work very well under ambient temperatures as low as -9 °C. Fig. 3 shows heat pump evaporator at operation with ambient temperature of 8 °C and relative humidity of 80%. It is an evidence that the air heat pump works stabile however the temperatures differences at surface of the evaporator are quite large. In authors opinion this problem could be solved by using better distribution system of refrigerant. Air source heat pump was tested during winter conditions from December till February.

Table 2. Poland Climate Zones [11]

Climate Zones	Temperature, °C
I	-16
II	-18
III	-20
IV	-22
V	-24

Temperature is determined as mean of coldest period, e.g. as 5 coldest days of every year during 25 years

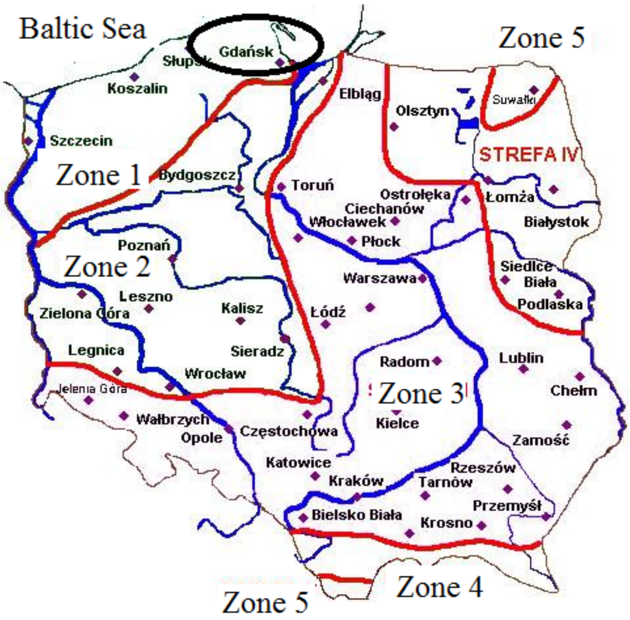

Fig. 2 Polish climatic zones map [11]

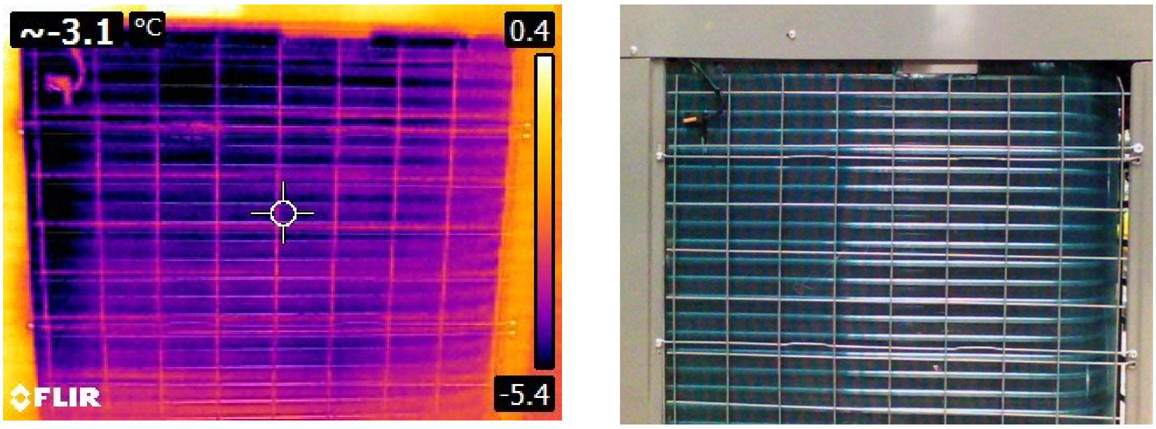

Fig. 3. Thermal image of working air source heat pump evaporator (left) and unit view (right)

Heat pump along with additional circulating pump power consumption was measured and recorded on daily basis. Fig. 4 shows view of detached house construction and schematically presented structure of testing system. This system has been consisted of computer data acquisition with National Instruments application (LabView 8.0) and electronic sensors to measure the basic parameter of working installation. It collected power consumption of air sourced heat pump, the daily time of work and outside parameter of air. Installation has been equipped with PLC regulator and a several temperature sensors used to regulations and control.

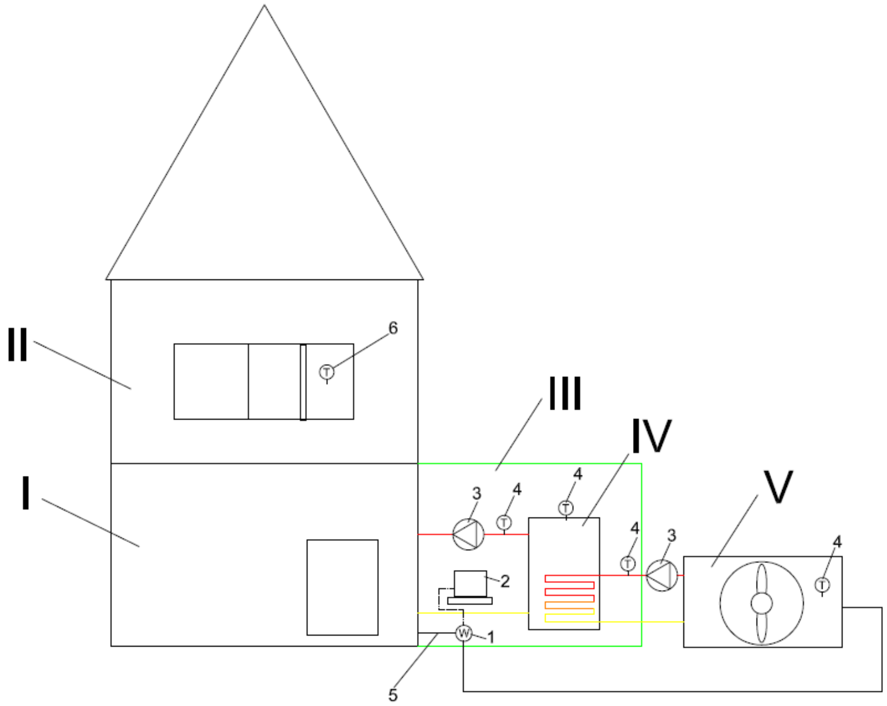

Fig. 4. Main elements of systems: I – first floor of building, II – second floor of building, III – boiler room, IV – water tank, V – Air Source Heat Pump; Test facility: 1 – wattmeter, 2 – PC, 3 – Pump, 4 – temperature sensor, 5 – electric grid, 6 – room temperature controller

Average daily power consumption was measured as 13 kWh. This consumption includes additional heat supplied in the system for heat pump defrosting. Furthermore it is worth to add that the heat pump covers, for most of the winter period, all building consumption for heat. Fig. 3 shows measured electrical energy consumption of an ASHP during tests. Fig. 5 shows daily power consumption for the air to water heat pump based heating system measured in 10.02.2015.

The average coefficient of heat performance was calculated as:

$$COP_h = \frac{\dot{Q}_h}{P} = \frac{13}{2} = 7{,}5\,[-], \tag{1}$$

where $\dot{Q}_h$ – heat energy consumption [kWh]; P – daily electric power consumption [kWh].

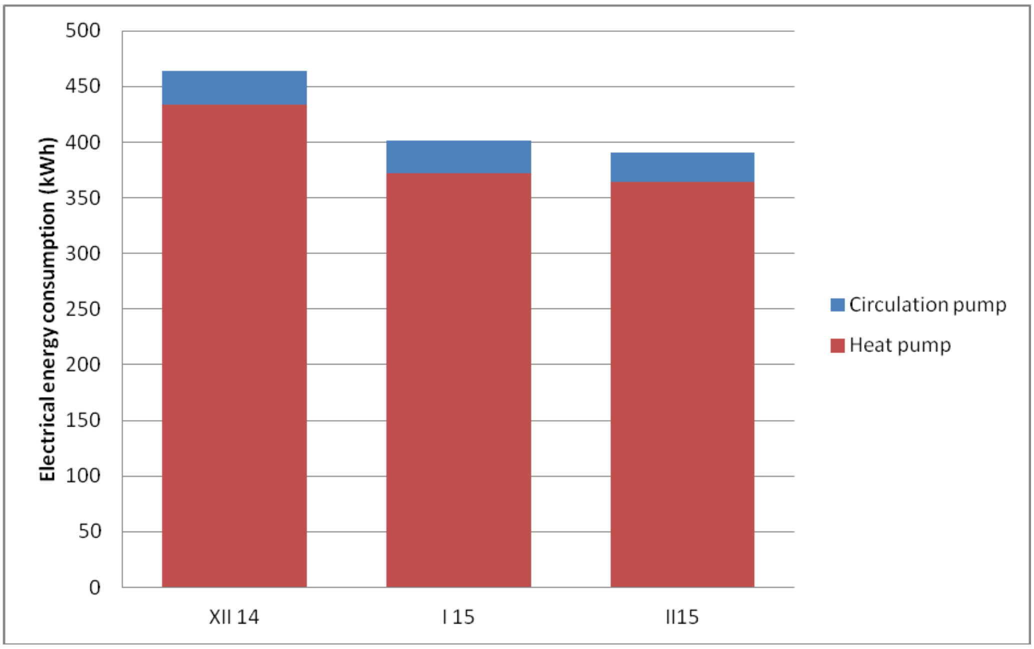

Fig. 3. Monthly electrical energy consumption for the air to water heat pump based heating system

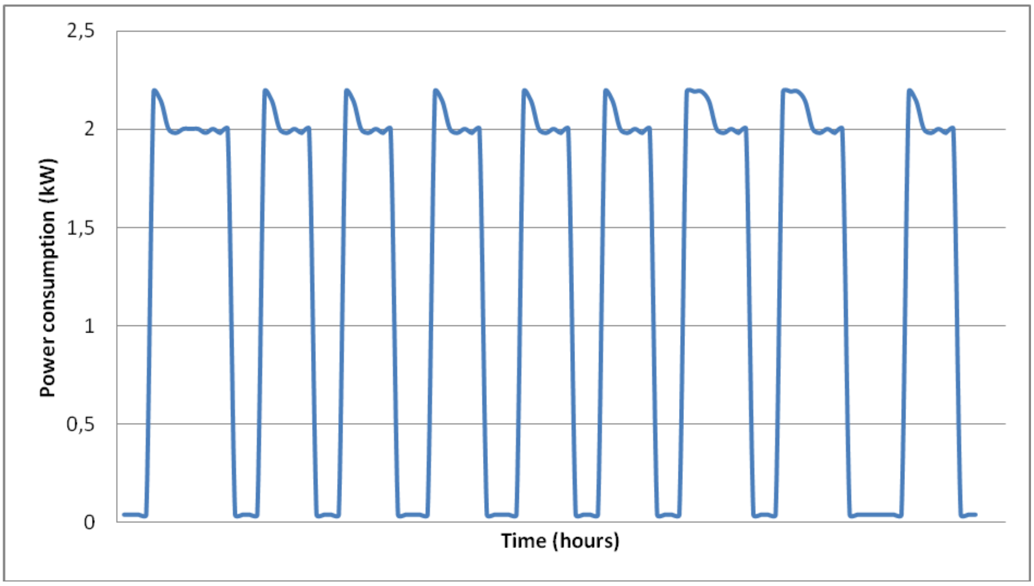

Fig. 4. Daily power consumption for the air to water heat pump based heating system in 10.02.2015

4. CONCLUSIONS

An experimental investigation was carried out to study air source heat pump effectiveness and power consumption in winter conditions in northern Poland. Feasibility of ASHP for heat supply in domestic applications in winter conditions was verified. Study shows that system operation resulted in average power consumption of 13 kWh daily for a 3 kW heat demand house (calculated for standard winter conditions in Gdansk). Further investigations are needed in order to optimize heat pump working cycle. Authors' future work will be focused on improvement of heat pump evaporator and condenser efficiency.

REFERENCES

1. OMER A.M. Ground-source heat pump systems and applications. Renew Sustain Energy Rev. 2007. doi:10.1016/j.rser.2006.10.003.
2. LUND J.W., FREESTON D.H. World-wide direct uses of geothermal energy. 2000. Geothermics 2001; 30: 29–68.
3. FLORIDES G., KALOGIROU S. Ground heat exchangers – a review of systems, models and applications. Renew Energy, 2007. doi:10.1016/j.renene. 2006. 12.014.
4. GUOYUAN MA, QINHU CHAI, YI JIANG. Experimental investigation of air-source heat pump for cold regions. International Journal of Refrigeration 2003; 26: 12e8.
5. CHEN YI-GUANG, GUO XIAN-MIN. Dynamic defrosting characteristics of air source heat pump and effects of outdoor air parameters on defrost cycle performance. Applied Thermal Engineering 2009; 29: 2701.
6. ROTH K., DIECKMANN J., BRODRICK J. Heat pumps for cold climates, ASHRAE Journal (February) (2009).
7. MORRISON G.L., ANDERSON T., BEHNIA M. Seasonal performance rating of heat pump water heaters. Solar Energy 2004; 76: 147–52.
8. MEI V.C., DOMITROVIC R.E., BREWER W.H., CHEN F.C. Experimental study of an R407C heat pump water heater. ASHRAE Trans 2001; 107(part 1): 224–9
9. MEI V.C., CHEN F.C., DOMITROVIC R.E., KILPATRICK J.K., CARTER J.A. A study of a natural convection immersed condenser heat pump water heater. ASHRAE Trans 2003; 109 (part2): 3–8.
10. RANKIN R., ROUSSEAU P.G., ELDIK M.V. Demand side management for commercial buildings using an inline heat pump water heating methodology. Energy Convers Manage 2004; 45: 1553–63.
11. http://www.hvacr.pl/strefy-klimatyczne-polski-i-temperatury-obliczeniowe-322

CYSENI 2015, May 27–28, Kaunas, Lithuania
ISSN 1822-7554, www.cyseni.com

BINARY VAPOR CONDENSATION ON THE WETTABLE NANOPARTICLES

A. Brin, Y. Belaya
A.V. Luikov Heat and Mass Transfer Institute
National Academy of Sciences of Belarus
P. Brovki str. 15, 220072 Minsk – Belarus
Phone +375 17 284-22-22
Email: brin@hmti.ac.by

ABSTRACT

An efficient method for the registration of nanoparticles is detecting of heterogeneous droplets, which are formed by means of the supersaturated vapor condensation on nanoparticles. Laminar flow diffusion chambers are widely used for investigation of such processes. The heterogeneous condensation of vapors of water and alcohol on nanoparticles and the growth of formed droplets are numerically studied under conditions of laminar flow diffusion chamber. A new mathematical model of a laminar flow diffusion chamber performance has been developed. The model represents a boundary-value problem for a system of ordinary differential equations, describing a change in the temperature field of the vapor-gas mixture and the field of the numerical vapor density, and an equation for droplet growth in a supersaturated vapor. The results of a numerical simulation of vapor condensation on nanoparticles introduced in laminar diffusion chamber for a mixture of air and vapors of water and alcohol are presented. Particularly, it was found that the heterogeneous droplets containing a nanoparticle inside grow to an optically detectable sizes (tens of microns), which allows the efficient use of this technology to the detection of the nanoparticles and trapping them from vapour-gas mixture.

Keywords: laminar flow diffusion chamber, heterogeneous condensation, temperature field, field of the numerical vapor density, numerical simulation, nanoparticle

1. INTRODUCTION

Nanotechnology important issue is the problem of extraction of the synthesized nanoparticles from the gas stream. One of the possible methods for solving of this problem – applying easily removable coating on the nanoparticles. If the radius of the coating is about 1 micron, further manipulations with particles are well established in the physics of aerosols. It is known that micron coating are rapidly formed by heterogeneous condensation of supersaturated steam environments. Effective device to create a stationary supersaturated gas media is laminar diffusion chamber (LDC), schematically shown in Fig. 1. The principle of operation of this chamber design is as follows. The cold gas stream with nanoparticles after saturator enters the cylindrical chamber (condenser) with wall temperature T_w and mixes with saturated water vapor penetrating into the chamber through the porous walls. Diffusion processes of vapor occur simultaneously with thermal conductivity in the radial direction of the chamber. Since the saturated vapor density depends exponentially on the temperature, even a small reduction in temperature of the gas mixture leads to the formation of a supersaturated environment in the chamber.

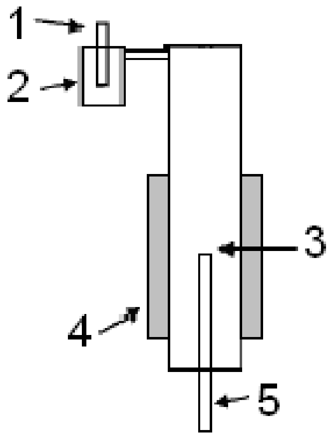

Fig. 1. Scheme of a laminar diffusion chamber: 1 – introduction of nanoparticles; 2 – saturator; 3 – condenser; 4 – porous walls; 5 – removal of the waste material

The Fig. 2 schematically shows the structure of heterogeneous droplet containing nanoparticle inside.

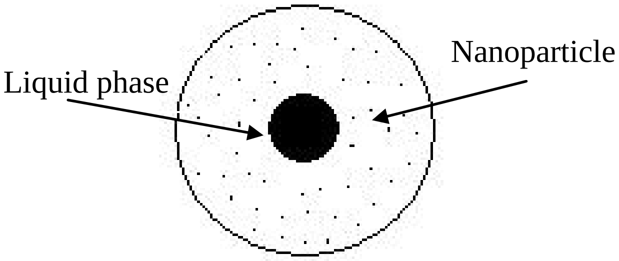

Fig. 2. Structure of heterogeneous droplet

This paper presents the results of a numerical study of the growth of coating on nanoparticles on the test substance during its motion in the LDC. It has been investigated the influence of binary vapor mixture of water and alcohol on droplet growth. Adding the second substance (alcohol) enhances the heat and mass transfer processes in comparing with pure water vapor condensation on nanoparticle [1]. For example, for pure water vapor condensation the heterogeneous droplets reach the size of one micrometer on the length of 6 radiuses of chamber (30 millimeters). After adding second condensing vapor (alcohol) we have reached the sizes of droplets about 20 micrometers on such length of the chamber.

To calculate the thickness of the coating on the nanoparticle, it is necessary to find the field supersaturation and nucleation temperature in the chamber. Calculation of fields of temperature and supersaturation and growth of heterogeneous droplets was carried out using mathematical models of LDC performance developed earlier in [2–4]. Note that the supersaturation of the vapor of the working substance should not be too high so as not started a homogeneous vapor condensation. In particular, the temperature difference between temperature of saturator T_s and temperature of porous walls T_w of the chamber should not exceed 20 degrees for the mixture of air and water vapor and alcohol.

The two-dimensional mathematical model of transport processes in the gas phase and the simultaneous growth of coatings on nanoparticles introduced in laminar diffusion chamber has been used for the numerical investigation of the problem.

2. MATHEMATICAL MODEL

In laminar flow diffusion chamber the flow of mixture of vapor with nanoparticles and carrier gas is arranged so that it is laminar. The velocity profile $u(r)$ at the entrance of the chamber has the form:

$$u(r) = 2u_0\left[1-\left(\frac{r}{R}\right)^2\right],$$

where u_0 – average cross-section flow velocity, R – radius of the channel of the chamber.

The equation for the temperature field of gas-vapor mixture is the equation of convective thermal conductivity with a source associated with the release of the latent heat of phase transition during the growth of the droplets.

$$u(r,z)\frac{\partial T(r,z)}{\partial z} = \frac{1}{\rho_m c_m}\left[\frac{1}{r}\frac{\partial}{\partial r}\left(\lambda(r,z)r\frac{\partial T}{\partial r}\right)\right] + I_t\left[n(r,z)-n_s(T(r,z))\right], \quad (1)$$

where $\lambda(r, z)$ – thermal conductivity of the mixture, ρ_m – density of the mixture, c_m – heat capacity of the mixture, r – radial coordinate, z – axial coordinate, $I_t\left[n(r,z)-n_s(T(r,z))\right]$ – heat source, $n_s(T)$ – the density of saturated vapor at temperature T.

Convective diffusion equation with source which corresponds to the condensation of vapor on droplets and depletion of vapor describes the field of numerical density of vapor.

$$u(r)\frac{\partial n(r,z)}{\partial z} = \frac{1}{r}\frac{\partial}{\partial r}\left(D(T(r,z))r\frac{\partial n}{\partial r}\right) + I_n(r,z)\left[n(r,z)-n_s(T(r,z))\right], \quad (2)$$

where $D(T(r, z))$ – binary vapor diffusion coefficient, depending on temperature, $I_n(r,z)\left[n(r,z)-n_s(T(r,z))\right]$ – diffusion source. We have to use two Equations (2) in our simulation: one for changing of number density of water vapor in air and another – for changing of number density of alcohol vapor in air.

Previously were made numerical estimations of the additional terms in the equations (1) and (2) which show that the sources I_n and I_t play a significant role only for a rather high initial numerical densities of nanoparticles in a gas flow: more than 10^8 droplets/m^3. For these conditions, there is a relationship between the growth of the droplets and the processes of heat and mass transfer in LDC due to exhaustion of vapor and releasing of the latent heat of the phase transition on the growing droplets.

The boundary conditions can be written in the following form. Since the condensed liquid thin film flows on the wall of the laminar diffusion chamber, the boundary conditions for the vapor on the wall have the form:

$$T(R, z) = T_w,\ n(R, z) = n_s(T_w), \quad (3)$$

where T_w – temperature of the cold wall and $n_s(T_w)$ – density of the saturated vapor at temperature T_w.

In the center of the flow, we have two standard conditions of symmetry of the problem:

$$\frac{\partial T(0,z)}{\partial r} = \frac{\partial n(0,z)}{\partial r} = 0. \quad (4)$$

In Equation (2) the integral term I_n is equal to:

$$I_n(r,z)=\frac{4\pi\rho_l}{m}\int_0^z N_d(z_0,r)R_d^2(z,z_0,r)L(R_d(z,z_0,r))dz_0, \tag{5}$$

where m – mass of the vapor molecule (water or alcohol), ρ_l – density of liquid phase, $R_d(z, z_0, r)$ – droplet radius, $N_d(z_0, r)$ – the number density of droplets formed on the interval (z_0, $z_0 + dz_0$). Thus, the dimension of $N_d(z_0, r)$ is equal to the inverse fourth power of length.

The function $L(R_d)$ has an interpolation character and depends on the Knudsen number:

$$Kn = \lambda_d/R_d,$$

where λ_d – the mean free path of the molecules of vapor and describes the isothermal mass transfer for various regimes of droplet growth, R_d – radius of the droplet. It accurately describes the growth of droplets in a free molecular and diffusion regimes:

$$L(R_d)=\frac{Dm}{\rho_l R_d}\left(\frac{1}{1+(D/R_d)\sqrt{2\pi m/kT}}\right),$$

where k – is a Boltzmann constant.

The temperature and concentration dependence of the diffusion coefficient D has been taken into the account during the calculations. For the number density of clusters per unit volume $N_d(z, r)$ we have a steady continuity equation with the source:

$$\frac{\partial N_d(z,r)}{\partial z}=\frac{J(z,r)}{u(z,r)}, \tag{6}$$

where $J(z, r)$ – the local velocity of nucleation.

We use the following equation to describe the growth of coating on the nanoparticle:

$$\frac{\partial R_d(z,r)}{\partial z}=L(R_d(z,r))\frac{n(r,z)-n_s(T(r,z))}{u(z,r)}. \tag{7}$$

In Equation (1) an integral parameter I_t is equal:

$$I_t=\frac{U}{\rho_m c_m+N_d 4\pi R_d^3\rho c_d/3}I_n, \tag{8}$$

where U – the latent heat of the phase transition for a single molecule of vapor; c_d – specific heat capacity of droplet.

Initial conditions for the gas mixture are the homogeneous distributions of density and temperature of the vapor at the inlet of nucleation chamber:

$$T(0, r) = T_c,\ n(0, r) = n_s(T_c), \tag{9}$$

where T_c – temperature of the gas-vapor mixture at the inlet of nucleation chamber of LDC.

The system of partial differential equations with variable coefficients (1), (2) and (7) was transformed into a system of ordinary differential equations using the method of lines [5]. Wherein the partial derivatives in the radial direction are replaced by finite differences. We also assume that the particle trajectories are straight lines parallel to the axis of the nucleation chamber. The resulting system of ordinary differential equations, which includes several Equations (7) for different radial positions, was numerically solved using adaptive method of Runge-Kutta of fourth order in Mathcad 14.

3. RESULTS

Some results of numerical simulation of laminar diffusion chamber operating at atmospheric pressure are shown in Fig. 3–6. Calculations were performed for the following parameters of laminar diffusion chamber: R = 5 mm, the condenser temperature T_c = 288 K, the chamber wall temperature T_w = 310 K, the initial temperature of the gas-vapor mixture T_s = 288 K, the initial velocity of the flow u_0 = 0.14 m/s, carrier gas – air and working substance – vapor mixture of water and alcohol. The nucleation chamber in the radial direction was divided into 7 radial positions from the center of the chamber: $r_1 = 0.14R$; $r_2 = 0.29R$; $r_3 = 0.43R$; $r_4 = 0.57R$; $r_5 = 0.71R$; $r_6 = 0.86R$. The initial radius of nanoparticles was taken to be $5 \cdot 10^{-9}$ m, the initial concentration – $N_d = 10^9$ droplets/m^3.

The profiles of supersaturation for the mixture of vapors of water and alcohol are shown in Fig. 3. The dimensionless parameter in the direction of the flow in the chamber was taken as the radius of nucleation chamber R.

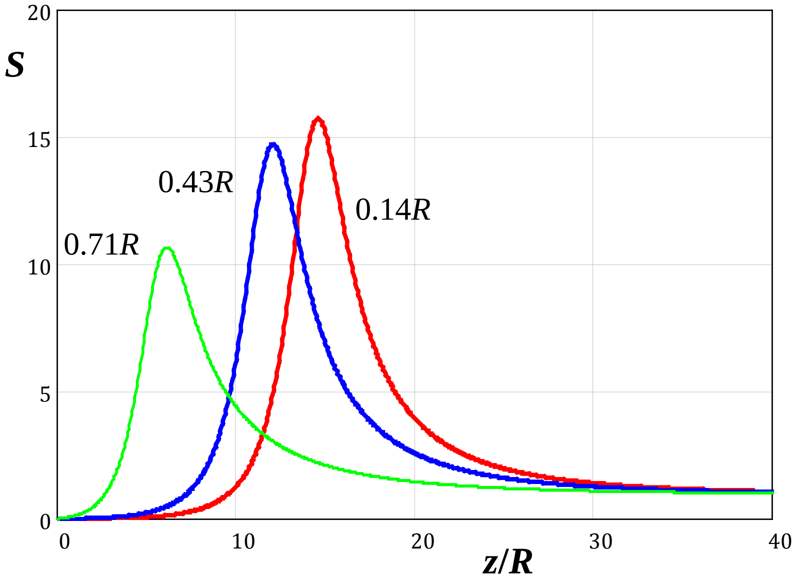

Fig. 3. Supersaturation S along the chamber for three radial positions

From the analysis of the data presented in Fig. 3, it follows that for gas-vapor mixture the supersaturation occurs for all radial positions and the most concentrated in the central region of the chamber, which is associated with the colder temperatures in the center.

The temperature profiles for the mixture of air and vapors of water and alcohol are presented in Fig. 4. It should be noted that the more rapid increase of temperature occurs near the chamber wall, which is associated primarily with the higher initial temperature of the walls than in the central region of the chamber.

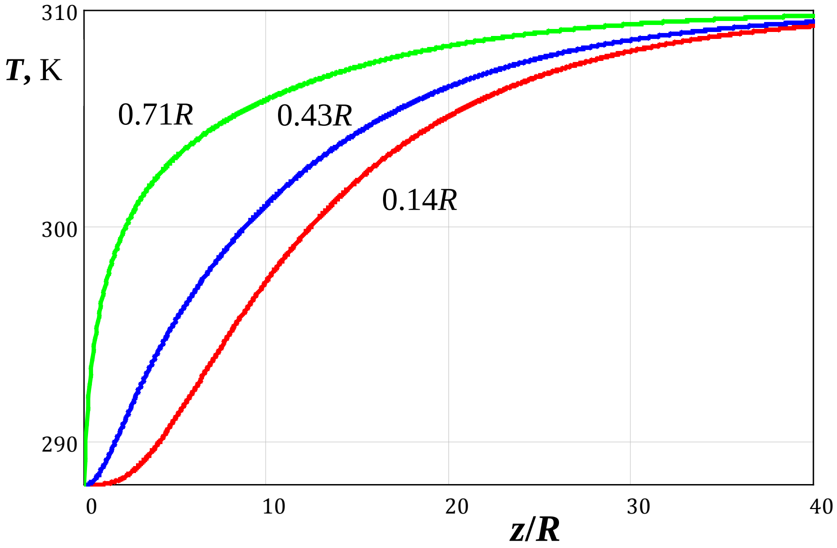

Fig. 4. Temperature profiles along the chamber for three radial positions

The profiles of number density for a mixture of air and vapors of water and alcohol are shown in Fig. 5. It is seen that the profiles of the numerical density reach the value *n* = 1 on about 40 of the chamber radiuses and also, as for the temperature profiles, they grow more rapidly near the hot wall.

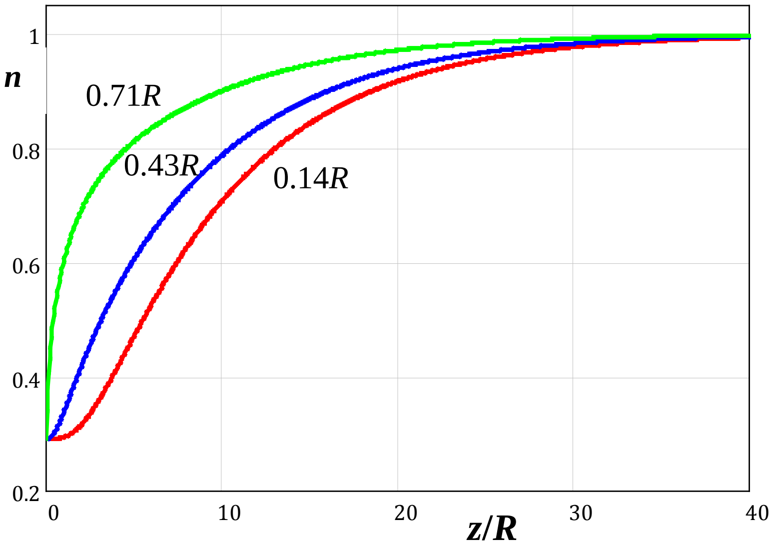

Fig. 5. Numerical density profiles along the chamber for three radial locations

The dependence of the radius of heterogeneous droplets or, actually, the thickness of the coating of vapor mixture of water and alcohol, from their position in the chamber is shown in Fig. 6. It is evident that the heterogeneous droplets containing the nanoparticles grow to an optically detectable size (tens of micrometers), which allows efficient use of this technology for the detection and trapping of the nanoparticles from the gas-vapor flow. Results are shown for two radial positions: near the chamber axis and the chamber wall.

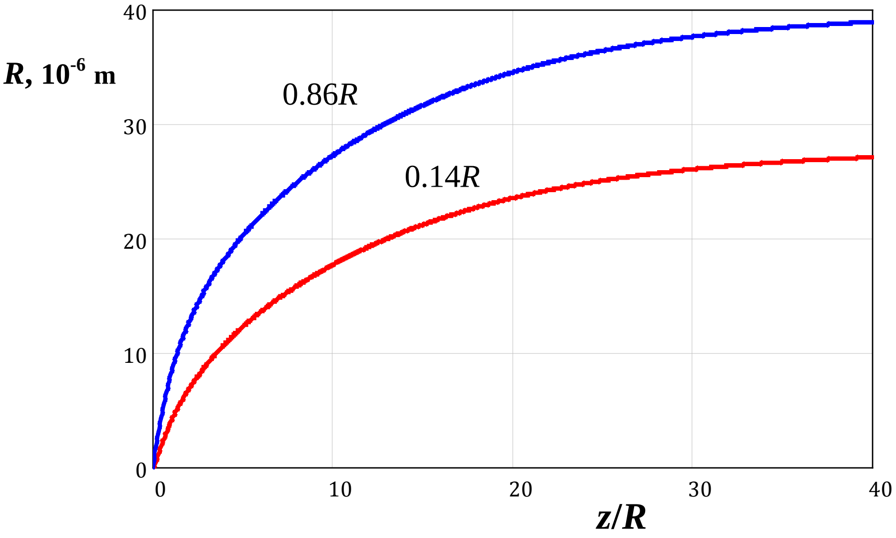

Fig. 6. Growth of heterogeneous droplets along the chamber

4. CONCLUSIONS

A mathematical model of a laminar flow diffusion chamber performance has been developed by including the processes of the heterogeneous condensation of vapors of water and alcohol on nanoparticles and the growth of formed droplets.

It was found that the heterogeneous droplets containing a nanoparticle inside grow to an optically detectable sizes (tens of microns), which allows the efficient use of this technology to the detection of the nanoparticles and trapping them from vapour-gas mixture.

REFERENCES

1. BRIN, A.A., FISENKO, S.P. Heterogeneous condensation of a steam on nanoparticles in a laminar diffusion chamber. *Journal of Engineering Physics and Thermophysics*, 2006. Vol. 79, № 2, p. 212–216.
2. BRIN, A.A., FISENKO, S.P. Heat and mass transfer and condensation interference in a laminar flow diffusion chamber. *International Journal of Heat and Mass Transfer*, 2006. Vol. 49, p. 1004–1014.
3. BRIN, A.A., FISENKO, S.P. Simulation of the operation of a laminar flow diffusion chamber to study homogeneous nucleation: Part I. *Technical Physics*, 2006. Vol. 51, No. 4, p. 418–422.
4. BRIN, A.A., FISENKO, S.P., SCHABER K. Growth and motion of heterogeneous water droplets in laminar diffusion chambers: 2. High nanoparticle concentrations. *Colloid Journal*, 2009. Vol. 71, No. 4, p. 455–458.
5. ВЕРЖБИЦКИЙ В. М. Основы численных методов. М.: Высшая школа, 2002, 848 с. (in Russian).

CYSENI 2015, May 27–28, Kaunas, Lithuania
ISSN 1822-7554, www.cyseni.com

THE INFLUENCE OF UNIQUE WATER PHYSICAL PROPERTIES ON THE CALCULATION OF WATER-VAPOR INTERFACE CONDENSATION

M. Drūlia
Lithuanian Energy Institute
Laboratory of Nuclear Installation Safety
Breslaujos str. 3, LT-44403 Kaunas – Lithuania
Phone +370 673 86228
Email: Mindaugas.Drulia@lei.lt

ABSTRACT

A short review is presented on some of the unique water physical properties that cause anomalous behaviour of water, affecting the condensation process intensity. The hydrogen bonding is one of such properties that cause water molecules to form into clusters. Hydrogen bonds are presented to prevent water molecules from evaporating by just two particles interaction. Condensation process is even more complex. Therefore it is suggested that the condensation rates cannot always be described by Maxwell distribution, also in cases under turbulent conditions. The resulting errors in the classical calculations and modelling are proposed to be caused by inaccurate initial assumptions about the physical reality.

Keywords: Condensation coefficient, Condensation rate, Hydrogen bonding, Water clusters

1. INTRODUCTION

Water is the most abundant and most common natural compound on Earth. However it has a series of properties that are unusual compared to analogous materials, e.g. other Group 6A hydrides, like H_2S, H_2Se, H_2Te and H_2Po. Due to the water's unique physical properties, it is widely used in technological installations. For example, one of the characteristics of water is high heat capacity (4.19 kJ/kgK); water for this reason is practical to use in nuclear reactors and thermal circuits as heat carrier. Pure water is a very good solvent, which is why it constantly has enough amount of solute salts to influence water features and condensation processes; that is why there are relatively few experiments made with pure water. The phase reversibility of water is used in vapor turbines cycle to generate electric power, etc. Although water has many areas of application in our environment, there still remain some unanswered questions, e.g. what is the water's behaviour during the process of condensation in the molecular level? It is now possible to predict the rates of the process, but yet the fundamental understanding of the physical mechanisms is incomplete. Knowing about water properties in a more extended manner may help to understand about condensation in deeper level. It is also important to know what is the influence of water properties on the water's behaviour, when the ambient conditions are changed.

The aim of this paper is to make a basic review on some of the unique water physical properties that cause anomalous behaviour of water, and influence the condensation process intensity at water-vapor interface.

2. LITERATURE REVIEW

2.1. Unique water physical properties

Considering the point of the molecular level, water molecules are made of one oxygen and two hydrogen atoms that are joined together by covalent bonds. When a liquid system is made of more water molecules they interact by weaker Van der Waals bonds and hydrogen bonds [1]. The latter ones are responsible for many unique and anomalous water physical properties. The study about unusual water properties in extended way is done by Chaplin [5], covering more than 60 water anomalies. They are classified basically to 5 groups that cover phase, density, material, thermodynamic and other physical anomalies. High melting, boiling and critical points belong to phase anomalies range. It also covers the property of hot water to freeze faster than cold water, the so-called Mpemba effect. It is connected with energy relaxation through H-bonds and covalent bonds compression and expansion. The property to shrink on melting is one example of density anomalies. Others could be that water density increases with temperature, up to 3.984 °C, or water having low compressibility. An example of material anomalies group is before-mentioned statement that no aqueous solution is ideal; it always contain some amount of impurities, like salts. Solutes have varying effects on properties, such as density and viscosity. From a thermodynamic point of view, water has one of the highest specific heats of the liquids, except ammonia. The specific heat capacity of water is about twice than that of ice or steam (comparison: at melting and boiling points it is 37.77 J/mol*K vs. 76.01 J/mol*K, and 37.47 J/mol*K vs. 75.95 J/mol*K, respectively). Other unique properties to be mentioned are the cohesiveness in water being large due to H-bonds that are three-dimensional, and for this reason high viscosity is achieved. The surface tension is high, so as a large self-diffusion. A complete list of anomalies may be found at water structure and science page [5]. Most of these unusual properties, not common to other materials, arise from hydrogen bonded network of water molecules.

All in all, one H_2O molecule may form 6 bonds with neighbouring molecules. By maximum, four of them may be based on hydrogen bonding. Due to hydrogen bonds water molecules can be formed to polymeric units called clusters (see Fig. 1). Because H_2O molecule has a polarity, when it forms into a cluster, it has a resultant polarity. The clusters are formed near one another, and the amount of them is characterized by the cluster density. It is calculated that clusters that are near the water-vapor interface are of a lower cluster density than those in the bulk of the liquid [10].

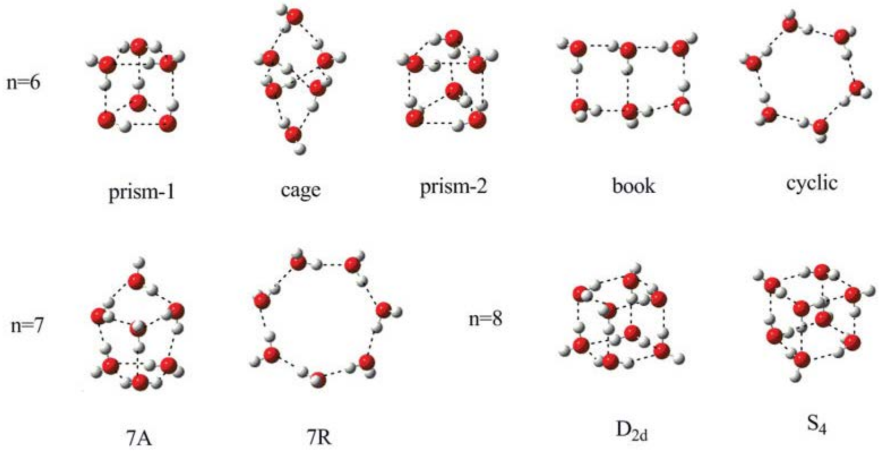

Fig. 1. Various types of low energy water clusters simulated. Adapted from [12]

Also, it is calculated that by average one H_2O molecule composes 3 hydrogen based bonds with other H_2O molecules [1]. Single cluster exists for 10^{-12}–10^{-9} seconds period by average [2]. It is a short duration, which depends on the electron moving rate around hydrogen nucleus and on rapid thermal vibrations [2]. But the formed bonds are quite strong, compared to the thermal energy (k_B*T) (k_B – Boltzmann constant) of water molecules. For example, under conditions of standard temperature and pressure, the strength energy of hydrogen bonding is 0.24 eV (i.e. 23.3 kJ/mol, [9]), while the thermal energy equals 0.023 eV, i.e. about 10 times less than hydrogen bond. Besides, under ambient conditions, water hydrogen bonding energy is still about 5 times greater than the average thermal collision fluctuation. When the cluster is broken, a new one is formed almost instantaneously. In 2006, Smith and co-workers wrote an article, based on a work about water cluster simulations [3]. They stated that hydrogen bonds between molecules break and re-establish so rapidly that all the liquid system can be considered as continuous network of hydrogen bonds. How could a hydrogen bond be connected with a condensation at water-vapor interface?

2.2. Water models

In order to define the behaviour of water molecules, the theoretical water models are composed and established [4]. They are operated under such conditions, when H_2O molecules are moving in liquid and in vapor, during the condensation or evaporation processes, or in other cases. Water models are used both for simplifying transitional processes calculations and making water structure view as close as possible to the physical reality (see Fig. 2). While creating the specific water model based on the needs, various parameters are related with a hypothetical molecule. It is done with a purpose to characterize a single H_2O molecule and to apply it for computational simulations between the groups of molecules. The parameters usually have an equivalent in physical reality, e.g. the length between bonds and their strength, the polarity of a molecule, attractive and repulsive forces with respect to other water molecules, the number of molecules, etc. The more precisely such a model predicts the physical properties of the material, the more precise structural view of the material is achieved. In fact, however, theoretical water models are not successful in recreating the real water properties, even though these models give some useful information about the behaviour of water [5], [11].

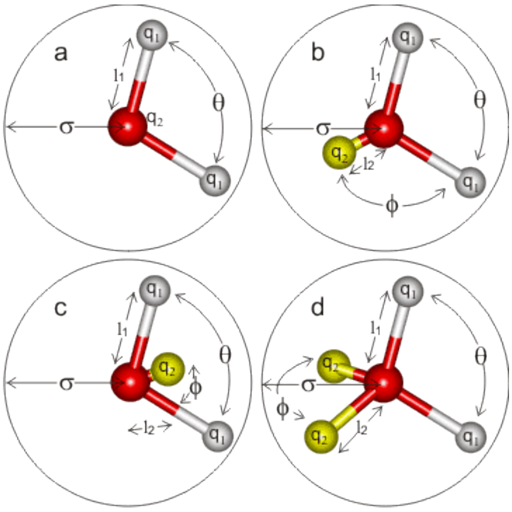

Fig 2. Various water molecular models [5]

2.3. Experimental observations

Water evaporation and condensation processes are being widely investigated for around a century, both creating theoretical models [4] and experimentally, for measuring the speed of processes. Marek & Straub [6] evaluated condensation coefficients used by various researchers in their experiments (see Fig. 3). The coefficients ranged by several orders of magnitude under the same pressure in different investigations. The errors may be neglected if results differed by few percents. In this case the blinking of the fact is inadequate. This presupposes an idea that the used condensations coefficients do not correspond to the physical reality. It may happen due to experimental results inaccuracy or due to misconstruction of assumptions done before the coefficients were accepted as the right ones.

At the beginning of the development of classical theory, based on Maxwell-Boltzmann distribution and applied to water, one of the logical assumptions were that the liquid water molecules can change into vapor phase, in a case when the average temperature of liquid molecules exceeded the average temperature of vapor molecules. However, the results in the experimental works of researchers Ward et al [7], and Badam et al [8] were contradicting to this theory. The temperature jumps across the water-vapor interface were detected both in cases of condensation and evaporation, while the temperature of vapor were higher than that of water surface by several degrees Celsius. And also, the same results were achieved under the special heating of vapor phase. In Badam et al experiment a lot of attention was paid to the improvement of measurements accuracy, so the results are reliable. Ward et al and Badam et al experiments support and strengthen the position that while solving the tasks of condensation, the coefficients used in the classical methodology are introduced because of the initial Maxwell-Boltzmann theory assumption for water is unsuitable.

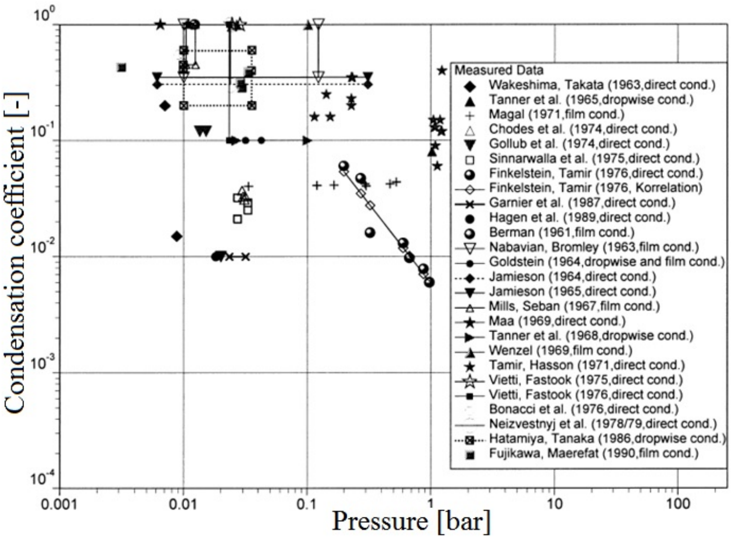

Fig. 3. Condensation coefficient of water as a function of pressure. Adapted from [6]

The fundamental of classical theory is that the event of H_2O molecule evaporation and condensation is caused by the interaction of two molecules. The theory is in good agreement with the experimental results, when the particles are assumed to be hard balls. The analytic techniques, used to measure the condensation fluxes and rates through the water-vapor interface, are often deduced from so-called Hertz-Knudsen-Schrage equation:

$$J = \left(\frac{2}{2-\alpha_e}\right)\sqrt{\frac{M}{2\pi R}}\cdot\left(\frac{\alpha_c \cdot P_{fi}}{\sqrt{T_{fi}}} - \frac{\alpha_e \cdot P_{gi}}{\sqrt{T_{gi}}}\right), \tag{1}$$

where J is the flux of condensation or evaporation; α_c and α_e are the condensation coefficient and evaporation coefficient; M is the molar mass of H_2O; R is the universal gas constant; P_{fi} and P_{gi} are pressures near interface from liquid side and from vapor side, respectively; T_{fi} and T_{gi} are the corresponding temperatures. Since the water molecule is strongly polar and quite non-spherical, and the molecules are tied by hydrogen-bond attractions, the analysis of water molecules as hard balls becomes complicated, and some correction factors must be set, in order to make results closer to the physical measurements. Under the development of calculations, the correction coefficients sometimes differ even though the experimental conditions are quite the same, as written by Marek & Straub [6]. The question arises, what theoretical model is appropriate for operating and rejecting the correction factors, or even reducing their influence in condensation rates calculations?

3. DISCUSSION

According to the comparison of intermolecular bonds strength vs water thermal energy amount, the assumption can be made: for a single H_2O molecule, in order to evaporate, the momentum impact of another single H_2O molecule is insufficient for breaking three hydrogen bonds. The moment, when a water molecule is not formed into hydrogen-bond based clusters, is very short and rare event. On the other part, the kinetic energy of water vapor molecule is usually lower than water surface tension forces. In order for a molecule to be inserted in between those bondings and to be condensed, there is possibly existing another mechanism than just two-molecules interaction. The verification of such hypothesis requires additional experiments shall be done.

4. CONCLUSIONS

Unique water physical properties are caused by intermolecular hydrogen bondings between H_2O molecules. The mentioned properties in turn make an influence for condensation processes.

The strength of hydrogen bond is about 10 times higher compared to the thermal energy of water under normal conditions.

The condensation of water vapor molecule cannot be caused by two molecules interaction event. The assumptions of classical Maxwell-Boltzmann distributions for water condensation are possibly incorrect.

REFERENCES

1. LENZ A., OJAMÄE L. Theoretical IR spectra for water clusters (H2O)n (n = 6-22, 28, 30) and identification of spectral contributions from different H-bond conformations in gaseous and liquid water. *J. Phys. Chem. A*, 110, (2006), p. 13388–13393.
2. LOWER S. A gentle introduction to water and its structure. Vancouver, Canada (2014) [referred on the 2nd of March, 2015 y]. Link to the internet <http://www.chem1.com/acad/sci/aboutwater.html>
3. SMITH J.D., CAPPA CH.D., WILSON K.R., COHEN R.C., GEISSLER P.L., SAYKALLY R.J. Unified description of temperature-dependent hydrogen bond rearrangements in liquid water. *Proceedings of the National Academy of Sciences* (2005).

4. WALLQVIST A., MOUNTAIN R.D. Molecular models of water: Derivation and description. *Reviews in Computational Chemistry* 13 (1999), p. 183–247.
5. CHAPLIN M. Water structure and science. London South Bank University, UK (2015) [Referred on the 2nd of March, 2015 y.]. Link to the internet <http://www1.lsbu.ac.uk/water/water_structure_science.html>
6. MAREK R., STRAUB J. Analysis of the evaporation coefficient and the condensation coefficient of water. *Int. J. Heat Mass Transfer* (2001). Vol. 44, p. 39–53.
7. WARD C. A., STANGA D. Interfacial conditions during evaporation or condensation of water. *Phys. Rev. E*, (2001), Vol. 64, p. 05159091-05159099.
8. BADAM V.K, KUMAR V., DURST F., DANOV K. “Experimental and theoretical investigation of interfacial temperature jumps during evaporation. *Experimental Thermal and Fluid Science*, (2007), Vol. 32, p. 276–292.
9. SURESH S.J., NAIK V.M. Hydrogen bond thermodynamic properties of water from dielectric constant data. *J. Chem. Phys.*, 2000, Vol. 113, p. 9727–9732.
10. CHAPLIN M. Theory vs Experiment: What is the Surface Charge of Water? *Water Journal* (2009), Vol. 1, p. 1–28.
11. GUILLOT B. A reappraisal of what we have learnt during three decades of computer simulations on water, *Journal of Molecular Liquids* (2002) Vol. 101, p. 219–260.
12. QIAN P., SONG W., LU L., YANG Z. Ab Initio Investigation of Water Clusters $(H_2O)_n$ ($n = 2$–34). *International Journal of Quantum Chemistry*, 2009, Vol. 110, No 10, p. 1923–1937.

EXPERIMENTAL STAND DEVICE MODELING FOR IEAC THERMAL PERFORMANCE STUDY

G. Frīdenbergs, **A. Lešinskis**
Riga Technical University
Azenes str. 16/2nd floor, LV-1010 – Latvia
Phone +371 26875297
Email: guntars@eigers.lv

ABSTRACT

This paper reported a review, calculations and measurements based study into Indirect Evaporative Cooling (IEC) stand device parts which have influence on thermal performance, which was undertaken from a variety of aspects including background, history, current status, and concept. Experimental stand device parts have been described as equations of heat and mass transfer in primary and secondary air and water flows. Model has been validated with self-made device measurements located in laboratory. The main goal have been to made working stand device for future researches of IEAC (Indirect Evaporative Air Cooling) device cooling efficiency, which mostly depends on mass flow rates ratios of primary and secondary air flows and spacing between plates of wet and dry passages.

Keywords: IEAC stand device, indirect evaporative air cooler, cooling efficiency, heat and mass transfer from water to air through thin wall

1. INTRODUCTION

To determine the parameters experimental stand device was studied (Fig. 1). The two main discovered parameters influencing on cooling performace are water consumption and water exchange cycle [1].

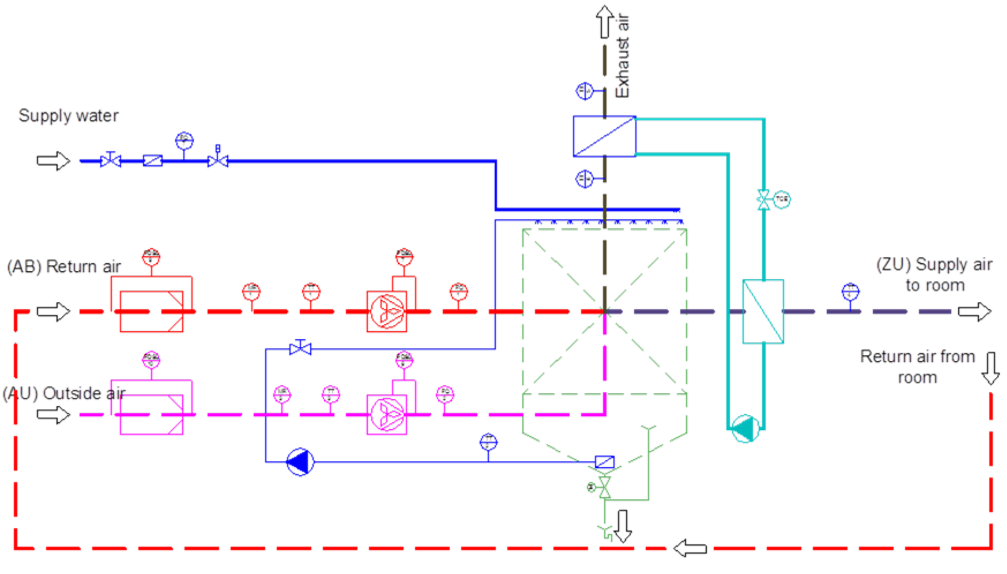

Fig. 1. Practical model of studied device [2]

1. The water consumption of evaporative air conditioners includes the water evaporated to provide the cooling effect.

2. Water exchange cycle – is water dumped off with predicted period of time for the purpose of cleaning and avoiding high salt concentration.

The aim of this paper is to clarify the interaction between the indoor humidity and the thermal performance of an indirect evaporative cooling system where the return air is used as secondary air [4–6].

So far no research was found on the interaction between the thermal performance of an indirect evaporative cooling system and the building moisture balance. In this paper firstly an integrated simulation approach is given. The necessary parameters to the model are defined by means of measurements. Next, the potential of IEC-systems to improve the thermal comfort in a typical application in Latvia region is investigated using dynamic simulations with MS Excel made simulation tool.

2. WATER EVAPORATION

The psychrometric chart in Fig. 2 illustrates the evaporation process (blue line) when air passes through the wet side of indirect evaporative air conditioner. At given entry air conditions (t_1, t') and evaporation effectiveness (ε_e), the dry-bulb temperature of the leaving air (t_2) can be calculated according the Eq. 1. In ideal conditions the wet-bulb temperature of the leaving air is the same as the wet-bulb temperature of the entering air. Then the humidity ratios of both entering and leaving air can be determined from the psychrometric chart (Fig. 1). The water consumption rate for cooling purpose can be estimated using Eq. 2 [3, 4, 5].

$$t_2 = t_1 - \frac{\varepsilon_e}{100} \times (t_1 - t'), \tag{1}$$

$$\dot{m}_e = \rho \dot{V} (w_2 - w_1) / 1000. \tag{2}$$

Where

$\dot{m}_e$ – water consumption rate, kg/h;

$\dot{V}$ – air volumetric flow rate, m^3/h;

ρ – air density, 1.2041 kg/m^3;

w_1, w_2 – humidity ratios of entering and leaving air, g moisture/kg dry air.

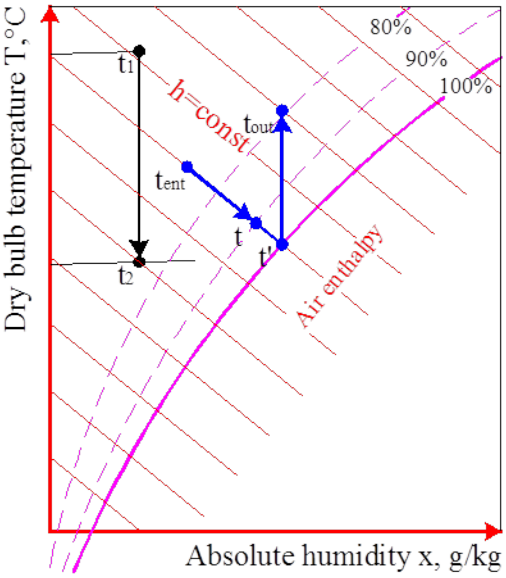

Fig. 2. Psychrometrics of two-stage evaporative cooler [2]

The water consumption rate due to evaporation varies depending on the air flow rate, the temperature and humidity of the outside air and the pad characteristics. Some manufacturers quote indicative figures for water consumption but these can only be used as approximate values. In an effort to provide independent values of the water required for evaporation, the water consumption rates for cooling purposes can be calculated in different locations. The design temperature and humidity can be based on typical historical data and be used to represent the maximum cooling conditions [6].

Furthermore, the amount of water consumption for cooling purpose has been calculated based on hourly weather conditions in a typical hot day and a typical summer day from one available climate data source in Riga, Latvia: (Table 1) data supplied by METEO [6]. It is assumed that cooling to be switched on at full speed during hours when the outside temperature exceeds 27 ^{o}C and represents the maximum water consumption on those days in the calculation. The total water consumption and the average consumption rate of the typical summer day are shown in Table 1.

Table 1. Evaporated water consumption in typical days in Riga

Location	Period requires cooling	Total daily water consumption (L/day) for random various air flow rates		Average hourly water consumption rate (L/hr) for random various air flow rates	
		9360(m^3/h)	16200(m^3/h)	9360(m^3/h)	16200(m^3/h)
Riga typical summer day	10:00am~19:00pm	481.5	833.3	48.1	83.3
	11:00am~20:00pm	538.8	932.5	53.9	93.3

The water consumption rate for cooling purposes is dependent on the humidity ratio difference of the entering and leaving air and the air flow rate. The sizes selected in Table 1 are based on maximum cooling requirements on the hottest part of the day. Typically, the fan utilised in residential evaporative air conditioners has a variable speed and runs on low speeds for the majority of operating time. The evaporated water consumption in Table 1 was calculated based on the maximum fan speed, thus it should be considered as overestimates.

3. SIMULATION SCHEME

The cell element selected for numerical analyses (Fig. 3) is shown in Fig. 4. The element consists of half the height of the dry channel, the plate wall and half the height of the wet channel. Energy balance equations were applied to each single element, with consideration of a pre-set boundary condition. This allowed the temperature and humidity distribution across the dry and wet channel sections to be established.

To simplify the modelling process and mathematical analysis, the following assumptions were made:

1. The heat and mass transfer is in steady state. The IEAC enclosure is considered as the system boundary.

2. The wet surface of the fibre-sheet is completely saturated. The water vapour is distributed uniformly within the wet channel.

3. A temperature gradient for the channel cross-section was set to zero. Heat transfer in the separating plate is considered in the vertical direction only. Within the working fluid, the cross-stream convective heat transfer is considered as the dominant mechanism of heat transfer.

4. Each element has a uniform wall surface temperature. An analysis carried out by Zhao et al. showed that the thermal conductivity of the plate wall has a little impact on the magnitude of the heat and mass transfer rates, due to its small thickness (0.24 mm). The temperature difference between dry and wet sides of the wall can be ignored [8].

5. Air is treated as an incompressible gas.

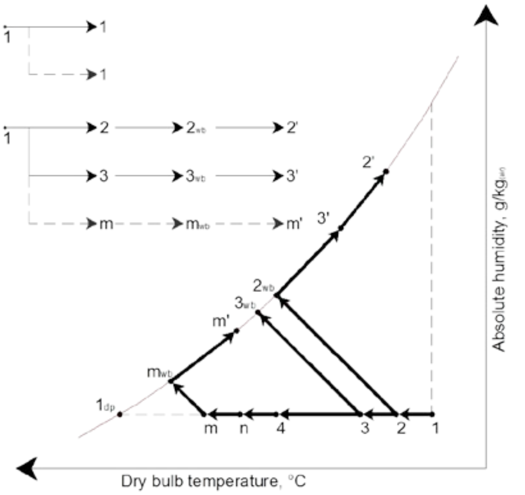

Fig. 3. Selected IEAC cooler operation cycle in H-x diagram [2]

The mass balance in the wet channel can be expressed by Eq. 3:

$$\left(\frac{m_{a,f2}}{2}\right) dw_{a,f2} = h_m\left(\rho_{w,a2} + \rho_{a,f2}\right), \tag{3}$$

where

$m_{a,f2}$ – air mass flow rate, kg/s,
$w_{a,f2}$ – humidity ratio of moist air, kg/kg dry air,
h_m – mass transfer coefficient, m/s,
ρ – density, kg/m^3.

The general energy balance within the element in Fig. 4 can be expressed as Eq. 4:

$$dQ_1 = dQ_1 + dQ_2, \tag{4}$$

where

Q – heat flux, W/m^2.

The energy balance in dry passages – dry passage air involves the forced convective heat transfer, leading to change of the enthalpy of the air. Energy balance in a dry passage could be written as Eq. 5:

$$dQ_1 = h_1\left(t_{a,f1} + t_w\right)dA = \left(\frac{m_{a,f1}}{2}\right) di_{a,f1}. \tag{5}$$

Where

A – heat transfer area, m^2
h – specific enthalpy of air, J/kg.

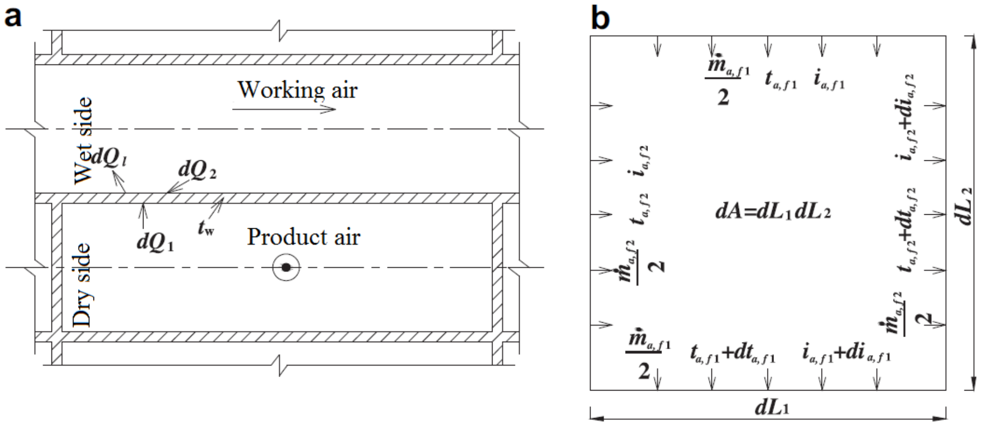

Fig. 4. Cell element (a) applied for numerical simulation, differential illustration (b)

The energy balance in wet passages – wet passage air involves the forced heat and mass exchange, which leads to a change of enthalpy of the air within the passages. The energy balance within the passages can be written as Eq. 6:

$$dQ_1 - dQ_2 = \left(\frac{m_{a,f2}}{2}\right) dw_{a,f2}, \tag{6}$$

where, for the forced convective heat and mass transfer occurring in the wet passages respective Eq. 7 and Eq. 8 can be written

$$dQ_2 = h_2\left(t_{a,f2} + t_w\right) dA, \tag{7}$$

$$dQ_1 = \left(\rho_{w,a2} + \rho_{a,f2}\right) \gamma dA, \tag{8}$$

The air flow within the pipes remains in a laminar flow state when $Re_D < 2300$ and becomes turbulent flow when $Re_D > 4000$. Due to the passage size and air velocity, the air flow within the passage is considered to be laminar. In this case, the thermal entry length for laminar flow can be calculated as follows (Eq. 9):

$$\frac{L}{d} = 0.05 Re \cdot Pr. \tag{9}$$

For both entry region and fully developed flow conditions, the Nusselt number can be calculated using the following Eq. 10:

$$Nu = 1.86 \left(\frac{Re \times Pr}{\frac{L}{d}}\right)^{1/3} \left(\frac{\eta_{a,f}}{\eta_{w,a}}\right)^{0.14}. \tag{10}$$

The thermal entrance Nusselt numbers are higher than those for the fully developed case. For the developing flow conditions in the entry region, the Nusselt number can be calculated as presented below by Eq. 11 [8]:

$$Nu = 3.66 + \frac{0.0688 \cdot Re \cdot \Pr\left(\frac{d}{L}\right)}{1 + 0.04\left[Re \cdot \Pr\left(\frac{d}{L}\right)\right]^{2/3}}. \tag{11}$$

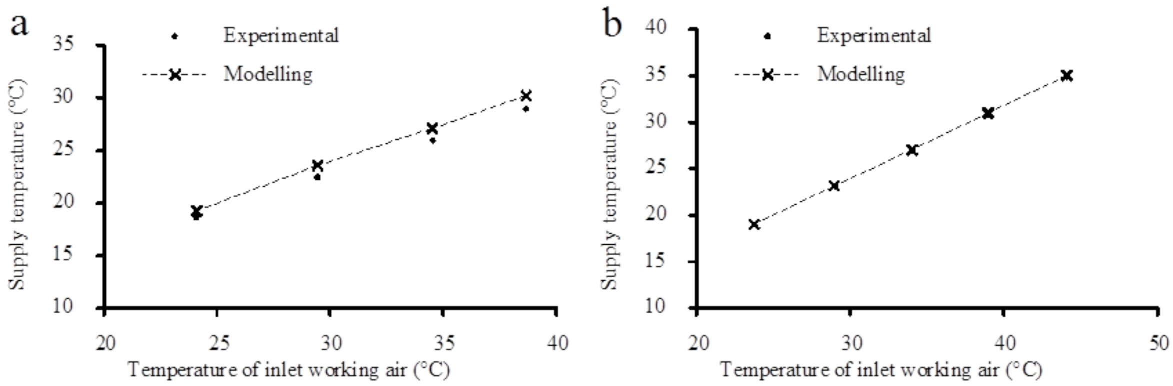

Fig. 5. Experimental validation of supply air temperature. (a) Case 1. (b) Case 2 [8]

Case 1 and Case 2 was modelled at constant air flow rate 150 m^3/h (to compare with C. Zhan past calculations) and dry bulb 25 till 40 °C. In Case 1 RH=35%, in Case RH=50%, that is main difference.

The mass transfer coefficient between wet passage air flow and the wet surface of the wall may be calculated using the following 12 equation:

$$\frac{h}{h_m} = \rho c_p Le^{2/3}. \tag{12}$$

The mathematical expression for wet-bulb effectiveness ε_{wb} can be written as follows (Eq. 13):

$$\varepsilon_{wb} = \frac{t_{db,wk,in} - t_{db,su}}{t_{db,wk,in} - t_{wb,wk,in}}. \tag{13}$$

The theoretical energy efficiency coefficient of performance (COP) of the system can be defined as the ratio of cooling capacity and fan power consumption:

$$COP = \frac{\Phi_0}{P}. \tag{14}$$

Cooling capacity (Φ_0) can be expressed as Eq. 15:

$$\Phi_0 = m_{pt}\left(i_{wk,in} - i_{wkpt,in}\right). \tag{15}$$

Where

m_{pt} – product air mass flow rate, kg/s,
$i_{wk,in}$ - specific enthalpy of inlet working air, J/kg,
i_{pt} – product air enthalpy, J/kg.

The theoretical fan power (P), can be written as Eq. 16:

$$P = \Delta p_{wk} V_{wk} + \Delta p_{pt} V_{pt}. \tag{16}$$

Where

Δp_{wk} – working air pressure loss, Pa,
V_{wk} – working air flow rate, m^3/s,
Δp_{pt} – product air pressure loss, Pa,
V_{pt} – product air flow rate, m^3/s.

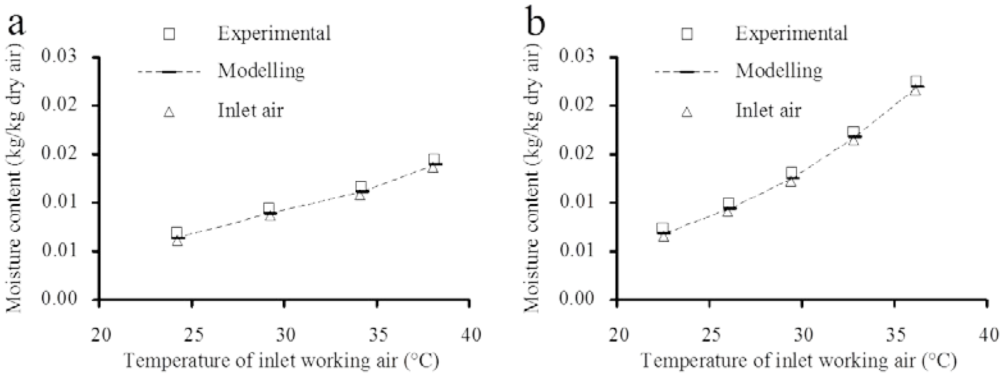

Fig. 6. Experimental validation of supply air moisture content in case 1 (a) and case 2 (b) [8]

It should be emphasized that the energy efficiency obtained from the simulation is an ideal value, which involves use of the theoretical fan power. Actual fan power will be 120–170 % of the ideal value, leading to a drop in the calculated efficiency by 60–80 %. It should be noted that in this paper all the subsequent Figures related to COP are 'ideal' rather than 'practical' values.

4. RESULTS

The result of the calculation is determined temperature distribution of the heat exchanger plates, which then will explore the heat transfer across the heat exchanger volume, as well as allow for the calculation of geometrical effects on the final parameters. Below (Fig. 5) there are presented three parameters calculation visualization graphs. The more accurate data needed for further research.

For this operating condition, the temperature profiles of dry, wet air and the exchanging wall are presented in Fig. 5 a, b, c, the heat flux in Fig. 5 a, b, c, it can be seen that the temperature of supply air in dry channels decreases along its direction of flow, and the temperature of working air in the dry channels.

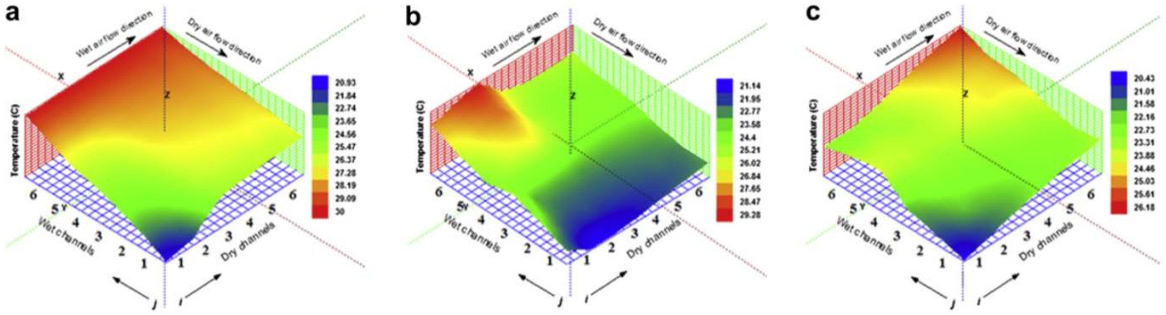

Fig. 5. Temperature distribution across the heat exchanger plate dry side (dry passages) (a), wet side (wet passages) (b) and wall (c)

As shown in Fig. 6 a, the convective heat transfer decreases along the flow path of dry air as a result of the observed (see Fig. 6 a and c) decrease in the temperature difference between the dry channel air and the wall. The heat transfer rate in dry channels is higher if they have bigger air mass flow rates [16–21]. Referring to Fig. 6 b, the wet air is not initially saturated and has a higher temperature than the wet wall close to the entrance of the wet channels (comparison of Fig. 5 b and c). These results in heat being transferred to the water reserved on the wet side of the wall leading to the evaporation of the water. After travelling to a critical point, the temperature of wet air is lower than that of the wet wall, so the convective heat flux has become negative (as shown in Fig. 6 b), this means that the wet air picks up both sensible and latent heat from the wall.

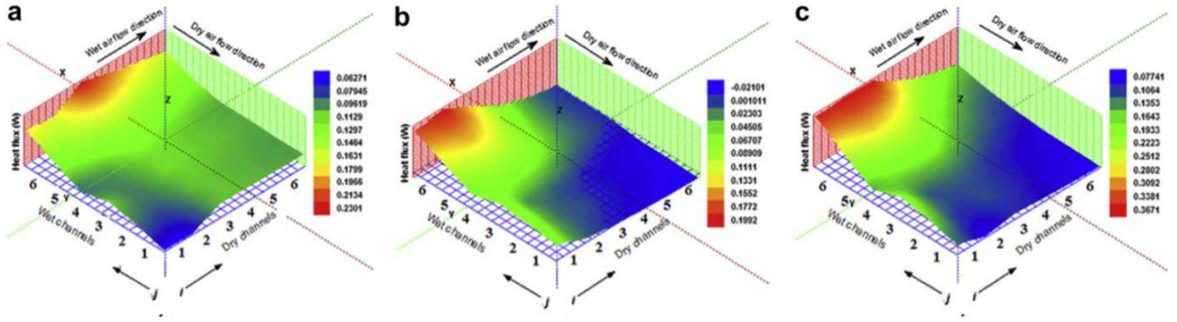

Fig. 6. Heat transfer rate across the heat exchanging plate dry (a),
wet (b) side and on the wall (c)

The supply air temperature and the return air temperature just behind the first part of the heat exchanger were in good agreement with the measured data. The model underestimated the temperature of the exhaust air because it does not take into account the fact that the return air is heated by the recirculated water in the second part of the heat exchanger (Fig. 7).

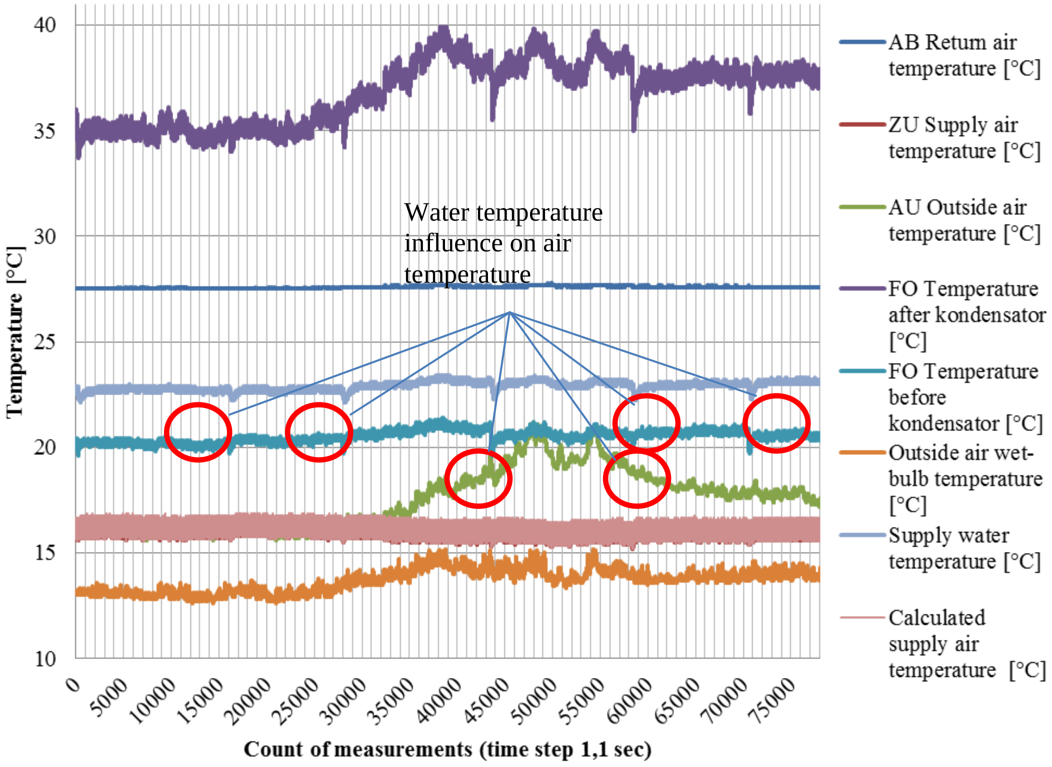

Fig. 7. The observed and calculated water temperature fluctations on IEAC heat exchanger

5. CONCLUSIONS

Comparing the two major components of water usage in evaporative air conditioners (water used for the cooling effect and water dumped/bled off), it may be concluded that if the water bleeding/dumping system is well designed, set and maintained, the total water consumption will be largely dominated by the moisture evaporation which is essential in operating the evaporative cooler. However, if not properly adjusted, the water bleeding/dumping rate is of the same order of magnitude as the evaporation rate and can lead to considerable wastage of valuable water.

An integrated simulation methodology of the building with its indirect evaporative cooling installation is necessary in order to take into account both heat and mass balance in building calculations. It is concluded that for future researches is not important to make calculations because of multiple available publications. In this way it is possible to study the interaction between the thermal performance of an indirect evaporative cooling system and the moisture balance of a room. The IEC-effectiveness was studied using measurements in an Air Handling Unit containing an indirect evaporative cooling system.

As new aspect in literature is found that the thermal effectiveness is independent of the inlet conditions of the outdoor and return air. It is important for future researches.

REFERENCES

1. SUPPLE, R.G., BROUGHTON, D.R. *“Indirect evaporative cooling – Mechanical cooling design”*, ASHRAE Transactions, Vol. 91, Part 1B – 1985. – p. 319–328.
2. FRĪDENBERGS, G., LEŠINSKIS, A. *Evaluation of indirect evaporative cooler in public buildings*, RTU, 2012 – p. 6–48.
3. FRĪDENBERGS, G., BRAHMANIS, A., LEŠINSKIS, A., Experimental device modeling for IEAC thermal performance study, RTU, Roomvent 2014, Sao-Paulo, Brazil, 2014 – p. 359–364.
4. HASAN A., SIREN, K. Theoretical and computational analysis of closed wet cooling-towers and its applications in cooling of buildings. *Energy and Building*s – 2002 – p. 34.
5. KALS, W.A. *Wet-surfaces air coolers*, Chemical Engineering – 1971. – p. 68.
6. Zhiyin, D., CHANGHONG, Z., ZHAN, C., RIFFAT, S.B. Indirect evaporative cooling: Past, present and future potentials, *Renewable and sustainable energy reviews* – 2012. – p. 1–28.
7. Latvijas Metroloģijas centra data base [referred on the 3th of January in 2012 y.]. <www.meteo.lv/pdf_base/meteor_2009.html>
8. ZHAO, X., DUAN, Z., ZHAN, C., RIFFAT, S.B. Dynamic performance of a novel dew point air conditioning system for the UK climate. *International Journal of Low Carbon Technology* 2009.
9. HALASZ, B.A general mathematical model of evaporative cooling devices, *Rev. Gén. Therm.*, FR, Vol. 37 – 1998. – p. 245–255.
10. COSTELLOE, B., FINN, D. Indirect evaporative cooling potential in air e water systems in temperate climates. *Energy and Buildings*, 2003.
11. SETHI, V.P, SHARMA, S.K. Survey of cooling technologies for worldwide agricultural greenhouse applications. *Solar Energy*, 2007.
12. CERCI, Y. A new ideal evaporative freezing cycle. *International Journal of Heat and Mass Transfer* 2003 – p. 1–11.
13. PARKER, R.O., TREYBAL, R.E. *The heat-and-mass transfer characteristics of evaporative coolers*, Chemical Engineering Progress Symposium Series – 1961 – p. 57.
14. PETERSON, J.L. *An effectiveness model for indirect evaporative coolers*, ASHRAE Transactions – 1993. – p. 99.

15. CIBSE KNOWLEDGE SERIES: *sustainable low energy cooling: an overview*. Plymouth PL6 7PY, UK: Latimer Trend & Co. Ltd, 2005.
16. STABAAT, P., MARCHIO, D. Simplified model for indirect-contact evaporative cooling-tower behaviour, *Applied Energy* 78 (2004), - 2003 – p. 433–451.
17. MACLAINE-CROSS, I.L., BANKS, P.J. A general theory of wet surface heat exchangers and its application to regenerative evaporative cooling, *Journal of Heat Transfer*, Vol.103, No. 3, – 1981 – p. 579–585.
18. MCCLELLAN, C. H. Estimated temperature performance for evaporative cooling systems in five locations in the United States, *ASHRAE Transactions*, 94 (2), – 1988. – p. 1071–1090.
19. MIZUSHINA RIT., MIYASHITA H. Characteristics and methods of thermal design of evaporative coolers, *International Chemical Engineering* – 1968 – p. 3–8.
20. MIZUSHINA RIT, MIYASHITA H. Experimental study of an evaporative cooler, *International Chemical Engineering* 1967. – p. 4–7.
21. NIITSU Y., NAITO K., ANZAI T. Studies on characteristics and design procedure of evaporative coolers, *Journal of SHASE*, Japan – 1969. – No.7 – p. 12–23.
22. SCHIBUOLA, L. High-efficiency recovery for air-conditioning applications in a mild climate: a case study, *Applied Thermal Engineering*, Vol. 17, No. 5 – 1997. – p. 447–454.
23. Rīga’s municipal government’s corporation “Rīgas Ūdens” data base [referred on the 4th of April in 2013 y.].
    < https://www.rigasudens.lv/par-uznemumu/vesture/>

CYSENI 2015, May 27–28, Kaunas, Lithuania
ISSN 1822-7554, www.cyseni.com

NUMERICAL STUDY OF TIME DEPENDENT BLOOD FLOW IN OPHTHALMIC ARTERY WITH APPLIED EXTERNAL PRESSURE

E. Misiulis, A. Džiugys
Lithuanian Energy Institute
Laboratory of Combustion Processes
Breslaujos str. 3, LT-44403 Kaunas – Lithuania
Phone +37060377878
Email: Edgaras.Misiulis@lei.lt

ABSTRACT

Fast and accurate measurement of intracranial pressure (ICP) is crucial after a brain trauma or stroke. These aforementioned situations are one of the leading causes of disability and death. Too high or too low ICP could cause severe brain damage and even can result in death. One way of ICP estimation is new non-invasive Two Depth Transcranial Doppler (TDTD) method, which is based on measurement of blood flow velocity in ophthalmic artery (OA). This method had already been certified in many countries such as USA, Japan and EU. The further device improvement is an increase in precision and extension of capabilities and applicability require fundamental understanding about pulsatile blood flow in the elastic OA and its interaction with the surrounding tissues when the outer wall of OA is exposed to varying pressure. Commercial COMSOL module Fluid-Structure Interaction (FSI) was used numerically to simulate arteries system, which consisted of Internal Carotid Artery (ICA) and OA. External Pressure (Pe) was applied as a function of time Pe(t) (range: [0, 40] mmHg) on OA's Extra Cranial (EC) part while ICP on OA's Intra-Cranial (IC) part was being held constant at {10, 15, 25, 35} mmHg. Simulations proved the possibility to measure ICP through differences in blood velocity on OA's IC and EC parts.

Keywords: hemodynamics, fluid-structure interaction, intracranial pressure, ophthalmic artery

1. INTRODUCTION

ICP – is a pressure inside human skull and thus in the brain tissue and cerebrospinal fluid (CSF). For a healthy patient in a supine position ICP is in a normal range from 7 to 15 mmHg [1]. In an event of traumatic brain injury (TBI) this pressure could reach higher or lower values [2]. This pressure deviation is a sign of compensatory autoregulation mechanism saturation [3] and could be the cause of disability or even can result in death. That is why knowing ICP is crucial.

Human skull, once the sutures and fontanelles have closed, becomes a structure that permits no further expansion. It's inside volume becomes constant and depends little on applied pressure [3]. Constant volume and different constituents: arterial blood, vein blood, cerebrospinal fluid (CSF)and brain tissue, give rise to ICP. Up to certain limits this pressure is autoregulated – if one of the constituent's volume increases, the other's decreases [4].

ICP measurement can be done in two different ways – invasive and non-invasive. When applying invasive method, a sensor of ICP is sticked in the patient head or in the back through physically drilled hole to reach brain tissue, or ventricle. This kind of method is slow, it is very hard to implement and also expensive. There is a risk of complications, for example, during surgery an infection could spread in the brain. Also these monitorings cannot be performed in the outdoor conditions.

Non-invasive absolute ICP (aICP) measurement is carried out by putting a special mask on the patients head. This mask is equipped with two depth Doppler ultrasound device. It surrounds eyeball and external pressure (Pe) could be applied on the outer skull segment of the ophthalmic artery (OA). Using two depth transcranial Doppler Ultrasound (TDTD) technique, velocities of the inner and outer segments of OA are measured. At any given moment blood flow rate in different segments is equal, but mean velocity differs, as it depends on the lumen diameter. That is why mean velocity could provide an information about ICP, as if there is no difference then following equation should be true: $ICP = Pe + \Delta P$, where ΔP is the normal vasculature pressure drop.

Today, numerical modeling method is being widely used and adopted for investigation on human vasculature, causes and process of disease, and the treatment options [5], [6].

Currently in Lithuania research on new non-invasive intracranial pressure measuring device is being conducted by [7] and [8]. Device working principle is based on the change in ophthalmic artery blood flow properties. For the further device improvement it is necessary to conduct not only experimental but also numerical research. Tekorius (2002) [9] performed a numerical investigation on simplified mathematical model, for the assessment of the direct and reverse blood flow in a blood vessel. Ragauskas et al. (2005) published a scientific article on “Innovative non-invasive method for absolute intracranial pressure measurement without calibration” [10]. This kind of ICP measuring device is unique in the world and has been patented.

Non-invasive intracranial pressure determination technique uses ophthalmic artery as the main sensor. For that reason it is necessary to know how changing internal and external parameters, for different patients, influences obtained results. In vivo determination of parameter influence is complicated and not always possible. It is possible to do any kind of parameter influence test using numerical modeling approach and there is no need for patients. It is a cheaper and faster method. This method could also be used for wide parameter range investigation.

The objective of this work is theoretical analysis of the properties of pulsatile blood flow in the OA by means of computational fluid dynamics at different pressures of cerebral fluid and the eye socket pressures, including different measurement conditions influencing the measurement accuracy.

2. METHODOLOGY

Numerical modelling was performed using COMSOL. This commercial software uses finite element method (FEM). Time-dependent study of blood flow in internal carotid (ICA) and OA was performed. Model geometry is shown in (Fig. 1).

Fig. 1. Model geometry in a plane

$l_{ICA_{s1}}$ corresponds to the ICA's inlet. $l_{ICA_{s3}}$ – distance from $l_{ICA_{s1}}$ to OA symmetry axis, this distance corresponds to artery's bifurcation and is equal to 0.1372 m. All of the ICA length is $l_{ICA_{s4}} = 0.148$ m. Starting diameter of ICA is $d_{s1} = 0.0056$ m. After length $l_{ICA_{s3}}$ it is 0.0049 m. From point s_1 diameter changes by given formula:

$$d(l_{ICA}) = \begin{cases} -0.0051433 \cdot l_{ICA} + d_{s1} & when\ l_{ICA} \leq l_{ICA_{s3}} \\ -0.1092437 \cdot (l_{ICA} - l_{ICA_{s3}}) + d_{s2} & when\ l_{ICA} > l_{ICA_{s3}} \end{cases} \tag{1}$$

Ophthalmic artery diameter d_{OA} was 0.00145 m, length 0.026 m. Ophthalmic artery was segmented in 3 different parts. From $l_{OA_{s1}}$ to $l_{OA_{s2}}$ was an internal part of OA. From $l_{OA_{s2}}$ to $l_{OA_{s3}}$ OA‘s segment that goes through the bone. From $l_{OA_{s3}}$ to $l_{OA_{s4}}$ external part of OA. Arteries lumen wall thickness was it‘s lumen diameter divided by 5.

2.1 Numerical model physics

Blood was modelled as a Newtonian fluid, it's dynamic viscosity was held constant 0.003675 kg/(m*s) [11]. It is a fairly good approximation for a blood flow in a relatively big arteries lumen diameter greater than 0.1 mm [11]. Period of the heartbeat or pressure wave was 0.917 s [12]. Systolic and diastolic pressures, P_{sys} and P_{dias} respectively, in internal carotid artery were taken as of a normal subject 120/80 mmHg.

Artery vessel walls exhibit viscoelastic behaviour [13]. Although simpler hyperelastic model was used [14].

Deformable, time-dependent systems are exposed to mechanical vibrations. In real world these mechanical vibrations are dissipated through heat or through mechanical energy transfer. In current model energy dissipation through heat can be neglected and only mechanical energy losses should be taken into account. For isotropic medium a constant of isotropical losses could be described. As of practical point of view it is accepted that value of 0.1 gives good results.

As shown in a (Fig. 2) 1–5 numbers mark boundaries that are immovable. 2, 4 boundaries mark places were arteries goes through skull bone. The ends of arteries are immovable because in a in vivo situation there is tissues that holds it, in this case as there is no enveloping tissue to have stability one has to prescribe immovable boundaries. The enveloping tissue influence could be prescribed in arteries tissue parameters by changing their value to fit experimental results.

2.2 Boundary conditions

1, 3, 5 numbers mark boundaries were different pressures were applied: *P_ICA_in*, *P_ICA_out*, *P_OA_out* respectively. Also displacement is set to be zero there.

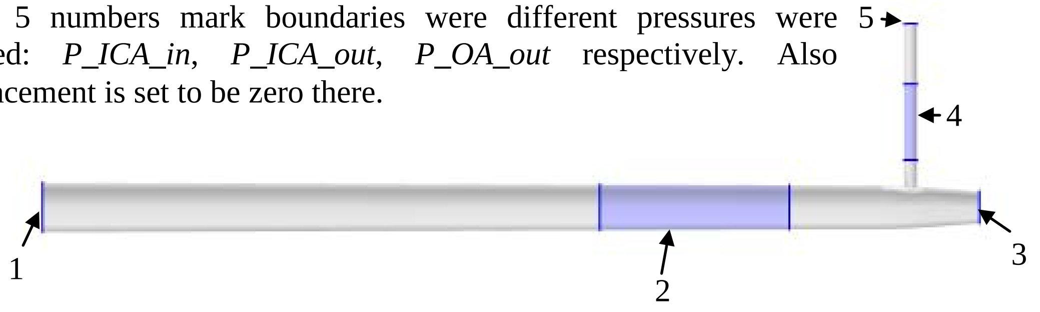

6, 7 numbers mark boundaries were different pressures were applied: *6 - ICP(t)* and 7 - *Pe(t).*

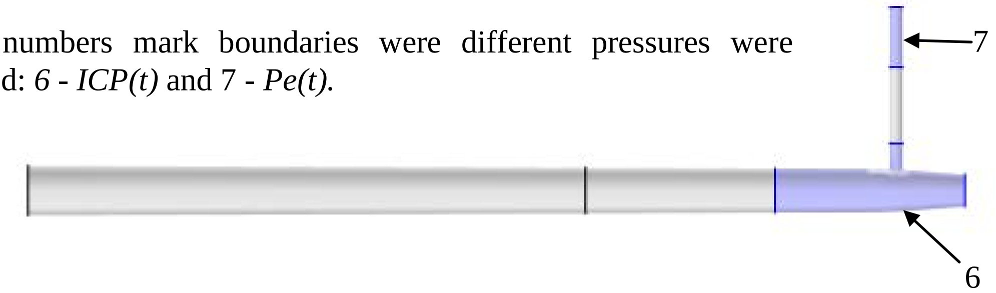

Fig. 2. Boundary conditions

Mathematically blood pressure wave was described as:

$$p(t) = A \cdot \begin{cases} s_f(t, T, t_{top}) & when\; t < T + t_{top} \\ a + b \cdot f_{cw}(t, T, t_{top}, c, d) & when\; t \geq T + t_{top}, \end{cases} \tag{2}$$

where A – is pressure amplitude, a - $\frac{P_{dias}}{P_{sys}}$, b - $1 - \frac{P_{dias}}{P_{sys}}$, c and d – parameters that change pressure function profile.

Numerical model that experience rapid change in variable values could become unstable. To counter this, a smooth function was implemented for pressure build up:

$$s_f(t) = \sin\left(\frac{\pi t}{2 \cdot (T + t_{top})}\right), \tag{3}$$

where T – pulse period, t_{top} – time of maximum pressure from the beginning of a period.

A twofold function for inlet laminar inflow pressure boundary condition mathematically was prescribed as:

$$f_{cw}(t) = \frac{1}{2} \cdot \begin{cases} 1 - \cos\left(\frac{\pi \cdot mod(t,T)}{T_{top}}\right) & mod(t,T) \leq T_{top} \\ \left(\frac{1}{2} + \frac{1}{2} \cdot \cos\left(\frac{\pi(mod(t,T) - T_{top})}{T - T_{top}}\right)\right)^c + \left(1 - \frac{mod(t,T) - T_{top}}{T - T_{top}}\right)^d & mod(t,T) > T_{top} \end{cases} \tag{4}$$

Example of $p(t)$ function (2):

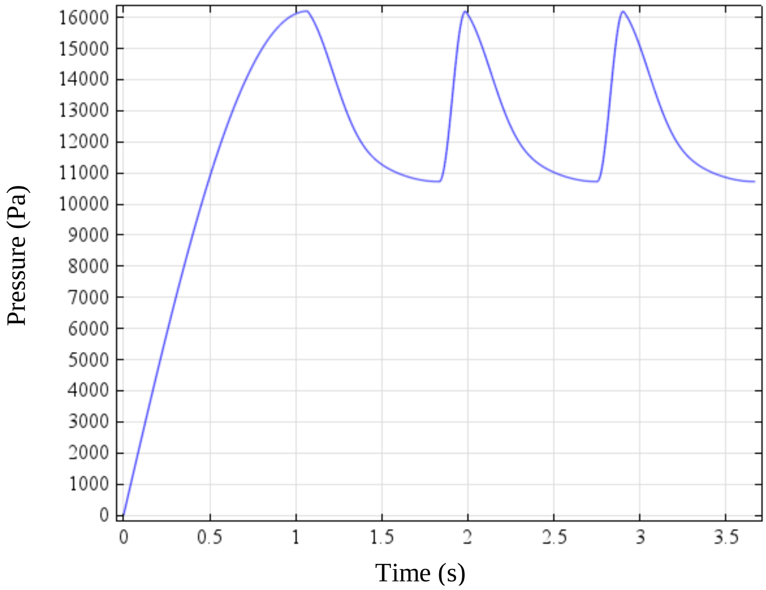

Fig. 3. Example of twofold inlet laminar inflow pressure boundary condition function

Functions for changing ICP and *Pe* could be seen in (Fig. 4). Every uneven period is for a slow pressure build up phase in an arterial system. Vice versa for constant ICP and *Pe* pressures.

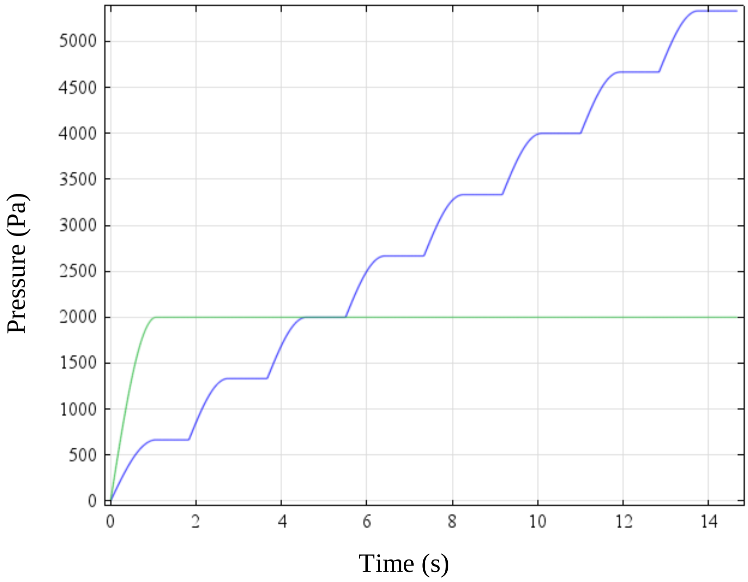

Fig. 4. Example of external pressures applied on different OA segments. ICP depicted as a green curve and *Pe* as a blue curve

Table 1. Calculated flow rates using Hagen-Poiseuille law

	Flow rate (m^3/s)		
	Systolic	Diastolic	Mean
ICA inlet	$1.08 \cdot 10^{-5}$	$3.00 \cdot 10^{-6}$	$5.00 \cdot 10^{-6}$
ICA outlet	$1.04 \cdot 10^{-5}$	$2.86 \cdot 10^{-6}$	$4.82 \cdot 10^{-6}$
OA outlet	$4.17 \cdot 10^{-7}$	$1.39 \cdot 10^{-7}$	$1.80 \cdot 10^{-7}$

ICA inlet pressure was prescribed using equation (2). Outlet had laminar outflow boundary condition with constant pressure and constant exit length.

Table 2. Inlet and outlet boundary conditions

	Pressure (Pa)		Inflow/Outflow length (m)
	Systolic	Diastolic	
ICA inlet	Prescribed by equation (2)		0.121
ICA outlet	8 645	8 645	0.760
OA outlet	8 029	8 029	0.540

2.3 Calculation

COMSOL program decides what time step it should take to meet relative and absolute error to 0.1. Mesh had 97831 elements, from which 74058 was for blood domain and the others for artery wall domain. The mean element quality was 0.639. Maximum size of an element was 2.25 mm, minimum 0.0783 mm. Part of the mesh, where OA bifurcation takes place, can be seen in (Fig. 5).

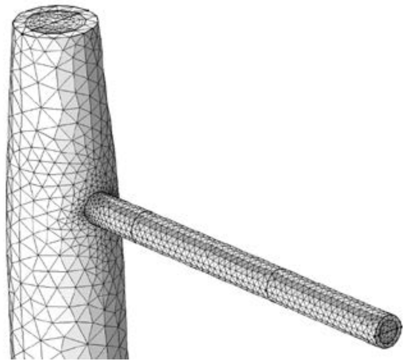

Fig. 5. Part of the ICA-OA model mesh, where OA bifurcates from ICA

3. RESULTS

The results from pressure build up phase was neglected in the analysis. Flow rates, seen in (Fig. 6), corresponded well with in vivo values from literature [15].

In literature, the flow rates obtained from in vivo ultrasonography measurements are given only extreme values, as also in this work.

Relation $ICP = Pe + \Delta P$ was estimated. The cross-sectional area at different parts of the OA: IC and EC dependence on applied pressure was plotted in (Fig. 7).

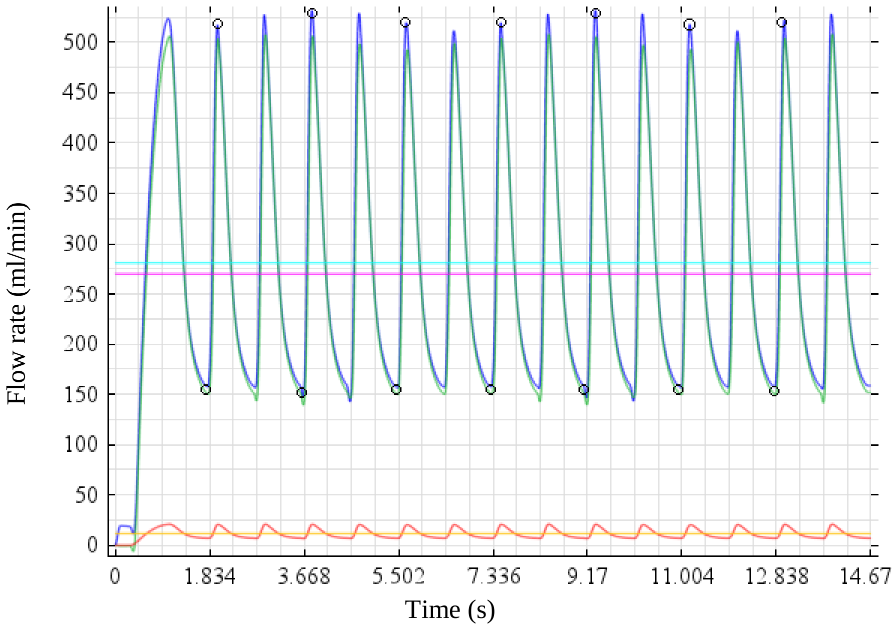

Fig. 6. Blood flow rate dynamics: blue curve corresponds to ICA inlet blood flow rate; green curve to blood outflow rate of ICA; red curve corresponds to blood outflow rate from OA. Lines corresponds to mean blood flow rate integrated over period (T_{blood}), colours: cyan corresponds to inflow of ICA; magenta to outflow of ICA; yellow to OA outflow. Circles corresponds to places were external pressure is constant and at these times results are taken for further analysis

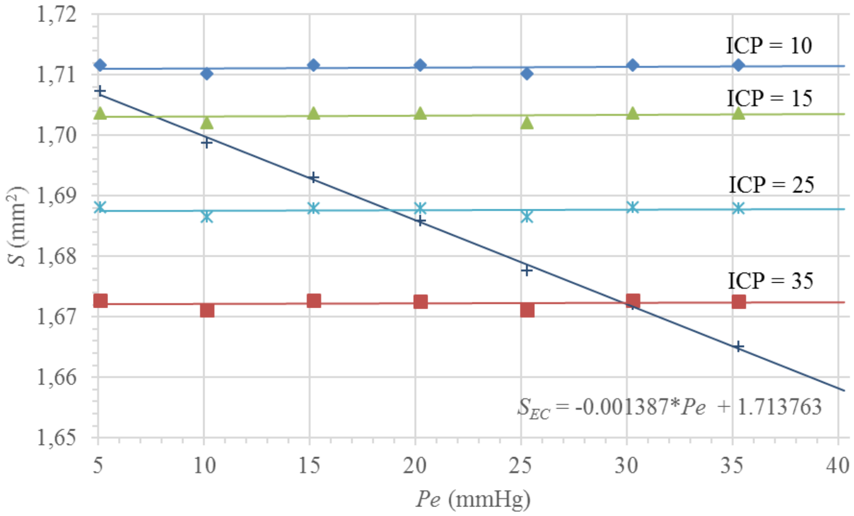

Fig. 7. Cross-sectional area of different OA parts and it’s dependence on pressure. Line with crosses depicts EC part and it’s cross-section area dependence on *Pe*

The ICP to *Pe* difference of different parts of OA was in a range of from about 5 to 6 mmHg.

ΔP pressure could be seen in (Fig. 8). It was obtained from taking difference of surface averaged pressure in different OA parts: IC and EC.

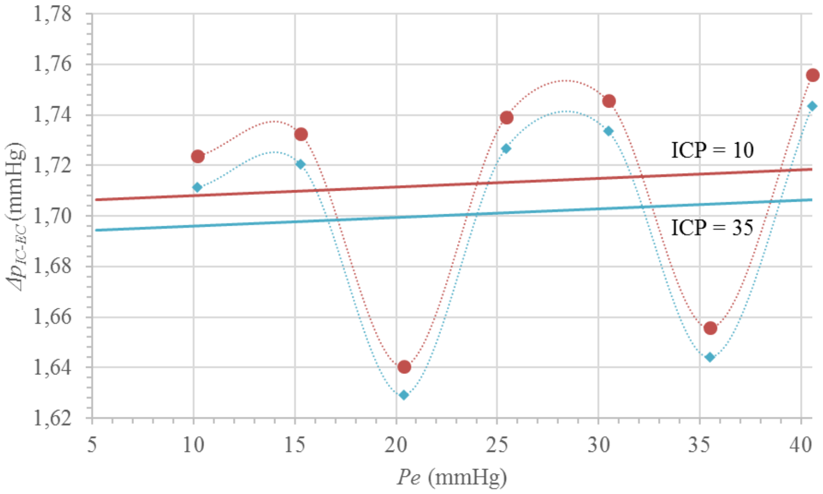

Fig. 8. Blood flow domain pressure difference from IC to EC

ΔP depends very little on ICP and *Pe*. The main dependence comes from blood flow pressure difference. *ΔP* changes rapidly at certain *Pe* values. From (Fig. 6) analysis it was obtained that these value variations follow low frequency wave of ~1 Hz. These variations are from the unknown sources and require further analysis.

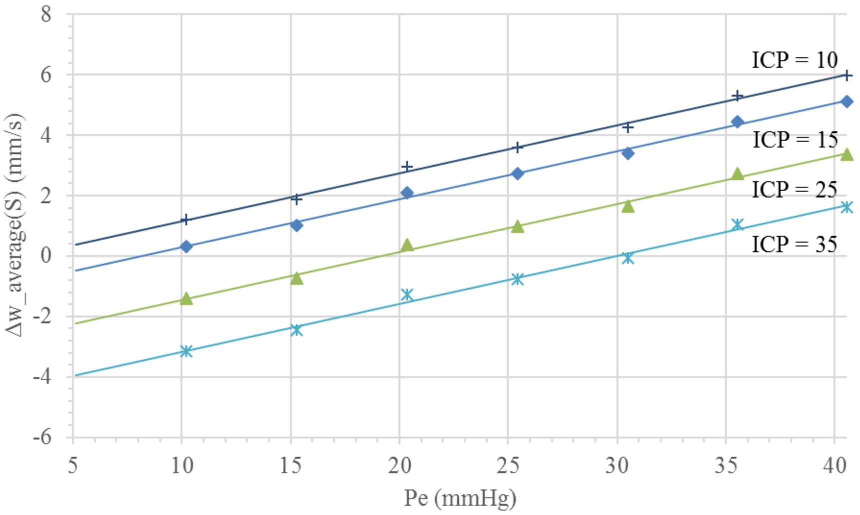

Fig. 9. Velocity difference in different OA segments averaged per cross-sectional area

Obtained velocity differences from IC and EC parts of OA, when $ICP = Pe$ differed in a range from 0.8 to 1.15 mm/s, were 1 mm/s corresponds to about 6.25 mmHg. *ΔP* was founded to be about 1.7 mmHg. The relation $ICP = Pe + \Delta P$ should incorporate another parameter *U* to form $ICP = Pe + \Delta P + U$ equation, were *U* is from an unknown source and needs further research. *U* values are in a range from about 3.3 to 5.5 mmHg.

4. CONCLUSIONS

Numerical time-dependent study was performed using COMSOL on ICA-OA arteries system to test $ICP = Pe + \Delta P$ relation. Different pressures were applied on IC and EC OA segments, ICP and *Pe*, respectively. ICP was held constant in a value range of {10; 15; 25; 35} mmHg, while *Pe* was rised and held constant every heart beat period in a range from 0 to 40 mmHg.

It was found that *S* depends on *Pe* and *ICP*, and it could be written in a linear equation form for both IC and EC parts.

For this kind of mechanical system, for example, the change in ΔP should follow linear form, although low frequency ~1 Hz disturbance was found, which requires additional research.

The tested relation $ICP = Pe + \Delta P$, after the study could be written $ICP = Pe + \Delta P + U$, where U is unknown parameter in a range from 3.3 to 5.5 mmHg for tested pressure values. This founding also requires additional research.

5. REFERENCES

1. STEINER, L.A., ANDREWS, P.J. „Monitoring the injured brain: ICP and CBF," *British Journal of Anaesthesia*, 2006 Vol. 1, No. 97, p. 26–38.
2. DUGDALE, D.C. SHETH, K., Increased intracranial pressure. *MedlinePlus*, 18 June 2011.
3. RODRIGUEZ, Boto G.; RIVERO, Garvia M.; GUTIERREZ, Gonzalez R., MARQUEZ, Rivas J. Basic concepts about brain pathophysiology and intracranial pressure monitoring. *Neurologia*, T. 1, Nr. 30, p. 16–22, 2012.
4. MOKRI, B., The Monro-Kellie hypothesis: applications in CSF volume depletion. *Neurology*, 2001, Vol. 12, No. 56, p. 1746–1748.
5. LI, E., LIU, G.R., XU, G.X., TAN, V., HE, Z.C., Numerical modeling and simulation of pulsatile blood flow in rigid vessel using gradient smoothing method. *Engineering Analysis with Boundary Elements*, 2012, Vol. 36, p. 322–334.
6. HO, H., MCGHEE, C. Numerical analysis for the blood flow in a patient-specific ophthalmic artery. *Medical Engineering & Physics*, 2012, Vol. 34, p. 123–127.
7. SIAUDVYTYTE, L., JANULEVICIENE, I., RAGAUSKAS, A., BARTUSIS, L., SIESKY, B. HARRIS, A. Update in intracranial pressure evaluation methods and translaminar pressure gradient role in glaucoma. *Acta Ophthalmologica*, 2014, p. 1–7.
8. RAGAUSKAS, A., MATIJOSAITIS, V., ZAKELIS, R. Clinical assessment of noninvasive intracranial pressure absolute value measurement method. *Neurology*, 2012, Vol. 78, p. 1684–1691.
9. TEKORIUS, T.A Simplified Mathematical Model of Forward and Reverse Blood Flow in Arteries. *Information technology and control*, 2002, Vol. 2, No. 23, p. 27–32.
10. RAGAUSKAS, A., DAUBARIS, G., DZIUGYS A. Innovative non-invasive method for absolute intracranial pressure measurement without calibration. *Acta Neurochir Suppl*, 2005, Vol. 95, p. 357–361.
11. MILNOR, W.R. *Cardiovascular physiology*. New York: Oxford University Press, Inc., 1990.
12. HOLDSWORTH, D.W., NORLEY, C. Characterization of common carotid artery blood-flow waveforms in normal human subjects. *Physiol. Meas.*, 1999, Vol. 20, p. 219–240.
13. ROSSET, E., BRUNET, C. Viscoelastic properties of human arteries Methodology and preliminary results. *Surgical and Radiologic Anatomy*, 1996, Vol. 18, p. 89–96.
14. AURICCHIO, F., CONTI, M., FERRARA, A., MORGANTI, S., REALI, A. Patient-specific finite element analysis of carotid artery stenting: a focus on vessel modeling. *International Journal for Numerical Methods in Biomedical Engineering*, 2012.
15. AMBARKI, K., HALLBERG, P. Blood Flow of Ophthalmic Artery in Healthy Individuals Determined by Phase-Contrast Magnetic Resonance Imaging. *Investigative Ophthalmology & Visual Science*, 2013, Vol. 4, No. 54, p. 2738–2745.

TWO PHASE THERMOSIPHON TO UTILIZE GROUND HEAT IN DOMESTIC BUILDING APPLICATIONS

T. Muszyński, R. Andrzejczyk
Gdansk University of Technology
Narutowicza 11/12, 80-233 – Gdansk, Poland
Phone 58 347 24-22
Email: tomasz.muszynski@pg.gda.pl, rafal.andrzejczyk@pg.gda.pl

ABSTRACT

Paper presents experimental investigations of passive heat elements such as thermosiphons, in use in domestic building applications, as in sidewalk deicing. Main goal of this article is to find the best working fluid to utilize low grade ground heat source, instead of high temperature heat source [1]. The paper presents an experimental test rig which was constructed to carry out investigations of two phase thermosiphon with new generation of refrigerants as working fluids. Sample experimental results for acetone as working fluid were presented.. Experimental data for acetone and HFE7100 were gathered. Conducted experimental research, will be used to verify the applicability of the existing correlations describing heat transfer coefficient for two-phase thermosiphons.

Keywords: heat pipe, thermosiphon, deicing, ground heat, heat recovery

1. INTRODUCTION

For the past many years, two-phase passive heat transfer devices like heat pipes and thermosyphons have played an important role in a variety of engineering heat transfer systems, ranging from electronics thermal management to heat exchangers and reboilers.

First systems based on renewable energy used to defrost the usable surface appeared in 1969 in the United States, New Jersey. This setup had a form of hybrid device using a heat pipe filled with ammonia and circulation system filled with a mixture of aqueous glycol. The scheme is presented in Fig. 1.

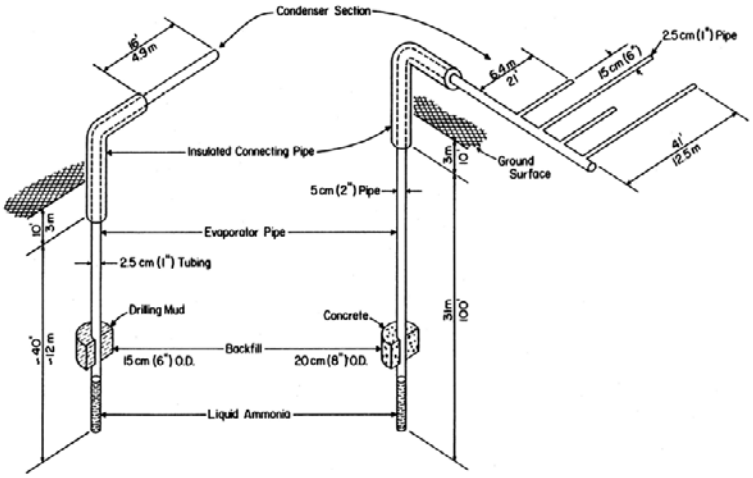

Fig. 1. Deicing system [1]

Heat pipe operation involves using the high efficiency of phase transformation and no need to provide an additional energy to the heat transfer [2]. If the heat pipe can be installed in a vertical position it is not required to fill it with porous material (wick). In the literature such an arrangement is often defined as two-phase thermosyphon. When the system has to operate in a horizontal configuration it is necessary to use a heat pipe equipped with a wick supporting circulation of the working medium inside the tube by capillary forces [3]. Fig. 2 presents example of the heat pipes operating in vertical and horizontal configurations.

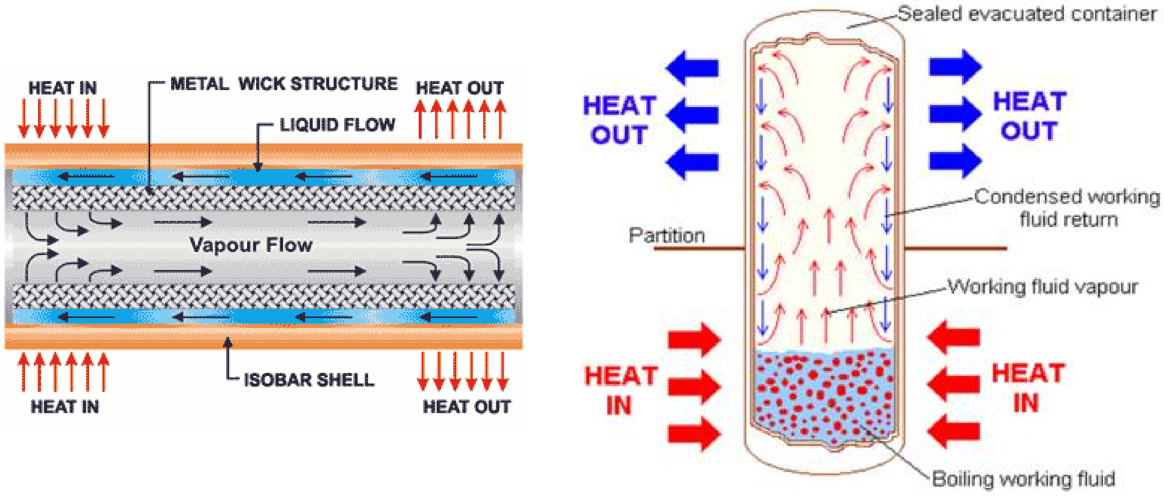

Fig. 2. Examples of heat pipes operation: horizontal configuration (left), vertical configuration (right) [1]

2. EXPERIMENTAL RIG SET-UP

Due to current interest of the issues related with maintaining proper quality of utility construction surfaces, in the Department of Energy and Process Equipment in Gdansk University of Technology, is carried out intensive work on the application of modern systems based on passive components (thermosyphons and heat pipes) using waste heat and renewable energy sources for defrosting and snow removal. The work is in the testing phase, so far was built the test-rig which scheme is presented on Fig. 3.

The considered element here is the heat pipe which is not filled with porous material, having an internal diameter of 6 mm, the outer of 10 mm, made of stainless steel. The total length of the pipe is 2 m, but heat is supplied to the length of 0.5 m. There is also 1 m long adiabatic section and cooling section over a length of 0.5 m. For the winter conditions temperature changes along with the depth, however, it is assumed that the temperature at the depth where the pipe is inserted (the part where heat is transferred) should range from 5 °C to 8 °C.

The elements of the test rig (Fig. 3) are insulated with polyurethane foam with a thermal conduction coefficient below 0.04 W/mK and a thickness of 20 mm. Tested item is insulated by double layer of polyurethane foam. Due to the assumed measurement parameters, as the working medium was chosen the refrigerant R365mfc. It is an uniform factor with a normal boiling point at 40.15 °C. Currently this refrigerant is used on an industrial scale as a foamer.

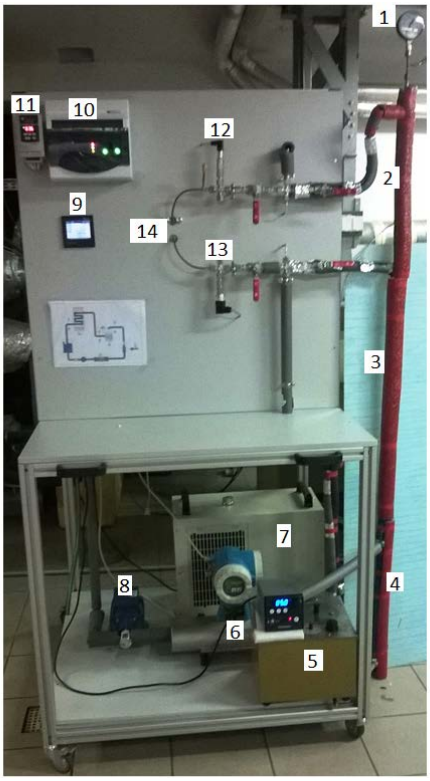

Fig. 3. The schematic of experimental rig: 1 – pressure transducer, 2 – cooling section, 3 – adiabatic section, 4 – heat supply section, 5 – high accuracy ultra thermostatic water bath, 6 –Coriolis flow meter, 7 – chiller, 8 – pulse-free gear pump with magnetic propulsion system, 9 – data acquisition system, 10 – electric switchboard, 11 – inverter, 12 – manometer, 13 – absolute pressure converter, 14 – differential pressure measurements by using a high-precision intelligent differential pressure converter

3. EXPERIMENTAL RESULTS

Thermocouple signals were validated with use of an infrared camera. Sample image is shown in Fig. 4. Fig. 5 shows the comparative results of transferred heat in thermosyphon with acetone, HFE7100 and R365mfc.

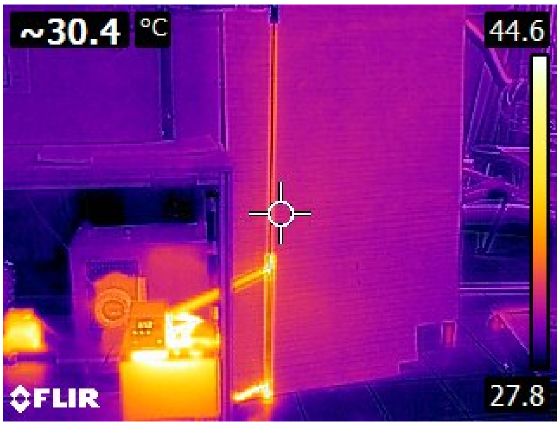

Fig. 4. Thermal image of working termosyphon

Lowest thermal performance obtained with HFE7100 as the working fluid. Similar results were obtained for R365mfc as a medium. Best performance was observed for acetone. In general, thermal performance slightly rises with rising source temperature.

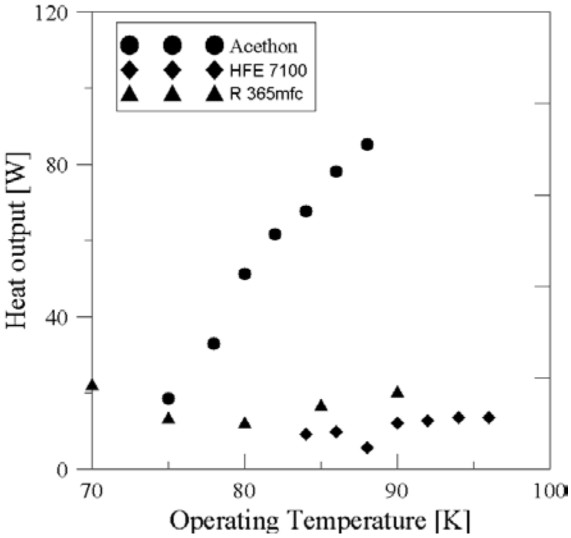

Fig. 5. Effect of operating temperature and fluid properties on transferred heat

4. CONCLUSIONS

A two-phase gravity assisted thermosyphon was designed, fabricated and tested with three refrigerants. Baseline thermal performance was obtained with HFE7100 as the working fluid. In general, it is observed that thermal performance slightly rises with rising source temperature. Maximum performance was observed for acetone while minimum was for HFE7100. Further investigations are needed in order to develop correlations to predict the heat transfer coefficients and performance of the termosyphone.

REFERENCES

1. NYDAHL, J., PELL K., LEE R., SACKOS J. 1984. Evaluation of an Earth Heated Bridge Deck, USDOT Contact No.DTFH61-80-C-00053, University of Wyoming, Laramie.
2. HUSSAM JOUHARA, Heat pipes and their applications tohvac systems&progress with the sirac kick startfunding, School of Engineering and Design, Brunel University.
3. MASOUD AMELI, Advanced 3D printed heat pipes for space applications, Heat Exchanger Action Group (HEXAG) meeting22 May 2013.

CYSENI 2015, May 27–28, Kaunas, Lithuania
ISSN 1822-7554, www.cyseni.com

LITHIUM SALT CONCENTRATION EFFECT ON ELECTRICAL RESESTIVITY AND THERMAL PROPERTIES OF POLYETHYLENE OXIDE COMPOSITE POLYMER ELECTROLYTE

A. Kiyanitsa, S. Gaidukov, I. Blaudums
Riga Technical University
Āzenes street 14/24, 1048 Riga - Latvia
Phone: +371 27180308, +37126270770, +37126190330
Email: alex.kijanica@gmail.com, gaidukov@gmail.com, inguss.blaudums@rtu.lv

ABSTRACT

Paper actuality is based on growing need for non-combustible and safe batteries, which operate portable electronic devices. The composites were prepared from PEO and salt solution by hot-pressing method. Influence of Lithium perchlorate and Lithium trifluoromethanesulfonate concentration on the electrical properties of Polyethylene oxide composite was investigated. Differential scanning calorimetry and thermogravimetric analysis measurements are made to determine composite's crystallinity and thermal properties. The salts addition affected the crystallinity degree and thus electrical properties of the composite.

Keywords: Composites, PEO, Lithium perchlorate, Lithium trifluoromethanesulfonate, Conductivity, TGA, DSC

1. INTRODUCTION

Nowadays people use wireless portative devices and electrical vehicles with polymer-Lithium batteries more and more [1, 2, 18, 19]. Nowadays polymer-Lithium batteries are light, non-toxic, do not content liquid volatile solvents and they are non-combustible in ambient temperature and pressure. At the same time the average discharge time of nowadays devices batteries have decreased, because of applications, which load processor.

Working of listed below applications leads to utilize more energy:

- the display lighting, which consume most of the energy;
- all sorts of data transmission – WiFi, mobile internet, Bluetooth, GPS and etc.;
- background applications, video and music playback and etc.

Latvian public opinion poll about "Battery discharge in mobile phone" in 2014 year show, that 70% of 849 respondent think, that batteries should be optimized (respondents from 15 till 74 year old) [2].

The term "battery" describes a device that converts the chemical energy contained in its active materials directly into electric energy through the electrolyte, which provides the essential ionic transfer [4, 16, 17]. Polymer molecules composed of large repeating unit, which are connected by covalent chemical bonds. Wide range of film-like solid polymer electrolyte designs are already utilized in batteries, mostly in portative electronics because of following material properties: light-weight, non-toxicity, non-combustibility, easy forming, mechanical stability [4–6, 17]. At the same time the investigation of solid polymer electrolyte composition is going on, with a goal to improve its electrical properties in wide range of temperatures without decrease in mechanical and thermal properties [1-19]. It means that there is the need for engineering of solid polymer electrolyte films with acceptable conductivity, mechanical properties, electrochemical stability and ease of handling.

For the solid polymer electrolyte system it is important that polymer has a strong coordination to the cations. For example polyethers, polythiols and polyimides have groups or atoms that can serve as electron donors. Polyethylene oxide (PEO) have no double bonds and have a “plenty” of space between its oxygen groups, which is preferable for many different types of cation solvatation and salt complexes formation. PEO as matrix for polymer electrolyte are widely selected, because of its advantages such as: ease of thin film manufacture, flexibility of size, shape, no-leakage of electrolyte, safety, effectiveness in solvating Lithium salts [17–20]. It should be mentioned, that polymer-Lithium salt electrolyte is a composite material, where macromolecules acts as a “solvent” for a salt, which becomes partially dissociated in macromolecules, leading to ionic conductivity. Nuclear magnetic resonance spectroscopy results of PEO-Lithium salt systems show that conductivity is dominated by the movement of lithium ion, i.e., the lithium transport number is 1.0 [21]. Differential scanning calorimetry (DSC) results indicate that addition of Lithium salt decrease important melting values, such as degree of crystallinity and melting temperatures [15, 16].

It was taken into account, that PEO is partially crystalline polymer, in which part of atoms, molecules or ions is arranged in an orderly repeating three-dimensional pattern (crystalline phase) and another part of atoms, molecules or ions are arranged irregularly (amorphous phase). Polymer and Lithium salt forms complexes, which are conductive only in the elastomeric state. Theoretically, ion moves in polymers between polymer segments by large amplitude polymer motions. Therefore ion transport probably occurs with the breaking of at most 1 or 2 cation-polar group interactions [4, 20]. It can be concluded, that increasing the amorphous phase amount and mobility of Lithium cations could increase the ionic conductivity of polymer electrolyte.

At the same time, the limit of conductivity for applications is 10^{-5} S cm^{-1} (in the range between 20°C and 100ºC). The limit for conductivity to amorphous phase is its glass transition temperature, but no higher than it. Some authors claim, that ionic conductivity in solid PEO-Lithium salt system reached averaged maximum 10^{-6} S cm^{-1} [22, 16]. However, ionic conductivity of PEO-alkali metal salt system was reached 10^{-7} S cm^{-1} at room temperature [24].

Molecular weight of PEO is also important factor to control physicochemical properties of the polymer electrolyte. PEO-Lithium salt system were revealed to be amorphous when the molecular weight was in range 300-750 g/mol, but system that was obtained with PEO higher than 1000 g/mol – partly crystallized [24]. This phenomenon is based in decrease of crystallite size, which occurs at higher PEO molecular weight, although it cannot explain the different activation energies in the systems [23]. It was found, that PEO-Lithium salt systems show highest conductivity with PEO molecular weight value lower than 300 000 g/mol. It was concluded, that optimal molecular weight for PEO-Lithium salt electrolyte should be about 100 000 g/mol.

Lithium trifluoromethanesulfonate (LiTrifl) with linear formula CF_3SO_3Li and Lithium perchlorate (LiCl) with linear formula $LiClO_4$ are widely used as ion source and plasticizer [3, 15–25]. The Lithium ion is the smallest in compare with other group ions. It is the stronger Lewis base of the group. It accepts the lone pairs on oxygen the quickest and easiest and has the highest (or the least shielded proton) relative exposed positive charge. Hence it will attract water, making the salts hygroscopic and therefore more flexible [26].

In the manufacturing process melting temperature of LiCl or LiTrifl polymer electrolyte salt must be taken into account. It is known, that LiCl start melting at 247° temperature and it does not decomposite till temperatures higher than 400°C. Studies show that hydrates still exist in LiCl after 12 h of drying at 300°C temperature [9, 10]. However LiTrifl start its decomposition at 290–300°C [11].

The aim of this paper is to explore Lithium perchlorate and Lithium trifluoromethanesulfonate salt concentration effect on electrical resistivity and thermal properties of PEO composites polymer electrolyte.

2. METHODOLOGY

2.1. Sample preparations

PEO was chosen as matrix of composite polymer electrolyte. LiCl and LiTrifl were chosen for composite polymer electrolyte as ion source. Properties of substance given above were supplied by manufacturer and are listed in Table 1.

Table 1. Material used in sample preparation

Substance	**Manufacturer**	**Substance properties**
Polyethylene oxide	Scientific Polymer Products	MW 100 000 g/mol density 1.21 g/cm^3 melting point 65°C
Lithium perchlorate	ChemPure	MW 60.41 g/mol
Lithium trifluoromethanesulfonate	Fluorochem	MW 156.01 g/mol

Solution casting technique was used to prepare composite films. 10% PEO solution was prepared by dissolving PEO in ethanol and then mixed by with magnetic stirrer at 60°C for 20 minutes. Suspension turned into a homogeneous translucent solution.

Lithium salts were dispersed in ethanol by magnetic stirring. It was added to 10% PEO solution and dispersed with ultrasound for 20 minutes. The polymer solution was casted as film and solvent was allowed to evaporate for 48 h at 25°C temperature with subsequent annealing in vacuum at 60°C for 24 h.

Films with average 500 μm thickness were prepared in mold at 90°C (6 minutes) by “Carver” heat-pressing equipment. Heat-pressing method was applied along with the additions of Lithium salts to improve the ionic conductivity of PEO polymer electrolytes.

LiCl salt concentrations in PEO-Lithium composite are 1, 5, 10, 15, 20, 25 % of dry PEO mass. Concentrations of LiTrifl are 1, 5, 10, 25 % of dry PEO mass.

2.2. Surface and volume resistivity measurements

The electrical conductivity of the sample was measured by sandwiching the samples between two electrodes – guarded electrode and ring electrode. The measurements for each sample were performed using “Keithley 6487” picoampermeter. Constant voltage equal to 500V for 60 seconds (according to the ASTM D257 standard) at 23°C temperature was applied.

Direct current conductivity measurements were made on prepared film sample. It should be noted that the electrical conductivity of solid material may be characterized using Ohm’s Law by volume resistance ρ_V and surface resistance ρ_S.

The specific surface resistance is a measure current flow along the surface of a polymer test specimen. The resistivity to the flow of current through a material, is known as volume resistivity.

In order to receive specific resistance values, we have to make calculations using the equations (1) and (2).

Specific volume resistance for the thin sample should be calculated using the following Equation:

$$\rho_V = R_V \cdot \frac{22.9cm^2}{h}, [\Omega \cdot cm] \tag{1}$$

R_V – measured volume resistance of the sample (V/I), [Ω];
h – thickness of the sample, [cm];
22.9 – surface area of the electrode, [cm^2].
Specific surface resistance should be calculated using the following equation:

$$\rho_S = R_S \cdot 53.4, [\Omega] \tag{2}$$

R_S – measured surface resistance of the sample (V/I), [Ω];
53.4 –diameter of electrodes divided by the distance between them.

2.3. Thermogravimetric analysis

"Mettler Toledo TG50" thermogravimeter was used to measure PEO samples. TG measurements were carried out in the air. The heating rate of samples specimens was 10°C/min. The TG analysis was performed at temperatures from 20°C to 600°C. Therefore we tracked changes in the mass of the sample as a function of time. Separate TGA run on each sample was made. Sample weight was in 2–4 mg range.

Following measurements were obtained, compared and analysed: decomposition temperature, mass loss in certain temperature, sample end mass.

2.4. Differential Scanning Calorimetry

Thermal analysis was performed on "Mettler Toledo DSC30" equipment. A specific amount (8–20 mg) from each composite sample was cut and put in an aluminium sample pan, which was hermetically sealed by compression moulding. DSC thermograms were obtained at heating and cooling rates of 10°C/min from 20°C to 100°C under a nitrogen atmosphere in order to reduce oxidation. Melting enthalpy and melting temperature were obtained. The endothermic peak temperature was taken as the melting temperature (T_m).

It is known, that completely (100%) crystalline PEO polymer melting enthalpy ($\Delta H°$) is equal to 213.7 J/g [5, 6]. Using the equation (3) from below, we can calculate degree of crystallinity of PEO composite samples:

$$\chi = \frac{\Delta H_m}{\Delta H_m^o} \cdot 100\% \tag{3}$$

X – degree of crystallinity of sample, [%];
ΔH_m – melting enthalpy of sample, [J/g];
$\Delta H_m°$ – completely (100%) crystalline PEO polymer melting enthalpy, [J/g].

3. RESULTS AND DISCUSSIONS

3.1. Surface and volume resistivity measurements

Calculated specific volume resistance and surface resistance values are summarized in Fig. 4 and Fig. 5. The difference of ionic conductivity between discovered PEO-Lithium salt systems was expected to be caused by the difference of the mobility of ions.

Volume resistivity results (Fig.1.) of the PEO/LiCl and PEO/LiTrifl composites show, that addition of 1% LiCl decrease resistivity of pure PEO from $8.56 \cdot 10^{10}$ Ωcm to $2.68 \cdot 10^{8}$ Ωcm, but addition of 1% LiTrifl – to $2.63 \cdot 10^{9}$ respectively. It can be concluded, that addition of only 1%

LiCl decreased the volume resistivity by 319 times, while addition of 1% LiTrifl decreased the volume resistivity only by 32 times. As it was mentioned in literature [7, 8], the presence of filler particles enhances the electric conductivity substantially. It can be assumed that decrease in the resistivity occurs as a result of filler addition, possible amorphous phase increase free ion higher mobility.

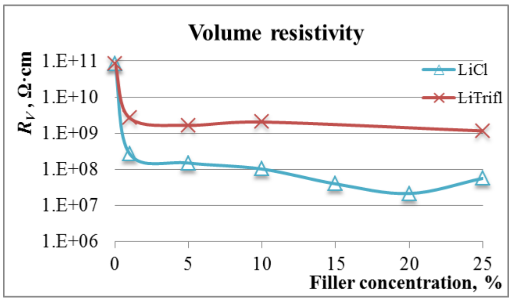

Fig. 1. Volume resistivity (at 24 °C) of the PEO based polymer composite films

It was observed, that increase of filler content up to 5% decrease volume resistivity in each filler case. At the same time 5% LiCl decrease resistivity by 11 times in comparison with 5% LiTrifl. Further addition of LiTrifl continues decrease volume resistivity; however further addition of LiCl raise volume resistivity, after it reached 20% filler content.

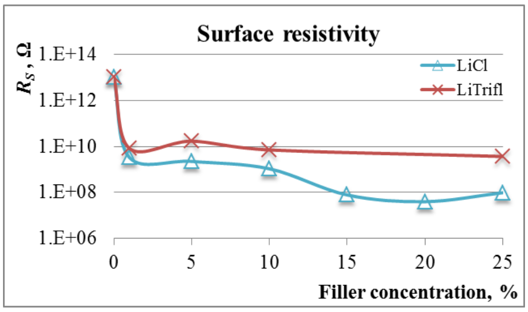

Fig. 2. Surface resistivity (at 24 °C) of the PEO based polymer composite films

Fig. 2 show results obtained from surface resistivity. The similar behaviour of the PEO/LiCl and PEO/LiTrifl composites is observed. Surface resistivity values of PEO/LiCl are lower than PEO/LiTrifl composites. Observed conduction behaviour could be attributed to less molecular weight of LiCl and its higher ion mobility.

It was observed, that maximum decrease in surface resistivity was obtained in PEO/20%LiCl ($3.98 \cdot 10^7$ Ω) and in PEO/25%LiTrifl ($3.68 \cdot 10^9$ Ω) composite. It can be concluded that the greater Lithium filler concentration in PEO-Lithium composite electrolyte, the more PEO-Lithium complex are formed thus increasing the mobility of ions and therefore decreasing the surface resistivity.

3.2. TGA studies

Thermal degradation of PEO based polymer LiCl composites films was made.

As it was proven by electrical resistivity measurements - significant changes occur after LiCl concentration reaches 20% content. These changes occurred because of the hygroscopic nature of both PEO and the Lithium salt; therefore increase of Lithium salt increase samples hygroscopicity. It was decided to compare pure PEO sample thermal degradation kinetic behaviour with PEO/5%LiCl and PEO/20%LiCl composite samples (Fig. 3).

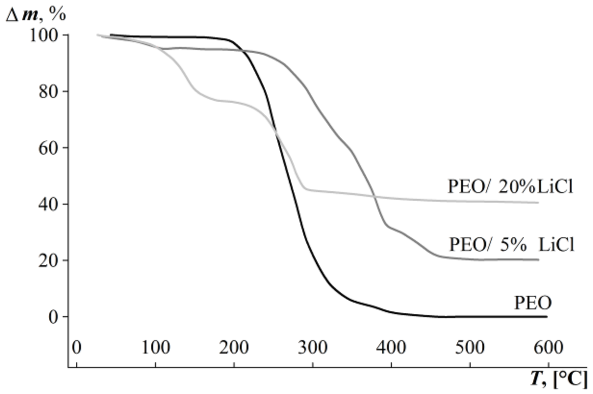

Fig. 3. Typical TG curve for pure PEO and PEO composite with 5% and 20% LiCl filler content

Decomposition temperature equilibrium is earlier if filler content is higher (Fig. 3).

Fig. 4 represent TGA results of PEO/LiCl composite, where the plot shows the percent of mass loss as a function of sample temperature. PEO composite with 5% LiCl is more thermally stable than pure PEO and other composites. PEO/5%LiCl thermal stability is higher in all heating range. It was observed, that addition of filler decreases thermal stability of all composites. It is observed proportional mass loss of composites with 15%, 20% and 25% filler concentration. Addition of 15% and more of LiCl decreases thermal degradation temperature compared with pure PEO, but opposite behaviour is observed for composites with LiCl content that is less than 15%.

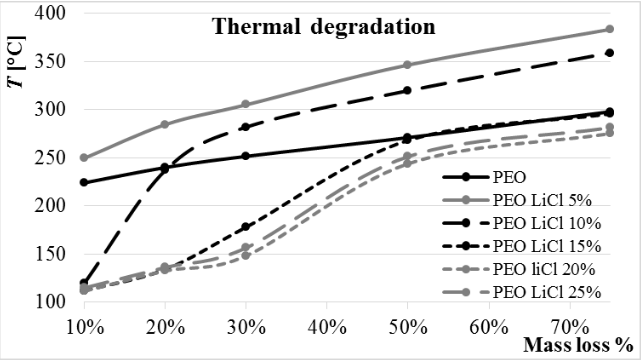

Fig. 4. Dependence of PEO/LiCl composite film mass loss as a function of sample temperature

3.3. DSC results

Concluding, we have tested the lowest and the highest content of the filler to see the characteristic changes. Resistivity measurements also concluded the provisional relative changes. However, the values of crystallinity and melting temperature for 10 and 15 will be remained between experimentally observed. Results obtained in DSC are summarized in Table 2. It consists of melting enthalpies, degree of crystallinities and melting temperatures values.

Table 2. DSC results for PEO composites with 5% and 25% filler content of LiCl and LiTrifl

Composition		**Melting enthalpy, mJ**	**Melting enthalpy, J/g**	**Degree of crystallinity, %**	**Melting temperature, ^{o}C**
PEO		1517	128.8	60	66.2
PEO	5% LiCl	199	14.9	7	62.9
PEO	25% LiCl	0	0	0	0
PEO	5% LiTrifl	608	119.2	53	61.5
PEO	25% LiTrifl	155	23.9	8	49.9

Initially, it was found that our PEO reached 60% of the theoretically possible crystallinity. But addition of 5% and 25% LiTrifl decrease it by 11% and 86% respectively. In case of 5% and 25% LiCl filler, crystallinity decreased much more – by 88% and 100% respectively.

Melting temperature "T_m" of the polymers is one of the most important technological parameters, because all processes and practical application of ready material are highly affected by it. It plays the most important role for polymer electrolytes in batteries [12]. Thus, it was interesting to explore melting temperatures of PEO composites. First, it should be noted, that bulk PEO melting temperature is higher than PEO film melting temperature. The difference between bulk (T_m=65°C) and film (T_m=66.2°C) PEO melting temperatures is equal to 1.2°C. We can suggest that this difference exist because of free volume theory and kinetic theory for structural relaxation, where dynamic displacements in film are higher than in bulk polymer [13, 14]. Addition of 5% LiCl reduce melting temperature by 3.3°C. At the same time addition of 5% LiTrifl reduce melting temperature by 4.7°C. In the case of 25% LiCl filler content it is not possible to determine PEO composite melting temperature as there is no crystalline areas. Different situation is observed in PEO with 25% LiTrifl content, where melting temperature reduced by 16°C.

4. CONCLUSIONS

This paper was focused on the electrical resistivity and the changes in relaxation behaviour of semicrystalline PEO around its melting temperature of obtained PEO-based electrolyte composites. We can conclude that LiCl, which have low lattice energy, is more effective than LiTrifl in electrical resistance reduction. Increasing of the Lithium salts content above 10% decreases electrical resistance, but visually it is evident that the mechanical properties (such as hardness) became worse and surface hygroscopicity increased, which makes material utilization more complicate at 23°C temperature. Experiments showed that the optimal addition of LiCl and LiTrifl salts for PEO-Lithium salts system are equal to 5%. A PEO sample with molecular weight 100 000 g/mol with 5% LiCl successfully reduced the crystallinity without loss of mechanical properties, which can be observed at external examination already. The phase transition based on the crystallization of PEO disappeared after the addition of 25% LiCl salts. Thus, the obtained PEO-Lithium salt system was confirmed to be amorphous by the DSC measurement.

REFERENCES

1. "EU Collaborative Project within the FP7 of greener and cheaper Li-Ion batteries" [referred on the 20 of April in 2015 y.]. Link to the internet < http://www.greenlionproject.eu/project-overview>

2. “Poll: 70% of smartphone users want to better batteries” [referred on the 3th of March in 2015 y.]. Link to the internet <www.tvnet.lv/tehnologijas/nozares_jaunumi/506665-aptauja_70_viedtalrunu_lietotaju_velas_labakas_baterijas>
3. WILLGERT, M., et al. Photoinduced free radical polymerization of thermoset lithium battery electrolytes. *Eur Polym J*, 2011, Vol. 47, No 12, p. 2732–2738.
4. YIN, Y. An Experimental study on PEO polymer electrolyte based all-solid-state supercapacitor. Open Access Dissertations. 2010, p. 440.
5. IBRAHIM, S., JOHAN, M.R. Thermolysis and Conductivity Studies of PEO Based Polymer Electrolytes Doped with Carbon Nanotube. 2012, Vol. 7, p. 2596–2615.
6. ALI, A.M.M., SUBBAN, R.H.Y., BAHRON, H., WINNIE, T., LATIF, F., YAHYA, M.Z. Grafted natural rubber based polymer electrolytes: ATR-FTIR and conductivity studies. *Ionics*, 2008, Vol.14, p. 491–500.
7. CHEW, K.W., TAN, K.W. The Effects of ceramic fillers on PMMA-based polymer electrolyte salted with lithium triflate, $LiCF_3SO_3$. *Int. J. Electrochem. Sci.*, 2011, Vol. 6, p. 5792–5801.
8. YAP, Y.L., YOU, A.H., TEO, L.L., HANAPEI, H. Inorganic filler sizes effect on ionic conductivity in PEO composite polymer electrolyte. *Int. J. Electrochem. Sci.*, 2013, Vol. 8, p. 2154–2163.
9. ШУМАХЕР И. *Перхлораты. Свойства*. Москва: ГХИ, под редакцией Генина Л.С. 1963, с. 236.
10. KURT. H.S. High temperature Properties and decomposition of inorganic salts. Part 4. Oxy-salts of the halogens. *J. Phys.Chem. Ref. Data*, 1974, Vol.3, No. 3.
11. LEIJONMARCKA, S., CARLSONB, T., LINDBERGHA. G. Solid polymer electrolyte-coated carbon fibres for structural and novel micro batteries. *Comp. Sci. and Tech.*, 2013, Vol. 89, p. 149–157.
12. NOOR., S.A.M. et al.. Solid polymeric electrolyte of poly(ethylene)oxide-50% epoxidized natural rubber-lithium triflate. *Natural Sci.*, 2010, Vol. 2, p. 190–196.
13. BECKER, J.S., BROWN, R.D., KILLELEA, D.R., YUAN, H., SIBENER, S.J. Comparative surface dynamics of amorphous and semicrystalline polymer films. Proceedings of the National Academy of Sciences of the USA, 2011, Vol. 108, No. 3, p. 977–982.
14. KAWASHIMA, K., INOUE, R., KANAYA, T. G. et al.. Distribution of glass transition temperature in a polymer thin film by neutron reflectivity. *J of Phys.: Conf. Ser*. 2009, Vol. 184, 012004.
15. KIM, H., CHOI, G., MOON, S., KIM. S. Electrochemical properties of Li ion polymer battery with gel polymer electrolyte based on polyurethane. *J Appl. Electrochem.*, 2003, Vol. 33, No. 6, p. 491–496.
16. MANUEL STEPHAN, A., NAHM., K.S. Review on composite polymer electrolytes for lithium batteries. *Polymer (Guildf).*, 2006, Vol. 47, No. 16, p. 5952–5964.
17. CHEW, K.W., NG, T.C., HOW, Z. H. *Int. J. Electrochem. Sci.*, 2013, Vol. 8, p. 6354–6364.
18. CHANDRA, An., CHANDRA, Ar., THAKUR, K. Preparation and characterization of hot-pressed Na+ ion conducting nanocomposite polymer electrolytes. *Indian J. of Pure & Applied Physics*. 2013, Vol. 51, p. 44–48.
19. DEY, A., KARAN, S., DE, K S. Effect of nanoadditives on ionic conductivity of solid polymer electrolyte. *Indian J. of Pure & Applied Physics*. 2013, Vol. 51, p. 281–288.
20. BRANDELL. D. Understanding ionic conductivity in crystalline polymer electrolytes. Acta Universitatis Upsaliensis. Digital Comprehensive summaries of Uppsala

dissertations from the faculty of science and technology 34. 63 pp. Uppsala. ISBN 91-554-6204-9.

21. GADJOUROVA, Z., ANDREEV, Y.G., TUNSTALL, D.P., BRUCE, P.G. Ionic conductivity in crystalline polymer electrolytes. *Nature*. 2001, Vol. 412, p. 520.
22. FM Gray. Fast ion transport in solids. Polymer electrolytes, RSC materials monographs. (Cambridge: The Royal Society of Chemistry. 1997); Armand MB, Chabagno JM, Duclot M. In: Vashista P, Mundy JN, Shenoy GK, editors. Amsterdam: Elsevier; 1979. p. 131.
23. STOEVA, Z., MARTIN-LITAS, I., STAUNTON, E., ANDREEV, Y.G., BRUCE, P.G. *J Am Chem Soc*. 2003, Vol. 125, p. 4619.
24. YOICHI T., NAOMI T., HIROYUKI O. Effect of added salt species on the ionic conductivity of PEO:sulfonamide salt hybrids. *Electrochimica Acta*. 2000, Vol. 45, p. 1285–1289.
25. ARMAND, M., GORECKI, W., ANDREANI, R. Proceedings of the second International Symposium on Polymer Electrolytes (ISPE-2), Elsevier, London, 1990, p. 31.
26. MUNSHI, M.Z.A. *Handbook of Solid State Batteries & Capacitors*. World Scientific publishing Co. Pte. Ltd. 1995. 716 p. ISBN 981-02-1794-3.

CYSENI 2015, May 27–28, Kaunas, Lithuania
ISSN 1822-7554, www.cyseni.com

ASPECTS OF INCORPORATING THE PRODUCTION OF LEVOGLUCOSAN INTO A WOOD-BASED BIOREFINERY

K. Meile, A. Zhurinsh
Latvian State Institute of Wood Chemistry
Dzerbenes str. 27, LV-1006 – Latvia
Phone +371 29137880
Email: kristine.meile@inbox.lv

ABSTRACT

Levoglucosan or 1.6-anhydro-β-D-glucopyranose is among the main products of the fast pyrolysis of lignocellulosic feedstock after acid pre-treatment, but despite its abundance and potential application in several fields, there are certain impediments for producing levoglucosan on an industrial scale. The most serious issue is the purification of levoglucosan, because the products of pyrolysis form a very complex mixture of numerous individual compounds. This study investigated both cation and anion exchange resins as sorbents for fractionation of the liquid products of pyrolysis. Levoglucosan with at least 70% purity was obtained by using cation exchange columns. Furthermore, the strongly acidic cation exchange resin in Ca^{2+} form enabled the separation of the isomer of levoglucosan – 1.6-anhydro-β-D-glucofuranose.

Keywords: biorefinery, renewable chemicals, levoglucosan, ion exchange chromatography

1. INTRODUCTION

The depletion of fossil resources has initiated a search for more sustainable alternatives for producing energy, fuels, chemicals and materials. Most renewable resources, such as wind or solar power can only be used to produce energy, while biomass – the only carbon containing renewable – can additionally be used to produce chemicals and materials therefore the utilization of biomass is the key to a bio-based society. Establishing a bio-based economy is a priority for the European Union, as stated in the European Biorefinery Vision for 2030 [1]. The basis for a bio-economy is biorefining, which is ’’the sustainable processing of biomass into a spectrum of marketable products and energy’’ [2].

There are various possible sources of biomass – crops, organic waste, agricultural and forestry waste, wood and aquatic biomass, all of which are beneficial, if produced in a sustainable way [3], but this article focuses on the possibility to use wood-based biomass in a biorefinery, producing levoglucosan among other products, because lignocellulosic materials such as forest residues are the most commonly used feedstock for commercial pyrolysis factories [4].

Levoglucosan or 1,6-anhydro-β-D-glucopyranose is an anhydrosugar, which is formed during the pyrolysis of carbohydrates – most often cellulose or starch [5]. At present, levoglucosan is not produced on an industrial scale, although it has the potential to be used for the synthesis of dextrans [6], bioethanol [7], various polymers [8], complex assimetric molecules [9], etc. Commercially available pure levoglucosan, produced from starch, is expensive (90 eur/g) [10]. The use of starch involves certain difficulties, such as the swelling of starch, which can disturb the production of levoglucosan on a large scale. Besides, since starch is an edible carbohydrate, there are ethical limitations for its use in producing non-food products. It is also possible to synthesize levoglucosan from glucose [11], but this method is not economically feasible for large scale production, but for research purposes only. So, in the end, pyrolysis of a cellulose containing material is the reasonable approach to produce levoglucosan on an industrial scale.

Pyrolysis is the thermal processing of wood or other feedstock in the absence of molecular oxygen, and in the last few decades it has become particularly interesting in context with the production of value-added products [12]. It can be applied to various feedstock, besides pyrolysis requires rather low capital investment and is easy to scale up for industrial processes [13]. The three main physical parameters of pyrolysis are the process temperature, residence time in the reactor, and heating rate [14]. Fast pyrolysis, which employs short hot vapour residence time in the reactor (less than 2 seconds) and high temperature (approximately 400-600 ºC) at fast heating rates, has a characteristically high yield of the liquid products or bio-oil (75%), but less gas (12%) and char (13%) [4]. Gas and char are essentially energy suppliers, but bio-oil consists of a mixture of chemicals, among which the most abundant single compound is levoglucosan [13].

Fig. 1 shows an example of a biorefining concept for the production of furfural and levoglucosan from lignocellulosic biomass [15]. This is a hybrid concept involving hot pressurized water treatment (aquathermolysis) and fast pyrolysis. During aquathermolysis an aqueous hemicellulose fraction is separated and converted mainly into furfural, acetic acid and hydroxymethylfurfural. The solid lignin-cellulose fraction is further subjected to fast pyrolysis to obtain gaseous products, char and bio-oil.

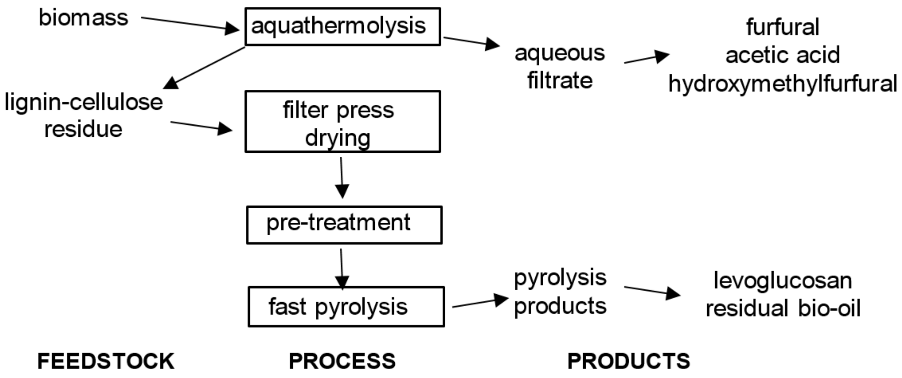

Fig. 1. A schematic illustration of a biorefinery for the production of levoglucosan, furfural and other chemicals from lignocellulosic biomass [15]

The parameters of pyrolysis for good yields of levoglucosan have been extensively studied and described [4, 12, 16], but at the moment the most problematic issue is the separation and purification of levoglucosan from pyrolysis liquids (bio-oil). Liquid pyrolysis products contain several hundreds of individual compounds, so it is very challenging to extract separate chemicals from this mixture. Various separation methods for levoglucosan have been proposed – solvent extraction, column chromatography with different sorbents, recrystallization [17]. However, in order to obtain a pure product a combination of several processes may be necessary. An economical method for the purification of levoglucosan still needs to be developed.

Ion exchange resin columns are successfully used for water purification [18], and there is information about ion exchangers used for the separation of carbohydrates in biomass hydrolysates [19]. Previous research [20] has shown that strongly acidic cation exchange columns are applicable for the fractionation of starch based pyrolysis liquids. But, since the chemical composition of the pyrolysis products depends greatly on the feedstock, it is important to investigate ways to fractionate pyrolysis liquids, obtained from wood.

Ion exchange resins belong to the solid, synthetic organic sorbents. The resins consist of a polymer matrix – most often a polystyrene-divinylbenzene copolymer, and functional groups. The matrix is built up of cross-linked polymer chains, which form macro- and micropores. The porosity of the matrix leads to separation of substances by size exclusion. Other retention mechanisms in ion exchange resin columns depend on the different functional groups: strongly acidic cationites are sulphonated, weakly acidic cationites are made of acrylic polymers which are hydrolyzed to form carboxylic acid groups, and anion exchange resins are aminated [21].

Ion exchange resins are used for carbohydrate purification even on an industrial scale [22], so this method could be applied to the separation of anhydrosugars from pyrolysis liquids as well. Compared to sequential crystallization of levoglucosan, ion exchange chromatography has a potential to supply replicable, stable separation results without the use of organic solvents. Preparative chromatography could also be used to obtain additional products besides levoglucosan, which would increase the profitability of a biorefinery. The purpose of this study is to develop a method for the separation of levoglucosan from pyrolysis liquids by ion exchange chromatography.

2. METHODOLOGY

2.1.1. Materials and Equipment

All chemicals (analytical grade) were purchased from Sigma-Aldrich and used without further purification.

Finex CA16GC (weakly acidic cation exchange resin in Na^+ form), Dowex 50WX4 (strongly acidic cation exchange resin in H^+ form) and Lewatit VPOC 1074 (weakly basic anion exchange resin in Cl^- form) were used for column chromatography. The strongly acidic cation exchanger was regenerated to Ca^{2+} form with a 5 % $CaCl_2$ solution. The weakly acidic anion exchanger was regenerated to OH^- form with a 2 % NaOH solution.

Iodometric titration was done with a Radiometer automatic burette (maximum volume 10 mL). Perkin Elmer UV/Vis spectrophotometer Lambda 25 (wave length range 190-1100 nm) was used to measure the absorption in the chromatographic fractions. Samples were dried in a Memmert heating oven (temperature range 20-150 °C, precision ± 0.5 °C).

Samples of pyrolysis liquids were obtained at the Latvian State Institute of Wood Chemistry from birch wood by fast pyrolysis after sulfuric acid pre-treatment as described in the literature [23]. The samples contained different amounts of levoglucosan: sample A 5.3±0.1 wt%, sample B 23.0±0.3 wt%, sample C 46.2±0.5 wt%, and sample D 58.9±0.4 wt%.

2.1.2. Fractionation of the pyrolysis liquids

Three types of ion exchange resins were used in the column chromatography experiments. One of them was a strongly basic anion exchange resin in OH^- form (further in the text SBA), the other two were cationites – a weakly acidic cation exchange resin in Na^+ form (WAC) and a strongly acidic cation exchange resin in Ca^{2+} form (SAC).

A suspension of the resin in the eluent of choice (water or a water/ethanol mixture volume to volume ratio 4:1) was poured into a glass column (60×2 cm). At first 10 mL of a solution of standard sugars – cellobiose, D-glucose and levoglucosan (0.5 wt% each) was separated, in order to establish the elution sequence of carbohydrates on the WAC column with flow rate 0.69 ± 0.02 mL/min. Afterwards about 1 g of pyrolysis liquids was dissolved in 15 mL of deionized water and filtered through a Whatman 95 filter paper. The filtrate was carried onto the column and separated in fractions after every 10 min. When separating the samples of pyrolysis liquids, the flow rate was 1.2 ± 0.2 mL/min. The experiments were performed at room temperature (21 ± 3 °C).

The WAC column was used to fractionate a total of 25 g of pyrolysis liquids (sample D). Two fractions were obtained (dividing the eluent at 90 min). The content of sugars and anhydrosugars was determined in these fractions. A sample of the second fraction was dried at 103 °C until a solid with constant mass (0.5421 g) was obtained. The solid was dissolved in 2 mL of deionized water. After the addition of 8 mL acetone, the sample was stored at 4 °C overnight. A sample of the pyrolysis liquids without separation on the WAC column was prepared and stored the same way.

2.1.3. Analytical Methods

The amount of sugars and anhydrosugars was determined by iodometric titration after oxidation with sodium periodate and the amount of anhydrosugars was calculated as levoglucosan [24]. 5 mL of the sample solution were measured into two 25 mL measuring flasks. 5 mL of 15 % sulfuric acid was added to the first flask and it was placed in the heating oven at 120 °C for 1.5 h to hydrolyze levoglucosan into glucose. Afterwards both measuring flasks were filled up with deionized water and 2 mL were transfered into 30 mL weighing glasses, 1 mL of 0.2 M sodium periodate solution was added and the glasses were placed in the heating oven at 40 °C for 4 h to oxidize the sugars and anhydrosugars. Then the excess of periodate was masked with 5 mL of 10 % ammonium molybdate solution. 1 mL of glacial acetic acid and 1 mL of 10 % potassium iodide were added and after 15 min and the resulting iodine was titrated with 0.1 M potassium thiosulfate solution, using starch as the indicator. Equation 1 was used to calculate the amount of sugars and Equation 2 for the amount of anhydrosugars, expressed as levoglucosan.

$$n_{sugars} = \frac{c \cdot \left(V_{before\ hydrolysis} - \frac{2}{3}\left(V_{after\ hydrol.} - V_{before\ hydrol.}\right)\right)}{5} \tag{1}$$

$$n_{levoglucosan} = \frac{c \cdot \left(V_{after\ hydrol.} - V_{before\ hydrol.}\right)}{3} \tag{2}$$

n – amount [mol];
c – molar concentration of potassium thiosulfate [mol/L];
V – volume of thiosulfate [L].

The purity of levoglucosan was calculated by Equation 3, and Equation 4 was used to calculate the yield of levoglucosan.

$$P\% = \frac{m_{levoglucosan}}{m_{total\ sample}} \cdot 100\% \tag{3}$$

$$Y\% = \frac{m_{levoglucosan\ obtained}}{m_{levoglucosan\ theoretical}} \cdot 100\% \tag{4}$$

P – purity [%];
Y – yield [%];
m – mass [g].

The content of dry matter in the fractions was determined gravimetrically, by drying at 103 °C until a constant mass was reached.

The content of phenolic substances was characterized by measuring the absorption at 275 nm [25].

3. RESULTS AND DISCUSSION

When the SBA column was used for the separation of a sample of pyrolysis liquids, the eluate practically contained levoglucosan alone, but the other components of the sample were permanently retained on the column. The eluent was distilled water, but the retained fraction (phenols, sugars etc.) could not be washed off the column with a 2 % NaOH solution. Allthough anion exchange resins have been reported to be suitable for the separation of sugars from wood hydrolysates [19], our experiments showed that pyrolysis liquid samples contaminated the column making it practically unsuitable. This could be explained by the fact that pyrolysis liquids contain hundreds of individual compounds [26], among which there is a noteworthy part of oxygenated compounds of high molecular weight [27], so pyrolysis liquids are more complicated samples than hydrolysates.

Since the SBA column could not be easily regenerated, it would not be suitable for industrial processes in a biorefinery.

Figure 2 shows a chromatogram of standard sugars, which was obtained on the WAC column with water as the mobile phase. The retention times of cellobiose, glucose and levoglucosan were 115 min, 148 min and 167 min, respectively. The selectivity of levoglucosan/glucose of 1.3 was acceptable for preparative chromatography.

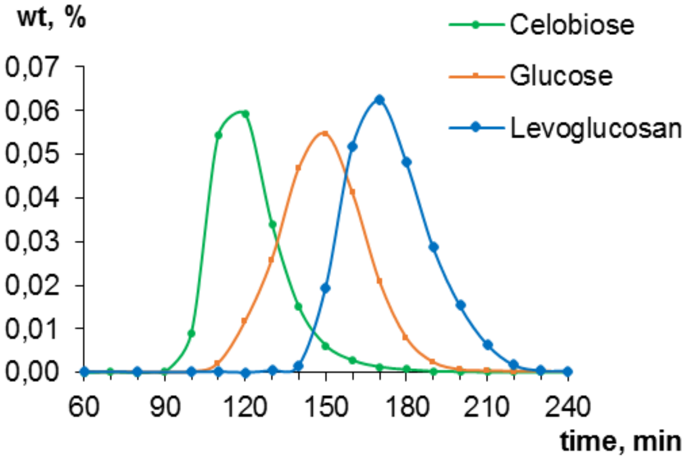

Fig. 2. A chromatogram of standard sugars – cellobiose, glucose, levoglucosan – obtained on a weakly acidic cation exchange resin in Na^+ form column with water as eluent

Although the separation of sugar mixtures on ion exchangers is generally a combination of various retention mechanisms [28], it is plausible that the weak retention of cellobiose, a disaccharide, was due to size exclusion, which was ensured by the macropores of the sorbent. The difference of the retention of glucose and levoglucosan was influenced by the polarity of these molecules and their complex formation ability (number of hydroxyl groups).

When pyrolysis liquid samples were separated on the WAC column, it was found that addition of ethanol to the mobile phase improved the separation of levoglucosan (selectivity for sugars/levoglucosan increased from 2.5 to 3.0), so Fig. 3A shows a chromatogram of sample D, which was obtained with a water/ethanol mixture (4:1) as the eluent. The effect of the addition of ethanol can be attributed to the fact that, WAC resins have an acrylic polymer matrix, which is relatively polar, compared to polysterene-divinylbenzene copolymers in SAC resins, which are completely nonpolar [29]. In this case hydrophobic-hydrophilic retention mechanisms were at work, so the change of the polarity of the eluent had an influence on the separation of the sample.

In Fig. 3A the first chromatographic peak consists of overlapping peaks of several compound groups, including sugars, other anhydrosugars besides levoglucosan, and phenolic compounds, which are the products of the thermal degradation of lignin and have an absorption at 275 nm. The phenol peak is expressed as the relative absorption, instead of mass fraction, because it is a mixture of different phenol derivatives and could not be determined as specific substances with a specific molecular weight. It is very likely that these were high molecular products of the condensation of phenols and aldehydes, so they were eluted first along with oligosaccharides due to size exclusion mechanisms. Fig. 3A also shows a large peak of levoglucosan, which was asymmetrical in favour of the smaller retention times, because there were actually other anydrosugars present in pyrolysis liquids, which had a smaller retention time.

Although the addition of ethanol increased the selectivity of the WAC column, if industrial processes are to be developed for the separation of levoglucosan, it would be favorable to avoid organic eluents, both for economical and safety reasons. But, when the SAC column was used, distilled water turned out to be the most selective eluent. Fig. 3B shows a chromatogram of the pyrolysis liquid sample, which was separated on a SAC column with water as the eluent. The most notable difference between the mentioned cation exchange resins is the fact, that the SAC column provided better separation between levoglucosan and other anhydrosugars – while in Fig. 3A there is only one asymmetrical peak of anhydrosugars, in Fig. 3B there are two separate anhydrosugar peaks. On the other hand the WAC column was more effective for the removal of phenols from the levoglucosan fraction.

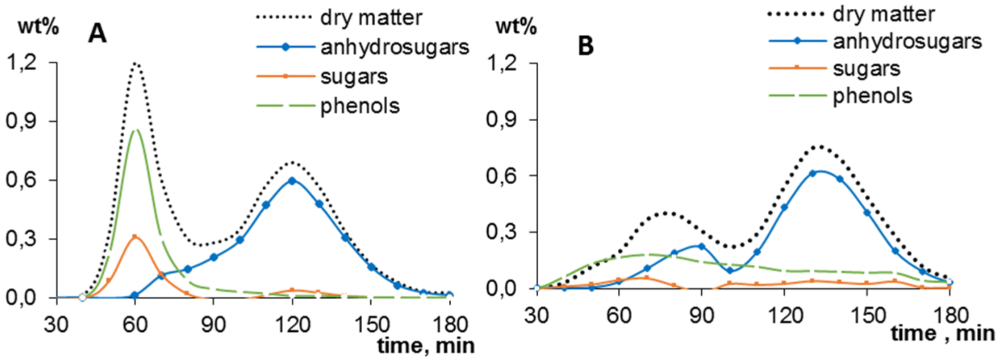

Fig. 3. Chromatograms of pyrolysis liquids (sample D): A – weakly acidic cation exchange resin in Na^+ form column with water/ethanol (v/v 4:1); B – strongly acidic cation exchange resin in Ca^{2+} form column with water as eluent

Four different samples of pyrolysis liquids were separated, using cation exchange resins, and fractions with an increased concentration of levoglucosan were collected (after 90 min). Table 1 shows the content of levoglucosan in each sample as they were to begin with, and after they had been separated on the column. Regardless of the initial mass concentration of levoglucosan in the samples (from 5.3 to 59 wt% in Table 1), the purity of the obtained levoglucosan fraction was not less than 70 wt%, keeping the yield at approximately 75 wt%. The purity of some sugars in wood hydrolysates after preparative column chromatography has been reported [22] to be lower (after a single separation: 41 % for galactose, 19 % for mannose, 7 % for rhamnose and 12 % for fucose).

Table 1. The purity and yield (with standard deviations) of levoglucosan after fractionation with cation exchange resins

Sample	Levoglucosan before fractionation wt% (purity)	Levoglucosan after fractionation wt% (purity)	Yield of levoglucosan after fractionation wt%
A	5.3 ± 0.1	70 ± 7	75 ± 4
B	23.0 ± 0.3	69 ± 8	73 ± 8
C	46.2 ± 0.5	86 ± 8	74 ± 4
D	58.9 ± 0.4	79 ± 5	73 ± 12

When 25 g of sample D were separated on the WAC column, two fractions were collected. Table 2 shows that, the second fraction contained mostly levoglucosan. The first fraction was a mixture of phenolic substances, sugars and other anhydrosugars, equivalent to 16.0 ± 0.2 wt% levoglucosan.

Table 2. The content of anhydrosugars expressed as levoglucosan in sample D, and the two fractions of this sample obtained with a weakly acidic cation exchange column

Sample fraction	Anhydrosugars (as levoglucosan) wt%
Unfractionated sample of pyrolysis liquids	58.9 ± 0.4
1st fraction (< 90 min)	16.0 ± 0.2
2nd fraction (> 90 min)	83.4 ± 0.4
Crystals from 2nd fraction	94.9 ± 0.9

The second fraction (rich with levoglucosan) showed signs of crystallization. It is known that pure levoglucosan is a white crystalline substance [10], but the colour of the second fraction was still brown, even though there were visible signs of crystallization. The addition of acetone to the levoglucosan rich fraction (83.4±0.4 wt% purity in Table 2), formed levoglucosan crystals with purity 94.9±0.9%. But crystallization was not observed, when acetone was added to the unfractionated pyrolysis liquid sample (58.9±0.4 wt% purity in Table 2). The crystallization took a long time (first crystals formed after storage at 4 °C overnight, but as more days went by more crystals gradually appeared) and the yield of levoglucosan was not sufficient, so further investigation should be done to develop an effective crystallization method.

4. CONCLUSIONS

The anion exchange resin was not suitable for the fractionation of pyrolysis liquids, because the phenol and aldehyde condensation products were strongly retained on the column, making it impossible to regenerate the sorbent. However, cation exchange columns proved to be effective for increasing the concentration of levoglucosan. The separation of different samples of pyrolysis liquids showed, that a high content of levoglucosan in the last fraction (at least 70%) was achieved regardless of the initial amount of anhydrosugars in the sample. Increasing the concentration of levoglucosan by column chromatography benefited its crystallization to obtain a product with higher purity. Furthermore, the use of a SAC column might enable the separation of other anhydrosugars, such as 1,6-anhydro-β-D-glucofuranose, which is the isomer of levoglucosan. This would require a different final purification step, because 1,6-anhydro-β-D-glucofuranose is not crystalline, but it is still a perspective research line, as including another product with added value to a biorefinery increases the economical benefit.

ACKNOWLEDGEMENTS

This work was supported by the Latvian National Programme ’’Forest and earth entrailed resources: research and sustainable utilization – new products and technologies’’ (ResProd) Project Nr. 3 ’’Biomaterials and products from forest resources with versatile applicability’’.

REFERENCES

1. *Joint European Biorefinery Vision for 2030 Star-Colibri.*; 2011:54. Available at: www.star-colibri.eu/files/files/vision-web.pdf*IEA Bioenergy Task 42 Biorefinery*, 2009. Availa*ble at: www.biorefinery.nl/fileadmin/biorefinery/docs/B*rochure_Totaal.
2. GOLDEMBERG, J., TEIXEIRA COELHO, S. Renewable energy—tradit*ional biomass vs. modern biomass. Energy Policy*, 2004, Vol. 32, No. 6, p. 711–714.
3. KERSTEN, S., GARCIA-PEREZ, M. Recent developments in fast pyrolysis of ligno-cellulosic materials. *Curr. Opin. Biotechnol.*, 2013, Vol. 24, No. 3, p. 414–420.
4. KWON, G., KIM, D., KIMURA, S., KUGA, S. Rapid-cooling , continuous-feed pyrolyzer for biomass processing Preparation of levoglucosan from cellulose and starch. *J. Anal. Appl. Pyrolysis*, 2007, Vol. 80, p. 1–5.
5. LIN, T., GOOS, E., RIEDEL, U. A sectional approach for biomass : Modelling the pyrolysis of cellulose. *Fuel Process. Technol.*, 2013, Vol. 115, p. 246–253.
6. 6. CHLUDZINSKI, M., MILAN, D., FOREST, R., STONE, A.E.M. Modified dextrans in a dental health method deactivating glucosyltransferase enzymes. Patent US4767614, 1988.
7. LUQUE, L., WESTERHOF, R., ROSSUM, G. VAN. Pyrolysis based bio-refinery for the production of bioethanol from demineralized ligno-cellulosic biomass. *Bioresour. Technol.*, 2014, Vol. 161, p. 20–28.

8. LAZDINA, B., STIRNA, U., TUPUREINA, V. Synthesis and biodegradation of poly(ester urethanes) based on levoglucosan monoacetate. *Polym. Sci. Ser. A,* 2004, Vol. 46, No. 4, p. 411–416.
9. ERMOLENKO, M.S. Convenient and Efficient Synthesis of 2 , 4-Dideoxy-levoglucosan. *Synth. Commun.,* 2013, Vol. 43, No. 21, p. 2841-2845.
10. Sigma aldrich levoglucosan. Available at: http://www.sigmaaldrich.com/catalog/product/aldrich/316555?lang=en
11. ALEXANDER, L., HOYT, C., MICHALCZYK, R., WU, R., DL, T., LA, S. Gram-scale synthesis and efficient purification of 13C-labeled levoglucosan from 13C glucose . *J. Label. Compd. Radiopharm.,* 2013, Vol. 56, No. 1, p. 27–9.
12. MEIER, D., BELD, B. VAN DE, BRIDGWATER, A.V., ELLIOTT, D.C., OASMAA, A., PRETO, F. State-of-the-art of fast pyrolysis in IEA bioenergy member countries. *Renew. Sustain. Energy Rev.,* 2013, Vol. 20, p. 619–641.
13. LI, Q., STEELE, P.H., YU, F., MITCHELL, B., HASSAN, E.M. Pyrolytic spray increases levoglucosan production during fast pyrolysis. *J. Anal. Appl. Pyrolysis,* 2013, Vol. 100, p. 33–40.
14. LIN, T., GOOS, E., RIEDEL, U. A sectional approach for biomass : Modelling the pyrolysis of cellulose. *Fuel Process. Technol.,* 2013, Vol. 115, p. 246–253.
15. HABETS, S., WILD, P.J. DE, HUIJGEN, W.J.J., ECK, E. VAN. The influence of thermochemical treatments on the lignocellulosic structure of wheat straw as studied by natural abundance 13 C NMR. *Bioresour. Technol.,* 2013, Vol. 146, p. 585–90.
16. BRIDGWATER, A. Renewable fuels and chemicals by thermal processing of biomass. *Chem. Eng. J.,* 2003, Vol. 91, No. 2–3, p. 87–102.
17. MIURA, M., TANAKA, R. Refinement of levoglucosan in wood pyroligneous liquor. *Mokuzai Gakkaishi,* 1996, Vol. 42, No. 3, p. 318–321.
18. PHETRAK, A., LOHWACHARIN, J., SAKAI, H., MURAKAMI, M., OGUMA, K., TAKIZAWA, S. Simultaneous removal of dissolved organic matter and bromide from drinking water source by anion exchange resins for controlling disinfection by-products. *J. Environ. Sci.,* 2014, Vol. 26, No. 6, p. 1294–300.
19. SAARI, P., HEIKKILA□, H., HURME, M. Adsorption Equilibria of Arabinose, Fructose, Galactose, Glucose, Mannose, Rhamnose, Sucrose, and Xylose on Ion-Exchange Resins. *J. Chem. Eng. Data,* 2010, Vol. 55, No. 9, p. 3462–3467.
20. GANDER, M., RAPP, K.M., SCHIWECK, H. Process for preparing 1,6-beta-D-anhydroglucopyranose (levoglucosan) in high purity. Patent US5023330, 1991.
21. HARLAND, C.E. Ion Exchange: Theory and Practise, RSC, 1994, 285 p.
22. SAARI, P. Industrial Scale Chromatographic Separation of Valuable Compounds from Biomass Hydrolysates and Side Streams. Aalto University, 2011.
23. ZHURINSH, A., DOBELE, G., RIZHIKOVS, J., ZANDERSONS, J., GRIGUS, K. Effect of pre-treatment conditions on the analytical pyrolysis products from birch wood lignocellulose. In: *Journal of Analytical and Applied Pyrolysis*., 2013,Vol. 103, p. 227–231.
24. MEILE, K., ZHURINSH, A., SPINCE, B. Aspects of Periodate Oxidation of Carbohydrates for the Analysis of Pyrolysis Liquids. *J. Carbohydr. Chem.,* 2014, Vol. 33, No. 3, p. 105–116.
25. WANG, Z., JIANG, J., WANG, X. Selective removal of phenolic lignin derivatives enables sugars recovery from wood prehydrolysis liquor with remarkable yield. *Bioresour. Technol.,* 2014, Vol. 174, p. 198–203.
26. MULLEN, C.A., BOATENG, A.A. Chemical Composition of Bio-oils Produced by Fast Pyrolysis of Two Energy Crops. *Energy & Fuels,* 2008, Vol. 22, No. 3, p. 2104–2109.
27. BERTERO, M., GOROSTEGUI, H.A., ORRABALIS, C.J., GUZMÁN, C.A., CALANDRI, E.L., SEDRAN, U. Characterization of the liquid products in the pyrolysis of residual chañar and palm fruit biomasses. *Fuel,* 2014, Vol. 116, p. 409–414.

28. CARUEL, H., RIGAL, L., GASET, A. Carbohydrate separation by ligand-exchange liquid chromatography Correlation between the formation of sugar-cation complexes and the elution order. *J. Chromatogr.*, 1991, Vol. 558, p. 89–104.
29. EITH, C., KOLB, M., SEUBERT, A. Practical Ion Chromatography: An Introduction, Metrohm, 2011, 161 p.

CYSENI 2015, May 27-28, Kaunas, Lithuania
ISSN 1822-7554, www.cyseni.com

KINETIC ANALYSIS OF OIL PALM EMPTY FRUIT BUNCH (OPEFB) PELLETS AS A FEEDSTOCK FOR PYROLYSIS

B.B. Nyakuma, A. Ahmad, A. Johari, T.A.T. Abdullah, O. Oladokun,
A. Bello, H. Alkali, S.I. Ahmed
Institute of Hydrogen Economy
Universiti Teknologi Malaysia
81310 Skudai, Johor Bahru – Malaysia
Phone +60133337635
Email: bbnyax1@gmail.com,bnbevan2@live.utm.my

ABSTRACT

The thermal behaviour and decomposition kinetics of pelletized oil palm empty fruit bunch (OPEFB) was investigated in this study using thermogravimetric analysis (TGA). The OPEFB pellets were heated from 30-1000 ºC at different heating rates; 5, 10 and 20 C min^{-1} under inert atmosphere. Thermal degradation occurred in three steps; drying, devolatization and char decomposition. Subsequently, the Popescu method was applied to the TG/DTG data to determine the kinetic parameters of the OPEFB pellets. The activation energy, *E*, for different degrees of conversion, α = 0.05 to 0.7 are 36.60 kJ/mol to 233.90 kJ/mol with high correlation R^2 values. In addition, the drying and decomposition of lignin reactions displayed lower *E* values compared to the devolatization characterized by high *E* value of 233 kJ/mol at α = 0.2. This indicates that the devolatization process is slower and requires higher energy requirement to reach completion than the other stages of thermal decomposition of the fuel under inert atmosphere.

Keywords: decomposition, kinetics, oil palm, empty fruit bunch, pyrolysis

1. INTRODUCTION

The inefficient disposal and management of waste in the Malaysian oil palm industry has resulted in increased environmental pollution, greenhouse gas (GHGs) emissions, and burden on the life cycle of palm oil production. In spite of this, lignocellulosic oil palm waste (OPW) can be converted into solid, liquid and gaseous biofuels. The potential of OPW as a renewable feedstock for clean biofuels production has been highlighted in literature [1–4].

However, the valorisation of OPW for energy applications is currently hampered by the poor fuel properties [5], low conversion efficiencies [6] and operational problems such as agglomeration [7]. The effective, efficient and sustainable utilization of biomass resources for energy applications can be improved by characterization and pre-treatment processes. Hence, knowledge of the thermochemical properties of lignocellulosic biomass resources is vital particularly in the design, optimization and scale up of future biomass conversion systems [8].

Therefore, this study is aimed at investigating the thermal behaviour and decomposition kinetics of oil palm empty fruit bunch (OPEFB) pellets using a thermogravimetric analyser (TGA). This will augment current scientific knowledge on thermochemical conversion of OPEFB currently hampered by operational problems [9].

2. EXPERIMENTAL

The OPEFB pellets were procured from a local oil palm mill in Kota Tinggi, Johor Malaysia. The pellets were pulverised in Panasonic Dry Miller^{TM} and sieved using a Retsch^{TM} analytical sieve to obtain homogenous particles below 250 μm in size. Ultimate analysis was determined using the LECO CHNS 932 elemental analyser according to ASTM D5291. The proximate of the OPEFB was determined using standard ASTM techniques E871, E872 and D1102 for determining moisture content, volatiles and ash respectively. The tests were repeated at least three times to ensure the reliability of the runs. The fixed carbon content of the fuel was determined by difference. For each TGA run 8-10 mg of powdered OPEFB pellets was placed in an alumina crucible and heated from 30-1000 ºC in a Netzsch 209 F3 TG Analyser at 5 °C/min, 10 °C/min and 20 °C/min heating rates using nitrogen (99.99%) N_2 (flowrate 50 ml/min) as purge gas. The TG/DTG data was deduced to investigate the thermal behaviour and decomposition kinetics of the OPEFB pellets using the Popescu method [10]. The kinetic method has been described and successfully applied to biomass materials [11-13]. Hence the method was applied in this study to determine the activation energy *E*, conversions, $\alpha = 0.05–0.7$ of the OPEFB pellets.

The rate of solid state thermal decomposition of the OPEFB pellets can be described by the modified Arrhenius equation expressed mathematically as;

$$\frac{d\alpha}{dt} = A\exp\left(-\frac{E}{RT}\right)f(\alpha) \tag{1}$$

Where, dα/dt is rate of conversion, *t* – time; *A* - pre-exponential or frequency factor; *E* – activation energy; *R* – universal gas constant, *f*(α) is the reaction model. At constant heating rate, *β*, given by the relation, dT/dt, can be substituted into Eq.1;

$$\frac{d\alpha}{dT} = \frac{A}{\beta}\exp\left(-\frac{E}{RT}\right)f(\alpha) \tag{2}$$

By integrating Eq. 2, we can obtain the integral form for the dependence function of conversion *f*(α) denoted by G(α) expressed as;

$$G(\alpha) = \int_0^{\alpha}\frac{d\alpha}{f(\alpha)} = \frac{A}{\beta}\int_0^{\infty}\frac{d\alpha}{f(\alpha)}exp\left(-\frac{E}{RT}\right)dT \tag{3}$$

Eq.3 is the general equation used to describe the temperature dependence of the kinetic parameters during solid state thermal decomposition of biomass species. Hence, it is the basis for numerous isoconversional models such as the (KAS) Kissinger-Akihara-Sunose [14] (Eq 4) from which the Popescu method is derived [13].

$$\ln\left(\frac{\beta}{T^2}\right) = \ln\left(\frac{AR}{G(\alpha)E}\right) = \frac{E}{RT} \tag{4}$$

The generalised expression for the Popescu method [10, 11], Eq.3 can be rewritten for the degrees of conversion a_m, and a_n undergoing thermal conversion at temperatures T_m, and T_n respectively;

$$G(\alpha)_{mn} = \int_{\alpha_m}^{\alpha_n}\frac{d\alpha}{f(\alpha)} = \frac{1}{\beta}\int_{T_m}^{T_n}k(T)dT = \frac{A}{\beta}H(T)_{mn} \tag{5}$$

The terms $(H)T_{mn}$, and T_δ are defined by Eq. 6–7 respectively;

$$H(T)_{mn} = (T_n - T_m)\,exp\left(-\frac{E}{RT_{\partial}}\right) \tag{6}$$

$$T_{\partial} = \left(\frac{T_n + T_m}{2}\right) \tag{7}$$

Consequently, the final equation for the Popescu method can be obtained by integrating Eq. 4 at temperatures T_m and T_n for degrees of conversion a_m and a_n respectively.

$$\ln\left(\frac{\beta}{T_n - T_m}\right) = \ln\left(\frac{A}{G(\alpha)}\right) - \frac{E}{RT} \tag{8}$$

Therefore the activation energy E, can be deduced from the slope of the plot of $In\ [\beta\ /\ (T_n\text{-}T_m)]$ vs $1/T_{\delta}$ for the decomposition of the biomass during thermal analysis.

3. RESULTS AND DISCUSSION

3.1 Chemical Fuel Properties

The heating value, ultimate and proximate analyses for OPEFB pellets are presented in Table 1. The oxygen and fixed carbon were obtained by diffrence from the ultimate and proximate analysis repsectively. The ultimate analysis is presentened in dry ash free (daf) basis while proximate and heating value are reported in as received (a.r) basis.

Table 1. Chemical fuel properties of OPEFB Pellets

Ultimate Analysis *(wt %) daf basis*	Carbon	C	49.44
	Hydrogen	H	6.57
	Nitrogen	N	1.38
	Sulfur	S	0.05
	Oxygen*	O	57.16
Proximate analysis *(wt % ar basis)*	Moisture	M	8.17
	Volatiles	V	71.83
	Fixed Carbon*	F	15.44
	Ash	A	4.56
Heating value (MJ/kg)	Higher Heating Value	HHV	17.57

The elemental *C, H, O* content for biomass generally range from; 42–71%, 3–11% and 16–49% respectively. The elemental composition of OPEFB pellets presented in Table 1 is in good agreement with reported literature values [15]. The study by Vassilev et al., (2010) also reveals that biomass *N* content ranges from 0.1–12% and 0.01–2.3% for *S* which suggests that the reported OPEFB properties are within the acceptable limits. Furthermore, it also indicates that the fuel has low susceptibility to NO_x and SO_x emissions during thermal conversion.

The volatiles and fixed carbon content of biomass are generally within 48–86 % and 1–38 % respectively [15]. Since volatiles and fixed carbon comprises condensable and noncondensable matter [16] namely CO, CO_2, H_2, moisture and tars [17], we can predict that thermal conversion of OPEFB pellets will yield reasonable solid, gaseous, and liquid products.

The heating value of the OPEFB pellets (17.57 MJ/kg) indicates the fuel contains sufficient calorific value for utilization as a solid biomass fuel (SBF) for future thermochemical energy applications. Furthermore, its low moisture and ash content is vital for efficient fuel conversion and minimal operating problems such as agglomeration and slagging [18] in gasifiers and biolers.

3.2 Thermal Analysis of OPEFB

Fig. 1–2 present the TG/DTG curves for OPEFB pellets indicating weight loss (mass loss fraction) and derivative weight loss under inert atmosphere. The curves show the typical inverted *S*-shaped temperature dependent weight loss phenomena typically observed for the decomposition of biomass materials during thermal analysis.

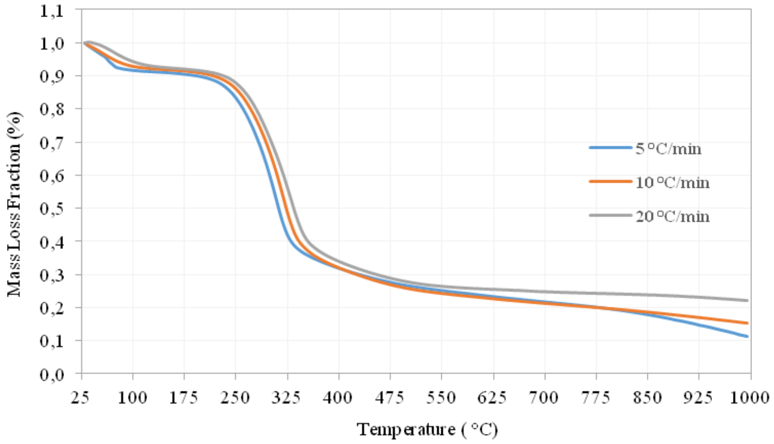

Fig. 1. TG curves for OPEFB pellets

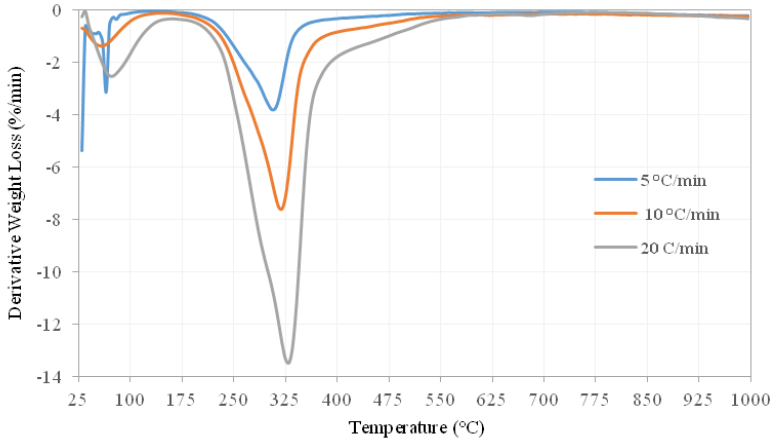

Fig. 2. DTG curves for OPEFB pellets

In addition, we can observe the curves shifted to the right with increasing heating rate from 5 °C to 20 °C during thermal analysis. This can attributed to the thermal lag resulting from the thermal resistance between the reacting and evolved species which occurs at higher heating rates during thermal analysis of biomass samples. This observation has been described by other researchers in literature and is this is considered as classic behaviour of biomass materials during in thermal analysis [19, 20].

The DTG curves in Fig. 2 also displayed the temperature dependency of the thermal decomposition process (TDP) observed in the TG curves of the sample with increase in heating rate. In addition, analysis of the curves also indicate that the TDP is a 3-step occurrence involving the loss of moisture or drying from (30-175 °C), active devolatization or loss of volatiles from (175–400 °C) and char degradation (400-1000 °C) denoted by the long tailing in the DTG curves. Similar trends have been reported for biomass samples in literature [21, 22].

3.3 Kinetic Analysis of OPEFB

The Popescu method was used to deduce the activation energy, *E*, from the slope of the plot of *In* $[\beta / (T_n\text{-}T_m)]$ vs $1/T_\delta$ presented in Figure 3 for the degrees of conversion a_m and a_n at temperatures T_m and T_n for respectively.

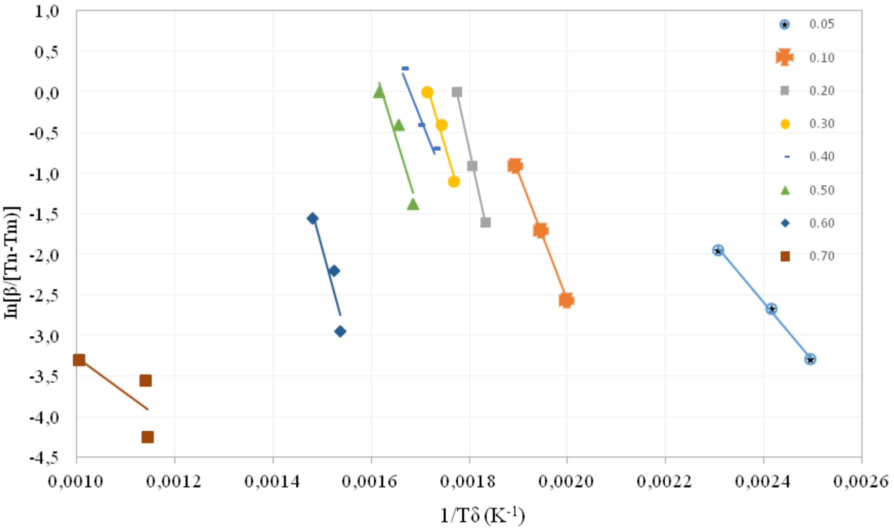

Fig. 3. Regression plots for OPEFB pellets

The values 0.05–0.70 represent the degree or extent of conversion of the OPEFB pellets at 5% to 70% during thermal-kinetic analysis. It is important to state that values above 0.7 (70% conversion) have been customarily excluded due to low correlation (R^2).

The activation energy, *E* was widely distributed for the degrees of conversion, a_n, a_m as presented in Table 2. The values of *E* ranged from 36.60 kJ/mol to 233.92 kJ/mol with high correlation (R^2) values. The results highlight the influence of temperature on the kinetics of OPEFB pellets decomposition.

Table 2. Activation Energy, *E*, of OPEFB from Popescu Method

Heating Rate, *β*	**R^2**	***E* (kJ/mol)**
0.05	0.9980	59.51
0.10	0.9985	131.25
0.20	0.9981	233.92
0.30	0.9657	169.97
0.40	0.9565	125.93
0.50	0.9055	164.24
0.60	0.8844	181.42
0.70	0.5225	36.60

The highest *E* was 233.93 kJ/mol at the degree of conversion α = 0.2 during the active devolatization or loss of volatiles from 175–400 °C. The reported *E* values for lignin (250–550 °C), hemicellulose (250–350 °C) and cellulose (300–430 °C) are 80, 100 and 200 kJ/mol [13]. Hence it will appear the predominant reaction during the thermal analysis of OPEFB pellets is the active devolatization or cellulose decomposition. However the overlapping temperature ranges and reactivity of the lignocellulosic biomass components mean that lignin and hemicellulose also undergo decomposition concurrently at low temperatures [23].

The lowest E values of were 59.51 kJ/mol at $\alpha = 0.05$ for drying and 36.60 kJ/mol at $\alpha = 0.70$ for lignin decomposition. This suggests that the drying and devolatization reactions require minimal energy to occur rapidly compared to active devolatization process during thermal analysis. Hence, we can infer that active devolatization of the OPEFB pellets is the slow reaction or rate determining step during thermal degradation.

4. CONCLUSION

The thermal kinetics and decomposition behaviour of oil palm empty fruit bunch (OPEFB) pellets was investigated at different heating rates under non-isothermal inert conditions. Thermal analysis revealed the widely reported three-step-reaction process; drying, devolatization and lignocellulosic char decomposition. Thermal kinetics was evaluated using the Popescu method, a modified form of the Kissinger-Akihara-Sunose (KAS) method to determine the kinetic parameters of the OPEFB pellets. The average activation energy, E, for overall decomposition of the fuel was 137.86 kJ/mol. In addition, the drying and decomposition of lignin reactions displayed lower E values compared to the devolatization stage which can be considered as the rate determining step of the process.

5. ACKNOWLEDGMENT

The authors will like to acknowledge the financial support of the Ministry of Education Malaysia for the Long Research Grant Scheme (LRGS VOT No. 4L817). The contribution of Syie Luing Wong, Muhamad Faizal and Dr Ahmad Romli of POCREST, Universiti Teknologi MARA, Shah Alam is gratefully acknowledged.

REFERENCES

1. YUSOFF, S. Renewable energy from palm oil – innovation on effective utilization of waste. *Journal of Cleaner Production*, 2006. 14(1): p. 87–93.
2. YANG, H., YAN, R., CHEN, H., LEE, D.H., LIANG, D.T., ZHENG, C. Pyrolysis of palm oil wastes for enhanced production of hydrogen rich gases. *Fuel Processing Technology*, 2006. 87(10): p. 935–942.
3. ATNAW, S.M., SULAIMAN, S.A., YUSUP, S. Syngas production from downdraft gasification of oil palm fronds. *Energy*, 2013. 61: p. 491–501.
4. CHANG, S.H. An overview of empty fruit bunch from oil palm as feedstock for bio-oil production. *Biomass and Bioenergy*, 2014. 62: p. 174–181.
5. ABDULLAH, N.; GERHAUSER, H.SULAIMAN, F. Fast pyrolysis of empty fruit bunches. *Fuel*, 2010. 89(8): p. 2166–2169.
6. HUSAIN, Z.; ZAINAL, Z., ABDULLAH, M. Analysis of biomass-residue-based cogeneration system in palm oil mills. *Biomass and Bioenergy*, 2003. 24(2): p. 117–124.
7. LAHIJANI, P., ZAINAL, Z.A. Gasification of palm empty fruit bunch in a bubbling fluidized bed: a performance and agglomeration study. *Bioresour Technol*, 2011. 102(2): p. 2068–2076.
8. NYAKUMA, B.B., MAZANGI, M., TUAN ABDULLAH, T.A., JOHARI, A., AHMAD, A., OLADOKUN, O. Gasification of Empty Fruit Bunch Briquettes in a Fixed Bed Tubular Reactor for Hydrogen Production. *Applied Mechanics and Materials*, 2014. 699: p. 534–539.

9. LAHIJANI, P.; ZAINAL, Z. A., Fluidized Bed Gasification of Palm Empty Fruit Bunch Using Various Bed Materials. *Energy Sources, Part A: Recovery, Utilization, and Environmental Effects*, 2014. 36(22): p. 2502-2510.
10. POPESCU, C., Integral method to analyze the kinetics of heterogeneous reactions under non-isothermal conditions A variant on the Ozawa-Flynn-Wall method. *Thermochimica Acta*, 1996: p. 309-323.
11. JEGUIRIM, M.; DORGE, S.TROUVE, G., Thermogravimetric analysis and emission characteristics of two energy crops in air atmosphere: Arundo donax and Miscanthus giganthus. *Bioresour Technol*, 2010. 101(2): p. 788-793.
12. LI, D.; CHEN, L.; ZHANG, X.; YE, N.XING, F., Pyrolytic characteristics and kinetic studies of three kinds of red algae. *Biomass and Bioenergy*, 2011. 35(5): p. 1765-1772.
13. SUN, W. G.; ZHAO, H.; YAN, H. X.; SUN, B. B.; DONG, S. S.; ZHANG, C. W.QIN, S., The Pyrolysis Characteristics and Kinetics of Jerusalem artichoke Stalk Using Thermogravimetric Analysis. *Energy Sources, Part A: Recovery, Utilization, and Environmental Effects*, 2012. 34(7): p. 626-635.
14. KISSINGER, H. E., Reaction kinetics in differential thermal analysis. *Anal. Chem.*, 1957. 29: p. 1702-1706.
15. VASSILEV, S. V.; BAXTER, D.; ANDERSEN, L. K.VASSILEVA, C. G., An overview of the chemical composition of biomass. *Fuel*, 2010. 89(5): p. 913-933.
16. BASU, P., *Biomass gasification, pyrolysis and torrefaction: practical design and theory*. 2013: Academic Press.
17. DEMIRBAS, A., Combustion characteristics of different biomass fuels. *Progress in Energy and Combustion Science*, 2004. 30(2): p. 219-230.
18. BASU, P., *Combustion and gasification in fluidized beds*. 2006: CRC press.
19. SLOPIECKA, K.; BARTOCCI, P.FANTOZZI, F., Thermogravimetric analysis and kinetic study of poplar wood pyrolysis. *Applied Energy*, 2012. 97: p. 491-497.
20. DAMARTZIS, T.; VAMVUKA, D.; SFAKIOTAKIS, S.ZABANIOTOU, A., Thermal degradation studies and kinetic modeling of cardoon (Cynara cardunculus) pyrolysis using thermogravimetric analysis (TGA). *Bioresour Technol*, 2011. 102(10): p. 6230-6238.
21. LI, B.; LV, W.; ZHANG, Q.; WANG, T.MA, L., Pyrolysis and catalytic pyrolysis of industrial lignins by TG-FTIR: Kinetics and products. *Journal of Analytical and Applied Pyrolysis*, 2014. 108: p. 295-300.
22. VHATHVAROTHAI, N.; NESS, J.YU, J., An investigation of thermal behaviour of biomass and coal during co-combustion using thermogravimetric analysis (TGA). *International Journal of Energy Research*, 2014. 38(6): p. 804-812.
23. VAMVUKA, D.; KAKARAS, E.; KASTANAKI, E.GRAMMELIS, P., Pyrolysis characteristics and kinetics of biomass residuals mixtures with lignite☆. *Fuel*, 2003. 82(15): p. 1949-1960.

CYSENI 2015, May 27–28, Kaunas, Lithuania
ISSN 1822-7554, www.cyseni.com

HYDROTHERMAL SYNTHESIS OF MOLYBDENUM DISULFIDE / MESOPOROUS CARBON NANOCOMPOSITE

L. Shyyko, V. Kotsyubynsky, I. Budzulyak
Vasyl Stefanyk Precarpathian National University
Shevchenko str. 57, 76018 Ivano-Frankivsk – Ukraine
Phone +380673436942
Email: liudmyla.shyiko@pu.if.ua

ABSTRACT

This paper presents the results devoted to the hydrothermal synthesis of molybdenum disulfide / mesoporous carbon composite using cetyltrimethylammonium cations. As precursors were used previously prepared ammonium tetrathiomolybdate, hydrazine hydrate, cetyltrimethylammonium bromide and mesoporous carbon obtained from raw material of plant origin and activated with orthophosphoric acid. Further the obtained material was annealed in Ar atmosphere at 500°C for 2 h. The samples were characterised by X-ray difractometry (XRD), Transmission electron Microscopy (TEM), Small angle X-ray scattering (SAXS) and porosimetry. It was confirmed that the composite MoS_2 has a structure of multilayer sheets dispersed in amorphous carbon. The sizes of nanoparticles of molybdenum disulfide and pores are in the vicinity of 52 nm and 5-20 nm respectively. The value of specific surface of synthesized composite is 430 m^2/g that is much lower than for mesoporous carbon material, which is 2200 m^2/g, but electric conductivity of the composite is 3 times higher (0.51 mS/m and 0.18 mS/m, respectively). The annealing has not significant effect on composite structure, that indicating the temperature stability of the material.

Keywords: molybdenum disulfide, mesoporous carbon, hydrothermal synthesis, nanocomposite

1. INTRODUCTION

The rapid development of chemical power sources and the need to improve their operating parameters stimulate researchers to study different materials that may be used as a cathode – active matrix paired with lithium or lithium containing anode. It is widely known, that a magnitude and type of conductivity of the material, as well as its structure, significantly affect the implementation processes of lithium [1]. In the best case host material must have sufficient both electronic and ionic conductivity. Porous carbon materials are widely used in separation, catalysis and energy storage and generation. However, its application in high-energy Li-ion batteries (LIBs) is largely hampered by the relatively low theoretical capacity (for graphite it is 372 mAh/g). Regarding molybdenum disulfide (MoS_2), which belongs to layered transition-metal dichalcogenides, as an electrode material for the same purpose, the feature of MoS_2 layered structure allows the Li+ ions to diffuse without a significant increase in volume expansion, but although its specific capacity is much higher than for graphite (approximately 700 mAh/g), there is still an effort of low ion/electron conductivity. According to latest tendencies the composite structure based on MoS_2 and carbonaceous matrix materials solved this problem and is highly promising as high-performance electrodes for LIBs. In addition, the feature of MoS_2 is the ability to form structures with different morphology and size, affecting the properties of this material. In particular, the flower-like particles [2], nanospheres [3], nanorods [4] and single layers [5] have been already synthesized. However, as in the most of nanoscale materials, there are the problems of aggregation and restacking during the repetitive cycling and even the drying process of electrodes, not forgetting also that MoS_2 is a semiconductor with a very low conductivity. All these issues would result in the loss of the unusual properties of the graphene-like MoS_2 and the negative effects on their properties. If the graphene-like MoS_2 nanosheets are uniformly dispersed in other medium such as carbon materials, their aggregation will be effectively inhibited, which leads to enhanced electrochemical properties. The amorphous carbon can stabilize the disordered structure of the MoS_2 nanoparticles throughout the cycling regime to accommodate more Li^+ ions, and also keep the active materials electrically connected [6,7].

We have investigated the possibility of obtaining the nanocomposite MoS_2 / C with high conductivity for high-energy electrochemical devices such as Li-ion batteries (LIBs). Here we present simple synthesis method of molybdenum disulfide / mesoporous carbon nanocomposite, that does not require significant energy, is low-cost and environmentally friendly. In addition we compare the electric conductivity of commercial MoS_2 (Merck, Germany), mesoporous carbon obtained from raw material of plant origin and synthesized molybdenum disulfide / mesoporous carbon nanocomposite.

2. MATERIALS AND METHODS

2.1. Materials preparation

2.1.1. Mesoporous carbon preparation

The powder of ground apricot seeds was used as the raw material for mesoporous carbon. 50 g of apricot seeds powder was mixed with 400 ml 30% H_3PO_4 and left for 1 h, after the mixture was thermally treated at the temperature of 550°C on air for 1 hour with the further annealing in Ar atmosphere at 500°C for 2 hours.

2.1.2. Precursor preparation

Molybdate ammonium $(NH_4)_2MoS_4$ was a precursor for MoS_2 synthesis, which was pre-prepared by following procedure: 5.88 g of $(NH_4)_2MoO_4$ was dissolved in 40.8 ml of 20% $(NH_4)_2S$. After stirring during 30 minutes at the room temperature the dark yellow precipitate of $(NH_4)_2MoS_4$ was formed (Eq.1):

$$(NH_4)_2MoO_4 + 4(NH_4)_2S \rightarrow (NH_4)_2MoS_4 + 8NH_4 \cdot OH \qquad (1)$$

2.1.3. Synthesis of MoS_2/C nanocomposite

Resulting $(NH_4)_2MoS_4$ was mixed with 1.98 ml of hydrazine hydrate $N_2H_4{\cdot}N_2O$ and 100 ml of distilled water. The pH level of the reaction medium was 7.6 and regulated by hydrochloric acid HCl. After adding 1 g of cetyltrimethylammonium bromide $C_{19}H_{42}BrN$ and 1 g of mesoporous carbon the solution was put into Teflon autoclave and stored at the temperature of 220°C for 24 hours. The resulting black precipitate was washed with distilled water and ethanol, and after centrifugation dried at 80°C. Additionally, the obtained material was annealed in argon atmosphere at 500°C for 2 hours. The experiment is based on the approaches of MoS_2 nanostructures synthesis, in particular [8].

2.2. Materials characterization

The synthesized material phase composition and structure were investigated by XRD and SAXS methods (DRON-3 diffractometer, Cu K_α radiation). Morphological characteristics and chemical composition were obtained by TEM and EDS (FEI Technai G2 X-TWIN microscope). The specific surface area and pore size distribution were measured by nitrogen adsorption at 77.2 K (Quantachrome NOVA 2200e porosimeter). Electrical conductivity σ as a function of frequency was measured by the method of impedance spectroscopy in the frequency range of 0.01–100 kHz (Autolab PGSTAT 12/FRA-2 analyser), all samples were made in pellet form with the diameter of $17 \cdot 10^{-3}$ m and thickness of $0.1 \cdot 10^{-3}$ m under pressure of 34 MPa at room temperature.

3. RESULTS AND DISCUSSION

According to XRD the synthesized material is nearly X-ray amorphous, however there are two areas of increased intensity of diffracted X-rays: in the angle 2θ about 33.4° and 58.2° and can be associated with (100) and (110) reflections of 2H-MoS_2 crystal structure, which belongs to hexagonal system and P63/mmc symetry group (Fig. 1, a). The (002) peak in the vicinity of 2θ =14-15° typical for this structure was not indentified. It, according to [9], indicates the lack of connection between the individual MoS_2 layers and the formation of graphene-like structure.

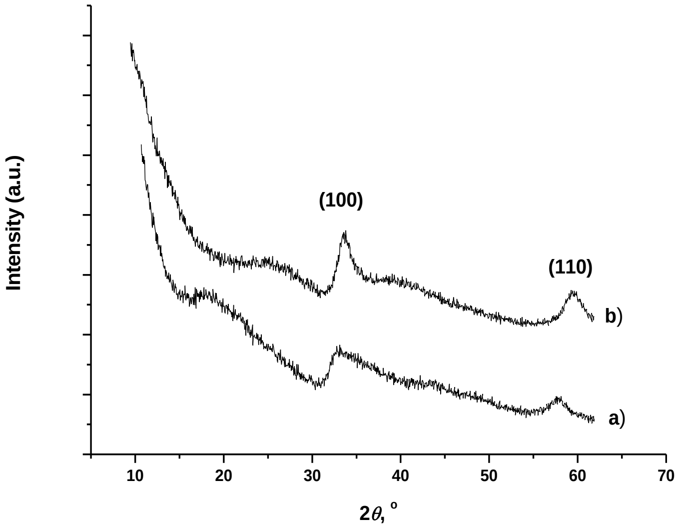

Fig. 1. Diffraction patterns of obtained materials after heat treatment at 80°C (a), 500°C (b)

After annealing in Ar atmosphere at 500°C during 2 hours, the reflex corresponding to the family of (110) planes, has shifted to higher angles by 2.2°, while the change in (100) reflex position is within acceptable error (Fig. 1, b). This fact shows the change of interatomic distances within (001) plane, i.e. along the layers formed by Mo atoms placed between two layers of S atoms, forming a trigonal prism. But in general it can be concluded that annealing did not significantly affect the morphology and composition of the nanocomposite.

TEM images (Fig. 2) show, that synthesized nanocomposite consists of stacked nanosheets (7–9) of MoS_2 characterized by crystalline order and dispersed in amorphous carbon (Fig. 2 a, b, c). According to EDS analysis the relative content of carbon atoms along 2 μm line is at least 35 at.% (Fig. 3 a). Concentrations of Mo, S and O in the sample along 2 μm line are shown in Fig. 3 (b, c and d respectively).

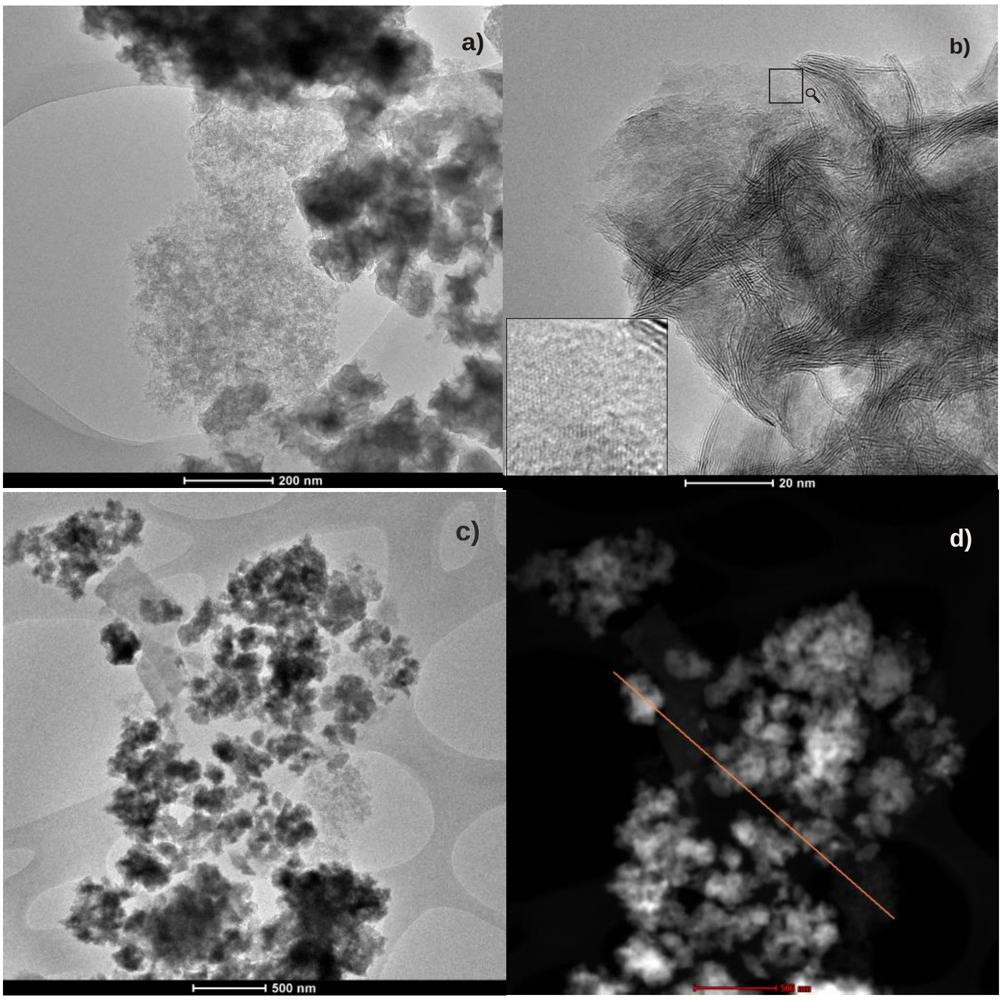

Fig. 2. TEM images of the material obtained by hydrothermal synthesis after heat treatment at 500°C

To explain the creation of such structure let's consider the processes occurring during the synthesis. Chemical reactions that take place in hydrothermal synthesis are (Eq. 2, 3):

$$2(NH_4)_2MoS_4 + N_2H_4 \rightarrow 2MoS_2 + 4H_2S + 4NH_3 + N_2, \qquad (2)$$

$$MoS_4^{2-} + N_2H_4 \rightarrow 2MoS_2 + N_2 + S^{2-} + H_2S \qquad (3)$$

In aqueous solution of $C_{19}H_{42}BrN$ there is the formation of spherical and lamellar micelles, and the dominance of second ones occurs when the surfactant excess concentration is over the value 0.05 g/cm^3 [10]. Under the applied experimental conditions in the reaction medium both types of micelles were present. The average size of lamellar micelles is about 44 nm, however, several authors, including [11], recorded significant flexibility of micelles, and in [12] there is observed a formation of the rings with diameters of 4.5–6 nm. The electrostatic interaction between the $[MoS_4]^{2-}$ complexes and positively charged parts of surfactant molecules is the driving force of adsorption on the micelle surface.

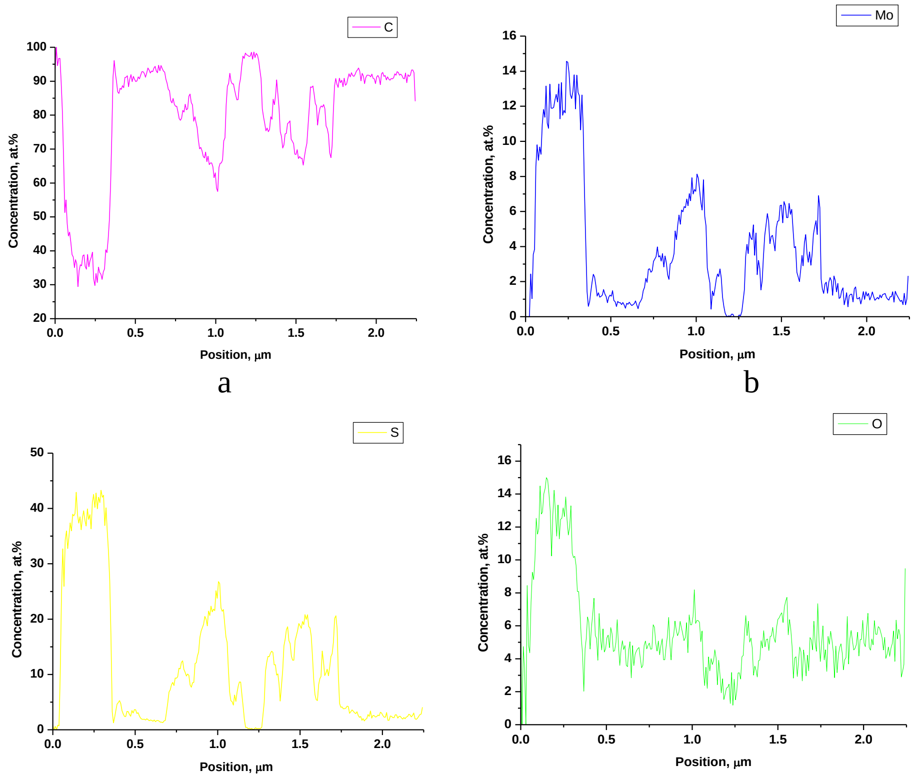

a b

c d

Fig. 3. The atomic content of components C, Mo, S and O in a fragment of the synthesized composite along the line of 2 µm by EDS

The results of nitrogen sorption, in particular, the pore size distribution of mesoporous carbon and synthesized nanocomposite (Fig. 4), confirmed that nanoparticles of molybdenum disulfide have localized in micro and mesopores of carbon material. Comparing the pore size distributions of carbon and nanocomposite (cyan and blue colors in Fig. 4), one can see the difference in the pore width range of 0–8 nm. The surface areas, calculated by the BET method from nitrogen sorption curves, of mesoporous carbon and MoS_2/C nanocomposite are 2200 m^2/g and 430 m^2/g, respectively.

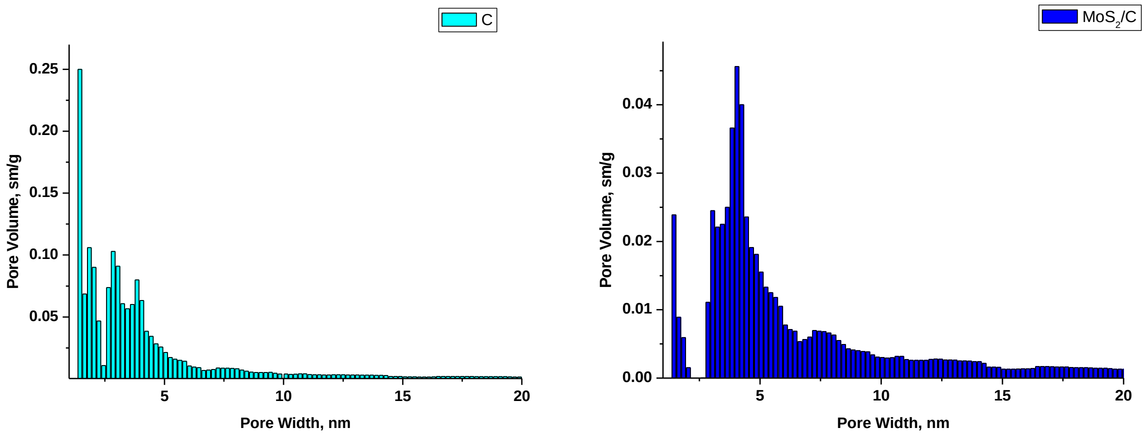

a b

Fig. 4. Pore size distributions for C (a) and MoS_2/C (b)

More information on the internal microstructure of the synthesized material we have obtained through the method of small-angle X-ray scattering (Fig. 5). Scattering intensity curves of the samples are presented in double logarithmic coordinates. The volumetric distribution function of inhomogeneities was calculated using GNOM (Institute of Crystallography RAS, Moscow) in the model of homogeneous polydisperse spheres [13].

As seen from the data scattering intensity curves of both samples show a similar character. The curves can be devided into three angular regions of $I(s)$ dependance (I is the scattering intesity, s is the module of the wave vector and $s = \frac{4\pi}{\lambda}\sin(\theta)$, 2θ is the scattering angle). In the ($s_{\min}$, s_1) range the scattering intensity is described by Guinier's law and corresponds to the scattering of X-rays by MoS_2 nanoparticles (Eq. 4):

$$I(s) \sim \exp(-\frac{1}{3}R_g{}^2 s^2) \qquad (4)$$

where R_g is a radius of inertia of the nanoparticles.

In the (s_1, s_2) range power law decline of the intensity is observed $I(s) \sim s^{-n}$, with $n \approx 4.0$. This result indicates the scattering by nanoparticles surface formed of carbon (graphene) layers. The value of $n \approx 4.0$ indicates the implementation of Porod's law of scattering by smooth (nonfractal) surface.

The (s_2, $s_{\max}$) range corresponds to scattering by polydisperse system of mesopores.

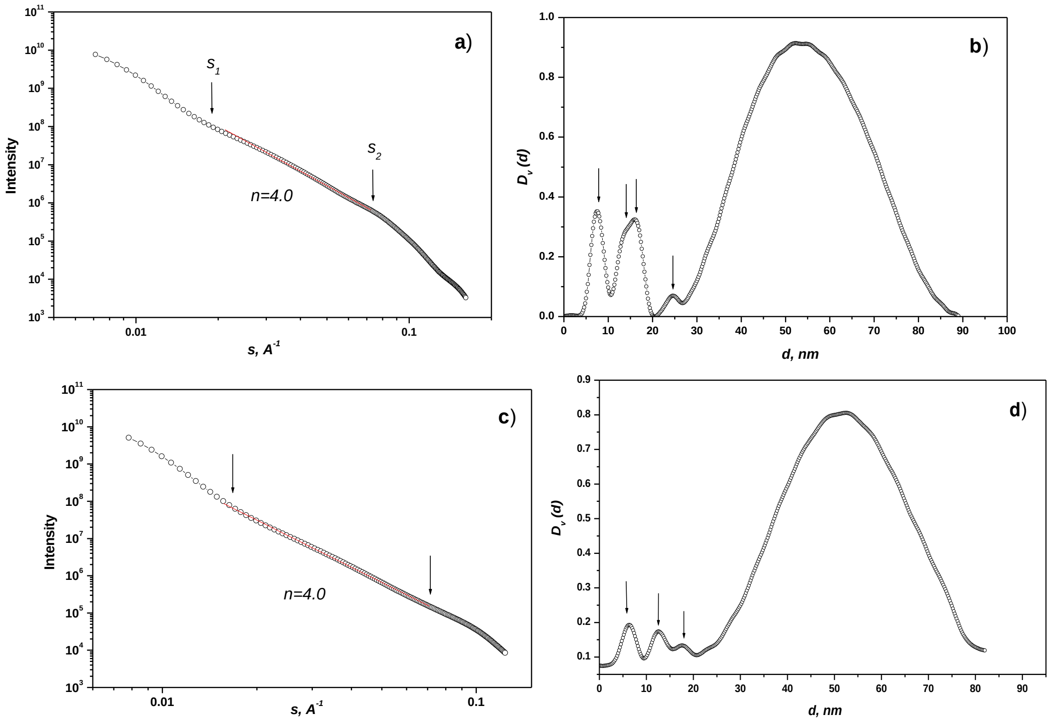

Fig. 5. The curves of scattering intensity of X-rays at small angles (a, c) and calculated scattering centers distribution function (b, d) for the material samples annealed at 80°C and 500°C, respectively

On the distribution function of scattering centers there is a broad symmetrical peak at $d \approx 52$ nm that corresponds to the most probable diameter of the MoS_2 nanoparticles. Along with it in the range of 0-25 nm there is a number of peaks corresponding to the most probable mesopore diameters. For the sample after annealing the intensity curve of X-ray scattering has not changed (Fig. 5 c), but on the distribution curve of inhomogenities the peaks mentioned above are reduced due to the decrease in the volume fraction of mesopores after annealing.

Fig. 6 shows the frequency dependence of the complex conductivity in logarithmic coordinates for mesoporous carbon before (-▲-) and after (-△-) annealing in Ar atmosphere at 500°C for 2 hours, nanocomposite MoS_2/C before (-●-) and after (-○-) annealing in Ar atmosphere at 500°C for 2 hours, and commercial MoS_2 (–) received from Merck KGaA, Germany. The curves for all samples, except for commercial MoS_2, can be divided into two areas: the linear frequency independent region, and the second one, where the conductivity increases sharply with frequency increasing.

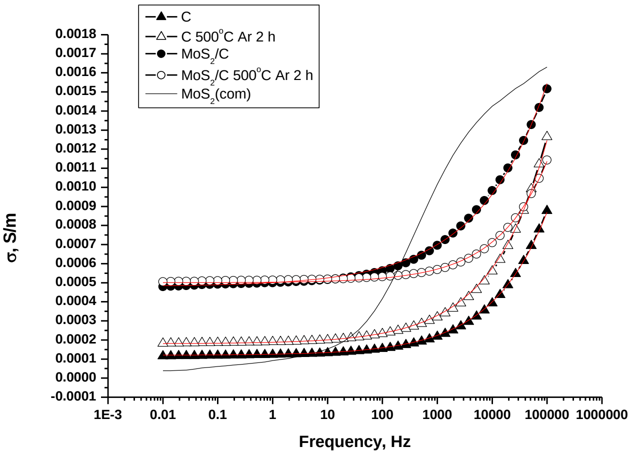

Fig. 6. Frequency dependent electrical conductivity of the samples.

Taking into account the geometrical parameters of pellets made of all samples we calculated the value of electrical conductivity by equation 7, which is derived from the following (Eq. 5 and 6) [14]:

$$\rho^* = \rho' - j\rho'', \tag{5}$$

where $\rho' = Z'S/d$ i $\rho'' = Z''S/d$, Z' and Z'' are real and imaginary parts of the complex impedance, S and d are cross-sectional area and thickness of the pellets made of the sample, respectively. The complex conductivity is the reciprocal of the complex resistance:

$$\sigma^* = \frac{1}{\rho^*} = \sigma' + j\sigma'', \tag{6}$$

where $\sigma' = \rho'/M$, $\sigma'' = \rho''/M$, and $M = |Z^*|^2(S/d)^2$, then:

$$\sigma^* = \sqrt{(\sigma')^2 + (\sigma'')^2}\ . \tag{7}$$

Conductivity of mesoporous carbon for the direct current approximation is 0.11 mS/m before and 0.18 mS/m after annealing in argon atmosphere. Such low conductivity of mesoporous carbon is due to a large number of pores and greatly depends on the graphitization degree [15]. At relatively low temperature of carbonization (below 600°C) organic base feedstock is burnt partially and a complex framework of condensed aromatic layers formed by carbon atoms is incomplete. As a result the impedance of the aggregated carbon particles, which depends on the electrical resistance of each particle and the contact resistance between them, remains quite high. Also, the presence of oxygen on nanoparticles surface affects the electrical resistance. According to [16] oxygen-containing compounds that are formed mainly at the edges of graphite fragments, enlarge the barrier for electron transfer from one crystal element to another. In addition, the electrical properties of carbon materials are directly related to their electronic and atomic structures. Typical values of electrical conductivity of amorphous carbon is in the range of 10^{-4} [17, 18] as a result of low ohmic contact between particles and carbon graphitization degree. The annealing leads to sintering and tightness of the particles that improved contact between them.

The conductivity of molybdenum disulfide, which refers to semiconductors, according to published data, at room temperature along the c axis, i.e. perpendicular to the layers, is about 10.4 mS/m [19], but for pressed pellets this value is smaller and lies in the range of 10^{-2}–10^{-4} mS/m [20, 21]. We measured the conductivity of commercial MoS_2 (Merck KGaA, Germany) with an average particle size of 10 μm and it is equal to 0.038 mS/m. The conductivity of the synthesized MoS_2/C nanocomposite is 0.48 mS/m before and 0.51 mS/m after the heat treatment in argon atmosphere at the temperature of 500°C for 2 hours (Fig. 6). The conductivity of nanocomposite increased by 3 times in comparison with carbon is due to a synergistic effect of these two materials, in particular carbon acts as a donor of electrons for molybdenum disulfide, which at low frequencies and room temperature is usually *n*-type semiconductor with hopping conductivity, i.e. the exchange of electrons between Mo ions. The excess electrons from the electron donor would be expected to reduce the hardness of the electron transfer and according to [22] in the partial electron transfer from graphene (or carbon layer) to MoS_2 layers each carbon atom donates ca. 0.027e to MoS_2 and the transferred electrons are located on sulphur atoms.

Table 1. The data obtained from Jonscher's power law approximation

Sample	**A**	***n***	**σ_{dc}, mS/m**
C	$5.4 \cdot 10^{-6}$	0.42	0.11
C (500°C, Ar)	$7.6 \cdot 10^{-6}$	0.42	0.18
MoS_2/C	$2.0 \cdot 10^{-5}$	0.34	0.48
MoS_2/C (500°C, Ar)	$2.7 \cdot 10^{-6}$	0.47	0.51

Obtained dispersion curves of dependence of conductivity on frequency ω of applied field (Fig. 6) were approximated by Jonscher's power law in disordered materials (Eq. 8) [21]:

$$\sigma(\omega) = \sigma_{dc} + A\omega^n, \tag{8}$$

where σ_{dc} is frequency independent part of conductivity, A is a temperature dependent constant that gives the information about the strength of the polarizability (or non-ideal conductivity) which comes from the diffusive motion of carriers in the sample. The exponent *n* is the slope of the linear section of the high-frequency dispersion (its value ranges from 0 to 1) and describes the process of charge transfer in disordered materials and is a measure of the interaction between charged particles involved in the processes of polarization and conductivity, and also depends on the temperature. The calculated values of A and *n* are presented in Table 1. For today the universal and exact relationship between these constants is not defined yet, a lot of researches tried to determine it empirically but still not a one assumption was proved. In our case the sample with the lowest *n* has the biggest A value. As to exponent *n*, Jonscher suggested that the range of $0 < n < 0.4$ [23] corresponds to material conductivity based on the existence of conducting grains separated by less conducting barriers. At low frequencies, each grain behaves as a macroscopic dipole, owing to the migration of a possible negative charge on its surface, which interacts strongly with its neighbors, giving rise to a strong dispersion. As the frequency is increased, this dipole has insufficient time to respond, and the bulk response of the grains predominates [24]. While the range of the exponent $0.4 < n < 0.6$ suggests multipolaron hopping of charge carriers across the interfaces of grains and grain boundaries or at the layers interfaces. This indicated the localized nature of the electronic charge carriers about the ionic sites of the crystal structure [25]. Thus, the annealing in inert atmosphere leads to the differences in the electric conductivity character as a result of microstructural changes in the nanocomposite material.

4. CONCLUSIONS

The method of MoS_2/C nanocomposite obtaining by hydrothermal method using cetyltrimethylammonium bromide and mesoporous carbon obtained from raw materials of plant origin was suggested and performed. The resulted nanocomposite consists of 7-9 stacked nanosheets of molybdenum disulfide with an average size of 52 nm dispersed in amorphous carbon, occupying most of the mesopores and filling the micropores. The surface area of mesoporous carbon is 2200 m^2/g and of synthesized nanocomposite is 430 m^2/g. Annealing in argon atmosphere at 500^oC has not significant impact on the morphology, composition and conductivity value of nanocomposites, confirming the thermal stability of the material.

The conductivity of synthesized MoS_2/C nanocomposite, which was obtained by direct current approximation, is three times higher than of carbon and almost 13 times higher than of the commercial MoS_2 with average particle size of 10 μm. The resulted high conductivity of the nanocomposite does not contradict the general patterns of nanoparticles conductivity, which is usually less than of microparticles due to the properties of the large specific surface at which the scattering occurs, and is explained by a synergistic effect between MoS_2 and carbon. This result is important for use in electrochemical electric energy generation devices.

REFERENCES

1. BROUSSELY, M., BIENSAN, Ph., SIMON, B. Lithium insertion into host materials: the key to success for Li ion batteries. *Electrochimica Acta*, 1999, Vol. 45, No.1, p. 3–22.
2. LI, H., LI, W., MA, L., CHEN, W., WANG, J. Electrochemical lithiation/delithiation performances of 3D flowerlike MoS_2 powders prepared by ionic liquid assisted hydrothermal route. *Journal of Alloys and Compounds*, 2009, Vol. 471, p. 442–447.
3. DING, Sh., ZHANG, D., CHEN, J., LOU, X. Facile synthesis of hierarchical MoS_2 microspheres composed of few-layered nanosheets and their lithium storage properties. *Nanoscale*, 2012, Vol. 4, No. 1, p. 95–98.
4. ZHENG, X., ZHU, L., YAN, A., BAI, Ch., XIE, Y. Ultrasound-assisted cracking process to prepare MoS_2 nanorods. *Ultrasonics Sonochemistry*, 2004, Vol. 11, p. 83–88.
5. MAK, K., LEE, C., HONE, J., SHAN, J.,HEINZ, T. Atomically thin MoS_2: a new direct-gap semiconductor. *Physical Review Letters*, 2010, Vol. 105, No. 13, p. 136805.
6. CHANG, K., CHEN, W., MA, L., LI, H., LI, H., HUANG, F., XU, Zh., ZHANGD, Q., LEED, J.-Y. Graphene-like MoS_2/amorphous carbon composites with high capacity andexcellent stability as anode materials for lithium ion batteries. *Journal of Materials Chemistry*, 2011, Vol. 21, No. 17, p. 6251–6257.
7. ZHU, Ch., MU, X., VAN AKEN, P.A., YU,Y., MAIER, J. Single-Layered Ultrasmall Nanoplates of MoS2 Embedded in Carbon Nanofibers with Excellent Electrochemical Performance for Lithium and Sodium Storage. *Angewandte Chemie International Edition*, 2014, Vol. 53, No. 8, p. 2152–2156.

8. LI, N., CHAI, Y., LI, Y., TANG, Z., DONG, B., LIU, Y., LIU, C. Ionic liquid assisted hydrothermal synthesis of hollow vesicle-like MoS_2 microspheres. *Materials Letters*, 2012, Vol. 66, p. 236–238.
9. LIANG, K., CHIANELLI, R., CHIEN, F., MOSS, S. Structure of poorly crystalline MoS_2 – A modeling study. *Journal of Non-Crystalline Solids*, 1986, V. 79, No. 3, p. 251–273.
10. REM-HUSSON, F., LUZZATI, V. The Structure of the Micellar Solutions of Some Amphiphilic Compounds in Pure Water as Determined by Absolute Small-Angle X-Ray Scattering Techniques. *The Journal of Physical Chemistry*, 1964, Vol. 68, No. 12, p. 3504–3511.
11. LIN, Z., CAI, J., SCRIVEN, L, DAVIS, H. Spherical-to-Worm like Micelle Transition in CTAB Solutions. *Journal of Physical Chemistry*, 1994, Vol. 98, p. 5984–5993.
12. IMAE, T., KAMIYA, R., IKEDA, S. Formation of Spherical and Rod-like Micelles of Cetyltrimethylammonium Bromide in Aqueous NaBr Solutions. *Journal of colloid and interface science*, 1985, Vol. 108, No. 1, p. 215–225.
13. SVERGUN, D. Determination of the regularization parameter in indirect-transform methods using perceptual criteria, *Journal of Applied Crystallography*,1992, Vol. 25, No. 4, p. 495–503.
14. ABDULLAH, M, YUSOFF, A. Complex impedance and dielectric properties of an Mg-Zn ferrite. *Journal of Alloys and Compounds*, 1996, Vol. 233, p. 129–135.
15. OSTAFIYCHUK, B., REVO, S., KUZYSHYN, M., BUDZULYAK, M., RACHIY, B. Influence of Degree of Compression on the Electrical Conductivity of the Composite Material. *Physics and Chemistry of Solid State*, 2013, V. 14, No. 4, p. 734–740.
16. BINIAK, S., SWIATKOWSKI, A., PAKULA, M. *Chemistry and physics of carbon.* New York: Marcel Dekker, 2001, 125 p. ISBN 0-8247-0246-8.
17. ROBERTSON, J. Amorphous carbon. *Advances in Physics*, 1986, Vol. 35, No. 4 , p. 317-374.
18. GODET, C. Hopping model for charge transport in amorphous carbon. *Philosophical Magazine B*, 2001, Vol. 81, No. 2, p. 205–222.
19. GUHA THAKURTA, S., DUTTAI, A. Electrical conductivity, thermoelectric power and Hall effect in p-type molybdenite crystal. *Journal of Physics and Chemistry of Solids*, 1983, Vol. 4, No. 5, p. 407–416.
20. BENAVENTE, E., SANTA ANA, M., GONZALEZ, G. Electrical conductivity of MoS_2 based organic–inorganic nanocomposites. *Physica Status Solidi B*, 2004, Vol. 241, No. 10, p. 2444–2447.
21. AHMAD, M., RAFIQ, M., IMRAN, Z., RASOOL, K., SHAHID, R, JAVED, Y., HASAN, M. Charge conduction and relaxation in MoS_2 nanoflakes synthesized by simple solid state reaction. *Journal of Applied Physics*, 2013, Vol. 114, No. 4, p. 043710.
22. KOROTEEV, V., BULUSHEVA, L., ASANOV, I., SHLYAKOVA, E., VYALIKH, D., OKOTRUB, A. Charge transfer in the MoS_2/carbon nanotube composite. *The Journal of Physical Chemistry*, 2011, Vol. 115, No. 43, p. 21199–21204.
23. JONSCHER, A. Frequency-dependence of conductivity in hopping systems. *Journal of non-crystalline solids*, 1972, Vol. 8, No. 10, p. 293–315.
24. FOURRIER-LAMER, A., FIZAZI, A., BELHADJ-TAHAR, N. Studies of semiconducting organic polymer-graphite composites from d.c. to microwave frequencies. *Synthetic Metals*, 1988, Vol. 24, p. 95–105.
25. NARESH, N., BHROWMIK, R. Structural, magnetic and electrical study of nano-structured α-$Fe_{1.4}Ti_{0.6}O_3$. *Journal of Physics and Chemistry of Solids*, 2012, Vol. 73, No. 2, p. 330–337.

CYSENI 2015, May 27–28, Kaunas, Lithuania
ISSN 1822-7554, www.cyseni.com

HIGH SURFACE ELECTRODE FOR ELECTROCHEMICAL ENERGY STORAGE DEVICES BASED ON NANOPOROUS TIN OXIDE

D. Solovei, S. Filatov, E. Batirev, G. Kuczynski
A.V. Luikov Heat and Mass Transfer Institute NAS Belarus
P. Brovka str. 15, 220072 Minsk – Belarus
Phone +375 17 2841251
Email: solovei@hmti.ac.by

ABSTRACT

A high surface electrode for ionistors and electrochemical power sources based on open nanoporous tin oxide architectures has been done. Self-organized nanoporous tin oxide matrixes were synthesized through electrochemical anodizing procedure of the tin metallic films deposited on the dielectric substrates. Cross section and surface morphology of the nanoporous matrixes were investigated by scanning electron microscopy. An electrochemical properties of the tin oxide electrode were measured by using galvanostatic charge/discharge technique and cyclic voltammetry. Open nanoarchitectures of the high surface area tin oxide electrode showed fast ions penetration and charge transport inside porous matrix films. Obtained results demonstrated promising applications of the nanoporous tin oxide films as electrodes for electrochemical energy storage devices.

Keywords: high surface electrode, ionistor, electrochemical power source, nanoporous tin oxide

1. INTRODUCTION

In the past few decades the development and widespread adoption of portable and stationary electronic devices operating in conditions of limited energy resources have revealed more extensive requirements for energy storage devices and power electrical supply. Typically electrochemical energy storage cells are more widely used for powering the most electronic gadgets and equipment. Furthermore, to increase the operation time and stability of such devices new alternative sources with high power density and power energy are needed [1]. The most typical alternative energy sources for mobile and portable devices are: batteries, fuel cells and supercapacitors, which operate on the principle of converting chemical energy into electrical energy [2]. Comparison of these energy sources showed that supercapacitors or ionistors (electric double layer capacitors) have the biggest power, charge rate, the number of charge-discharge cycles, as well as maximum lifetime (up to 20 years)

One way to improve the efficiency of electrochemical energy sources is the use of electrode materials with a large and well-developed active surface area for the electrochemical reaction and exchange charge. Therefore more nanostructured materials applied in the fabrications of electrodes for electrochemical energy storage devices. One of the most popular materials for producing nanostructured electrodes are carbon nanomaterials [3], transition conductive metal oxides [4] and conductive polymers [5], as well as composites of these materials [6–8]. Commercial attractiveness for using of nanostructured materials is based on the low cost production of these materials and the safety for the environment. On this basis the most promising candidate for use as a nanostructured electrode for electrochemical energy sources are transition valve metal oxides obtained by the electrochemical methods [9].

This paper describes the formation and investigation of the nanoporous tin oxide matrix applied as a planar electrode with advanced surface area for electrochemical storage devices. The results of cyclic voltammetry and galvanostatic charge-discharge process of fabricated metal oxide electrode are described.

2. EXPERIMENTAL

The thin film layers of a metallic tin were formed by using thermal vacuum evaporation on a preliminarily cleaned glass substrate with size 26×76 mm. Chemically clean granulated tin were used as the metal source. Thermal sputtering was performed by using vacuum chamber providing vacuum $3\cdot10^{-3}$ Pa and a tungsten boat for evaporation. The thickness of the deposited tin layers was about 1.5 μm. To improve the adhesion of the metallic tin films to the glass substrate vacuum annealing was applied at 200 °C for 2 hours.

Nanoporous tin oxide matrixes were formed by one-step electrochemical anodization process of deposited metallic thin-film layers in two electrode electrochemical cell, platinum foil comparable in size with the anode was used as the counter electrode. The process carried out in aqueous solutions of oxalic acid at a concentration of 0.4 M by galvanostatic mode at ambient temperature. The current density 8 mA/cm^2 was applied and 4.7–4.8 V anodizing potential was measured in an electrochemical system while process performed. After the anodization procedure obtained films were thoroughly washed by distilled water and dried in a stream of a hot air. The anodically formed nanoporous tin oxide films were annealed at 240 °C for 2 hours for removing of all water molecules incorporated inside porous matrixes and for complete oxidation of all remaining metallic tin parts.

Surface morphology and samples cross section of the porous matrix were investigated by the scanning electron microscope Supra 55 at accelerating voltage 3 kV. Microanalysis of the obtained materials was carried out by using energy dispersive x-ray spectroscopy system (EDX-analysis) Inca 350 based on the electron microscope described above.

The charge-discharge behavior of the tin oxide thin films was investigated using cyclic voltammetry and galvanic chronopotentiometry in a three electrode electrochemical system comprising Pt electrode as counter, Ag/AgCl as a reference and nanoporous tin oxide films as working electrode. All electrochemical investigations were performed by using 0.5 M KCl aqueous electrolyte and IPC-Compact potentiostat with specialized software installed.

3. RESULTS AND DISCUSSION

3.1. Morphology and structural film investigation

Fig. 1 shows the scanning electron microscopy (SEM) images of the surface (Fig. 1 a) and cross section (Fig. 1 b) of porous tin oxide matrixes obtained after electrochemical process and thermal annealing at 240 °C. As seen from the Fig. 1 a, nanopores have an average diameter 40–60 nm and are not strictly round shapes, more over pore walls don't have continuous morphology of the tin oxide material. Pore walls consist from the pseudo nanospheres with average diameter of about 10–20 nm and connected together. Such nanostructure differs considerably from the morphology of unannealed nanoporous matrixes described in previous works [9–11]. These phenomena associated with the water molecules loss embedded in the tin oxide nanoporous matrix structure during the thermal annealing process. For the determination of tin and oxygen atoms aspect ratio inside metaloxide film the EDX measurements were performed. According to EDX investigations atomic ratio of tin and oxygen was determined in the ratio of 1:1 and thereby as a result a formation of tin monoxide SnO took place.

The thickness of the nanoporous tin oxide matrix (about 2 μm) was measured by using cross section SEM images (see Fig. 1 b). In comparison with initial metallic layer (about 1.5 μm) the thickness of anodized and annealed tin oxide film increases by 1.33 times. Investigation of the pores walls structure in the depth of the films shows transformation of the morphology from continuous walls to merged nanospheres like on the film surface and as a result increasing of the film porosity up to 60% as well. In spite of the temperature morphology modification of the matrix cellular-porous structure the open nanoarchitectures completely remained and the access of electrolyte and charge exchange throughout the depth of the nanoporous film has been provided.

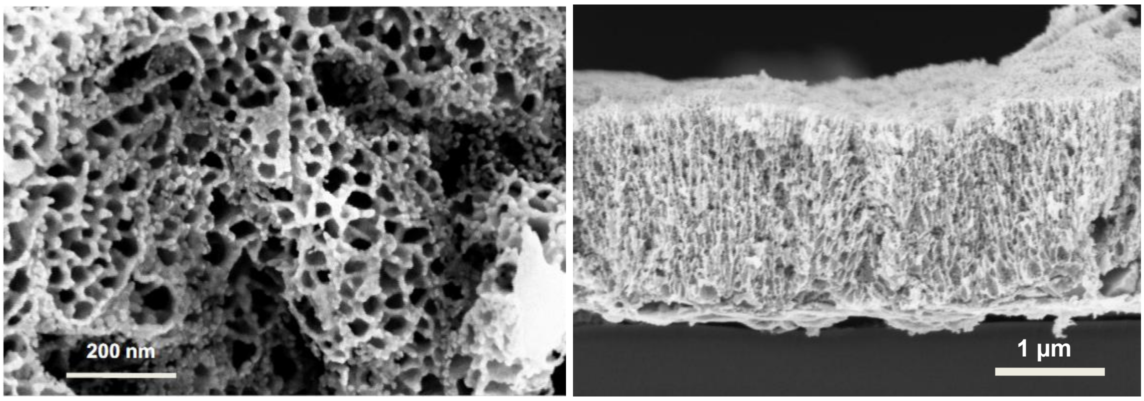

a b

Fig. 1. SEM images of the tin oxide nanoporous matrix fabricated by electrochemical µm anodizing process in 0.4 M oxalic acid electrolyte and thermal annealed at 240 °C:
a – detailed view of the surface, b – cross section view

3.2. Electrochemical film investigation

Electrochemical measurements were performed at 0.5 M KCl aqueous electrolyte. For limiting of the current level the size of samples for measurements was 3 cm^2. The choice of potassium chloride electrolyte was caused by fully chemical inertness of tin oxide towards KCl water solution that allows providing long-term electrochemical operation for the metal oxide electrodes. Fig. 2 a show the cyclic voltammograms obtained in the interval -400 -800 mV with scan rate from 10 to 400 mV·s^{-1}. The shape of the voltammograms corresponds to the supercapacitors behavior of nanoporous tin oxide film in the investigated range of potentials. The difference between positive and negative current level is caused by the occurrence of pseudocapacitive faradaic electrochemical process flowing between potassium ions and tin monoxide, which leads to an additional current increasing. In this faradaic charge transfer specifically adsorbed potassium ions takes part in the redox reaction and can be cause of the capacitance increasing. The dependence of the specific capacitance estimated from the adsorbed charge at different potential sweep rate is shown on Fig. 2 b. The maximum of specific capacitance 210 F·g^{-1} was obtained at 10 mV·s^{-1}, subsequent sweep rate increasing leads to decreasing of the capacitance. So increasing of the potential scan rate till 100 mV·s^{-1} capacity is drops to half, while increasing the scan rate to 400 mV·s^{-1} capacity decreases to 36% from the initial maximum value. The reached maximum value of the specific capacitance is less than mentioned in previous reports [4, 12], but in our case we investigated planar thin film electrode formed on the dielectric substrate causing greater resistance in comparison with bulk materials.

The stability of the charge-discharge process was investigated by using a 500 repeated cyclic voltammograms with scan rate at 50 mV·s^{-1} (see Fig. 2 c). As seen from the picture some deviation of the current takes place. First few tens cycles have 15% higher negative current level in comparison with last cycles. The cause of this phenomenon can be an adaptation of the oxide matrix surface to adsorption of electrolyte ions of opposite signs and mutual compensation of their charges during multiple charge-discharge oxide surface process. In general, this test did not reveal any falling of the capacity or destruction of the electrode surface. Fig. 2 d shows results of the galvanostatic charge-discharge investigations performed at current density 0.5 mA·cm^{-2} with 2 second period. As seen from the picture diagram have standard sawtooth shape, corresponding to the stable charge-discharge process inside of electrode potential window.

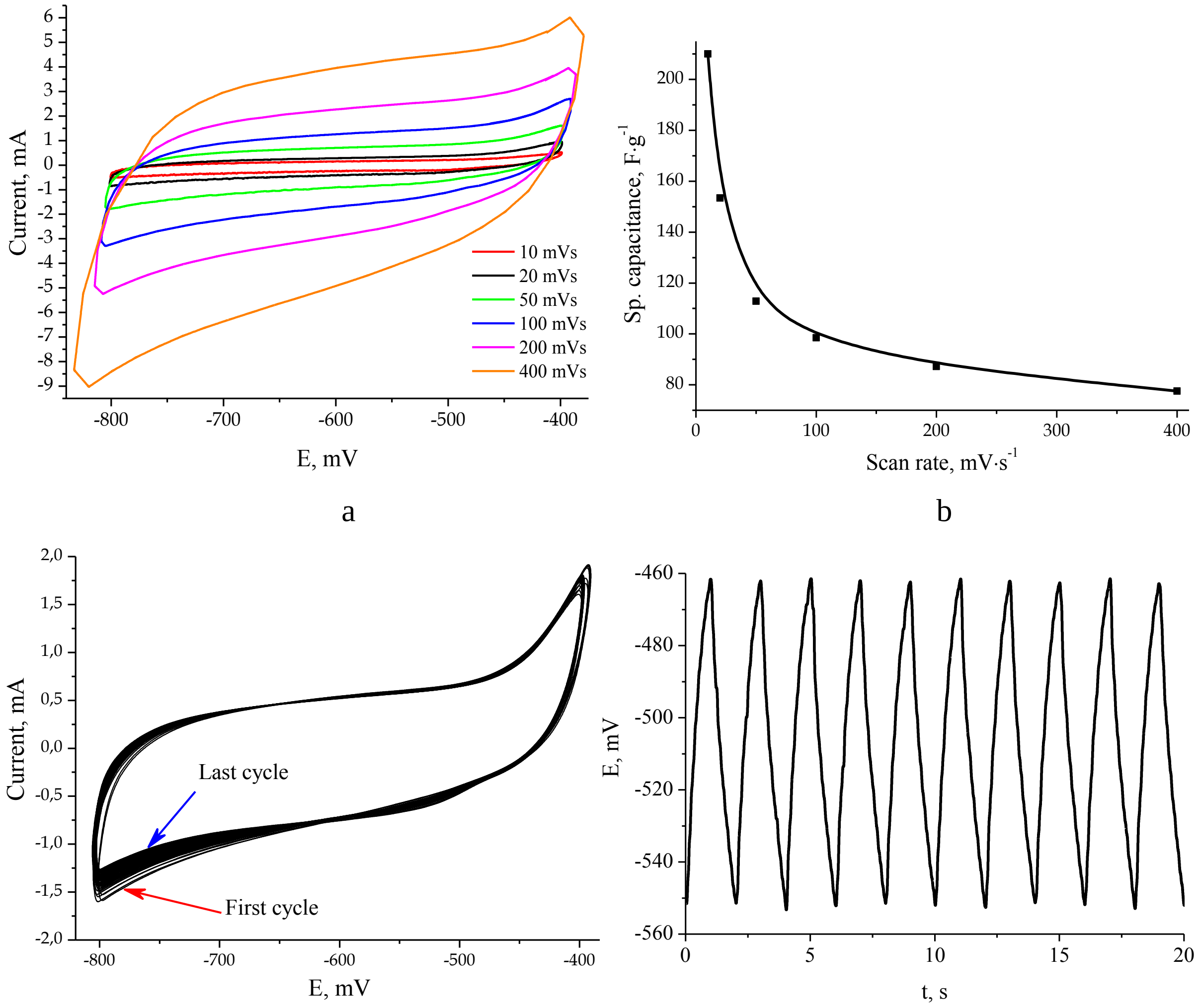

a

b

c

d

Fig. 2. Electrochemical performance of the anodic thin films nanoporous tin oxide matrix measured in 0.5 M KCl aqueous electrolyte: a – cyclic voltammograms at various scan speed (10–400 mV·s^{-1}); b – modification of the specific capacitance under different scan rate speed (10–400 mV·s^{-1}); c – voltammograms stability test at 50 mV·s^{-1} under 500 cycles; d – galvanostatic charge-discharge graph at 0.5 mA·cm^{-2}

4. CONCLUSIONS

Thin film planar nanoporous tin oxide electrode formed on a glass substrate by electrochemical anodization and thermal annealing process has been investigated as a base for energy storage devices. Fabricated thin film electrode is nanoporous tin monoxide (SnO) matrix with average pore diameters about 50 nm. Thermal transformation at 240 °C leads to the modification of the pores walls from continuous shape to chain of the nanospheres merged together throughout the entire thickness of the matrix while the porosity of the film increases up to 60%.

The open pores morphology with continuous high surface area demonstrates supercapacitors behaviour with the maximum of specific capacitance 210 $F \cdot g^{-1}$ reached at 10 $mV \cdot s^{-1}$. The ion charge mobility and adsorption on the surface of pores walls inside oxide matrix provides uniform distribution of the electric double layer on the wall-electrolyte interface. The stability of the planar thin film nanoporous tin oxide matrix for charge-discharge process was confirmed by 500 cycles obtained in potassium chloride electrolyte. The use of microelectronics technology as well as simple electrochemical anodization techniques it is possible to fabricate low cost electrodes based on planar thin films with high surface area for creation of effective electrochemical power sources.

REFERENCES

1. BAGOTSKY, V.S., SKUNDIN, A.M., VOLFKOVICH, Y.M. Electrochemical Power Sources: Batteries, Fuel Cells, and Supercapacitors. John Willey & Sons, 2015. 400 p. ISBN: 978-1-118-46023-8.
2. CHEN, S.-M., RAMACHANDRAN, R., MANI, V., SARASWATHI, R. Recent Advancements in Electrode Materials for the High-performance Electrochemical Supercapacitors: A Review. Int. J. Electrochem. Sci., 2014, Vol. 9, p. 4072–4085.
3. LI, X., WEI, B. Supercapacitors based on nanostructured carbon. Nano Energy, 2013, Vol. 2, p. 159–173.
4. LOKHANDE, C.D., DUBAL, D.P., JOO, Oh-Shim. Metal oxide thin film based supercapacitors. Current Applied Physics, 2011, Vol. 11, p. 255–270.
5. MASTRAGOSTINO, M., ARBIZZANI. C., SOAVI, F. Polymer-based supercapacitors. Journal of Power Sources, 2001, Vol. 97–98, p. 812–815.
6. CHENG, Q., TANG, J., MA, J., ZHANG, H., SHINYA, N., QIN, L.-C. Graphene and nanostructured MnO2 composite electrodes for supercapacitors. Carbon, 2011, Vol. 49, p. 2917–2925.
7. SONIA, T.S., MINI, P.A., NANDHINI, R., SUJITH, K.I., AVINASH, B., NAIR, S.V. and SUBRAMANIAN, K.R.V. Composite supercapacitor electrodes made of activated carbon/PEDOT:PSS and activated carbon/doped PEDOT. Bull. Mater. Sci., 2013, Vol. 36, p. 547–551.
8. LIU, L., NIU, Z., ZHANG, L., ZHOU, W., CHEN, X., XIE, S. Nanostructured graphene composite papers for highly flexible and foldable supercapacitors. Adv. Mater., 2014, Vol. 26, p. 4855–4862.
9. SOLOVEI, D.V., BATIREV, E.V., FILATOV, S.A., KUCZYNSKI, G.S. Thermal transformation and Raman structural investigation of the nanoporous tin oxide. CYSENI 2014. Proceedings of the 11-th annual conference of young scientists on energy issues. [CD]. Kaunas: Lithuanian Energy Institute. 2014 May 29–30, p. VII-314–VII-321.
10. WANG, M., LIU, Y., XUE, D., ZHANG, D., YANG, H. Preparation of nanoporous tin oxide by electrochemical anodization in alkaline electrolytes. Electrochimica Acta, 2011, Vol. 56, p. 8797–8801.
11. ZARASKA, L., CZOPIK, N., BOBRUK, M., SULKA, G. D., MECH, J., JASKUŁA, M. Synthesis of nanoporous tin oxide layers by electrochemical anodization. Electrochimica Acta, 2013, Vol. 104, p. 549–557.
12. SHINDE, D.V. LEE, D.Y., PATIL, S.A., LIM, I., BHANDE, S.S., LEE, W., SUNG, M.M., MANE, R.S., SHRESTHA, N.K., HAN, S.-H. Anodically fabricated self-organized nanoporous tin oxide film as a supercapacitor electrode material. RSC Advances, 2013, Vol. 3, p. 9431–9435.

CYSENI 2015, May 27–28, Kaunas, Lithuania
ISSN 1822-7554, www.cyseni.com

FORMATION OF SiO_2 LAYER ON THE SURFACE OF EXPANDED POLYSTYRENE FOAM

Š. Varnagiris, D. Milčius
Lithuanian Energy Institute
Breslaujos str. 3, LT-44403 Kaunas – Lithuania
Phone +37066243136
Email: Sarunas.Varnagiris@lei.lt

E. Brazys
Vytautas Magnus University
K. Donelaičio st. 58, LT- 44248 Kaunas-Lithuania
Phone +37061633926
Email: edgaras.brazys@gmail.com

ABSTRACT

Structure expanded polystyrene foam is generally flammable material. This article presents the results of uniform SiO_2 coatings formation on the surface of expanded polystyrene foam. Expanded polystyrene was treated with argon plasma in order to achieve better surface adhesion. Plasma was generated in 9×10^{-2} mbar pressure using pulsed DC power source (frequency – 20kHz, voltage – 400 V). Formation of SiO_2 layer was done using magnetron sputtering in reactive atmosphere without extraction of polystyrene samples into the atmospheric pressure. Mixture of argon and oxygen gas was used in order to form SiO_2 layer (argon – 80 %, oxygen – 20 %). Vacuum pressure was 6×10^{-3} mbar during SiO_2 formation process. All samples were analysed using scanning electron microscope, X-ray energy dispersive spectroscope and X-ray photoelectron spectroscope. Results showed that Si and O particles distributed uniformly after SiO_2 formation. However, SiO_2 particles formed not only separate layer on the surface of polystyrene, but also penetrated into the interface layer between surface and the bulk. Depth of SiO_2 penetration was about 157 µm. Morphology results showed negligible changes after SiO_2 formation. These results show that SiO_2 coating might potentially work as a good fireproof coating in the future.

Keywords: SiO_2 layer, expanded polystyrene, penetration, plasma treatment

1. INTRODUCTION

Polymer materials are used for widely type of products. Expanded polystyrene foam is the polymer materials that are commonly used for thermal insulation of buildings. The use of expanded polystyrene foam is driven by it remarkable combination of properties (thermal insulation, low weight, low cost, etc.). However polystyrene has relatively high flammability. Burning polystyrene can destruct the property or even kill people. Because of this, materials which reduce the flame ability are used in manufacturing process of polystyrene. These materials are called flame retardants [1–3].

There are three basic ways how to incorporate flame retardant in polystyrene. First is mechanical incorporation of flame retardant into the bulk polymeric matrix. It is low cost and fast blending technique, but it can change some bulk properties of polystyrene (strength, elasticity, etc.) [4–5]. Second way is to bind units chemically. Flame retardant elements become an integral part of the polystyrene chain and could change the surface morphology and physical properties of the bulk. Higher efficiency and longer durability could be observed using this method. However, there are many difficulties in industrial manufacturing [6–7]. Third method is the use of fireproof coatings. This method mostly involves surface modification. Fireproof coatings could be used in various commercial applications. It is one of the most convenient, economical and most efficient way to protect substrates against fire [5, 8]. Normally flame retardant coatings are applied by means of dip, spray, brush or roller techniques. The main problem of these methods is delamination of coatings because of limited polymer adhesion [9]. Problem with adhesion could be solved using advanced techniques like physical vapour deposition (PVD), chemical vapour deposition (CVD), sol-gel etc.

This article presents the results of SiO_2 coatings formation using PVD technique on the surface of expanded polystyrene foam. However, polystyrene has a low surface energy. Plasma activation was used to solve this problem. It is very important, that plasma activation and SiO_2 deposition processes were done continuously without sample extraction to the atmosphere.

2. METHODOLOGY

2.1. Preparation of materials

Experiments were done using expanded polystyrene foam. The foam was cut into small pieces of about 20×35×10 mm. Plasma treatment and SiO_2 formation were done using the system of physical vapour deposition (KJLC, PVD 75).

2.2. Plasma treatment

Argon (99.99 % pure) plasma treatment was done using vacuum chamber. Pressure was 9×10^{-2} mbar during plasma treatment process. Plasma was generated by using pulsed DC generator (frequency – 20 kHz, voltage – 400 V, power – 110 W). Distance between samples and the plasma plate was about 40 mm. Time of plasma treatment process – 40 s.

2.3. SiO_2 formation

SiO_2 layer was formed without samples extraction to the atmospheric pressure after plasma treatment process. SiO_2 formation was done using mixture of argon and oxygen gas (argon – 80%, oxygen – 20%, purity of both gases – 99.99%). Pressure was 6×10^{-3} mbar during SiO_2 formation process. Pulsed DC generator was used to generate plasma. Voltage of SiO_2 formation was 282 V (power – 141 W respectively). Distance between samples and the Si cathode was about 40 mm.

Expanded polystyrene is very sensitive for high temperature. In order to do not overheat surface of polystyrene, breaks were done in the process of SiO_2 formation. SiO_2 formation was done using this principle:

$$SiO_2\ formation = (5\min\ deposition + 5\min\ cooling) \times 8\ times\ . \tag{1}$$

2.4. Measurement of SiO_2 deposition ratio

Polystyrene is very soft and porous material. It is very hard to evaluate thickness of SiO_2 layer on the surface of polystyrene. Because of this deposition ratio was measured by using silicon plate. The same SiO_2 deposition conditions were used for this measurement. Thickness of SiO_2 layer was measured by using Profilometer (XP-200) on the surface of silicon plate. Deposition rate was calculated by using (2) formula:

$$v = d / t, \quad [nm/\min] \tag{2}$$

d – thickness of SiO_2 layer, [nm];

t – deposition time, [min].

2.5. Surface morphology and concentration of chemical element

Measurements of surface morphology were done using scanning electron microscope (SEM, Hitachi S-3400N). Type of measurement – BSE3D. Measurement of surface concentration was done by using X-ray energy dispersive spectroscope (EDS, Bruker Quad 5040).

2.6. Chemical state analysis

Chemical analysis of supplied samples was done by XPS measurements using ULVAC-PHI Versaprobe 5000 apparatus. Main X-ray parameters were: monochromated 1486.6 eV Al radiation; 25 W beam power; 100 μm beam size; and 45º measurement angle. Spectral window was recorded with 0.2 eV step for 20 eV window. The energy throughput window at the detector for each element was 23.5 eV. Sample charging was compensated using dual neutralisation system consisting of low energy electron beam and ion beam. Energy calibration was done by measuring 1s peak of adventitious carbon and fixing it at 284.8 eV.

3. RESULTS AND DISCUSSION

Atomic concentration of polystyrene is shown in Table 1. before and after SiO_2 formation on the surface of polystyrene.

Table 1. EDS information of polystyrene atomic concentration

Chemical elements	Concentration, atom. %	
	Untreated polystyrene	Polystyrene after SiO_2 formation
C	94.96	33.04
O	5.04	56.39
Si	-	10.57

Untreated polystyrene consist of carbon and oxygen. Carbon covers the biggest part of polystyrene (94.96 atomic %). However, atomic concentration of carbon decreased till 33.04 atomic % after SiO_2 formation. On the other hand, concentration of oxygen increased over 51.35 atomic %. Also, atomic concentration of silicon was 10.57 % after SiO_2 formation. These results showed that additional oxygen was incorporated into the top layer of polystyrene. Sputtered silicon particles could form compounds with oxygen ions inside a plasma. These compounds deposit on the surface of polystyrene (or penetrate between surface and the bulk). Also, some of oxygen molecules might be adsorbed on the surface of polystyrene. Because of these two processes, atomic concentration of oxygen increased drastically.

Result that carbon covers about 33 atomic % after SiO_2 formation means that all information comes not only from SiO_2 coating, but also from interface layer between surface and bulk, where carbon particles were observed.

Calculated SiO_2 deposition ratio was 6 nm/min. approximately. Measured thickness on the surface of silicon plate was about 240 nm. However, it is hard to evaluate real deposition ratio on the surface of polystyrene, because both materials have different adhesion.

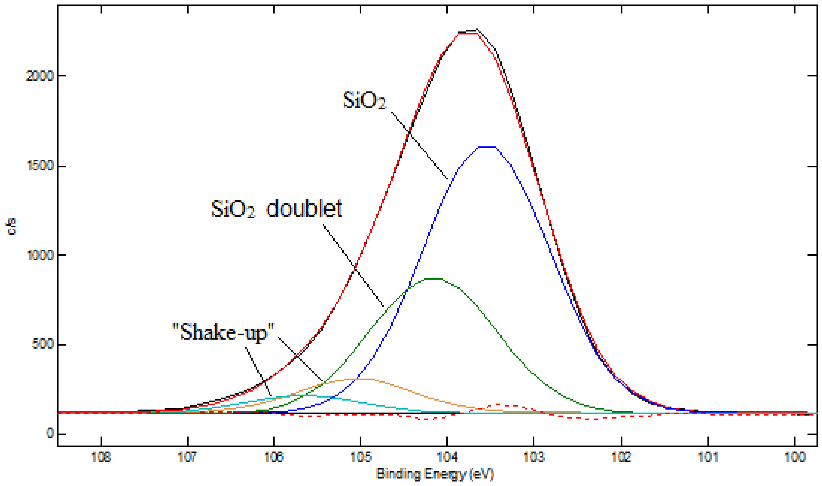

Fig. 1. XPS fitting of Si 2p chemical bond. Black line – measured peak, red line – calculated line. Dashed line shows difference between measured and calculated lines

Si 2p peak was fitted in order to investigate silicon chemical bonds (Fig. 1.). This peak consists of two main parts: Si 2p 3/2 and Si2p 1/2 doublet. It was analyzed that both parts correspond the same chemical bond – SiO_2. Position of the main part (Si 2p 3/2) is 103.55 eV. Separation between Si 2p 3/2 and Si2p 1/2 doublet is 0.61 eV. Also, two shake-up lines were observed (105.05 eV and 105.66 eV). Binding energy of pure Si 2p peak is at 99.4 eV. There was no single Si 2p peak observed at this point. This means that all silicon particles formed SiO_2 compound. This result leads to expect that such a formation of SiO_2 compound could give uniform formation of SiO_2 coating on the surface of polystyrene.

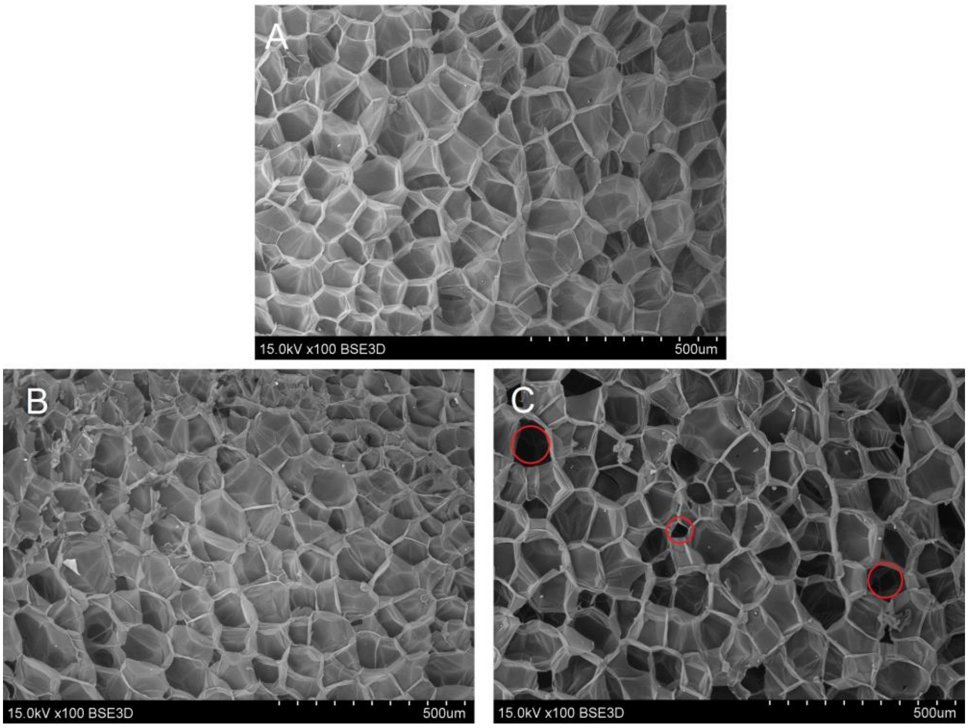

Fig. 2. SEM views of polystyrene morphology: A – untreated polystyrene, B – after plasma treatment, C – after SiO_2 formation (red circles show examples of wells)

Fig. 2 shows morphology of polystyrene. It can be seen that polystyrene foam consists of grains, which are connected in one structure. Dimensions of polystyrene grains remain relatively stable before and after plasma treatment. However, polystyrene has negligible changes after SiO_2 formation. Small wells were observed in some parts of polystyrene after SiO_2 formation (Fig. 2 C, see red circles). These wells could be formed because of vacuum and temperature influence in SiO_2 formation process. On the other hand, these wells might help to introduce SiO_2 particles into the interface layer between surface and the bulk. Because of this, polystyrene might have a thicker layer of a fireproof coating which could show better results of resistance to fire.

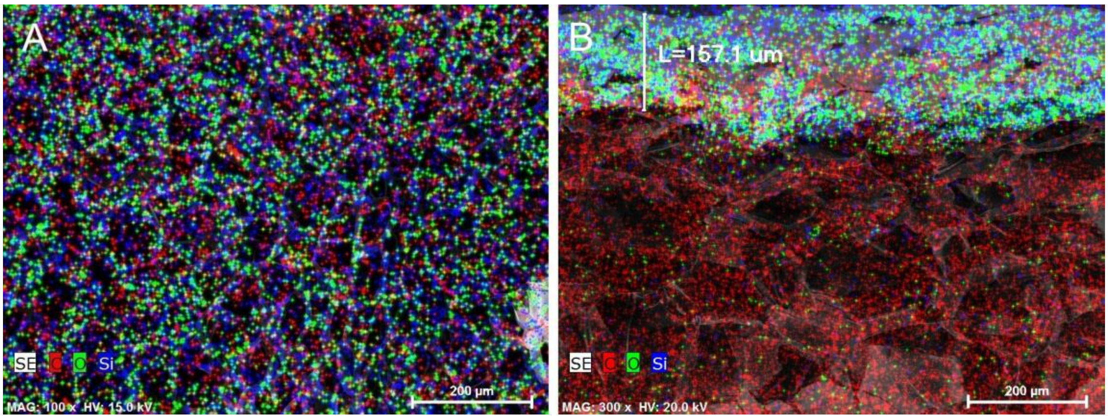

Fig. 3. SEM views of polystyrene mapping after SiO_2 formation: A – surface mapping, B – cross-section mapping

Surface mapping was done in order to observe distribution of elements (oxygen and silicon) on the surface of polystyrene. Results of surface mapping are shown in Fig. 3 A. It can be seen that the biggest part of elements was formed on the boundaries between grains. Smaller amount of these elements were observed into the wells. Particles of carbon were observed into the wells as well. It is possible that oxygen and silicon penetrated into the interface layer and carbon particles went to the top layer respectively. However, both elements (oxygen and silicon) distributed relatively uniformly on the all surface of polystyrene.

Cross-section mapping was done in order to understand how deep oxygen and silicone penetrated into the polystyrene bulk. (Fig. 3 B). Result showed that depth of penetration was about 157 µm. It means that oxygen and silicon particles penetrated into the interface layer between the surface and the bulk. Carbon, oxygen and silicon were mixed in this layer.

Penetration of these particles is initiated of several processes. Sputtered silicon particles have a high kinetic energy. Generally, when particles deposit on the solid substrate surface, they are stopped and kinetic energy became thermal energy, which heated surface of substrate. However, expanded polystyrene foam is relatively soft and very porous material. Because of this, particles are not stopped immediately, when it deposit on the surface of polystyrene. Just a part of kinetic energy became thermal energy. Other part of kinetic energy leads to penetrate into polystyrene [12, 13].

This distribution of elements created a double fireproof structure: coating on the surface of polystyrene and interface layer, which might work as a fireproof layer. Such type of structure could exhibit higher efficiency and longer durability of fire retardant materials.

4. CONCLUSIONS

SiO_2 layer was formed using activation and deposition processes without samples extraction to the atmosphere. XPS results showed that all silicon particles formed SiO_2 compound. It was observed that oxygen and silicon distributed relatively uniformly on the all surface of polystyrene. Also, small wells were observed in some parts of polystyrene after SiO_2 formation, which might help to introduce SiO_2 particles into the interface layer between surface and the bulk. Cross-section result showed that depth of silicon and oxygen particles penetration was about 157 μm. It means that both elements penetrated into the interface layer between the surface and the bulk.

5. ACKNOWLEDGMENTS

This research was funded by a grant (Nr. VP1-3.1-ŠMM-10-V-02-019) from the project "nanoPUTPLAST".

REFERENCES

1. WANG, S., CHEN, H., LIU, N. Ignition of expandable polystyrene foam by a hot particle: An experimental and numerical study. *Journal of Hazardous Materials*, 2015, Vol. 283, p. 536–543.
2. KATANCIC, Z., TRAVAŠ-SEJDIC, J., HRNJAK-MUGIC Z. Study of flammability and thermal properties of high-impact polystyrene nanoparticles. *Polymer Degradation and Stability*, 2011, Vol. 96, p. 2104–2111.
3. HAMDANI, S., LONGUET, C., PERRIN D., etc. Flame retardancy of silicone-based materials. *Polymer Degradation and Stability*, 2009, Vol. 94, p. 465–496.
4. DU L., XU G., ZHANG, Y., QIAN, J., CHEN J. Synthesis and Properties of a Novel Intumescent Flame Retardant (IFR) and Its Application in Halogen-Free Flame Retardant Ethylene Propylene Diene Terpolymer (EPDM), *Polymer-Plastics Technology and Engineering*, 2011, Vol. 50, p. 372–378.
5. LIANG, S., NEISIUS, N., GAAN S. Recent development in flame retardant polymeric coatings, *Progress in Organic coatings*, 2013, Vol. 76, p. 1642–1665.
6. LAOUTID, F., BONNAUD, L., ALEXANDRE, M., LOPEZ-CUESTA, J.M., DUBOIS P. New prospects in flame retardant polymer materials: From fundamentals to nanocomposites, *Materials Science and Engineering*, 2009, Vol. 63, p. 100–125.
7. WEIL, E.D., LEVCHIK, V. Flame retardants in commercial use or advanced development in polyurethanes, *Flame Retardants for Plastics and Textiles*, 2009, p. 153–178.
8. CHATTOPADHYAY, D.K., RAJU K.V.S.N. Structural engineering of polyurethane coatings for high performance applications, *Progress in Polymer Science*, 2007, Vol. 32, p. 352–418.
9. THOMAS, J.O., SCHIELDS J. The effect of surface coating on fire growth over composites materials, *Fire Safety Journal NIST United States Department of Commerce Building and Fire Research Laboratory; National Institute of Stan-dards and Technology, Gaithersburg*, 1996, p. 173–193.
10. VESSEL A. Modification of polystyrene with a highly reactive cold oxygen plasma, *Surface and Coatings Technology*, 2010, Vol. 205, p. 490–497.
11. MOULDER J.F., Handbook of X-ray photoelectron spectroscopy, 1995.
12. MATTOX, Donald M. *Handbook of physical vapour deposition (PVD) processing. Film formation, adhesion, surface preparation and contamination control*. Westwood, New Jersey, U.S.A., 1998. 294, 344-354 p. ISBN: 0-8155-1422-0.
13. MARTIN, Peter M. *Handbook of deposition technologies*. The Boulevard, Langford Lane, Kidlington, Oxford, U.K. 2002. 280-295 p. ISBN–13: 978-0-8155-2031-3.

CYSENI 2015, May 27–28, Kaunas, Lithuania
ISSN 1822-7554, www.cyseni.com

EXPERIMENTAL INVESTIGATION OF CATALYTIC FIBERS PRODUCED BY PLASMA SPRAYING METHOD

V. Astašauskas
Kaunas University of Technology
Studentų str. 50, LT-51368, Kaunas – Lithuania
Phone +37061263302
Email: v.astasauskas@gmail.com

V. Grigaitienė, R. Kėželis, M. Milieška
Lithuanian Energy Institute
Breslaujos str. 3, LT-44403, Kaunas – Lithuania
Phone +370837401898
Email: Viktorija.Grigaitiene@lei.lt

ABSTRACT

Plasma spraying method can be used to deposit a wide range of metals, ceramics and even composite materials for many different applications. In this research the most attention has been focused on the deposition and investigation of micro- and nanostructured fibres and films from metal and metal oxide materials and their mixtures: zeolites, Cu, CuO, Cr_2O_3 and etc., for catalytic application. Micro sized fibers have been deposited employing atmospheric pressure plasma flow. Determination of microstructure, element and phase composition of the obtained products were carried out using the scanning electron microscopy (SEM), energy-dispersive X-ray spectroscopy (EDX) and surface area analysis (BET). The investigation of catalytic properties of produced different fiber samples was performed employing a specific and newly designed test bench. The experiments and measurements were performed at atmospheric pressure under chosen conditions of gas temperatures, flow rates and concentrations. All of the samples of fibres were tested as catalysts in CO oxidation. The best results were achieved by Cu supported catalysts when the conversion rate of CO gas was nearly 80% at the temperature range of 300-400 ^{o}C.

Keywords: catalytic coatings, catalytic fibre, plasma spray deposition, catalytic oxidation of CO

1. INTRODUCTION

During the last years a significant progress has been made in development of plasma spraying technology [1] where the plasmas in general can be produced by the application of a sufficient high level of energy. The different types of particles can exist in plasma, e.g. ions, electrons and neutral particles (non-excited and excited atoms, molecules and radicals) which can be grouped in accordance to different temperatures. Plasma spraying process is involved in the production of variety of coatings, fine mineral fiber, synthesis of micro- and nanostructured particles and plasma polymer products [2–4].

The traditional production methods of fibers such as melting of raw materials in furnace chamber and further mechanical treatment requires quite complex equipment and uninterrupted fabrication technologies. The conventional powder-based processing requires also multi-step operations with high temperature initial material sintering process to provide the final properties and dimensions of the product. Upcoming demands for high quality and new functionality products often means that traditional production methods are finding it increasingly difficult to produce refractory or compact fiber for catalytic applications. On-stream technological process is required for these purposes. So, traditional technologies are unusable for high temperature catalytic fibers production [5]. The catalytic reactors prepared by chemical deposition of platinum group metals are expensive and often fail because of the fusion of ceramic honeycombs caused by overheating [6]. Alternatively, the synthesis of catalytic reactors containing much cheaper metal oxides, zeolites and other materials that serve as active catalytic coatings have been proposed by authors of present study [7]. Recently the authors realized a novel technology for the deposition of mineral fiber made of inorganic metal oxides in plasma ambient. Consequently, the main objective of this work was to obtain catalytic fiber including different phases with highly developed surface for environmental application. This study contains results of an investigation of the deposition process of microfiber by plasma spray technology. The main goals of this research 1) to realize melting of mixtures in plasma torch enriched by zeolite, Cu, CuO, Cr_2O_3 powder at atmospheric pressure; 2) to obtain catalytic microfiber on the steel mesh and 3) to identify physical properties and catalytical effects in the flow of CO gas over the prepared catalytic surface.

2. EXPERIMENTAL SETUP AND TECHNICAL DETAILS

The specific plasma technology was applied and properties of the produced catalytic fiber were discussed for the case of plasma spraying of zeolites powder doped with various selected catalytic materials. The schematic presentation of atmospheric pressure plasma spraying process is shown in Fig. 1. The plasma generator (PG) consists of hot hafnium cathode and a water cooled copper anode and is discussed by authors elsewhere [8].

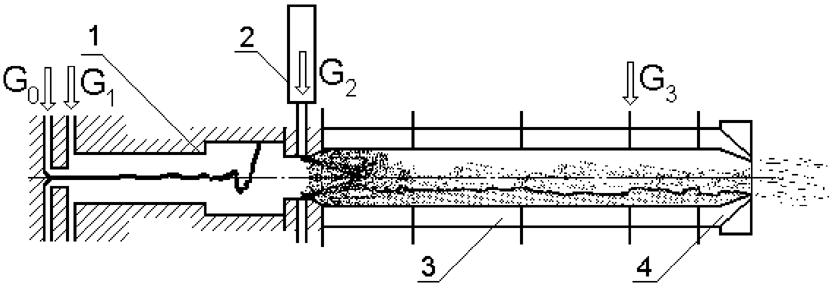

Fig. 1. Plasma spraying system: 1 – plasma generator, 2 – feeding of raw material, 3 – section of the plasma-chemical reactor, 4 – melt flow. G_0 is the injection place of electrode protective gas (argon); G_1 – plasma forming gas (air, propane); G_2 – mixture air and dispersed particles, G_3 – propane gas

The power to the PG is supplied from the voltage rectifier and it includes current stabilization and precise regulation systems. The process begins after the arc ignition between two electrodes while gas is introduced into the arc. The gas passes through the arc with dissociation-ionization process until it forms plasma, which is stabilized by a low-voltage, high-current source. The geometry of the copper anode lets rapidly expanding gas to accelerate and a high velocity, high temperature flow is generated. The raw material is injected as a mixture of powder (50–100 μm in diameter) into the entrance of plasma-chemical reactor (PCR) connected to the plasma torch.

The chamber of the PCR is divided into five sections with 0.016 m inner diameter. The length of the first section which is connected to the plasma torch was 0.09 m and other sections were 0.05 m in length. All the sections are water cooled and insulated from each other, so no heat transfer between the cooling water of each section takes place [8].

The mixture of air and propane was used as plasma forming gas. Propane gas influences higher temperature of the plasma flow and higher intensity of heat transfer between plasma flow and injected particles. The values of the main parameters used in the production of fiber are given in Table 1.

Table 1. Technical parameters of plasma torch

Power, *P* (kW)	50–120
Arc current, I (A)	175–250
Arc voltage, U (V)	350–450
Cooling water flow rate, G_v (kg/s)	0.16–0.18
Source gas flow rate, G (kg/s):	
cathode, G_N	1.0–2.0
neutrode, G_1	7.0–24
anode, G_3	1.0–9.6
Additional gas (propane) flow rate (kg/s):	up to 1.2
Plasma jet average mass temperature T_f (K)	1460–4200
Plasma jet velocity, w_f (m/s)	500–1200
Efficiency, η	0.78–0.82

The efficiency η of used plasma torch was calculated according

$$\frac{1-\eta}{\eta} = 0.71\left(\frac{I^2}{Gd_2}\right)^{0.8} \cdot \left(\frac{G_1}{G}\right)^{0.14} \cdot \left(\frac{G}{d_2}\right)^{0.21} \cdot \frac{d_2}{I}\left(l/d_0\right)^{0.95}. \qquad (1)$$

Here *l* – the characteristic arc distance, d_2 – the diameter of the anode of PG.

In the following, Cu, CuO, Cr_2O_3 and their mixtures with 70, 90 and 95% of zeolites were injected into the plasma jet (as shown in Fig. 1., position 2). Dispersed particles of raw material are injected into the plasma jet by air flow using powder feeder. The air and powder was injected through a 9.5 mm diameter cylindrical tube with a flow rate about $0.4 \cdot 10^{-3}$ kg/s. After the injection dispersed particles are rapidly heated and melted by high temperature flow. Catalytic fibers were produced at the exit of plasma-chemical reactor, directly connected with a plasma torch. Inside PCR the particles are melted and form a liquid flow which flux along the plasma flow direction near the walls of the reactor until it reaches the outlet. At the exit nozzle of the reactor the viscosity of melted substance is high enough, so, plasma flow kinetic energy disturbs the surface of the melted mass and pull single jets and droplets, which are then cooled and solidified [9]. The distance between the PG and fiber collecting device was equal to 0.9–1.2 m.

The determination of microstructure, elemental and phase composition of the obtained fibers was carried out using SEM, energy-dispersive X-ray spectroscopy (EDX), X–ray diffraction (XRD), BET analysis. Also the results of catalytic behavior of produced zeolite and Cu/CuO/Cr_2O_3 fibers in the conversion of CO emissions were obtained.

3. RESULTS AND DISCUSSION

3.1 Parameters of the flow

The investigation of plasma flow parameters is very important in the deposition process of catalytic fibers because the kinetic energy of the flow is employed to convert the melted mixture to fiber. Energy characteristics also serve as a criterion of plasma conditions to establish required fiber formation regime, the viscosity of the melt and facilitate the movement of the molten mass. The properties of fibers are also in strong dependence on the parameters of the PG, the plasma injector and the geometry of the experimental technological equipment.

The velocity and temperature of the powder flowing in the PCR chamber depend on how it is injected: directly into the arc reaction zone or into plasma flow after the anode. A commercial zeolite powder of chemical composition (mass %): Al_2O_3 – 40.9; SiO_2 – 55.2; Fe_2O_3 – 0.9; TiO_2 – 1.4; CaO – 0.5, MgO – 0.49, Na_2O – 0.2) was used for the production of fiber and additional relatively small quantities (5–10%) of catalytic powder were injected. After being sieved and dried the powders of 50–100 µm in size were used to form the two-phase plasma jet. Distribution of temperatures and velocities of different component size particles in the flow were evaluated in dependence on the coordinates. It follows that the maximum velocity depends on the powder material density and the powder size. The chemical composition of zeolite is multipartite, so the simplified example – the simulation of hardly melting Al_2O_3 particles is presented in Fig. 2.

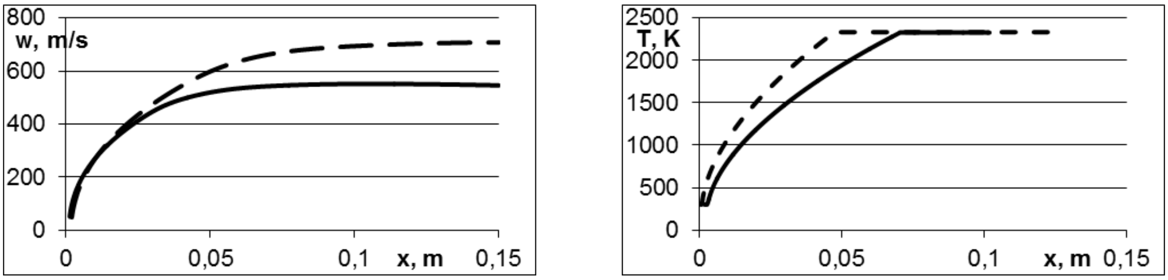

a

b

Fig. 2. Velocity (a) and temperature (b) of Al_2O_3 particle, injected in plasma jet flow obtained by numerical simulation. Particle size: dash line – 50 µm, solid – 100 µm

As it is seen from the curves of velocities (Fig. 2a), the velocity of dispersed particles in the center of the plasma jet reaches the average gas jet velocity at $x/d \geq 6$ and depending on the sizes of particle reaches 540–700 m/s. It can be noticed, that the size of particles has the influence on its accelerating. The difference of the velocity of solid Al_2O_3 particle of 50 µm in diameter in comparison of 100 µm particle can be up to 25%.

After mixing with the plasma jet, the solid particles have lower temperature than the jet, and certain time is needed to heat them up. Particles have to be rather fine in order to quickly heat up. Heating of particles in the plasma jet occurs while releasing heat by convection, whereas inside of the particles the heat is transferred by conduction. Particle temperature evaluation shows (Fig. 2b), that those comparatively small particles (50 µm in size) reaches the melting temperature somewhere at the distance $x \geq 3 \cdot 10^{-3}$ m from the injection place. Al_2O_3 particles of 100 µm in size reaches the melting temperature at $x = 5 \cdot 10^{-3}$ m.

Multiphase plasma and dispersed particle flow was studied using high speed optical camera (in this research recording speed was 15400 frames per second). This method provides the opportunity to observe and record the kinetics of fiber formation. The observation shows that multiphase flow in the environment of plasma chemical reactor outlet nozzle consists of a trickle of melt in different sizes or partially molten granules and gas phase plasma flow (Fig. 3).

The fiber formation begins at the spraying distance $x = 2 \cdot 10^{-3}$ m. The melted mass (Fig. 3, pos. 1) is stretched into many small and tiny filaments. Big and heavy granules (Fig. 3, pos. 2) have slow motion and are separate from any fiber filament. Granules move with the velocity of 40–50 m/s, because they were stopped by melted mass. Small fast granules and fiber filaments (Fig. 2, pos. 3, 4), which can be seen on high speed video move with the velocity of 300–400 m/s.

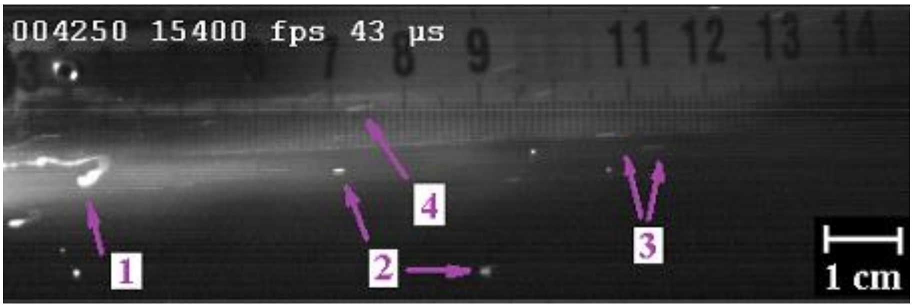

Fig. 3. The behavior of melted zeolite particles during the plasma spraying process. The power of plasma torch is 90 kW

3.2 Fiber structure and properties

The best condition for fibre production is achieved when the melt viscosity is about 5 Pa [6]. It strongly depends on what kind of material is melted. Experimental tests showed that Al_2O_3 powder, injected into high temperature air jet is not melted properly, so, for the improvement of melting process and increase temperature of the flow the propane gas was supplied and optimal fibrillation conditions has been achieved. The typical views of fibers obtained by scanning electron microscope (SEM) with different magnifications are presented in Fig. 4. It can be seen, that the thickness of fibers was 0.5–2 microns and the average length was about 0.07 m. However, there appeared same of non-fibre melt inclusions, because catalytically active materials were injected separately at the end of the plasma torch. It ensured having the catalytic materials on the top of the filaments of the fibers. And the pictures obtained from scanning electron microscope reveal a quite homogeneous distribution of components on the surface.

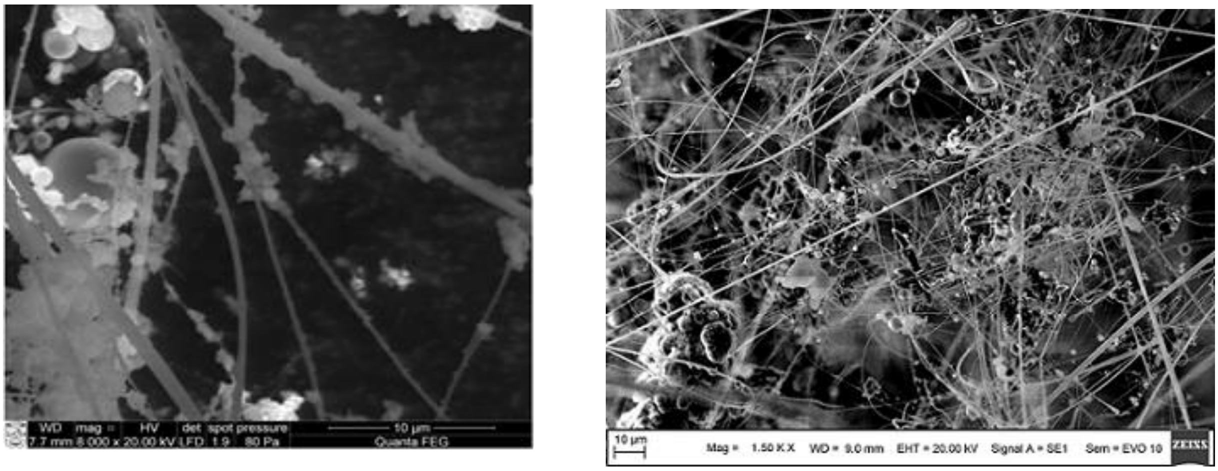

Fig. 4. SEM micrograph of fiber doped by: a) Cu and b) CuO, Cr_2O_3. The power of plasma torch and the air flow rate is 90 kW and 0.019 $kg \cdot s^{-1}$, respectively

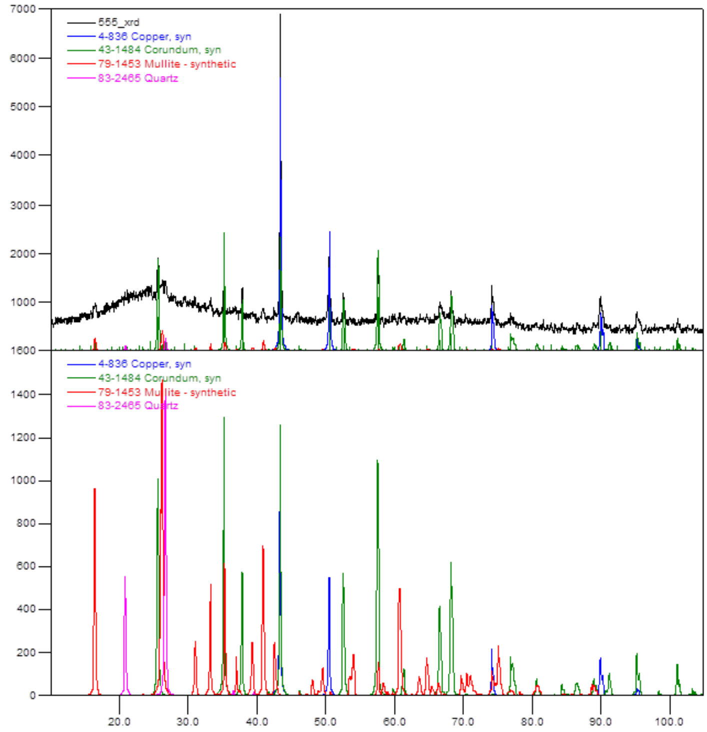

Fig. 5. XRD pattern of zeolite + Cu catalytic fiber produced by plasma spraying. Corundum: Al_2O_3, mullite formula: $Al_{4.64}$ $Si_{1.36}$ $O_{9.68}$

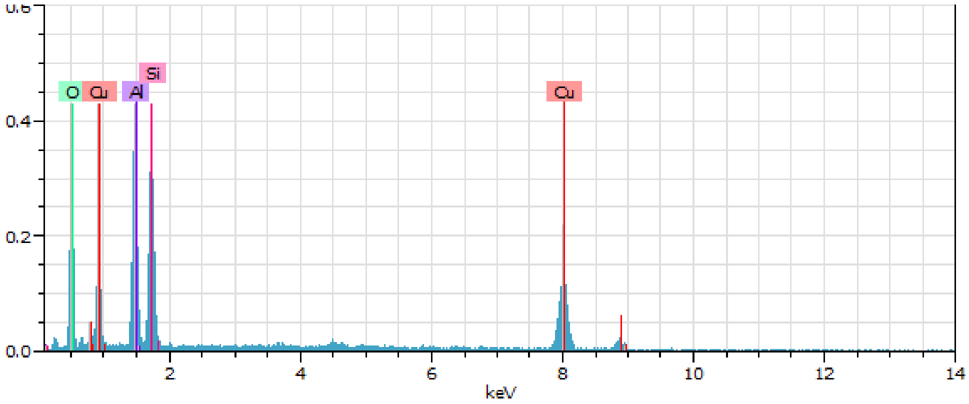

Fig. 6. EDX pattern of zeolite + Cu catalytic fiber produced by plasma spraying

X–ray analysis (Fig. 5) shows that formed zeolite fiber catalyst doped by Cu powder mainly includes SiO_2, corundum (aluminum oxide) and copper phases. Additional EDX analysis (Fig. 6) gives the elemental composition on the surface of the sample and it can be confirmed, that catalytically active copper is on the surface of the fibers. It is very important and has the essential influence on catalytic behaviour of the prepared catalyst. BET analysis results showed the surface area 4.33–5.85 m^2/g.

3.3 Catalytic combustion behavior

The catalytic properties of prepared fiber catalysts (Fig. 7) for the reduction of combustion product CO were established using a specific test bench. In all considered cases converters including zeolite fiber doped with Cu, CuO and Cr_2O_3 demonstrated that the level of environmentally aggressive component CO in the exhaust gases could be reduced. Catalytic activity of fibers has been investigated in the range of temperatures 200–450 ^{o}C, which was controlled in the channel by precise three heating zone furnace. The concentration of CO in the initial flow through the catalyst was 3%. The typical reaction profile as a function of temperature is given in Fig. 7. The best selected samples containing different amount of catalytic material (Table 2) show different activity at moderate temperature of 400 ^{o}C. In comparison, the commercial catalyst supported by platinum metals group, removed from automobile, showed the highest activity and the shortest duration of ignition, however the ignition temperature differs only slightly.

Table 2. The composition of initial mixture

Sample No.	Amount of used substances in the mixture, %			
	Zeolite	CuO	Cr_2O_3	Pure Cu
1	70	20	10	0
2	90	10	0	0
3	95	0	0	5

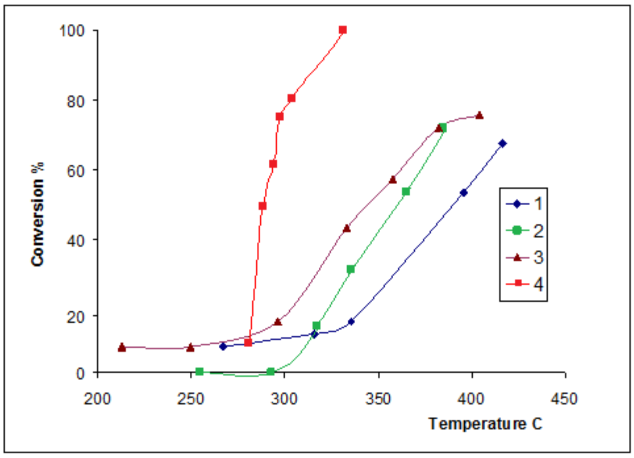

Fig. 7. CO conversion as a function of flow temperature. Numbers in the legends correspond to date given in Table 2. Legend 4 shows the activity of commercial automotive platinum based comb catalyst

However, it is important to notice that in many cases the use of zeolite as initial material for fiber production doesn’t provide the expected results. In many cases the CO conversion over such catalyst was not sufficient. The possible explanation of this fact is that all components of the catalytic mixture have very different densities. The component having bigger density may sink in the bulk melt.

The other reason of low activity of some zeolite based fiber catalysts is the poor mixing of melted batch components on the walls of PCR. This means that the initial viscosity of the melted mass is too low to produce the required catalytic fiber. The increase of the amount of catalytic material certainly improves the combustion of CO. This is related with the increase of catalytic substance on the fibre filament surface.

4. CONCLUSIONS

The use of the plasma spraying technology at atmospheric pressure demonstrates the ability to obtain catalytic fiber with controlled characteristics suitable for environmental applications.

The mineral fibre was successfully deposited from inorganic metal oxides: zeolites doped by catalytic Cu, CuO, Cr_2O_3 and their mixtures at atmospheric pressure employing specific plasmachemical facility with stream reactor and linear DC plasma torch 70–120 kW of power. By using properly designed plasma jet reactor it is possible to produce mineral fiber consisting of fine filaments when their diameter appears only 0.5–2 micrometers.

The steady operating regime of the equipment is reached immediately after the start of plasma torch. Distribution of thermal and heat transfer characteristics in PCR allows the effective fibrillation process and low energy consumption. It was demonstrated that the yield of final product depend on the viscosity of melted mass. The interaction of plasma flow and dispersed particles lasts up to 1.1 ms.

Catalytic fibers, generated by plasma spray technology with active component Cu, CuO and Cr_2O_3 can reduce effectively the amount of CO in the exhaust gas and according to the activity are comparable to the catalysts containing noble metals. It was determined that fiber catalysts, depending of their chemical properties and structure operate optimally when the temperature of feed gas is 350–370 ^{o}C (CO concentration is 3%). Unfortunately, CO conversion degree did not exceed 80% in any of the experiments described, but it is possible that the degree of pollutant conversion would increase on increasing the catalytic surface area. Nevertheless, information accumulated on the basis of the obtained research results could be used in creating, designing and calculating CO oxidizing catalysts, they can also enlarge experimental data on the processes occurring in such sort of fiber catalysts. The research is continued.

REFERENCES

1. FRIDMAN A. *Plasma Chemistry*, Cambridge University Press, Cambridge, 2008, ISBN 9781107684935.
2. NIELSEN E.R., AUGUSTESEN, M., STAHL K., Devitrification and high temperature properties of mineral wool, *Materials science forum*, 2007, Vol. 558–559, p. 1255–1260.
3. VALINČIUS V., GRIGAITIENĖ V., SNAPKAUSKIENĖ V., VALATKEVIČIUS P., KĖŽELIS R. Interaction of dispersed ceramic particles and melted domains with turbulent plasma jet. Proceedings of the sixth international symposium on turbulence, heat and mass transfer 6 (THMT'09), Rome, Italy, September 14–18, 2009. New York, Wallingford (UK): Begell House, Inc., 2009, ISBN 978-1-56700-262-1, p. 1–12.
4. TANAKA K. Unsolved problem in catalysis, *Catalysis Today*, 154, 2010, p.105–112.
5. SINGHA K. A Short Review on Basalt Fiber, *International Journal Textile Science*, 2012, Vol. 1, No. 4, p. 19–28.
6. TWIGG, M. V., “Progress and Future Challenges in Controlling Automotive Exhaust Gas Emissions”, *Applied Catalysis B Environmental*, 2007, B 70, p. 2–15.
7. VALINČIUS V., KĖŽELIS R., SNAPKAUSKIENĖ V., GRIGAITIENĖ V., VALATKEVIČIUS P., TAMOŠIŪNAS A. The influence of plasma spraying regime and initial substance injection location on the structure of deposited coatings, *Surface & coatings technology*, ISSN 0257-8972. 2011. Vol. 205, Suppl. 2, p. 359–363.
8. VALINCIUS, V. KRUSINSKAITE, P. VALATKEVICIUS, VALINCIUTE V. Electric and thermal characteristics of the linear, sectional DC plasma generator, *Plasma Sources Science and Technology*, Vol.13, No 2, 2004, p. 199–206.
9. GRIGAITIENĖ V., KĖŽELIS R., VALINČIUS V., MILIEŠKA M. Diagnostic of plasma spray process using high speed imaging and numerical simulation, Proceedings of 15th international symposium on flow visualization (ISFV-15), Minsk, Belarus, 25–28 June, 2012, ISBN 978-985-6456-75-9, p. 1–7.

INVESTIGATION OF RUBBER WASTE PROCESSING IN SCREW REACTOR

A. Lozhachnik, V. Sauchyn, H. Dalholenka
A. V. Luikov Heat and Mass Transfer Institute
National Academy of Sciences of Belarus
P. Brovka str. 15, 220072 Minsk – Belarus
Phone (+37517) 284-12-17
Email: lozhechnikav@mail.ru, v.sauchyn@gmail.com

ABSTRACT

Investigation of modified technology for thermal processing of rubber waste is based on analyse of different methods described in literature and results of experimental research of steam conversion carried out in A.V. Luikov Heat and Mass Transfer Institute.

As raw material rubber crumb is used. Temperature of the process is 500 °C. Medium in reactor is nitrogen and steam with some amount of light hydrocarbons (non-condensed part of products of pyrolysis). As a result of rubber waste processing we obtain 36–38% solid carbon residue, 54‑56% liquid hydrocarbon phase and 6–9% non-condensed gases. Abstained quantitative dependence of gas content in the reactor.

Analysis of pyrolysis gases by gas chromatography shows that the main gases produced by the pyrolysis process are H_2 and hydrocarbons: CH_4, C_2H_4, C_3H_6, C_4H_8, C_2H_6, C_3H_6, $C_3H_6O_2$, C_4H_{10} and small amount H_2S, CO, CO_2. Non-condensed gases will be used as a fuel for reactor heating and process realization.

Keywords: rubber waste, screw reactor, technology of treatment

1. INTRODUCTION

Relevance of the problem is due to both an increase in environmental pressures on the environment, as well as economic reasons. Because the demand for natural resources is constantly growing, as supplies are limited, and the development of new deposits and operation of existing becoming more expensive. Attempts to create processes which would combine solutions of these two problems, involving waste in to numerous manufacturing processes by their deep processing are promising and noteworthy [1, 2].

Previous research [3–5] shows that in modern conditions scrap tires pyrolysis is most effective. Destruction of hazardous and hardly decomposing waste and obtaining products, such as carbon black, and mixtures of liquid hydrocarbons is an important advantage of this technology.

As it is seen from [1–6] periodic process is organized with produced gases atmospheric afterburning. According to this we modified technology for thermal processing of rubber waste.

This paper presents description of the continuous technology of rubber waste treatment, products analysis of the pyrolysis process, quantitative dependence of gas content from start of material feeding. Modified technology includes gas circulation in close loop what prevents emissions to the environment.

2. METHODOLOGY

Experimental set was designed on the base of experimental results obtained in previous research [4, 5]. Set with screw reactor diagram is shown in Fig. 1.

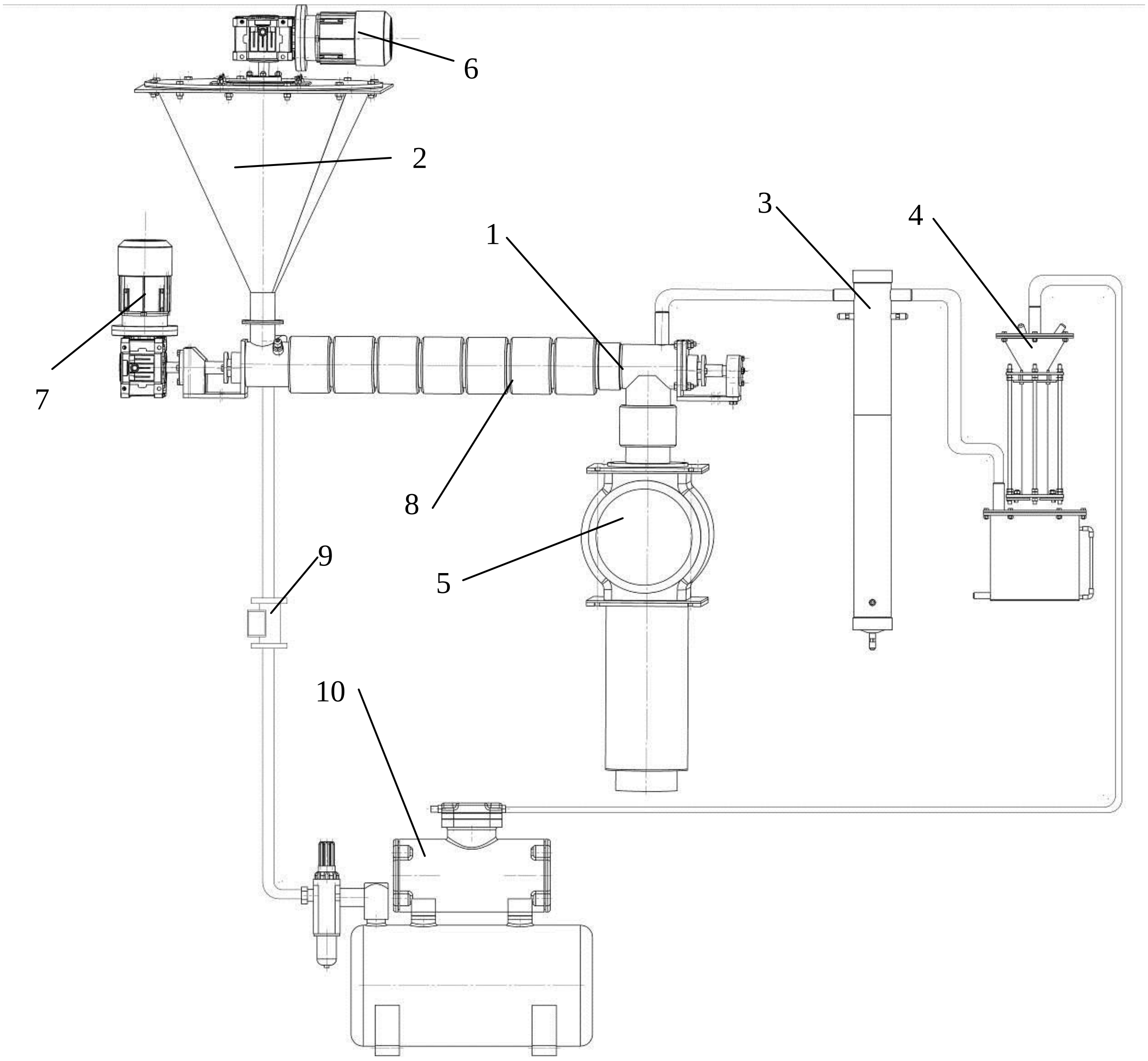

Fig. 1. Set diagram: 1 – screw reactor; 2 – feeder; 3 – tubular condenser (K1); 4 – tank for drops trapping (K2); 5 – gateway for unloading solid carbon; 6 – feeder gear-motor drive; 7 – reactor gear-motor drive; 8 – heaters; 9 – input gas adjusting; 10 – compressor

According to suggested method material is loaded from feeder with screw to the reactor where it is heated by electrical heaters. Because of high temperature material decomposes and organic vapour is released. Temperature of reactor heating is controlled by thermocouples placed between heaters and heated surface. Nitrogen and water steam is fed to the beginning zone of the reactor. It is used to pull out air from the reactor before start operation and as a transport gas during decomposition process. Steam is condensed in tubular condenser and after separation redirected to the reactor. Steam-gas mixture was used as working medium as it intensify heat- and mass transfer. It increase process speed and decrease energy for scrap tires decomposition [7].

Separation of reaction mixture occurs after destruction process. Solid part is collected in tank for carbon for cooling and analysing. Collecting condensed organic substances occurs in the tubular condenser K1 and tank for drops trapping K2. After that mixture of non-condensed gases and transport gas (nitrogen) is pumped to the beginning zone by compressor, in these way closed loop is organized. Closed loop prevent emissions to the environment. Extra non-condensed gases collected in special tank or can be burned for material heating.

Operation of the set is controlled by automated control system connected to PC.
Set is connected to supply systems:

- power supply system;
- water supply system;
- nitrogen and steam supply system;
- control panel.

Technical characteristic of experimental set is presented in Table 1.

Table 1. Technical characteristic of experimental set

Laboratory reactor efficiency, kg/h	5–10
Temperature, °C	400–600
Power, up to kW	25
Voltage, V	380/220
Gas consumption, kg/h: non-condensed gases steam	 0.94 0.8
Extra non-condensed gases, kg/h	0.8–1.5

3. RESULTS AND DISCUSSIONS

Use of pyrolysis as a method for recycling waste tires depends on the market for pyrolysis products. For this reason, characterization of pyrolysis products and possibilities of their application in other processes is very important.

Tires are composed of rubber compounds and textile or steel cords. We use scrap rubber 1–5 mm dimension with textile cord as raw material. Its average composition is presented in Fig. 2 [8]. Due analysing different rubber compounds, various authors report different results of elemental analysis, as shown in Table 2. For obtaining the average content of elements in tires each part of tire must be analysed.

Table 2. Elemental analysis of scrap tire rubber

Author	C (wt%)	H (wt%)	N (wt%)	S (wt%)	O (wt%)	Ashes (inorganic)
This paper	86.7	7.5	0.4	1	-	4.4
Gonzales et al.[8]	86.7	8.1	0.4	1.4	1.3	2.9
Williams and Bottrill[9]	85.8	8.0	0.4	1.0	2.3	2.4

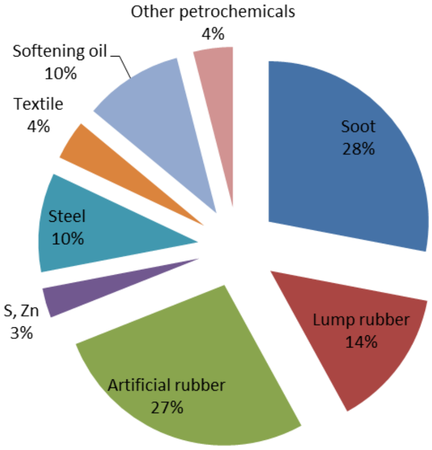

Fig. 2. Scrap rubber from car wheel average composition

Table 3. Influence of some process conditions on char, liquid and gas yields presented by different authors

Author	Temperature (°C)	Heating rate (°C/min)	Pressure MPa	Sample sizes, mm	Solid (wt.%)	Liquid (wt %)	Gas (wt.%)
This paper	500	50	0.1	1–5	36–38	54–56	6–9
González et al.[8]	350–700	5–20	0.1	0.2–1.6	37–40	55	4–11
Williams et al. [10]	300–720	5–50	0.1	-	35	55	10
Roy et al. [11]	25–500	15	0.08-2.8	-	35–36	62	1–3

The solid residue contains carbon black and the mineral matter initially present in the tire. Elemental analysis shows: C – 86–89%; H – 0.4–0.9%; S – 1.8–2.5%. Also inorganic components were found: zinc oxide as a main component and some additives of titan dioxide (according to radiographic-phase analysis). Sorption surface solid residue of is estimated at a ~15 m^2/g (colorant sorption).

The liquid phase is the most important product of tire pyrolysis process. Gas chromatography/Mass spectroscopy (GC/MS) is the most often method used for analysing pyrolysis liquid product. The liquid phase contains over 50 individual components that can be separated but in many cases it is economically inexpedient and technically not always possible.

According to literature data [3] while analysing pyrolysis gases by gas chromatography, found that the main gases produced by the pyrolysis process are H_2 and hydrocarbons: CH_4, C_2H_4, C_3H_6, C_4H_8 and small amount H_2S, CO, CO_2. In Fig. 3 presented quantitative dependence of gas content from star of material feeding. It can be seen that after 50 minutes in the reactor partial pressure of mentioned gases achieves saturation vapour pressure. These conditions make gases to dilute in liquid phase.

Experimental research shows that in non-condensed phase the equilibrium concentration of ethane – 6.4%, propylene – 5.1%, methyl acetylene – 5.3%, n-hexane –0.9%, i-butane – 0.3%, n-butane – 0.6%, i-pentane –0.1%, n-pentane – 0.1%.

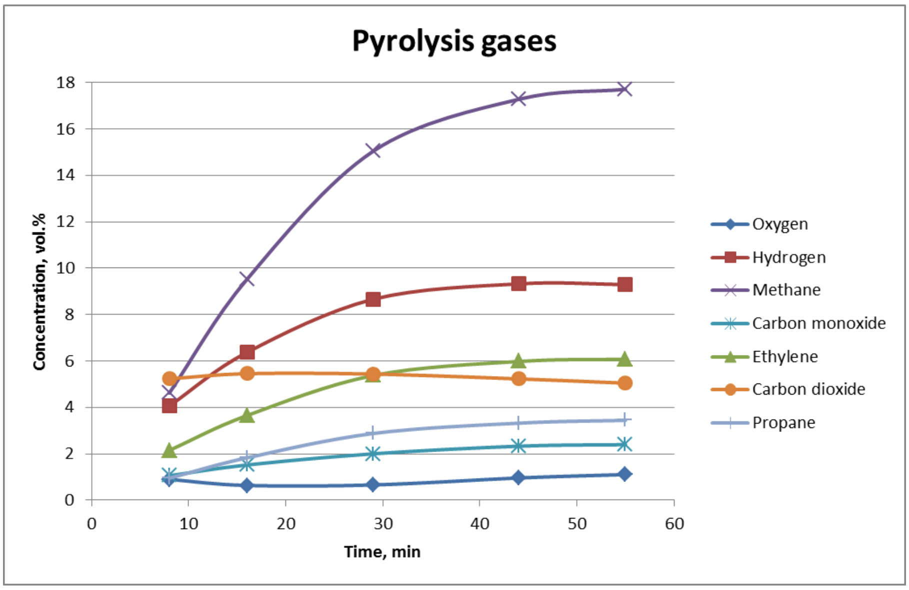

Fig. 3. Main gases produced by the pyrolysis process

4. CONCLUSIONS

Continuous technology with gas circulation in close loop prevents emissions to the environment.

During the pyrolysis process that occurs at 500 °C and scrap rubber 1-5 mm dimention with textile cord as raw material, weight distribution of the process product was determined as solid carbon – 36–38%, liquid phase – 54–56% and non-condensed gases – 6–9%.

At present time, the main application for solid char is its use as active carbon, as reinforcement in rubber industry and as smokeless fuel. The liquid product is used as a fuel, or a source of chemicals, and the gas fraction as a fuel in the pyrolysis process.

Analysis of pyrolysis gases by gas chromatography shows that the main gases produced by the pyrolysis process are H_2 and hydrocarbons: CH_4, C_2H_4, C_3H_6, C_4H_8, C_2H_6, C_3H_6, $C_3H_6O_2$, C_4H_{10} and small amount H_2S, CO, CO_2. Non-condensed gases will be used as a fuel for reactor heating and process realization.

Obtained quantitative dependence of gas content from start of material feeding shows that after 50 min. in the reactor partial pressure of mentioned gases achieves equilibrium concentration.

REFERENCES

1. LYAHEVICH G.D., LYAHEVICH A.G. Technology and economics of processing of secondary rubber materials, including tires with metal cord. *Minsk: BGPA*, 1999. – 244 p.
2. BOBOVICH B.B.; DEVIATKIN V.V. Waste treatment of production and consumption: Reference Edition. *M: IntermetInzhiniring*, 2000. – 496 p.
3. Juma M., et al. Pyrolysis and combustion of scrap tire. *Petroleum & Coal,* 2006, Vol. 48, № 1, p. 15–26.
4. ZHURAVSKY G.I., MATVEICHUK A.S. Thermal technology for production of fuels from organic waste. *XIV Minsk International Forum on Heat and Mass Transfer*. Minsk, September 2012, Vol. 2, 62 p.
5. LOZHACHNIK A.V., SAUCHYN V.V., NIKANCHUK A.N., DOLHOLENKA G.V. Technology of rubber waste treatment. CYSENI 2014. Proceedings of annual conference of young scientists on energy Issues. [CD]. Kaunas: Lithuanian Energy Institute. 2014 May 29−30.
6. Mini-factories “PROMETHEUS” to produce naphtha and diesel fuel various kinds of raw materials and waste [referred on the 2th of March in 2015 y.] Link to the internet <http://www.potram.ru/index.php?page=111>
7. BABENKO V.A., JDANOK V.A. Mathematical model of thermodestruction of automobile tires in overheated steam medium. *Journal of Engineering Physics and Thermophysics.* V. 82, № 1, 117 p.
8. JUAN F. GONZÁLEZ, JOSÉ M., ENCINAR, JOSÉ L. CANITO, JUAN J. RODRÍGUEZ. Pyrolysis of automobile tyre waste. Influence of operating variables and kinetics study. *Journal of Analytical and Applied Pyrolysis*, 2001, Vol. 58–59, № 1, p. 667–683.
9. PAUL T.WILLIAMS AND RICHARD P. BOTTRILL. Sulphur-polycyclic aromatic hydrocarbons in tyre pyrolysis oil. *Fuel*, 1995, Vol. 74, № 5, p. 736–742.
10. PAUL T. WILLIAMS, BESLER S., TAYLOR D.T. *The pyrolysis of scrap automotive tyres: The influence of temperature and heating rate on product composition*. *Fuel*, 1990, Vol. 69, p. 1474–1482.

ROY C., CAUMIA B., CAUMIA B. D. Recycling of scrap tires to oil and carbon black by vacuum pyrolysis. *Resour. Conserv. Recy.*, 1990, Vol. 4, p. 203–213.

CYSENI 2015, May 27–28, Kaunas, Lithuania
ISSN 1822-7554, www.cyseni.com

SPEED MEASUREMENTS OF MACRO PARTICLES LAUNCHED BY MAGNETOPLASMA ACCELERATOR

A. Makhnach
A.V. Luikov Heat and Mass Transfer Institute
National Academy of Sciences of Belarus
P. Brovki Str. 15, 220072 Minsk – Belarus
Phone+37529-6202099
Email: mahnach_anna@mail.ru

ABSTRACT

This paper presents two optical methods for measurements of high velocities of small bodies launched by magnetoplasma accelerator. These methods were used in the testing of the gas-discharge installation for acceleration of micro and macro particles, which provide an increasing of the temperature and pressure of the working gas by the discharge energy in magnetoplasma compressor. A launching of particles occurs in vacuum. The velocities in the range of 0.8–4.3 km/s were measure using the developed methods. The velocities of particles were also evaluated using the ballistic limit equation. The difference between the velocity measured by the optical methods and evaluated using the ballistic limit equations is no more than 20%.

Keywords: velocity measurement, magnetoplasma accelerator

1. INTRODUCTION

Energy, aviation, rocket and other industries require an experimental study of the phenomena occurring during high-speed collisions of bodies with barriers and the motion of bodies with high speeds in different gas mixtures, as well as other similar processes. For the experimental study of such phenomena they use different types of throwing systems, one of which are magnetoplasma accelerator [1–5]. In such systems, particle acceleration occurs due to the energy of heated and compressed plasma. Such launchers allow to accelerate small bodies (~mm) up to several km/s.

To measure the speed of projectile the method of high-speed photography on the background of luminous screen is widely used [6, 7]. However, it is applicable to the case where the ratio of the longitudinal dimension of the body to its velocity less than exposure time. A simple registration system to measure high velocity by means of film sensors was developed in [8]. Each sensor consists of two charged parallel plate capacitors spaced by a certain distance. Projectile pierces the capacitor plates shorting plates causing electric impulses. Projectile velocity was calculated from the time shift between electric impulses in the parallel plate capacitors. To prevent the loss of projectile momentum and its destruction in a collision with a sensor in [9] they proposed to use thin (5 mm) lavsan films with a surface metallization. A system of two sensors described above was used to measure the speed during the tests of small bodies electrodynamic launcher. The projectile was not destroyed upon contact with the sensor and left holes with enough smooth edges in lavsan films. Projectile speed decrease was insignificant. However, the described method has a low protection against electrical interference, especially in launchers with high current pulse amplitude. In this regard, quite relevant is the task of developing noise immunity simple and reliable method of projectile speed registration [9].

2. OPTICAL METHODS FOR MEASURING THE VELOCITY OF PROJECTILE

To measure the projectile velocity two optical methods were developed. They were used for velocity measurements of small bodies (graphite or steel spherical projectile 4 mm in diameter) accelerated by gas discharge launcher which provide an increasing of the temperature and pressure of the working gas by the discharge energy in magnetoplasma compressor. Plasma expands and pushes the particle in the launcher barrel. A launching of particles occurs in vacuum. An optical setup of developed velocity detector is shown on Fig. 1.

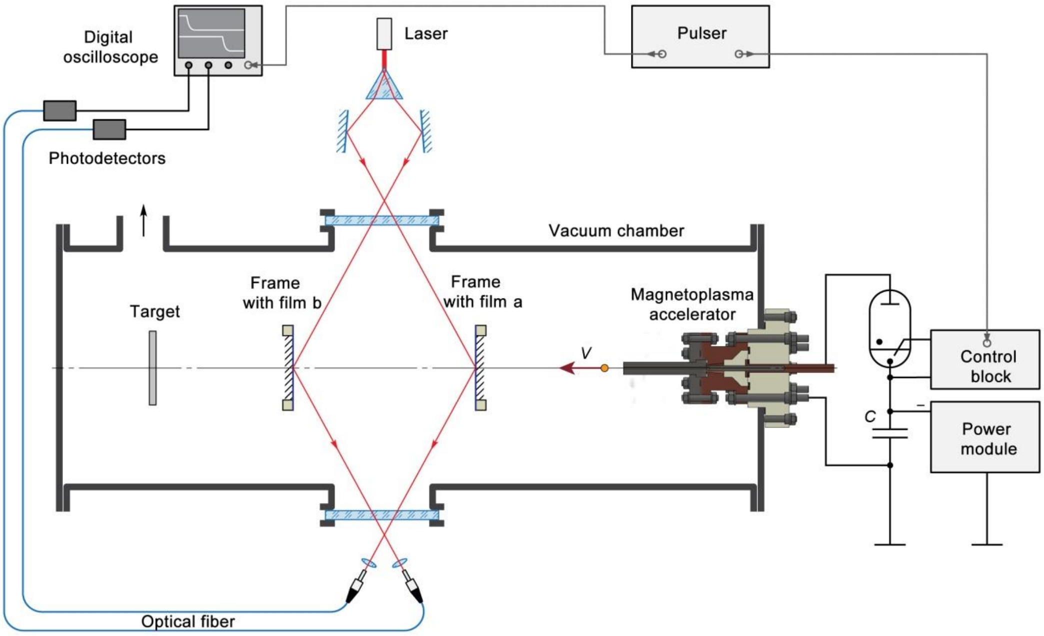

Fig. 1. Scheme of projectile velocity measurement by means of the first optical method

Two frames with reflective coating thin films were placed on the path of the projectile body at a certain distance from each other. Laser beams were directed to each film at some angle and after reflection were transmitted on the photosensors by means of optical fiber. To form two beams, a semiconductor laser radiation was passed through the separation prism and then was directed to the thin films by means of mirrors. To focus the radiation onto the surface of the photodetector the lens were placed in front of the optical fiber ends.

When the projectile moves it perforates thin film hence the rays geometry are changed and signals on optical sensors are interrupted sequentially. The projectile speed can be calculated from the time interval between the interrupt signals and known distance between two frames.

Typical oscillograms of signals from photodetectors are shown in Fig. 2.

The velocities in the range of 0.8–2.6 km/s were measured by the using of this method.

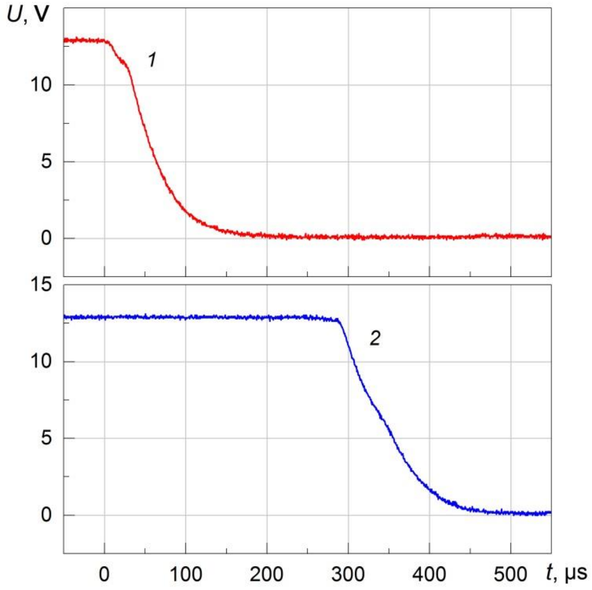

Fig. 2. Typical oscillograms of signals from the photodetectors:
1 – the signal corresponding to the ray reflected from the film *a*,
2 – a signal corresponding to the reflected beam from the film *b*

An optical setup of the second velocity detector is shown on Fig. 3.

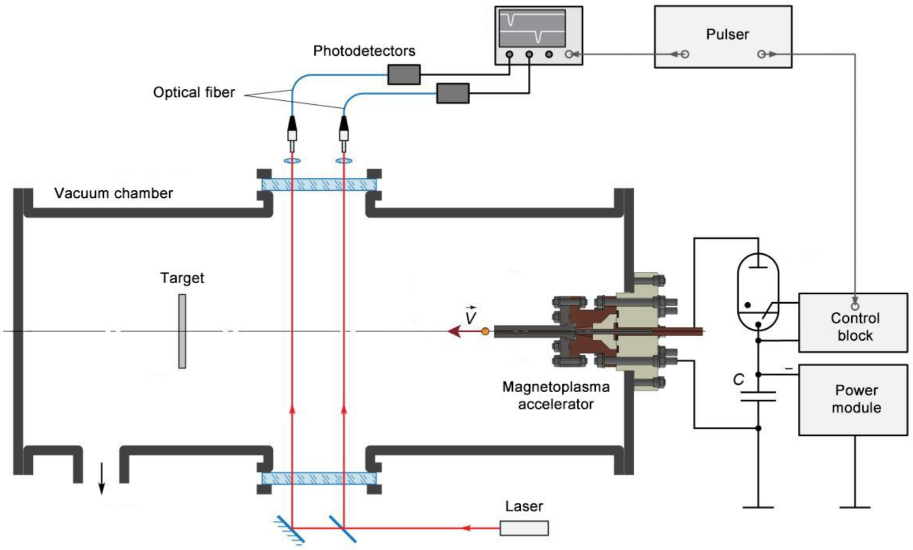

Fig. 3. Scheme of projectile velocity measurement by means of the second optical method

Trajectory of projectile motion was intersected perpendicularly by laser beams at a certain distance from each other. At the exit from the vacuum chamber, they were directed on the photosensors by an optical fiber. To form two beams a semiconductor laser radiation was passed through the beam-splitting plate and then was directed to the lens placed in front of optical fiber edge for focusing the radiation onto the surface of the photodetector.

When the projectile moves it crosses the area of the rays and signals on optical sensors are interrupted sequentially. The projectile speed can be calculated from the time interval between the interrupt signals and known distance between two laser beams. In fact, the proposed measurement method is the laser ballistic chronometer.

Typical oscillograms of signals from photodetectors are shown in Fig. 4.

With the designed detector, projectile velocity measurements were made in the range of 0.8–4.3 km/s.

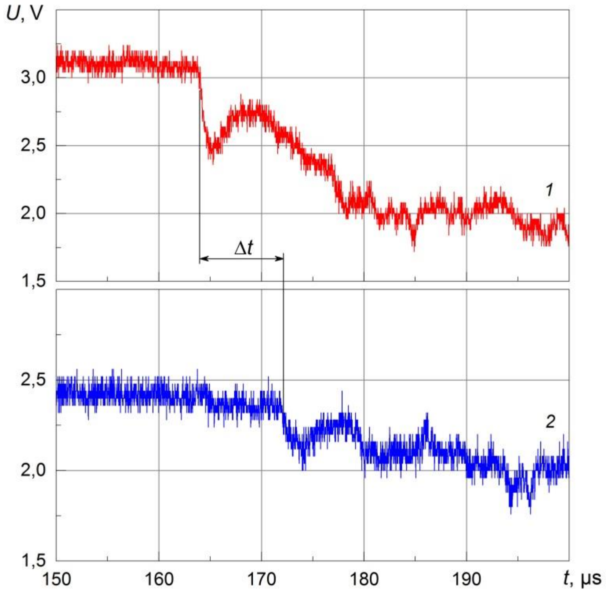

Fig. 4. Typical oscillograms of signals from the photodetectors: 1– the signal corresponding to the first beam which the projectile crosses, 2 – a signal corresponding to the second beam

In the experiments we used duralumin target of 2-8 mm thickness, which were placed in the path of the particle behind the velocity sensor. Speed of launched particles were evaluated using ballistic limit equations given in [10], which represent a semi-empirical relationships obtained in the analysis of a large number of experimental data. This equations express a dependence of the crater depth in target, formed when collision with a particle, from the particle velocity and other parameters of the particle and the target:

$$\Delta h = 5,24 d^{19/18} \left(HB\right)^{-1/4} \left(\rho_0 / \rho_t\right)^{1/2} \left(u / C\right)^{2/3}, \qquad (1)$$

where Δh – the penetration depth into a semi-infinite target, d – projectile diameter, HB – Brinell hardness of target, ρ_0, ρ_t – density of projectile and target, u – projectile velocity, C – Speed of sound in target

The difference between the velocities measured by sensors and evaluated by the formula (1) is no more than 20%.

3. COMPARISON OF METHODS

Optical method using thin films is well suited for measuring of relatively low velocities of launched bodies (no more than 3 km/s). When the speed is about 3 km/s and more this case corresponds to high-speed regime, and the signal analysis is complicated. In this case punching the film the projectile hardly causes its oscillation. If the hole in the film is not consist with the location of laser beam falling the corresponding signal is interrupted only after reaching and deformation of the film by the plasma outflowing after projectile from the acceleration channel.

A second optical method is well applicable for both cases. The plasma flow partly overlaps rays of laser ballistic chronograph, but it doesn't complicate the signal analyzes.

4. CONCLUSIONS

Presented methods were used to measure the velocity of small particles (4mm), throwing by magnetoplasma accelerator in range of 0.8 - 4.3 km/s. This methods are noise immunity and simple way of projectile speed registration that especially actual for launchers with high current pulse amplitude. The difference between the velocity measured by the optical methods and evaluated using the ballistic limit equations is no more than 20%. Thus, the two proposed methods are well suited for measurement of the velocity of particles, launched by magnetoplasma accelerator and also by other throwing systems.

REFERENCES

1. МЕРЖИЕВСКИЙ Л.А., ТИТОВ В.М., ФАДЕЕНКО Ю.И., ШВЕЦОВ Г.А. Высокоскоростное метание твердых тел. *Физика горения и взрыва*, 1987. Т. 23, № 5, с. 77–91.
2. Под ред. ГЕРАСИМОВА А.В. *Теоретические и экспериментальные исследования высокоскоростного взаимодействия твердых тел*. Томск: Изд-во Томского университета, 2007.
3. ГОЛУБЯТНИКОВ А.Н., ПИЛЮГИН Н.Н, ЛЕОНТЬЕВ Н.Е. Методы повышения эффективности легкогазовых установок. *Успехи механики*, 2003. Т. 2, № 2, с. 97–124.
4. IGENBERGS E., SHRIVER E. *J. Appl. Phys*., 1973, Vol. 44, 2177 p.
5. ИГЕНБЕРГС Е.Б., ДЖЕКС Д.В., ШРАЙВЕР Е.Л. Новый двухкаскадный ускоритель для исследования удара при гиперскоростях. *Ракетная техника и космонавтика*, 1975. Т. 13, № 8, с. 73–81.
6. ДРОБЫШЕВСКИЙ Э.М., ЖУКОВ Б.Г., НАЗАРОВ Е.В. и др. *Препринт ФТИ-1315*. Л., 1989.
7. КОНДРАТЕНКО М.М., ЛЕБЕДЕВ Е.Ф., ОСТАШЕВ В.Е. и др. *ТВТ*, 1988 Т. 26, № 1, с. 159–164.
8. EICHELBERGER R.J. *J. Appl. Phys*, 1956. Vol. 27, No. 1; p. 63–68.
9. ДРОБЫШЕВ Э.М., ЖУКОВ Б.Г., САХАРОВ В.А. Измерение больших скоростей тел малых геометрических размеров. *Письма в ЖТФ*, 1993. Т. 19, № 17, с. 45–48.
10. CHRISTIANSEN E.L. Meteoroid/Debris Shielding. Report TP-2003-210788. NASA, Johnson Space Center, Houston, Texas. 2003.

CYSENI 2015, May 27–28, Kaunas, Lithuania
ISSN 1822-7554, www.cyseni.com

PLASMA METHOD FOR MINERAL AND GLASS FIBERS PRODUCTION

V. Sauchyn, A. Lozhachnik, H. Dalholenka, D. Skamarokhau

A.V. Luikov Heat and Mass Transfer Institute
National Academy of Sciences of Belarus
P. Brovka str. 15, Minsk, 220072 – Belarus
Phone +375-29-7759560
Email: v.sauchyn@gmail.com

ABSTRACT

Traditional technologies for mineral fiber production are associated with enormous energy costs and it is not possible to obtain melting with physical and mechanical properties required to obtain high-quality fibers. It is connected with the materials high melting point (1600–1900 °C). Use of concentrated stream of thermal plasma as a source of thermal energy reduces the melting formation time due to the high temperature effect on materials (3000–5000 °C).

In this paper alternative one-stage method for mineral fibers production in plasma facility is presented. Designed plasma facility has a number of advantages in compare with equipment, used for inorganic materials processing. It contains plasma torch and plasma reactor with rectangular resection combined in one unit. DC arc plasma torch that generates turbulent plasma flow with temperature 4000-6000 K is used for heating and melting of mineral raw materials. Tests show good results of producing fine and superfine fiber from glass and minerals.

Keywords: plasma, plasma torch, plasma set, mineral material melting, glass fibers, mineral fibers

1. INTRODUCTION

Mineral fibers are fibers obtained from inorganic compounds [1]. Glass fiber is the fiber made of thin glass threads. Glass of such form shows unusual properties: it doesn't crash, doesn't break, and it is easy to bend. It allows weaving fiberglass cloth. Continuous glass fibers looks like silk thread, and spun glass is like cotton or wool fiber. Properties of the glass fibers are determined by their chemical composition and characterized by a combination of high heat resistance (e.g., heat resistance of quartz, silica, kaolin fibers is above 1000 °C), low thermal conductivity and high mechanical strength. Glass fiber hygroscopicity is almost equal to zero. Glass fibers are used for industrial purposes and for production of decorative cloths.

Depending on the used technology and raw materials stone wool (popularly called mineral), slag wool and glass wool are distinguished. Raw materials for the stone wool production are various rocks such as basalt, dolomite, limestone and diabase. Slag wool is made of slags of ferrous and non-ferrous metallurgy. Silica sand, limestone, dolomite and waste glass production (cullet) are used in the glass wool production.

Common technology for mineral fibers production is realized in several steps [2]:

1. Selection of raw materials (batch) and its preparation (drying, grinding, dosing). As a rule, each manufacturer selects its own unique composition of the batch, based on the local natural resource base. The quantitative and qualitative composition of the used defines future consumer properties of mineral wool, such as durability and water repellency.

2. Batch melting. Dosed raw material is fed into the melting unit, where it melts at a temperature of about 1500 ° C. Melt viscosity depends on melting temperature and determines

the length and width of the future fiber - the key parameters, and strength and thermal properties of mineral wool depend on it.

3. Fiber forming and binder input.

Two-stage and single-stage methods for mineral super thin fiber producing are known [3].

Two-stage method for mineral super-thin fiber production, including mineral raw material melting, melt homogenization and its processing using platinum or its alloys spinnerets in primary threads (fibers) or a trickle and its following blowing into superfine fiber by energy carrier has the disadvantage of a poor performance.

The single-stage method for superfine mineral fibers production eliminates the step of obtaining the primary filaments (fibers) or jets and does not require spinnerets of platinum or its alloys. It is more productive.

Traditional technologies for mineral fiber production are associated with enormous energy costs and it is not possible to obtain melting with physical and mechanical properties (viscosity, surface tension) required to obtain high-quality fibers. It is connected with the materials high melting point (1600–1900 °C). Use of concentrated stream of thermal plasma as a source of thermal energy reduces the melting formation time due to the high temperature effect on materials (3000–5000 °C).

Disadvantages of traditional two-stage methods are high energy consumption (up to 20 kW·h/kg batch), increased fire and explosion hazards, insufficient quality of the mineral fiber obtained, need of significant production areas.

In this paper alternative one-stage method for mineral fibers production in plasma facility is presented. Plasma reactor has a number of advantages in compare with equipment, used for inorganic materials processing. Firstly, equipment is very compact, secondly, the feed material is used almost without preparation, except of mechanical fractional treatment, thirdly, the melting of raw materials and fibers is combined in one device, thus providing a single-stage production, fourthly, design of the device allows wide range of operating parameters adjustment (reactor rotation speed, thermal energy source power), which provides the ability to create an automatic process control system.

Melts obtained in plasma reactors have a high crystallization upper limit temperature (above 1750 °C), in particular they are used for the manufacturing of high-temperature kaolin wool and ceramic wool comprising 95–98% of $SiO_2 + A1_2O_3$.

2. METHODOLOGY

We propose plasma technology and equipment to realize the process of mineral fiber production in one stage.

Dispersed raw material is fed as fluidized solids in top part of reactor. High temperature plasma flow melts the material that forms liquid film on inside surface of the reactor and moves down. Obtained melt is blown by plasma flow and preheated compressed air.

The formation of mineral fibers is determined by the factors:

- State of a melted mineral material with fiber-forming temperature interval less or equal to the temperature of heated gases.
- Thermal-physical characteristics of the melt: viscosity and superficial tension, and their ratio, ensuring a steady fiber formation from the mineral.
- The velocity of high-temperature gas flow is sufficient for stretching of fibers from the melt and the extent of the zone of its influence on melt spurts with viscosity that allows stretching of fibers.

Thickness of the melt film moving along the inner surface of the cylindrical reactor at a fixed material consumption is linearly depended on the movement speed of the material in the liquid phase of the film, and determining thin films motion factor is the friction force of plasma stream to the film surface (gravity force begin to prevail only at thicknesses of 2 mm and higher [4]). The main parameter of the friction force is the velocity of the plasma flow, which at constant other parameters is quadratic inversely proportional function of the reactor diameter, i.e. reactor diameter increases, the velocity of the plasma stream, frictional force of the film and the melt flow rate of the film decrease and it results in film thickening as the amount of material is constant. Simultaneously as the frictional force increase with plasma flow speed increase convective heat transfer coefficient into the reactor channel increases which is proportional to $Re^{0.8}$ [4]. This results in higher material film heating, reducing its viscosity, reducing friction forces and therefore increasing the flow velocity.

According to proposed technology plasma facility was designed. It consists of plasma reactor, plasma torch, raw material feeding system, compressed air supply system, cooling water supply system.

Non-transferred DC arc plasma torch is used as source of heat. Plasma torch power can be varied from 30 to 100 kW. Plasma forming gas is air.

Plasma reactor consists of two quill cylinders that are arranged aligning. Inside diameter of the reactor is 40 mm. Diameter of outlet nozzle is 20 mm. Length of reacting zone 300 mm.

According to technological scheme raw material is fed as fluidized solids in top part of reactor. Plasma flow with high temperature melts the material and forms melted film on the inside surface of the reactor. Obtained melt goes down to the nozzle where fibers formation takes place. It should be mentioned that compressed air is used for reactor wall cooling. The air is heated to temperature up to 700 °C. Hot air and plasma are used for blowing.

Blown fibers are cooled quickly with atmospheric air and form staple fiber.

Parameters of plasma facility operation (see Fig. 1):

Current strength – 190–250 A.

Voltage – 380–400 V.

Compressed air consumption – 8–12 g/s.

Additional air for blowing – 14-–20 g/s.

Temperature of plasma jet – 3000–5000 K.

Plasma jet speed – 50–130 m/s.

Temperature of the reactor wall (inside) up to – 900–1000 °C.

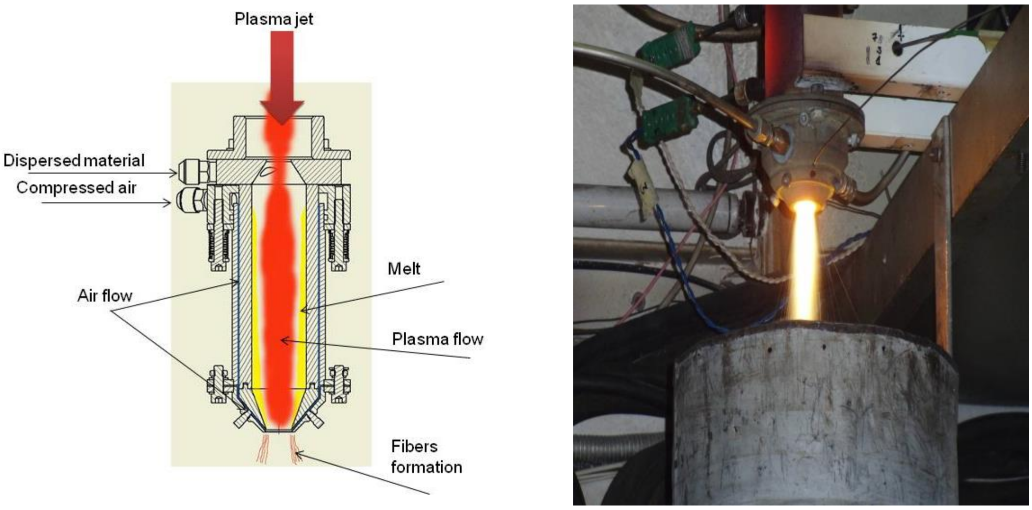

Fig. 1. Plasma reactor

3. RESULTS AND DISCUSSIONS

Experimental tests of mineral fibers formation were conducted. From the very beginning glass powder was used as raw material for fiber production. Size of glass powder is from 40 μm up to 200 μm (see Fig. 2).

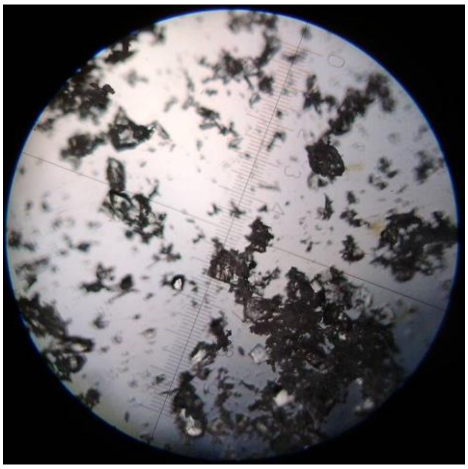

Fig. 2. Raw material (glass powder)

As a result of experiments glass fibers were obtained. Photos of glass fibers from different tests are shown in Fig. 3, 4. Colour of fibers is white.

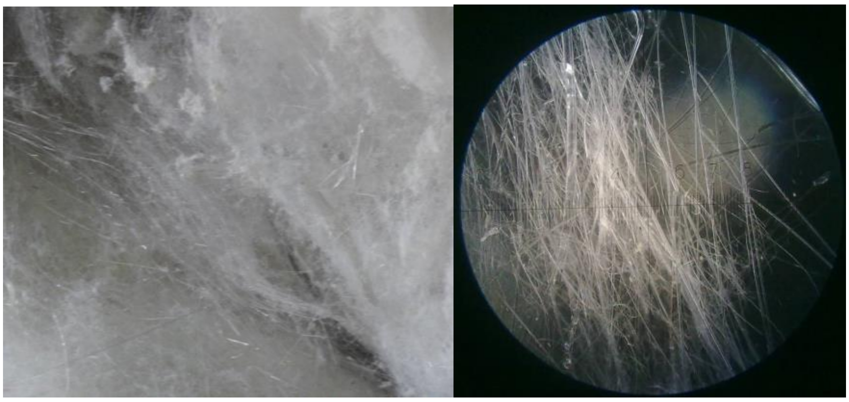

Fig. 3. Glass fiber

Fig. 4. Quartz-Glass fiber

Main mechanical parameters of obtained fibers:
Diameter of fiber is from 3 to 25 µm (photo of one of samples is shown in Fig. 5).
Length of fiber is from 3 to 10 cm (in general), up to 30 cm.
Nonfibrous inclusions is about 10–15 %.

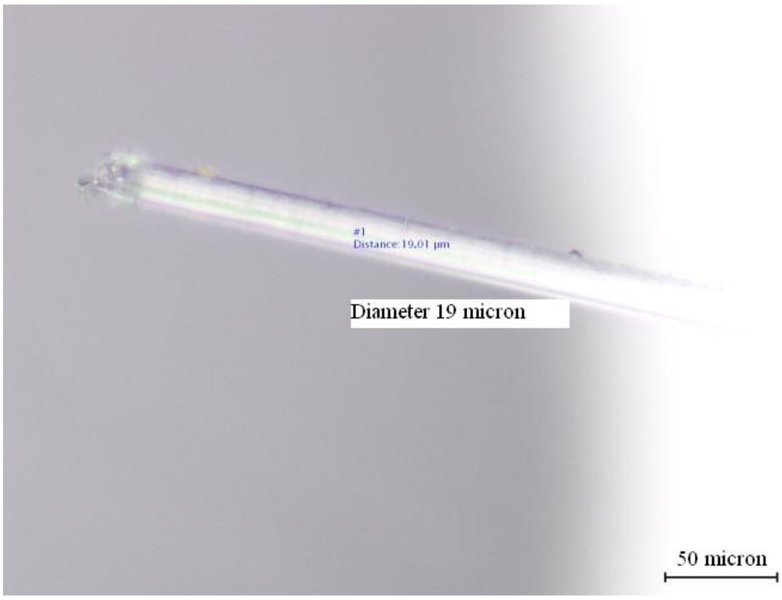

Fig. 5. Glass fiber after test on strength

Tests of produced fibers on strength were made with Instron electromechanical testing system – INSTRON 5942 (some results are presented in Table 1). Base for measurement is 10 mm; speed of tension 1 mm/min.

Table 1. Results of fibers test on strength

№	**Diameter, µm**	**Force, cN**	**Tensile strength , GPa**
1	16.31	25.824	1.24
2	16.30	19.273	0.92
3	8.95	7.847	1.25
4	8.96	6.647	1.05
5	19.01	29.248	1.03
6	14.45	21.457	1.31
7	19.66	36.04	1.19
8	15.27	18.907	1.03
9	12.13	15.188	1.32
10	26.69	52.624	0.94
11	41.18	57.822	0.43
12	33.33	69.418	0.80

As can be seen from the Table 1 strength of thicker fibers is lower. It can be explained by defects and nonisomorphic inclusions in fibers. This fact will be investigated in future work.

4. CONCLUSION

Alternative plasma method to common technologies of mineral fibers production is proposed. Use of concentrated stream of thermal plasma as a source of thermal energy reduces the melting formation time due to the high temperature effect on materials. Dispersed raw material is fed as fluidized solids in top part of reactor. High temperature plasma flow melts the material. Obtained melt is blown by plasma flow and preheated compressed air.

According to the proposed technology plasma facility was designed and manufactured. The power of plasma reactor is up to 100 kW. Experimental researches show the possibility to produce fine mineral fibers from glass and quartz.

Developed laboratory facility will be used for further investigation of properties of different minerals to possibility of fine fibers production.

5. ACKNOWLEDGMENT

The work was supported by A.V. Luikov Heat and Mass Transfer Institute (Belarus), project KACST-HMTI/21.

REFERENCES

1. KAMINSKAS, A.J. Chemistry and Technology of mineral fiber. *Russian Journal of Chemistry*. 2003, Vol. 47, No 4, p. 32–38.
2. BOBROV, Yu.L. *Durability of Heat-Insulating Mineral Wool Materials*. Moscow: Stroiizdat, 1987. 168 p.
3. VOLOKITIN, G.G. Plasma technology in building industry. VI International Conference «Plasma Physics and Plasma Technology». Minsk: Institute of Physics of NAS of Belarus. 2009 September 28–October 2.
4. LAKTYUSHIN, A.N., SERGEEV, V.L., Khvedchin, I.V. Analysis of the processes of heat and mass exchange in a slag-lined plasma reactor in production of microfibers from powder minerals. *Journal of Engineering Physics and Thermophysics*, 1997, Vol. 12, No. 4, p. 616–619.

CYSENI 2015, May 27–28, Kaunas, Lithuania
ISSN 1822-7554, www.cyseni.com

FLOW VISUALIZATION IN A TEST CHAMBER OF RAPID COMPRESSION MACHINE BY OBSERVATION OF BURNING PARTICLES DISPLACEMENT

V. Leschevich, O. Penayzkov, S. Shimchenko
Heat and Mass Transfer Institute
P.Brovki str. 15, 220072 Minsk – Belarus
Phone +375 17 2841520
Email: v.leschevich@dnp.itmo.by, penyaz@dnp.itmo.by, sergey.shimchenko@gmail.com

ABSTRACT

The rapid compression machine (RCM) is important experimental tool for investigation ignition and combustion processes. The question about uniform temperature distribution in test volume of RCM is one of the most serious because there is no possibility for direct temperature measurements. It can be only estimated from pressure measurements using assumption of adiabatic compression process. A complex flow of gas generated during compression stroke can significantly effect on adequacy of this assumption application. It is well known that during piston motion the roll-up vortex can be formed in cylinder. It causes mixing of cold gas from boundary layer with hot gas from core region. To minimize this phenomenon it is necessary to study it dependence on different operation parameters of rapid compression machine and gas mixture properties. One of the most convenient experimental methods for studying gas flows is Particle Image Velocimetry (PIV), but it is rather difficult to integrate it in RCM study. Moreover, this method gives information in one cross-section and application of Stereo Scanning PIV is probably impossible task. In this work the perspectives of new similar to PIV experimental method were considered. It was previously found that at definite conditions in test volume of RCM the ignition of small particles is always preceded to the ignition of reactive gas mixture. Moreover, the motion of these particles is not stochastic and probably correlates with motion of gas media. As result addition of easily reactive particles in oxygen contained gas media is a simple method to obtain bright trackers in all test volume. The proposed method was tested in this study and data analysis algorithm was developed. Experiments were carried for heated by compression coal dust-air mixture. Direct light emission from test chamber of RCM was visualized by high speed camera. Velocities of burning particle were measured using every two successive frames from video. The distributions of radial velocities along chamber radius obtained at different time moments clearly showed changes of gas flow structure. It is believed that proposed method will be subsequently used for optimization of aerodynamics inside RCM.

Keywords: rapid compression machine, roll-up vortex, auto-ignition, burning particles

1. INTRODUCTION

Now different kinetic mechanisms are available to describe chemical reactions. Such mechanisms are usually verified by ignition delay time data measured in experiments. The results of predictions agree well with experimental data at high temperatures. However, at temperatures lower 1100 K, there is significant discrepancy between experimental data and results of calculations that were obtained by known kinetic models of chemical reactions. It caused numerous experimental and theoretical studies aimed to explain the failure of models to predict experimental ignition delay times. Analysis of kinetic mechanisms has shown results of calculations can be approached to experimental data only by unreasonably changing of reaction rate constants. The uncertainties in the rates of elementary reactions are not entirely explaining the model’s failure [1]. It is now considered that ignition delay times measured at low temperatures are not the result of pure chemical kinetic processes under the ideal conditions of constant pressure and temperature but are affected by phenomena which are facility-specific [2]. Thus, models failure connected with inability to take into account experimental non-idealities that are caused by the presence of contaminants in the reactants or on facility surfaces, compressible fluid dynamic affects, inhomogeneous mixing, and catalysis from particles or surface materials [3, 4]. The different contribution of each phenomenon as well as different their combination for various facility complicates the correct experimental data interpretation and precludes direct cross-comparison of experimental data collected in different venues. It is likely that inside the rapid compression machine gasdynamic fluctuation associated with the movement of a piston are one of the main reason. It was shown on the schlieren photographs of inert and reactive mixtures in the earlier works [5]. It is seen there is inhomogeneity of the temperature distribution in the chamber at the end of compression. Numerical and various diagnostic optical methods have shown complex vortex flow of the gas mixture is formed inside of the chamber when speeds of the piston are high. This vortex affects on inhomogeneity of the temperature distribution within a test at the end of compression. It means that the adiabatic approximation can't be used for estimation of gas temperature in test volume. In this way, ideally to create experimental conditions that will completely destroy the vortex or will minimize influence of the vortex to the reactive mixture. Many researchers have solved this problem by using a creviced piston [6], whereby an annular gap is formed between the piston and the cylinder wall. As a result many researchers used this configuration of the compression piston without adaptation it for specific parameters of their experimental setups. In a recent work [7, 8] influence of size and gap geometry, parameters of test mixtures and RCM configuration (compression stroke, chamber height etc.) to a process of vortex formation was studied by CFD (computational fluid dynamics) calculations. It was found that the vortex decreases with increasing of the final compression pressure and the chamber or with decreasing of the compression stroke. What is more, simultaneous reduction in the piston stroke and height of the chamber are more effective for one degree of compression. Increasing of the length of the annular gap also proved positive. Development and testing of a suppression method of stable vortex formation or his damage must be additionally supported by experimental observations. Different techniques are used to flow visualization: Laser Induced Fluorescence Technique (LIF) [9], Planar Laser-Induced Fluorescence (PLIF) [10, 11] and Particle Image Velocimetry (PIV) [12, 13]. But realization of these techniques is quite difficult. The main goal of this study is to determine the possibility of using the easier method for the flow visualisation. This method is based on the observation of the movement of burning particles. The apparent advantage of this technique is that there is no necessity to illuminate dust and we can observe the movement of particles in all test volume.

2. METHODOLOGY AND EXPERIMENTAL SETUP

Frames were obtained with hot spots. Every two consecutive photos were processed. The hot spot was found on the first frame and its coordinates were determined. Then area with centre coordinate from the first frame was selected on the second frame. The hot spot was found with new coordinates in this area. Thereby the displacement was defined. Thereby the vector projection of displacement of burning particle was defined on perpendicular plane to cylinder axis. Also knowing the time span between two frames, we can calculate the projection of particle velocity on the image plane. This technique has several shortcomings. The first one is two and more points can be in the area in the second picture. Then the displacement of particle was not determined. And moreover, the particle extinguishes and a new particle ignites in the same time in the same place. However, this technique rather good determines the displacement of each particle. The camera «La Vision HighSpeedStar X» was used to derive these frames. Video registration lasted during compression stroke and ignition process. A frame rate was 12500 fps and the resolution was 1024 × 1024 pixels. Camera was installed in front of the compression cylinder. The end of the chamber, the “cylinder head”, was fitted with an optically flat, fused silica window (50 mm diameter × 25 mm thick). This window permitted a full view of the chamber cross section. The recording time was synchronized with the ignition process by signal from photomultiplier without the filter before the photocathode. The combustion of these particles progressed in adiabatically heated stoichiometric methane/air and air mixtures at temperatures close to 1000 K and pressures 1.3–2 MPa. The rapid compression machine was used to generate these conditions. The test chamber (Fig. 1) was 50 mm in diameter and about 20 mm high. The RCM chamber was equipped with a high-temperature quartz pressure sensor Kistler 6031U18, a gas inlet/outlet valve, and quartz window in a cylindrical wall (5 mm diameter × 30 mm thick). The chemiluminescence at ignition and combustion was recorded through the bifurcated optical fiber light guide connected to the mandrel of the quartz window. Emissions of CH radicals at λ = 431.5 nm were detected by one photomultiplier and the second photomultiplier was used for natural light recording.

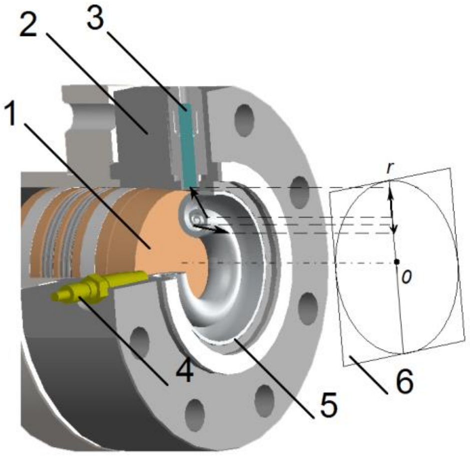

Fig. 1. Combustion chamber design of the RCM and roll-up vortex: 1 – compressing piston, 2 – cylindrical combustion chamber, 3 – quartz window for photometric measurements, 4 – pressure sensor, 5 – roll-up vortex, 6 – image plane and radial velocity projections of particles moving in the vortex

3. RESULTS AND DISCUSSION

Previously we found that ignition of methane-air mixtures is non-homogeneous and starts from the local point [14]. As it turned out, these hot spots are extraneous burning particles that almost always are in the test volume even after thorough cleaning of the inner surface of the compression cylinder and filtering the test mixture. The experiment set was carried out with unclean compression cylinder. As a result it was discovered that bright points appear in the end of compression stroke and continue to shine in the induction period until the ignition of the mixture. Burning time of some motes (bright points) was 400 µs. It was enough to overcome the distance comparable to the radius of the chamber. Later it was noticed, the motion of burning particles was not chaotic but had some direction. And worth noting no one particle did not cross the chamber diagonally. The motion of particles had the preferential direction – from the centre of the chamber to the border and back. Thereby, it was supposed that these particles are carried along by flow. Based on this assumption the idea occurred to use them for flow visualization. The algorithm has been developed to trace the displacement of each particle.

The typical oscillogram of experiment which illustrates dynamic of pressure, emission of radicals CH and natural light is in Fig. 2. The pressure in the end of compression stroke was 1.36 MPa, the temperature was 990 K. Also timestamps of selected frames for further analysis with developed algorithm marked with vertical lines.

Clearly visible that the ignition of motes occurs before the ending of compression stroke and continues until the time of ignition of methane (the temperature in the end of compression stroke is about 990 K). The idea of this algorithm was to monitor displacements of each particle. At the inlet we had the array that contains information about the coordinates of each particle and coordinates of their displacement vector. On frames (Fig. 2) arrows are attached to each point. Arrows point the direction of motion, and the length of arrows is proportional to the velocity of the displacement. I found, the maximum velocity was about 10–12 m/s. It coincides with the average speed of the piston motion. An availability of adjacent oppositely directed arrows indicates a complex three-dimensional structure of the motion of the gas.

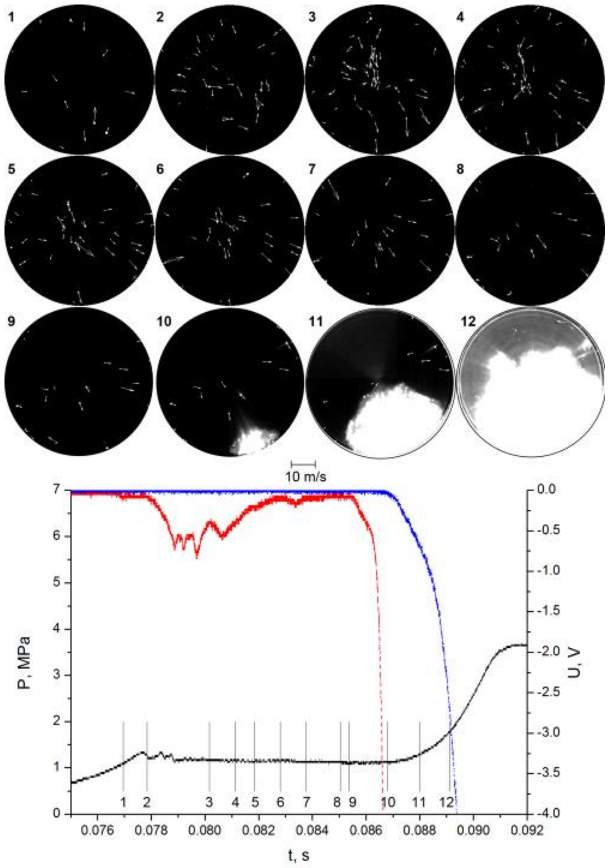

Fig. 2. Pressure-time (black line), emission of CH radicals (blue line) and natural light (red line) in the RCM and selected frames of high-speed video

To increase the number of luminous spots foreign particles are put to the compression cylinder by spraying on the inner surface of the compression cylinder and the piston. Different materials and sizes of particles were tried. The ability of ignition and time of combustion were the main criteria. On the one hand, the smaller particle, the faster it ignites and the better follows the gas flow, but on the other hand, in the same time the combustion time is reduced. Therefore, this parameter was selected by changing the initial material of particles. Carbon particles (size 20–32 microns) were the most optimal.

The experimental results of ignition of these particles are shown in Fig. 3 similarly to Fig. 2. The air was heated by rapid compression. Parameters of the experiment (the initial pressure, the compression ratio, the height of the combustion chamber, the average speed of the piston) were similar to experiment that is shown on Fig. 2. From these frames can be seen the ignition of particles begins on the compression stroke when the air temperature is about 860 K. As we can see, at first the number of particles is very small. With further compression of air and at the same time with increase of temperature the number of particles increases and fills evenly the entire volume. Advantageously particles move from the centre to the border of the chamber and vice versa. It is seen that the velocity depends on the location of the particle in the chamber. In this case the velocity is a projection of speed on the plane which is perpendicular to the axis of the chamber. In the centre of the cylinder the velocity is minimal and then it begins to increase. The maximum velocity is at the distance equal to 0.5R–0.7R (R is a radius of the cylinder). Then it begins to decrease until reaches the border of the chamber. Almost all motes extinguished when had reached the border of the chamber. The same speed change is characteristically for motes that moved from the border of chamber to the centre.

This velocity distribution can be easily explained. If particles are removed by the vortex (the structure of the vortex is toroidal form and rotation axis coincides with the compression cylinder axis — Fig. 1), the projection of the moving velocity on the chamber radius of single mote will at first increase with the motion picture on the plane from the centre to the border and then will decrease to zero and will change the direction. Then, if the particle is removed by the vortex and the particle is in the centre or on the border of the chamber, its velocity vector is directed tangentially to the vortex, i.e. the velocity vector is perpendicular to the plane of the camera. Therefore, the projection of the particle velocity has minimal values in these points. If the point is located on a distance about 0.5 R–0.7 R, velocity vector of the point is parallel to the plane, and projection has a maximum value.

Based on the above, projections of velocities of all particles on the radius of the combustion chamber were defined for the analysis of changes in the structure of the vortex motion in time. A positive value was assigned to the velocities of dust particles moving from the centre to the edge, and negative value was assigned to the particles moving vice versa.

The distribution of radial velocities for different moments of time measuring from the end of the compression stroke is shown on the Fig. 4. Each distribution was obtained by using four frames, i.e. time of exposure of one picture is 0.24 ms. Since the image of the volumetric figure on the plane of camera matrix is the central projection, so radial displacement of the point on the plane of image will be determined by the displacement along the optical axis, when the point moves away from the optical axis of the lens. Therefore, the error of measurement of the velocity of radial movement of dust particles is bigger near walls of the chamber. This effect of image perspective can be minimized using a long lens.

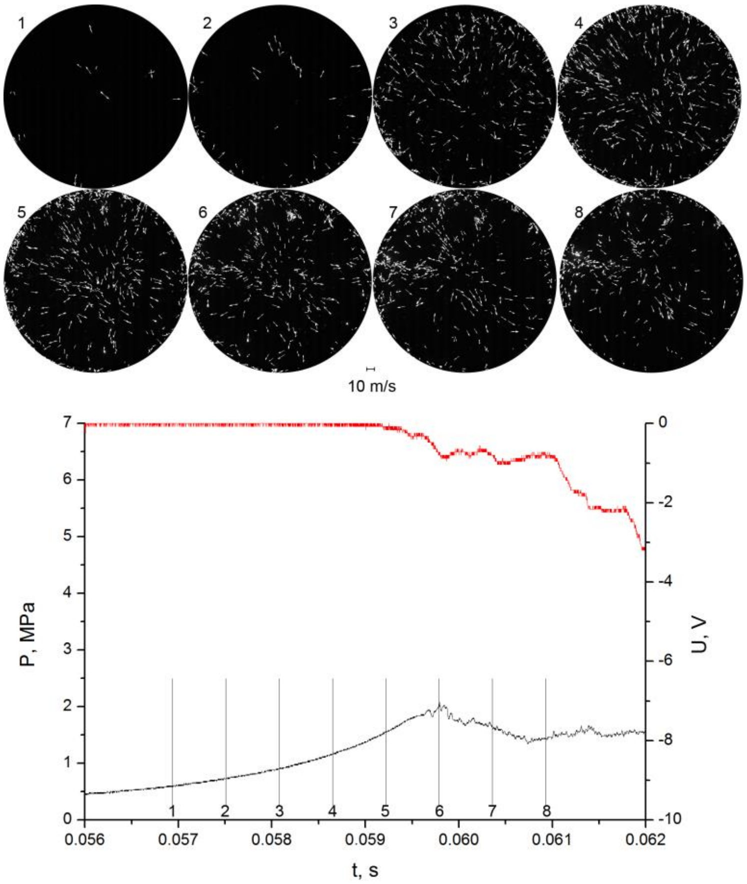

Fig. 3. Pressure-time (black line), natural light (red line) is recorded by fast compression of air with carbon dust in the RCM

Obtained radial velocity distributions show the number of motes with low radial speed increases as the end of the compression stroke (for example, -0.43 ms) in the centre and near walls of the chamber (R = 0 and R = 25 mm). Number moving particles is bigger near the walls of the chamber due to the dust was initially dispersed on the inner surface of the cylinder. Therefore ignition of particles starts usually near it. And not having reached the centre of the chamber, a lot of particles completely burned. The number of dust particles with high speed increases when the radius is about 15 mm. This is consistent with the vortex movement that is shown in Fig. 1. Over time empty area in the vicinity of this radius begins evenly to be filled by points. And the distribution of velocity projections becomes more homogeneous. It indicates orderly movement is destroyed. We can also see how this area (without points) appears in the radius about 20 mm in 1.63 ms before the end of the compression stroke. Then the area moves along the radius to the centre of the chamber. It can illustrate the beginning of the vortex formation and its growth. But the strict connection of the development of gas dynamic phenomena and behaviour of the set of points on the image is unacceptable because of the large scatter of the points. Using of averaging or any approximations for the obtained array of values of velocity projections is difficult since the proposed method of representation does not consider the internal structure of the vortex motion because of its two-dimensionality. This structure can be quite complicated (for example, closed circular or spiral tracks can be in a section of the vortex). Moreover, as has been experimentally shown [15], vortex structure can change over time and depends on the flow Reynolds number. Nevertheless, in our opinion, this method of flow visualization in the chamber of RCM is easy to implement so has a right to exist and can be applied:

1) for assess the order of the gas movement

2) for development of measures to suppress vortex formation and optimization of aerodynamics inside the existing RCM.

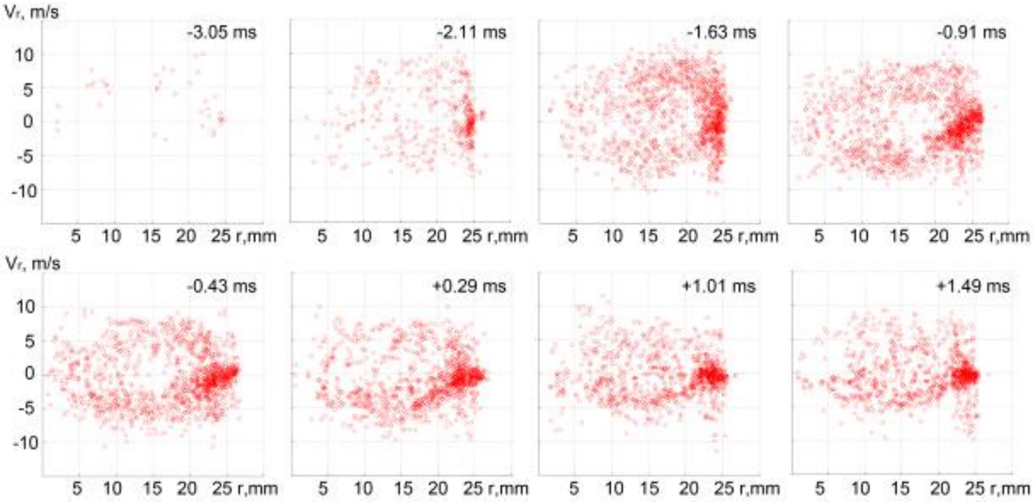

Fig. 4. Radial velocity distributions along the radius of the chamber at different time points

4. CONCLUSIONS

The presence of particles in the test volume of the RCM was finally confirmed in this work. It was also found that these particles can be autoignited before the end of the compression stroke and during the induction period. Moreover they move through test volume and this motion is not stochastic and likely caused by gas flow. Based on these observations, the simple method of flow visualization inside the test volume was proposed and tested. But application of technique is limited because it is necessary to achieve the conditions of gaseous medium required for ignition of dust. The results of performed data analysis agree with presentation of flow field generated during compression stroke in a form of roll-up vortex. This method allows to estimate the geometrical and velocity features of this vortex and their variation in time. The maximum velocity of particles displacement along radius is about 10 m/s. It proves the reliability of technique used for flow visualization because this value agrees with average speed of piston motion.

REFERENCES

1. PETERSEN, E.L., KALITAN, D.M., BARRET, A.B., REEHAL, S.C., MERTENS, J.D., BEERER, D.J., HACK, R.L., McDONELL, V.G. New syngas/air ignition data at lower temperature and elevated pressure and comparison to current kinetic models. *Combustion and Flame*, 2007, Vol. 149, p. 244–247.
2. CHAOS, M., DRYER, F.L. Chemical-kinetic modeling of ignition delays: considerations in interpreting shock tube data. *International Journal of Chemical Kinetics*, 2010, Vol. 42, No. 3, p. 143–150.
3. DRYER, F.L., CHAOS, M. Ignition of syngas/air and hydrogen/air mixtures at low temperatures and high pressures: Experimental data interpretation and kinetic modeling implications. *Combustion and Flame*, 2008, Vol. 152, p. 293–299.

4. PANG, G.A., DAVIDSON, D.F., HANSON, R.K. Experimental study and modeling of shock tube ignition delay times for hydrogen–oxygen–argon mixtures at low temperatures. *Proceedings of the Combustion Institute*, 2009, No. 32, p. 181–188.
5. LIVENGOOD, J.C., LEARY, W.A. 1951. Autoignition by rapid compression. *Industrial and Engineering chemistry*, 1951, Vol. 43, No. 12, p. 2797–2805.
6. LEE, D., HOCHGREB, S. Rapid compression machines: heat transfer and suppression of corner vortex. *Combustion and Flame*, 1998, Vol. 114, p. 531–545.
7. MITTAL, G., RAJU, M.P., SUNG, C.J. Vortex formation in a rapid compression machine: Influence of physical and operating parameters. *Fuel*, 2012, No. 94, p. 409-417.
8. GRIFFITHS, J.F., JIAO, Q., SCHREIBER, M., MEYER, J., KNOCHE, K.F. Development of thermokinetic models for autoignition in a CFD code: experimental validation and application of the results to rapid compression studies. *Proceedings of the Combustion Institute*, 1992, No. 24, p. 1809–1815.
9. CLARKSON, J., GRIFITHS, J.F., MACNAMARA, J.P., WHITAKER, B.J. Temperature fields during the development of combustion in a rapid compression machine. *Combustion and Flame*, 2001, Vol. 125, p. 1162–1175.
10. STROZZI, C., SOTTON, J., BELLENOUE, M., MURA, A. Self-ignition of a lean methane-air mixture at high pressure in a Rapid Compression Machine. Third European Combustion Meeting. Chiania: Mediterranean Agronomic Institute of Chania. 2007 April 11 – 13.
11. STROZZI, C., SOTTON, J., MURA, A., BELLENOUE, M. Characterization of a two-dimensional temperature field within a rapid compression machine using a toluene planar laser-induced fluorescence imaging technique. *Measurement Science and Technology*, 2009, Vol. 20, p. 1–3.
12. GUIBERT, P., KEROMNES, A., LEGROS, G. An Experimental investigation of the turbulence effect on the combustion propagation in a Rapid Compression Machine. *Flow, Turbulence and Combustion*, 2010, Vol. 84, p. 79–95.
13. STROZZI, C., MURA, A., SOTTON, J., BELLENOUE, M. Experimental analysis of propagation regimes during the autoignition of a fully premixed methane–air mixture in the presence of temperature inhomogeneities. *Combustion and Flame*, 2012, Vol. 159, p. 3323–3341.
14. KRIVOSHEYEV, P.N., LESCHEVICH, V.V., PENYAZKOV, O.G., SHIMCHENKO, S.Yu. High-speed imaging of premature ignition in rapid compression machine. *Advances in Nonequilibrium Processes: Plasma, Combustion, and Atmosphere*, 2014, p.137–147.
15. TABACZYNSKI, R.J., HOULT, D.P., KECK, J.C. High Reynolds number flow in a moving comer. *Journal of Fluid Mechanics*, 1970, No. 42, p. 249–255.

CYSENI 2015, May 27–28, Kaunas, Lithuania
ISSN 1822-7554, www.cyseni.com

GREEN OFFICES: COST SAVING AND ENVIRONMENTAL BENEFIT

V. Varanavičius
Lithuanian Energy Institute
Breslaujos str. 3, 44403 Kaunas – Lithuania
Phone +370 614 71864
Email: v.varanavicius@lei.lt

ABSTRACT

Regarding the nowadays increasing consumption it is vital important to focus companies to environmental friendly behaviour. Since companies are becoming more and more distrustful, it is important to prove the financial interest in order to reach their attention. Thus, one of the major challenge that companies face is the integration of theoretical solutions to the practical level. In this paper, the author undertook examination of research studies in order to reach a broad overview and understanding the behaviour and tendencies of green offices, what kind of factors are influencing energy and cost saving, how the environment is influenced, what energy consumption trends are captured and what possible solutions can be incorporated in offices. It could be constituted that the current study is extensive in terms of presented latest energy consumption trends in green offices, also defined factors and solutions. Hence, the significance of the article lies on the fact that it is a systematic approach which puts forward an important foundation for future theory and practice investigations.

Keywords: green office, energy saving, greenhouse gas, cost saving, environment

1. INTRODUCTION

More than a decade ago the discussion about green offices begun. This concept appeared when it was started to implement the idea of sustainable consumption in the work place – in the office. The green offices can be seen as ecological and economical buildings [2, 9, 13 11], or also highlighting the different behaviour in the office and systematically covering both aspects [4].

In order to objectively evaluate green offices concept implementation possibilities, there is a lack of researches about their environmental benefits. Also most scientists are oriented to do the researches related to certificates of green offices and their benefits (the real estate price, the benefit for staff and etc.), however there are not much implemented researches that defines how green office behaviour practically influence employees, or maybe they face additional inconvenience, time, costs. The researches of behaviour in offices and its effect on energy usage and Greenhouse Gas (GHG) emission as considered as a lifestyle, however there are some of the researches oriented to clear working style and behaviour that makes influence to energy consumption [17].

According to Bin (2012) commercial buildings are of four main energy users, they had more than 18% of U.S. energy consumption in 2009. During the previous three decades commercial energy consumption was growing by 2 percent annually, which is more than total average growth, while transport sector consumption was growing by 1.3%, household sector 1.1%, in industry the consumption was decreasing by 0.1%.

The working style in offices consist of the set of provisions and behaviour in a work place. Often in depends on personal attitudes, but the influence is also made by his/her tasks, management, colleagues and various other factors. The emergence of certain working style the reason can be business actions, business type, building type, company's terms and conditions by the managers and overall workplace culture. Looking at the green movement in the offices is seen that environment friendly behaviour in workplace is in development process and there is a lack of comprehensive experiments, modulated and theory-based interventions [5]. Even though the environment friendly and energy saving initiatives are implemented in various working places, the efficiency is rarely measured. The research in United Kingdom where 147 office buildings were investigated found that only 15% were evaluating their influence on environment [23] and according to Gardner, Stern (2002), the intervention based on providing feedback and knowledge, which is promoted through monetary or other expression, can be successful.

The aim of the study is to investigate the tendencies for cost saving and environmental benefits in green offices.

The objectives of the study are:

1) to analyze the cost saving in green offices through the academic perspective,
2) to analyze the environmental benefit in green offices through the academic perspective,
3) to analyze the cost saving and environmental benefit in green offices in particular case.

2. THE IMPORTANCE OF IMPLEMENTATION THE GREEN OFFICES

In order to justify the importance and need of green offices, there is a need to evaluate the current situation and the potential of green buildings.

According to Airaksinen (2011), Armitage (2011), in the buildings are consumed approximately 40 percent of total energy consumption in Europe and about 36 percent of CO_2 emission also come from the buildings.

Wilkinson (2006) argues that 12 percent of greenhouse gas emission is produced by commercial buildings including office buildings. In 2005 in Melbourne (Australia) the research was made of various types, ages and sizes of the office buildings and evaluated their GHG emission. The outcome of this research states that positive correlation exist between increased energy consumption, CO_2 emission and smaller size of office building. The energy consumption and CO_2 emission of older offices dramatically increase with age. The emission levels are associated with office space per employee - a higher level of employment means lower emissions. That is why Airaksinen (2011) highlight that current office buildings become more and more energy efficient.

It is worth to mention data from 2002 Green Seal report. In USA 1 600 000 disposable pens are discarded every year; 24 trees are needed to produce one ton of printing and office paper, but one ton of paper produced from recycled paper would save 4100 kilowatt-hours of energy, 26500 litres of water, 30 kilograms of emission and 3 cubic meters of landfill space. Sending the printer and copier cartridges for refilling or recycling USA companies could save 1.5 milliard dollar and not less as 100 000 barrels of oil every year. Two thirds of USA companies have the waste recycling policy, however only 40 percent have policies for recycled materials acquisition. As we can see, there is great potential to carry out green office policy, thus ensuring a comprehensive sustainable development.

Scot (2007) points out that a representative office computers and other electronic office equipment consume about 26% of energy consumption. However, the use of certified energy-efficient appliances can reduce energy consumption by up to 40% and provide savings.

Australian study revealed that most of the offices are not implementing conservation practices to reduce energy consumption, greenhouse gas emission and waste. The research was made where office employees were interviewed. The results of the study are:

- 74 percent of respondents say that air conditioning in office is turned on all the time,
- 14 percent of respondents are not turning off the light in office at night,
- 25 percent are using only recycled paper,
- 85 percent prefer printing the document copy and not correcting it on the screen,
- 35 percent are not turning off computer during the night,
- 20 percent do not have containers for paper recycling,
- 50 percent do not have containers for aluminum cans, plastic bottles, and for other secondary material to collect.

It is said that air conditioning cause highest amount of CO_2 emission and consist of almost half energy usage in a building. The turned on equipment, such as computers, are responsible for 280 tons of GHG emission every year. It is seen that even in Australia, which is one of the leaders of green offices in the world, have no policy of green offices and there is a huge potential to implement sustainable development.

Because of the World's climate change the sustainability and environmental interests are increasing, more and more organizations are engaged in a green practice. The goal of Neha.org (2008) survey was to find out how organizations and offices are getting involved into the green movement. The research results revealed that 104 respondents or 49 percent introduced couple sustainable simple things in their office, 35 percent indicated that nothing has changed in the last year. 14 percent indicated that most green means were implemented and two percent have not implemented green practice, but are seeking for changes in this way.

Interesting fact was enclosed in the research made by Patrick (2012), 74 percent of companies located in green buildings think that their organization could improve their green activity.

Looking at the outcome of the researches results, the conclusion can be made that involvement to sustainable development assurance is very important and there is a big potential. If more offices in the world would be carrying about the green policy, the climate change problem would not be so sensitive [3].

3. ECONOMIC BENEFITS OF GREEN OFFICE

In year 2004 journal "The Economist" announced report where says that green offices save money, decrease long-term energy consumption: the research in United States of America of 99 green offices showed that in average this kind of buildings consume 30 percent less energy than traditional buildings. So any kind of additional costs when building green building can pay back quickly: to reach certificate's LEED Gold requirements need to increase the building costs by 2 percent, this investment pays back in 2 years by lower ongoing costs. While decreasing the costs by building the standard office results are opposite – it can cause a higher bills for energy and wasted materials [11].

Edwards (2006) was analyzing the green offices and green buildings that were built since year 1990 in United Kingdom. This scientist paid most of his attention analyzing technical characteristics of the building, emphasized the architectural side, and however in the research extracted the useful information analyzing also the green office benefit by saving operating expenses and increasing the productivity of employees. He recognized that green offices provide financial and life cycle benefits, including those that reduce energy bills. The research was confirmed by increased productivity of employees in green offices that can be even more important than GHG emission reduction.

Miller (2008) made a study about the benefit of certificated (LEED and Energy Start) office buildings. This analysis showed that lots of benefits in a green and high quality office building cannot reflect the higher rental price. However, in recent years, the tenants began to appreciate the cleaner air, more natural light and more easily transformed space benefits. In 2007 after investigation was made of 500 corporations, it was revealed that 75 percent of managers answered that their companies are willing to invest more money into environmental programs.

Edwards (2008) notes that during the last 25 years the thinking of managers has changed, they are not scared to invest, implement the policy of green offices. Also it is thought that it helps to attract investors, as a sample can be taken Wal-Mart and IBM.

It is said that economic benefit of green offices need to be evaluated also through less visible aspects. Example, by using natural day light in the office are also decreasing the energy costs, also the employees are working more efficient. Michigan University Environment psychologists made a research and found out that employees that have the possibility to see a natural landscape have higher satisfaction for the work, experience less stress, and has less diseases. Also it was found out that truancies are decreased by 15 percent when it was moved to green office building. So the economic benefit of green office need to be calculated taking into the account the employees' performance, decreased truancies and how those parameters increase the profit of the company [11].

It is important to have a natural light and constant ventilation in the office, if there is a wish to reach the efficiency of energy consumption. The fact is that green offices help not only to decrease the energy expenditures, but also help to decrease and a part of employee costs, that leads to competitive advantage. Service companies that have their offices in green buildings have to pay their attention to increase the satisfaction of employees, but not just calculate the financial benefit and efficiency of energy consumption. Also it is important to seek for highest satisfaction for employee. Also green offices can help to attract and hold the high qualification employees. The economic benefit coming from employees' productivity by profit would exceed the saving of energy by 6 times in 20 years [7].

From the provided results is seen that the main economic benefit is reached through decreased expenses for energy, also there is a visible increase of employees productivity which generates the profit for the company.

4. THE PRACTICE OF GREEN OFFICES IN FINLAND

An initiative to reduce ecological footprints called World Wildlife Fund (WWF) Green Office runs a program with a goal to help for offices in Finland to become green. This program helps to increase the ecology and decrease the GHG emission for the companies through renovations of the offices [12].

Fig. 1 shows the tenancies of green offices growth in Finland. From the Figure is seen that the biggest interest in green offices started in 2007.

The office surroundings and workplaces have an important role in energy consumption and sustainable decisions. The scheme of green office influence the employees to cooperate and make ecological work together at the same time developing the organization activities in other spheres. The network of green offices in Finland in year 2011 consisted of 193 organizations, 53 000 employees in total [12].

In WWF (2011) report announced about green offices advantages in Finland during 2010. It is said that green offices saved 2810 tons of GHG emission during the 2010 comparing to 2009. During this year green offices compensated 242 kg GHG emission for one person. The electricity consumption was decreased by 32 percent for one person, in total 296 GW/h was saved which can be compared to 2300 tons of GHG emission. The paper consumption in green offices decreased by 15670 paper sheets that made GHG emission decrease by 200 tons.

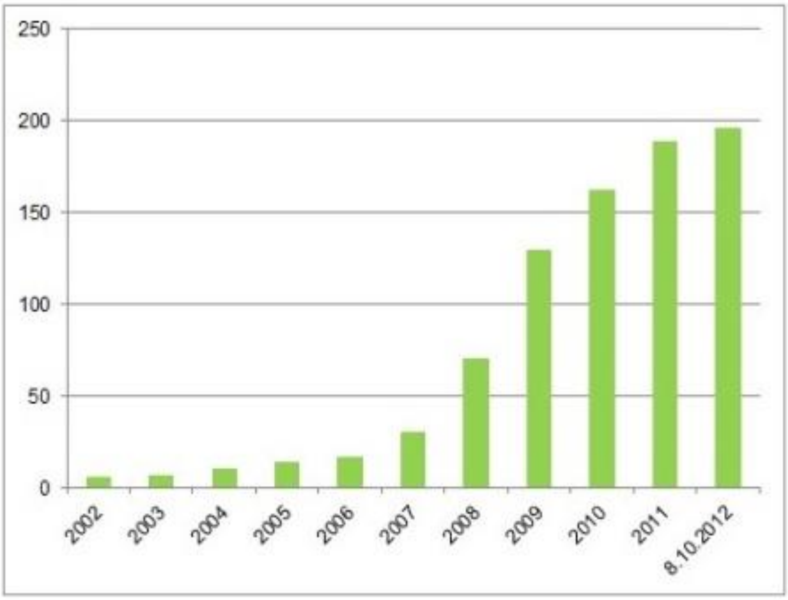

Fig. 1. Green Offices growth in Finland [12]

All in all, analyzing the sample of Finland is seen that the quantity of green offices increases, as increases the popularity and willingness to establish the office in such a building, which provide direct and indirect benefits.

5. CONCLUSION

1. Buildings consume approximately 40 percent of total energy consumption in Europe and about 36 percent of CO_2 emission also come from the buildings, so looking at the outcome of the researches results is seen that sustainable development assurance is very important for the future of planet, also the big potential of sustainable development is seen. If more offices in the world would be taking care about green policy, the climate change problem would not be so sensitive.
2. 12 percent of greenhouse gas emission is produced by commercial buildings including office buildings. Positive correlation exist between increased energy consumption, CO_2 emission and smaller size of office building. The energy consumption and CO_2 emission of older offices dramatically increase with age. Current office buildings become more and more energy efficient.
3. Office computers and other electronic office equipment consume about 26% of energy consumption. The air conditioning cause highest amount of CO_2 emission and consist of almost half energy usage in a building. The turned on equipment, such as computers, are responsible for 280 tons of GHG emission every year.
4. The sample of Finland show that the quantity of green offices increases every year, as increases the popularity and willingness to have the office in such a building. It has been evaluated, that green offices significantly increase countries environmental care, save energy and costs.

REFERENCES

1. AIRAKSINEN, M., MATILAINEN, P. *A Carbon Footprint of an Office Building.* VTT Technical Research Centre of Finland, 2011. Vol. 4, pp. 1197-1210, ISSN 1996-1073.
2. ARMITAGE, L., MURUGAN, A., KATO, H. *Green offices in Australia: a user perception survey.* Journal of Corporate Real Estate, 2011. Vol. 13 Iss: 3, p. 169–180.
3. BIN, S. *Greening work styles: an analysis of energy behavior programs in the workplace.* American Council of an Energy-Efficient economy, report number B121, 2012.
4. BROWN, Z., COLE, R.J., ROBINSON, J., DOWLATABADI, H. *Evaluating user experience in green buildings in relation to workplace culture and context.* Facilities, 2010. Vol. 28, Issue: ¾.
5. DAVIS, M., CHALLENGER, M., CLEGG, C. *Understanding and promoting green behaviour in the use of existing buildings*. A Report to Arup, 2008.
6. DIETZ, T, GARDNER, G.T. *Household actions can provide a behavioral wedge to rapidly reduce US carbon emissions.* Proceedings of the National Academy of Sciences of the United States of America, 2009. Vol. 106, Issue 44, p. 18452–18456, 5 p. ISSN: 00278424.
7. EDWARDS, B. *Benefits of Green Offices in the UK: Analysis from Examples Built in the 1990s.* InterScience, 2006 Vol. 14, p. 190–204. DOI: 10.1002/sd.263.
8. EDWARDS, C. *The green office myth.* Engineering & Technology, 2008. Vol. 3, Issue 20, p. 74–77, 4 p.
9. EICHHOLTZ, P., KOK, N., QUIGLEY, J.M. *Doing Well By Doing Good? Green Office Buildings.* American Economic Review University of California Energy Institute, 2009.
10. GARTNER, G.T., Stern, P.C. *Environmental problems and human behavior*. 2nd ed. Boston, MA: Pearson Custom Publishing, 2002.
11. HERZOG, T., MCDONOUGH, W., FOSTER, N, HEINZ, K.T. *The rise of the green building.* Economist, 2004. Vol. 373 Issue 8404, p. 17–23, ISSN 00130613, AN 15263155.
12. JULKUNEN, H. *WWF*, 2011 [referred on the 3th of March in 2015 y]. Link to the internet <http://wwf.fi/mediabank/1416.pdf>
13. KATO, H., TOO, L., RASK, A. *Occupier perceptions of green workplace environment: the Australian experience.* Journal of Corporate Real Estate, 2009. Vol. 11 Iss: 3, p. 183–195.
14. MAKOWER, J. *Three Ways to Green Up Your Office on the Cheap*. Scientific American, 2011 [referred on the 3th of March in 2015 y]. Link to the internet <http://www.scientificamerican.com/article.cfm?id=three-ways-to-green-up-yo>
15. MILLER, N., SPIVEY, J., FLORANCE, A. *Measuring the Green Premium for Office Buildings. Does Green Pay Off?* Green Design, 2008. Vol. 15, No. 1.
16. *Neha.org*. The National Environmental Health Association, 2008 [referred on the 3th of March in 2015 y.]. Link to the internet <http://www.neha.org/research/index.html>
17. PATRICK X.W., ZOU, P.X., COUANI, P. *Managing risks in green building supply chain*, 2012. Vol. 8, p. 143–158.
18. SAN DIEGO STATE UNIVERSITY *Green Building Saves Green*. San Diego Business Journal, 2008, p. 31, ISSN: 87506890.

19. SCHIPPER, L., MEYERS, S. *Energy Efficiency and Human Activity: Past Trends, Future Prospects*. Cambridge Energy and Environment Series, 1992. ISBN 0 521 43297 9.
20. SCOT, C. *Offices go green.* Government Procurement, 2007. Vol. 15 Issue 5, p. 26–29, 4 p. ISSN: 10780769.
21. WILKINSON, Sara J., REED, Richard G. *Office building characteristics and the links with carbon emissions.* Emerald Group Publishing Limited, 2006. Vol. 24, No. 3, p. 240–251, DOI 10.1108/02630800610678887.
22. World Commission on Environment and Development. *Our Common Future.* Oxford: Oxford University Press, 1987, p. 27. ISBN 019282080X.
23. ZIBARRAS, R., BALLINGER, C. *Promoting environmental behaviour in the workplace.* A survey of UK organisations. In: Bartlett D (ed.). The psychology of sustainability in the workplace. Leicester: BPS Publications, 2011.

CYSENI 2015, May 27–28, Kaunas, Lithuania
ISSN 1822-7554, www.cyseni.com

ADJUSTMENT FACTORS IN BAYESIAN RELIABILITY ASSESSMENT FOR DEMO FUSION TECHNOLOGY

T. Iešmantas, R. Alzbutas
Lithuanian Energy Institute
Breslaujos str. 3, LT-44403 Kaunas – Lithuania
Phone +370 37 401801
Email: Tomas.Iesmantas@lei.lt, Robertas.Alzbutas@lei.lt

ABSTRACT

DEMO fusion plant is supposed to be the first fusion reactor to generate electrical power. Therefore many of its technologies will be first of its kind. As a consequence, there is little or no knowledge about the reliability characteristics of such systems. There is a possibility to reuse statistical data and expert knowledge accumulated by nuclear power plant operating community, especially since many designs will be adapted from NPP systems. However, many differences will be present as well. This makes to consider approaches of reliability assessment other than already in use. In this paper we are presenting analysis of failure rates of Primary Heat Transfer System for Helium Cooled Pebble-Bed blanket, one of several concepts under consideration for DEMO reactor. Failure rate adjustment factors will be considered as the main vehicle to translate the impact of different conditions in DEMO plant. For example, the failure rates of pipelines – there is a vast amount of data from NPP industry for reliability of pipelines with water as a cooling fluid, but in DEMO it might be helium. In addition, all analysis will be carried out by employing Bayesian approach due to its abilities to incorporate different kinds of information and an intuitive treatment of uncertainty.

Keywords: Fusion, DEMO, reliability, Bayesian, HCPB, Cooling system

1. INTRODUCTION

DEMO fusion plant is supposed to be the first fusion reactor to generate electrical power. Therefore many of its technologies will be first of its kind. As a consequence, there is little or no knowledge about the reliability characteristics of such systems. There is a possibility to reuse statistical data and expert knowledge accumulated by nuclear power plant community, especially since many designs will be adapted from NPP systems. However, many differences will be present as well. This leads to consider approaches of reliability assessment other than already in use. In this paper we will consider analysis of failure rates of Primary Heat Transfer System for Helium Cooled Pebble-Bed (HCPB) blanket, one of several concepts under consideration for DEMO reactor. Failure rate adjustment factors will be considered as the main vehicle to translate the impact of different conditions in DEMO plant. For example, the failure rates of pipelines – there is a vast amount of data from NPP industry for reliability of pipelines with water as a cooling fluid, but in DEMO it might be helium. In addition, all analysis will be carried out by employing Bayesian approach due to its abilities to incorporate different kinds of information and an intuitive treatment of uncertainty.

The plan of the paper is as follows: we review the main aspects of the HCPB blanket as well as the main cooling system. Then we discuss the notion of adjustment factors and how it might be applied in the context of HCPB. Next we briefly present the Bayesian approach to the DEMO plant reliability assessment and then proceed with the application of this approach to the adjustment factors for DEMO HCPB coolant pipelines.

2. COOLED PEBBLE BED BLANKET

2.1. HCPB blanket concept

As expressed in [14], the helium cooled pebble bed (HCPB) ceramic blanket [9] is one of several blankets chosen for a European DEMO reactor and has seen steady development over the past years. Key points of the development have been the design of a HCPB test module for ITER [1], continuing work on characterising physical properties of Beryllium and ceramic breeder pebble beds [10, 19] and the exploration of blanket manufacturing technology [18]. Following information about the current state of the HCPB concept is directly adapted from [22].

According to the total blanket power and design temperatures at blanket inlet and outlet, the total He mass flow rate is 2143 kg/s from energy balance. From the neutron power calculation the total neutron power is 1547 MW. Neutron power generation in each blanket module is different and it will be calculated by neutronic analyses. Based on the neutron power results in each blanket module He flow distribution can be determined. The heat load to the FW under normal steady-state operation is expected to be in the range of 0.5–15 MW/m² and a considerable amount of energy (>90%) is radiate by light impurities injected into plasma boundary [17]. Heat loads above 0.5 MW/m² could mainly be expected due to interaction with hot charge-exchange neutral atoms and due to convective radial plasma losses, associated with unstable convective cells in the SOL (Scrape Off Layer) region.

As shown in Fig. 1 Multi Module Segments (MMS) are used for the blanket arrangement. The whole blanket system inside the VV in all-round toroidal direction is divided in 16 sections due to the defined 16 ports. Each section is divided into 3 segments on outboard (OB) side and 2 segments on inboard (IB) side in the toroidal direction. In each segment 10 MMS are arranged for IB or OB in the poloidal direction. Thus totally 800 blanket modules are designed. For example, Fig. 1 shows one OB equatorial blanket module. The outer dimensions of the module are 800 x 1000 x 1430 mm (radial x poloidal x toroidal). The blanket module is composed by the first wall (FW), caps, Horizontal and Vertical Stiffening Grids (HSG and VSG), breeding zone, manifolds (MFs) between Back Plates (BPs) and Back Supporting Structures (BSST) with He feed lines. Bending plates are constructed for blanket montage. The stiffening grids divide the breeding zone into 35 breeding units (7x5 BUs). Each BU is filled with lithium ceramic pebbles (Li_4SiO_4) in the U-shape canister and Be pebbles in the environment of the canister up to the walls of the stiffening grids. The BUs on the edge of the area have smaller sizes than the central BUs. An average W-layer with 2 mm thickness adheres to the FW as PFC. Using W armour physical sputtering is expected to be the controlling erosion mechanism during normal operation. He cooling channels are imbedded in the FW, caps, grids and BUs for heat removal. He flows through the blanket via MFs. To achieve efficient heat transfer required for the FW ($h \geq 5$ kW/m²K), a high flow velocity (> 100 m/s) should be achieved by increasing the pressure drop, for which large circulator power is required [17]. If any gases or materials for an enhanced radiative heat transfer either in the main plasma or divertor to protect the FW and divertor walls, they could be activated and are then the part of the exhaust gas.

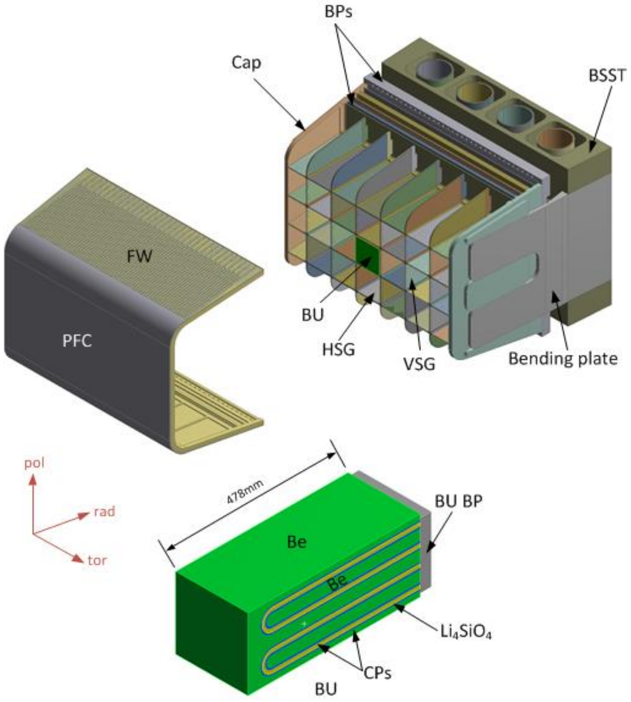

Fig. 1. Scheme of one blanket module

2.2. HCPB cooling system

The main helium coolant system is relatively similar to that of High Temperature Helium Cooled Reactors (HTR) and even more to that of a Gas Cooled Fast Reactor (GCFR) due to the high pressure and lower temperature of the helium in comparison of these values for the HTR, so that industrial experience is available for the design of these systems. The main design of the helium cooling system will be briefly presented as adapted from [22, 6].

Fig. 2 shows a scheme of the blanket-PHTS, which is designed in [6] based on the concept in [8]. He cooling circuits from the 48 OB segments are connected to two ring headers A and B to complete separation of the two independent cooling systems for the redundancy. Six He lines are connected to each header, each line being provided with its own circulator and SG. Five of them are operation line while the sixth line is the reserved line for replacement of a malfunctioning line as required. The same arrangement is adopted for the 32 IB segments, however only three He lines are departing from each ring header (C or D): two in operation and one in reserve. Table 1 shows some data of the blanket-PHTS. He inventory is taken from the previous concept and it will be defined for the current concept after completion of piping and components design.

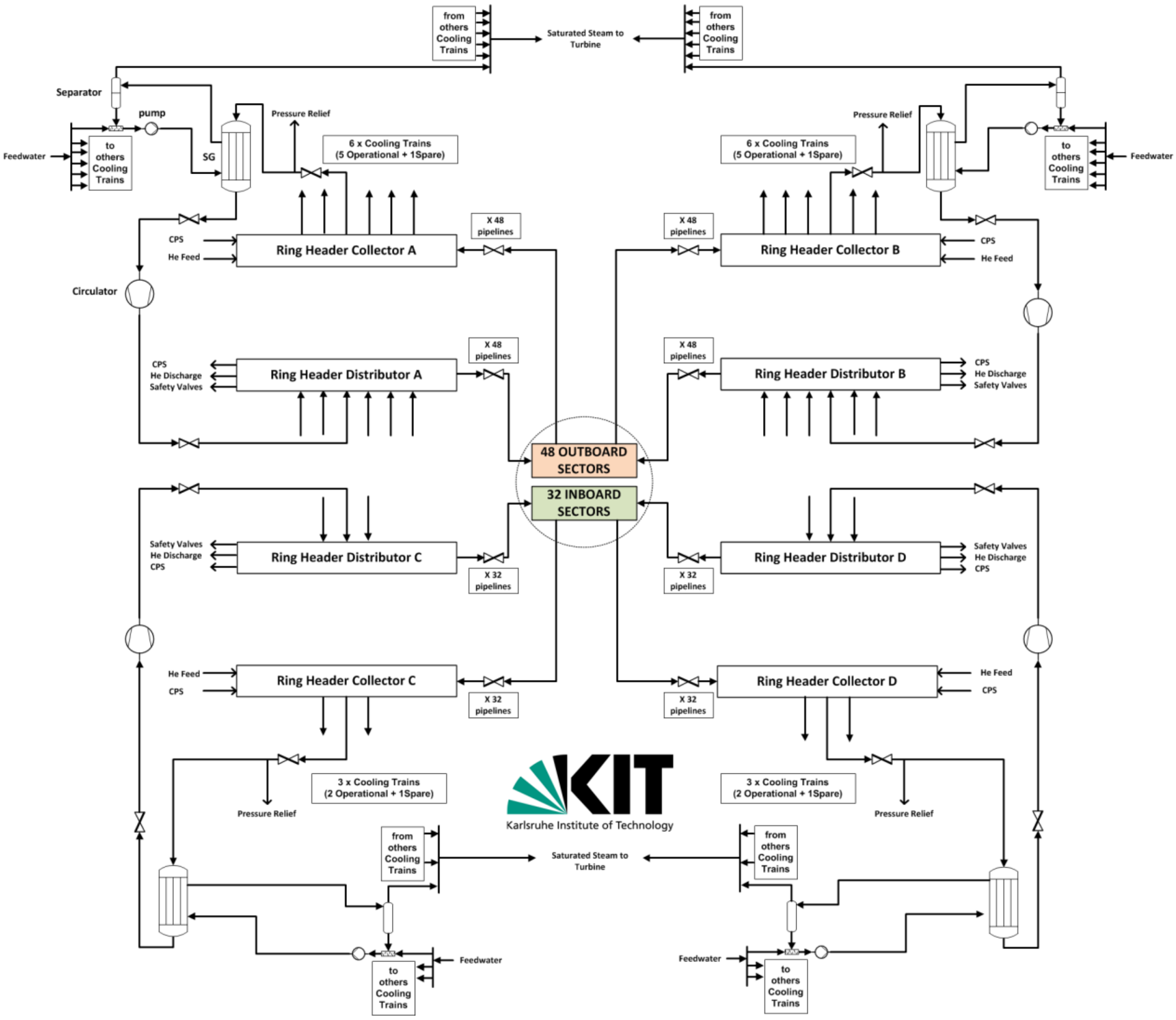

Fig. 2. Scheme of the blanket-PHTS [7]

Table 1. Some data of the blanket-PHTS (information was collected from refs. [10, 19, 20, 12])

		Value
Pressure (MPa)		8
Mass flow rate (kg/s)		2143
Temperature blanket in-/outlet (°C)		300/500
Primary coolant inventory (kg)		22600
Concentration Ci (vppm)	HT	0.023
	HTO	0.0012
HT partial pressure pHT (Pa)		0.185

3. FAILURE RATE ADJUSTMENT FACTORS FOR DEMO HCPB BLANKET PRIMARY HEAT TRANSFER SYSTEM

The basic approach to reliability is to use component operating experiences to calculate component failure rates, and use these failure rates with a model of a new system to predict the reliability of the new system. However, there are instances when the available component operating experiences are collected under environmental conditions and service parameters that are different than those of the new system to be modelled. For example, one might reuse extensive pipeline reliability data collected over many NPPs', but the cooling fluids differ: primary cooling loop of HCPB uses helium instead of water. The concept of adjustment factors, the multiplicative factors applied to a failure rate to adjust it for varying environments and service conditions, has been used in reliability studies for many years (one of the first analysis where this concept was used were passive device failure rate models for mil-hdbk-217b [21]).

There are models providing the needed adjustment factor depending of operating temperature, system dimensions, coolant and flow media, neutron radiation, vibrations, etc.

The Primary Cooling System/PHTS is considered to consist of the Main Coolant Pumps, Steam Generators, Pressurizer, and In-Vessel Coolant Loops. These systems will be affected by the inner and outer reactor environment to varying degrees. The overall adjustment factor for the PHTS of pulsed tokamak was suggested to be 3 [2]. Just In-Vessel Coolant Loops will be considered further.

Blankets system in the HCPB concept exploits Helium as coolant with Inlet/Outlet Temperature of 300/500 °C, a Nominal Pressure of 8 MPa, a Flow Rate of 2143 kg/s and a Pressure Drop of 0.4 MPa. The total length of HCPB main heat transfer system was estimated [11] to be 4200 m. The power to remove has been estimated in 2227 MW, of which 1603 on the outboard side and 624 on the inboard. Therefore, the coolant temperature ranges are comparable to those in fission reactors (except for HTR). The experience in fission reactor may be directly transferable to the pipelines of Coolant Loops and thus no adjustment factor is required (i.e. $k = 1$). This is agreement with the observations of Cadwallader [5] made for ITER reactor.

Due to its pulsating regime, DEMO reactor will cause additional stress to the systems. However, the many start-stop cycles of the heat transport system were expected to have small effects on reliability. As noted in [4], the piping will not suffer these effects to the extent that pump motors and frequently cycling valves will. Therefore no adjustment factor was given to it as well.

Another aspect that needs a separate consideration is that the Helium is considered to the coolant material for HCPB blanket. Thus, the knowledge, about how differently pipelines would be affected by helium as compared to water, is needed. However, there is lack of literature about the effect on failure rate of helium coolant. There is no database for gas components and no compilation of component failure rate data from past helium-cooled fission reactors such as the Peach Bottom and Fort St. Vrain units, nor from the German AVR and Thorium High Temperature Reactor (THTR) plants. On the other hand, helium gas is highly inert and the corrosion will be much less severe than would be if water coolant is used instead. The main cause of corrosion would be impurities of helium – water steam, small particles, etc. It is difficult to give any conclusive adjustment factor in this case, because of large uncertainty about the helium impact on the pipeline walls. Having in mind that it is much more inert than water, the factor probably is less than 1. However, due to the reasons of conservativeness, for the time being we state the adjustment factor equal to 1.

At this point we observe that the overall adjustment factor for the pipelines of Primary Cooling Loop is approximately 1. The uncertainty about the true effects of reactor operating conditions on the reliability of Primary Cooling Loop poses a significant problem. Hence in order to account for this level of uncertainty we will provide guidelines on how to treat this problem in a Bayesian fashion. Bayesian methods will allow us to include the uncertainty about the adjustment factor.

4. BAYESIAN RAMI WITH UNCERTAIN ADJUSTMENT FACTORS

4.1. Bayesian uncertainty treatment for DEMO technology

The Bayesian approach toward inference offers many advantages. Among these, it allows us to pool information obtained from related experiments into the joint estimation of quantities of interest from each, and it allows us to incorporate expert opinion and subject matter expertise into the analysis of an experiment in a coherent way. Perhaps as importantly, it provides a remarkable degree of flexibility in modelling the phenomena that contribute to reliability and lifetime. With the advent of Markov chain Monte Carlo (MCMC) algorithms, fitting complicated statistical models to data and evaluating the uncertainty in fitted values is now almost routine.

In Bayesian reliability analysis, the statistical model consists of two parts: the likelihood function and the prior distribution. The likelihood function is typically constructed from the sampling distribution of the data, defined by the probability density function assumed for the data. In Bayesian analysis, the parameters in the likelihood function are treated as unknown quantities, and we use a probability density function to describe our uncertainty about them.

Bayesian analysis differs from classical frequency-based analysis in several key ways. One major philosophical difference is the notion of probability. Classical methods are rooted in the notion of probability as the limiting relative frequency of an event in a repeated series of identical trials. In contrast, the cornerstone of Bayesian methods is the notion of subjective probability. Bayesian methods consider probability to be a subjective assessment of the state of knowledge (also called degree of belief) about model parameters of interest, given all available evidence.

As a direct consequence of its use of subjective probability, Bayesian methods permit us to incorporate and use information beyond that contained in experimental data. Whether a reliability analyst does or does not have such test data available, he will often have other relevant information about the value of the unknown reliability parameters. Such relevant information is an extremely useful and powerful component in the Bayesian approach, and thoughtful Bayesian parameter estimates reflect this knowledge. This relevant information is often derived from combinations of such sources as physical/chemical theory, engineering and qualification test results, generic industry-wide reliability data, computational analysis, past experience with similar devices, previous test results obtained from a process development program, and the subjective judgment of experienced personnel.

After the test data have been obtained, the posterior distribution fully describes the uncertainty associated with the parameter. We calculate the posterior distribution via Bayes' Theorem using the likelihood function and the prior distribution. The logical sequence of likelihood function, prior distribution, Bayes' Theorem, and posterior distribution makes Bayesian reliability methods easy to describe and the derived estimates easy to interpret and use. For example, a Bayesian interval estimate may be directly interpreted as a probability statement about a parameter. In contrast, a corresponding frequency-based confidence interval has no such direct interpretation.

Because Bayesian posterior distributions are true probability statements about unknown parameters, they may be easily propagated through complex system models, such as fault trees, event trees, and other logic models. Except in the simplest cases, it is difficult or impossible to propagate classical confidence intervals through such models. Features and nuisances of real-world reliability problems, such as complex censoring and random hierarchical effects, can easily be accommodated and modelled by Bayesian methods. Such considerations are often either difficult or impossible to consider when using classical methods [13].

4.2. Updating state of knowledge of DEMO RAMI

As already mentioned, Bayesian approach allow to incorporate various sorts of information, whether it is subjective opinion of expert, or statistical sample observed over some period of time. The nature of Bayesian approach is such that once new data/information becomes available there is no need to incorporate it into previously obtained information and perform inference anew. One can just use previously obtained results as its prior state of knowledge and update it with new information.

Having stated a model for observed reliability data, for elicited subjective insights of experts as well as for information contained in various RAMI data sources, one has to push these parts through the Bayes formula in order to obtain posterior state of knowledge, i.e. RAMI state of fusion devise after all relevant information is taken into account.

Such joint analysis process can be simply visualized as in Fig. 3 (for more information on this please refere to the paper [16]). This process can be extended to the cyclic procedure, where posterior distribution becomes prior distribution after new statistical data or new expert opinion is available. Then such adjustments of current state of knowledge about RAMI can be repeated over and over again.

Although for engineering use of Bayesian formalism simplicity of posterior calculations is preferred, it can be quite difficult to stick to it however. Taking into account all the information available – expert subjective experiences, raw statistical data – requires different levels of complexity and non-trivial sub-models. Hence, knowledge of computational methods like family of Markov Chain Monte Carlo algorithms is of great advantage. Although, this necessity can be partially relieved with freely available software like OpenBUGS or Stan.

5. BAYESIAN RELIABILITY OF HCPB COOLING SYSTEM

The data, extracted from FCFR database (presented in the Table) is failure rates of pipelines of various diameters (generic failure mode). This data will be used to estimate failure probability of HCBP water cooling cycle. Entries with upper and lower bounds give additional information about the probabilistic mechanism that, assumingly, produced respective failure rate. Hence, we could divide the available data into two parts: the one, with complete information about the stochastic nature of the data, and the part where just family of probability distributions is known. The second part could be easily assumed as data coming from parameterized distribution and we just have to estimate parameters of it. We could drop the information about upper and lower bounds in the first part and merge failure rate with the second part. We would loose some amount of information but would not have to bother ourselves any more with the question of how to use that additional information.

Another way could be to see that partial information as some kind of opinion elicited from a set of “virtual experts”. Let’s assume that the failure rate estimates are distributed according to log-normal distribution with unknown parameters $\left(ms^{2} \right)$. And the bounds are given for this distribution. Hence, we will view these quantiles as provided by different (subjective) experts. According to our methodology, we will produce a prior distribution obtained from these quantiles and will use it together with failure rate estimates to obtain a posterior distribution and related estimates.

Table 2. Failure rate and related data

Failure rate [1/(m*h)]	Source	Model	Lower bound	Upper bound
2.78E-10	IAEA-TECDOC-478	Log-Normal	3.00E-12	3.00E-09
2.50E-10	INEEL/EXT-98-00892	Exponential	1.25E-10	5.00E-10
2.50E-11	INEEL/EXT-98-00892	Exponential	8.33E-13	7.50E-10
8.86E-09	AICHE	Log-Normal	4.70E-10	1.00E-07
6.56E-08	RAGUSA	NA	NA	NA
2.78E-10	WASH 1400	Log-Normal	3.00E-12	3.00E-09
2.86E-11	INEL EGG-FSP-8709	Log-Normal	NA	NA
2.86E-10	INEL EGG-FSP-8709	Log-Normal	NA	NA
7.00E-10	INEL EGG-FSP-8709	NA	NA	NA
3.75E-09	INEL EGG-FSP-8709	Log-Normal	NA	NA

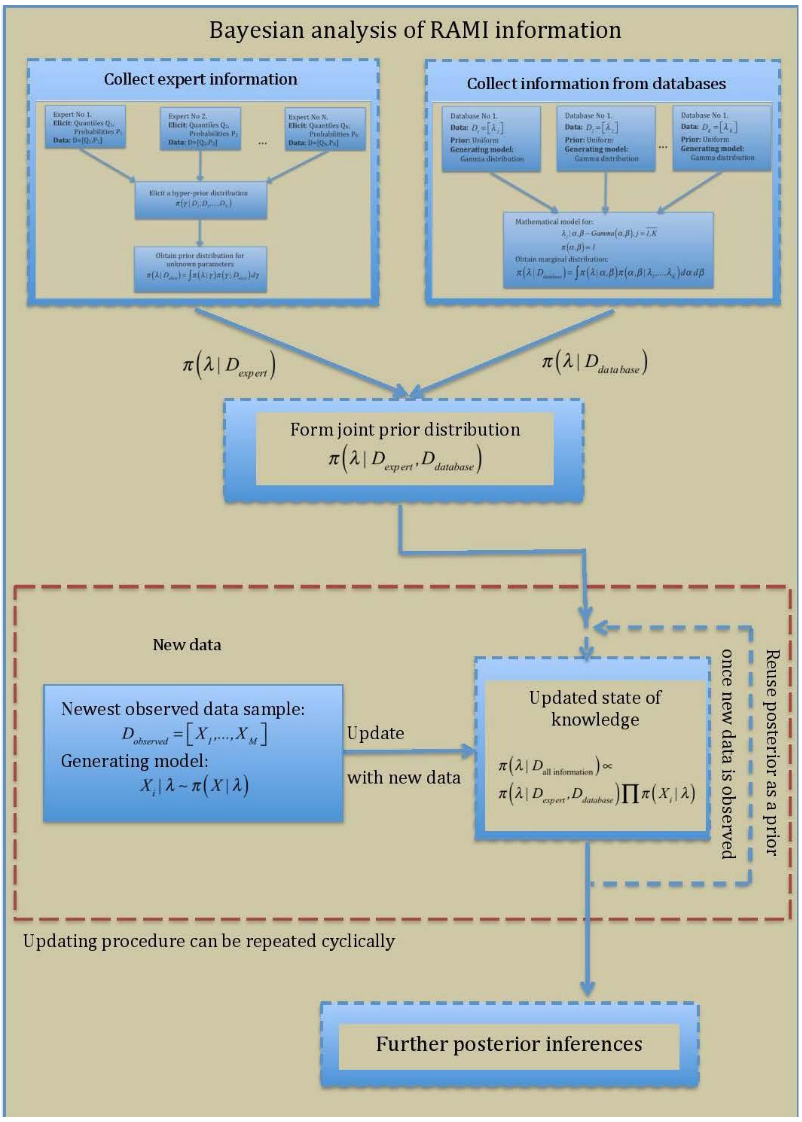

Fig. 3. Scheme of Bayesian analysis of RAMI information procedure [15]

Quantiles can easily be converted to the lognormal distribution parameters:

$$\sigma = \frac{1}{\Phi^{-1}(p_1) - \Phi^{-1}(p_2)} log\left(\frac{F^{-1}(p_1)}{F^{-1}(p_2)}\right),$$

$$\mu = F^{-1}(p_1) - \sigma \cdot \Phi^{-1}(p_1)$$

where $\mathsf{F}^{-1}(p)$ is a p-quintile of standard normal distribution, $p_1 = 0.05$ and $p_2 = 0.95$, $F^{-1}(p)$ p-quintile of lognormal distribution, η and s are parameters for the log-normal distribution.

To make our lives a bit easier, let’s take a natural logarithm of s^2. Hence, the data from which we will form a prior is as in table:

Table 3. Data for prior formation

P(η)	Q($log(s^2)$)
-24.2	1.1306
-22.1	-2.0769
-24.4	1.1078
-19.9	0.6296
-24.2	1.1306

Previous Bayesian analysis of this data sample is provided in [15]. The failure rate posterior distribution, obtained by merging statistical data (failure rate column in Table) and virtual expert opinions (lower and upper bound columns in Table) were found to have the following expression

$$\pi(\mu,\sigma^2 \mid \lambda) \propto \pi(\mu,\sigma^2)\pi(\lambda \mid \mu,\sigma^2)$$

$$\pi(\mu,\sigma^2) \propto \sigma^{-2}\left(\left[(n+1)\left((\mu - C_1)^2 + 2b_1\right) + 2b_1\right] \cdot \left[(n+1)\left((log\,\sigma^2 - C_2)^2 + 2b_2\right) + 2b_2\right]\right)^{-(n+2)}$$

$$\pi(\lambda \mid \mu,\sigma^2) \propto \sigma^{-10} exp\left[-\frac{1}{\sigma^2}\sum(\lambda_i - \mu)^2\right],$$

where C_1, C_2, b_1 and b_2 are constants depending on the prior expert information.

In order to investigate the effect of the adjustment factors, we need to form a prior distribution for it. It was concluded that this factor is around 1, but might be smaller due to less corrosive properties of helium gas. On the other hand it might be higher than 1 due to the cyclic thermal load. It is reasonable to expect that higher than 1 adjustment factor should be adopted as the cyclic loadings, radiative effects and other factors makes the operating environment harsher than that found in fission reactors. Therefore the probability distribution describing the uncertainty of the adjustment factor most likely should be asymmetric putting more weight on the values above k=1. A reasonable choice for this distribution is a log-normal probability distribution with parameters α (location) and β (scale), as it is defined on positive values only and may be forced to adopt an asymmetric form. The mode is assumed to the 1. Hence if the variance of the lognormal distribution is assumed to be zero, we would obtain expectation to be equal to 1. We will investigate the sensitivity to the variance as well, so that we leave this value undefined for now.

Just to remind, our main assumption was that failure rates are data points generated from lognormal distribution:

$$\lambda_i \mid \mu\sigma^2 \sim LN(\mu,\sigma^2).$$

The multiplication of random variable λ_i by an adjustment factor k yields a distribution:

$$k\,\lambda_i \mid \mu\sigma^2 \sim LN\left(\mu + \log k\sigma^2\right).$$

Now, consider that we vary the variance $\frac{1}{\alpha}$ of adjustment factor within the interval [0.2; 6]. The corresponding 0.95 credibility intervals are plotted in Figure.

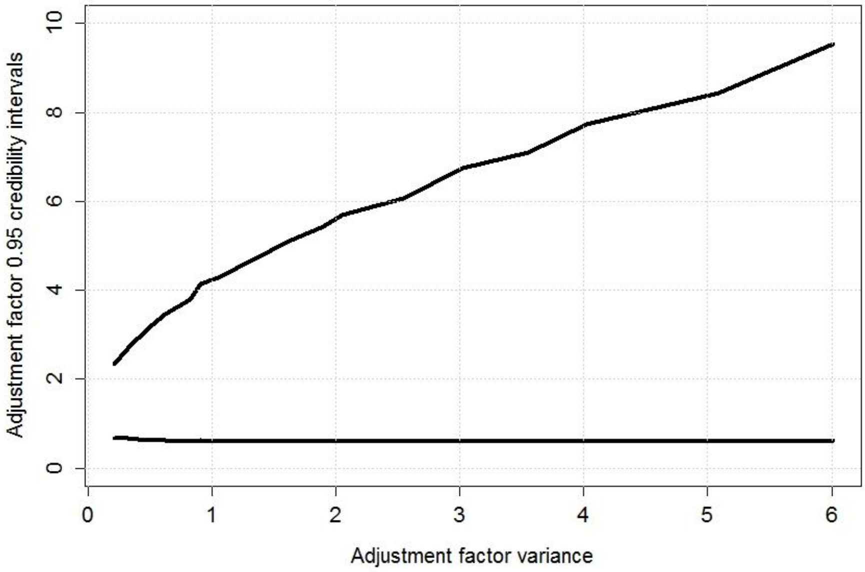

Fig. 4. credibility intervals of size 0.95 for each considered value of the AF variance

Then, probability of failure of PHTS pipelines within a year responds to the changes of AF variances as in the plot.

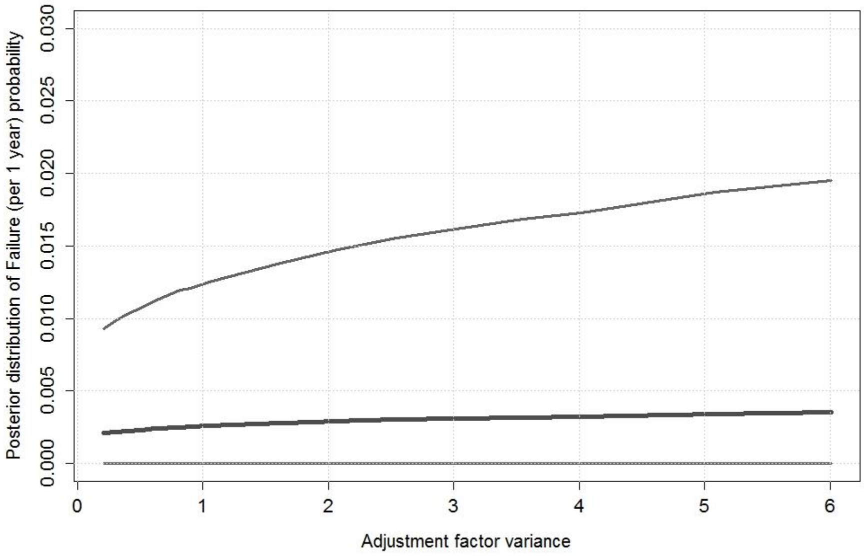

Fig. 5. Failure probability dependence on the AF variance (lighter grey marks 95% credibility intervals, while darker grey is for the expectation of probability estimate)

By increasing the variance of AF, we increase the likelihood of larger than 1 values for the AF. However, from Fig. 5 we observe that the influence on the upper 0.95 bound of the failure probability estimate is not very significant. In extreme cases of high variance it is only two times higher than at the small variance. This implies a conclusion that the effect of adjustment factor to the failure probability may be neglected.

6. CONCLUSIONS

We close this brief analysis with the main conclusion that the posterior failure rates are not significantly sensitive to the variations in the adjustment factor. This basically means that the unreliability data of pipelines obtained (for example) by nuclear power industry is sufficient for the DEMO HCPB main cooling system reliability assessment. The impact of AF of failure rates is not significant.

Of course, we were here concerned with the impact on the magnitude or the order of failure rate. The exact (or as accurate as possible) value at this stage of DEMO design is not relevant and would be impossible to obtain by any means, since currently there is not exact dimensions of the future cooling system.

7. ACKNOWLEDGEMENT

This work has been carried out within the framework of the EUROfusion Consortium and has received funding from the European Union‘s Horizon 2020 research and innovation programme under agreement number 633053. The views and opinions expressed herein do not necessarily reflect those of the European Commission.

REFERENCES

1. BOCCACCINI, L.V., (ed.) European Helium Cooled Pebble Bed (HCPB) Test Blanket, ITER Design Description Document, FZKA 6127, 1999.
2. CADWALLADER, L.C. Investigation of component failure rates for pulsed versus steady state tokamak operation. Idaho, 1992.
3. CADWALLADER, L.C. Preliminary Failure Modes and Effects Analysis of the US DCLL Test Blanket Module. Idaho, 2007.
4. CADWALLADER, L.C. Selected Component Failure Rate Values from Fusion Safety Assessment Tasks. Idaho, 1998.
5. CADWALLADER, L.C. Failure Rate Adjustment Factors for High Technology Components. 25th Symposium on Fusion Engineering, 2013.
6. CARLONI, D., DONGIOVANNI, D., PINNA, T., JIN, X., BOCCACCINI, L.V. Definition of DEMO safety requirements and compilation of preliminary safety design guidelines D2 FFMEA for the DEMO HCPB concept, EFDA WP13-SYS04-T02, EFDA_D_ 2L48QQ V2.0, 2013.
7. CARLONI, D., KECSKE, S. DEMO HCPB 2013, EFDA WP13-DAS02-04, 2013.
8. DALLE, D.M. (Ed.), European DEMO BOT solid breeder blanket, KfK 5429, Forschungszentrum Karlsruhe, 1994.
9. DALLE, D. M., (Comp.). European DEMO BOT Solid Breeder Blanket, KfK 5429, Forschungszentrum Karlsruhe, 1994.
10. DALLE, D.M., GORAIEB, A., PIAZZA, G., SORDON, G. Measurements of the effective thermal conductivity of Li_4SiO_4 Pebble Bed, ISFNT-5, Rome, September 1999.
11. DONGIOVANI, D., PINNA, T., CARLONI, D. RAMI analysis for DEMO: Helium Cooled Pebble Bed cooling system. Report for Task Agreement WP13-DTM-02-T01-ENEA, 2013.

12. FRANZA, F. Tritium transport analysis in HCPB DEMO blanket with the FUS-TPC Code”, KIT-report 7642, 2013.
13. HAMADA, M.S., WILSON, A.G., REESE, C.S., MARTZ, H.F. Bayesian Reliability. Springer, 2008.
14. HERMSMEYER, S. Improved Helium Cooled Pebble Bed Blanket, FZKA 6399, 1999;
15. IESMANTAS, T.; ALZBUTAS, R., Method to evaluate and integrate diverse RAMI input data. Sub-report for TA WP13-DTM02-T02, 2013.
16. IESMANTAS, T., ALZBUTAS, R. Bayesian methodology for fusion plant reliability data analysis // 11th international conference of young scientists on energy issues (CYSENI 2014), Kaunas, Lithuania, May 29–30, 2014. Kaunas: LEI, 2014. ISSN 1822-7554, p. 181–193.
17. IGITKHANOV, Y., BAZYLEV B., LANDMAN, I., FETZER, R. Design Strategy for the PFC in DEMO Reactor, KIT Scientific Reports 7637, 2013.
18. LECHLER, T., FIEK, H.-J., GERDEEV, S., SCHLEISIEK, K. Manufacturing of a Semi-scale Blanket Box Mock-up of the European HCPB Blanket, ISFNT-5, Rome, September 1999.
19. SCAFFIDI-ARGENTINA, F. Beryllium R&D for fusion applications, ISFNT-5, Rome, September 1999.
20. SEDANO, L.A. Tritium Cycle Design for He-cooled Blankets for DEMO, CIEMAT, 2007.
21. US MIL-HDBK 2017. Reliability prediction of electronic equipment, Version A, Dec. 1, 1965.
22. XUE, Z. J., CARLONI, D., BOCCACCINI, L.V. Source terms and critical event sequences for the blanket concept HCPB. Report for Task Agreement WP13-SYS04-T03, 2013.

CYSENI 2015, May 27–28, Kaunas, Lithuania
ISSN 1822-7554, www.cyseni.com

DEFINITION OF THERMAL STATE OF SPENT NUCLEAR FUEL ASSEMBLY AT DRY STORAGE

S. Alyokhina[1, 2]
[1] A. M. Pidgorny Institute for Mechanical Engineering Problems
of the National Academy of Sciences of Ukraine
2/10 Dm. Pozharsky Str., UA-61046 Kharkiv – Ukraine
Phone +380572942794
Email: alyokhina@ipmach.kharkov.ua
[2] V. N. Karazin Kharkiv National University
4 Svobody Sq., UA-61022 Kharkiv – Ukraine

ABSTRACT

The safety of Dry Spent Nuclear Fuel Storage Facility (DSNFSF) consist of three main components – Nuclear safety, Radiation safety and Safe thermal condition. This work is devoted to third part of this complex conception. In particular to the definition of thermal state of spent nuclear fuel assembly. For definition of thermal state of spent fuel assemblies the multi-stage approach was proposed. On each level of multi-stage approach the solving of conjugate heat transfer problems were used.

The maximal temperatures are observed in fuel assemblies which are placed in center of storage basket. The results of investigation allow to detect fuel rods with maximal temperatures and the next stage of calculations should be carried out for these fuel rods for detecting temperature of fuel cladding during all period of storage. The results which were presented in this work will be used for estimation and the improving of safety level of DSNFSF on Zaporizhska NPP. \

Keywords: thermal fields, conjugate heat transfer problems, spent nuclear fuel assembly

1. INTRODUCTION

More than 250 tons of spent nuclear fuel is produced by Ukrainian NPPs each year. The issue of spent nuclear fuel (SNF) storage according to Energy Strategy of Ukraine till 2030 is temporary solved by storage until acceptable decision about disposal or reprocessing will be reached. This approach today is used for six WWER-1000 reactors of Zaporizhska NPP [1].

The Dry Spent Nuclear Fuel Storage Facility (DSNFSF) on Zaporizhska NPP has been operating for more than 10 years [2]. The long and the safe operation of DSNFSF can be ensured only with full scientific support, which should give clear understanding of processes and mechanisms of equipment work at the different stages of operation.

The safety of Dry Spent Nuclear Fuel Storage Facility consists of three main components – Nuclear safety, Radiation safety and Safe thermal condition. This work is devoted to third part of this complex conception. In particular, to the definition of thermal state of spent nuclear fuel assembly.

The problem of thermal state of containers with spent nuclear fuel is solved by many researchers but all of these works have some limitations. Mostly authors consider problems with simplified geometry structure and use equivalent thermal properties for storage basket or for spent fuel assemblies [3, 4] but this way of investigations does not allow to obtain the detailed information about thermal processes inside storage containers. Another problem of existing publications is the consideration of the problem in engineering definition [5] which means simulation part of object only for specific operation conditions. This way of investigations does not allow to make large series of numerical experiments due to limitations of computational time or necessity to redefine problem for each new situation.

The goal of this work is to develop numerical approach by solving the direct conjugate heat transfer problem for definition detailed thermal state of spent nuclear fuel assemblies of reactors WWER-1000 which are placed inside of the hermetic basket for dry storage.

2. PROBLEM DEFINITION

The spent nuclear fuel assemblies after storage in water pool are loaded in tight storage basket. The basket is placed inside concrete container and this system is then moved to storage platform. The basket with spent nuclear fuel is cooled by natural convection (Fig. 1). The atmospheric air which comes through the ventilating system is cooling and removes decay heat from spent nuclear fuel.

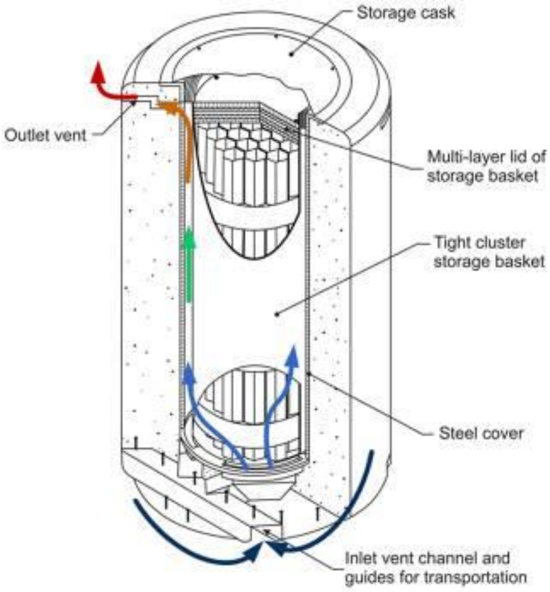

Fig. 1. Storage container cooling

Storage containers have the passive cooling system, so cooling only by atmospheric air takes place. The thermal safety criteria for the temperature of spent nuclear fuel cladding inside storage basket is 350 °C maximum. The ventilating air on an exit from channels should not be heated more than on 61 degrees (the safety criteria for considered type of containers [6]). The temperature measurements are carried out only on exit of ventilation channels.

The storage facility is designed for 50 years operation. The most dangerous time is at the beginning of storage because the spent fuel assemblies have the maximum decay heat and accidents with exceeding of critical temperature are more probable. So the next calculations were carried out for this period and decay heat of each fuel assembly was 909 W.

3. METHODOLOGY

For definition of thermal state of spent fuel assemblies the multi-stage approach was proposed. On each level of multi-stage approach the solving of conjugate heat transfer problems were used [7].

At usage of multi-stage approach on each next stage the part of investigated object is considered. The geometrical model of this part has more detailed structure in comparison with previous stage of current investigations. The boundary conditions on each next stage for part of object is defining on base of calculation results of previous stage.

The multi-stage approach for current problem consists of the following. At the first stage the thermal state of storage container is defined and the storage basket with spent fuel assemblies was considered as being solid body with equivalent thermal properties. At next stage the heat transfer conditions on surface of basket were obtained and this information was used for next (third) stage where thermal state of storage basket was calculated. At third stage of investigation the detailed structure of storage basket was considered and the received numerical information was used for definition of boundary conditions on surfaces of guiding tubes. At the last (forth) stage these boundary conditions are used for calculation thermal state of spent fuel assemblies.

The definition of thermal fields of solid body and fields of pressure, velocity and temperature of the cooling or the heating medium by solving of the differential equations at known single-valuedness conditions is object of the direct conjugate heat transfer problem. This type of problems is lying in base of multi-stage approach at detailed definition of thermal state of containers with spent nuclear fuel.

The system of differential equations which describe the conjugate heat transfer problem consists of the following equations [8, 9, 10]:

– continuity equation

$$\frac{\partial}{\partial x}(\rho u)+\frac{\partial}{\partial y}(\rho v)+\frac{\partial}{\partial z}(\rho w)=0\,,$$

where u, v, w – the Cartesian components of velocity vector;

– equation of motion of viscous gas

$$\rho u\frac{\partial u}{\partial x}+\rho v\frac{\partial u}{\partial x}+\rho w\frac{\partial u}{\partial x}=-\frac{\partial p}{\partial x}+2\frac{\partial}{\partial x}\left(\mu_{\text{ef}}\frac{\partial u}{\partial x}\right)+$$

$$+\frac{\partial}{\partial y}\left(\mu_{\text{ef}}\left(\frac{\partial u}{\partial y}+\frac{\partial v}{\partial x}\right)\right)+\frac{\partial}{\partial z}\left(\mu_{\text{ef}}\left(\frac{\partial w}{\partial x}+\frac{\partial u}{\partial z}\right)\right)-\frac{2}{3}\frac{\partial}{\partial x}\left(\mu_{\text{ef}}\left(\frac{\partial u}{\partial x}+\frac{\partial v}{\partial y}+\frac{\partial w}{\partial z}\right)\right),$$

$$\rho u\frac{\partial v}{\partial x}+\rho v\frac{\partial v}{\partial x}+\rho w\frac{\partial v}{\partial x}=-\frac{\partial p}{\partial y}+2\frac{\partial}{\partial y}\left(\mu_{\text{ef}}\frac{\partial v}{\partial y}\right)+$$

$$+\frac{\partial}{\partial x}\left(\mu_{\text{ef}}\left(\frac{\partial u}{\partial y}+\frac{\partial v}{\partial x}\right)\right)+\frac{\partial}{\partial z}\left(\mu_{\text{ef}}\left(\frac{\partial w}{\partial y}+\frac{\partial v}{\partial z}\right)\right)-\frac{2}{3}\frac{\partial}{\partial y}\left(\mu_{\text{ef}}\left(\frac{\partial u}{\partial x}+\frac{\partial v}{\partial y}+\frac{\partial w}{\partial z}\right)\right),$$

$$\rho u\frac{\partial w}{\partial x}+\rho v\frac{\partial w}{\partial x}+\rho w\frac{\partial w}{\partial x}=-\rho g-\frac{\partial p}{\partial z}+2\frac{\partial}{\partial z}\left(\mu_{\text{ef}}\frac{\partial w}{\partial z}\right)+$$

$$\frac{\partial}{\partial x}\left(\mu_{\text{ef}}\left(\frac{\partial w}{\partial x}+\frac{\partial u}{\partial z}\right)\right)+\frac{\partial}{\partial y}\left(\mu_{\text{ef}}\left(\frac{\partial v}{\partial z}+\frac{\partial w}{\partial y}\right)\right)-\frac{2}{3}\frac{\partial}{\partial z}\left(\mu_{\text{ef}}\left(\frac{\partial u}{\partial x}+\frac{\partial v}{\partial y}+\frac{\partial w}{\partial z}\right)\right),$$

where ρ – density; p – pressure; μ_{ef} – effective (with turbulent component μ_{t}) dynamic viscosity;

– energy equation for fluids

$$c_p\rho\left(u\frac{\partial T}{\partial x}+v\frac{\partial T}{\partial x}+w\frac{\partial T}{\partial x}\right)-\left(u\frac{\partial p}{\partial x}+v\frac{\partial p}{\partial x}+w\frac{\partial p}{\partial x}\right)=\frac{\partial}{\partial x}\left(\lambda_{\text{ef}}\frac{\partial T}{\partial x}\right)+\frac{\partial}{\partial y}\left(\lambda_{\text{ef}}\frac{\partial T}{\partial y}\right)+\frac{\partial}{\partial z}\left(\lambda_{\text{ef}}\frac{\partial T}{\partial z}\right),$$

where T – temperature, c_p – specific thermal capacity at constant pressure, λ_{ef} – effective (with turbulent component λ_{t}) thermal conductivity of gas environments;

– energy equation for solids

$$\frac{\partial}{\partial x}\left(\lambda\frac{\partial T}{\partial x}\right)+\frac{\partial}{\partial y}\left(\lambda\frac{\partial T}{\partial y}\right)+\frac{\partial}{\partial z}\left(\lambda\frac{\partial T}{\partial z}\right)+q_V=0,$$

where λ – thermal conductivity of solid bodies, q_V – the power of inner heat source;

– equations of turbulence model (k-ε model was chosen according to [11]) [12]:

$$\frac{\partial(\rho ku)}{\partial x}+\frac{\partial(\rho ku)}{\partial y}+\frac{\partial(\rho ku)}{\partial z}=$$

$$\frac{\partial}{\partial x}\left(\left(\mu+\frac{\mu_t}{\sigma_k}\right)\frac{\partial k}{\partial x}\right)+\frac{\partial}{\partial y}\left(\left(\mu+\frac{\mu_t}{\sigma_k}\right)\frac{\partial k}{\partial y}\right)+\frac{\partial}{\partial z}\left(\left(\mu+\frac{\mu_t}{\sigma_k}\right)\frac{\partial k}{\partial z}\right)+G_k+G_b-\rho\varepsilon,$$

$$\frac{\partial(\rho\varepsilon u)}{\partial x}+\frac{\partial(\rho\varepsilon u)}{\partial y}+\frac{\partial(\rho\varepsilon u)}{\partial z}=$$

$$\frac{\partial}{\partial x}\left(\left(\mu+\frac{\mu_t}{\sigma_\varepsilon}\right)\frac{\partial\varepsilon}{\partial x}\right)+\frac{\partial}{\partial y}\left(\left(\mu+\frac{\mu_t}{\sigma_\varepsilon}\right)\frac{\partial\varepsilon}{\partial y}\right)+\frac{\partial}{\partial z}\left(\left(\mu+\frac{\mu_t}{\sigma_\varepsilon}\right)\frac{\partial\varepsilon}{\partial z}\right)+C_{1\varepsilon}\frac{\varepsilon}{k}\left(G_k+C_{3\varepsilon}G_b\right)-C_{3\varepsilon}\rho\frac{\varepsilon^2}{k},$$

where k – turbulent kinetic energy, ε – velocity of dissipation of turbulent kinetic energy, G_k – the term of equation which describes the generation of turbulent kinetic energy which caused by velocity gradient (according to Boussinesq hypothesis $G_k = \mu_t S^2$); G_b – the term of equation which describes the generation of turbulent kinetic energy which caused by buoyancy force (for ideal gas: $G_b=-\frac{\mu_t}{\rho\,\mathrm{Pr}_t}\left(g_x\frac{\partial p}{\partial x}+g_y\frac{\partial p}{\partial y}+g_z\frac{\partial p}{\partial z}\right)$); $C_{1\varepsilon}$, $C_{2\varepsilon}$, $C_{3\varepsilon}$ – the constants which equal respectively 1.44, 1.92, 0.09; $\sigma_k = 1.0$ – the turbulent Prandtl number for k; $\sigma_\varepsilon = 1.3$ – the turbulent Prandtl number for ε.

The turbulent component of dynamic viscosity determined by expression

$$\mu_\mathrm{t}=0.09\rho\frac{k^2}{\varepsilon},$$

and turbulent component of thermal conductivity of moving medium

$$\lambda_\mathrm{t}=\frac{c_p\mu_\mathrm{t}}{\mathrm{Pr}_\mathrm{t}},$$

where $\mathrm{Pr}_\mathrm{t} = 0.85$ – the turbulent Prandtl number.

As the equation of state the Mendeleev-Clapeyron equation is used [13]

$$\rho=\frac{p}{RT},$$

where R – gas constant.

During the spent nuclear fuel storage the radiative heat transfer play an important part so, the heat flux from one body to another described as

$$Q_{12}=\sigma_0\varepsilon_\mathrm{r}\left(T_1^4-T_2^4\right)F_{12},$$

where $\sigma_0 = 5.672\cdot10^{-8}$ Wt/(m^2·K^4) – the Stefan-Boltzmann constant; ε_r – the reduced emissivity coefficient; T_1 – the surface temperature of hotter body; T_2 – the surface temperature of colder body; F_{12} – the area of mutual surface of irradiation which can be defined from expression

$$F_{12} = \int_{F_1} dF_1 \int_{F_2} \frac{\cos\theta_1 \cos\theta_2}{\pi R_{12}^2} dF_2 \ ,$$

where F_1, F_2 – the areas which take part in heat exchange of surfaces; θ_1 and θ_2 – the angles between line which connects the centers of elemental areas dF_1 and dF_2 and the respective normals to these areas; R_{12} – the distance between these elemental areas.

The reduced emissivity coefficient can be defined as

$$\varepsilon_r = [1 + (1/\varepsilon_1 - 1)\varphi_{12} + (1/\varepsilon_2 - 1)\varphi_{21}]^{-1},$$

where ε_1 and ε_2 – emissivity coefficient of surface 1 and surface 2 respectively; $\varphi_{12} = F_{12}/F_1$ and $\varphi_{21} = F_{12}/F_2$ – the irradiation coefficients or angular coefficients of radiation which show what part of radiation from one body gets on another.

For the solving of described equations the commercial (ANSYS Fluent, STAR-CD, PHOENICS etc.) and non-commercial (OpenFOAM etc.) program complexes could be used.

4. RESULTS

The verification of developed methodology could be carried out by comparison of measured and calculated data. Unfortunately only temperatures in outlet channels can be used for it. The Fig. 2 shows the result of verification for single container in calm condition. For the day of operation (13.02.2006) the calculated and measured temperatures differ on 0.1 degree. After two months of container operation (03.04.2006) this value became 2.9 degree which can be explained by decreasing of decay heat. In both cases the calculated results give good accuracy. So the developed methodology can be used for the next calculations.

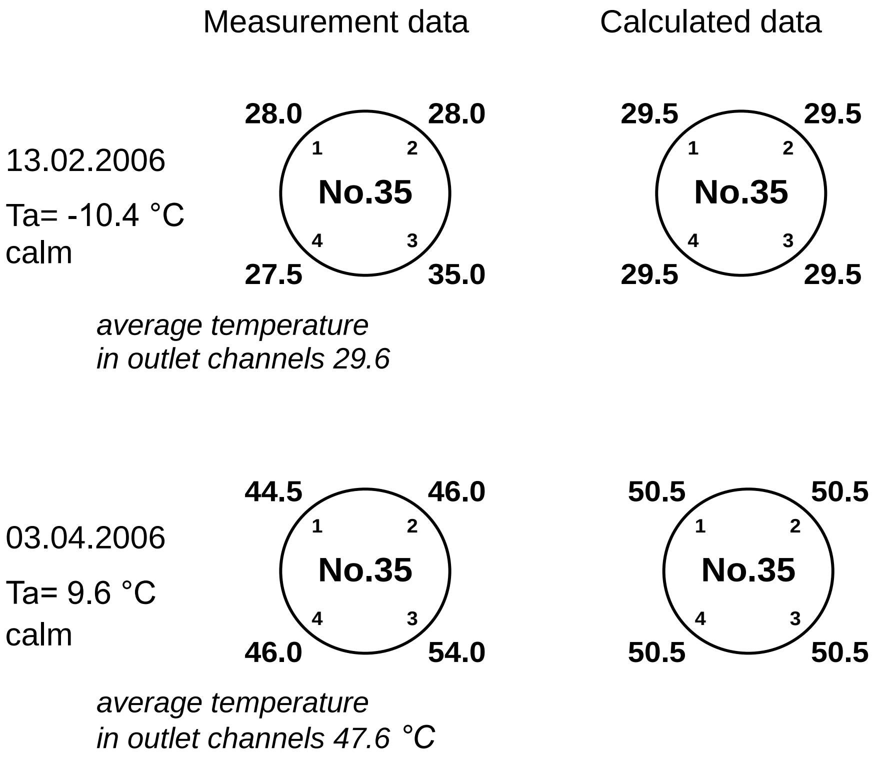

Fig. 2. Calculated and measured temperatures for single container at calm conditions

For each of fuel assembly inside storage basket the conjugate problem was solved. the thermal state of fuel assemblies at 40 ºC of ambient air temperature was considered. The nuclear fuel rods were considered as solid bodies with equivalent heat conductivity coefficient [14]. The temperature field of fuel rods, guiding tubes and helium which filled space between fuel rods and tubes are shown on Fig. 3.

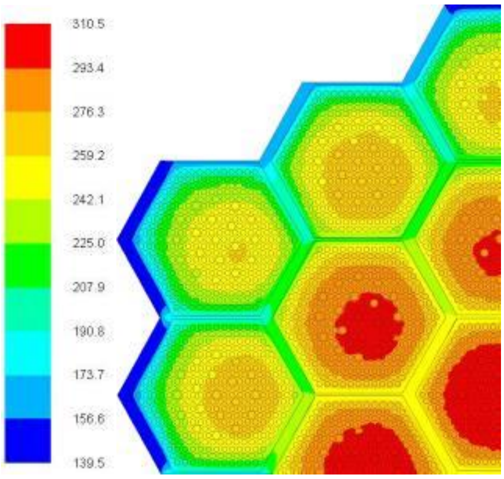

Fig. 3. Temperature field in horizontal cross section of storage basket on the maximal temperature level at 40 ºC of ambient air temperature

The places of the hottest fuel assemblies are shown on Fig. 4 (dark points). As opposed to results which presented by other authors [3, 4, 5 etc.] the described approach allowed to detect exact places of the maximum temperatures inside storage basket and the hottest fuel rods are placed not in center of fuel assemblies. The loading of storage basket should be carried out on base of information about places with the hottest fuel rods. The real fuel assemblies have the non-uniform decay heat and the hottest assemblies parts should be placed out of calculated dangerous places.

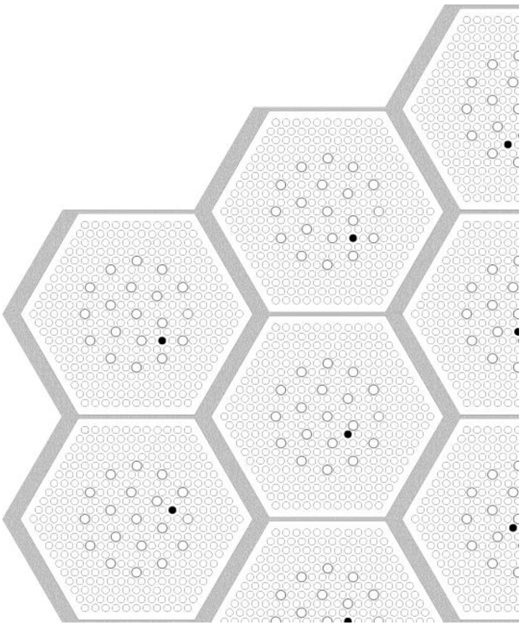

Fig. 4. The places of the hottest fuel assemblies

The developed approach was tested on containers which used on Zaporizhska NPP. The presented results were obtained for calm conditions of operation at high ambient temperatures but described numerical approach could be easy used for any operational conditions.

5. CONCLUSIONS

The developed numerical approach is allowed to detect the places of the hottest fuel rods of fuel assemblies which are placed in center of storage basket. It gives more detailed information about temperature fields inside container. The next stage of calculations should be carried out for the hottest fuel rods with purpose of the detecting temperature of fuel cladding during all period of storage. The described methodology and results which were presented in this work could be used for estimation and the improving of safety level of DSNFSF on Zaporizhska NPP in particular for modernization of container ventilation system, for control and improving operation conditions, for developing new temperature measurement system etc.

REFERENCES

1. *“Energy strategy of Ukraine till 2030”* authorized by the order of Ukrainian Cabinet of Ministers No. 145, p. 15 March 2006.
2. RUDYCHEV, V.G., ALYOKHINA, S.V., GOLOSCHAPOV, V.N. and other Spent Nuclear Fuel Dry Storage Safety, V.N. Karazin Kharkiv National University, 2013–200 p. ISBN 978-966-623-945-0.
3. GREINER, M., GANGADHARAN, K.K., GUDIPATI, M. Use of fuel assembly/backfill gas effective thermal conductivity models to predict basket and fuel cladding temperatures within a rail package during normal transport. *Proceedings of 2006 ASME Pressure Vessels and Piping Division Conference.* July 23–27 2006: 1–10.
4. LI, J., MURAKAMI, H., LIU, Y., GOMEZ, P.E.A., GUDIPATI, M., GREINER, M. Peak cladding temperature in a spent fuel storage or transportation cask. *Proceedings of the 15th International Symposium on the Packaging and Transportation of Radioactive Materials PATRAM 2007.* October 21-26 2007, p. 1–11.
5. DAS, K., BASU, D., SOLIS, J., ZIGH, G. Computational fluid dynamics modeling approach to evaluate vsc–17 dry storage cask thermal designs. *Proceedings of the CFD for Nuclear Reactor Safety Applications (CFD4NRS-3) Workshop*. 14-16 September 2010, p. 1–12
6. *Safety Analysis Report of Dry Spent Nuclear Fuel Storage Facility on Zaporizhska NPP*, Zaporizhska NPP, 2008, Ref. No. 1526(3) – 624 p.
7. ALYOKHINA, S.V., GOLOSHCHAPOV, V.N., KOSTIKOV, A.O., MATSEVITY, Yu.M. The solving of conjugate heat transfer problem at investigation of thermal state of ventilated concrete container with spent nuclear fuel. *Mechanical engineering problems*, Kharkov, 2005, Vol. 8, No.4, p. 12–20.
8. PERELMAN, T.L. On conjugated problems of heat transfer, *Int. J. Heat Mass Transfer*, No. 3, 1961, p. 293–303.
9. LUIKOV, A.V., PERELMAN, T.L., LEVITIN, R.S., GDALEVICH, L.B. Heat transfer from a plate in a compressible gas flow, *Int. J. Heat Mass Transfer*, No. 13, 1971, p.1261–1270.
10. PATANKAR, S.V. 1980, Numerical Heat Transfer and Fluid Flow. Taylor & Francis.

11. WATARU, M., TAKEDA, H., SHIRAI, K., SAEGUSA, T. Thermal hydraulic analysis compared with tests of full-scale concrete casks. Nuclear Engineering and Design (2008), No. 238, p. 1213–1219.
12. WILCOX, D.C. Turbulence modeling for CFD, California: DCW Industries Inc., 1994. – 537 p.
13. MORAN, M.J., SHAPIRO, H.N., Fundamentals of Engineering Thermodynamics, Wiley, 4th Ed, 2000 – 920 p.
14. CHIRKIN, V.S., Thermal physical properties of nuclear engineering materials, M.: Atomizdat, 1967. – 474 p.

CYSENI 2015, May 27–28, Kaunas, Lithuania
ISSN 1822-7554, www.cyseni.com

BURN-UP CREDIT APPROACH FOR CRITICALITY ASSESSMENT OF NEW RBMK-1500 SPENT NUCLEAR FUEL STORAGE CASK

V. Barkauskas
Centre for Physical Sciences and Technology
Savanorių ave. 231, Vilnius, 02300 – Lithuania
Phone +37061001442
Email: vytenis.barkauskas@gmail.com

ABSTRACT

Criticality calculations of spent nuclear fuel in CONSTOR® RBMK-1500/M2 cask, foreseen to be used in a new interim spent nuclear fuel storage facility near Ignalina NPP, were performed using pre-generated ORIGEN-ARP spent nuclear fuel composition libraries and results of RBMK-1500 burn-up credit impact on effective neutron multiplication factor (k_{eff}) and its uncertainties were obtained and are presented in the paper. SCALE 6.1 code package with STARBUCKS burn-up credit evaluation tool was used for modelling. ARP (Automatic Rapid Processing) cross-section libraries based on ENDF/B-VII cross section library were used for fast burn-up inventory modelling for criticality safety calculations. CONSTOR® RBMK-1500/M2 SNF cask consists of a cylindrical basket 32 M containing 102 fuel bundles, a surrounding ring basket containing 80 fuel bundles and other structural and shielding elements. Detailed geometrical model of CONSTOR® RBMK-1500/M2 SNF cask for Monte Carlo simulations of neutron transport was created. Different conditions in SNF cask were modelled: 2.0–2.8% initial enrichment fuel of various burn-up and water density inside cavities of SNF cask. Fuel composition was chosen taking into account main actinides used in burn-up credit calculations. Results show decrement of k_{eff} due to change of fuel composition during burn-up. Water density inside SNF cask is significant factor affecting k_{eff} value.

Keywords: CONSTOR RBMK-1500/M2, nuclear fuel, burn-up credit, criticality safety

1. INTRODUCTION

Two RBMK-1500 reactors of Ignalina nuclear power plant (NPP) are permanently shutdown. One of the most important remaining issues regarding nuclear safety is spent nuclear fuel (SNF) storage. There are about 22000 assemblies of SNF which have to be safely stored until final decision regarding SNF management – reprocessing or disposal – is made. Part of SNF assemblies is stored at existing interim dry type SNF storage facility containing 20 CASTOR® RBMK-1500 and 100 CONSTOR® RBMK-1500 storage casks containing 2% ^{235}U initial enrichment uranium SNF bundles.

A new dry type storage facility for remaining RBMK-1500 SNF is under construction in the vicinity of Ignalina NPP. Up to 200 of new design CONSTOR® RBMK-1500/M2 type casks for storage and transportation are planned to be stored there. One of the key elements of design of these facilities is SNF characterization regarding composition and related activity and neutron emission. These characteristics allows to evaluate if the proposed design of storage cask is sufficiently safe, which means that main objectives of sufficient sub-criticality, proper heat removal, containment of radioactive materials and control of external radiation levels are achieved.

Safety analysis and design justification was performed on new interim dry type SNF storage facility [1, 2]. It claims that SNF storage facility and its components are sufficiently safe. According to Lithuanian national regulations effective multiplication factor (k_{eff}) shall not exceed 0.95 during normal operation and postulated accident scenarios. However only conservative – fresh fuel – assumption regarding SNF composition were used in this analysis.

Lithuanian regulations regarding SNF storage allows possibility of burn-up credit (BUC) implementation in safety justifications of SNF storage facilities [3]. BUC approach calculations may be shortly described as taking into account reduced SNF configuration reactivity due to depletion of fissile isotopes and the creation of neutron-absorbing isotopes when the fuel is irradiated in the reactor [4]. BUC application primarily is related with positive economical effect, e.g. possible increment of number of SNF assemblies kept in wet storage facility or increment of number of SNF bundles allowed to store in the same SNF storage cask. BUC application is encouraged by International Atomic Energy Agency (IAEA) and industry [5, 6].

Availability of accurate and validated versus experiments calculation results is essential for possible use of burn-up credit in SNF storage facilities analysis. SNF composition determination using direct or indirect experimental techniques is rather expensive and complicated. Therefore computer simulations are often used to obtain information needed. New computational codes, improved computational speed and improved capabilities (e.g. 3D modelling geometry) for burn-up analysis allows to evaluate fuel depletion more precisely and to extend the understanding of fuel burn-up in the reactor.

MCNP and ORIGEN codes were used for depletion calculations for RBMK-1000 fuel and comparison with experimental data was performed and presented in 2005 [7]. RBMK-1500 type reactor SNF depletion calculations and SNF storage cask criticality calculations were performed and presented in 2001 and 2004[8, 9]. Burn-up credit application in criticality analysis in CASTOR® RBMK-1500 and CONSTOR® RBMK-1500 was presented in 2002 [5].

One of the possible ways of taking burn-up credit into account is the use of actinide-only burn-up credit. This approach is less conservative than fresh fuel assumption but more conservative compared to burn-up credit calculations taking into account fission products. Actinide-only approach reduces unnecessary conservatism and also gives acceptable safety margin in criticality calculations. Actinides used for actinide-only calculations may be different in different countries, but most of them are the same [10].

Criticality calculations of spent nuclear fuel in CONSTOR® RBMK-1500/M2 cask were performed using pre-generated one-group ORIGEN-ARP spent nuclear fuel composition libraries and obtained results of actinide-only burn-up credit impact on k_{eff}.

2. MODELLING TOOLS AND PROCEDURE

2.1. SCALE 6.1 modules

SCALE 6.1 code package was used for calculations [11]. STARBUCS analysis sequence for automating criticality safety calculations of spent fuel systems employing burn-up credit was used. It automatically performs all necessary calculations to determine spent fuel compositions, self-shielded cross sections, and the k_{eff} of the spent fuel configuration [12].

A depletion calculation for each of the burn-up-dependent regions of a spent fuel bundle is performed using the ORIGEN-ARP sequence. The region dependent nuclide concentrations and cross-sections are applied in a three-dimensional criticality safety calculation using the KENO IV code. ENDF/B-VII 238 energy group data library was used for calculations. ARP reads previously prepared one group RBMK fuel depletion libraries and interpolates a problem-dependent library for ORIGEN-S using defined parameters. This procedure simplifies and accelerates calculations. Library for RBMK-1000 fuel depletion modelling is also available with SCALE6.1 package, however there are no libraries for erbium fuel used in

RBMK-1500 type reactors therefore we generated our own. Comparison of concentrations of actinides obtained from these libraries show acceptable agreement with experimental values.

KENO-VI, a functional module in the SCALE system, is a Monte Carlo criticality program used to calculate the k_{eff} of three-dimensional (3-D) systems. Energy of average lethargy causing fission (EALF) is additional parameter besides k_{eff} which is calculated by KENO IV. EALF is defined as the energy of the average fission group. EALF is measure of “similarity” between physics of critical systems.

2.2. Simplified geometrical model of CONSTOR® RBMK-1500/M2 cask

CONSTOR® RBMK-1500/M2 SNF cask consists of a cylindrical basket 32M containing 102 fuel bundles, a surrounding ring basket containing 80 fuel bundles and other structural and shielding elements [1, 13]. Detailed geometrical model of CONSTOR® RBMK-1500/M2 SNF cask for Monte Carlo simulations of neutron transport was created in KENO-VI.

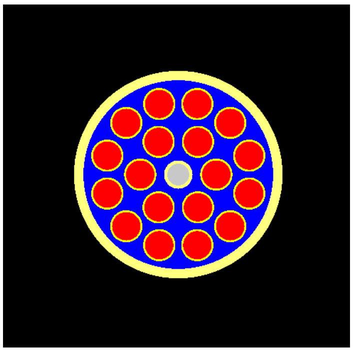

Fig. 1. Configuration of fuel rods of RBMK-1500 fuel bundle

RBMK-1500 fuel bundle consists of 18 fuel rods arranged in two concentrical rings with central carrier rod at the centre (see Fig. 1) [14]. Fuel rod is treated as zirconium alloy tube homogeneously filled with uranium dioxide with or without burnable erbium absorber. Fuel pellet density was reduced to ensure that amount of fuel material inside the tube corresponds to design value. Central carrier rod was defined as hollow tube made from zirconium alloy. Triangular pitch with half-pitch h=0.802 cm was chosen for lattice cell parameters to assist self-shielding calculations [15].

CONSTOR® RBMK-1500/M2 SNF cask inner 32M basket contains 102 fuel bundles (see Fig. 2). It is a stainless steel basket with a hollow 194 mm diameter central tube, 102 position tubes, a cylindrical shell and a closed bottom. The position tubes in 32M are arranged in triangular pitch of 125 mm and have an outer diameter of 102 mm with 2 mm thick wall. Fuel bundle is assumed to be centred in its position tube. Ring basket is modelled as 454 mm thick ring of 1482 mm inner diameter made of aluminium alloy with 80 cylindrical holes with 2 mm thick stainless steel position tubes. All remaining cavities inside cask were assumed to be filled with water.

The sidewall of cask consists of two steel with 40 mm wall thickness cylinders of different size. The 340 mm thick annulus space between them is filled with heavy concrete CONSTORIT. The bottom of the cask is CONSTORIT filled cylinder between two steel plates. The top of the cask body consists of a metallic head cylinder which is modelled as a 355 mm thick steel plate. Dimensions of the cask are: diameter – 2630 mm and height – 4850 m, and mass of the loaded cask is up to 116 tons.

Several SNF loading schemes for the cask are foreseen in the cask design. However only scenarios with completely filled cask with one specified enrichment fuel were modelled.

Fresh and different burn-up fuel with 2 % ^{235}U enrichment and with 2.4%, 2.6% and 2.8% enrichment with erbium burnable absorber was modelled. Also water density in the cavities of the cask was changed.

Actinide-only approach was used for fuel composition – only most important actinides were included in k_{eff} calculations: ^{234}U, ^{235}U, ^{236}U, ^{238}U, ^{238}Pu, ^{239}Pu, ^{240}Pu, ^{241}Pu, ^{242}Pu, ^{237}Np, ^{241}Am, ^{242m}Am, ^{243}Am [10]. All k_{eff} values except those for evolution were calculated 5 years after fuel bundles removal from reactor. Random errors associated with Monte Carlo method are evaluated and does not exceed 0.0011.

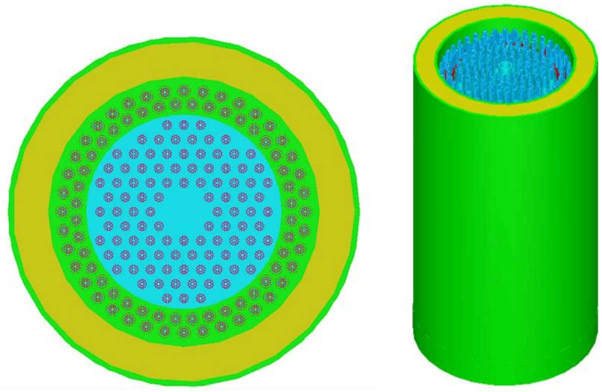

Fig. 2. CONSTOR® RBMK-1500/M2 SNF cask geometrical model with design configuration of fuel bundle positions

3. RESULTS AND DISCUSSION

3.1. k_{eff} of different enrichment fuel

k_{eff} calculation results for fuel enrichment 2.0–2.8% are given in Figs. 3 and 4. Fig. 3a shows k_{eff} dependency on water density inside SNF cask cavities for 0.45 GWh/tU burn-up fuel. Maximum values are achieved at water density values from 0.35 to 0.4 g/cm^3, with maximum k_{eff} = 0.940 for 2.8% fuel enrichment. This trend may be explained using SNF cask neutron spectra analysis (Fig. 3b) – as water density increases we have increasing neutron slowing down. However at certain point absorption by other than fissile isotopes also begin to significantly increase. This causes reduction of k_{eff}. Calculated trends show that drying SNF causes most risky condition as well as untightness during storage.

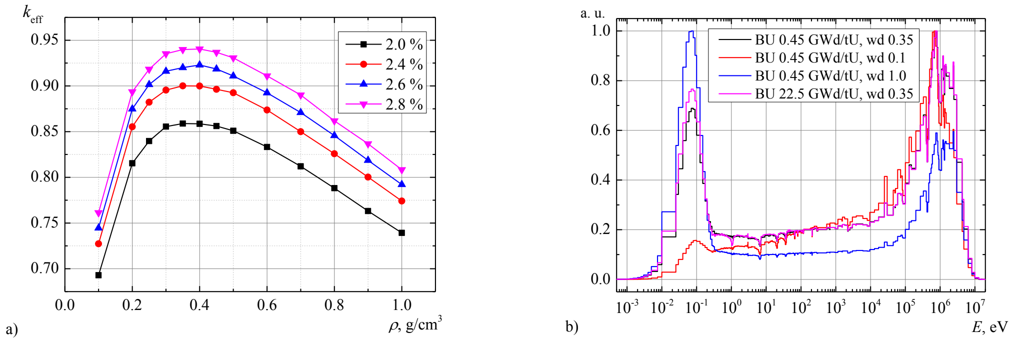

Fig. 3. Effective multiplication factor as a function of water density inside SNF cask cavities (a) and neutron spectrum in SNF cask for 2.8 % enrichment fuel different cask water density and burnup values (b)

k_{eff} dependency on burnup shows clear trend of reduction of reactivity with increasing burn-up (Fig. 4a). As actinide-only BUC approach is considered, erbium is not included in criticality analysis of the cask. Erbium is included in SNF composition calculations, then most important actinides are picked up and criticality calculations are performed. Therefore change of k_{eff} (with increasing burn-up), which is typical for SNF with erbium burnable absorber is not noticed. EALF increases due to burn-up for each type of fuel. However as enrichment (and erbium concentration) increases, increment of EALF is slower. It happens due to relatively higher neutron absorption in ^{239}Pu in lower enrichment fuel of high burnup.

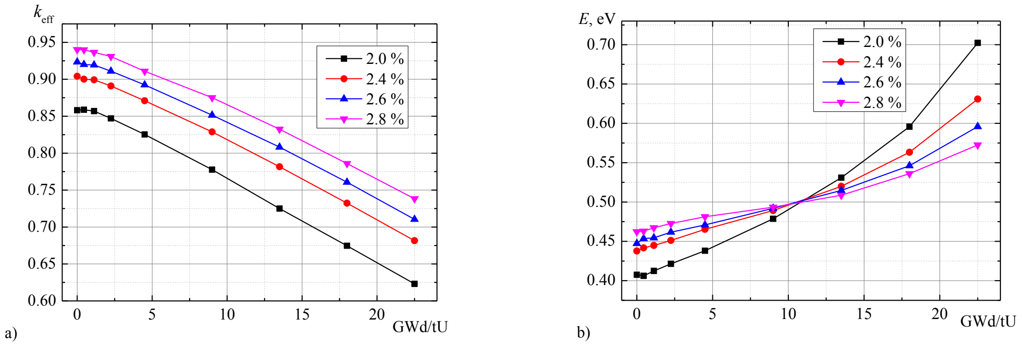

Fig. 4. Effective multiplication factor as a function of fuel burn-up (a) and energy of average lethargy causing fission as a function of burn-up (b) for different fuel enrichment

3.2. k_{eff} evolution

Evolution of k_{eff} for 2.8% enrichment fuel for 100 years is evaluated and presented in Fig. 5a. k_{eff} evolution was modelled increasing SNF storage time, resulting in changes of fuel composition - concentration changes due to decay of isotopes. Then water density inside cask cavities corresponding to most reactive conditions (~0.35 g/cm^3) was taken and used for criticality evaluation. For low burn-up fuel k_{eff} does not change in this period of time. For higher burn-up fuel (13.5 GWd/tU) decrease of reactivity is observed for 30 years.

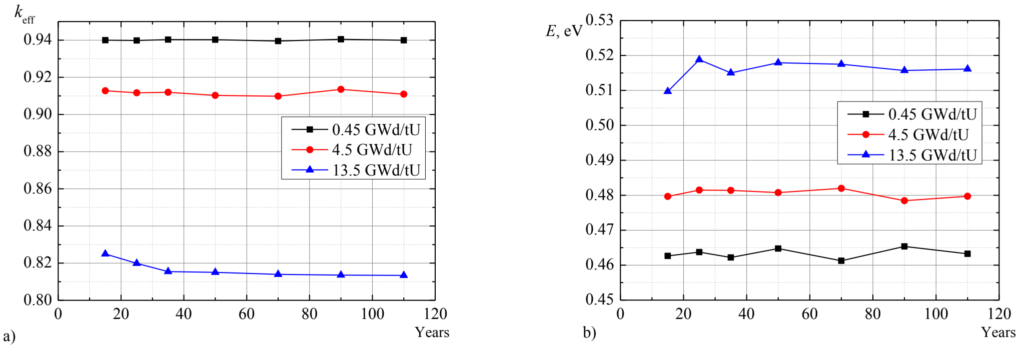

Fig. 5. Evolution of effective multiplication factor (a) and evolution of energy of average lethargy causing fission (b) for different burnup 2.8 % enrichment fuel inside SNF cask

It may be associated with beta decay of ^{241}Pu and buildup of ^{241}Am. Significant amount of ^{241}Pu forms after sufficient period of irradiation of fuel in the reactor, therefore this effect is not noticeble for lower burnup fuel. EALF does not show significant changes during evaluated period (Fig. 5b).

3.3. k_{eff} as a function of fuel burnup and water density inside SNF cask

k_{eff} of SNF cask filled with 2.0 and 2.8% enrichment fuel as a function of water density inside SNF cavities and fuel burnup with corresponding EALF values are given in Fig, 6 and 7. Most critical region is identified: 0–6 GWh/tU burn-up and 0.2–0.6 g/cm^3 water density. EALF is almost independent from burnup, only 2.0% high burnup fuel does not follow this trend.

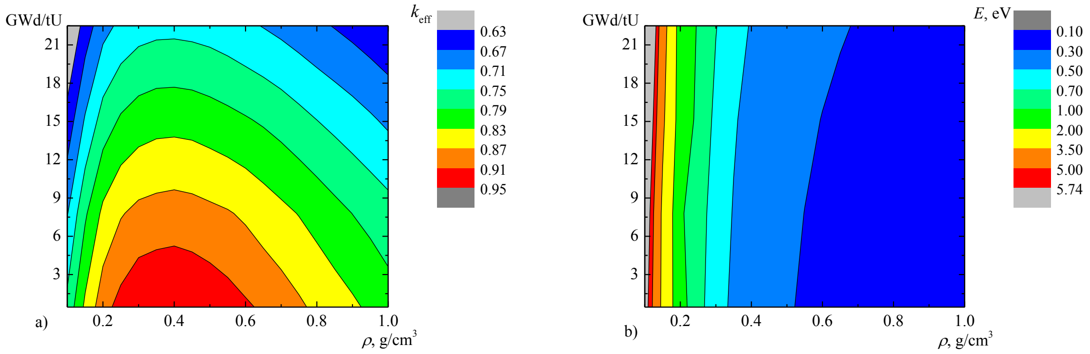

Fig. 6. Effective multiplication factor (a) and EALF (b) as functions of water density and burn-up for 2.8% enrichment fuel

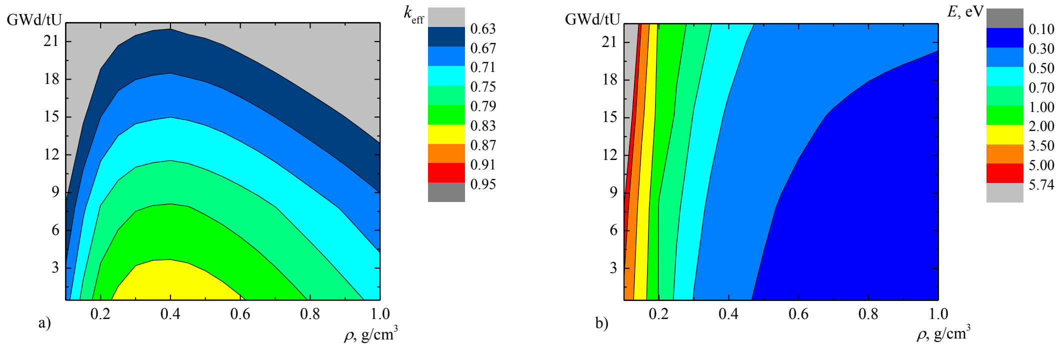

Fig. 7. Effective multiplication factor (a) and EALF (b) as functions of water density and burn-up for 2.0 % enrichment fuel

4. CONCLUSIONS

Detailed geometrical model of CONSTOR$^{®}$ RBMK-1500/M2 SNF cask for Monte Carlo simulations of neutron transport was created in SCALE 6.1 environment for criticality assessment using actinide-only burn-up credit approach. k_{eff} calculations of 2.0–2.8% initial enrichment fuel of various burn-up and water density inside cavities of SNF cask were performed. Pre-generated one-group ORIGEN-ARP spent nuclear fuel composition libraries were used for SNF composition evaluation. Maximum k_{eff} = 0.940 value was obtained for 2.8 % fuel enrichment and 0.4 g/cm^3 water density in SNF cask cavities. k_{eff} dependency on burnup shows reduction of reactivity with increasing burn-up. For low burn-up fuel k_{eff} does not change in 100 years period, for higher burnup fuel changes are not significant. Analyzing k_{eff} as a function of water density inside SNF cavities and fuel burnup most critical region was identified: 0–6 GWh/tU burn-up and 0.2–0.6 g/cm^3 water density. Despite maximum k_{eff} obtained is higher than specified in safety analysis of SNF storage facility, it may be seen, that inclusion of validated burnup credit approach gives suitable confidence that SNF cask filled with sufficiently irradiated 2.8% SNF should be subricritical even in most reactive conditions.

REFERENCES

1. *Interim Storage of RBMK Spent Nuclear Fuel from Ignalina NPP Units 1 and 2*, Environmental Impact Assessment Report, Consortium GNS – NUKEM, Lithuanian Energy Institute, 2007.
2. *Preliminary Safety Analysis Report Interim Storage Facility for RBMK Spent Nuclear Fuel Assemblies from Ignalina NPP Units 1 and 2* (B1), Consortium GNS – NUKEM, Lithuanian Energy Institute, 2007.
3. *General Requirements for Spent Nuclear Fuel Storage Facility of the Dry Type*, Nuclear Safety Requirements BSR-3.1.1-2010, State Nuclear Power Safety Inspectorate (VATESI).
4. MAHMOUD, R.F., SHAAT, M.K., NAGY, M.E., AGAMY, S.A., ABDELRAHMAN, A.A. Burn-up credit in criticality safety of PWR spent fuel, *Nuclear Engineering and Design*, December 2014, Vol. 280, p. 628–633.
5. *Practices and developments in spent fuel burnup credit applications*, Proceedings of a Technical Committee meeting held in Madrid, 22–26 April 2002, IAEA Tecdoc-1378.
6. *Advances in Applications of Burnup Credit to Enhance Spent Fuel Transportation, Storage, Reprocessing and Disposition*: Proceedings of a Technical Meeting held in London, 29 August–2 September 2005, IAEA Tecdoc-1547.
7. PLUKIS, A., PLUKIENĖ, R., REMEIKIS, V., RIDIKAS, D. MCNP and ORIGEN codes validation by calculating RBMK spent nuclear fuel isotopic composition, *Lithuanian Journal of Physics*, 2005, Vol. 45, No. 4, p. 281–287.
8. ŠMAIŽYS, A., POŠKAS, P. Konteinerių CASTOR RBMK-1500 ir CONSTOR RBMK-1500 su panaudotu branduoliniu kuru kritiškumo įvertinimas, *Energetika*, 2001, Vol. 4.
9. ŠMAIŽYS, A. Analysis of nuclear and radiation characteristics of RBMK-1500 spent nuclear fuel casks and storage facilities, *PhD thesis*, 2004, Kaunas.
10. *Spent Nuclear Fuel Assay Data for Isotopic Validation*, NEA State of the art Report, OECD, 2011.
11. BOWMAN, S.M., SCALE 6: Comprehensive Nuclear Safety Analysis Code System, *Nuclear Technology*. May 2011, Vol. 174(2), p. 126–148.
12. GAULD, I.C., BOWMAN, S.M., STARBUCS: A Prototypic SCALE Control Module for Automated Criticality Safety Analyses Using Burnup Credit, ORNL/TM-2001/33, Oak Ridge National Laboratory, October 2001.
13. ŠIMONIS, V., ŠMAIŽYS, A., POŠKAS, P. Naujų panaudoto branduolinio kuro saugojimo konteinerių naujojoje Ignalinos AE saugykloje šiluminis įvertinimas, *Energetika*, 2011, Vol. 57, No. 3, p. 163–171.
14. ALMENAS, K., KALIATKA, A., UŠPURAS, E. *Ignalina RBMK-1500. A source book*, 1998, Lithuanian Energy Institute.
15. PLUKIENĖ, R., PLUKIS, A., GERMANAS, D., REMEIKIS, V. Numerical sensitivity study of irradiated nuclear fuel evolution in the RBMK reactor, *Lithuanian Journal of Physics*, 2009, Vol. 49, No. 4, p. 461–469.

CYSENI 2015, May 27–28, Kaunas, Lithuania
ISSN 1822-7554, www.cyseni.com

ENVISIONING A SUSTAINABLE FUTURE FOR EUROPE: THE LEAD FAST REACTOR AND THE ALFRED PROJECT

G. Grasso
Italian National Agency for New Technologies, Energy
and Sustainable Economic Development (ENEA)
Via Martiri di Monte Sole 4, 40129 Bologna – Italy
Phone +39 051 6098438
Email: giacomo.grasso@enea.it

ABSTRACT

Energy availability is needed for development, the primary condition for aiming at wellness. This legitimate ambition is growing along with the vision of a sustainable scenario, for which affordable, acceptable and environmental-friendly energy sources are deemed necessary.

In this perspective, nuclear energy can play a relevant role, provided it overcomes the social concerns blasted out after the Fukushima events, with safety enhancement and waste management in the spotlight of public opinion. For this, breakthroughs are to be conceived, developed and qualified in view of the deployment of a fleet of Nuclear Energy Systems (NES) of a new Generation.

Among the candidate concepts identified by the Generation-IV International Forum, Lead-cooled Fast Reactors (LFRs) are a very promising option, thanks to the exploitation of the favourable intrinsic properties of lead for safety (practically eliminating severe accidents), sustainability (coping with extreme flexibility with the closure of the fuel cycle), proliferation resistance (allowing long-lived battery cores) and physical protection (retaining into the coolant almost the whole potential radioactive inventory).

In the roadmap towards the deployment of commercial LFRs, the Advanced LFR European Demonstrator (ALFRED) is envisioned to prove the viability of lead technology for use in a future Gen-IV NES. All the achievements of ALFRED and of its supporting program, will allow significant advancements for Europe in mastering the nuclear lead technology. Indeed, the ALFRED reactor together with all its supporting infrastructures, to be built in Romania, will be offered to the whole Europe as a unique open-access technology park, for universities, research organizations, industry, safety authorities and utilities all together to get prepared to the advent of a safe, secure and sustainable energy future.

In this paper the ALFRED Project, the ALFRED reactor and the features of the European LFR concept are presented, and the perspectives discussed.

Keywords: Nuclear Energy System, Generation-IV, Sustainability, Safety, ALFRED

1. INTRODUCTION

Aiming at sustainable, yet secure – and competitive! – energy with a long-term vision, the European Union prepared in 2010 a policy oriented to transform the entire energy system towards a low-carbon scenario.

The Strategic Energy Technology Plan (SET-Plan) [1] tackles this challenge, establishing the energy technology policy needed to meet the objective and all its far-reaching implications.

In this scenario, nuclear energy is reckoned as a key component of the mix to be pursued, notably relying on a wide implementation of fast-reactor-based technologies, so as to target the actual closure of the fuel cycle.

The mandate of the SET-Plan is assigned, to what concerns nuclear energy, to the Sustainable Nuclear Energy Technology Platform (SNETP) [2], which is called to sustain the development of innovative fast reactor technologies for their deployment in the long term.

The SNETP mandate is formulated sharing the perspective put forward in 2002, when an international panel of experts set the Generation-IV International Forum (GIF) [3]. The experts identified 12 design goals, in the four areas of safety, sustainability, economics and proliferation resistance and physical protection, thanks to which a new generation of nuclear energy systems would have emerged, bringing people closer to this energy source.

The ambition behind this vision is so high, that only breakthroughs will allow the fulfilment of all goals, representing a steep improvement with respect to present systems. Out of more than one hundred of proposals, the panel of experts identified only six concepts candidate to give body to Generation-IV nuclear energy systems.

The European scientific community started three actions for research and development programs on Sodium-, Lead- and Gas-cooled Fast Reactors (SFR, LFR and GFR, respectively), supported by the European Sustainable Nuclear Industrial Initiative (ESNII) [4], one of the three pillars SNETP is based upon. ESNII was launched in 2010 with the mandate of facilitating the deployment of a fleet of fast reactors, having the SFR technology as reference, thanks to the accumulated operative experience, and the LFR as most credible short-term alternative [5].

2. THE EUROPEAN LFR CONCEPT

Following the European vision and the ESNII mandate, a relevant number of the researches have been conducted for more than 20 years on the lead technology through both national initiatives and international cooperative actions supported by the EC since its 5th EURATOM Framework Programme (FP5), have been finalized to the development of for the deployment of a fleet of industrial Generation-IV systems.

These studies on one side provided elements showing the technical and technological viability of a lead-cooled nuclear system; on the other suggested the potential for LFRs to be significantly safer and more economical of general SFR and GFR systems. According to this, the idea of a reference European LFR (ELFR) of new Generation was consolidated, as a nuclear energy system design complying with economics, improved intrinsic and passive safety, enhanced sustainability and proliferation resistance. The number of collaborative research projects on lead systems and lead technology increased exponentially in the 6th and 7th EURATOM Framework Programmes (FP6 and FP7), extending the scopes of some relevant national R&D programs (the Italian and the Czech ones being the largest, with about 18 M€ and 17 M€ invested over the past 9 years, respectively).

2.1. The design philosophy

The design mainstream for the LFR of European concept, hence of all R&D actions in support to the design itself, is the magnification of the unique properties of lead as coolant, to fulfil all the Generation-IV objectives under the general leitmotif of simplicity [6].

Simplicity, because:

- simple is safe: nothing added on but rather embedded in;
- simple is reliable: the less the parts, the less the potential failures;
- simple is robust: what a fool can do, any fool can do;
- simple is economic: ça va sans dire.

Although simplicity is often acknowledged as an asset only proper of academic reactors [7], in the process of stepping towards a practical reactor it was reckoned that bringing simplicity into the LFR concept is the main key for the steep technology improvement that is necessary to achieve the high vision behind the Generation-IV statement.

Considering the sustainability concept at large, particular attention was spent on two aspects: the protection of people and of the environment. Accordingly, and to put in place simplicity into a real system, the design being elaborated is based on two ideas to be integral part of it: the so called “walk away reactor” and “adiabatic reactor” concepts.

2.1.1. The Walk-away reactor concept [8]

The actual protection of people is achieved by the elimination of the need for off-site emergency responses. In other words: no matter the accidental condition the plant might be called to face, it has to withstand without releasing any amount of radioactivity potentially harmful for the population living in the surrounding.

Learning the lessons drawn after the Fukushima events, in which plant monitoring and remote controls were completely unavailable, and considering the spreading risk of cyber-attacks, through which the indications to operators might be mystified to induce erroneous countermeasures as initiators of a potential accident, to target the ambitious objective mentioned above, human intervention is to be made unnecessary. In this the “walk away reactor” concept envisages the extensive use of intrinsic features and natural laws, to achieve a system able to react autonomously and passively to any potential initiator, bringing the plant back in safe conditions without the need for any operators’ action. Operators that might be hence allowed to quietly walk away from the plant (instead of rushing towards, or just running away…).

2.1.2. The Adiabatic reactor concept [9]

The second concept, the one envisaging an “adiabatic reactor”, is based on the idea of multi-recycling for the closure of the fuel cycle, but arranged so as that the system can be fed with uranium only (either natural, depleted or recovered), continuously recycling all actinides to produce energy while releasing as waste only fission products.

The advantages of this approach are twofold: on one side, uranium stocks are saved by a factor 100, since only the amounts strictly needed for energy production are reintegrated in the fuel; on the other, the waste is not only strongly reduced in volume, but its radio-toxicity lowered so as to be comparable to that of ore uranium after few centuries, instead of one hundred thousand years, with a strong simplification on waste management.

But even more can be done. Instead of a system preserving exactly the inventories of plutonium and Minor Actinides (MAs), as previously described, it is possible to achieve different operative conditions also with differential Pu and MAs breeding or burning, simply by defining beforehand the desired performances.

On top of all, the real power of the theory underneath this concept comes from the possibility to anticipate the composition of the fuel at equilibrium before the system is defined, so that the designer is allowed to seek – from the very beginning of the design process – for a core and plant configuration remaining within the aimed safety margins during the entire plant life.

2.2. The general design approach

To provide the highest safety levels, it was decided to extend the design of the system so as to consider events typically assumed for Design Extension Conditions (DEC) as Design Basis Accidents (DBA): indeed, embedding safety features as much as possible into the design was reckoned as the only approach allowing to target a system helping nuclear energy to get rid of the risk of another Fukushima.

As mentioned, to achieve this ambition, the intrinsic properties of lead have been exploited in choosing the main design options with the aim to target simplicity; at the same time, design or engineered provisions have been taken to address the drawbacks, to ensure a sound and reliable configuration.

2.2.1. Lead features and their impact on system design

Lead has an extremely high boiling point (1743 °C at ambient pressure [10]), well above the melting temperature of structural materials. This a) leaves enormous safety margins before reaching the onset of boiling in any accident scenario (including uncontrolled power ramps and flow blockages); b) strongly reduces the positive reactivity potentially inserted in the system; c) allows the operation of the primary system without pressurization to reduce the loads on the structures.

Lead does not react violently with air or water. This allows a) a significant reduction of the potential energy stored in the primary system, with evident safety benefits, b) the elimination of the intermediate cooling circuit, reducing capital costs and increasing plant efficiency; c) the elimination of fire risks on the nuclear island; d) the easy use of air and water as ultimate heat sinks for Decay Heat Removal (DHR) systems without safety threats intrinsic to these systems; e) the declassification of coolant leakages from a safety point of view, simplifying the requirements for leak monitoring systems.

Lead has optimal thermal properties [10]. In particular, the high thermal capacity of lead can accommodate large energy releases into the primary system with modest temperature increases, protecting the structures and providing a significant grace time for provisions (either intrinsic or engineered) to actuate.

Lead has a high density (11.34 g/cm^3 solid at room temperature [10]). Higher than the density of oxide fuels, letting envisage the possibility of fuel dispersion in spite of sinking in case of core disruption, avoiding the need for a core catcher in favour of a natural creation of a cold melting pot retaining the fuel. Moreover, although the thermal expansion coefficient is modest, high density variations are caused even by small temperature excursions, facilitating the onset of natural circulation.

Lead has excellent neutronic properties [11], notably a minimum moderating power and very low absorption cross-section. The former allows for a significantly hard neutron spectrum, which promotes criticality (because of the high value of $\bar{\nu}$) and can be exploited to easily introduce the design methodology at the basis of the adiabatic reactor concept.

Lead has excellent retention capabilities, notably for iodine and cesium, among fission products the two typically responsible for the main contamination and public exposure in case of releases. First of all, this greatly reduces the potential source term within the reactor building in case of loss of the first two engineered barriers (cladding and primary system), the coolant becoming a further, very effective one. Then, this allows to have the cover gas atmosphere extremely clean, hence the possibility of performing refueling, inspection and replacement of internals by opening the reactor cover. minimum moderating power and very low absorption cross-section.

Lead is an excellent γ-shield. This reduces the needs for engineered shielding around the reactor and provides self-protection to sensible components or instruments operating within the main vessel.

2.2.2. Lead drawbacks and provisions

Lead has a high density (11.34 g/cm^3 solid at room temperature [10]). This may pose concerns on the loads to the structures, notably during earthquakes. For this reasons plant size limitations are usually considered along with the use of seismic insulators for the reactor building.

Lead has a high melting point (327 °C [10]). To prevent the risk of freezing a relevant use of heaters is to be considered, notably when no burnt fuel is loaded in the core. Anyway, investigations are being performed to assess whether freezing should be considered a safety issue or just a potential threat for investment protection.

Lead is corrosive. This property, associated to the chemical compatibility with structural material, is a function of temperature. For structural materials commonly used in the nuclear industry (austenitic and ferritic-martensitic stainless steels), below 400 °C no relevant effect is observed; below 500 °C corrosion can be inhibited by passivation of the surfaces through self-formed oxide scales; above 500 °C proper barriers must be applied through coating techniques [12].

Lead is erosive. This mechanical effect is a function of the speed of jets impinging orthogonally on the surfaces. Unless special materials (like MAXTAL) or protective coatings are used, for steels of common use it is required to limit the normal component of lead velocity to 3 m/s, which is practically translated, for common applications, to a limit on lead bulk speed to 2 m/s. The impact of this limitation on heat removal from the core can be minimized by enlarging the pitch between fuel pins, with very low impact on core performances thanks to the excellent neutronic properties of lead.

3. THE ALFRED PROJECT

In order to show the effectiveness of the European LFR concept, a demonstration reactor, completely representative of the concept, is envisioned as main step following the R&D phase. ALFRED – the Advanced Lead Fast Reactor European Demonstrator – is the solution proposed by the European scientific community working on LFRs for years. Conceived so as to rely as much as possible on already available technologies to speed up design and construction, ALFRED, implementing all design provisions foreseen for the commercial reactor, is hence expected to prove – to the largest extent – the viability of the technology for use in an innovative nuclear energy system, from qualification of components and licensing to construction, operation, grid connection, inspection and maintenance.

The results obtained through the operation of ALFRED will provide relevant evidences on all matters of nuclear energy production in front of all potential stakeholders.

3.1. ALFRED design

ALFRED is a pool-type reactor, conceived so as to have all components easily removable for inspection and repair through the reactor cover [6]. The primary circuit is revolutionized by placing the Primary Pumps (PPs) in the hot leg, with suction directly from core outlet. The Steam Generators (SGs) are directly connected one-to-one with the PPs in a single unit. The cold lead exiting the SGs fills the main vessel in the annulus outside a cylindrical Inner Vessel (IV) containing the core. A scheme of the ALFRED reactor block, with coolant path indicated, is shown in Fig. 1.

Around the main vessel, a safety vessel – realized as a liner of the reactor cavity – is foreseen as a countermeasure against failure of the main vessel. In case of coolant leakage, the gap between the two vessels ensures both the core and the SGs remain under the new coolant level despite the lowering of the latter, to ensure heat removal from the core. The width of the gap also allows the insertion of robots to remotely inspect the status of the main vessel.

The positioning of the PPs in the hot leg allows to simplify the IV design, still ensuring that the main vessel walls face only cold coolant, reducing the thermal stresses on it. Two options are envisioned for the PP: a traditional centrifugal pump, even though a careful design is required to reduce the coolant speed at the impeller, and an Archimedean one, whose design is presently being optimized.

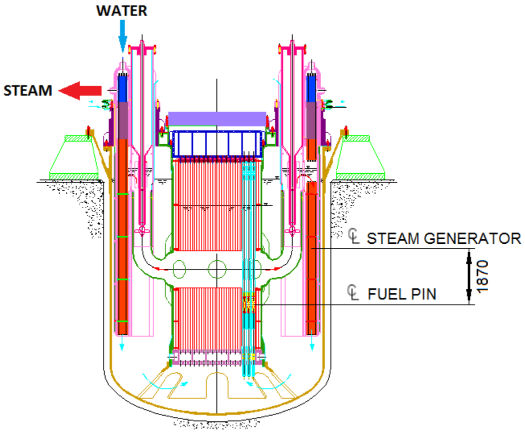

Fig. 1. ALFRED reactor block [dimension in mm]

The SG is made of straight, double-walled bayonet tubes (Fig. 2), arranged in a triangular lattice with a large pitch over the diameter to lower pressure drops. The internal double-walled tube separates cold feedwater, descending within the innermost tube, from the annulus where water – raising in counter-current to lead – boils to produce superheated steam. Between its two walls an insulator is foreseen to prevent steam condensation on the inner tube. The operating pressure is 180 bar, with water entering at 335 °C (to maintain a margin against lead freezing) and steam exiting at 450 °C. The external double-walled tube is set to as safety provision provide against Steam Generator Tube Rupture (SGTR). The gap between these two tubes is filled by highly-conducting powder and pressurized with inert gas to have a continuous monitoring of the integrity of these two tubes.

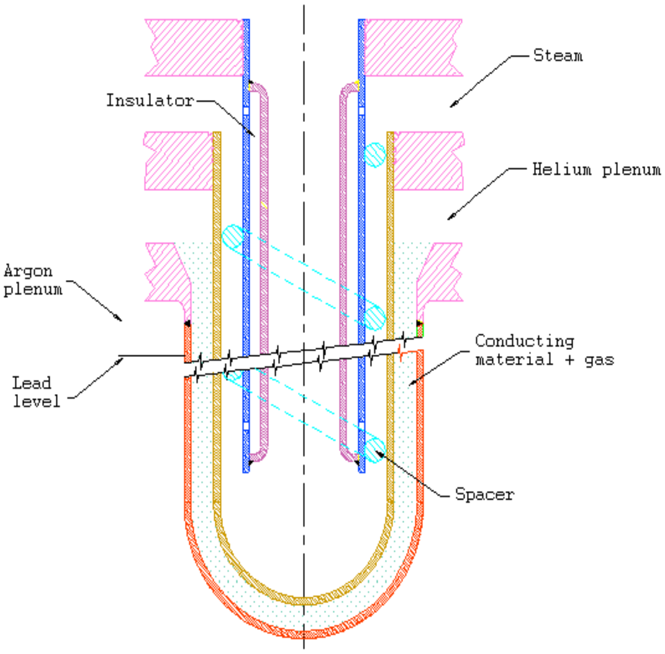

Fig. 2. Scheme of the double-walled bayonet tubes of the ALFRED SG

The IV is a block made of a vessel and two diagrids (Fig. 3). The vessel is made of a cylindrical, structural element, provided of eight “L” pipes to connect the PP-SG units, and a shroud following the core perimeter to constrain the latter. The lower diagrid is a box structure made of two horizontal plates with holes for the insertion of the sub/assemblies (S/As) and vertical elements providing stiffness to the structure. The connection between the vessel and the lower diagrid is made by pins, to eliminate weldings. The upper diagrid has the same box structure, but is more stiff. Instead of holes, cup connections are used to engage the S/As, each one provided with springs to accommodate the differential thermal expansions of the S/As. The cups have holes to cable instrumentation in the core region. The upper diagrid is placed above the lead level, since the S/As extend up to the reactor roof to compensate the buoyancy of the elements in lead and to exploit the possibility of refueling in the cover gas, in full visibility.

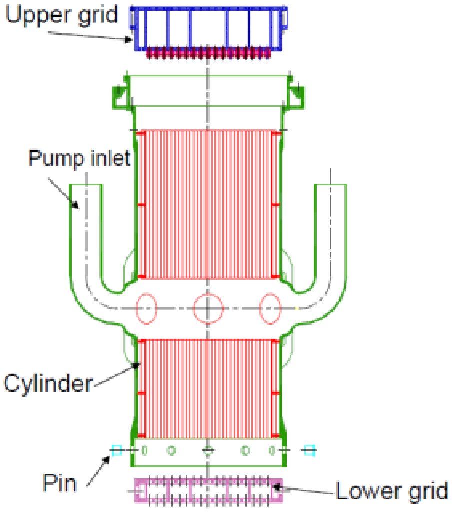

Fig. 3. The Inner Vessel block of ALFRED (disassembled)

On the diagrids 295 positions are retrieved for the S/As (Figure 4) [13]. 171 positions are necessary to host the Fuel Assemblies (FAs) to provide 300 MW$_{th}$ (converted to about 125 MW$_e$ as net output by the Balance of Plant). Within the active region, 12 positions are reserved in the outermost part for Control Rods (CRs). 4 more positions, close to the core centre, are reserved for Safety Rods (SRs). The remaining 108 positions surrounding the active region host dummy elements for neutrons reflection and IV shielding.

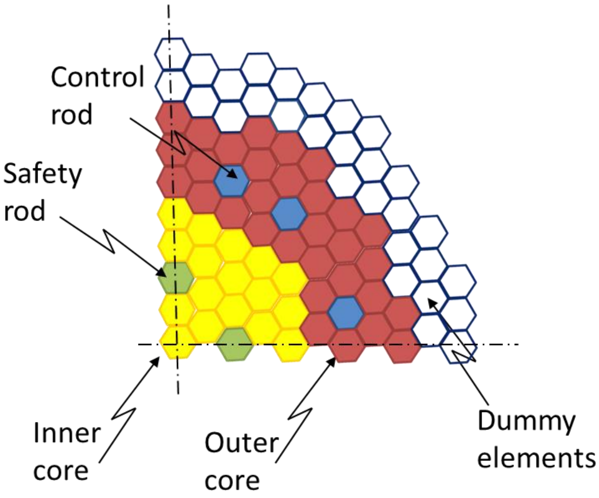

Fig. 4. ALFRED core map

The hexagonal wrapped S/As (Fig. 5) are made of:

- a spike engaging the holes in the lower diagrid. The spike is provided of two series of holes: the lower one to let the coolant enter from the lower plenum to feed the S/As in nominal conditions, preventing the sudden blockage at the inlet; the upper one to feed the volume within the lower diagrid (hence the by-pass between the S/As) in nominal conditions, and reversed as coolant intake in case of complete blockage of the first series of holes.
- a lower shroud containing the fuel, absorber or reflector pins bundles.
- a cylindrical section defining the volume for the upper plenum.
- an upper shroud extending up to the cover gas to engage the upper diagrid. The extension is foreseen to host a tungsten ballast as measure to compensate the buoyancy of the S/As in lead. The ballast is dimensioned to force every S/As on the lower diagrid when the pumps are off (refuelling); when forced circulation is on, the drag force is compensated by the spring pack at each cup connection on the upper diagrid.

The hexcan is bumped at several heights to form pads providing contact points between adjacent FAs to prevent core compaction and promote core flowering.

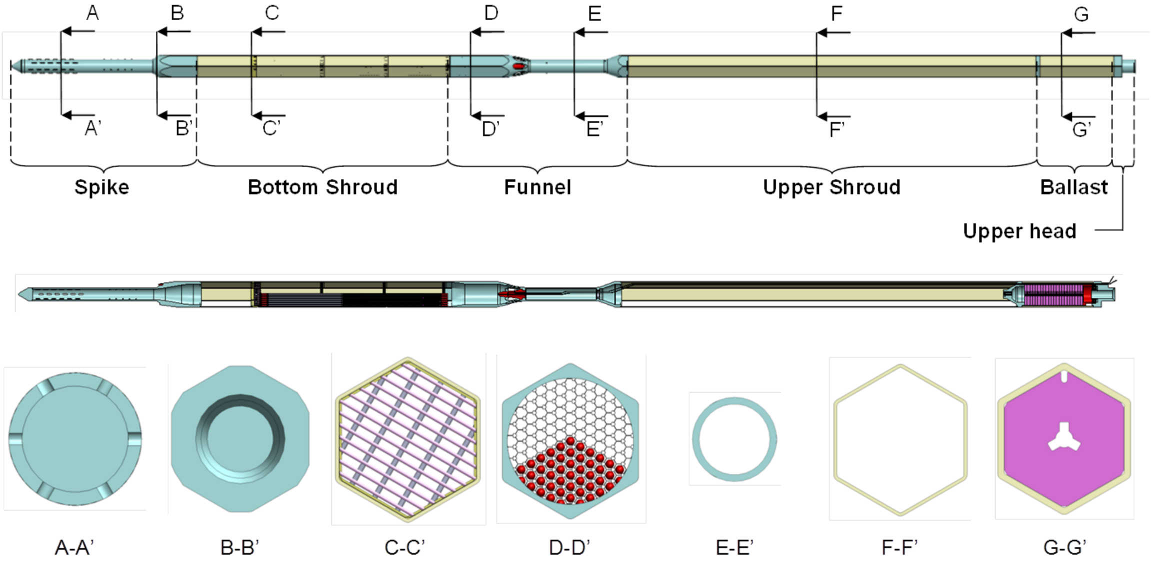

Fig. 5. Vertical cross-section of an ALFRED S/A

The bundle in the FAs is made of 127 pins arranged in a triangular lattice with a pitch-over-diameter ratio of 1.32. The pins are 139 cm long, while the length of the active region is only 60 cm (left frame of Figure 6). The coolant flow velocity through the core is 1.4 m/s, lower than the allowed limit (2 m/s) to reduce the pressure drops so as to exploit a geometry promoting natural circulation in case of loss of the PPs. The coolant, entering at 400 °C, exits from the core 80 °C hotter (on average), so as to limit the hot spots on the cladding below 550 °C which is the limit allowed by the candidate coating selected at the beginning of the design[1].

---

[1] The present reference option for the coating proved to withstand corrosion excellently up to 600 °C.

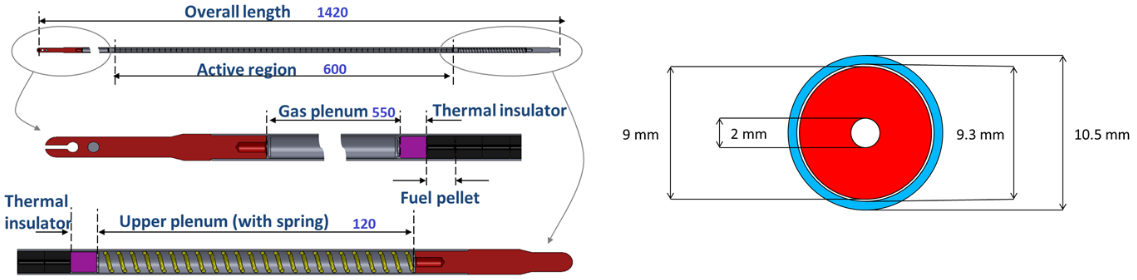

Fig. 6. Vertical (left) and horizontal (right) cross sections of the ALFRED fuel pin

The cladding has an outer diameter of 10.5 mm to enlarge the fuel inventory for criticality, and a thickness of 0.6 mm to withstand swelling and internal gaseous fission products pressure (set by design at 5 MPa). The fuel pellet has an outer diameter of 9 mm and a central hollow with a diameter of 2 mm to reduce the maximum temperature and the pellet-cladding mechanical interaction (right frame of Fig. 6). To achieve criticality and flatten the power/FA distribution, two enrichment zones are found on the core map: the 57 innermost FAs have an enrichment (Pu+Am/Pu+Am+U) of 21.7 at.%, while the 114 outermost FAs have a Pu+Am content of 27.8 at.%. The FAs are apportioned in 5 groups, homogeneously distributed throughout the core map, undergoing refuelling every year.

The CRs are made of a bundle of 19 pins with B_4C enriched up to 90% in ^{10}B as absorber. The bundle is extracted downwards and enters the core by motors during operation or by buoyancy for SCRAM. The reserve of anti-reactivity they provide (more than 6800 pcm) is sufficient for compensating the cold zero power to hot fuel power transition (about 1400 pcm) and the swing during one cycle (about 2600 pcm). The SRs are made of a bundle of 12 absorbing pins using the same B_4C 90% enriched in ^{10}B. The SRs are placed still atop the core, entering only in case of SCRAM. To overcome buoyancy and ensure their insertion, a tungsten ballast is positioned above the bundle. To speed up the insertion, the SCRAM signal – unlocking the electromagnet holding the bundle – triggers a passive pneumatic system.

3.2. The safety performances of ALFRED

Due to its size, ALFRED will not be operated as an adiabatic reactor, although some tests on single fuel pins or assemblies will be planned during its operation lifetime to prove the effectiveness of this design option.

Accordingly, ALFRED will be called to demonstrate the safety performances envisioned for the European LFR and ensured by the design methodology, which borrows the same criteria formulated for the commercial reactor.

The proposed ALFRED configuration has therefore been stressed through extensive analyses, to assess its behaviour both against DBA and DEC. Within the LEADER project [8], a list of accidents has been compiled analyzing all the potential initiators. Out of this list, 19 transients were selected as the most challenging conditions for the plant, and successively grouped into 3 extreme conditions reckoned to encompass all these: an Unprotected Loss Of Flow (ULOF), an Unprotected Transient Of Power (UTOP) and an Unprotected Loss Of Offsite Power (ULOOP – a Fukushima-like condition complicated by the failure of the SCRAM actuation).

During a ULOF (Fig. 7), the maximum temperature reached by the cladding in the initial flow undershot (in the transition from forced to natural circulation) reaches about 750 °C for few seconds, to then quickly reduce below 650 °C, hence complying with the 30 minutes grace time assumed by design for the manual actuation of the SCRAM. The feedback coefficients – mainly the ones due to coolant density and core expansion at the level of the diagrid and pads – are capable to reduce the power to a level (about 200 MW_{th}) complying with the onset of natural circulation at acceptable temperatures.

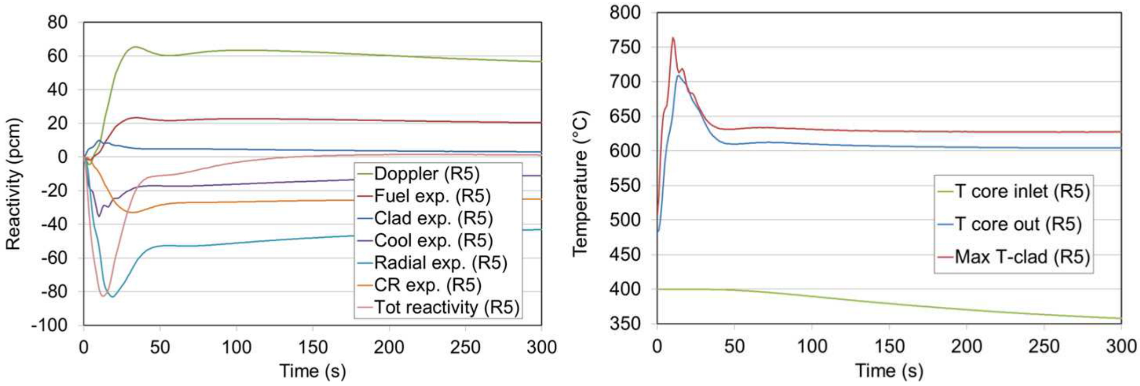

Fig. 7. Feedback responses (left) and main system temperatures (right) during a ULOF transient

During a UTOP (Fig. 8), the margins left on the peak fuel temperature – through the design limit on the maximum linear power – lead to no generalized melting of the fuel, which involves only the inner region of few pellets in the hottest pins. The prompt intervention of the Doppler feedback arrests the power ramp bringing back the plant in controllable conditions with no damages.

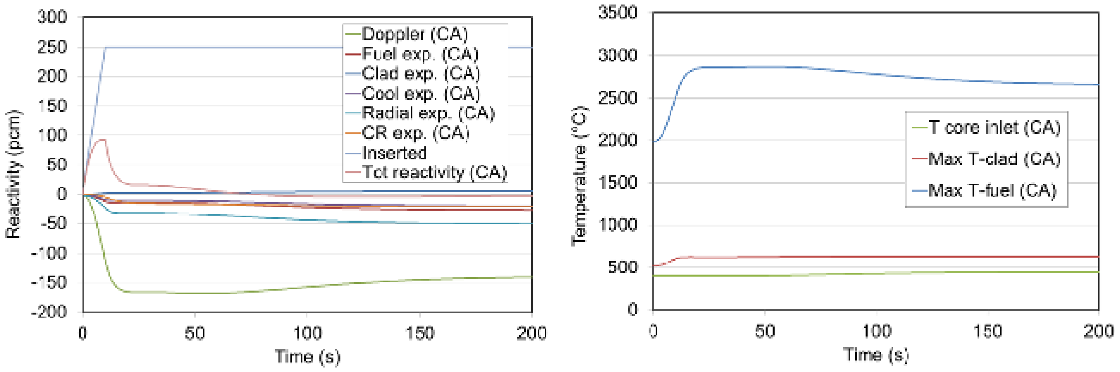

Fig. 8. Feedback responses (left) and main system temperatures (right) during a UTOP transient

In case of ULOOP (Fig. 9), the tendency of all system temperatures to increase exceeding the design limits is interrupted by the reactivity feedback promptly reducing the core power to 160 MW_{th} in few seconds, and then progressively approaching 20 MW_{th}, the power of the DHR. This results in no expected failure of the cladding, although a potential threat for the main vessel can be envisioned in the long term.

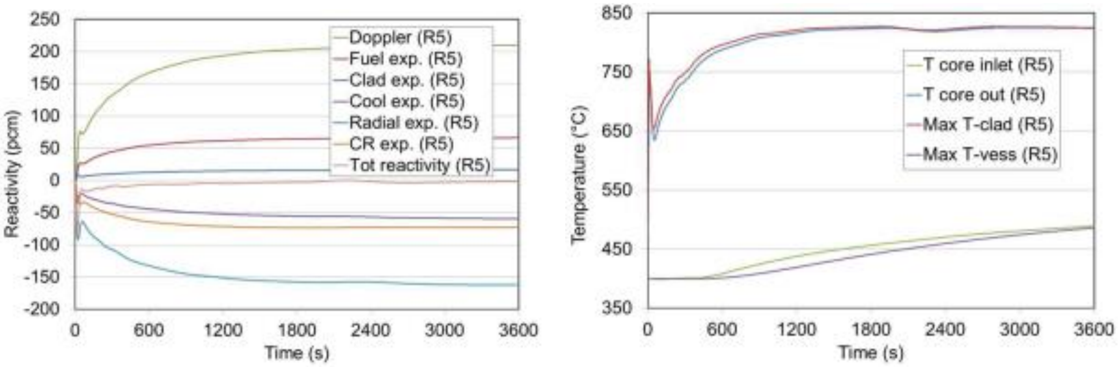

Fig. 9. Feedback responses (left) and main system temperatures (right) during a ULOOP transient

It is worth mentioning that – whatever the situation investigated – once the SCRAM is actuated (that means: in case all these events happen in Protected conditions), the deviation of plant operation is such to pose no concerns, the grace time of the plant before any action from operators (typically: refilling the heat sinks of the DHRs) being of three days.

3.3. FALCON

According to the willingness of Romania to host ALFRED, and due to the strong commitment of Italian organization (mainly Ansaldo Nucleare as general architect and designer of the primary system, and ENEA as core designer and coordinator of the supporting R&D program), an International Consortium (FALCON – Fostering ALFRED Construction) was established in December 2013 to coordinate all the actions necessary for committing to the ALFRED realization, including R&D, management and financial assessment, sitting and licensing preparation and promotion.

Presently FALCON numbers four full members (Ansaldo Nucleare, ENEA, ICN and CVR) and 10 partners associated through a Memorandum of Agreement: LeadCold reactors (SE) and SRS (I) as industry; GRS (D) as Technical Safety Organization; KIT (D), NRG (NL), IIT (I) and CRS4 (I) as research organizations; CIRTEN (I) and the University of Genova (I) as universities and SYMLOG (F) as institute for social sciences.

Currently FALCON is pursuing two main objectives in parallel: the inclusion of iCRADLE (Infrastructure for Cooperative Research to Advance up to Demonstration the Lead technology in Europe) in the ESFRI roadmap, and a financing from European Structural and Investment Funds in Romania for setting the first basis of a new centre of excellence for researches on the lead technology.

The former foresees the creation of a distributed research infrastructure, gathering the existing ENEA centre of excellence at Brasimone (Italy), the CVR centre of excellence under construction at Rez (Czech Republic) and a new one, planned in Romania. The latter will be provided, in a first phase, of a number of relevant facilities extending the scopes of the investigations possible at the other nodes of the distributed research infrastructure to the remaining aspects needed for the full qualification of the technology needed for building ALFRED and for supporting the licensing of the latter. In a second phase, through the construction of the reactor, the infrastructure will be the largest and the only one in the World offering a real reactor for researches and studies on innovative reactor operation, inspection and maintenance.

4. CONCLUSIONS

The vision that led to the concept of the European LFR fully complies with the European policies for secure, safer, more sustainable and competitive energy sources, providing an innovative design for a Nuclear Energy System cooled by lead.

The general philosophy behind this vision led to the design of a very promising solution that raised the interests of a number of partners – ranging from academia and up to industry, utilities and safety organizations – supporting the initiative for advancing the readiness level of the lead technology up to its maturity, so as to let industry take the lead for the commercial deployment of this concept in the long term.

The demonstration of the viability of the general design formulated for the European LFR, and of all the features envisioned for it – notably the safety features envisioned for the systems of European LFR concept – passes through the construction and successful operation of ALFRED.

Indeed, ALFRED has been developed embedding as much as possible safety provisions by design, so as to target very ambitious goals. Preliminary safety analyses confirm the effectiveness of this approach, reporting no core damage, nor relevant concern for the protection of the plant, in any transient simulated, not even unprotected.

In order to prepare for this demonstration phase, a number of the remaining supporting actions must be anticipated to fully qualify the technology options to be used in the reactor.

The FALCON International Consortium is working to prepare this perspective, coordinating all the efforts to target the goal.

REFERENCES

1. *Towards a European Strategic Energy Technology Plan*. European Commission, 2007. <http://ec.europa.eu/energy/technology/set_plan/set_plan_en.htm>
2. *The Sustainable Nuclear Energy Technology Platform: A vision report*. Directorate-General For Research And Directorate J-Energy (EURATOM) of European Commission, 2007. Special report EUR 22842. <http://www.snetp.eu/www/snetp/images/stories/Docs-VisionReport/sne-tp_vision_report_eur22842_en.pdf>
3. *A Technology Roadmap for Generation IV Nuclear Energy Systems*. U.S. DOE & Generation IV International Forum, GIF-002-00. <http://www.gen-4.org/Technology/roadmap.htm>
4. A contribution to the EU Low Carbon Energy Policy: Demonstration programme for Fast Neutron Reactors – Concept paper. SNETP, 2010. <http://s538600174.onlinehome.fr/snetp/wp-content/uploads/2014/05/ESNII-Folder-A4-oct.pdf>
5. *Strategic Research and Innovation Agenda*. SNETP, 2013. <http://www.snetp.eu/wp-content/uploads/2014/05/sria2013_web.pdf>.
6. *Lead-cooled European Advanced DEmonstration Reactor (LEADER)*. EURATOM FP7 project, Grant agreement no. FP7-249668. <http://www.leader-fp7.eu/>.
7. RICKOVER, H.G. http://ecolo.org/documents/documents_in_english/Rickover.pdf
8. BANDINI, G., et al. Safety analysis results of representative DEC accidental transients for the ALFRED reactor. FR13. Proceedings of international conference of fast reactors. Paris. 2013 March 4–7.
9. ARTIOLI, C., GRASSO, G., PETROVICH, C. A new paradigm for core design aimed at the sustainability of nuclear energy: the solution of the extended equilibrium state. *Annals of Nuclear Energy*, 2010, Vol. 37, p. 915–922.

10. *Handbook on Lead-bismuth Eutectic Alloy and Lead Properties, Materials Compatibility, Thermal-hydraulics and Technologies*. Paris: OECD, 2007. ISBN 978-92-64-99002-9.
11. CINOTTI, L., SMITH, C.F., ARTIOLI, C., GRASSO, G., CORSINI, G. Lead-Cooled Fast Reactor (LFR) Design: Safety, Neutronics, Thermal Hydraulics, Structural Mechanics, Fuel, Core, and Plant Design. CACUCI, D.G. (ed). *Handbook of Nuclear Engineering*. Springer, 2010. ISBN 0-387-98130-6.
12. WEISENBURGER, A., et al. Materials for ALFRED and ELFR – selection and challenges. FR13. Proceedings of international conference of fast reactors. Paris. 2013 March 4–7.
13. GRASSO, G., et al. The core design of ALFRED, a demonstrator for the European lead-cooled reactors. *Nuclear Engineering and Design*, 2014, Vol. 278, p. 287–301.

CYSENI 2015, May 27–28, Kaunas, Lithuania
ISSN 1822-7554, www.cyseni.com

VALIDATION OF CODES DRAGON4 AND DONJON4 BY CALCULATING K_{EFF} OF A SLOWPOKE-2 REACTOR

O. Jai, O. Elhajjaji, J. Tajmouati
Sidi Mohamed Ben Abdellah University
Atlas, Postal Address: B.P. 1796 Fez - Morocco
Phone +212651546099
Email: otmanway@gmail.com, othajjaji@gmail.com, jatajm@yahoo.fr

A. Hebert
Nuclear Engineering Institute
Downtown, C.P. 6079, Montreal - Canada
Email: alain.hebert@polymtl.ca

ABSTRACT

Several neutronic calculation codes must be used to solve the equation for different levels of discretizatiоn which all necessitate a specific modelisation. This chain of such models, known as a calculation scheme, leads to the knowledge of the neutron flux in a reactor from its own geometry, its isotopic compositions and a cross-section library. Being small in size, the “Slowpoke-2” reactor is difficult to model due to the importance of the leaking neutrons.

In the paper, the simulation model is presented (geometry, cross section library, assumption, etc.), and the results obtained by **DRAGON4/DONJON4** codes were compared to the calculations performed with Monte Carlo code MCNP using detailed geometrical model of the reactor and the experimental data. Criticality calculations have been performed to verify and validate the model. Since created model properly describes the reactor core it can be used for calculations of reactor core parameters and for optimization of research reactor application.

Keywords: transport equation, Dragon4, Donjon4, neutron flux, effective multiplication factor

1. INTRODUCTION

Research reactors are commonly used as sources of neutrons for scientific investigations or as means for use in nuclear analytical studies. The Slowpoke-2 criticality benchmark experiment was performed at Royal Military College (RMC) in Kingston and at École Polytechnique of Montreal for newly developed Low Enrichment Uranium (LEU) fuel, and was thoroughly evaluated [1]. All these experiments were thoroughly analysed and obtained results were employed for various purposes: for testing of cross section libraries [1], to optimise irradiation facilities activity by using the Monte Carlo transport code MCNP 4A [13].

Deterministic codes such as DRAGON [7] and DONJON [5] treat neutron scattering in a different way. As the Slowpoke-2 benchmarks are highly sensitive to the scattering nuclear data , they were chosen to perform comparison of reactor physics parameters calculated by two different codes Monte Carlo neutron transport code MCNP 4A and deterministic codes DRAGON and DONJON.

The main objective of this work is to build the simulation model of the Slowpoke-2 research reactor located at the École Polytechnique of Montreal by using the DRAGON4 neutron transport code and DONJON4 diffusion code, and to verify calculated K_{eff} with experimental data.

In the first part of the paper, the computational model is presented (geometry, cross section library, etc.). In the second part, the DRAGON and DONJON results are compared against the experimental values and MCNP 4A calculations results.

2. SLOWPOKE-2 RESEARCH REACTOR

SLOWPOKE is an acronym for Safe Low Power Critical Experiment (Fig. 1). It is a low-energy, pool-type research reactor developed by Atomic Energy Canada Limited (AECL) in the late sixties as a Neuron Source for experiment, limited isotope production and Neutron Activation Analysis. Low cost, inherent safety (due to its limited excess reactivity and large negative temperature coefficient of reactivity) and simplicity of operation were primary consideration. The reactor provides a usable thermal neutron flux of $10^{12} neutron.cm^{-2}.s^{-1}$ at approximately $20Kw$ thermal power. Slowpoke-2 has five sample places in the beryllium radial reflector and five more sites in the water surrounding section of the reflector.

Irradiation capsule is transferred to and from the reactor using a compressed gas system in tube extending from the loading station to the sample site. Fig.1 shows the Slowpoke-2 reactor assembly.

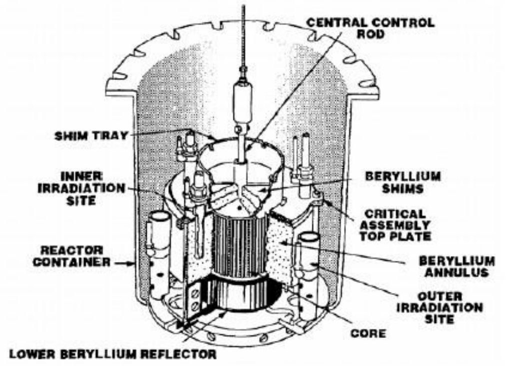

CRITICAL ASSEMBLY

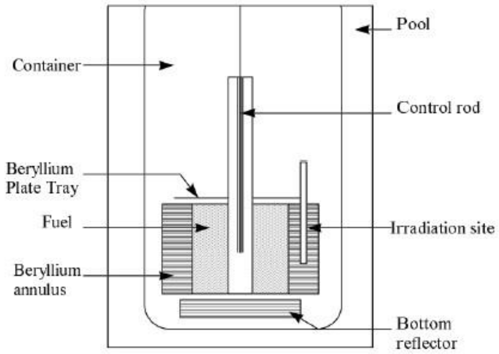

Fig. 1. Critical assembly and representation of the LEU SLOWPOKE-2 reactor

After twenty years of operating with Highly Enriched Uranium fuel (HEU), the HEU-fuelled SLOWPOKE reactor, installed at École Polytechnique of Montréal in 1976, will be replaced by Low Enriched Uranium fuel in September 1997. The Newly developed LEU fuel was used for the first time in the SLOWPOKE installed at the Royal Military College (RMC) in Kingston, Ontario in 1985 [13]. The newer LEU fuel is constructed in the same manner as CANDU (for CANada Deuterium Uranium) fuel, Zircalloy-Clad, but with 20% enrichment instead of Natural Uranium oxide [2]. The pool, reactor water container, light water moderator, beryllium reflector, Cadmium control rod and irradiation sites are the same as for the HEU-fuelled reactors. The details of the two types of SLOWPOKE-2 reactor cores are given in Table 1.

Table 1. SLOWPOKE-2 Design specifications

Core	**HEU**	**LEU**
Core diameter (mm)	220	220
Core height (mm)	228	234
Fuel	$U-Al$	UO_2
Cladding	Aluminium	Zircaloy-4
Number of fuel pins	296	198
Fuel density (g/cm^3)	3.45	10.6
Total mass of Uranium ((Kg)	0.9	5.6
Total mass of U^{235} (Kg)	0.82	1.12
Enrichment ($(\%\ of\ U^{235})$	93	19.89
Fuel length (mm)	225	234
Fuel pin diameter (with cladding) (mm)	5.23	5.26
Volume of water in core (L)	7.8	8.1

3. SIMULATION MODEL OF THE SLOWPOKE-2 REACTOR

Neutron distribution in the reactor can be predicted using the three main steps depicted in Fig. 2 [3]. The transport calculations were performed with the DRAGON4 (release 4.0.7) lattice code. The diffusion code DONJON4 was then used to compute multiplication factors.

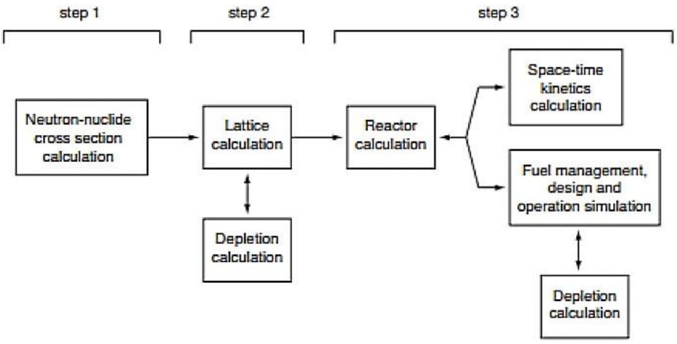

Fig. 2. Global computational scheme

3.1. Nuclear Data Library

IAEA Nuclear data Libraries updated in **WLUP** (**W**IMS **L**ibraries **U**pdates **P**roject) Project were used [11]. When the transport equation is solved and the thermal regions are homogenized, macroscopic properties are condensed to 4, 6 and 8 energy groups, as shown in Table 2, and then stored in the **COMPO** files. This file is directly accessed in the DONJON computation.

Table 2. The utilized energy spectra, with the upper and lower energy limits indicated

Groups	**Energy Spectra**	**4 Energy Groups**	
		Upper Energy (eV)	Lower Energy (eV)
1	Epithermal	1.0000E+07	5.5300E+03
2		5.5300E+03	4.0000E+00
3	Thermal	4.0000E+00	6.2500E-01
4		6.2500E-01	1.0000E-05

Groups	**Energy Spectra**	**6 Energy Groups**	
		Upper Energy (eV)	Lower Energy (eV)
1	Epithermal	1.0000E+07	8.2100E+05
2		8.2100E+05	5.5300E+03
3		5.5300E+03	4.0000E+00
4	Thermal	4.0000E+00	6.2500E-01
5		6.2500E-01	1.0000E-01
6		1.0000E-01	1.0000E-05

Groups	**Energy Spectra**	**8 Energy Groups**	
		Upper Energy (eV)	Lower Energy (eV)
1	Epithermal	1.0000E+07	8.2100E+05
2		8.2100E+05	5.5300E+03
3		5.5300E+03	2.7700E+01
4		2.7700E+01	4.0000E+00
5	Thermal	4.0000E+00	6.2500E-01
6		6.2500E-01	2.2000E-01
7		2.2000E-01	5.0000E-02
8		5.0000E-02	1.0000E-05

The WIMSD-IAEA-69 library is the WIMS Library Update Project 69-group nuclear data library [11], which was basically originated with the aim to introduce the most recent evaluated nuclear data files into research and power reactors neutronic calculations. The library has advantages over the older ones, and specifically it has been chosen as it is updated through the use of new and revised evaluated nuclear data files, it is well tested and benchmarked, and the library contains increased number of materials, resonance absorbers, etc.

For the proposed calculations the following libraries have been used: IAEA (WIMS library on 69 energy groups), ENDFB7 (WIMS library on 69 energy groups, based on ENDF/BVII.0 evaluated nuclear data library), JEFF31 (library on 69 energy groups, based on JEFF- 3.1 evaluated nuclear data), ENDFB6 (WIMS library on 69 energy groups, based on ENDF/B-VI evaluated nuclear data Library, JENDL3 (library on 69 energy groups, based on JENDL-3.2 evaluated nuclear data), JEF22 (library on 69 energy groups, based on JEF2.2 evaluated nuclear data).

3.2. DRAGON4 Modelling of the SLOWPOKE-2 Reactor

The DRAGON Transport Cell and Lattice Calculations Code (Fig. 3) is a multigroup transport theory lattice, cell and supercell code that can simulate the neutron flux distribution inside a unit cell or a fuel assembly in a nuclear reactor. It has been developed and continuously maintained at Institut de Génie Nucléaire, École Polytechnique de Montréal. It includes all of the functions that characterize a lattice cell code, namely: the interpolation of microscopic cross sections supplied by means of standard libraries; resonance self-shielding calculations in multidimensional geometries; multigroup and multidimensional neutron flux calculations.

This code is divided into many calculation modules, which are linked together by using the GAN generalized driver [8]. Here the exchange of information is ensured by well defined data structures. This is done so that new calculation techniques can be implemented in this code. It consists of many modules, which can be modified independently. It can be installed on workstation that support a FORTRAN compiler.

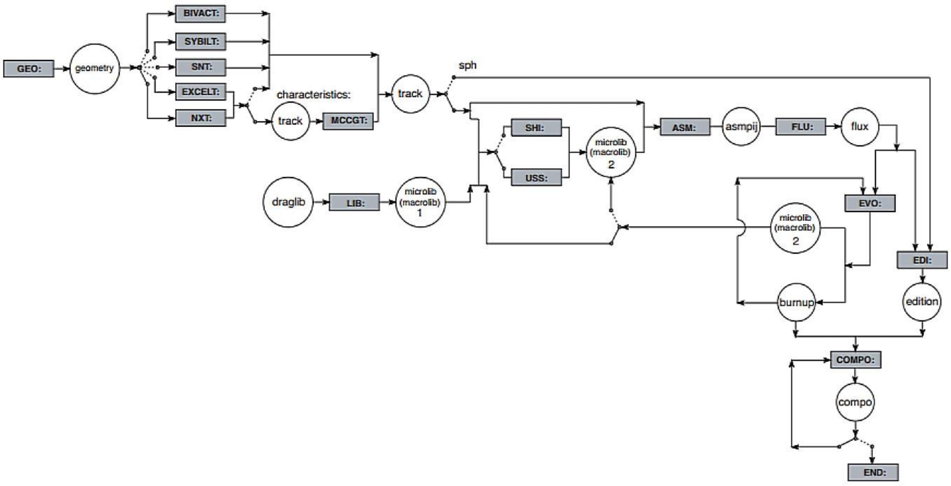

Fig. 3. Data flow diagram of DRAGON4 code

A SLOWPOKE model [4] is used to compute neutron transport. The geometry of the reactor core loaded by LEU is composed of eight different circular regions (Fig. 4).

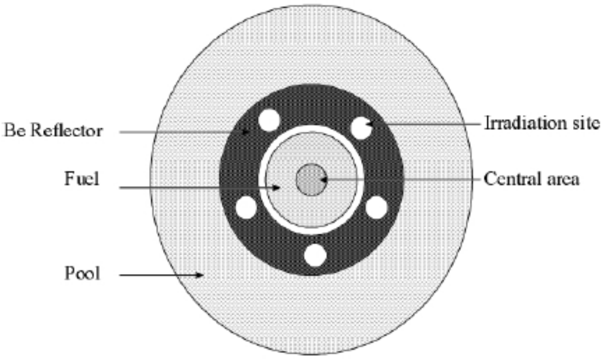

Fig. 4. 2D Transport model (DRAGON4)

For accounting the leakage effects, a B_1 homogeneous model [8] is used in DRAGON4. After having fixed an initial value of buckling B^2 and a first estimate of the cross section, flux and the eigenvalue K_{eff} are calculated by solving the transport equation. Then a new value of B^2 is calculated along with a new group-dependent leakage coefficient d_g. The total cross section is increased by amount of $d_g B^2$:

$$\Sigma_{t,g}^{corr} = \Sigma_{t,g} + d_g B^2 \tag{1}$$

A new B^2 value is then calculated. The iteration ends when the value of K_{eff} becomes equal to one. The value of B^2 is then used to calculate the diffusion coefficients. The nuclear properties are homogenized and condensed with 4, 6 or 8 energy groups. The intervals of energy of the groups are presented in Table 2.

3.3. Diffusion Calculations for the SLOWPOKE-2 reactor using DONJON4 code

DONJON is its sister code, designed to for the full reactor core modelling in 3D Cartesian and other geometries. The modelling of the fuel lattice is done through defining the number of channels and bundles for each channel and each channel is recognized by specified names. Using either instantaneous or time-average methods, the interpolation of fuel properties with respect to fuel burnup can be achieved [2] (Fig. 5).

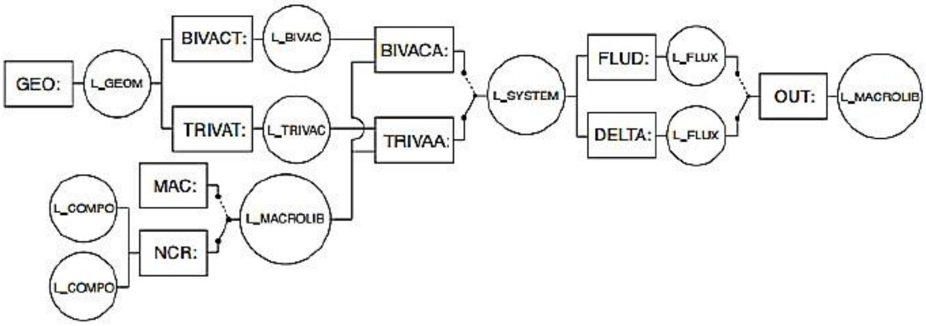

Fig. 4. Data flow diagram of DONJON4 code

The COMPO file and the 3D diffusion model (Fig. 5) are used in the DONJON code to solve the multigroup diffusion equation:

$$A_{gg}\vec{\phi}_g = \sum_{\substack{h=1 \\ h\neq g}}^{G} A_{gh}\vec{\phi}_h + \frac{1}{K_{eff}}\sum_{h=1}^{G} B_{gh}\vec{\phi}_h, \qquad (2)$$

where: A_{gg}: Matrices composed of the diffusion terms; A_{gh}: Scattering matrices; B_{gh}: matrices containing the neutron production terms; K_{eff} : Eigenvalue; $\vec{\phi}_g$: Fluxes

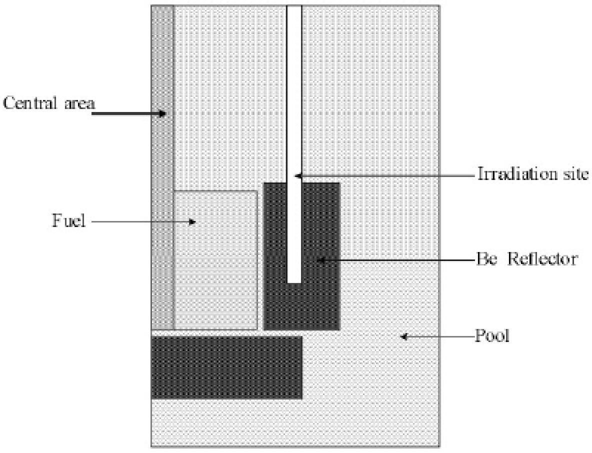

Fig. 5. 3D diffusion model (DONJON4)

The values of the coefficient K_{eff}, as well as fluxes at the various points of the reactor are calculated. Using the **INIRES** module in the DONJON4 code we recovered the flux values in the holes of interest [2].

3.4. Reactivity calculations of the SLOWPOKE-2 research reactor

The reactivity multiplication factor K_{eff} is by far the most important parameter in the reactor analysis and it depends on the material composition and its distribution in the core, and the geometry of the core, also excess reactivity of the core which is a measure of the departure from criticality, which is given in two equivalent units, mk and pcm, by:

$$\rho = \frac{K_{eff} - 1}{K_{eff}} \tag{3}$$

The reactivity and effective multiplication factors were calculated using the diffusion code DONJON4 in 3D geometry, based on macroscopic cross sections libraries generated using the DRAGON4 lattice calculation code, and IAEA Nuclear data Libraries updated in WLUP (WIMS Libraries Updates Project) Project. The effective multiplication factors were calculated for water moderator temperature varying from 10°C to 80°C, and for fuel temperature up to 300°C without the control rod using the 4, 6 and 8 energy groups condensed libraries.

4. RESULTS AND DISCUSSIONS

Experiments and Monte Carlo simulation were done in the LEU Slowpoke-2 reactor at Royal Military College (RMC) [13]. The results of excess reactivity are presented in the Table 3.

Table 3. Criticality calculations results at 20°C

	Experimental reactivity	MCNP 4A calculated reactivity
Excess reactivity in (mK)	3.15	3.17
Multiplication factor K_{eff}	1.003159954	1.003180081

The multiplication factor of the reactor was determined for the control rod in its fully out position , for water temperature over a range of temperature from 10°C to 80°C , and for fuel temperature up to 300°C. The excess reactivity is calculated by equation 3.

Table 4. Comparison of calculated K_{eff} for 6 energy groups

Water Temperature in °C	IAEA	ENDFB7	ENDFB6	JEF22	JENDL3	JEFF31
10	0.9992397	0.9968133	0.9968586	0.9873284	0.9973431	0.9982668
20	1.000005	0.9975605	0.9975725	0.9879614	0.9980869	0.9989496
30	1.000312	0.997824	0.9978272	0.9881198	0.9983872	0.999168
40	1.000236	0.9976966	0.9977014	0.9879002	0.9982942	0.9989946
50	0.9998402	0.9972276	0.9972412	0.9873366	0.9978672	0.9984828
60	0.9991221	0.9964401	0.9964766	0.9865912	0.9971423	0.9977437
70	0.9981301	0.9953685	0.995428	0.9855618	0.9961377	0.996707
80	0.9968938	0.9940504	0.9941283	0.9842524	0.9948805	0.9954075

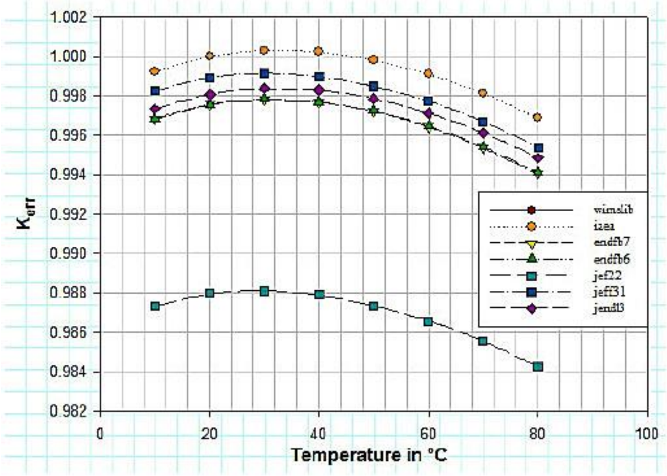

Fig. 6. K_{eff} as a function of moderator temperature and cross section library for SLOWPOKE-2 reactor with 6 energy groups

Table 4. Comparison of Excess reactivity for 6 Energy groups

Water Temperature in °C	IAEA	ENDFB7	ENDFB6	JEF22	JENDL3	jeff31
10	-0.7608785	-3.19688752	-3.15129949	-12.8342302	-2.66397792	-1.7362092
20	0.00499998	-2.44546571	-2.4334071	-12.1852939	-1.91676697	-1.0515045
30	0.31190269	-2.1807453	-2.17753134	-12.0230361	-1.61540533	-0.8326928
40	0.23594432	-2.3087179	-2.30389573	-12.2479983	-1.70871473	-1.00641185
50	-0.15982554	-2.78010757	-2.76643203	-12.8258185	-2.13735856	-1.51950539
60	-0.87867139	-3.57261816	-3.53585824	-13.5910395	-2.86588985	-2.2614024
70	-1.87340308	-4.6530506	-4.59299919	-14.6497155	-3.8772752	-3.30387968
80	-3.11587854	-5.9852096	-5.90638049	-15.9995546	-5.14584415	-4.61368836

Table 5. Comparison of criticality calculations results for SLOWPOKE-2 reactor at 20°C

	Experimental reactivity (mK)	MCNP 4A calculated reactivity (mK) (ENDF/B-V library)	DRAGON4/DONJON4 calculated reactivity (mK)		DRAGON4/DONJON 4 calculated K_{eff}	
4 Energy Groups	**3.15** (K_{eff} =1.003159954)	**3.17** (K_{eff} =1.003180081)	**IAEA**	23.6701411	**IAEA**	1.024244
			ENDFB7	20.9161679	**ENDFB7**	1.021363
			JENDL3	23.250544	**JENDL3**	1.023804
6 Energy Groups			**IAEA**	0.00499998	**IAEA**	1.000005
			ENDFB7	-2.44546571	**ENDFB7**	0.9975605
			JENDL3	-1.91676697	**JENDL3**	0.9980869
8 Energy Groups			**IAEA**	-1.6025641	**IAEA**	0.9984
			ENDFB7	-4.09308505	**ENDFB7**	0.9959236
			JENDL3	-3.7209945	**JENDL3**	0.9962928

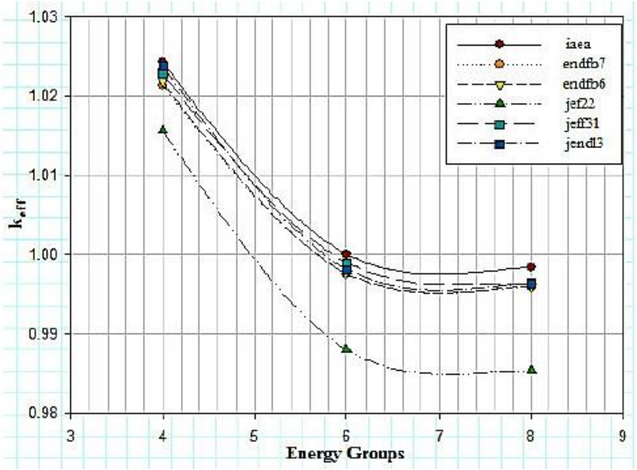

Fig. 7. K_{eff} as a function of energy groups number for SLOWPOKE-2 reactor with 6 energy groups

Generally, the criticality calculations results show good agreement with the references specially for six and eight energy groups calculations, as shown in Table 5 and Fig. 7.

The reactivity feedback effect due to temperature changes were calculated by treating the four variables: coolant temperature, cross section library, number of energy groups (condensed) and the tracking module. A series of DRAGON4/DONJON4 calculations were done for coolant temperature varying from 10°C to 80°C for IAEA Nuclear data Libraries updated in WLUP, 4, 6 and 8 energy groups and finally for EXCELT and NXT tracking modules.

This Simulation clearly display the inherent safety of the LEU fuelled SLOWPOKE-2 research reactor and the validity of this calculational route to simulate the neutronic behaviour of research reactor.

5. CONCLUSION

The simulation of the SLOWPOKE-2 research reactor employing deterministic method was successfully accomplished using the calculation approach: IAEA Nuclear data Libraries updated in WLUP (WIMS Libraries Updates Project) Project / DRAGON4 lattice and cell calculations code/ DONJON4 core calculations code. The main advantages of DRAGON4/DONJON4 codes namely: the interpolation of microscopic cross sections supplied by means of standard libraries; resonance self-shielding calculations in multidimensional geometries; multigroup and multidimensional neutron flux calculations.

REFERENCES

1. HAJJAJI, O EL. (1999). La physique du réacteur SLOWPOKE-2 de l'école polytechnique. PhD. École Polytechnique de Montréal, Montréal.
2. NOCEIR S., HAJJAJI O. EL, VARIN E., ROY R., ROZON D. Diffusion Calculations for SLOWPOKE-2 Reactor Using DONJON, Proceeding 18th Annual Conference of the Canadian Nuclear Society, Toronto, Ontario, June (1997), Vol. 2.
3. HÉBERT, A. (2009). Applied reactor physics (3éd). Montréal: Edition de école Polytechnique de Montréal.

4. MARLEAU, G., NOCEIR, S., ROY, R. (1997). DRAGON modelling of the SLOWPOKE-2 reactor at Ecole Polytechnique. Annual Conference of the Canadian Nuclear Association. (Vol. 1, p.227–239). Montréal.
5. SEKKI, D., HEBERT, A. et CHAMBON, R. (2011). A user guide DONJON Version 4.
6. TOWNES, B.M., HILBORN, J.M. The SLOWPOKE-2 reactor with low Enrichment uranium oxide fuel. Annual Conference of the Canadian nuclear society, (1985), (p., 1–7), Ottawa.
7. MARLEAU, G., HEBERT, A. et ROY, R. (2011). A user guide for DRAGON Version 4.
8. ROY, R. et HEBERT, A. (2000). The GAN generalized driver. Rapport technique IGE 158, Institut de Génie Nucléaire.
9. BELL, G.I., GLASSTONE, S. (1970). Nuclear reactor theory. New York: Van Nostrand Reinhold Company.
10. ZKIEK, A. et MARLEAU, G. (2007). DRAGON Verification: the NXT: Module. Technical Report IGE-299, Revision 0, Institut de Génie Nucléaire, école polytechnique de Montréal.
11. IAEA (2005). WIMS. Website. <http://www-nsd.iaea.org/wimsd/>.
12. S. NOCEIR, E., VARIN, ROY R. (1996), « HEU and LEU fuelled SLOWPOKE Reactor Modelling », Report IGE-216, école Polytechnique de Montréal.
13. PIERRE, J.R.M., BONIN, H.W. (1999). Monte Carlo Simulation of the LEU-Fuelled SLOWPOKE-2 Nuclear Reactor MCNP A4. Nuclear Technology, Vol. 125.

UNCERTAINTY ANALYSIS OF SEVERE ACCIDENT IN THE SPENT FUEL POOL

A. Šutas
Lithuanian Energy Institute
Breslaujos str. 3, LT-44403 Kaunas
Phone +37062951775
Email: Antanas.Sutas@lei.lt

V. Vileiniškis
Lithuanian Energy Institute
Breslaujos str. 3, LT-44403 Kaunas
Phone +37037401928
Email: Virginijus.Vileiniskis@lei.lt

ABSTRACT

The wider research of the phenomena of severe accidents in the spent fuel pools due to the loss of water was started after the accident in Fukushima Daiichi NPP. The main measure to prevent an occurrence of such an accident is a restoriation of a water supply. Moreover, it is extremely important to restore cooling function until fuel bundles are not yet dangerously overheated, when the temperature of fuel rods exceeds the threshold of the intensive steam-zirconium reaction. Otherwise, exothermic steam-zirconium reaction will take place and significant amounts of additional heat will be released, which accelerates breaching of the fuel rods, as well as generation of significant amounts of hydrogen, which can cause an explosion.

The purpose of this paper is to analyze phenomena that occur in a spent fuel pool during a severe accident due to loss of collant and to determine the impact of uncertainties of spent fuel pool model parameters on the amounts of generated hydrogen.

This paper presents a numerical analysis of phenomena that occur during a severe accident due to loss of water in the spent fuel pool. The analysis was performed with ASTEC programe package. Processes which take place during a restoration of a water supply as well as uncertainties of spent fuel pool model parameters and it's influence on accidents consequencies are also discussed.

Keywords: spent fuel pool, hydrogen generation, ASTEC computer code.

1. INTRODUCTION

The significant technical aspects of spent fuel pools (SFP) are:

- Permanent cooling is necessary due to decay heat from spent fuel rods;
- Water layer above spent fuel assemblies in SFP is necessary due to cooling function assurance as well as plant personel protection from ionizing radiation.

The main reason for a severe accident in a spent fuel pool is loss of coolant scenario. According to the NRC data, the probability of such an event is about 10^{-6} per pool per year [1].

Critical time moment in a SFP accident scenario is time when water level drops below the top of fuel bundles. This increases ionizing radiation dose to pool service personal and limits personal actions to manage an accident. For example, water levels drop in three meters induces 9-fold increase in radiation dose [2].

The Tsunami that followed the earthquake at the Fukushima Daiichi nuclear plants in Japan [3] showed that a loss of heat removal in the spent fuel pools may lead to very serious consequences. During Fukushima accident water level in SFP decreased about 7 m and only

1.5 m thickness water layer left above the top of spent fuel assemblies. Water leakage was stoped and nondesign water injection sources were used to restore the initial water level [4].

This paper describes a severe accident scenario at Ignalina NPP SFP due to a loss of water analysis as well as the influence of model parameters uncertainties on accidents consequencies and generated hydrogen amounts when water supply is restored at two different time moments and calculations are performed using maximum and minimum values of uncertain parameters. The results of this analysis can be used for evaluation of accident management strategies used in other nuclear power plants with RBMK reactors under operation as well as for plants with other types of reactors.

2. METHODOLOGY

2.1 SFP design

The whole complex of storage pools of the spent fuel storage and handling system comprises 12 pools (see Figure 1) which are detailly described in the SAFETY ANALYSIS REPORT FOR INPP UNIT 2 [5]. They are as follows:

- Two pools (Rooms 236/1, 236/2) intended to store spent fuel assemblies after they are extracted from the reactor;
- Five pools (Rooms 336, 337/1, 337/2, 339/1, 339/2) intended to store spent fuel fragmentized assemblies placed in baskets;
- Pool (Room 234) intended to accumulate spent fuel assemblies prepared to be fragmentized, to cut suspension brackets from the spent fuel assemblies, transport spent fuel assembly to the “hot” cell and full 102 placed transport baskets from the “hot” cell to the storage pools;
- Two pools (Rooms 338/1, 338/2) intended to perform operations to load the transport baskets with the spent fuel assemblies into the transport casks and store the 102 placed transport baskets when the storage pools hall is under repair;
- Transport corridor (Room 235) intended to transport spent fuel assemblies and transport baskets loaded with spent fuel assemblies between the pools;
- Transport corridor (Room 157) intended to transport fresh fuel and reactor assemblies from the fresh fuel assembly preparation bay of Storage Pools Hall to the reactor and return spent fuel and reactor assemblies from the reactor to the storage pools.

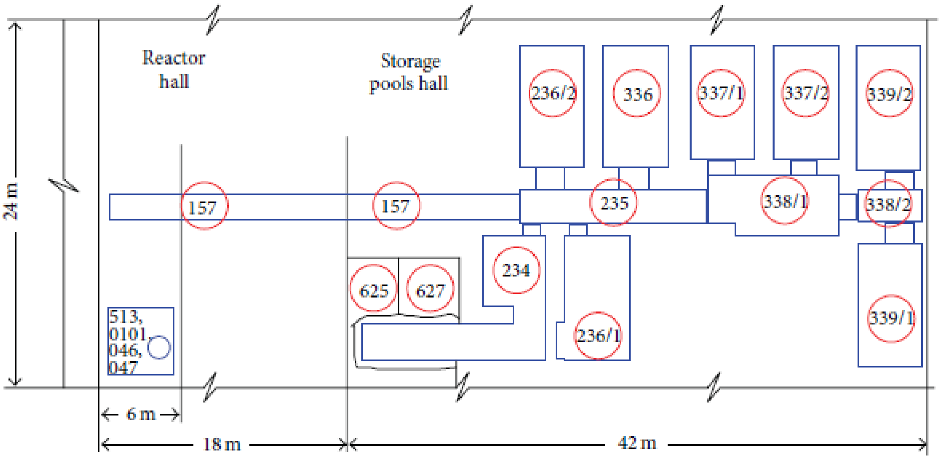

Fig. 1. Layout of buildings in storage pools hall at Ignalina NPP Unit 2

2.2 Modelling methodology

The numerical modelling was performed using ASTEC program package [6]. ASTEC code has a modular structure and was designed to evaluate an accident source term. The modeling was performed with ICARE module which is a part of ASTEC V2.0R2 code. The ICARE module simulates in-vessel core degradation and thermal-hydraulics. It computes behaviour of in-vessel structures, thermal-hydraulics for water, steam and non-condensable gases, chemical reactions between materials, thermal and mass transfers between components.

Table 1 presents general parameters of water, water level dynamics and pool structure, which model is presented at Fig. 2. The initial water leakage rate is 21.1 kg/s. It is assumed that water leakage rate decreases due to decreasing volume of water mass in the pool. At the time t = 76.7 h all water is leaked from the pool. Further no operator actions is done up to time moments of t_1 = 93.1 h and t_2 = 101.9 h ($t_{1;2}$ is a start moment of water injection for different calculations) when water injection with injection rate of 27.8 kg/s starts.

Table 1. General modelling parameters

Total power of SFA, kW	4253
Water level, m	16.9
Water volume in SFP, m^3	5070
Initial water temperature, °C	50
Water leakage rate, kg/s	21.111
Outside wall thickness, m	0.5
Cooling of outside wall of SFP	Constant heat transfer coefficient (5W/m^2)

The main data used in calculations for fuel rod models “ROD1”, “ROD2”, “ROD3” and “ROD4” is presented in Table 2.

Table 2. Parameters of groups of Spent Fuel Assemblies (SFA) in ASTEC model, according situation at 2009

Groups	**Group of SFAs in ASTEC model**	**Assumed storage time in SFP**	**SFA decay heat, kW**	**Amount of SFAs in group**	**Group power, kW**
SFAs in 236/2 room	ROD1	8 days	5.21	166	864.9
SFAs in 236/2 room	ROD2	137 days	1.281	1182	1514.1
SFAs in 236/1 and 234 rooms	ROD3	2 years	0.489	892	436.2
SFBs in shipping casks	**ROD4**	3 year	0.254	5661	1437.9
Total:				7901	4253

In ASTEC code al rooms of SFPs and fuel assemblies are modeled as a single pool with 4 different groups of spent fuel assemblies (Table 2 and Fig. 2). It is assumed that heat from the pool to the environment is transferred through the walls of SFP. In the model SFP and a hall is modeled as a single element with a direct connection between SFP and the environment. Heat removal from outside of SFP to the environment is modeled through the heat structure POOLWALL using selected heat transfer coefficient. As it is mentioned above, all fuel assemblies are divided into 4 groups with different decay heat levels (Table 2). These decay values of spent fuel assemblies in the pool presents the situation at the moment of final shutdown of Ignalina NPP Unit 2 at the end of year 2009 [7].

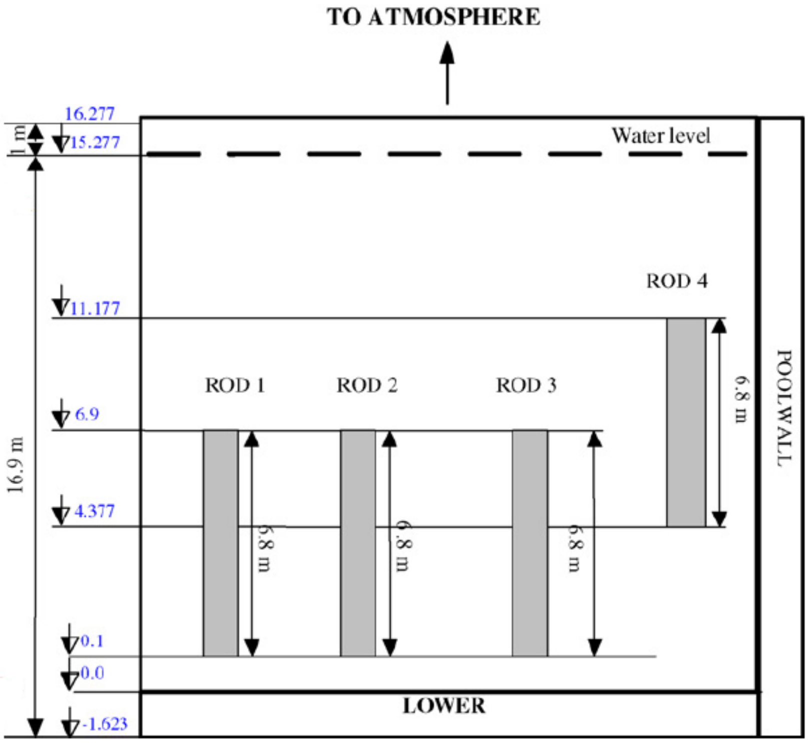

Fig. 2. SFP and SFAs nodalization scheme in ASTEC model.

2.2.1. Selection of uncertain parameters

Table 3 presents 9 parameters which can be considered as uncertain. Uncertainty range is set equal to 10 %, except for pool wall outer temperature and water temperature which uncertainty range is 5 K, what is also equal to 10 % if temperatures are taken in °C. Methodology of setting of uncertainty range is not discussed in this paper as this uncertainty analysis is a first step of full uncertainty – sensivity analysis which will be performed in the future. 10 % uncertainty range for all uncertain parameters is set as probable according to previous experience on evaluation of values of these 9 parameters. Pool wall thickness and pool model upper coordinate can be considered as uncertain because practically surface of ceiling and wall of spent fuel pool are not flat and contains various cavities for equipment. Pool wall outer temperature and water temperature in the model is an average temperature which differs in different points and setting of average value is a approximation which gives some uncertainties. Setting of maximum power of fuel assemblies in the same group is also a process with some uncertainties as power of each fuel assembly in the same group can differ from the average value which is set for that group. Thermal properties of zirconium and uranium dioxide is dependant on the temperature which varies in a range of several thousands of degrees in these calculations.

Table 3. Uncertain parameters and it’s variation limits

Parameter	**Basic value**	**Variation limits**
Power of fuel assembly	4.25 MW	±10 %
Pool wall outer temperature	298.15 K	±5 K
Pool wall thickness	0.5 m	±10 %
Water temperature	323.15 K	±5 K
Pool model upper coordinate	16.27 m	±10 %
Zirconium specific heat	285-340 J/(kg*K)	±10 %
Zirconium thermal conductivity	17-33.4 W/(m*K)	±10 %
Uranium dioxide specific heat	261-662 J/(kg*K)	±10 %
Uranium dioxide thermal conductivity	8.15-3.0 W/(m*K)	±10 %

Figs. 3 and 4 presents temperaturical dependence of thermal conductivity and specific heat for zirconium and uranium dioxide. 3 values are represented: basic value (middle line) with minimum and maximum values for A and B calculations, which are defined in the next paragraph.

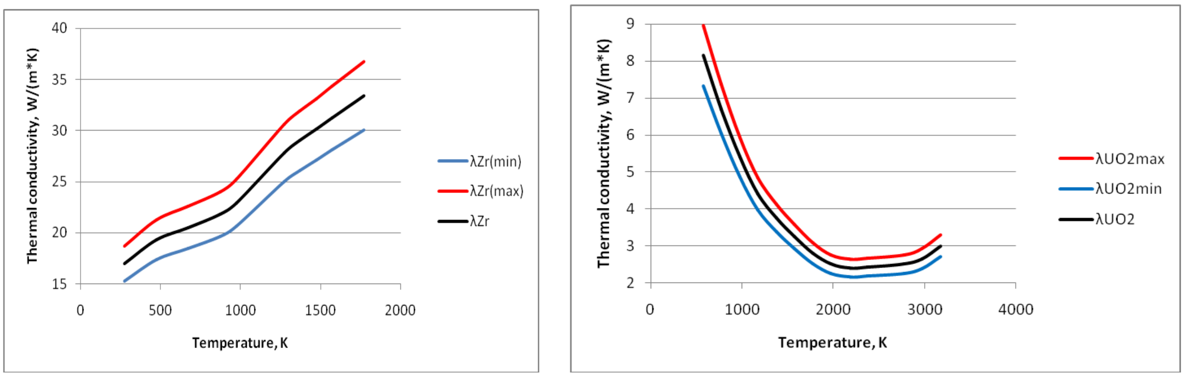

Fig. 3. Thermal conductivity of zirconium and uranium dioxide and it’s variation limits

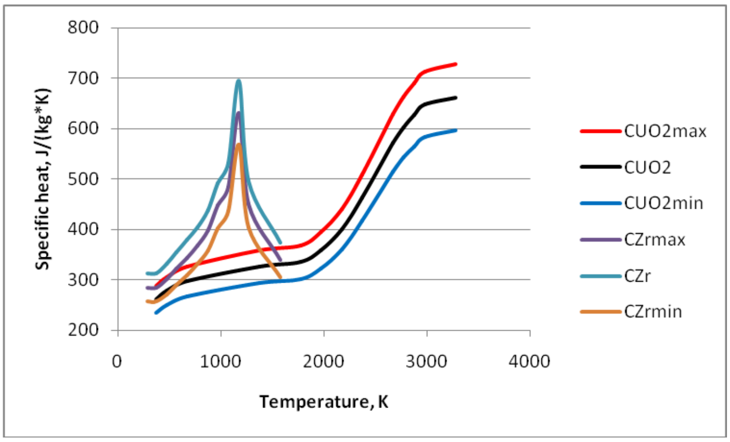

Fig. 4. Specific heat of zirconium and uranium dioxide and it’s variation limits

2.2.2. Setting of a uncertainty influence interval

First of all, it is important to emphasize that 6 different calculations were performed. Calculation with minimum values of uncertain parameters No. 1–4, maximum values of parameters No. 5–9 and without water supply restoration is called "A" calculation and calculation with maximum values of uncertain parameters No. 1–4, minimum values of parameters No. 5–9 and without water supply restoration is called "B" calculation. Increasing values of parameters No. 1–4 leads to more intense heating in the pool: fuel assemblies with higher power generates more heat, thicker pool wall with higher outer temperature determines the lower heat transfer throw pool wall coeficient, higher initial water temperature determines greater amount of heat accumulated in a system at the start of calculations. On the other hand, increase in parameters No. 5–9 leads to the conditions when better heat transfer in fuel assemblies is achieved (higher thermal conductivity of zirconium and uranium dioxide) and more heat is needed to increase the temperature of a system (greater specific heat of zirconium and uranium dioxide and greater volume of a pool when pool height is increased). Parameters of "A" calculation is selected in a such a way as to obtain the lowest (minimum) temperatures in the pool. "B" calculation is an opposite case to "A" calculation. For setting of water supply restoration time for A and B calculations a temperature of 1500 K was chosen as a critical point when rapid zirconium oxidation reaction starts. Time moment when maximum temperature of spent fuel assembly reaches value of 1500 K was chosen for a start of water supply from the bottom of a pool for calculations using maximum (B-1 calculation) and minimum (A-2 calculation) values of parameters, i.e. calculation A with water supply restoration at time moment t2=101.9 h is calculation A-2 and calculation B with water supply restoration at time moment t1=93.1 h is calculation B-1. Calculation A-1 is compiled using calculation A with water supply restoration at time t1 and calculation B-2 is the same calculation B just with restoration of water supply at time moment t2. This methodology is presented in Fig. 5. Values of uncertain parameters with time moments for water supply restoration for all 6 calculations is presented in Table 4.

Table 4. Values for uncertain parameters and time moments for setting of water supply restoration moment

	Calculations					
Parameter	**A**	**B**	**A-1**	**A-2**	**B-1**	**B-2**
Power of fuel assembly	-10%	+10%	-10%	-10%	+10%	+10%
Pool wall outer temperature	-10%	+10%	-10%	-10%	+10%	+10%
Pool wall thickness	-10%	+10%	-10%	-10%	+10%	+10%
Water temperature	-10%	+10%	-10%	-10%	+10%	+10%
Pool height	+10%	-10%	+10%	+10%	-10%	-10%
Zirconium specific heat	+10%	-10%	+10%	+10%	-10%	-10%
Zirconium thermal conductivity	+10%	-10%	+10%	+10%	-10%	-10%
Uranium dioxide specific heat	+10%	-10%	+10%	+10%	-10%	-10%
Uranium dioxide thermal conductivity	+10%	-10%	+10%	+10%	-10%	-10%
Time moment, when maximum temperatures reached 1500K, h	101.9	93.1	96.7	101.9	93.1	93.1
Time moment, when the water injection starts, h	-	-	93.1	101.9	93.1	101.9

This methodology encloses how particular uncertainties of some parameters can influence on actions of operator who observes a temperature of fuel assemblies as the only characteristic of severe accident state. The results of such analysis is presented in the next paragraph.

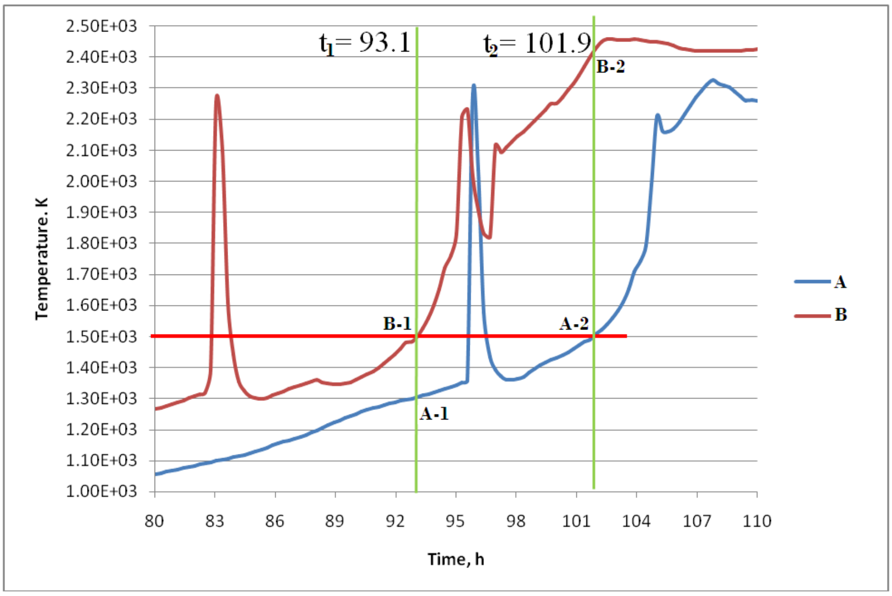

Fig. 5. Maximum temperatures of fuel assemblies for sets with maximum and minimum modelling parameters and setting of a time moment of water supply restoration

3. MODELLING RESULTS AND DISCUSSION

A progression of severe accident in spent fuel pool with loss of water incident, fuel assemblies overheating and restoration of water supply can be divided into 7 stages, which are separated by these moments:

- "I" moment: uncovering of SFA's in ROD4 group;
- "II"moment: all fuel assemblies in a SFP become fully uncovered;
- "III" moment: deformation and balooning of fuel rods claddings (T>1100K);
- "IV" moment: temperature reaches 1500 K – start of strong hydrogen generation reaction;
- "V" moment: start of fission product release;
- "VI" moment: start of water injection;
- "VII" moment: temperature of overheated (A and B) or cooled (A-1;2, B-1;2) fuel rods reaches constant value.

Table 4 presents masses of generated hydrogen and time moments of the abovementioned events occurrence in each of 6 calculations.

Table 5. Generated hydrogen and accident phases occurrence moments for 6 modelling cases

Case Nr.	**Accident phase and it's occurrence time moment (hours)**							**Generated hydrogen mass (M_{H2}), kg**	***$M_{H2}/M_{H2(theor.)}$**, %***
	I	**II**	**III**	**IV**	**V**	**VI**	**VII**		
A	**15.8**	**69.75**	82.8	95.33	95.83	-	319.4*	260	2
B	**15.7**	**61.25**	67.7	82.56	82.8	-	232.8*	331	3
A-1	**15.8**	**69.75**	82.8	93.4	93.9	93.1	116.7	1603	14
A-2	**15.8**	**69.75**	82.8	93.4	93.9	101.9	119.7	1713	15
B-1	**15.8**	**61.25**	67.7	82.54	82.8	93.1	118.9	9331	80
B-2	**15.8**	**61.25**	67.7	82.54	82.8	101.9	120.6	8179	70

*temperature of overheated rods reaches constant value of T=2450 K;

**For theoretical evaluation of maximum hydrogen mass $M_{H2(theor.)}$ generated during zirconium oxidation reaction it is necessary to analyse an equation of pure zirconium and water vapour reaction:

$$Zr + 2H_2O \rightarrow ZrO_2 + 2H_2. \tag{1}$$

If expressed (1) equation through moles and molar masses one may write:

$$1\,\text{mol} \times 91.2\frac{g}{\text{mol}} + 2\,\text{mol} \times \left(2 \times 1\frac{g}{\text{mol}} + 16\frac{g}{\text{mol}}\right) \rightarrow 1\,\text{mol} \times \left(91.2\frac{g}{\text{mol}} + 2 \times 16\frac{g}{\text{mol}}\right) + 2\,\text{mol} \times 2 \times 1\frac{g}{\text{mol}}. \tag{2}$$

After simplification (2) Equation can be expressed in grams:

$$91.2\text{ g } Zr + 36\text{ g } H_2O \rightarrow 123.2\text{ g } ZrO_2 + 4\text{ g } H_2. \tag{3}$$

From (3) Equation it is obvious, that 91.2 g of reacted zirconium gives 4 g of hydrogen generated. To sum up it can be stated that during a reaction of 1 kg pure zirconium with water steam 43.9 g of hydrogen gass is generated.

For theoretical evaluation of maximum hydrogen quantity which can be generated in Ignalina NPP spent fuel pool from all 7901 fuel assemblies, overall mass of zirconium in a system should be multiplied by 43.9 g of hydrogen. This gives that theoretically 11.637 kg of hydrogen can be generated if all zirconium in a system of SFP is oxidized.

Accident phases I–V in "B" calculation occure earlier than in "A" calculation. The main difference between A and B type calculations appears with a start of water injection at time moments t_1 and t_2. Analyzing generated hydrogen amounts (Fig. 6), A and B calculations give the difference of 27%. These two calculations are unfavourable for hydrogen generation (only 2–3% of total theoretical mass of hydrogen is generated) due to lack of water. However, operator can not choose this accident management mode due to uncontrolable overheating of fuel rods and further melting and melt debris accumulation on the floor in a pool.

Taking into account calculations with water supply restoration and the results of generated hydrogen mass, dramatic distinctions are observed. The difference between A-1;2 and B-1; 2 calculations in generated hydrogen mass is equal to 5–6 times. B-1 and B-2 calculations present situation when 70–80% of the whole zirconium in a pool is oxidized. From this it can be concluded that for a severe accident management it is essential to have an equipment with the highest possible accuracy and also qualitative methodologies for determination and monitoring spent fuel pool parameters. Even slight uncertainties can determine severe consequencies with a huge amount of generated hydrogen which can react with air oxygen and cause an explosion in a spent fuel building – loss of the only physical barrier between SFP and environment causes huge amounts of radionuclides releases.

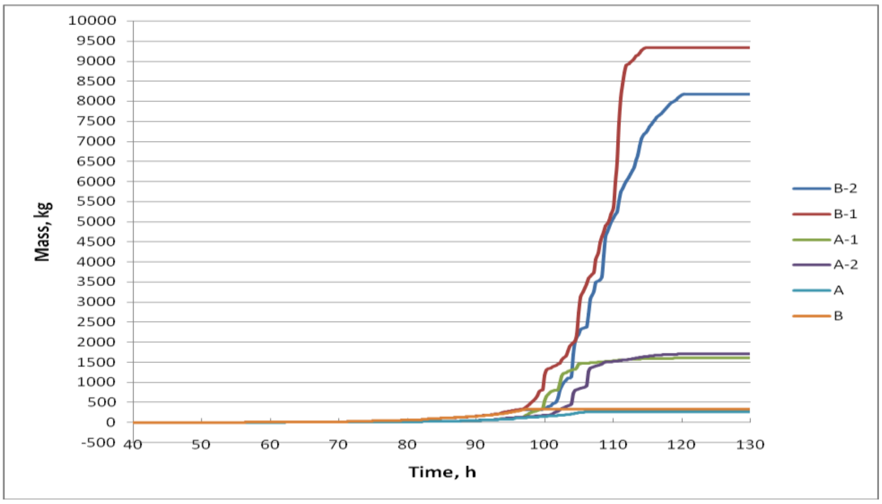

Fig. 6. Generated hydrogen masses for 6 modelling cases

As it can be seen from Fig. 6, the amount of generated hydrogen in B-1 calculation is higher than in B-2 calculation despite the fact that temperatures of fuel rods just before the start of water supply is higher in calculation B-2 (Fig. 7) and at this case fuel bundles are kept overheated for t_2-t_1= 8.8 h longer than in B-1 calculation. This fact can be explained as the result of longer preoxidation phase in B-2 than in B-1 what gives thicker zirconium oxide film when claddings are oxidizing in air atmosphere. If comparing mass of zirconium dioxide (oxidized zirconium) which was generated before temperature reaches 1500 K with the overall mass generated, B-2 case gives 0.92% and B-1 case gives 0.78%. This means that zirconium oxidation reaction during preoxidation phase (the result of which is formation of an oxide film) in B-2 case was also more intensive than in B-1 case. Thicker oxide film ensures better protection for further zirconium oxidation when water is supplied to a pool and quenching of overheated bundles is performed.

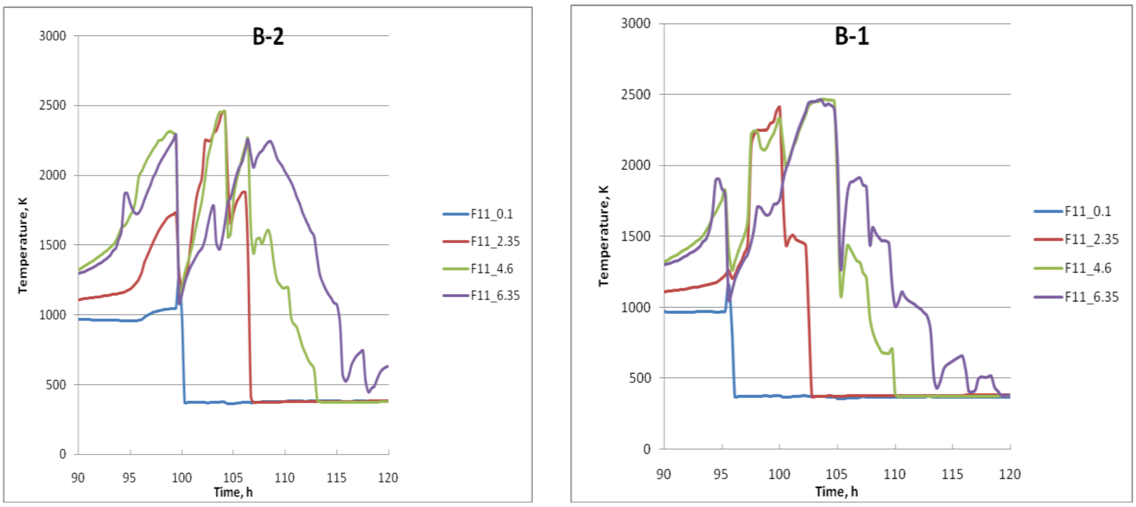

Fig. 7. Temperatures of ROD1 group fuel claddings at 4 different elevations (m) for B-1 and B-2 calculations

4. CONCLUSIONS AND RECOMMENDATIONS

For a selected ranges of uncertainties, time difference for a start of rapid zirconium oxidation and fission product release is up to 11 hours.

Generated hydrogen amount is very sensitive to the range of uncertainties (10 % range of uncertainties results in from 5 to 6 times difference in generated hydrogen mass) so it is extremely important for spent fuel pool parameters determination to select equipment and methods as exact as possible.

REFERENCES

1. COLLINS, T.E., HUBBARD G. "Technical study of spent fuel pool accident risk at decommissioning nuclear power plants," Tech. Rep. NUREG-1738, NRC, Washington, DC, USA, 2001.
2. Electric Power Research Institute, Vol. 2: The Physics of Accident Progression, Final Report, California, USA, October 2012.
3. http://fukushima.ans.org/
4. YANG R., RAHN F. "Fukushima Technical Evaluation," Final Report, EPRI, California, USA, February 2013.
5. PENKOV V. "System for storing and handling of spent nuclear fuel", Safety analysis report for Ignalina NPP UNIT 2, System for storing and handling of spent nuclear fuel safety analysis report for inpp unit 2, chap. 16, sect. 16.5, p. 6, 2002.
6. J. VAN DORSSELAERE, SEROPIAN C., CHATELARD P., et al. "The ASTEC integral code for severe accident simulation," Nuclear Technology, vol. 165, no. 3, p. 293–307, 2009.
7. The maintenance instruction of a complex of systems for storage and handling with nuclear fuel in the fuel pools – 1, 2 at Ignalina NPP, Code of document PTOed-0912-286V3, Ignalina NPP.

CYSENI 2015, May 27–28, Kaunas, Lithuania
ISSN 1822-7554, www.cyseni.com

INVESTIGATION OF DEMO STRUCTURAL MATERIAL CHARACTERISTICS INDUCED BY NEUTRON IRRADIATION

A. Tidikas
Lithuanian Energy Institute
Breslaujos str. 3, LT 44403 Kaunas - Lithuania
Phone +370 401941
Email: Andrius.Tidikas@lei.lt

ABSTRACT

In this work examination of possible structural materials for DEMO nuclear fusion reactor is being carried out. Main subjects of interest are reduced activation ferritic/martensitic and other steels that are used in reactor design (divertor, first wall and breeding blanket). Simulation of neutron irradiation in bulk material is being performed by using activation system program “FISPACT”. Neutron flux is selected in accordance with real neutron flux of the DEMO fusion reactor. After the irradiation certain properties of materials are being analyzed such as induced total activity, fission heat output, gamma dose rate as well as possible ingestion and inhalation doses by released radionuclides. Research is concluded by comparison between different materials as well as experiment validation with regard to other scientific papers.

Keywords: nuclear fusion, DEMO, FISPACT, neutron activation, irradiation

1. INTRODUCTION

DEMO is a future nuclear fusion reactor project, designed as intermediate between experimental and commercial reactors. Unlike fission reactors fusion devices don’t produce transuranic or other long-lasting fission waste. However some fusion reactor’s components will become radioactive in the process of operation due to interaction with neutrons generated during fusion processes. There are few approaches to resolve this issue. One of the possible solutions lies on material engineering. Having certain chemical compositions it is possible to reduce activity of the materials drastically. Reactor’s construction materials must exhibit low activity, be mechanically strong, resistant to long exposures of high neutron and heat fluxes and be cost efficient. Among variety of materials that were created for this purpose in last few decades, most notably is reduced activation EUROFER 97 steels. Depending on their crystallinitystainless steels also are classified to austenitic, ferritic and martensitic. The main goal of this study is to evaluate residual activity and decay heat after irradiation of materials mentioned above with the prospect of their application in DEMO fusion reactor constructions.

2. METHODS AND MATERIALS

European Activation System: Easy-2007 is used as a main tool for the determination of dominant radionuclides in structural materials after irradiation. Its code FISPACT is being utilized for simulation of irradiation process. Model of irradiation is simplified: infinite slab of material is being irradiated by neutron flux in pulses corresponding to operation of fusion device. FISPACT uses external libraries of reaction cross sections and decay data for all relevant nuclides to calculate nuclides produced as a result of the irradiation. Its output contains amount of radionuclide (number of atoms and grams), the activity (Bq), α-, β- and γ-energies (kW), γ dose-rate (Sv h^{-1}) as well as potential ingestion and inhalation doses (Sv). [1]

Input data: composition, density and mass can be expressed either as the percentage elemental composition or explicitly as the number of atoms of each nuclide. For this study EUROFER 97, F82H, F82-IAE, JLF-1, Manet, Manet II, Optifer 1a, Optifer II, la12lc, la12talc, T91[2, 3, 4, 5, 6, 7, 8, 9] and various configurations of 316 stainless steel were selected. Two extreme material's composition cases were analyzed additionally to optimal/ achievable composition when investigating EUROFER 97: Composition with a lot of possible impurities and completely pure alloy. All of these iron based alloys were considered for fusion reactor construction design (divertor, first wall or breeding blanket).

Neutron flux (Fig. 1) is presented as it is described in program, which uses vitamin-J energy structure groups. 175 groups represent energy range from 1E-05 eV to 2E+7 eV. Long time exposure and a series of neutron irradiation pulses are considered. First irradiation sequence is 1841 day long with 0,3 MW m^{-2} load on the slab surface. Another sequence consists of 17 pulses: material is exposed to 1 MW m^{-2} load for 4 hours and after that it has 1 hour of cool down until repeat. Sequences are performed one after another with one hour delay.

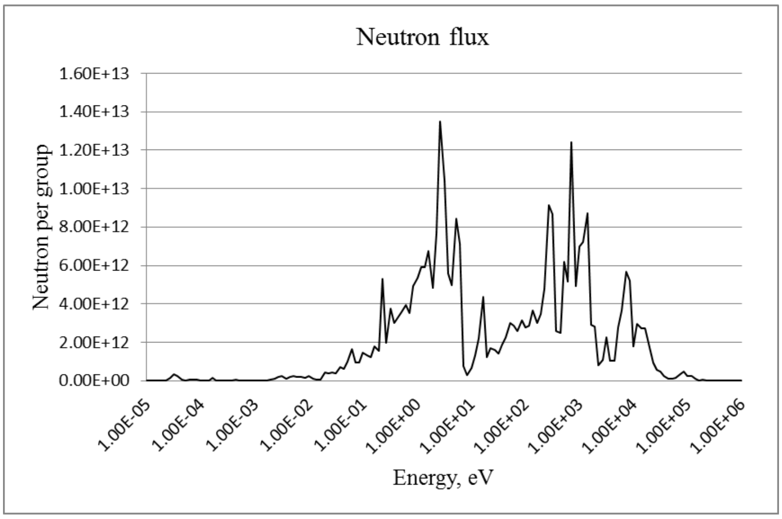

Fig. 1. Neutron spectra. Spectra is defined by vitamin-J energy structure groups

3. RESULTS AND DISCUSSION

Activity, dose rate and heat output of alloys are being examined. The period of interest spans up to 100 years after irradiation. Such length was selected taking into account previous studies that dealt with recycling of materials of fusion devices. Whole period is separated in two interest sections:

– early period – covers the first year of cool-down and calculated data might be useful for device operation, maintenance and decommissioning;

– late period – covers the last 50–100 year of cool-down and calculated data might be useful for disposal and recycling of the device materials.

Figs. 2 and 3 shows that F82H alloy exhibits lowest activity followed by Optifer II Optifer 1a and EUROFER 97 (target) in the late period. While in early period EUROFER 97 has lowest activity followed by Optifer II and Manet 2.

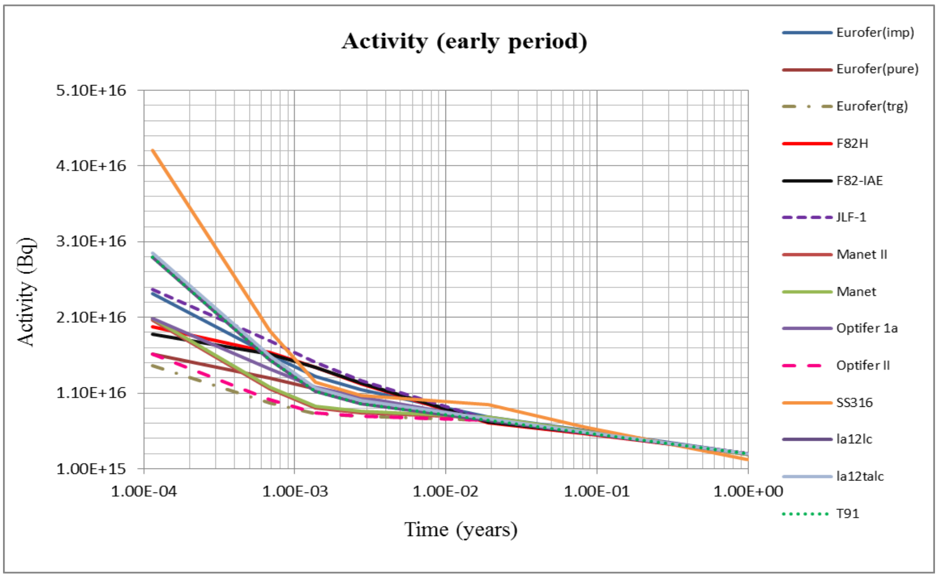

Fig. 2. Activity dependence on cool down time (early period)

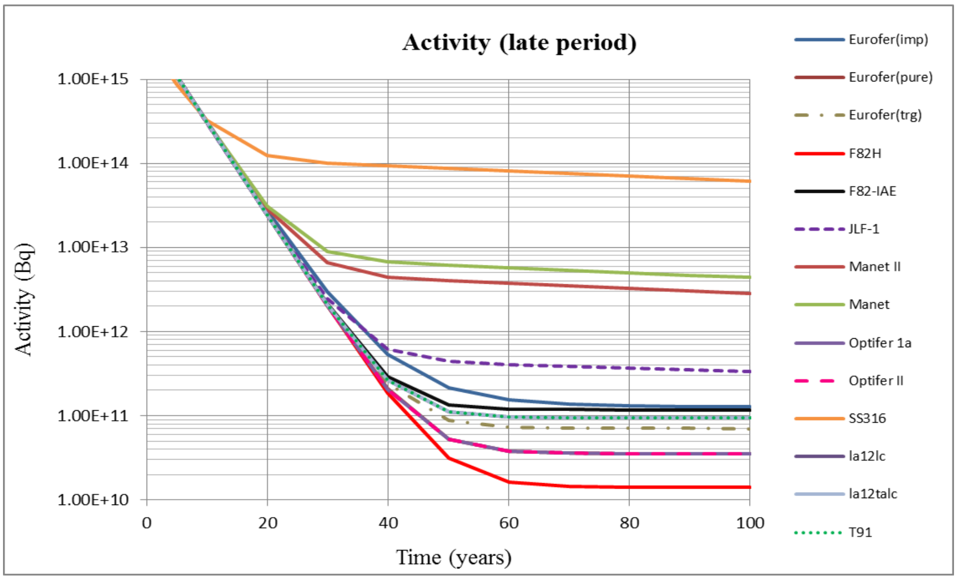

Fig. 3. Activity dependence on cool down time (late period)

The dose rate was calculated near the surface of the slab. Figs. 4 and 5 shows that the lowest dose rate in the early period corresponds to F82-IAE followed by F82H and EUROFER 97. In late period it is hard to distinguish which alloy has lowest dose rate due to very high gradient, however EUROFER with impurities exhibit worst characteristics followed by Manet and SS316. In order to get clearer results of this area another more detailed simulation is needed.

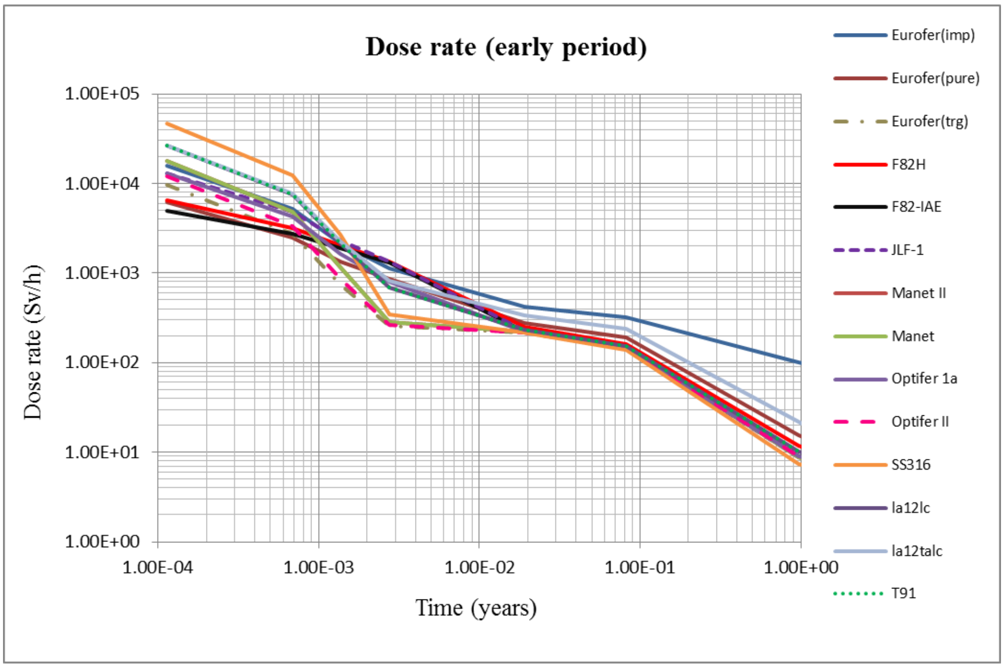

Fig. 4. Dose Rate dependence on cool down time (early period)

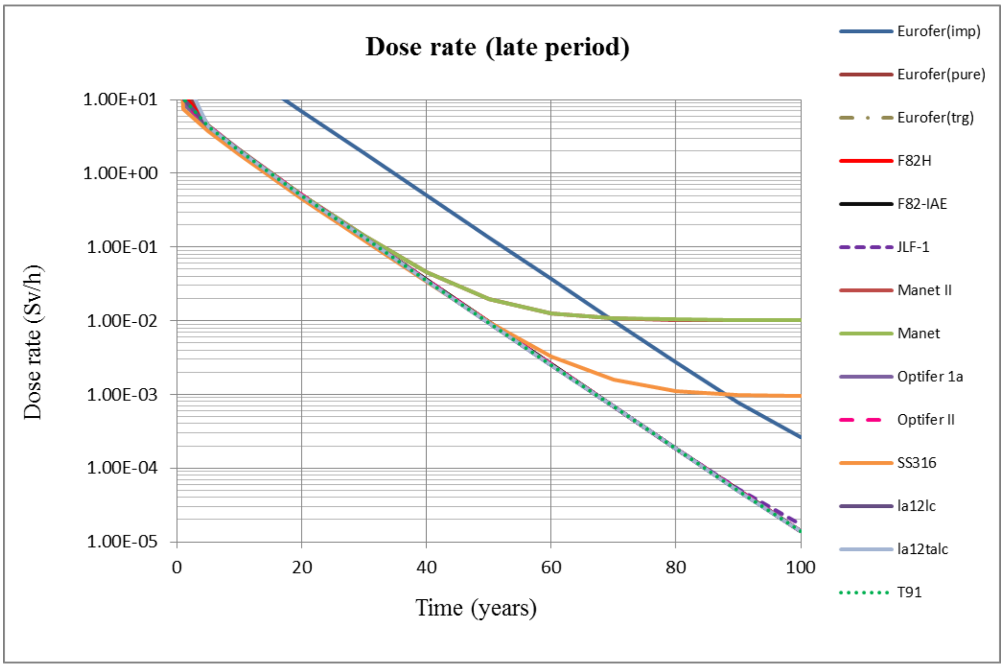

Fig. 5. Dose Rate dependence on cool down time (late period)

Heat output is shown in Figs. 6 and 7. F82-IAE has the lowest heat output followed by F82H and EUROFER (target) in early period. Lowest heat output in late period coincides the value of F82H followed by Optifer II/ Optifer 1a and EUROFER (target).

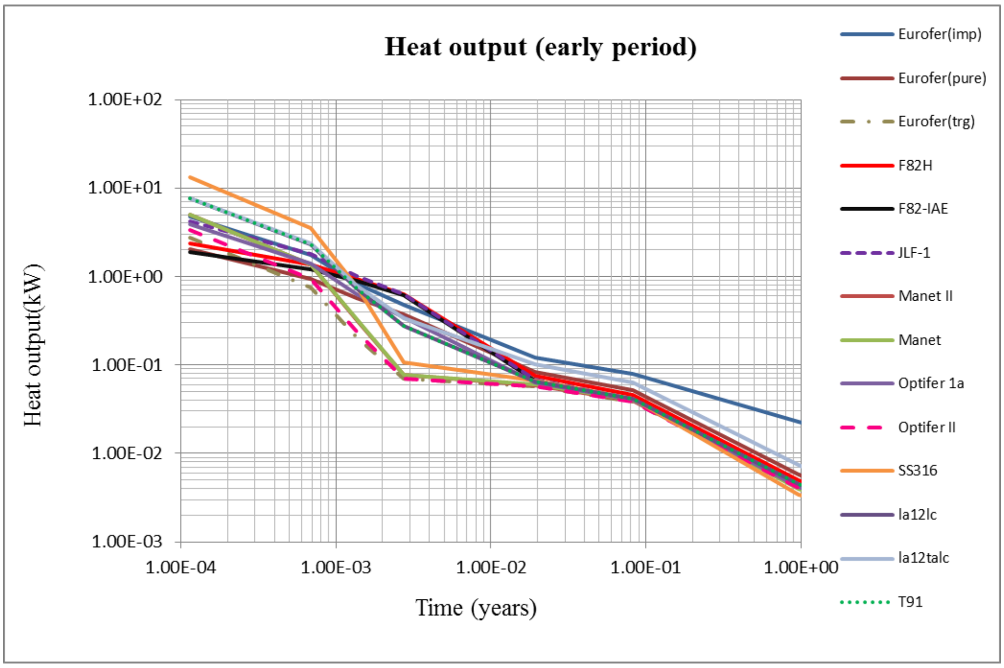

Fig. 6. Heat output dependence on cool down time (early period)

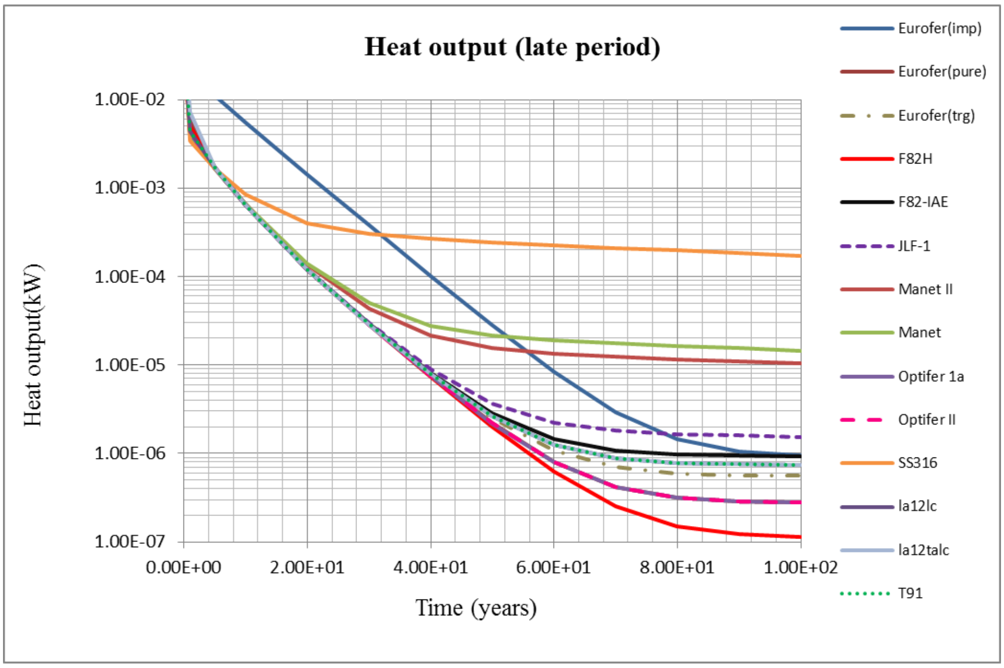

Fig. 7. Heat output dependence on cool down time (late period)

Activity and dose rate are some quantities used to judge the potential hazard of an irradiated material. However, activity takes no account of the biological impact on human beings. Therefore FISPACT code includes tools to estimate the dose received by a man over his lifetime (50 years). Such estimation includes radiation protection calculation because radiation type has different effect on human body as well as the effect of radiation differs for different organs. These data were obtained from reports published by International Commission on Radiological Protection and the National Radiological Protection Board [1].

Ingestion and inhalation doses are needed for regulatory control and further decommissioning, recycling or disposal. Dosimetric calculations reconsider short-lived radionucles and its daughter products, noble gasses and long-lived alpha emitters. Results are shown in Fig. 8 and Fig. 9. Both graphs have similar tendencies – at the early period EUROFER 97, Optifer II and Manet has lowest doses, while in late period F82H exhibit lowest dose followed by Optifer II and EUROFER 97.

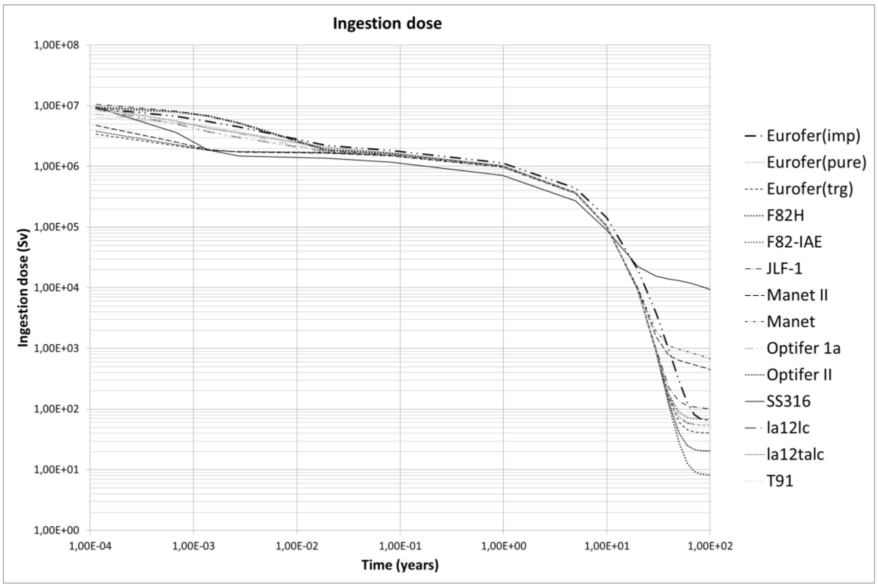

Fig. 8. Ingestion dose dependence on cool down time

Further processing of waste materials depends on the length of time since shutdown, the type of material and the amount of neutron flux. For materials with low activation, disposal with no special measurements is possible. The clearance of a radioactive material depends on the clearance index for that material being less than 1. A clearance index, based on International Atomic Energy Agency (IAEA) guidelines, is calculated from the clearance level value for each radioactive nuclide, and the radioactive inventory [1].

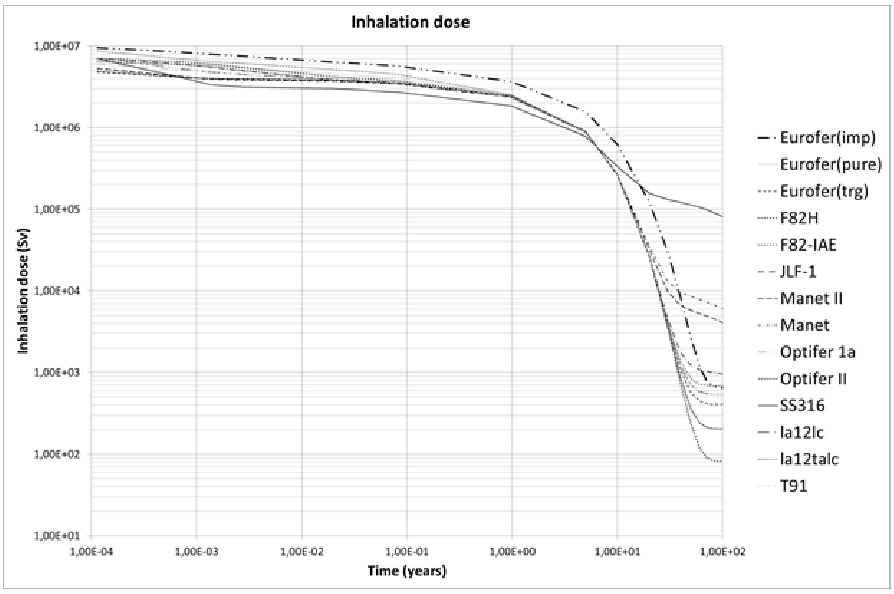

Fig. 9. Inhalation dose dependence on cool down cool down time

Fig. 10 shows the Activity of 316 austenitic stainless steel configurations. Dose rate and heat output graphs were not presented here because they are even less informative than activity graph. While SS316 doesn't have as good characteristic as reduced activation alloys, it might be still usable in fusion devices design. First of all it easier and cheaper to produce such materials in comparison to most of reduced activation steels, secondly some construction elements are not heavily affected by neutrons [10]. 316 Stainless steel material and other six configurations were analyzed.

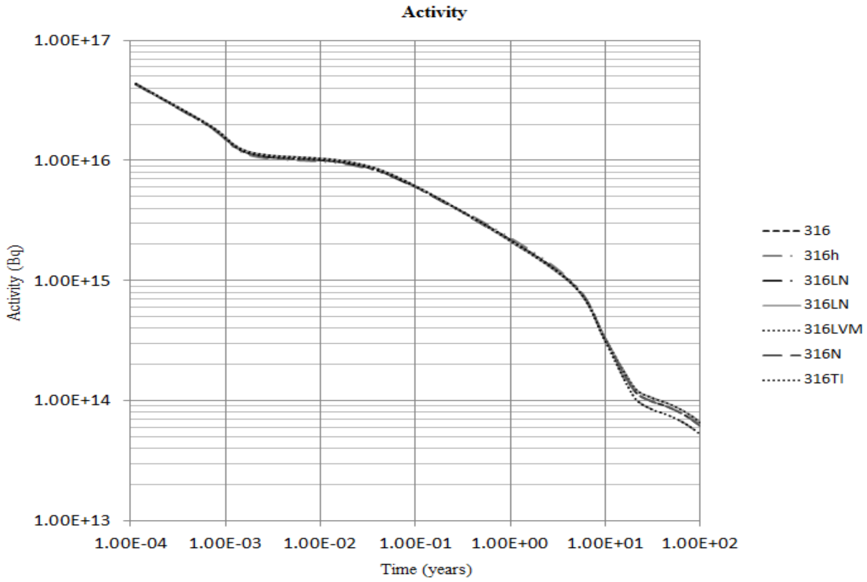

Fig. 10. Activity dependence on cool down time

It is known that 316h has significantly higher carbon percentage ~ 0.1%, 316L is has lower carbon percentage ~ 0.03%, 316LN has lower carbon ~0.035% but higher nitrogen percentage ~0.1%, 316 LVM has lower carbon ~0.035% and lower impurities percentage, 316N is enriched with nitrogen ~0.135% and 316Ti has titanium impurities ~0.7%. Only small changes are visible in graphs and data, so regarding the activity 316 Ti and 316 h has it generally lower. Difference between dose rate is indistiguishable. Heat output is also lower for 316 Ti, 316 h. Both materials have higher fraction of carbon in its structure. However the difference in activity is relatively small and might be outweighted by the mechanical and economical factors.

4. CONCLUSION

DEMO is one of the most recent and experimental fusion reactor projects and to this extent there is a lot of uncertainty regarding its design and operation. In this study certain irradiation scenario was investigated. Examination of different potential alloys for DEMO fusion reactor constructions was conducted in terms of their activity, dose rate, heat output. These values were calculated for the period of 100 year after neutron irradiation sequences. The period was divided into two sections – early (for maintenance and operation) and late (for disposal and recycling).

In the early period lowest activity was exhibited by EUROFER 97 alloys, while lowest dose rate and heat output was exhibited by F82H/ F82-IAE alloys.

In the late period lowest activity and output hear was exhibited by F82H. Overall most desirable characteristics were exhibited by F82H and EUROFER 97 alloys.

Second part of the study was focused on SS316 steel. 7 configurations of steel were examined. Results were mostly inconclusive indicating that small changes (mostly regarding carbon, nitrogen, titanium) on composition has only small influence on after irradiation characteristics of materials.

REFERENCES

1. FOREST R.A. *FISPACT-2007: User manual.,* EURATOM/UKAEA Fusion Association, Culham Science Centre, Abingdon, Oxfordshire UK 234 2007.
2. DANON A., SERVANT C., ALAMO A. BRACHET J.C. *Heterogeneous austenite grain growth in 9Cr martensitic steels: influence of the heating rate and the austenitization temperature.,* Materials Science and Engineering A348, 122/132, 2003.
3. STORK D. et al. *Developing structural, high-heat flux and plasma facing materials for a near-term DEMO fusion power plant: The EU assessment.,* Journal of Nuclear Materials 455 277–291, 2014.
4. CHEN, X., HUANG, Y., MADIGAN, B., ZHOU, J. *An overview of the welding technologies of CLAM steels for fusion application.,* Fusion Engineering and Design 87 1639–1646, 2012.
5. GAGANIDZE, E., AKTAA, J. *Assessment of neutron irradiation effects on RAFM steels,* Fusion Engineering and Design 88 118–128 2013.
6. STORK, D. et al. *Materials R&D for a timely DEMO: Key findings and recommendations of the EU Roadmap Materials Assessment Group.* Fusion Engineering and Design 89 1586–1594 2014.
7. LEE S.K.,YUN S.-H., JOO H.G., NOH S.J. *Deuterium transport and isotope effects in type 316L stainless steel at high temperatures for nuclear fusion and nuclear hydrogentechnology applications,* Current Applied Physics 14 1385e1388 2014.
8. KIMURA A. *Current Status of Reduced-Activation Ferritic/Martensitic Steels R&D for Fusion Energy.,* Materials Transactions, Vol. 46, No. 3, p. 394–404, 2005.
9. YOUSSEF M.Z., et al. *Current Status of Reduced-Activation Ferritic/Martensitic Steels R&D for Fusion Energy Verification of ITER shielding capability and FENDL data benchmarking through analysis of bulk shielding experiment on large SS316/water assembly bombarded with 14 MeV neutrons,* Fusion Engineering and Design, Volume 42, Iss. 1–4, p. 235–245, 1998.

CYSENI 2015, May 27-28, Kaunas, Lithuania
ISSN 1822-7554, www.cyseni.com

OVERVIEW OF LIFE CYCLE ASSESSMENT METHOD IN NUCLEAR ENERGY FIELD

K. Zakuciová
Research Centre Rez.,
Hlavni 130, 250 68, Husinec-Rez – Czech Republic

University of Chemistry and Technology Prague
Technicka 5, 166 28, Prague – Czech Republic
Phone + 420 775 364 032
Email: Kristina.Zakuciova@cvrez.cz

V. Kočí
University of Chemistry and Technology Prague
Technicka 5, 166 28, Prague – Czech Republic
Phone +420 220 44 3277
E-mail: Vlad.Koci@vscht.cz

ABSTRACT

Energy production by nuclear systems is considered as one of the most sustainable options. Sustainability of nuclear systems is expressed by environmental-friendly technology, safety and reliability, and by reasonable economic costs. Nuclear energy production is going through significant progress mainly by the development of new reactor technologies. It means shifting from currently most used technologies of Generation II and III Light Water Reactors (LWR) to Generation IV Fast Reactors (FR) which is promising a steep increase of nuclear technology sustainability once achieved their technical, economic and industrial viability. A suitable tool for sustainability evaluation of any energy system is LCA (Life Cycle Assessment). Using LCA method for nuclear power plants and their processes is a rare approach in comparison with LCA studies in other energy sectors (e.g. fossil fuels). Some commonly known LCA studies (usually not complete) in nuclear field were made for construction of a plant, for operation of sub-systems in once-through fuel cycle, for plant decommissioning and also for the back-end of the fuel cycle (reprocessing, storage/disposal). The better understanding of using LCA in the nuclear field and the identification of the gaps in the analysis require an overview of currently published LCA studies. This overview paper summarizes in which phases of nuclear energy production was LCA already applied and where further could the individual results lead to. This analysis is also essential for pointing out the required and missing data for subsequent complete LCA analysis.

Keywords: Life Cycle Assessment, Nuclear energy, Sustainability

1. INTRODUCTION

In the recent years there is a huge discussion about emission-free (or carbon-free) power generation systems. It is well known that nuclear energy and renewables have total life cycle of greenhouse gas (GHG) emissions much lower than from fossil fuels energy systems. Generally, plants with wind turbines, photovoltaic plants and nuclear power plants do not contribute to global warming. However, extraction, conversion of raw materials, construction plus other processes produces indirect GHG emissions [1]. Life Cycle Assessment (LCA) is considered as an analytical tool which can perfectly described whole life cycle of the systems processes and evaluate GHG emissions.

LCA tool for the environmental impact evaluation is becoming an operational requirement in almost all industrial sectors. Understanding the methodology and different impact factors in the technological processes can significantly influence total environmental burden. This paper should help to understand how LCA in nuclear sector has been already used, where the main gaps in the methodology are and what factors could influence the whole environmental impact.

Life cycle of the systems and products includes raw material acquisition and input materials production through product production, utilization and removal or recycling. Environmental impacts of product are evaluated on a basis of impact evaluation of material and energetic flows. Important contribution of LCA is specification of environmental impact by so-called impact category. Impact category is the specific environmental problem as global warming, eutrophication, etc. Precise specification of environmental impacts by impact category helps to identify undesirable transferring of problem from place to place. It means transferring of problem from one category to another [2]

LCA study is described by 4 phases:

1. Goal and scope definition;
2. Inventory analysis;
3. Impact assessment;
4. Interpretation.

The goal and scope of the LCA study include determination of functional unit, product system boundary, data quality requirements and data allocation. Inventory analysis requires modelling of products system and determination of environmental profile of product. Impact assessment means evaluation in impact categories. Interpretation includes identification of key findings, evaluation of LCA study, critical analysis, and suggestions for innovation of the product system [2].

LCA is commonly used in different areas of energy sector. It is important method how to gain results and data which could show concrete potential environmental harm. LCA in nuclear field has been already used and described in nearly 300 papers and scientific journals. Documents about Life Cycle Inventories of different energy systems of different countries usually include assessment of oil, natural gas, coal, nuclear, hydro power, photovoltaic and wind power energy systems [3, 4]. Data included in these reports are subjects to the Ecoinvent database terms of use.

The main goal of LCA methodology for electricity production from nuclear power is to estimate the current GHG footprint of nuclear power based largely on the global average nuclear fuel cycle [5]. This paper is reviewing selected papers and documents which are critically assessing different LCA approaches from various literature sources.

2. DESCRIPTION OF NUCLEAR FUEL CYCLE IN THE SENSE OF LCA METHOD

LCA methodology requires knowledge of described product system. In a case of electricity production from nuclear power it means description of nuclear fuel cycle which is briefly showed below in a figure 1. The focus is on open fuel cycle (once through) because the reference LCA methods were made for currently operating NPP`s. All stages of nuclear fuel cycle can be aggregated into three main processes:

1. Upstream – Mining and Milling, Conversion, Enrichment, Fuel Fabrication;
2. Core (Operational phase) – Operation of NPP, Operation of Fuel Storage, Operation of Waste Repository, Construction and Decommissioning of facilities;
3. Downstream – Electricity distribution. [6, 7].

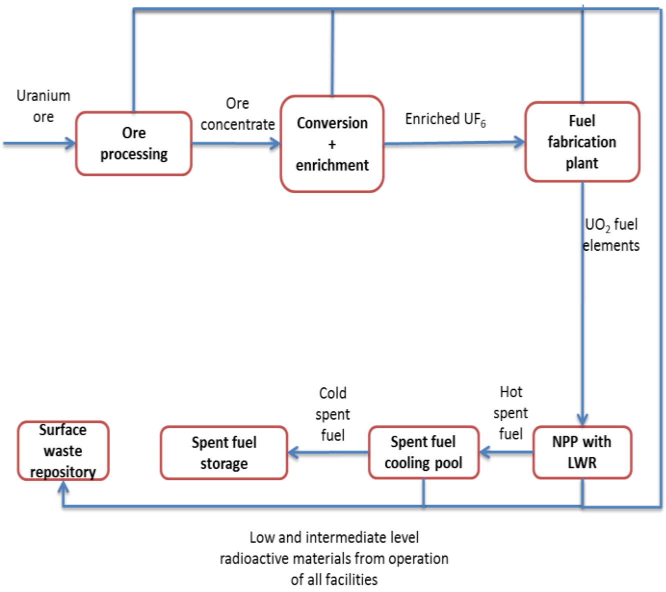

Fig. 1. Scheme of open fuel cycle

After the systems definition, specification of the functional unit is required. Functional unit is specification and quantification of the products function. Functional unit depends on the purpose and goal of the LCA method. For instance, Lenzen [8] defines functional unit as actual quantity in kWh of delivered electricity. On the other hand, Norgate [5] defines functional unit as 1MWh of electricity produced by a 1GWe PWR nuclear reactor, hence, GHG footprint is reported as kg CO_2eq/MWh. Functional unit should be connected also with time range (distribution of electricity during the reference period) in a scope of years [7].

Complexity of LCA study is defined by system boundaries. System boundary means determination of processes which will be included in a product system. It is important to define which stages of the products life cycle will be the subject of the analysis. System boundary can be narrowed [2]. For instance, Environmental Product Declaration for Sizewell B nuclear power station [7] excluded infrastructure upstream processes as construction and dismantling. Norgate [5] defines system boundary in nuclear energy from uranium ore mining through to electricity generation in NPP and waste disposal, including NPP construction. Also, other literature sources [3, 6] consider whole processes of nuclear fuel cycle.

Allocation is another important process in LCA. It is a distribution of environmental impacts of one process among two or more products which are the outputs from this process [2]. Allocation of nuclear fuel cycle is straightforward because most of the stages are mono-functional. However, mining can result in mixed products, as copper and uranium, where the allocation is made according to relative revenues from the products produced [5]. Allocation rule was also defined in treatment and handling with spent fuel which is based on polluter pays allocation method [7].

Life cycle Inventory (LCI) purpose is to gain environmentally important information about processes included into product system [2]. Data from LCA studies, reports and websites can be helpful but databases as EcoInvent or SimaPro are considered as main data source [4, 6, 7, 8, 9, 16].

2.1 Impact category for nuclear energy production

Impact category is the specific problem in the environment which is caused by human activity. The choice of the impact category is very important step for LCA which shows how the study will be complex and objective. Impact category provides tools how to calculate the harm of specific categories [2].

In general there are 10 basic impact categories, what could be assessed on midpoint and/or endpoint level:

1. Global warming and/or climatic change;
2. Stratospheric ozone depletion;
3. Acidification;
4. Eutrophication;
5. Photochemical ozone creation potential (POCP);
6. Terrestrial toxicity;
7. Aquatic toxicity;
8. Human toxicity and/or human health;
9. Resource depletion;
10. Land use [9].

According to Poinssot [10] studies selected eight indicators to describe the nonradioactive impacts: the green-house-gases emissions (GHG, g CO_2eq/kWhe), the atmospheric pollution (SOx and NOx, mg/kWhe), the water pollution (mg/kWhe), the landuse (m^2/GWhe), the water consumption and withdrawal (L/MWhe), and the production of technological waste (g/MWhe).

Three indicators were selected addressing the radioactivity specificity:

- Radioactive gaseous and liquid releases (Bq/kWhe);
- The solid radioactive waste production (g/MWhe or m^3/MWhe);
- Footprint of the required repository is also considered.

Additional 5 indicators for NOx and SOx releases: acidification, eutrophication and POCP. Also, eco-toxicity and human toxicity was assessed to show the maximum potential impact of both chemicals and radioactive release [16].

In LCA review article [3] indicators of SO_2, NOx and GHG emissions were selected based on their contribution to several impact categories. This study confirms that NOx and SO_2 are largely responsible for acidification in addition with NH_3 and eutrophication (NOx and NH_3).

The Swiss report [4] follows the same indicators of SO_2, NOx and GHG emissions which are noted above. Radioactive air emissions are in this case selected into four categories: radon (Rn-222, Rn-226), other gases and nobles (Ar, Kr, Xe) and non-noble gases (H-3, C-14), aerosols. Radioactive water emissions are distributed also into four categories: radium, tritium, mixed nuclides and actinides. Similar, radioactive solid waste production is monitored [16].

Vattenfall study [6] monitored main GHG emissions (CO_2, SO_2, NOx), acidifying substances (NH_3), emissions (hydrocarbons, SO_2, NOx, CO, non-methane volatile organic compounds, methane) contributing to POCP, emissions of eutrophicating substances ($PO_4^{\ 3-}$).

2.2 LCA methodology used for nuclear fuel cycle

Two most frequently used methodologies for evaluation in nuclear energy sector which are noted in the literature sources are Input- Output analyses (IOA) and Process Chain Analyses (PCA). IOA is considered as top-down approach and describes material and energetic inputs and outputs expressed in monetary units. PCA is bottom-up that requires the collection of data on the main production processes, or steps in the life cycle, which are then aggregated up in order to assess the impacts of the product as a whole [11]. The methodology needs to meet the following set of requirements:

- complete representation of the life cycle system from mining to final waste disposal for nuclear power,
- an explicit depiction of the elementary mechanism on the input–output interaction across the system boundary in the methodology [12].

In Voorspools study [11] both methodologies were applies for 1000MW NPP (type PWR) with a lifetime about 40 years. Results show that for the PCA, the steel products are the dominant factor in energy use and GHG emissions. Materials other than steel and concrete are hardly contributing to the total energy use and GHG emissions. Maintenance and demolition (including recycling and storage of radioactive equipment) also largely contribute to the overall energy use and GHG emissions.

Nians in his dissertation thesis [12] used similar approach Process Energy Input Analyses and Process Carbon Emission Analyses. Process energy input factors are computed by taking the ratio of total process energy input and the life cycle electrical energy output of the whole system life cycle (GJ/GWh). Process Energy Input Analyses can provide two indications which can be considered as alternative LCA datasets for nuclear power:

1. the distribution of process energy input across the LCA System;
2. the direction of proportionality (e.g. positively correlated or negatively correlated) [12].

Process carbon emission factors measured by t-CO_2/GWh are obtained by taking the ratio of the process carbon emissions and life cycle electrical energy output of the LCA System. The use of process carbon emission factor can give direct quantification on the amount of carbon emissions produced by a given process of the LCA System for each unit of electricity produced. This can also help to express LCA dataset for nuclear power system [12].

Another study where the PCA was used is study of uranium grade impact of GHG footprint in nuclear energy [5]. If data are not available or scarce, it is possible to use hybrid LCA methodology, which means combination of the methods (e.g. PCA+IOA). In the result these methodologies are showing which parts of the nuclear fuel cycle and how they are influencing the GHG footprint and energy consumption.

3. OVERVIEW OF THE RESULTS

In several literature sources the choice of enrichment technology and uranium ore grade are the main factors which can significantly change environmental footprint in nuclear energy production. Nian [12] states that with gaseous diffusion technology, the share of enrichment process energy input captures more than 80% of the overall upstream energy input factor. He considers that more efficient gaseous centrifuge technology reduces energy input share to between 15% and 30%. Other source [3] explains differences in USA and Japan nuclear technology in utilization of gaseous diffusion enrichment. When all uranium fuels are enriched using gaseous diffusion method in the USA, the Life Cycle Emission factor (LCE) increase to 30 and 27 g-CO_2/kWh while in Japan the LCEs decrease to 10 and 11 g-CO_2/kWhe.

The second influencing factor is the uranium concentration in the ore. The concentration of uranium has to be above 0.002% for the extracted fuel. If the uranium concentration in the ore decreases, the energy from mining and milling increases [13].

Norgate confirms the same fact that as the grade of the uranium ore mined for nuclear power production falls, a greater amount of energy and other material inputs are required in the mining and milling stage and this will cause increase of GHG footprint of nuclear power [5].

There are also other stages besides enrichment which highly contributes to the overall GHG emissions. According to Poinssot [10] the total GHG emissions for the global fuel cycle are estimated to be 5.29 g CO_2eq/kWhe. The main contributions come from the plants operation (40%), the mining activities (32%) and the enrichment (12%). On the other hand, conversion, disposal and reprocessing operations count with 5, 2 and 7%, whereas fuel fabrication has negligible impact.

In Norgates results GHG emissions were estimated to be 33.9 kg CO_2eq/MWhe where the fuel enrichment contributes in a greatest proportion of 56%. Then, plant construction (25%) and plant operation (9.4%) contribute to the overall GHG emissions. Mining and milling phases result in 1.3 kg CO_2eq/MWhe [5].

Another study [13] shows different ranges of non-radioactive emissions in particular stages of nuclear fuel cycle. The literature review in this study states that Storm and Smith's estimates is 17 g CO2eq/kWhe for construction and 31 g for operation which are based on input-output analysis [14].

Hondo estimates of 2.8 g CO_2eq/kWhe for construction which shares 11.7% and of 3.2 g CO2eq/kWh for operation in a share of 86.6% where 61.9% belongs to enrichment process. Remaining percentage belongs to decommissioning process [3]. Dones et al. corresponds that European modelled energy chains associated with LWRs shows a range of 5 and 12 g CO2eq/kWhe [4]. Vattenfall's study claims 5.3 g CO2eq/kWhe for whole nuclear fuel cycle process from process-based analyses. In Vattenfalls study upstream processes, mainly uranium extraction, conversion, enrichment contributes to GHG emissions with total of 51%. Construction counts with 15% contribution [6].

Lenzen et al. obtained higher greenhouse gas emissions of 57.7 g CO2eq/kWhe where 25% refers to operation and maintenance of the power plant and 28% to the enrichment [8].

The total greenhouse gas emissions per kWh according to EDF [7] have been calculated to be 6.04 g CO_2eq/kWhe where CO_2 emissions are dominated by the construction in a share of 42% mining and milling phases 23%.

All results of GHG emissions from operation phase and upstream processes from different literature sources are showed in the figure below.

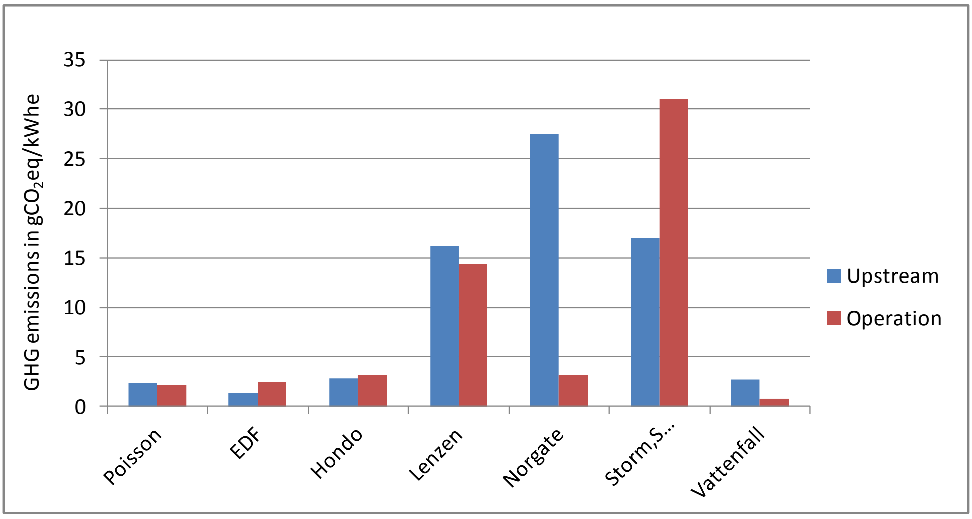

Fig. 2. GHG emissions result of operation and upstream processes according different literature sources

Results are clearly showing following findings:

- According to Storm and Smith`s calculation of GHG emissions, operation phase shows the highest level of g CO_2eq/kWhe.
- The highest GHG emission in upstream processes is showed in Norgates study.
- The lowest values in upstream processes appears in EDF study.
- The lowest GHG emissions in operation phase appears in Vattenfall.

4. DISCUSSION

Differences in results can be influenced by uncertainties in data sources. Norgates [5] data were mostly taken from general publicly available data, where age of data, different operating parameters and technologies, lack of transparency in the assumptions and secondary source of data were used. EDF states that construction and operation are large contributors to GHG emissions mainly because of used materials (steel and concrete). On the other hand, uncertainties are also caused by the limitation and lack of available data [7]. Differences in uranium mining process and technology have possible impact on data uncertainties too. Differences between different mining technologies among different literature sources are very well and deeply described in Beerten et al. study [1]. This study also discusses other technological differences which might influence final amount of GHG emissions.

Choice of the assessment methodology (LCA, PCA vs. I/O analysis) is also important factor which can influence final results. Storms and Smith`s high values are related to the energy expenditures which are far higher than the results obtained by PCA method. The main issue is that authors take into account large range of cost data [14, 15]. Variations in the results could be also influenced by the choice of different system boundaries, electricity mix used in different countries and geography range [2].

Results are showing that the operational and construction phase in nuclear fuel cycle are significant in the environmental footprint contribution. This is explained by the:

- High electricity consumption mainly in upstream processes.
- Land occupation mainly in a phase of uranium ore extraction.
- Radioactive waste production in upstream and core processes.
- CO_2, SO_2 and NOx production in upstream and core processes.

The overview of electric supply technologies made by Weisser [9] suggest following improvements for reducing emissions in nuclear technologies:

- Reduction of electricity input for enrichment process (diffusion vs. centrifuge, laser technology).
- Utilization of electricity based on low or non-carbon fuels.
- Extension of nuclear technology lifetime and burn-up.

5. CONCLUSION

LCA methodology can provide the key to the solutions which can reduce emissions production. In nuclear energy sector main processes which contribute to GHG emissions production are enrichment, mining and milling, conversion, operation phase, construction + decommissioning. It is also important to use right methodology which is usually influenced by the availability of dataset and information gained from the processes. Choice of the systems boundary and clear product system description are also part of the whole LCA methodology which needs to be clearly defined.

To be able to make comparative analyses of different nuclear technology (Light Water Reactors vs. Lead-cooled Fast Reactors), the generic LCA methodology is required. However, this is very hard to define because of lot of technological differences and mainly lack of data. That is why further research in LCA in nuclear technologies should be focused on defining clear system boundaries in the same time horizon which would result in generic system definition on the life cycle system, input-output and system boundaries.

6. ACKNOWLEDGEMENT

This work has been supported by the SUSEN Project CZ.1.05/2.1.00/03.0108 realized in the framework of the European Regional Development Fund (ERDF).

REFERENCES

1. BEERTEN, J., LAES, E., MESKENS, G., D'HAESELEER, W. Greenhouse gas emissions in the nuclear life cycle: A balanced appraisal, *Energy Policy*, 2009, Vol. 37, No. 12, p. 5056–5068.
2. KOČÍ, V. *Environmentální dopady:Posuzování životního cyklu,* VŠCHT, Praha, 2013, 131 p., ISBN: 978-80-7080-858-0.
3. HONDO, H. (2005). Life cycle GHG emission analysis of power generation systems: Japanese case. *Energy*, 2005, Vol 30, No.12, p. 2042–2056.
4. DONES R., BAUER C., BOLLIGER R., BURGER B., FAIST EMMENEGGER M., FRISCHKNECHT R., HECK T., JUNGBLUTH N., RÖDER A., TUCHSCHMID M. Life Cycle Inventories of Energy Systems: Results for Current Systems in Switzerland and other UCTE Countries. Ecoinvent report No. 5. Paul Scherrer Institut Villigen, Swiss Centre for Life Cycle Inventories, Dübendorf, 2007.
5. NORGATE, T., et al. The impact of uranium ore grade on the greenhouse gas footprint of nuclear power. *Journal of Cleaner Production*, 2014, Vol. 84, p. 360–367.
6. VATTENFALL A.B. Certified Environmental Product Declaration EPD® of Electricity from Ringhals Nuclear Power Plant. Group 171 – Electrical Energy, Germany, 2014.
7. EDF Energy Nuclear generation Ltd. Environmental Product Declaration of electricity from Sizewell B nuclear power station No. 4, Gloucester, 2014.
8. LENZEN, M. (2008) Life cycle energy and greenhouse gas emissions of nuclear energy: A review. *Energy Conversion and Management*, 2008, No. 49, p. 2178–2199.
9. WEISSER, D.A guide to life-cycle greenhouse gas (GHG) emissions from electrici supply technology. *Energy*,2007, Vol. 32, No. 9, p. 1543–1559.
10. STAMFORD, L., AZAPAGIC, A. (2011). Sustainability indicators for the assessment of nuclear power. *Energy*, 2011. Vol. 36, p.6037–6057.
11. POINSSOT, C., et al. Assessment of the environmental footprint of nuclear energy systems. Comparison between closed and open fuel cycles. *Energy*, 2014, Vol. 69, p. 199–211.
12. VOORSPOOLS, K.R., et al. (2000). Energy content and indirect greenhouse gas emissions embedded in 'emission-free' power plants: results for the Low Countries. *Applied Energy*, 2000, Vol. 67, No. 3, p. 307–330.
13. NIAN, V., et al. (2014). Life cycle analysis on carbon emissions from power generation – The nuclear energy example. *Applied Energy*, 2014, Vol. 118, p. 68–82.
14. FTHENAKIS, V.M., KIM, H.C. (2007).Greenhouse-gas emissions from solar electric- and nuclear power: A life-cycle study. *Energy Policy*, 2007, Vol. 35, No. 4, p. 2549–2557.
15. STORM VAN LEEUWEN, JW., SMITH, PH. Nuclear power – the energy balance, Ceedata, Chaam (The Netherlands), February 2008.

   SOVACOOL, B.K. Valuing the greenhouse gas emissions from nuclear power: A critical survey. *Energy Policy*, 2008, Vol. 36, No.8, p. 2950–2963.

CYSENI 2015, May 27–28, Kaunas, Lithuania
ISSN 1822-7554, www.cyseni.com

EVALUATION OF RADIATION CONSEQUENCES OF RELEASES IN ACCIDENTS WITH SPILLS OF LIQUID RADIOACTIVE MATERIALS IN AREAS WITH FORCED VENTILATION

O. Slepchenko, V. Bogorad, Y. Kyrylenko
State Scientific and Technical Center for Nuclear and Radiation Safety
35/37 V. Stusa Str., 03142, Kyiv – Ukraine
Phone +308 0444500500
Email: nrs@sstc.kiev.ua

ABSTRACT

This report focuses on assessment of radiation consequences of releases in accidents with spills of liquid radioactive materials in areas with forced ventilation. During the study, characteristic dependences between parameters of liquid radioactive materials and air exchange in areas with forced ventilation and associated radiation consequences were determined.

The proposed approach is based on the theory of non-stationary heat and mass transfer in surface evaporation of liquid heated below the boiling temperature. The physical model includes: liquid radioactive material, steam-aerosol radioactive mixture, air of forced ventilation, airborne filters, and floor of the emergency area. The key aspects of the model are evaporation of liquid material, its removal with exhaust ventilation and partial trapping on airborne filters. It is considered that the steam-aerosol radioactive mixture is released to the environment after filters.

The advantage of this model is the possibility to determine integral release of radionuclides to the environment and activity concentration of air in the emergency area at any moment after beginning of the accident, effective dose received by an adult during 14 days for a wide range of input thermodynamic and geometrical parameters, different operating modes of the ventilation system and different productivities of the filtering system.

Results from assessment of radiation consequences for the selected accident are presented and the associated effect of filtering systems is analyzed.

Keywords: liquid radioactive materials, radiation consequences

1. INTRODUCTION

Nowadays, one of the priorities in nuclear industry is to minimize actual radiation exposure on the population during normal operation of the facilities as well as potential one in case accidents. In case of an accident, the minimization is based on the dependence of radiation consequences on parameters that caused them. Such minimization is performed through analysis of the physical foundations incorporated in accident scenarios and identification of the main factors influencing their radiation consequences.

This work is devoted to the class of accidents involving spills of liquid radioactive materials (LRM) in areas with forced ventilation, assessment of activity and power of releases as well as assessment of the radiation consequences of such releases.

Worldwide there have been more than 22 significant accidents with spills of liquid radioactive materials at nuclear fuel cycle facilities for the last 60 years [1]. Among there is the accident at research reactors, nuclear power plants, nuclear complexes, pilot plants and chemical plants.

Many special computer codes and methods are currently developed to assess, with sufficient accuracy, parameters of releases for various accidents at nuclear fuel cycle facilities (e. g. [2] for NPP). But, these codes often require a large amount of input data and calculation time. The advantage of the approach developed in this paper is rapid assessment of radiation consequences.

2. LRM AS AN OBJECT OF STUDY

LRM are liquid solutions, which include impurities of radioactive elements (possibly bound in high-molecular complexes). The isotopic composition of LRM is determined primarily by the source of radioactive impurities.

The main sources of LRM at nuclear power plants and nuclear complexes are as follows:

- primary coolant that is discharged for operational reasons;
- water that is used to backflush filters and ion exchangers;
- floor drains that collect water that has leaked from the active liquid systems and fluids from the decontamination of the plant and fuel flasks;
- leaks of secondary coolant;
- laundries and changing room showers;
- and chemistry laboratories.

At nuclear power plants and nuclear complexes, LRM are mainly aqueous solutions of decay products of nuclear fuel [3], [4].

Pilot plants and chemical plants may contain a full range of isotopes and solvents.

3. MODEL OVERVIEW

The proposed approach is based on the theory of non-stationary heat and mass transfer in surface evaporation of liquid heated below the boiling temperature. The physical model includes: active liquid medium, steam-aerosol radioactive mixture (SARM), air of forced ventilation, airborne filters, and the floor of emergency area. The key aspects of the model are evaporation of liquid material, its removal with exhaust ventilation and partial trapping on airborne filters. It is considered that SARM is released to the environment after filters.

The model is developed to assess the radiation consequences in an accident with spill of LRM and describes the spread of radioactive material by two consecutive ways: releases within the emergency area and further transfer of SARM into the atmosphere. In this paper, we focus on the relationship of these pathways and study the process of evaporation as special one for accident with spill of LRM.

3.1. Basic principles and assumptions of the model

The model of LRM evaporation describes the transport of radionuclides within the emergency area. It takes into account processes such as:

- evaporation of the radioactive material;
- drainage of LRM;
- cooling of LRM by evaporation and heat transfer from floor;
- entrainment of SARM via ventilation;
- cleaning of SARM to remove radioactive aerosols on the filtration facility;
- release of LRM to the atmosphere.

Key assumptions in modeling the thermal evaporation processes:

- temperature of LRM is always higher than the temperature of involved air;
- condensation of SARM on surfaces of equipment and building designs is neglected;

- pressure in the airspace of the area is constant and equals atmospheric pressure;
- LRM's heat transfer coefficient relative to the floor does not depend on LRM temperature;
- convection flows within LRM are absent;
- concentration gradient of radionuclides in LRM is absent;
- heat transfer through the evaporation surface to the air of ventilation is neglected;
- velocity fields of aerodynamic flow and thermodynamic parameters of the air over the entire surface of evaporation are constant.

3.2. Description of LRM evaporation

The process of evaporation that occurs in direct contact of the supplied air and liquid surface is complex. It combines the effects of heat and mass transfer. The mass flow of SARM released from the surface of the liquid is determined by the Dalton [5] equation:

$$dm_w = -\beta_{sw} \cdot (p_{sw} - p_m) \cdot S dt, \tag{1}$$

where m_w – mass of LRM, *kg*;

β_{sw} – mass transfer coefficient for normal atmospheric pressure, $\frac{kg}{Pa \cdot m^2 \cdot s}$;

p_{sw}, p_m – saturation pressures of LRM for temperature of liquid surface T_{sw} and temperature of involved air T_m (Fig. 1), Pa;

S – area of evaporation surface, m^2;

t – time, *s*.

Accordingly, the heat flow which is directed from the liquid to the supplied air is:

$$dQ_{ev} = -r_w \cdot \beta_{sw} \cdot (p_{sw} - p_m) \cdot S dt \tag{2}$$

where r_w – heat of LRM evaporation, *J/kg*

In this case, if the temperature of LRM is always higher than the temperature of the supplied ventilation air in the boundary liquid layer, it gives rise to the temperature gradient, the nature of which depends on the intensity of heat and mass transfer.

The experimental data [6] show that the intensity of water transfer during evaporation depends on hygrothermal state of the incoming air flow (Fig. 1).

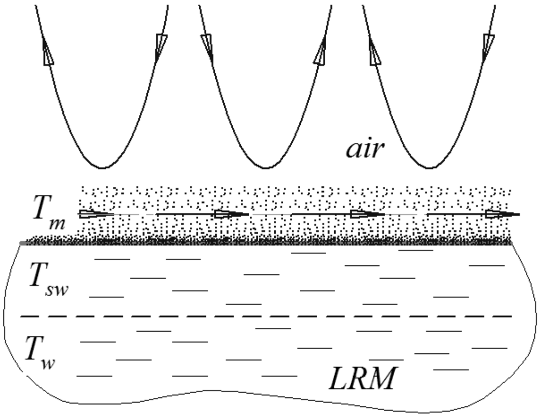

Fig. 1. The temperature gradient on the surface of LRM

On the basis of experimental studies [5], [6], the dependence of surface temperature of the evaporating liquid on hygrometric conditions and hydrodynamic process when the heat flow is directed from liquid surface to the environment was established. According to (1) and (2), the parameters β_{sw} and p_{sw} are functions of temperature of the liquid surface T_{sw}, and value r_w is functions of temperature within the liquid T_w.

The model of evaporation also describes the heat transfer from liquid to the floor of emergency area. According to [7], the heat transfer from the liquid to the floor is described by the expression:

$$dQ_f = k \cdot F \cdot (T_w - T_f)dt \tag{3}$$

where k – heat transfer coefficient for floor (this value can be found according to [7]), $\frac{W}{m^2 \cdot K}$;

F – area of contact surface of LRM with the floor, m^3.

Then the heat balance for LRM can be written as

$$dQ_w = -dQ_{ev} - dQ_f \tag{4}$$

At the same time

$$dQ_w = c_p m_w dT_w \tag{5}$$

where c_p – isobaric heat capacity of LRM (value c_p is function of temperature T_w), $\frac{J}{kg \cdot K}$

In view of (2), (3) and (5), heat balance for LRM (4) can be written as

$$c_p m_w dT_w = -r_w \beta_{sw}(p_{sw} - p_m)Sdt - kF(T_w - T_f)dt \tag{6}$$

Functions $\beta_{sw}(T_{sw})$, $p_{sw}(T_{sw})$, $p_m(T_m)$, $r_w(T_w)$ and $c_p(T_w)$ are polynomials. They are compiled according to the table values [8], [9].

In model, the performance of forced ventilation unit is determined by the flow rate of involved air. After the exhaust ventilation pipe, SARM partially settles on filters. This phenomenon accounts for the coefficient of filtration. It determines the relative amount of SARM that is deposited on the filter material. SARM further passes through the ventilation stack into the atmosphere.

Another method to confine LRM is to drain the spilled liquid by drainage pumps or by gravity. This process is characterized by the flow rate of LRM through the drainage channel.

The partial removal of radioactive substances from the liquid by evaporation depends on physicochemical properties of radioactive impurities and the solvent.

3.3. Modeling of the LRM evaporation

To solve the problem of unsteady LRM evaporation, using equations (1)-(6), four balance differential equations (7) were written to relate the main parameters of LRM and air space of area over time.

$$\begin{cases} \frac{dm_w}{dt} = -\beta_{sw}(p_{sw} - p_m)S - G_d \\ \frac{dm_a}{dt} = \beta_{sw}(p_{sw} - p_m)S - G_V \cdot \frac{m_a}{V} \\ \frac{dm_q}{dt} = G_V \frac{m_a}{V}(1-\psi) \\ \frac{dT_w}{dt} = -\frac{r_w \beta_{sw}(p_{sw} - p_m)S + kF(T_w - T_f)}{c_p m_w} \end{cases} \tag{7}$$

where m_a – current mass of SARM in air of the area, *kg*;

G_d – flowrate of LRM through the drainage channel (it also includes the volume of LRM leakage from the area), *kg/s*;

V – air volume in the area, m^3;

G_V – flow rate of involved air of forced ventilation (this parameter includes SARM leakage through the gaps or clearances in walls of the emergency area) m^3/s;

ψ – coefficient of filtration (efficiency of filtration);

m_q – mass of released SARM into the atmosphere, *kg*.

This system of nonlinear differential equations includes polynomial functions. Using the Mathcad sphere for solving the system of equations (7) provides the desired functions in matrix form (the values of the functions at particular moments of accident).

Average activity concentration of the radionuclide in the area air A_{air} (Bq/m^3) is given by the formula

$$A_{air} = \frac{A_w}{V} H \cdot m_a \tag{8}$$

where A_w – concentration of radionuclide in LRM, *Bq/kg;*

H – fraction of carried away solute with solvent vapours during evaporation.

The ultimate objective of the model is to determine the dynamics of LRM evaporation, SARM activity in the air space and the integral release of radioactive substances into the atmosphere. The mass fraction of a radionuclide in the release relative to its original content in radioactive liquid is commonly used in practice:

$$q = \frac{A_w}{m_0} H \cdot m_q \cdot 100\% \tag{9}$$

where m_0 – initial mass of LRM, *kg*.

This value is used as an input parameter for the assessment of doses to the population from atmospheric release.

3.4. Description of SARM atmospheric transport

There are a considerable number of theoretical and experimental studies devoted to the dispersion of pollutants released into the atmosphere. Simplified approaches may be used in calculations for dispersion modelling. One of such approaches is the Pasquill-Gifford method [10]. The calculation with this method involves selecting conservative categories of atmospheric stability and wind speed depending on the effective height of SARM release. These parameters are crucial in the distribution of radioactive substances in the territory surrounding the emergency facilities. Using method the Pasquill-Gifford method, we find fields of volume activity concentration in air and surface activity concentration on the ground of radionuclides. These parameters define the effective doses to the public.

3.5. Assessment of effective dose

The effective dose includes 3 special effective doses. It finds as

$$D_{ef} = \sum_i \left(D_i^{air} + D_i^{srf} + D_i^{ing} \right) \tag{10}$$

where D_i^{air} – effective dose due to inhalation and external irradiation from cloud (for *i*-th radionuclide), *Sv*;

D_i^{srf} – effective dose due to external irradiation from ground surface (for *i*-th radionuclide), *Sv;*

D_i^{ing} – effective dose due to ingestion (for *i*-th radionuclide), *Sv*.

Assessment of effective dose during 14 days received by an adult D_{ef} is based on the method [11].

3.6. Results of assessment of radiation consequences

The assessment resulted in a series of basic parameters of the radiation environment within and outside the emergency area:

- average activity concentration of the radionuclide in the area air A_{air},
- mass fraction of the radionuclide in the release relative to the original content in radioactive liquid *q*,
- effective dose received by an adult during 14 days as a result of SARM release D_{ef}.

4. ANALYSIS OF THE INFLUENCE OF INITIAL ACCIDENT CONDITIONS ON THE RESULTS OF ASSESSMENT

During the study, we assessed radiation consequences with the aim of briefly analysis of some results obtained for the hypothetical accident with spills of LRM in the storage area of liquid radioactive waste with a forced ventilation system, according to the input data specified in Table. 1.

Table 1. Input data of assessment

No	Parameter	Value
1	Initial mass of LRM m_0, *kg*	$2.0 \cdot 10^5$
2	Initial temperature of LRM T_{w0}, ^0C	98
3	Area of evaporation *S*, m^2	200
4	Area of contact surface of LRM with the floor *F*, m^2	210
5	Average temperature of the floor T_f, ^0C	20
6	Air volume in the area *V*, m^3	1000
7	Efficiency of filtration ψ	0
8	Heat transfer coefficient for the floor*, $\frac{W}{m^2 \cdot K}$	15.4
9	Average activity concentration of radionuclide in LRM A_w, *Bq/kg*: ^{137}Cs ^{60}Co	 $3.7 \cdot 10^8$ $4.7 \cdot 10^7$

*It was found for layered floor according to [7]: the outer layer - polymer (2 *mm*), the inner layer - concrete (1 *m*)

SARM released into the atmosphere through the ventilation stack (100 *m* height) in the following weather conditions:

- wind speed of 1 *m/s*;
- class of atmospheric stability "B" (the most conservative class for release height of 100 *m*);
- roughness of the underlying surface soil – 10 *cm*.

To analyze the influence of the initial accident conditions on the final results of the assessment, a number of input parameters were chosen: flow rate (G_V) and temperature (T_m) of supplied ventilation air, LRM drainage flow rate (G_d). Unlike other parameters, these values can be adjusted during an accident. These data are represented as a series of values in Table 2.

Table 2. Input parameters of operating modes of ventilation and drainage systems

No	G_V, m^3/s	T_m, ^0C	G_d, kg/s
1	0.001	10	0
2	0.75		
3	1.5		
4	2.25		
5	0.75	5	0
6		25	
7		45	
8	0.75	10	0
9			50
10			100
11			150

4.1. Results of assessment

Some results of the assessment of radiation consequences are shown in Table 3 (for the mix ^{137}Cs+^{60}Co) and Figs. 2–4 (only for ^{137}Cs).

Curves of Figs. 2–4 for ^{137}Cs are similar to ^{60}Co, cause, according to (8), the values of activity concentration A_{air} of both radionuclides are linearly dependent. According to (9), it is the same for mass fraction q. Therefore, for the analysis we showed the curves only for ^{137}Cs.

Table 3. Values of the maximum effective dose to the human body during 14 days depending on the operating modes of ventilation and drainage systems

No	Effective dose D_{ef}, μSv
1	1.94
2	14.90
3	15.53
4	16.15
5	16.50
6	15.53
7	12.53
8	14.83
9	3.13
10	1.88
11	1.39

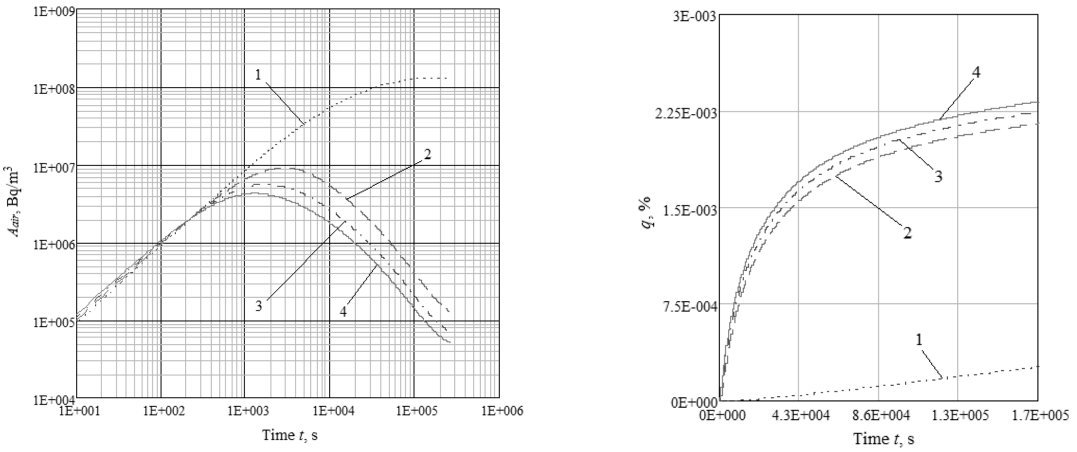

a) b)

Fig. 2. Changes in average activity concentration in the air of emergency area (a) and mass fraction of ^{137}Cs released to the environment (b) for the following ventilation flow rates: $G_V = 0.001\ m^3/s$ (1); $G_V = 0.75\ m^3/s$ (2); $G_V = 1.5\ m^3/s$ (3); $G_V = 2.25\ m^3/s$ (4)

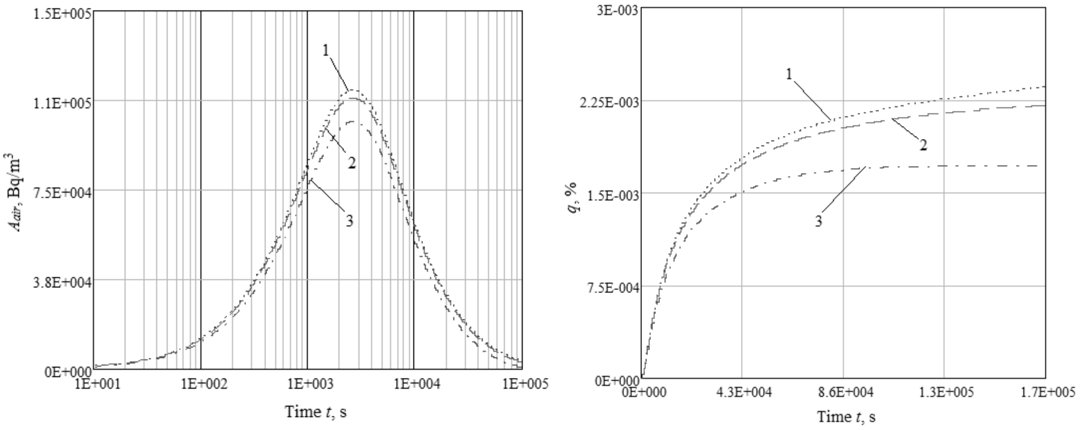

a) b)

Fig. 3. Changes in average activity concentration in the air of emergency area (a) and mass fraction of ^{137}Cs released to the environment (b) for the following supply air temperature: $T_m = 5^0C$ (1), $T_m = 25^0C$ (2), $T_m = 45^0C$ (3)

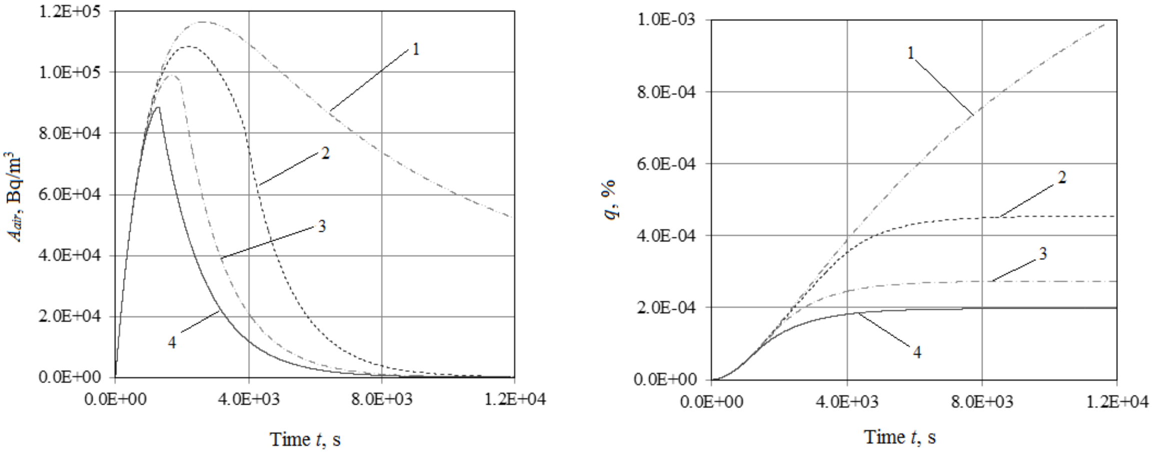

a) b)

Fig. 4. Changes in average activity concentration in the air of emergency area (a) and mass fraction of ^{137}Cs released to the environment (b) for the following drainage flow rates: $G_d = 0\ kg/s$ (1), $G_d = 50\ kg/s$ (2) , $G_d = 100\ kg/s$ (3), $G_d = 150\ kg/s$ (4)

4.2. Analysis

According to the assessment results (Fig. 2a), with higher flow rate, the activity concentration in the air of emergency area reduces and the release of radionuclides into the atmosphere (Fig. 2b) slightly increases with further growth of the flow rate. Therefore, there is the minimum flow rate that may provide sufficient reduction in SARM activity in the air of area. In this accident, atmospheric release is eliminated only if the ventilation system is inactive and the emergency area is completely confined.

The results presented in Fig. 3 indicate that heating of supply ventilation air (to the temperature of LRM surface T_{sw}) helps to suppress the evaporation process. The activity concentration of SARM in the air of emergency area and integral SARM release into the atmosphere decrease with increasing temperature of supply air.

The calculated data show (Fig. 4) that drainage of LRM is the most effective way to confine and prevent the release of radioactive substances into the air of emergency area and the environment. In the absence of drainage (curve 1, Fig. 4b), the integral release of SARM is rapidly growing even in 2 hours from the beginning of the accident.

It is interesting to note that curves 2–4 in Fig. 4a are not smooth. Each of them has the point of "breaking". At these times, the confinement of LRM and the evaporation process are terminated. Clearing of SARM remaining in the air of area begins.

In all cases, the effective dose to the public and personnel from a particular radionuclide is directly proportional to the size of release and activity concentration in the emergency area, respectively. Assessment of effective doses to the public has showed that this accident cannot cause significant radiation consequences (Table 3). High flow rate and low temperature of supplied ventilation air contribute to increase effective doses to the public.

5. CONCLUSIONS

The developed model can be used directly during an accident and with a reasonable degree of conservatism to give an adequate assessment of the radiation consequences for the set of initial conditions of accidents with spills of LRM in areas with forced ventilation.

During the study, characteristic dependences between parameters of liquid radioactive materials and air exchange in areas with forced ventilation and associated radiation consequences for the public were determined. The analysis of the influence of initial accident conditions on the results of assessment showed that there is a minimum set of countermeasures and facilities that can significantly reduce the radiation consequences of accidents with spills of LRM in areas with forced ventilation system, thereby reducing the dose to the public and facility personnel. Thus, in case of an accident with leakage of a radioactive water solution with a temperature close to the boiling point, rapid drainage of LRM and ventilation of the emergency area with heated air can ensure the minimum activity concentration of SARM within the area and the release of radioactive substances into the environment.

REFERENCES

1. The XIII Scientific and Practical Conference “Modern problems of scientific power ware” of Post graduate Students, Masters of Arts and Students. National Technical University of Ukraine “Kyiv Polytechnic Institute” 21-24.04.2015.
2. MELCOR Computer Code Manuals. Office of Nuclear Regulatory Research U.S. Nuclear Regulatory Commission Washington, NUREG/CR-6119, Vol. 3.

3. IAEA safety standards series. Radiation protection aspects of design for nuclear power plants. No NS-G-1.13, IAEA, Vienna, 2005.
4. Materials on environmental impact assessment of the proposed activity on the operation of a nuclear facility, a complex of nuclear materials intended for radiochemical reprocessing of spent nuclear fuel. Federal State Unitary Enterprise "Production Association "Mayak" FSUE" PA "Mayak", 2012.
5. NESTERENKO, Aleksey, V. *Fundamentals of thermodynamic calculations ventilation and air conditioning*. Moscow: Vysshaia Shkola, 1971. 460 p.
6. NESTERENKO, Aleksey V. Experimental study of heat and mass transfer during evaporation of the liquid with a free surface. *Material science*. Technical Physics. Academy of Sciences of the USSR. Vol. 24, No. 4, 1954.
7. ISACHENKO, Victor P, OSIPOVA, Varvara A., SUKOMEL, Aleksandr S. *Heat transfer*. Moscow: Energiya, 1975. 488 p.
8. VOLKOV, Oleg D. *Designing of industrial building ventilation*. Kharkov: Vyscha Shkola, 1989. 240p. ISBN 5-11-000656-3.
9. RIVKIN, Solomon L., ALEKSANDROV, Aleksey A. Thermodynamic properties of water and steam. *Directory*. Moscow: Energiya, 1984. 80 p.
10. GUSEV, Nicolay G., BELYAEV, Valentin A. *Radioactive releases in the biosphere*. Moscow: Energoatomizdat, 1991. 256 p. ISBN 5-283-03025-3.
11. Standard of National Nuclear Energy Generating Company "Energoatom". Procedure for setting the size of the sanitary protection zone NPP, 2014.

CYSENI 2015, May 27–28, Kaunas, Lithuania
ISSN 1822-7554, www.cyseni.com

NUCLEAR FUEL DEMAND EFFECT ON THE FRONT-END URANIUM MARKET

A. Auzans, A. Teder, A.H. Tkaczyk
University of Tartu
Ravila 14C, Tartu 50411, Estonia
Phone +372-737-4602
Email: aris.auzans@gmail.com, *allan.teder@gmail.com, alan@ut.ee*

ABSTRACT

This paper demonstrates the effect of a major demand shock to the natural uranium (NU) market based on real market supply and demand analysis. The uranium market is modelled as front-end nuclear fuel cycle, where the final low-enriched uranium (LEU) consumers are nuclear reactors which have relatively stable demand. Enrichment facilities are provided with NU, which comes from uranium mines.

NU enrichment facilities have an option to vary NU demand by adjusting the separative work unit (SWU) rate. When the price of NU increases enrichment facilities demand less NU and use more SWU to produce the same amount of LEU. However, when NU becomes cheap, enrichment facilities consume more NU and use less SWU to produce the same amount of LEU.

For simulation we use a mine-based uranium market clearing model [1, 2]. The mine-based uranium model is built around databases of primary and secondary uranium supply as a time-dependent simulation that determines the uranium and enrichment market conditions by calculating the intersection between the supply and demand curves in each user-defined time period (usually one year) [3]. The model simulates a time period from 2010 until 2030.

The market supply of NU is the sum of the supply functions of all individual uranium producers with their respective marginal costs. Uranium mines' operational decisions are based on the economic characteristics of individual mines. A new mine will not begin to operate unless its average total cost of producing uranium is less than or equal to the mine’s marginal costs (MC). Through this approach, this work models nuclear fuel demand effects on the front-end uranium market, and the results are relevant for uranium producers, consumers, as well as policymakers.

Keywords: market modelling, nuclear fuel cycle economics

1. INTRODUCTION

Unlike other commodities, natural uranium is not traded on an organized commodity exchange market. The uranium market mainly works on fixed long term supply contracts based on direct negotiations between uranium mine operators and facilities, but some 20% of all natural uranium part is traded under free market conditions [4-6]. The current simulation relies on the spot market price, which is based on current supply and demand and is subject to speculative effects.

The objective of this paper is to demonstrate the effect of a major demand shock to the natural uranium (NU) market based on real market supply and demand analysis in the perfect market competition conditions. A summary of a mine based market clearing model is presented. At each time step, U and enrichment market clearing states are solved; hence the model responds to shifts in supply and demand, for instance closure of a major mine. The market demand for uranium is the sum of the demand functions of all individual uranium consumers. Investments in nuclear energy reactors have long payback periods and are often with strategic importance for the country therefore we expect the demand for natural uranium to remain relatively stable regardless of the price (the demand is non-elastic). The individual supply curves are made from the available information in the uranium mine and enrichment plant databases, and the NU supply curve is augmented by secondary sources of uranium which are generally assigned zero production cost.

In a mine based market model, each uranium mine acts like an individual agent that is capable of deciding under which conditions it is economical to continue operation, suspend U mining or open a new uranium mine. Decisions are partly based on the current time period's U market price: for instance, if the price exceeds a prospective mine's total operating costs, the model opens the mine. To make these decisions, the model must have additional information about U mine's economic characteristics, specifically its total overnight capital cost (TOC) of construction, operation and maintenance (OM) and decommissioning (DD) costs.

One representative mine of each type, underground (UG), open pit (OP) and in-situ leach (ISL), is chosen from this data set. The Generation-IV Economic Modeling Working Group (EMWG) unit cost calculation procedure is used to compute unit production costs–UC ($/kg U), for these mines [7]. All other mines of that type are assumed to adhere to the same relative distribution of capital, operating and decommissioning costs. The EMWG calculations takes into account a sinking fund amortization factor (SFF), total construction period and discount rate.

This treatment of mine opening and re-opening decisions is a simplification of a lengthy and involved process. Therefore companies planning to operate mines must undertake a complex licensing process and provide the regulator with a long term financial management and decommissioning plan. In case of unexpected closure, the mine owner must obtain license renewal prior to re-opening [8].

Individual agents make decisions based only upon conditions in the current time step and not knowing what others are doing. Since this gives rise to unrealistically myopic behaviour, a time rollback function has been implemented to allow the simulator to move back in time in order to change agent decisions. This rollback function simulates the ability of entities to make long-run market forecasts; by rolling back the simulation clock to change a decision, an agent is modifying its strategy based upon the projected evolution of the market and the future actions it expects other entities to take. In this implementation, marching backward and forward in time creates a simulation strategy where uranium mines operate throughout their lifetimes rather than, say, shut down early due to over construction of capacity. The rollback function is used only in cases, if mine after opening causes significant market price fluctuations and in the second year after entering in market is forced to quit market.

This paper starts with the methodology section, which describes the improved agent decision making process.

Once the methodology is developed, test cases are presented next in Section 3, Results. The test case implements the realistic depiction of the world's uranium and enrichment markets described in ref. 1 and demonstrates the shock case. The final results are compared in the conclusion section.

2. METHODOLOGY

The aim of the work is to present demand effect shock to the natural uranium market. NU demand directly affects U mines, meanwhile enrichment facilities can adjust to the different market conditions. Assuming that uranium price increases (the reason might be shortage of supply). Enrichment facilities will demand less uranium and use more SWU to produce the same amount of enriched uranium. However when uranium becomes cheap, enrichment facilities order more NU and use less SWU to produce the same amount enriched uranium. Based on enrichment facilities' ability to adjust NU consumption we can expect that enrichment demand will drop more than NU demand. Mines will not have ability to reduce production in a short term, therefore the supply of NU on the market will be relatively high.

A mine-based market model allows U mines to produce between sort-run break-even point and long run shutdown point in a long run, which is rather unrealistic. Therefore, the paper presents a new agent decision making algorithm, to limit the time period in which mines can operate with losses. The model compares production costs with U market prices over the last 4 years. If U market price in the last 4 years was below to the short-run mine's MC, U mine will be shutdown.

Each mine in every time step undergoes such decision making process.

1. The mine is checked for availability. Any mine not currently able to operate in the given year is unavailable.
   a. If the mine is not available, skip to the next mine.
   b. If the mine is available, proceed to step 2.
2. The mine is checked for operation in the previous time step.
   a. If the mine operated in the previous time step, go to step 3.
   b. If no uranium was produced by the mine in the previous time step, proceed to step 4.
3. The minimum value of average variable costs (E_2) of the mine is checked against the current market price.
   a. If E_2 is greater than or equal to the market price proceed to step 6.
4. If E_2 is less than market price the mine enters temporary shutdown and the model restarts at step 1 with the next mine.
5. Checks determine if the mines are not running more than four years below short-run mine's MC (E_1).
6. If the mine did not operate in the previous time-step, the current market price is checked against the mine's E_1.
   a. If E_1 is greater than or equal to the market price, a new mine is opened and the model proceeds to step 5.
   b. If E1 is less than the market price, the loop restarts with the next mine.
7. The mine is flagged to produce uranium during the current time step.
8. A check is made to determine if the current mine is the last mine in the simulation (n = N).
   a. If true, the loop ends.
   b. If false, the loop is restarted with the next mine in the list.

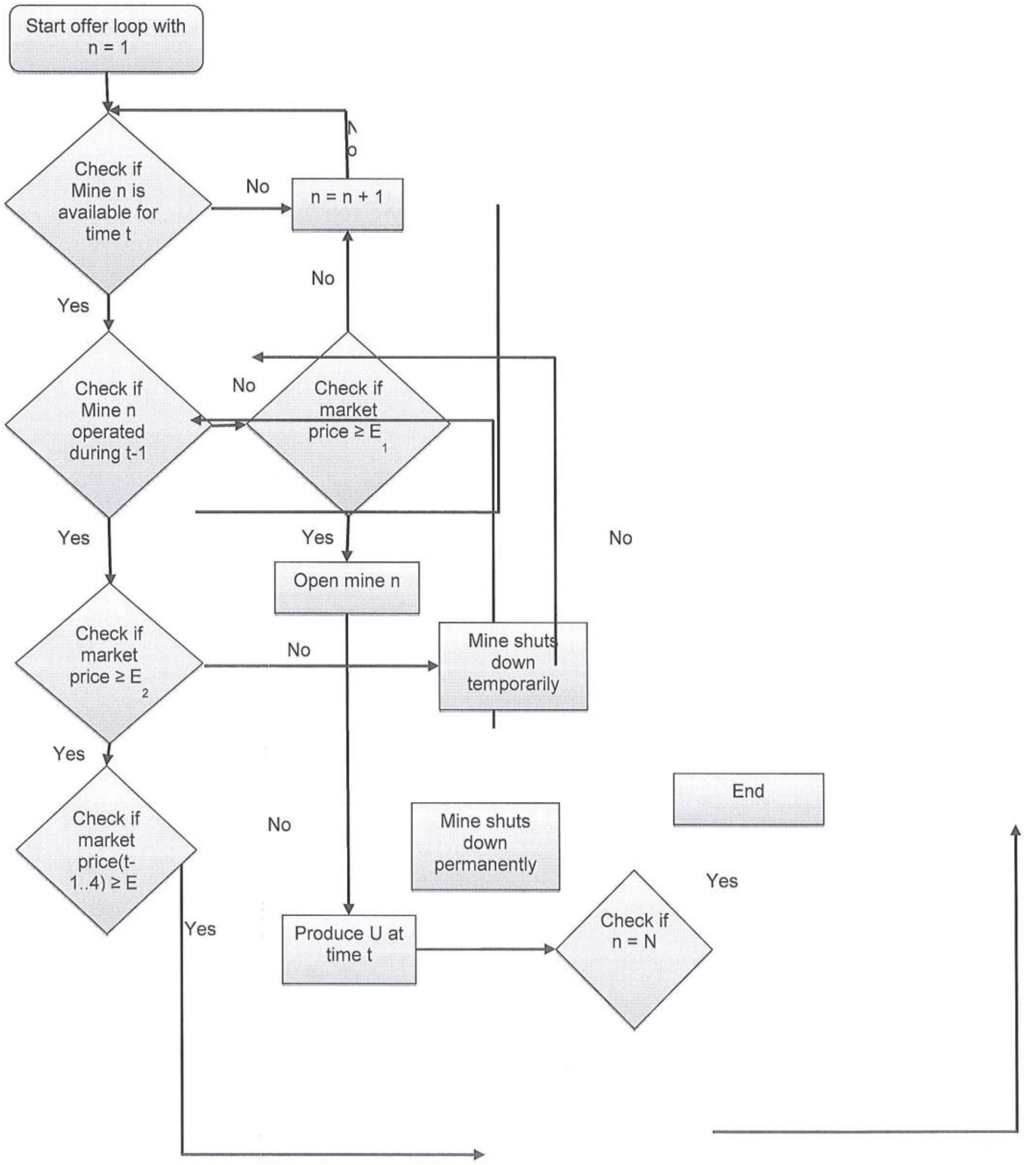

Fig. 1. Uranium mine decision making event chain

3. RESULTS

The real world scenario utilizes the reference-case uranium and enrichment industries described
in [1, 2] and results are given below in the Figures 2-5.

This test case assumes that with the demand shock starting from 2018 until 2023, NU demand fall each year by 5%. After year 2023 demand is projected to increase by 2.6% annually. In addition, all enrichment plant capacities are assumed to grow at a rate equal to that of LEU demand, an average of 2.6% per year, in each year after 2018.

Comparing the reference case and demand shock case we can see that content of tails (Fig. 2) is higher in the demand shock case, because more uranium is available in the market with a relatively small price and enrichment facilities use more NU and less SWU to produce enriched uranium. Also the SWU price (Fig. 3) is relatively lower because there is more NU in the market compared to the reference case. Figures 4 and 5 show annual SWU consumption and annual NU consumption, which is in line with the expected results — the fall of demand affecting NU and enrichment markets.

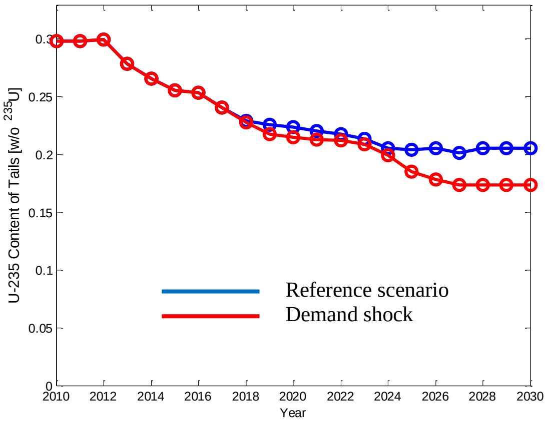

Fig. 2. Uranium U235 content in waste after enrichment

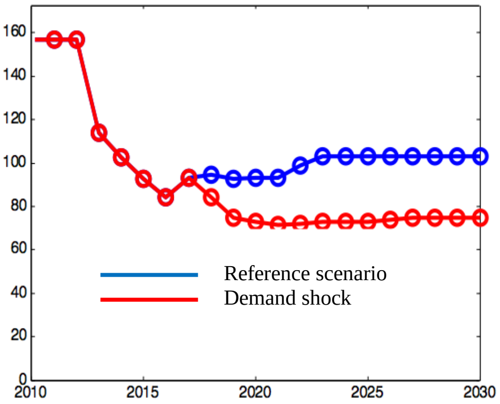

Fig. 3. Annual SWU price

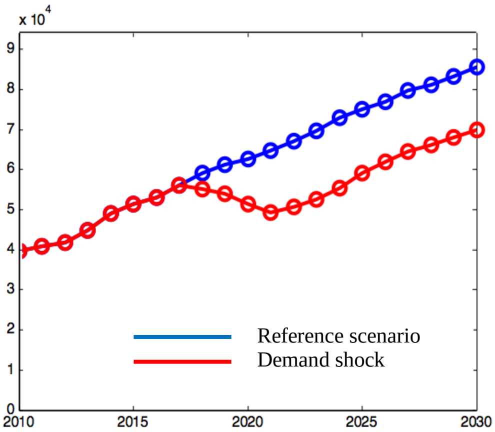

Fig. 4. Annual SWU consumption

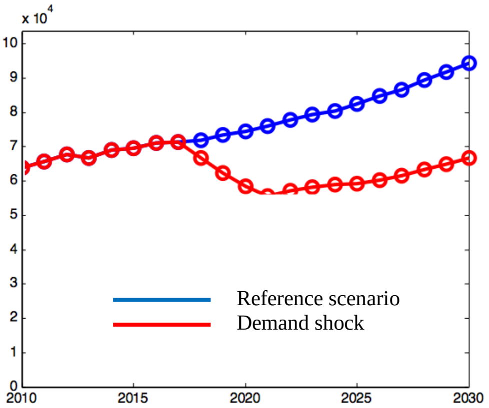

Fig. 5. Annual NU consumption

4. CONCLUSIONS

Using the uranium industry as an example, this paper has demonstrated a demand shock. Based upon their unique characteristics, the uranium mine entities made yearly decisions to commence or continue production, or alternatively to enter into short-term or permanent shutdown. The decisions were based upon the economic theory of individual firms with unique supply curves participating in a competitive market.

Demand shock analysis demonstrates effect on NU market and enrichment industry. Enrichment industry can react on NU price change by adjusting uranium U235 content in waste after enrichment process. In a case of small changes in NU price or demand, enrichment industries will adjust production. In a large demand shock case enrichment services and mines will reduce production output proportionally. U mine's directly depends from the enrichment industry output.

ACKNOWLEDGMENTS

This article is based on work supported by Award No. ESP1-7030-TR-11of the U.S. Civilian Research & Development Foundation (CRDF) and by the National Science Foundation under Cooperative Agreement No. OISE-9531011.Specifically, we acknowledge support from the CRDF Global and Estonian Science Foundation 2010 Energy Research Competition (CRDF-ETF II), including award ESP1-7030-TR-11 and ETF award 22/2011. “This research was supported by European Social Fund’s Doctoral Studies and Internationalisation Programme DoRa”.

REFERENCES

1. SCHNEIDER, E.A., PHATHANAPIROM, U., EGGERT, B.R., SEGAL, E. A market-clearing model of the uranium and enrichment industries. *Nucl. Technol.* 2013, 183, 160–177.
2. AUZANS ARIS, SCHNEIDER, ERICH A., FLANAGAN, ROBERT, TKACZYK, ALAN H. (2014). A Mine-Based Uranium Market Clearing Model. *Energies*, 7(11), 7673–7693.
3. EGGERT, R., GILMORE, A., SEGAL, E. Expanding Primary Uranium Production: A Medium-Term Assessment,” Colorado School of Mines Report. *Colorado School of Mines*: Colorado, USA. 2011.
4. *2013 Uranium Marketing Annual Report*; U.S. Department of Energy: Washington, DC, USA, 2014.
5. *The Global Nuclear Fuel Market*: Supply and Demand 2011–2030; World Nuclear Association: London, United Kingdom, 2008.
6. *Nuclear Energy Data*; OECD Technical Report NEA-6893; OECD Nuclear Energy Agency Paris, France, 2010.
7. Economic Modeling Working Group (EMWG) of the Generation IV International Forum. *Cost Estimating Guidelines for Generation IV Nuclear Energy Systems*; OECD Nuclear Energy Agency: Issy-les-Moulineaux, France, 2007.
8. *Licensing Process for New Uranium Mines and Mills in Canada*; Minister of Public Works and Government Services Canada Catalogue Number CC172-40/2007E-PDF; Canadian Nuclear Safety Commission: Ottawa, Canada, 2007.